

AD-A166 178

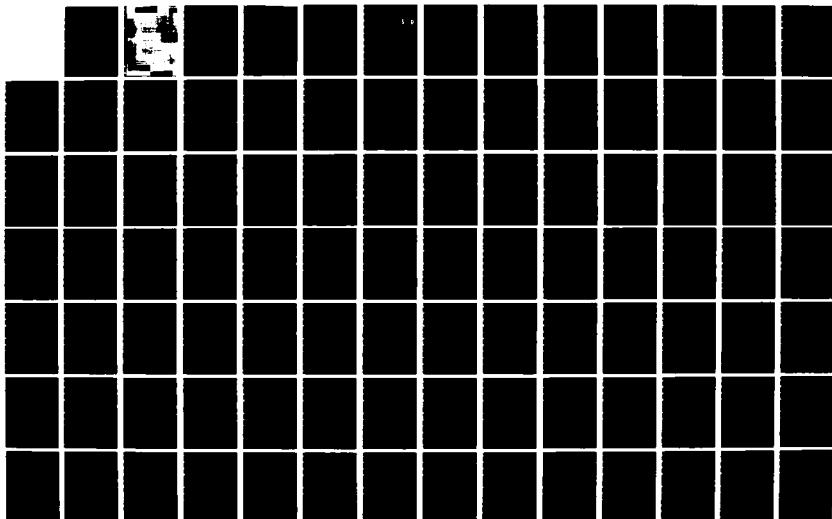
UNITED STATES AIR FORCE SUMMER FACULTY RESEARCH PROGRAM
1985 TECHNICAL RE. (U) UNIVERSAL ENERGY SYSTEMS INC
DAYTON OH R C DARRAH ET AL DEC 85 AFOSR-TR-86-0141
F49620-85-C-0013

1/11

UNCLASSIFIED

F/G 5/9

NL





MICROCOPY RESOLUTION TEST CHART
NATIONAL BUREAU OF STANDARDS-1963-A

AFOSR-TR-86-0141

①

AIR FORCE OFFICE OF SCIENTIFIC RESEARCH

AD-A166 178

UNITED STATES AIR FORCE

SUMMER FACULTY
RESEARCH PROGRAM

CONDUCTED BY
UNIVERSAL ENERGY SYSTEMS
U.E.S.

DTIC
ELECTE
APR 03 1986
S D

DTIC FULL COPY

1985
TECHNICAL REPORT
VOLUME 3 OF 3

RODNEY C. DARRAH
PROGRAM DIRECTOR, UES

SUSAN K. ESPY
PROGRAM ADMINISTRATOR, UES

DISTRIBUTION STATEMENT A

Approved for public release
Distribution Unlimited

86 4 11 51

UNCLASSIFIED

SECURITY CLASSIFICATION OF THIS PAGE

REPORT DOCUMENTATION PAGE

1a. REPORT SECURITY CLASSIFICATION UNCLASSIFIED		1b. RESTRICTIVE MARKINGS	
2a. SECURITY CLASSIFICATION AUTHORITY		3. DISTRIBUTION/AVAILABILITY OF REPORT APPROVED FOR PUBLIC RELEASE; DISTRIBUTION UNLIMITED	
2b. DECLASSIFICATION/DOWNGRADING SCHEDULE		5. MONITORING ORGANIZATION REPORT NUMBER(S) AFOSR-TR- 86-0141	
4. PERFORMING ORGANIZATION REPORT NUMBER(S)		7a. NAME OF MONITORING ORGANIZATION AFOSR/XOT	
6a. NAME OF PERFORMING ORGANIZATION Universal Energy Systems	6b. OFFICE SYMBOL (If applicable)	7b. ADDRESS (City, State and ZIP Code) Building 410 Bolling AFB, DC 20332-6448	
8a. ADDRESS (City, State and ZIP Code) 4401 Dayton-Xenia Rd. Dayton, Ohio 45432		9. PROCUREMENT INSTRUMENT IDENTIFICATION NUMBER F49620-85-C-0013	
8a. NAME OF FUNDING/SPONSORING ORGANIZATION AFOSR	8b. OFFICE SYMBOL (If applicable) XOT	10. SOURCE OF FUNDING NOS.	
8c. ADDRESS (City, State and ZIP Code) Building 410 Bolling AFB, DC 20332-6448		PROGRAM ELEMENT NO. 61102F	PROJECT NO. 2301
11. TITLE (Include Security Classification) United States Air Force Summer Faculty Research Program - Volume 3 - 1985		TASK NO. D5	WORK UNIT NO.
12. PERSONAL AUTHOR(S) Rodney C. Darrah, Susan K. Espy			
13a. TYPE OF REPORT Annual	13b. TIME COVERED FROM _____ TO _____	14. DATE OF REPORT (Yr., Mo., Day) December 1985	15. PAGE COUNT
16. SUPPLEMENTARY NOTATION			
17. COSATI CODES		18. SUBJECT TERMS (Continue on reverse if necessary and identify by block number)	
FIELD	GROUP	SUB. GR.	
19. ABSTRACT (Continue on reverse if necessary and identify by block number) See Attached			
20. DISTRIBUTION/AVAILABILITY OF ABSTRACT UNCLASSIFIED/UNLIMITED <input checked="" type="checkbox"/> SAME AS RPT. <input type="checkbox"/> DTIC USERS <input type="checkbox"/>		21. ABSTRACT SECURITY CLASSIFICATION UNCLASSIFIED	
22a. NAME OF RESPONSIBLE INDIVIDUAL Major Amos Otis, Program Manager		22b. TELEPHONE NUMBER (Include Area Code) (202) 767-4970	22c. OFFICE SYMBOL XOT

The United States Air Force Graduate Student Summer Support Program (USAF-GSSSP) is conducted under the United States Air Force Summer Faculty Research Program. The program provides funds for selected graduate students to work at an appropriate Air Force Facility with a supervising professor who holds a concurrent Summer Faculty Research Program appointment or with a supervising Air Force Engineer. This is accomplished by the students being selected on a nationally advertised competitive basis for a ten-week assignment during the summer intersession period to perform research at Air Force laboratories/centers. Each assignment is in a subject area and at an Air Force facility mutually agreed upon by the students and the Air Force. In addition to compensation, travel and cost of living allowances are also paid. The USAF-GSSSP is sponsored by the Air Force Office of Scientific Research, Air Force Systems Command, United States Air Force, and is conducted by Universal Energy Systems, Inc.

The specific objectives of the 1985 USAF-GSSSP are:

- (1) To provide a productive means for the graduate students to participate in research at the Air Force Weapons Laboratory;
- (2) To stimulate continuing professional association among the Scholars and their professional peers in the Air Force;
- (3) To further the research objectives of the United States Air Force;
- (4) To enhance the research productivity and capabilities of the graduate students especially as these relate to Air Force technical interests.

During the summer of 1985, 92 graduate students participated. These researchers were assigned to 25 USAF laboratories/centers across the country. This two volume document is a compilation of the final reports written by the assigned students members about their summer research efforts.

UNCLASSIFIED

AFOSR-TR. 86-0141

Approved for public release;
distribution unlimited.

①

DTIC
ELECTE
APR 03 1986
S D

UNITED STATES AIR FORCE
SUMMER FACULTY RESEARCH PROGRAM
1985
PROGRAM TECHNICAL REPORT
UNIVERSAL ENERGY SYSTEMS, INC.
VOLUME III of III

Program Director, UES
Rodney C. Darrah

Program Manager, AFOSR
Major Amos L. Otis

Program Administrator, UES
Susan K. Espy

DISTRIBUTION STATEMENT A
Approved for public release;
Distribution Unlimited

Submitted to
Air Force Office of Scientific Research
Bolling Air Force Base
Washington, DC
December 1985

86 4 1 151

PREFACE

The United States Air Force Summer Faculty Research Program (USAF-SFRP) is a program designed to introduce university, college, and technical institute faculty members to Air Force research. This is accomplished by the faculty members being selected on a nationally advertised competitive basis for a ten-week assignment during the summer intersession period to perform research at Air Force laboratories/centers. Each assignment is in a subject area and at an Air Force facility mutually agreed upon by the faculty members and the Air Force. In addition to compensation, travel and cost of living allowances are also paid. The USAF-SFRP is sponsored by the Air Force Office of Scientific Research, Air Force Systems Command, United States Air Force, and is conducted by Universal Energy Systems, Inc.

The specific objectives of the 1985 USAF-SFRP are:

- (1) To provide a productive means for Scientists and Engineers holding Ph.D. degrees to participate in research at the Air Force Weapons Laboratory;
- (2) To stimulate continuing professional association among the Scholars and their professional peers in the Air Force;
- (3) To further the research objectives of the United States Air Force;
- (4) To enhance the research productivity and capabilities of Scientists and Engineers especially as these relate to Air Force technical interests.

During the summer of 1985, 154-faculty members participated. These researchers were assigned to 25 USAF laboratories/centers across the country. This three volume document is a compilation of the final reports written by the assigned faculty members about their summer research efforts.

LIST OF PARTICIPANTS

NAME/ADDRESS

DEGREE, SPECIALTY, LABORATORY ASSIGNED

Dr. Phillip Ackerman
Assistant Professor
University of Minnesota
Dept. of Psychology
Elliott Hall
75 E. River Rd.
Minneapolis, Minnesota 55455
(612) 376-3139

Degree: Ph.D., Philosophy in
Psychology, 1984
Specialty: Human Abilities, Cognitive
Processes, Research
Methodology
Assigned: HRL/MO

Dr. Samuel Adams
Associate Professor
Iowa State University
Dept. of Industrial Engineering
212 Marston Hall
Ames, Iowa 50011
(515) 294-5065

Degree: Ph.D., Industrial
Engineering 1966
Specialty: Human Factors
Engineering
(Ergonomics), Biomechanics
Assigned: AMRL

Dr. Vernon Allen
Professor
Tennessee Technological Univ.
Dept. of Chemistry
Box 5055
Cookeville, Tennessee 38505
(615) 528-3425

Degree: Ph.D., Polymer Science,
1960
Specialty: Polymer Structure -
Property Relationship
Assigned: AFWAL/ML

Dr. Jihad Alsadek
Assistant Professor & Chairman
Tougaloo College
Department of Economics
Tougaloo, Mississippi 39174
(601) 956-4941

Degree: Ph.D., Economics, 1983
Specialty: Economics
Assigned: HRL/OT

Dr. Deborah Armstrong
Assistant Professor
University of Texas
Division of Life Sciences
San Antonio, Texas 78285
(512) 691-4458

Degree: Ph.D., Neuroscience,
1982
Specialty: Neurophysiology
Assigned: SAM



Accession For	
NTIS CRA&I	<input checked="" type="checkbox"/>
DTIC TAB	<input type="checkbox"/>
Unannounced	<input type="checkbox"/>
Justification	
By	
Distribution	
Availability Codes	
Dist	Avail and/or Special
A-1	

Dr. Lucia Babcock
Assistant Professor
Louisiana State University
Department of Chemistry
Baton Rouge, Louisiana 70803
(504) 388-4694

Degree: Ph.D., Inorganic Chemistry,
1978
Specialty: Ion-Molecule Chemistry,
Kinetics
Assigned: AFGL

Dr. Francesco Bacchialoni
Associate Professor
University of Lowell
Dept. of Electrical Engr.
1 University Avenue
Lowell, Massachusetts 01854
(617) 452-5000

Degree: Ph.D., Engineering, 1946
Specialty: Control Systems, Digital
Signal Processing, Micro-
processors
Assigned: AFGL

Dr. Mukul Banerjee
Professor
Meharry Medical College
Physiology Department
Nashville, Tennessee 37208
(615) 327-6288

Degree: Ph.D., Animal Physiology,
1964
Specialty: Respiratory Physiology,
Environmental Physiology
Assigned: SAM

Dr. Rex Berney
Associate Professor
University of Dayton
Physics Department
300 College Park
Dayton, Ohio 45469
(513) 229-3012

Degree: Ph.D., Solid State Physics,
1978
Specialty: Digital Electronics, Photo-
chromic Materials
Assigned: AFWAL/AL

Dr. Richard Bertrand
Professor of Chemistry
University of Colorado
Department of Chemistry
P. O. Box 7150
Colorado Springs, Colorado 80933-7150
(303) 593-3139

Degree: Ph.D., Chemistry, 1969
Specialty: NMR Spectroscopy, Atomic
Spectroscopy
Assigned: FJSRL

Dr. Peter Binkert
Associate Professor
Oakland University
Linguistics and Classics
Department of Linguistics
Rochester, Michigan 48063
(313) 370-2175

Degree: Ph.D., Linguistics, 1970
Specialty: Linguistic Theory, Natural
Language Understanding by
Computers
Assigned: HRL/IO

Dr. Zinny Bond
Associate Professor
Ohio University
Linguistics Department
204C Gordy Hall
Athens, Ohio 45701
(614) 594-6539

Degree: Ph.D., Linguistics, 1971
Specialty: Speech Acoustics, Speech
Perception
Assigned: AMRL

Dr. Kevin Bowyer
Assistant Professor
University of South Florida
Computer Science & Engr. Dept.
Tampa, Florida 33620
(813) 974-3032

Degree: Ph.D., Computer Science,
1980
Specialty: Software Engineering,
Computer Architecture,
Computer Networks
Assigned: AD

Dr. Eugene Brown
Associate Professor
Virginia Polytech Institute
and State University
Blacksburg, Virginia 24060
(703) 961-7199

Degree: Ph.D., Mechanical
Engineering, 1968
Specialty: Fluid Mechanics,
Computational Fluid
Dynamics
Assigned: WL

Dr. Linda Buehner
Assistant Professor
Wittenberg University
Education Department
P. O. Box 720
Springfield, Ohio 45501
(513) 327-6421

Degree: Ed. D., Curriculum and
Instruction, 1983
Specialty: Learning and Developmental
Handicaps, Reading
Assigned: HRL/LR

Dr. Connie Carrington
Assistant Professor
University of South Carolina
Mechanical Engineering Dept.
College of Engineering
Columbia, South Carolina 29208
(803) 777-7144

Degree: Ph.D., Engineering
Mechanics, 1983
Specialty: Dynamics and Controls
Assigned: AFWAL/FDL

Dr. Robert Chamberlain
Assistant Professor
University of Alabama
Dept. of Aerospace Engr.
241 Hardaway Hall
University, Alabama 35486
(205) 348-7300

Degree: Ph.D., Aeronautical and
Astronautical Engineering,
1984
Specialty: Computational Fluid Dynamics
Assigned: AFWAL/FDL

Dr. Jharna Chaudhuri
Assistant Professor
Wichita State University
Mechanical Engr. Department
Box 35
Wichita, Kansas 67208
(316) 689-3402

Degree: Ph.D., Materials Science,
1982
Specialty: Materials Science,
Metallurgy, Thin Films,
Electronic Materials
Assigned: AFWAL/AL

Dr. Lea Chen
Assistant Professor
The University of Iowa
Dept. Mechanical Engineering
2206 EB
Iowa City, Iowa 52242
(319) 353-5695

Degree: Ph.D., Mechanical
Engineering, 1981
Specialty: Combustion
Assigned: AFWAL/APL

Dr. David Choate
Assistant Professor
Xavier University
Mathematics Department
New Orleans, Louisiana 70125
(504) 486-7411

Degree: Ph.D., Mathematics, 1982
Specialty: Algebra and Number Theory
Assigned: RADC

Dr. Karen Chou
Assistant Professor
Syracuse University
Dept. of Civil Engr.
Syracuse, New York 13210
(315) 423-3314

Degree: Ph.D., Philosophy, Struc-
tural Engineering, 1983
Specialty: Structural Engineering,
Structural Reliability,
Application of Probability
and Statistics in Chemical
Engineering
Assigned: ESC

Dr. Louis Chow
Assistant Professor
Washington State University
Mechanical Engineering Dept.
Pullman, Washington 99164-2920
(509) 335-1327

Degree: Ph.D., Mechanical
Engineering, 1978
Specialty: Heat and Mass Transfer,
Fluid Mechanics
Assigned: AFWAL/APL

Dr. Derald Chriss
Instructor
Southern University
Department of Chemistry
Baton Rouge, Louisiana 70813
(504) 771-3990

Degree: M.S., Chemistry, 1981
Specialty: NMR Spectroscopy, X-Ray
Crystallography, Gas
Chromatography, Magnetic
Susceptibility Studies
Assigned: AFWAL/ML

Dr. David Chung
Professor
Howard University
Department of Physics
Washington, D.C. 20059
(202) 636-7903

Degree: Ph.D., Solid State
Physics, 1966
Specialty: Fiber Optics Sensors,
Ultrasound, Solid State
Electronics
Assigned: RADC

Dr. Gale Clark
Associate Professor
Middle Tennessee State Univ.
Chemistry Department
P. O. Box 137
Murfreesboro, Tennessee 37132
(615) 898-2300

Degree: Ph.D., Analytical
Chemistry, 1968
Specialty: HPLC using Electro-
chemical and Fluore-
scent Detection
Assigned: ESC

Dr. David Cochran
Assistant Professor
Clemson University
Electrical and Computer
Engineering Department
Clemson, South Carolina 29631
(803) 656-3190

Degree: Ph.D., Electrical
Engineering, 1981
Specialty: Solid State
Assigned: RADC

Dr. Alvin Compaan
Professor
Kansas State University
Department of Physics
Cardwell Hall
Manhattan, Kansas 66506
(913) 532-6786

Degree: Ph.D., Physics, 1971
Specialty: Laser Interaction with
Semiconductors
Assigned: AFWAL/AL

Dr. Thomas Connolly
Professor
Embry-Riddle Aeronautical
University
Aeronautical Science
Regional Airport
Daytona Beach, Florida 32014
(904) 252-5561

Degree: Ed.D., Technical Education,
1979
Specialty: Aviation Education,
Instructional Technology
Assigned: HRL/OT

Dr. Hobert Corley
Instructor
Davis and Elkins College
Computer Science Dept.
Elkins, West Virginia 26241
(304) 636-1900

Degree: M.S. Computer Science, 1980
Specialty: Computer Science
Assigned: HRL/LR

Dr. Billy Covington
Assistant Professor
Sam Houston State University
Physics Department
Huntsville, Texas 77341
(409) 294-1606

Degree: Ph.D., Physics, 1978
Specialty: Solid State Physics
Assigned: AFWAL/ML

Dr. Dennis Cravens
Instructor
Vernon Regional Jr. College
Science and Math. Dept.
4400 College Drive
Vernon, Texas 76384
(817) 552-6291

Degree: Ph.D., Molecular Bio-
physics, 1977
Specialty: Mathematic Models,
(numerical calculations)
Assigned: RPL

Dr. Parviz Dadras
Associate Professor
Wright State University
Mechanics Systems Engineering
Dayton, Ohio 45435
(513) 873-2944

Degree: Ph.D., Mechanical
Engineering, 1972
Specialty: Mechanics, Deformation
Processing, Material
Properties
Assigned: AFWAL/ML

Dr. Charles Davis
Assistant Professor
University of Toledo
Department of Math.
Toledo, Ohio 43606
(419) 537-2297

Degree: Ph.D. Statistics, 1976
Specialty: Statistics
Assigned: AMRL

Dr. Vito DelVecchio
Professor of Biology
University of Scranton
Scranton, Pennsylvania 18510
(717) 961-6117

Degree: Ph.D., Biochemical
Genetics, 1967
Specialty: Immunochemistry and
Recombinant DNA Probes
Assigned: SAM

Dr. Hermann Donnert
Professor
Kansas State University
Department of Nuclear Engineering
Ward Hall
Manhattan, Kansas 66506-7039
(913) 532-5960

Degree: Ph.D., Mathematics and
Physics, 1951
Specialty: Radiation Physics, Nuclear
Weapon Effects, Plasma
Physics
Assigned: FJSRL

Dr. Melvin Druelinger
Professor
University of Southern Colorado
Chemistry Department
2200 N. Bonforte Blvd.
Pueblo, Colorado 81001
(303) 549-2166

Degree: Ph.D. Chemistry, 1967
Specialty: Organic Chemistry
(Mechanisms, Synthesis,
Photochemistry, Energetic
Materials Fluorinations)
Assigned: RPL

Dr. Charles Drummond, III
Associate Professor
The Ohio State University
Dept. of Ceramic Engineering
2041 College Road
Columbus, Ohio 43210
(614) 422-2960

Degree: Ph.D., Applied Physics, 1974
Specialty: Glass Structure and Proper-
ties and Composites
Assigned: AFWAL/ML

Dr. Leroy Eimers
Associate Professor
Cedarville College
Dept. of Science and Math.
Cedarville, Ohio 45314
(513) 766-2211

Degree: Ph.D., Theoretical Physics,
1970
Specialty: Mathematics, Physics
Assigned: AFWAL/APL

Dr. Hudson Eldridge
University of Central Arkansas
Physics Department, LSC 149
Conway, Arkansas 72032
(501) 450-3146

Degree: Ph.D., Nuclear Physics,
1967
Specialty: Experimental Nuclear
Physics, Computing,
Digital Electronics
Assigned: WL

Dr. Harry Emrick
Associate Professor
Colorado School of Mines
Dept. of Engineering
Golden, Colorado 80401
(303) 273-3675

Degree: Ph.D., Geodetic/Computer
Science, 1973
Specialty: Positional Geodesy -
Computer Applications
Assigned: FJSRL

Dr. John Erdei
Assistant Professor
University of Dayton
Dept. of Physics
300 College Park
Dayton, Ohio 45469
(513) 229-2318

Degree: Ph.D., Condensed Matter
Theory, 1983
Specialty: Critical Phenomena and
Field Theory
Assigned: AFWAL/APL

Dr. Dah-Nien Fan
Professor
Howard University
Dept. of Mechanical Engr.
Washington, D.C. 22059
(202) 636-6607

Degree: Ph.D., Aerospace
Engineering, 1966
Specialty: Fluid Mechanics, Aero-
dynamics, Tensor Theory,
Applied Mathematics
Assigned: AFWAL/FDL

Dr. Mack Felton
Chairman and Professor
Southern University at
New Orleans
Biology Department
6400 Press Drive
New Orleans, Louisiana 70126
(504) 282-4401

Degree: Ph.D., Microbiology, 1973
Specialty: Virus Adsorption, Micro-
bial Ecology, Physiology
Assigned: SAM

Dr. Edna Fiedler
St. Mary's University
Department Head - Psychology
One Camino Santa Maria
San Antonio, Texas 78284
(512) 436-3314

Degree: Ph.D., Psychology, 1972
Specialty: Social and Clinical
Psychology
Assigned: HRL/MO

Dr. John Flach
Assistant Professor
University of Illinois
at Urbana-Champaign
Aviation Research Laboratory
Willard Airport
Savoy, Illinois 61874
(217) 333-7749

Degree: Ph.D., Psychology, 1984
Specialty: Human Performance and
Engineering Psychology
Assigned: AMRL

Dr. John Fleming
Assistant Professor
Texas A&M University
Dept. of Electrical Engr.
College Station, Texas 77843
(409) 845-7441

Degree: Ph.D. Electrical
Engineering, 1977
Specialty: Systems, Control, Applied
Mathematics, and Digital
Signal Processing
Assigned: RADC

Dr. Dennis Flentge
Assistant Professor
Cedarville College
Math and Science Dept.
Cedarville, Ohio 45314
(513) 766-2211

Degree: Ph.D., Physical Chemistry,
1974
Specialty: Catalysis, Infrared
Spectroscopy
Assigned: AFWAL/APL

Dr. Bessie Foster
Professor
Grambling State University
Department of Physics
Grambling, Louisiana 71245
(318) 274-2574

Degree: Ph.D., Science, Radiological Science, 1968
Specialty: Radiological Science (Health Physics and Radiation Biology)
Assigned: WL

Dr. James Gallas
Assistant Professor
University of Texas
1604 Loop/Rt. 10
San Antonio, Texas 78250
(512) 691-5446

Degree: Ph.D., Physics, 1981
Specialty: Interaction of Light (lasers) with Biological and Polymeric Materials
Assigned: SAM

Dr. Chester Gardner
Professor
University of Illinois
Electrical and Computer Engr.
1406 W. Green
Urbana, Illinois 61801
(217) 333-4682

Degree: Ph.D., Electrical Engineering, 1973
Specialty: Laser Remote Sensing, Optical Communications, Fiber Optics
Assigned: AFGL

Dr. Doris Ginn
Associate Professor
Jackson State University
English Department
1400 John R. Lynch Street
Jackson, Mississippi 39217
(601) 968-2116

Degree: Ph.D., Linguistics, 1979
Specialty: English as a Second Language and Sociolinguistics
Assigned: WL

Dr. Ramana Grandhi
Assistant Professor
Wright State University
Mechanical Systems Engineering
School of Engineering
Dayton, Ohio 45435
(513) 873-2079

Degree: Ph.D., Engineering Mechanics, 1984
Specialty: Structural Optimization
Assigned: AFWAL/FDL

Dr. Alwin Green
Associate Professor
State University College - Buffalo
Mathematics Department
1300 Elmwood Avenue
Buffalo, New York 14222
(716) 878-4420

Degree: Ph.D., Mathematics, 1972
Specialty: Graph Theory, Networks, Combinatorics, Mathematics Modeling
Assigned: RADC

Mr. Mahesh Greywall
Professor
Wichita State University
Mechanical Engineering Dept.
Box 35
Wichita, Kansas 67208
(316) 689-3402

Degree: Ph.D., Mechanical
Engineering, 1962
Specialty: Fluid Mechanics
Assigned: AFWAL/APL

Dr. Vijay Gupta
Associate Professor
Central State University
Chemistry Department
Wilberforce, Ohio 45384
(513) 376-6423

Degree: Ph.D., Chemistry, 1969
Specialty: Physical Chemistry
Assigned: AFWAL/ML

Dr. Barry Haack
Associate Professor
Ball State University
Dept. of Geography
Muncie, Indiana 47306
(317) 285-1776

Degree: Ph.D. Geography, 1977
Specialty: Digital Processing of
Remotely Sensed Data
Assigned: RADC

Dr. Je-Chin Han
Associate Professor
Texas A&M University
Mechanical Engr. Department
College Station, Texas 77843
(409) 845-3738

Degree: Sc.D., Mechanical Engineer-
ing Heat Transfer, 1976
Specialty: Heat Transfer
Assigned: AFWAL/APL

Dr. Donald Hanson
Associate Professor
University of Mississippi
Electrical Engineering Dept.
University, Mississippi 38677
(601) 232-5389

Degree: Ph.D., Electromagnetics,
1976
Specialty: Electromagnetic Field
Theory and MOSFET VLSI
Design
Assigned: RADC

Dr. David Hart
Assistant Professor
University of Florida
Dept. of Mathematics
201 Walker Hall
Gainesville, Florida 32611
(904) 392-6162

Degree: Ph.D., Mathematics, 1980
Specialty: Nonlinear Differential
Equations
Assigned: AFWAL/FDL

Dr. Albert Heaney
Professor
California State University
Electrical Engineering Dept.
Shaw and Cedar Avenues
Fresno, California 93740
(209) 294-2157

Degree: Ph.D. Electrical
Engineering, 1972
Specialty: Computer Engineering
Assigned: RADC

Dr. Carolyn Heising
Associate Professor
Northeastern University
Industrial Engineering Dept.
360 Huntington Ave.
Boston, Massachusetts 02115
(617) 437-4948

Degree: Ph.D., Mechanical
Engineering, 1978
Specialty: Reliability Analysis/Risk
Assessment
Assigned: ESD

Dr. Troy Henson
Associate Professor
Louisiana Tech University
Electrical Engr. Dept.
Tech Station
Ruston, Louisiana 71272
(318) 257-4715

Degree: Ph.D. Electrical
Engineering, 1975
Specialty: Communications and Control
Systems Theory, Digital
Signal Processing
Assigned: AMRL

Dr. Astor Herrell
Professor and Chairman
Winston-Salem State University
P. O. Box 13236
Winston-Salem, North Carolina
27110
(919) 761-2098

Degree: Ph.D., Inorganic
Chemistry, 1973
Specialty: Chemistry and Physical
Science
Assigned: AEDC

Dr. Albert Hsui
Associate Professor
University of Illinois
Dept. of Geology
245 Nat. Hist. Bldg.
1301 W. Green Street
Urbana, Illinois 61801
(217) 333-7732

Degree: Ph.D., Geophysics and
Mechanics, 1972
Specialty: Geophysics, Applied
Mathematics, Computer
Simulation
Assigned: AFGL

Dr. Clifford Johnston
Assistant Professor
University of Florida
Soil Science
2169 McCarty Hall
Gainesville, Florida 32611
(904) 392-1951

Degree: Ph.D., Soil Physical
Chemistry, 1983
Specialty: Vibrational Spectroscopy
(laser Raman and FTIR)
Assigned: ESC

Dr. Betty Jones
Associate Professor and
Director of the Institute
of Electron Microscopy
Morehouse College
Department of Biology
830 Westview Drive, S.W.
Atlanta, Georgia 30314
(404) 681-2800

Degree: Ph.D., Biology, 1978
Specialty: Medical Parasitology
Tropical Medicine and
Electron Microscopy
Assigned: SAM

Dr. Jeremy Jones
Assistant Professor
The University of West Florida
Systems Science Department
Pensacola, Florida 32514-0103
(904) 474-2551

Degree: M.S., Physics, 1970
Specialty: Artificial Intelligence,
Computer Science Department
Assigned: AFWAL/AL

Dr. Patrick Jones
Assistant Professor
The Ohio State University
Chemistry Department
140 W. 18th Avenue
Columbus, Ohio 43210
(614) 422-9489

Degree: Ph.D., Chemical Physics,
1980
Specialty: Chemical Dynamics
Assigned: AFWAL/AL

Dr. Walter Jones
Assistant Professor
University of Tennessee
Dept. of Engineering Science
and Mechanics
310 Perkins Hall
Knoxville, Tennessee 37996-2030
(615) 974-7684

Degree: Ph.D., Engineering
Mechanics, 1982
Specialty: Mechanics of Composite
Materials
Assigned: AFWAL/FDL

Dr. Prasad Kadaba
Professor
University of Kentucky
Electrical Engineering Dept.
Room 453 Anderson Hall
Lexington, Kentucky 40506
(606) 257-2966

Degree: Ph.D., Physics, 1950
Specialty: Dielectric Relaxation
and Magnetic Resonance:
Microwave and Millimet
Wave Measurements
Assigned: AFWAL/ML

Dr. James Kane
Associate Professor
Wright State University
Chemistry Department
Dayton, Ohio 45435
(513) 873-2352

Degree: Ph.D., Chemistry, 1960
Specialty: Organic, Physical Organic,
Polymer Chemistry
Assigned: AFWAL/ML

Dr. Amir Karimi
Assistant Professor
University of Texas
San Antonio
Division of Engineering
San Antonio, Texas 78285
(512) 691-5514

Degree: Ph.D. Mechanical
Engineering, 1982
Specialty: Thermal Sciences, Conden-
sation, Heat Exchanger
Design, Heat Transfer, Phase
Change Processes, Metastable
Thermodynamics
Assigned: SAM

Dr. Daisy Kimble
Instructor
Southern University
Chemistry Department
P. O. Box S.U.
Baton Rouge, Louisiana 70813
(504) 771-3990

Degree: B.S., Chemistry, 1974
Specialty: Chemistry-Analytical
Assigned: FJSRL

Dr. David Kohfeld
Professor
Southern Illinois University
at Edwardsville
Edwardsville, Illinois 62026
(618) 692-2582

Degree: Ph.D., Experimental
Psychology, 1966
Specialty: Human Performance
and Reaction Time, Math
Models
Assigned: HRL/OT

Dr. Stephan Kolitz
Assistant Professor
University of Massachusetts
Boston
Harbor Campus
Boston, Massachusetts 02125
(617) 929-8051

Degree: Ph.D. Industrial
Engineering, 1983
Specialty: Operations Research
Assigned: ESD

Dr. Lawrence Koons
Professor
Tuskegee Institute
Chemistry Department
Tuskegee Institute, Alabama 36088
(205) 727-8835

Degree: Ph.D., Physical
Chemistry, 1956
Specialty: Electrochemistry
Assigned: FJSRL

Dr. Arthur Kovitz
Professor
Northwestern University
Mechanical and Nuclear Engr.
2145 Sheridan Road
Evanston, Illinois 60201
(312) 491-7066

Degree: Ph.D., Aerospace
Engineering, 1957
Specialty: Fluid Mechanics, (Inter-
faces, Combustion, Compu-
tation)
Assigned: WL

Dr. Kurt Kraiger
Assistant Professor
University of Colorado
at Denver
Department of Psychology
1100 14th Street
Denver, Colorado 80202
(303) 556-8351

Degree: Ph.D., Industrial/
Organizational Psychology,
1983
Specialty: I/O Psychology, Performance
Appraisal, Job Attitudes,
Meta-Analysis
Assigned: HRL/MO

Dr. Madakasira Krishna
Professor
South Carolina State College
Mathematics and Computer Science
Box 1814, State College
Orangeburg, South Carolina 29117
(803) 536-7120

Degree: Ph.D., Numerical Analysis,
Fluid Mechanics Computer
Science, 1974
Specialty: Computational Fluid
Mechanics, Numerical
Analysis, Pde
Assigned: AD

Dr. Paul Lee
Associate Professor
North Carolina A&T State Univ.
Dept. of Business Administration
Greensboro, North Carolina 27411
(919) 379-7744

Degree: Ph.D., Resource
Economics, 1973
Specialty: Statistics, Management
Science and Computer
Sciences
Assigned: LMDC

Dr. Benjamin Lev
Professor and Chairman
Temple University
Department of Management
School of Business Admin.
Philadelphia, Pennsylvania 19122
(215) 787-8188

Degree: Ph.D., Operations
Research, 1970
Specialty: Production Management,
Mathematical Programming
Assigned: RADC

Dr. Edward Lewis
Professor
Belmont College
Computer Information Systems/
Management Science
1900 Belmont Blvd.
Nashville, Tennessee 37203
(615) 383-7001

Degree: Ph.D., Met. Science (Opera-
tions Research and
Statistics), 1978
Specialty: Mathematical Modeling,
Decision Support,
Statistical Analysis
Assigned: LMC

Dr. Michael Lewis
Assistant Professor
Troy State University
CIS Department
Troy, Alabama 36082
(205) 566-3000

Degree: M.S., Computer and
Information Science,
1985
Specialty: Advanced Microcomputer
Applications
Assigned: LMC

Dr. Philip Lewis
Professor
Auburn University
Department of Psychology
Auburn University, Alabama 36849
(205) 826-4424

Degree: Ph.D., Clinical
Psychology, 1968
Specialty: Marital Dynamics,
Personality Development,
Leadership
Assigned: LMDC

Dr. Irene Little-Marenin
Assistant Professor
Wellesley College
Astronomy Department
Whitin Observatory
Wellesley, Massachusetts 02181
(617) 325-0320

Degree: Ph.D., Astrophysics, 1970
Specialty: Astrophysics, Cool Stars
Assigned: AFGL

Dr. Dar-Biau Liu
Associate Professor
Old Dominion University
Dept. of Computer Sciences
Norfolk, Virginia 23508
(804) 440-3901

Degree: Ph.D., Applied Mathematics
and Computer Sciences,
1972
Specialty: Computer Science
Assigned: RADC

Dr. Carl Looney
Associate Professor
University of Nevada
EE/Computer Science Dept.
Reno, Nevada 89557-0030
(702) 784-6918

Degree: Ph.D., Mathematic
Analysis, 1972
Specialty: Artificial Intelligence,
Tracking, Filtering
Assigned: AFWAL/AL

Dr. James Marsh
Associate Professor
University of West Florida
Department of Physics
Pensacola, Florida 32514
(904) 474-2270

Degree: Ph.D., Physics, 1966
Specialty: Optics (Physical),
Electromagnetic Theory
Assigned: AD

Dr. Charles Mastin
Professor
Mississippi State University
Mathematics and Stat. Dept.
Drawer MA
Mississippi State, Mississippi 39762
(601) 325-3414

Degree: Ph.D., Mathematics, 1969
Specialty: Computational Fluid Dynamics
Assigned: AEDC

Dr. Odis McDuff
Professor
The University of Alabama
Electrical Engineering
P. O. Box 6169
University, Alabama 35486
(205) 348-6351

Degree: Ph.D., Electrical
Engineering, 1966
Specialty: Lasers and Optics,
Electromagnetics
Assigned: SAM

Mr. Bernard McIntyre
Associate Professor
University of Houston
Electrical Electronics Dept.
University Park
4800 Calhoun St.
Houston, Texas 77004
(713) 749-4753

Degree: Ph.D., Solid State Physics,
1970
Specialty: Space Plasma Physics
Assigned: AFGL

Dr. Leathem Mehaffey
Associate Professor
Vassar College
Biology Department
Box 410
Poughkeepsie, New York 12601
(914) 452-7000

Degree: Ph.D., Biophysics, 1971
Specialty: Neurobiology and Physiology
of Vision
Assigned: SAM

Dr. Ivor Mitchell
Professor
Marketing Department
Atlanta University
223 Chestnut Street, S.W.
Atlanta, Georgia 30337
(404) 681-0251

Degree: Ph.D., Marketing and
Statistics, 1977
Specialty: Marketing, Statistics
Assigned: LMDC

Dr. James Moore
Professor
University of Arkansas
Civil Engineering Dept.
Fayetteville, Arizona 72701
(501) 575-6027

Degree: Ph.D., Environmental Health
Engineering, 1972
Specialty: Environmental Engineering
Assigned: ESC

Dr. Osoma Mostafa
Associate Professor
California State University
Electronics Engineering Dept.
C. S. U. C. #930
Chico, California 95929
(916) 895-5374

Degree: Ph.D., Electrical
Engineering, 1975
Specialty: Systems, Automation,
Artificial Intelligence
Assigned: AD

Dr. Rex Moyer
Associate Professor
Trinity University
Biology Department
715 Stadium Drive
San Antonio, Texas 78284
(512) 736-7242

Degree: Ph.D., Microbiology,
1965
Specialty: Molecular Biology,
Experimental Oncology
Assigned: SAM

Dr. James Mrotek
Associate Professor
Meharry Medical College
Department of Physiology
1005 D. B. Todd Blvd.
Nashville, Tennessee 37208
(615) 327-6979

Degree: Ph.D., Biology, 1973
Specialty: Environmental Influences
on Cultured Mammalian
Cells, Endocrine Cell
Intracellular Exchanges
Assigned: SAM

Dr. Maurice Neveu
Associate Professor
State University College of N.Y.
Chemistry Department
Fredonia, New York 14063
(716) 673-3285

Degree: Ph.D., Physical-Organic
Chemistry, 1959
Specialty: Physical-Organic Chemistry,
Synthetic Organic Chemistry,
Chemical Kinetics, Reaction
Mechanisms, Explosives,
Aviation Fuels
Assigned: AD

Dr. Robert Niebuhr
Associate Professor
Auburn University
Dept. of Management
Auburn, Alabama 36849
(205) 826-4591

Degree: Ph.D., Management, 1977
Specialty: Management Processes,
Organizational Behavior
Assigned: LMDC

Dr. Marion Noble
Professor
Kansas State University
Physical Education Dept.
203 Ahearn Gym
Manhattan, Kansas 66506
(913) 532-6765

Degree: Ph.D., Biomechanics, 1970
Specialty: Biomechanics
Assigned: AMRL

Dr. Robert O'Connell
Assistant Professor
University of Missouri-Columbia
Electrical and Engr. Dept.
Columbia, Missouri 65211
(314) 882-8373

Degree: Ph.D., Electrical
Engineering, 1975
Specialty: Applied Optics, Laser
Effects
Assigned: FJSRL

Dr. Ralph Oberly
Professor and Chairman
Marshall University
Physics Department
Huntington, West Virginia 25701
(304) 696-6738

Degree: Ph.D., Physics (Molecular Spectra), 1970
Specialty: Molecular Spectroscopy, Optical Devices
Assigned: AFWAL/APL

Dr. Won Park
Professor
Wright State University
Mathematics and Statistics Dept.
Dayton, Ohio 45435
(513) 873-2837

Degree: Ph.D., Mathematics, 1969
Specialty: Stochastic Processes, Time Series, Reliability
Assigned: AFWAL/AL

Dr. Desmond Penny
Assistant Professor
Southern Utah State College
Physical Science Department
Cedar City, Utah 84720
(801) 586-7708

Degree: Ph.D., Civil Engineering, 1975
Specialty: Continuum Mechanics
Assigned: ESC

Dr. John Pierce
Associate Professor
University of North Alabama
Department of Chemistry
Florence, Alabama 35632
(205) 766-4100

Degree: Ph.D., Environmental Health, 1978
Specialty: Thermal Absorption of Toxicants, Analytical Methods Development
Assigned: OEHL

Dr. Boake Plessy
Professor
Dillard University
Division of Natural Science
2601 Gentilly Blvd.
New Orleans, Louisiana 70122
(504) 283-8822

Degree: Ph.D., Physical Chemistry, 1974
Specialty: Biopolymers, Proteoglycans from Corneal Tissue
Assigned: SAM

Dr. Arnold Polak
Professor
University of Cincinnati
Dept. of Aerospace Engr. and Engr. Mechanics
ML 70
Cincinnati, Ohio 45221
(513) 475-5133

Degree: Ph.D., Aerospace Engineering, 1966
Specialty: Fluid Mechanics
Assigned: AFWAL/APL

Dr. Justin Poland
Associate Professor
University of Maine Orono
Mechanical Engineering Dept.
209 Boardman Hall
Orono, Maine 04469
(207) 581-2123

Degree: Ph.D., Mechanical
Engineering, 1979
Specialty: Thermal Sciences, Thermo-
dynamics, Heat Transfer,
Fluid Mechanics
Assigned: AEDC

Dr. Kuldip Rattan
Associate Professor
Wright State University
Electrical Systems Engineering
Department
Fawcett Hall, Room 354
Dayton, Ohio 45435
(513) 873-2497

Degree: Ph.D., Electrical
Engineering, 1975
Specialty: Digital Control Systems
Assigned: AFWAL/FDL

Dr. Hemen Ray
Assistant Professor
North Carolina A&T State Univ.
Mechanical Engr. Dept.
112 Cherry Hall
Greensboro, North Carolina 27411
(919) 379-7621

Degree: Ph.D., Engineering
Mechanics, 1979
Specialty: Advanced Composites
Assigned: AFWAL/FDL

Dr. John Renie
Assistant Professor
University of Illinois
Dept. of Mechanical and
Industrial Engineering
1206 W. Green Street
Urbana, Illinois 61801
(217) 333-6199

Degree: Ph.D., Combustion/
Engineering, 1982
Specialty: Combustion and Fluid
Dynamics
Assigned: RPL

Dr. Michael Rhodes
Instructor
Clark College
Department of Physics
240 Brawley Drive, S.W.
Atlanta, Georgia 30314
(404) 681-3080

Degree: Ph.D., Physics, 1983
Specialty: Plasma Physics, Numerical
Analysis
Assigned: AFGL

Dr. Robert Ricci
Professor and Chairman
Holy Cross College
Chemistry Department
Worcester, Massachusetts 01610
(617) 793-3380

Degree: Ph.D., Chemistry, 1961
Specialty: Physical Chemistry,
Analytical Chemistry
Assigned: AFGL

Dr. James Riehl
Associate Professor
University of Missouri
Department of Chemistry
8001 Natural Bridge Road
St. Louis, Missouri 63121
(314) 553-5328

Degree: PH.D., Physical Chemistry,
1975
Specialty: Physical Chemistry,
Theoretical Chemistry,
Laser, Spectroscopy
Assigned: AFGL

Dr. Michael Ross
Associate Professor
Slippery Rock University
Computer Science Department
Slippery Rock, Pennsylvania
16057
(412) 794-7133

Degree: Ph.D., Applied Mathematics,
Specialty: Computer Simulation,
Operating Systems,
Numerical Analysis
Assigned: AMRL

Dr. Samuel Russell
Assistant Professor
University of South Carolina
Mechanical Engineering Dept.
Columbia, South Carolina 29208
(803) 777-3241

Degree: Ph.D., Engineering
Mechanics, 1982
Specialty: Nondestructive Testing of
Composite Materials
Assigned: AFWAL/ML

Dr. Sally Sage
Assistant Professor
West Georgia College
Department of Math
and Computer Science
Carrollton, Georgia 30118
(404) 834-1380

Degree: M.S., Computer
Science, 1979
Specialty: Programming Languages and
Computer Simulation
Assigned: AD

Dr. Joseph Saliba
Assistant Professor
University of Dayton
Civil Engr. Dept.
300 College Park
Dayton, Ohio 45469
(513) 229-3847

Degree: Ph.D., Solid Mechanics,
1983
Specialty: Solid Mechanics - Structures
Assigned: AFWAL/FDL

Dr. Gordon Schrank
Associate Professor
St. Cloud State University
Dept. of Biology Sciences
St. Cloud, Minnesota 56301
(612) 255-2036

Degree: Ph.D., Medical Microbiology,
1974
Specialty: General Microbiology,
Medical Microbiology,
Electron Microscopy
Assigned: SAM

Dr. Ronald Segal Assistant Professor University of Colorado Department of Electrical Engr. Colorado Springs, Colorado 80933-7150 (303) 593-3510	<u>Degree:</u> <u>Specialty:</u> <u>Assigned:</u>	Ph.D., Electrical Engineering, 1982 Electromagnetics FJSRL
Dr. Paul Seybold Professor Wright State University Chemistry Department Dayton, Ohio 45435 (513) 873-2407	<u>Degree:</u> <u>Specialty:</u> <u>Assigned:</u>	Ph.D., Biophysics, 1968 Structure-Activity Relations AMRL
Dr. Shawky Shamma Professor University of West Florida Pensacola, Florida 32504 (904) 474-2281	<u>Degree:</u> <u>Specialty:</u> <u>Assigned:</u>	Ph.D., Applied Mathematics, Applied Mathematics AD
Dr. Ralph Sheets Professor Southwest Missouri State Univ. Department of Chemistry Springfield, Missouri 65804 (417) 836-5611	<u>Degree:</u> <u>Specialty:</u> <u>Assigned:</u>	Ph.D., Physical Chemistry, 1971 Chemistry (surface chemistry and catalysis environmental) OEHL
Dr. Kyle Siegrist Assistant Professor University of Alabama Mathematics Department Huntsville, Alabama 35899 (205) 895-6470	<u>Degree:</u> <u>Specialty:</u> <u>Assigned:</u>	Ph.D., Applied Mathematics, 1979 Probability and Stochastic Processes RADC
Dr. Ricardo Silva Professor California State University 18111 Nordhoff Street Northridge, California 91330 (818) 885-3378	<u>Degree:</u> <u>Specialty:</u> <u>Assigned:</u>	Ph.D., Chemistry, 1961 Organic Chemistry, Synthesis and Analysis RPL
Dr. S. Ballou Skinner Professor University of South Carolina Coastal Carolina College Physics Department P. O. Box 1954 Conway, South Carolina 29526 (803) 347-3161	<u>Degree:</u> <u>Specialty:</u> <u>Assigned:</u>	Ph.D., Physics, 1970 Nuclear and Radiation Physics, Gamma Ray Spec- troscopy, Neutron Activation Analysis AEDC

Dr. Terrill Smith
Professor
Central State University
Chemistry Department
100 N. University Drive
Edmond, Oklahoma 73034
(405) 341-2980

Degree: Ph.D., Organic Chemistry,
1959
Specialty: Organic, Polymer, Fluorine,
Industrial Chemistry
Assigned: AFWAL/ML

Dr. Siavash Sohrab
Assistant Professor
Northwestern University
MNE Department
Technical Institute
Evanston, Illinois 60201
(312) 491-3572

Degree: Ph.D., Engineering Physics,
1981
Specialty: Combustion
Assigned: RPL

Dr. Richard Stebbins
Assistant Professor
University of Southern Maine
Chemistry Department
96 Falmouth Street
360 Science Building
Portland, Maine 04103
(207) 780-4232

Degree: Ph.D., Physical Chemistry,
1970
Specialty: Analysis of Trace Organics
by ECD Gas Chromatography
Assigned: OEHL

Dr. Bob Stewart
Assistant Professor
University of Cincinnati
Dept. of Mechanical Engr.
M.L. #72
Cincinnati, Ohio 45221
(513) 475-4781

Degree: Ph.D., Physics, 1981
Specialty: General Relativity,
Thermodynamics, Biomechanics
Assigned: WL

Dr. Lowell Stockstill
Assistant Professor
Wittenberg University
Dept. of Business Administration
P. O. Box 720
Springfield, Ohio 45501
(513) 327-7903

Degree: J.D./MBA, Law, 1982
Specialty: Small Business Law
Assigned: BRMC

Dr. William Stone
Assistant Professor
Meharry Medical College
Dept. of Pediatrics
Nashville, Tennessee 37208
(615) 327-6506

Degree: Ph.D., Molecular and
Cellular Biology, 1973
Specialty: Lipid Biochemistry,
Nutrition, Hyperbaric
Medicine
Assigned: SAM

Dr. James Sturm
Professor
Lehigh University
Department of Chemistry #6
Bethlehem, Pennsylvania 18015
(215) 861-3477

Degree: Ph.D., Physical Chemistry,
1957
Specialty: Photochemical Kinetics
Assigned: AFGL

Dr. Thomas Sudkamp
Assistant Professor
Wright State University
Computer Science Department
Dayton, Ohio 45435
(513) 873-2491

Degree: Ph.D., Mathematics, 1978
Specialty: Computer Science,
Mathematics
Assigned: AFWAL/AL

Dr. William Sutton
Assistant Professor
University of Oklahoma
School of Aerospace
Mechanical and Nuclear Engr.
Department
865 Asp Ave., Rm. 212
Norman, Oklahoma 73019
(405) 325-5011

Degree: Ph.D., Mechanical
Engineering, 1981
Specialty: Heat Transfer, Thermal
Radiation
Assigned: AEDC

Dr. Robert Swanson
Assistant Professor
Virginia Polytechnic Institute
and State University
Materials Engineering Dept.
Blacksburg, Virginia 24061
(703) 961-5600

Degree: Ph.D., Metallurgical
Engineering and Materials
Science, 1983
Specialty: Fracture Mechanics,
Environmental Cracking,
Corrosion
Assigned: AFWAL/ML

Dr. Patrick Sweeney
Professor
University of Dayton
Engineering Management and
Systems Dept.
KL 361
Dayton, Ohio 45469
(513) 229-2238

Degree: Ph.D., Mechanical
Engineering, 1977
Specialty: Simulation, Costing,
Management Systems
Assigned: BRMC

Dr. Charles Taylor
Professor
University of Florida
Dept. of Engineering Science
231 Aerospace Eng. Building
Gainesville, Florida 32611
(904) 392-0961

Degree: Ph.D., Theory and
Application Mechanics, 1953
Specialty: Optical Methods of
Experimental Stress
Analysis
Assigned: AD

Dr. Joseph Tedsco
Assistant Professor
Auburn University
Dept. of Civil Engineering
210 Ramsay Hall
Auburn, Alabama 36849
(205) 826-4320

Degree: Ph.D., Civil Engineering,
1982
Specialty: Structural Dynamics;
Concrete Structures
Assigned: ESC

Dr. Walter Trafton
Associate Professor
Gallaudet College
Chemistry Department
Kendall Green
Washington D.C. 20002
(202) 651-5536

Degree: Ph.D., Chemistry, 1973
Specialty: Physical Chemistry, Kinetics
and Gas Phase Reactions
Assigned: FJSRL

Dr. Larry Vardiman
Associate Professor and
Dept. Chairman
Christian Heritage College
Physical Sciences Dept.
2100 Greenfield Drive
El Cajon, California 92021
(619) 440-3043

Degree: Ph.D., Atmospheric Science,
1974
Specialty: Cloud Physics and Weather
Modification
Assigned: AFGL

Dr. Daniel Voss
Assistant Professor
Wright State University
Dept. of Math and Stat.
Dayton, Ohio 45435
(513) 873-2958

Degree: Ph.D., Statistics, 1984
Specialty: Experimental Design, Con-
founding in Factorial
Exper's
Assigned: LC

Dr. Christian Wagner
Assistant Professor
Oakland University
School of Engineering and
Computer Science
138 Dodge Hall
Rochester, Michigan 48063
(313) 370-2215

Degree: Ph.D., Educational
Psychology and Artificial
Intelligence, 1982
Specialty: Artificial Intelligence,
Cognitive Psychology
Assigned: HRL/IO

Dr. Richard Walker
Chairman
Miami University
Aeronautics Department
219 Culler Hall
Oxford, Ohio 45056
(513) 529-5919

Degree: Ph.D., Aerospace
Engineering, 1970
Specialty: Aircraft Design, Perform-
ance Analysis, Propulsion
Aerodynamics
Assigned: AFWAL/FDL

Dr. Doris Walker-Dalhouse
Director of Independent/Home
Study Programs
Associate Professor of Reading
Jackson State University
P. O. Box 17120
Jackson, Mississippi 39217
(601) 968-2378

Degree: Ph.D., Reading Education,
1977
Specialty: Education
Assigned: WL

Dr. Yin-min Wei
Professor
Ohio University
Computer Science Dept.
Morton Hall 573
Athens, Ohio 45701
(614) 594-6574

Degree: Ph.D., Electrical
Engineering, 1966
Specialty: Signal Processing
Assigned: AMRL

Dr. Isaac Weiss
Associate Professor
Wright State University
School of Engineering
Dayton, Ohio 45435
(513) 873-3021

Degree: Ph.D., Metallurgy, 1978
Specialty: Thermomechanical Process-
ing, Deformation Processing
Assigned: AFWAL/ML

Dr. Shih-sung Wen
Professor
Jackson State University
Psychology Department
1325 J. R. Lynch Street
Jackson, Mississippi 39217
(601) 968-2371

Degree: Ph.D., Educational
Psychology, 1971
Specialty: Cognitive Psychology,
Psychological Testing,
Statistics
Assigned: SAM

Dr. David Wilson
Associate Professor
University of Florida
Mathematics Department
311 Walker Hall
Gainesville, Florida 32611
(904) 392-6035

Degree: Ph.D., Mathematics, Rutgers,
1969
Specialty: Geometric Topology, Grid
Generation (Computer Flight
Dynamics)
Assigned: AD

Dr. Jesse Williams
Associate Professor
Cheyney University
Math/CIS Department
Cheyney, Pennsylvania 19319
(215) 399-2348

Degree: M.B.A., Computer Science,
1975
Specialty: Computer Science
Assigned: LMC

Dr. Arthur Woodrum
Head, Dept. of Physics
Georgia Southern College
Landrum Box 8031
Statesboro, Georgia 30460
(912) 681-5292

Degree: Ph.D., Physics, 1968
Specialty: Atmospheric Physics
Assigned: SAM

Dr. Billy Wooten
Associate Professor
Brown University
Psychology Department
89 Waterman Street
Providence, Rhode Island 02912
(401) 863-2330

Degree: Ph.D., Experimental
Psychology, 1970
Specialty: Color Vision
Assigned: HRL/OT

Dr. Carl Wulfman
Chairman
University of the Pacific
Department of Physics
Stockton, California 95211
(209) 946-2220

Degree: Ph.D., Organic Chemistry,
1957
Specialty: Chemical Physics
Assigned: FJSRL

Dr. Hsi-Han Yeh
Associate Professor
University of Kentucky
Dept. of E.E.
Lexington, Kentucky 40506
(606) 257-4289

Degree: Ph.D., Electrical
Engineering, 1967
Specialty: Multivariable Control
Assigned: AFWAL/FDL

Dr. Juin Yu
Professor
West Virginia Institute
of Technology
Mechanical Engineering Department
Montgomery, West Virginia 25136
(304) 442-3248

Degree: Ph.D., Mechanical
Engineering
Specialty: Thermofluid Processes
Assigned: AEDC

APPENDIX II C
PARTICIPANT LABORATORY ASSIGNMENT

C. PARTICIPANT LABORATORY ASSIGNMENT (Page 1)

1985 USAF/UES SUMMER FACULTY RESEARCH PROGRAM

AERO PROPULSION LABORATORY (AFWAL/APL)
(Wright-Patterson Air Force Base)

- | | |
|----------------------|-----------------------|
| 1. Lea Der Chen | 6. Mahesh S. Greywall |
| 2. Louis C. Chow | 7. Je-Chen Han |
| 3. Leroy E. Eimers | 8. Ralph E. Oberly |
| 4. John E. Erdei | 9. Arnold Polak |
| 5. Dennis R. Flentge | |

AEROSPACE MEDICAL RESEARCH LABORATORY (AMRL)
(Wright-Patterson Air Force Base)

- | | |
|---------------------|--------------------|
| 1. Samuel K. Adams | 6. Marion L. Noble |
| 2. Zinny S. Bond | 7. Michael D. Ross |
| 3. Charles B. Davis | 8. Paul G. Seybold |
| 4. John M. Flach | 9. Yin-min Wei |
| 5. Troy F. Henson | |

ARMAMENT LABORATORY (AD)
(Eglin Air Force Base)

- | | |
|--------------------------|----------------------|
| 1. Kevin W. Bowyer | 6. Sally A. Sage |
| 2. Madakasira V. Krishna | 7. Shawky E. Shamma |
| 3. James S. Marsh | 8. Charles E. Taylor |
| 4. Osana M. Mostafa | 9. David C. Wilson |
| 5. Maurice C. Neveu | |

ARNOLD ENGINEERING DEVELOPMENT CENTER (AEDC)
(Arnold Air Force Station)

- | | |
|----------------------|----------------------|
| 1. Astor Y. Herrell | 4. S. Ballou Skinner |
| 2. Charles W. Mastin | 5. William H. Sutton |
| 3. Justin H. Poland | 6. Juin S. Yu |

AVIONICS LABORATORY (AFWAL/AL)
(Wright-Patterson Air Force Base)

- | | |
|---------------------|-------------------|
| 1. Rex Barney | 5. Jeremy Jones |
| 2. Jharna Chaudhuri | 6. Carl Looney |
| 3. Alvin Compaan | 7. Won Park |
| 4. Patrick Jones | 8. Thomas Sudkamp |

BUSINESS RESEARCH MANAGEMENT CENTER (BRMC)
(Wright-Patterson Air Force Base)

- | |
|-------------------------|
| 1. Lowell E. Stockstill |
| 2. Patrick J. Sweeney |

C. PARTICIPANT LABORATORY ASSIGNMENT (Page 2)

ELECTRONICS SYSTEMS DIVISION (ESD)

(Hanscom Air Force Base)

1. Carolyn D. Heising
2. Stephan E. Kolitz

ENGINEERING AND SERVICES CENTER (ESC)

(Tyndall Air Force Base)

1. Karen Chai-Kwan Chou
2. Gale J. Clark
3. Clifford T. Johnston
4. Desmond N. Penny
5. Joseph W. Tedesco

FLIGHT DYNAMICS LABORATORY (AFWL/FDL)

(Wright-Patterson Air Force Base)

- | | |
|--------------------------|-----------------------|
| 1. Connie K. Carrington | 7. Kuldip S. Rattan |
| 2. Robert R. Chamberlain | 8. Hemen Ray |
| 3. Dah-Nien Fan | 9. Joseph E. Saliba |
| 4. Ramana V. Grandhi | 10. Richard C. Walker |
| 5. David C. Hart | 11. Hsi-Han Yeh |
| 6. Walter F. Jones | |

FRANK J. SEILER RESEARCH LABORATORY (FJSRL)

(USAF Academy)

- | | |
|------------------------|---------------------------|
| 1. Richard D. Bertrand | 5. Lawrence F. Koons |
| 2. Hermann J. Donnert | 6. Ronald M. Sega |
| 3. Harry W. Emrick | 7. Walter E. Trafton, Jr. |
| 4. Daisy W. Kimble | 8. Carl E. Wulfman |

GEOPHYSICS LABORATORY (AFGL)

(Hanscom Air Force Base)

- | | |
|-----------------------------|----------------------|
| 1. Lucia M. Babcock | 7. Michael B. Rhodes |
| 2. Francesco L. Bacchialoni | 8. Robert W. Ricci |
| 3. Chester S. Gardner | 9. James P. Riehl |
| 4. Albert Tong-Kwan Hsui | 10. James E. Strum |
| 5. Irene R. Little-Marenin | 11. Larry Vardiman |
| 6. Bernard McIntyre | |

HUMAN RESOURCES LABORATORY/LR (HRL/LR)

(Wright-Patterson Air Force Base)

1. Linda J. Buehner
2. Hobert H. Corley

HUMAN RESOURCES LABORATORY/OT (HRL/OT)

(Williams Air Force Base)

1. Thomas J. Connolly
2. David L. Kohfeld
3. Billy R. Wooten

C. PARTICIPANT LABORATORY ASSIGNMENT (Page 3)

HUMAN RESOURCES LABORATORY/MO (HRL/MO)

(Brooks Air Force Base)

1. Phillip L. Ackerman
2. Jihad A. Alsadek
3. Edna R. Fiedler
4. Kurt Kraiger

HUMAN RESOURCES LABORATORY/ID (HRL/ID)

(Lowry Air Force Base)

1. Peter J. Binkert
2. Christian C. Wagner

LEADERSHIP AND MANAGEMENT DEVELOPMENT CENTER (LMDC)

(Maxwell Air Force Base)

1. Paul S.T. Lee
2. Philip M. Lewis
3. Ivor S. Mitchell
4. Robert E. Niebuhr

LOGISTICS COMMAND (LC)

(Wright-Patterson Air Force Base)

1. Daniel T. Voss

LOGISTICS MANAGEMENT CENTER (LMC)

(Gunter Air Force Base)

1. Michael M. Lewis
2. Edward N. Lewis
3. Jesse Williams

MATERIALS LABORATORY (AFWAL/ML)

(Wright-Patterson Air Force Base)

- | | |
|-----------------------------|-----------------------|
| 1. Vernon R. Allen | 7. Prasad K. Kadaba |
| 2. Derald Chriss | 8. James J. Kane |
| 3. Billy C. Covington | 9. Samuel S. Russell |
| 4. Parviz Dadras | 10. Terrill D. Smith |
| 5. Charles H. Drummond, III | 11. Robert E. Swanson |
| 6. Vijay K. Gupta | 12. Isaac Weiss |

OCCUPATIONAL AND ENVIRONMENTAL HEALTH LABORATORY (OEHL)

(Brooks Air Force Base)

1. John T. Pierce
2. Ralph W. Sheets
3. Richard G. Stebbins

C. PARTICIPANT LABORATORY ASSIGNMENT (Page 4)

ROCKET PROPULSION LABORATORY (RPL)
(Edwards Air Force Base)

1. Dennis J. Cravens
2. Melvin L. Druelinger
3. John P. Renie
4. Ricardo A. Silva
5. Siavash H. Sohrab

ROME AIR DEVELOPMENT CENTER (RADC)
(Griffiss Air Force Base)

- | | |
|---------------------|---------------------|
| 1. David B. Choate | 7. Donald F. Hanson |
| 2. David Y. Chung | 5. Albert A. Heaney |
| 3. David R. Cochran | 6. Benjamin Lev |
| 4. John A. Fleming | 7. Dar-Biau Liu |
| 5. Alwin C. Green | 8. Kyle T. Siegrist |
| 6. Barry N. Haack | |

SCHOOL OF AEROSPACE MEDICINE (SAM)
(Brooks Air Force Base)

- | | |
|-------------------------|-----------------------|
| 1. Deborah L. Armstrong | 9. Leathem Mehaffey |
| 2. Mukul R. Banerjee | 10. Rex C. Moyer |
| 3. Vito G. DelVecchio | 11. James J. Mrotek |
| 4. Mack Felton | 12. Boake L. Plessy |
| 5. James M. Gallas | 13. Gordon D. Schrank |
| 6. Betty R. Jones | 14. William L. Stone |
| 7. Amir Karimi | 15. Shih-sung Wen |
| 8. Odis P. McDuff | 16. Arthur Woodrum |

WEAPONS LABORATORY (WL)
(Kirtland Air Force Base)

- | | |
|-----------------------|---------------------------|
| 1. Eugene F. Brown | 5. Arthur A. Kovitz |
| 2. Hudson B. Eldridge | 6. Robert M. O'Connell |
| 3. Bessie R. Foster | 7. Bob W. Stewart |
| 4. Doris O. Ginn | 8. Doris Walker-Dalhousie |

RESEARCH REPORTS
1985 SUMMER FACULTY RESEARCH PROGRAM

<u>Technical Report Number</u> Volume I	<u>Title</u>	<u>Professor</u>
1	Individual Differences in Abilities, Learning, and Cognitive Processes	Dr. Phillip L. Ackerman
2	Maximum Voluntary Hand Grip Torque for Circular Electrical Connectors	Dr. Samuel Adams
3	Properties and Processing of a Perfluorinated Polyalkylene Linked Polyimide	Dr. Vernon R. Allen
4	Quantifying Experience in the Cost of Human Capital	Dr. Jihad A. Alsadek
5	The Effects of Raphe Stimulation and Iontophoresis of Serotonergic Agents on Granule Cell Activity in Rat Lateral Cerebellar Cortex	Dr. Deborah Armstrong
6	Temperature Dependence of Ion-Molecule Association Reactions: Halide Ion Addition Reactions	Dr. Lucia Badcock
7	Active Control of Flexible Structures	Dr. Francesco Bacchialoni
8	Gas Exchange in the Rabbit Using High Frequency Ventilation in High Altitude	Dr. Mukul R. Banerjee
9	Computer Automated Test Mirror Registration System for the Ring Laser Gyro	Dr. Rex L. Berney
10	²⁷ Al Spin Lattice Relaxation Measurements in Alkylammonium- Chloroaluminate Room-Temperature Electrolytes	Dr. Richard Bertrand
11	Natural Language Understanding Using Residential Grammar and It's Use in Automatic Programming	Dr. Peter J. Binkert
12	Speech Effects of High Sustained Acceleration: A Preliminary Study	Dr. Zinny S. Bond

13	Automatic Determination of Object Orientation in 2-D Images	Dr. Kevin W. Bowyer
14	Stimulation of Jet Injection Using RAVEN	Dr. Eugene F. Brown
15	The Impact of Cognitive Styles & Subject Matter on Instructional Design	Dr. Linda J. Buehner
16	Polynomial Feedback Control for Robotic Manipulators	Dr. Connie K. Carrington
17	Modification and Evaluation of Heat Transfer Calculations Using the AFWAL PNS Code	Dr. Robert R. Chamberlain
18	Optical and X-Ray Topographic Characterization of Undoped Semi-Insulating GaAs	Dr. Jharna Chaudhuri
19	Visualization of Jet Flames	Dr. Lea D. Chen
20	Splines and the Fourier Transform	Dr. David B. Choate
21	Protection From Nonnuclear Weapons: A Probabilistic Approach	Dr. Karen C. Chou
22	Fluid Recirculation, Deployment, and Retraction of the Expandable Radiator	Dr. Louis Chow
23	Applications of Internal Reflection Spectroscopy to the Characterization of Thermoset Polymers	Dr. Derald Chriss
24	Applications of Fiber Optics of Low Temperatures	Dr. David Y. Chung
25	Evaluation of Selected Parameters Which Affect K_d When Measured Using HPLC Instrumentation	Dr. Gale J. Clark
26	Dipole Moment of InP in the Melt	Dr. David R. Cochran
27	Laser Raman Laboratory Research	Dr. Alvin D. Compaan
28	Aeronautical Decision-Making for Air Force Pilots	Dr. Thomas J. Connolly
29	Feasibility Study on the Logistics Operational Assessment Model	Dr. Hobert H. Corley
30	Photo-Hall Study of Doped and Undoped Semi-Insulating GaAs.	Dr. Billy C. Covington

31	Spin Formed Mirrors	Dr. Dennis J. Cravens
32	High-Temperature Across-Ply Testing of C/C Composites	Dr. Parviz Dadras
33	Statistical Descriptions of Shape in R^2 and R^3	Dr. Charles B. Davis
34	An Assessment of the Development of a DNA Probe for Mycoplasma hominis and Ureaplasma urealyticum	Dr. Vito G. DelVecchio
35	Effects of Nuclear Radiation on the Optical Characteristics of Laser Components	Dr. Hermann J. Donnert
36	Energetic Materials via Alkoxy-fluorinations of Alkenes with Xenon Difluoride	Dr. Melvin Druelinger
37	Metal Alkoxide Synthesis of High Temperature Matrices	Dr. Charles H. Drummond
38	Computer Modeling of GaAs and AlAs-GaAs Solar Cells	Dr. Leroy E. Eimers
39	Analyzing Gamma Ray and Neutron Emission Spectra	Dr. Hudson B. Eldridge
40	Geophysical Perturbing Forces on the Frank J. Seiler Large Passive Resonant Ring Laser Gyro	Dr. Harry W. Emrick
41	Quasiparticles and the Transition to Turbulence	Dr. John E. Erdei
42	Statistical Biases in IRLV Measurements of Turbulent Flows	Dr. Dah-Nien Fan
43	Analytical Methods for the Determination of Cholesterol and Cholesterol Esters in Salivary Fluids	Dr. Mack Felton
44	Personality Correlates of Pilot Performance	Dr. Edna Fiedler
45	Transfer of Training Between Alternative Motion Simulators	Dr. John Flach
46	Control of Adaptive Optical Systems	Dr. John A. Fleming

47	Electrochemical Analysis of the Degradation of Synthetic Lubricants	Dr. Dennis R. Flentge
48	Induced Nuclear Radiation Dose in a Simulated Standard Man with Implications on Aircrew Survivability	Dr. Bessie Ruth Foster
49	Determination of Thermal Properties of Melanin Using Photoacoustic Techniques	Dr. James M. Gallas
50	Lidar Measurements of the Mesospheric Sodium Layer at the Air Force Geophysics Laboratory	Dr. Chester S. Gardner
51	AFWL History	Dr. Doris O. Ginn
Volume II		
52	Optimum Design of Structures with Multiple Constraints	Dr. Ramana Grandhi
53	Descriptive Exploration of Patterns in Optical Turbulence Profiles	Dr. Alwin C. Green
54	Modular Modeling of Solid-Fuel Ramjet Combustor Flow	Dr. Mahesh S. Greywall
55	Thermal Stability Characteristics of Some Advanced Synthetic Base Fluids	Dr. Vijay K. Gupta
56	Use of Texture Measures in Multi-spectral Scanner Data Numerical Classifications	Dr. Barry N. Haack
57	Effect of High Free-Stream Turbulence From a Free Jet on Flat Plate Turbulent Boundary Layer Flow and Heat Transfer	Dr. Je-chin Han
58	A Study of Coplanar Waveguide and its Application to Phased Arrays of Integrated Circuit Antennas	Dr. Donald F. Hanson
59	Three-Dimensional Grid Generation for High-Performance Aircraft	Dr. David Hart
60	Analysis of the Report on Filan Performance Metrics	Dr. Albert A. Heaney
61	Methods for Reliability Warranty Verification	Dr. Carolyn D. Heising

62	Artificial Intelligence and Robotics Perception System	Dr. Troy Henson
63	The Thermodynamic, Physical and Optical Properties of Aluminum Oxide	Dr. Astor Y. Herrell
64	Geoid Modelling and Interpretation	Dr. Albert T. Hsui
65	FTIR Spectroscopic Study of Hydrazine Interactions with Clay Minerals	Dr. Clifford T. Johnston
66	Experimental Studies Related to III-V Semiconductor Growth and Characterization	Dr. Patrick L. Jones
67	A Preliminary Study of Learning Nets and Massive Parallelism	Dr. Jeremy Jones
68	Approximate Mathematical Solutions for Unidirectional Composites Containing Broken Fibers	Dr. Walter F. Jones
69	Long Term Life Expectancy Radiation Effects: An Ultrastructural Study of Brain Tumors Developed in Macaca Mulatta following Exposure to Proton Radiation	Dr. Betty Jones
70	Design Considerations for Phase Dependent Voltage Contrast Technique for Application to SEM Analysis and Electrical and Optical and Characterization of Certain Doped Organic Polymers	Dr. Prasad K. Kadaba
71	Synthesis of Novel Polybenzimidazole Monomers	Dr. James J. Kane
72	A Thermal Evaluation of a Portable, Battery-Powered Vapor-Compression Colling System	Dr. Amir Karimi
73	Mechanistic Studies of Energetic Materials: Analysis of 2,4,6-Trinitrotoluene Thermal Decomposition Products	Dr. Daisy W. Kimble
74	Role of Stimulus Uncertainty in Visual Contrast Sensitivity	Dr. David Kohfeld
75	The Multi-Weapon Multi-Target Multi-Phase Assignment Problem	Dr. Stephan E. Kolitz

- | | | |
|----|---|-----------------------------|
| 76 | A Study of the Electrochemical Behavior of the Bromine/Bromide Couple in Melts Composed of Aluminum Chloride and 1-Methyl-3-Ethylimidazolium Chloride | Dr. Lawrence F. Koons |
| 77 | The Thermal Layer: A Simplified Model | Dr. Arthur Kovitz |
| 78 | Analysis of Relationships Among Self, Peer, and Supervisory Ratings of Performance | Dr. Kurt Kraiger |
| 79 | Numerical Study of Detonation Near a Barrier | Dr. Madakasira V. Krishna |
| 80 | Sampling Plan for the Organizational Assessment Package Survey | Dr. Paul S. T. Lee |
| 81 | Route Planning Problem | Dr. Benjamin Lev |
| 82 | Statistical Performance Measures: Relating Air Force Mission Capability to Base Supply Measures | Dr. Edward Lewis |
| 83 | Testing the Effectiveness of some User Friendly Algorithms | Dr. Michael Lewis |
| 84 | Family Factors and the Career Intent of Air Force Enlisted Personnel | Dr. Philip M. Lewis |
| 85 | An Analysis of Low Dispersion IRAS Spectra of Carbon Stars, S Stars and M Variable Stars | Dr. Irene R. Little-Marenin |
| 86 | Preliminary Investigation on Resource Control Strategies on Distributed Computer Systems Real-Time vs. Non-Real Time | Dr. Dar-Biau Liu |
| 87 | Modelling/Analysis of Space Based Kinetic Energy Weapon Projectile Elyouts | Dr. Carl G. Looney |
| 88 | Image Formation and Processing in Superposition Eyes: Precision Location of Point Objects Using the Moire Effect | Dr. James S. Marsh |
| 89 | Control Functions in Grid Generation | Dr. C. Wayne Mastin |
| 90 | Active Mode-Locking Techniques for Ultra-Short Pulses in Nd:YAG Lasers | Dr. Odis P. McDuff |

91	Plasma Parameter Data for BERT 1 Chamber Testing	Dr. Bernard McIntyre
92	Fourier Analysis of the Pattern Electroretinogram	Dr. Leathem Mehaffey
93	Profiling Air Force Family Work Groups to Optimize Service Satisfaction and Career Commitment Impact	Dr. Ivor Mitchell
94	No Report Submitted	Dr. Osoma Mostafa
95	Chlamydomonas Photoaxis as a Simple System for Vision Research	Dr. Rex Moyer
96	Normobaric Oxygen Concentration Effects on Cultured Mouse Macrophage Responses	Dr. James Mrotek
97	Isothermal Differential Scanning Calorimetric Studies of Thermal Decomposition of 1,4-Butanediammonium Dinitrate	Dr. Maurice C. Neveu
98	A Study of the Relationship Between Leadership and Job Satisfaction/Career Commitment Among Air Force Personnel	Dr. Robert E. Niebuhr
99	A Review of Research Literature on the Measurement of Forces/Pressure on the Plantar Surface of the Foot During Gait Using Ambulatory Transducers	Dr. Marion L. Noble
100	A Silicon Vidicon System for Profiling 1.06 μ m Laser Pulses	Dr. Robert O'Connell
101	Free Radical Spectra of PO	Dr. Ralph Oberly
102	ATR Performance vs Image Measurements	Dr. Won J. Park
Volume III		
103	Blast Propagation Through a Composite Wall Section	Dr. Desmond Penny
104	Novel Means of Formaldehyde Analysis Adapted to USAF Laboratory Needs	Dr. Thomas Pierce
105	Raman Spectroscopy of Glycosaminoglycans from Cornea	Dr. Boake Plessy
106	Prediction of Surface Roughness Effects on Heat Transfer and Skin Friction	Dr. Arnold Polak

- | | | |
|-----|--|-----------------------|
| 107 | The Influence of Condensed Water
Revaporization on Wind Tunnel
Test Results | Dr. Justin H. Poland |
| 108 | Study of System Impairment Detection
and Classification Algorithm for Unmanned
Research Vehicle | Dr. Kuldip S. Rattan |
| 109 | Nonlinear Analysis of Composite Supports
for Armor | Dr. Hemen Ray |
| 110 | Diagnostics of Solid Propellant
Combustion | Dr. John P. Renie |
| 111 | Construction of Approximate Formulae
for the Calculation of Conductivity
Coefficients in Partially Ionized Gases | Dr. Michael B. Rhodes |
| 112 | A Literature Survey on the Formation and
LUMinescence of NO(A ² Σ) in a Hydrazine
N ₂ O ₄ Propellant System | Dr. Robert W. Ricci |
| 113 | Numerical Modeling and Inversion of
63 μm Earthlimb Emission From Atomic
Oxygen | Dr. James P. Riehl |
| 114 | No Report Submitted | Dr. Michael Ross |
| 115 | Nondestructive Evaluation of Advanced
Composites by Strain Field Analysis
Acquired Through Correlation of
X-Radiographs | Dr. Samuel S. Russell |
| 116 | Infrared Radiation Target Modeling
System | Dr. Sally Sage |
| 117 | Modeling of Tire/Soil Interaction | Dr. Joseph E. Saliba |
| 118 | Bacteriologic Techniques for the
Isolation of Legionellae From
Aquatic Environments | Dr. Gordon D. Schrank |
| 119 | Chemical Laser Research on the Iodine
Monofluoride (IF) System | Dr. Ronald Segal |
| 120 | Modeling the Tissue Solubilities of
Halogenated Methanes, Ethanes, and
Ethylenes | Dr. Paul G. Seybold |
| 121 | Digital Simulation of Surface-to-Air
Missiles and Smoothing of Cinetheo-
dolite and Radar Data | Dr. Shawky E. Shamma |

122	Indoor Radon Pollution	Dr. Ralph W. Sheets
123	Reliability of Systems with Markov Transfer of Control	Dr. Kyle Siegrist
124	The Synthesis of Reactive Intermediates	Dr. Ricardo Silva
125	Possible Targets for Testing the Neutral Particle Beam at Low Energies in the Mark I Aerospace Chamber	Dr. S. Ballou Skinner
126	Preparation of Non-Flammable Model Compounds	Dr. Terrill D. Smith
127	Studies on Combustion of Liquid Fuel Sprays in Stagnation Flows	Dr. Siavash H. Sohrab
128	Monitoring Environmental Quality by Metabolite Analysis	Dr. Richard G. Stebbins
129	Analysis of Geometric Attenuation in Ground Motion Testing	Dr. Bob W. Stewart
130	Competition Guide for Base-Level Buyers 1985	Dr. Lowell E. Stockstill
131	The Role of Antioxidants in Hyperbaric Oxygen Toxicity to the Retina	Dr. William L. Stone
132	Assessment of Maximum Entropy Method Software for Treatment of Data From the AFGL Labcede Facility	Dr. James E. Sturm
133	Inference Propagation in Emitter, System Hierarchies	Dr. Thomas A. Sudkamp
134	Particle Scattering in Plumes	Dr. William Holt Sutton
135	Thermal Stability of Aluminum-Iron-Cerium Alloys	Dr. Robert Swanson
136	The F-15 SPD Support Equipment "Tiger Team"	Dr. Patrick J. Sweeney
137	Studies in Holographic Procedures	Dr. Charles E. Taylor
138	Dynamic Stress Analysis of Layered Structures	Dr. Joseph W. Tedesco
139	An EPR Study of the Decomposition of Various Dinitrotoluenes and the Synthesis of Azo Compounds	Dr. Walter E. Trafton

140	A Comparison of Measured and Calculated Attenuation of 28 GHZ Beacon Signals in Three California Storms	Dr. Larry Vardiman
141	Allocation and Assessemnt of Logistics Resources	Dr. Daniel T. Voss
142	Natural Language Understanding Using Residential Grammar and Its Use in Automatic Programming	Dr. Christian C. Wagner
143	Stability and Control Computer Program for Conceptual Aircraft Design	Dr. Richard C. Walker
144	Compilation of Select Aspects of the Air Force Weapons Laboratory's 1984 History	Dr. Doris J. Walker-Dalhous
145	The Planning of A R & D Office Information System	Dr. Yin-min Wei
146	Development of High Strength Titanium Alloys VIA Rapid Solidification Processing	Dr. Isaac Weiss
147	"POPCORN" As a Tool for Future Cognitive Workload Assessment: A Conceptual Analysis	Dr. Shih-sun Wen
148	Labeling the Topographic Features of a Gray-Level Image	Dr. David C. Wilson
149	The Warehouse Layout Program	Dr. Jesse Williams
150	A Summer's Study on Nuclear Debris Cloud Radiation and Laser Transmission in the Atmosphere	Dr. Arthur Woodrum
151	The Effect of Wavelength on Light Scatter in the Human Eye	Dr. Billy Wooten
152	Molecular Operators That Move Nuclei Along Paths of Constant Orbital Energy	Dr. Carl Wulfman
153	The LQG/LTR Design Via H ₂ -Optimization	Dr. Hsi-Han Yeh
154	Heat Transfer Correlation for Nosetips With Stagnation-Point Gas Injection	Dr. Juin S. Yu

1985 USAF-UES SUMMER FACULTY RESEARCH PROGRAM/
GRADUATE STUDENT SUMMER SUPPORT PROGRAM

Sponsored by the
AIR FORCE OFFICE OF SCIENTIFIC RESEARCH

Conducted by the
UNIVERSAL ENERGY SYSTEMS, INC.

FINAL REPORT

Blast Propagation Through a Composite Wall Section.

Prepared by: Desmond N. Penny

Academic Rank: Assistant Professor

Department and Physical Science

University: Southern Utah State College, Cedar City, UT 84720

Research Location: Head Quarters, Air Force Engineering
and Services Center (HQ AFESC),
Facility Systems and Analysis Branch (RDCS),
Tyndall Air Force Base, FL 32403

USAF Research: John R. Hayes Jr., P.E.

Date: August 1985

Contract No: F49620-85-C-0013

Blast propagation through a composite wall section.

by

Desmond N. Penny Ph.D., P.E.

ABSTRACT

This report concerns the appropriate design for the outside walls of a protective structure. The threat considered here is that of a conventional bomb. The blast wave from such a device impinges on the wall of the structure and propagates into its interior, causing spalling, fragmentation and structural weakening.

Dissipation of this blast energy is a primary consideration of this investigation. A composite wall section is proposed to cause partial reflection of the blast energies at different interior boundaries of the wall. This partial reflection prevents a large build-up of tensile stresses at any boundary, and thus prevents spalling. A finite element model is developed using the ABAQUS code, to analyse this structural wall section.

ACKNOWLEDGEMENTS

The author would like to express his appreciation to the Research Engineering Division, Air Force Engineering & Services Laboratory, Engineering and Services Center, Tyndall AFB, Florida for their hospitality during his stay as a Summer Fellow. Special thanks are due to Dr. Joseph Tedesco who collaborated with the author on a main portion of the report. The author is also grateful for the advice and guidance given by Mr. John R. Hayes Jr., Mr. Harry R. Marien, Capt Paul L. Rosengren Jr. and LCDR Thomas J. Hilferty.

The author is grateful to Lt Col Thomas A. Brocato and Col Robert E. Boyer for their help in minimizing bureaucratic problems.

Appreciation is also extended to the Air Force Systems Command, Air Force Office of Scientific Research for its sponsorship and to Universal Energy Systems Inc. for the efficient administration of the program.

SECTION 1

INTRODUCTION

The author is an assistant professor in the physical science department of Southern Utah State College. He received his bachelors degree in Mathematical Physics at University College, Cork, Ireland. His masters degree was in elasticity and electromagnetic theory at the same university. He received his Ph.D. in civil engineering from the University of Utah, where his research was in the continuum mechanics area.

Ater graduation the author taught at University College, Cork, Ireland and at Lamar University, Texas. His research interests have included the characterisation of permanent memory materials, and the computer modeling of material and structural problems. Prior to his current position, he worked as a design engineer for Penn Engineering, Orange, Texas, where his chief responsibilities involved the analysis and design of offshore oil structures.

The author performed the attached study at the Air Base Survivability Branch, Research Engineering Division of the U.S. Air Force Engineering and Services Center, Tyndall AFB. One of the Branch's objectives is to develop design specifications for Air Force shelters to withstand various nonnuclear weapons attack. Safety of personnel, integrity of shelters, construction constraints, and cost effectiveness are among the areas of concern in the specifications.

SECTION II

OBJECTIVES

The initial objectives of my research efforts were as follows:

1. Examine the main work that has been done in the protection from nonnuclear weapons field and recommend fruitful areas for continued research.
2. Examine some of the finite element codes, in particular ABAQUS, and judge their applicability to problems in this area.

As my reading progressed I became intrigued with the possibilities offered by composite wall construction. In addition to the above I decided to propose a composite wall for use in protective structures and to perform an analysis of it using ABAQUS.

SECTION III

INITIAL DISCUSSIONS

This report concerns the problem of the appropriate design of the outside walls of a protective structure. The threat considered here is that of a conventional bomb. A Mark 83, 1000 lb. bomb, will be used in the analysis. The blast wave from such a device impinges on the wall of the structure and propagates into its interior.

Dissipation of the blast energy is a primary consideration of this investigation. The effects of the blast causes fragmentation of the outer surface of the wall, and tensile failure of materials at interior boundaries. Fragmentation can be greatly reduced by berming the outer wall surface, and will not be discussed here. The tensile failure at interior boundaries, called spalling, is one main concern of this report. As an initial effort to reduce spalling, a composite wall model is proposed in Section IV.

In Section V, the model is translated into a finite element computer model using the ABAQUS code which is installed on the CYBER computer at Tyndall. For the benefit of the staff at Tyndall, listings of the job streams and input files are included. It is hoped that this will facilitate the use of this computer model to analyze other materials in composite wall construction.

In Section VI, a discussion of the computer results is given. Section VII contains a summary of the conclusion arrived at in the report, and finally in Section VIII, recommendations are given about the ABAQUS code and fruitful areas for continued research.

SECTION IV

COMPOSITE WALL MODEL

The pressure wave from the blast impinges on the outer surface and imposes a compressive stress on the outer portion of the wall. This pressure history is shown in Figure 1 (Ref 1).

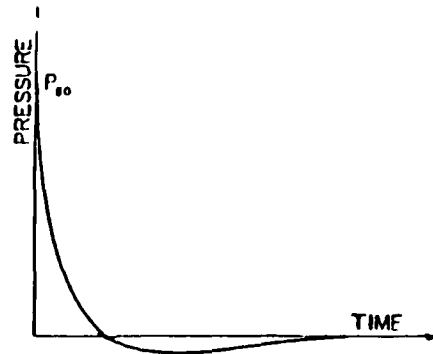


Figure 1: Blast pressure history

The compressive stress propagates into the interior of the wall and suffers reflection and refraction whenever the stress wave meets an interface between two materials. The equations giving the transmitted and reflected energies are (Ref 2):

$$\frac{\sigma_T}{\sigma_I} = \frac{2\rho'c'_1}{\rho'c'_1 + \rho c_1} \quad (1)$$

$$\frac{\sigma_R}{\sigma_I} = \frac{\rho'c'_1 - \rho c_1}{\rho'c'_1 + \rho c_1} \quad (2)$$

where ρ, ρ' = Densities of first and second materials respectively.

c_1, c'_1 = Speeds of wave

$\rho c_1, \rho'c'_1$ = Acoustic resistances

σ_I = Incident stress

σ_T = Transmitted stress

σ_R = Reflected stress

Consider the case of a stress wave moving from one material to a less dense one. In this situation $\rho c_1 > \rho' c'_1$.
 We see from Eqn 2, that $\frac{\sigma_R}{\sigma_I} < 0$.
 Thus, if $\sigma_I < 0$ then $\sigma_R > 0$.

Thus a compressive wave is reflected as a tensile wave.

Consider the case where steel and aluminum meet at an interface. The acoustic resistance of steel is 452, while that of aluminum is 165. In figure 2 below, an incident compressive wave of magnitude 1, impinges on the boundary. The reflected wave is tensile of magnitude 0.46, while the transmitted wave is compressive of magnitude 0.54 (Ref 2).

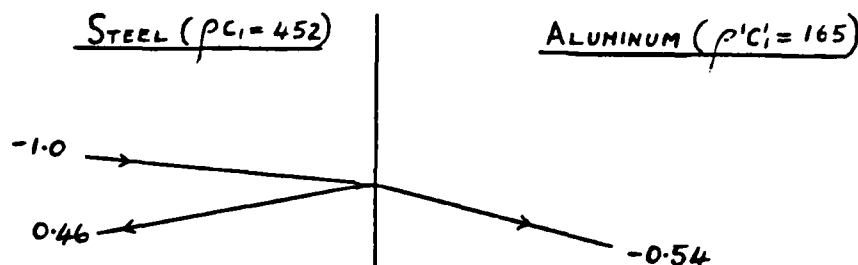


Figure 2: Reflection and refraction at an interface.

Equations 1 and 2 are strictly correct only for infinite media in contact at an interface, however, we can use them to guide our design for the composite wall section.

A common problem in protective structures design is the prevention of spall. This phenomenon occurs at the interior of walls and is characterized by the concrete failing locally and being ejected from the wall at high speed. It is generally thought that this occurs because of the reflection of the compressive blast wave from the concrete-air interface. The reflected wave from such an interface is seen from the above equations to be a tensile wave of equal magnitude to the compressive stress. The concrete therefore fails in tension in the described fashion.

From the above discussion we are led to a consideration of the following simplified model:

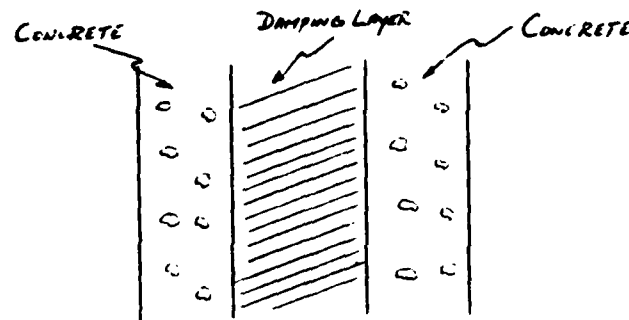


Figure 3: Simplified model.

Here we see two layers of concrete, separated by a damping material. This damping material should have an acoustic resistance such that only a portion of the incident stress is transmitted from the first to the second layer. A stiff rubber-like material comes to mind. This simplified model will be analysed in the next section.

For the simplified model shown in Figure 3, one damping layer is utilized. Since we now have two faces where spall can occur in the concrete, it is advisable to have equal sharing of the tensile reflected waves at these faces. This condition leads to the requirement that a 50 percent reduction of the transmitted stress occur at the first interface.

We will now derive the condition for transmission of just half of the incident stress. From Eqn 1, we see

$$\frac{\sigma_T}{\sigma_I} = \frac{2\rho'c_i}{\rho'c_i + \rho c_i} = \frac{1}{2}$$

$$\therefore 4\rho'c_i = \rho'c_i + \rho c_i$$

$$\therefore \rho'c_i = \frac{\rho c_i}{3}$$

Thus, 50% of the incident stress is transmitted, if the acoustic resistance of the damping layer is just one third that of the concrete layer.

In this case, for the reflected wave, we have from Eqn 2:

$$\frac{\sigma_R}{\sigma_I} = \frac{\frac{\rho C_1}{3} - \rho C_1}{\frac{\rho C_1}{3} + \rho C_1} = \frac{\rho C_1 (\frac{1}{3} - 1)}{\rho C_1 (\frac{1}{3} + 1)}$$

$$= -\frac{1}{2}$$

Thus, the reflected wave is tensile and has just half the magnitude of the incident wave.

Using the above ideas and some others, a composite wall model will now be proposed. Though the analysis of this model is beyond the scope of this present work, its design can be guided by the analysis of the simplified model to be performed in the next section.

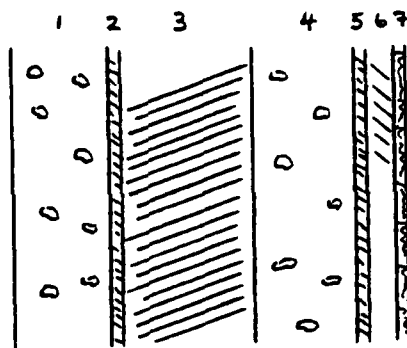


Figure 4: Composite wall model.

One of the primary benefits of this composite wall system is the partial reflection of the incident pressure at each boundary. This prevents large tensile stresses from occurring at any boundary, and thus minimizes the possibility of spalling. This multi-layer model utilizes the central idea of the simplified model - that of the partial reflection of the incident stress - and it also introduces some other promising features. I will now treat each layer separately and indicate its function.

Layers 1 and 4: Structural Layers.

We can have one or more reinforced concrete layers for structural strength.

Layer 3: Damping Layer.

The purpose here is to provide a layer where large compression can occur and thus dissipate energy. The transmitted compressive stress and the reflected tensile stress should be about 50% of the incident value. This layer would not only dissipate energy but also tend to isolate the interior layers from the compression blast.

Layers 2 and 5: Fabric Layer.

A double layered fabric material, similar to that used by Tom Hilferty in his HYPAR structures. This layer should be bonded to the interior surface of each structural layer to provide strong tension reinforcement at the point of maximum tensile stress.

Layer 6: Fragmentation Layer.

A correct choice of material can result in an advantageous fragmentation of this layer. The correct material would be one with low tensile strength that fragments in very small particles. Since the kinetic energy of the fragments is given by $\frac{1}{2} m v^2$, it follows that much of the incident energy will be dissipated if we can arrange for this layer to fragment in a large number of particles, each particle having a high velocity. This layer could be easily replaced after an attack and could also be retrofitted to existing structures.

Layer 7: Protective Curtain.

A final decorative cloth facing would minimize the possibility that these fragments could injure personnel. This facing could again be made from a fabric material such as that in layers 2 and 5. In this case, however,

Layer 7: Protective Curtain (continued).

it is not advantageous to bond the curtain to the previous fragmentation layer. The object here is to allow spalling to occur while preventing the fragementents from entering the work environment.

The composite wall system presented herein incorporates a number of promising featuers for use in protective structures:

1. A fragmentation layer for the inner surface.
2. Fabric layer to provide tension reinforcement and prevent spalling.
3. Provision of a damping layer.
4. Final protective curtain for spall containment.

These features deserve further analysis with a possible test program to follow.

I feel that this system has good prospects for maintaining the integrity of the structure after the blast. The only damage that should occur is to the fragmentation layer, and this can easily be replaced.

SECTION V
ANALYSIS OF THE SIMPLIFIED MODEL

In this section of analysis of the simplified model of Figure 13 is performed, using the ABAQUS finite element code. The incident pressure is arbitrary, since we are studying the decrease in this pressure as it propagates into the wall interior. The assumed pressure - time history propagating into the wall, is shown in Figure 5. Because of the small size of the model, the variation of the peak pressure across the wall is minimal and will be neglected.



Figure 5: Assumed blast history.

An overview of the situation is shown in Figure 6, Part (a). In order to produce an axisymmetric situation, a circular model with fixed boundary conditions is assumed in Part (b).

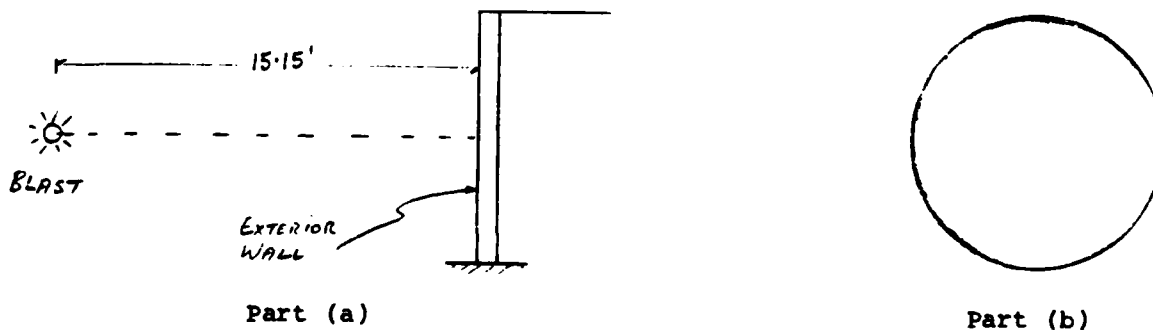


Figure 6: Blast configuration and assumed circular model.

A computer analysis of the model was run using the ABAQUS code, running on a CYBER 760 computer, with the NOS 2.2 operating system. For simplicity, linear elastic materials were used for the three layers. The phenomena of interest, namely, reflection and refraction of pressure waves, are local, small deformation events. The linear elastic assumption, should therefore not affect the character of the results.

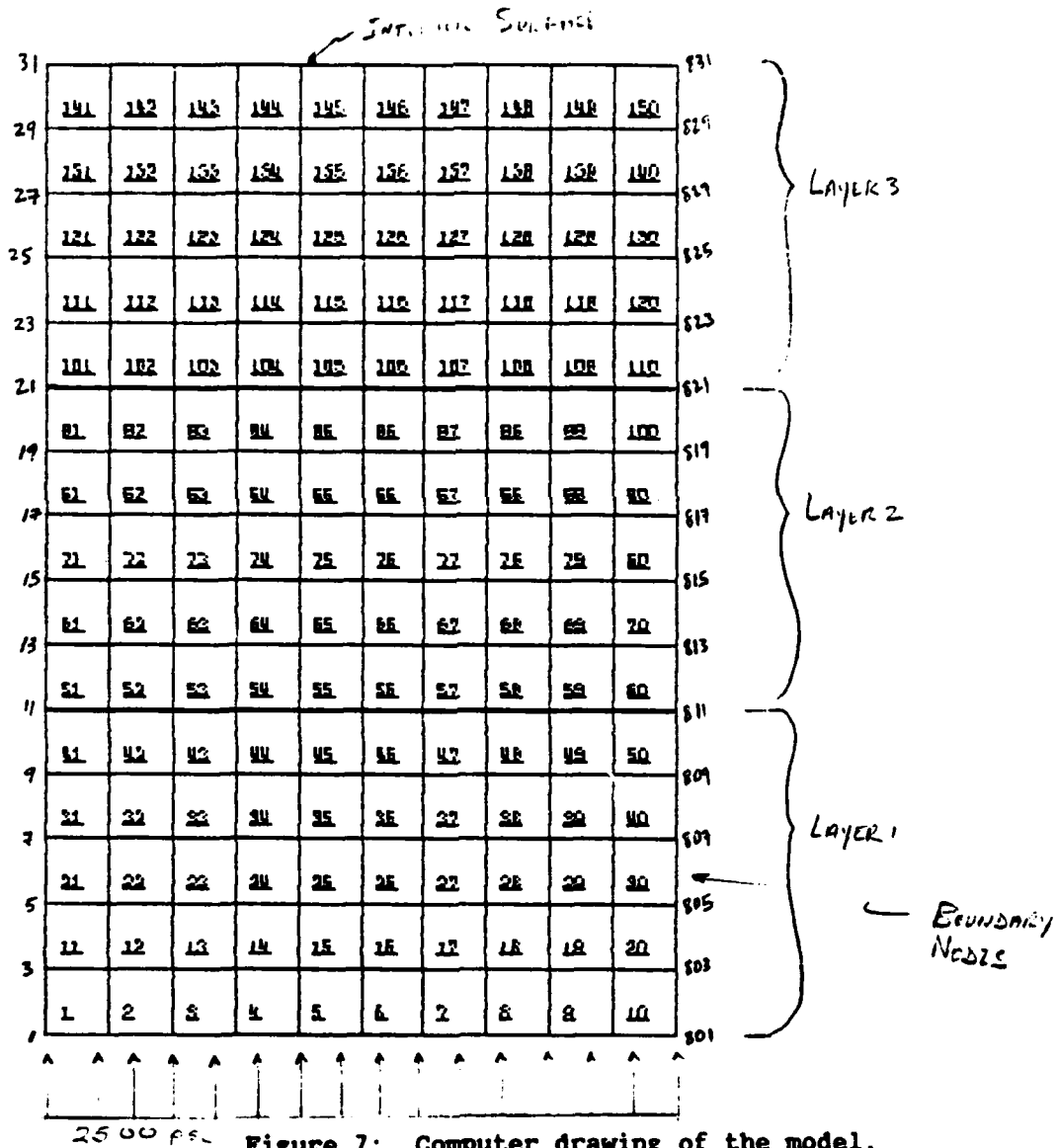


Figure 7: Computer drawing of the model.

Figure 7 shows the computer drawing of the model under the 2500 psi uniform load on the exterior face. It depicts a cross section of the plate, from the center, at nodes 1 - 31, to the boundary, at nodes 801 - 831. The boundary nodes are fully fixed. Since we have axial symmetry in the problem,

8-node axisymmetric elements, type CAX8, are used. The model has a radius of 20" and a total thickness of 30". The radius of 20" was sufficiently large to remove the influence of the boundary conditions on the behavior of the central elements. A first version of the model was run with a uniform material throughout. This was then compared with a second version which has steel in the front and back layers and a weaker material in the interior layer. The critical elements involved at the center of the model, from exterior to the interior face, are: 1, 11, 21, 31, 41 (Layer 1 elements); 51, 61, 71, 81, 91, (Layer 2 elements); 101, 111, 121, 131, 141 (Layer 3 elements). Non-linear analysis was used throughout.

For simplicity, the material chosen for layers 1 and 3, was steel. ABAQUS does allow the modelling of concrete, and this change to the model will not be difficult. The Youngs modulus of layer 2 material was chosen to be one-third the value for steel. This is consistent with the previous discussion in section iv.

The assumption of axial symmetry greatly simplifies the analysis. There is little loss of generality in this assumption since the effect we are analysing is local in nature. The assumption of fixed boundary conditions is not critical since we are only interested in what occurs at the center of the model, a sufficiently large distance from the boundary.

For completeness, the ABAQUS model, called ABAIN, is shown in Figure 8. The job stream, named ABARUN, that controls the execution of ABAIN, is shown in Figure 9. When ABARUN is submitted as a batch job, ABAIN is read, the model is constructed and the analysis is performed. The results are written to a file called TAPE8OL.

A post-processing run was executed. The job stream, called ABARUNP, and the input file, called ABAINP, are shown in figures 10 and 11 respectively. This run accesses TAPE8OL and performs various plots of the data.

```

*HEADING
NONLINEAR, CAX8, FINE MESH
*NODE
1,0,0
31,0,30
801,20,0
831,20,30
*NGEN,NSET=CENTER
1,31,1
*NGEN,NSET=BDRY
801,831,1
*NGEN
1,801,40
2,802,40
3,803,40
4,804,40
5,805,40
6,806,40
7,807,40
8,808,40
9,809,40
10,810,40
11,811,40
12,812,40
13,813,40
14,814,40
15,815,40
16,816,40
17,817,40
18,818,40
19,819,40
20,820,40
21,821,40
22,822,40
23,823,40
24,824,40
25,825,40
26,826,40
27,827,40
28,828,40
29,829,40
30,830,40
31,831,40
*ELEMENT,TYPE=CAX8
1,1,81,83,3,41,82,43,2
*ELGEN
1,10,80,1,15,2,10
*ELSET,ELSET=LAYER1,GENERATE
1,50,1
*ELSET,ELSET=LAYER2,GENERATE
51,100,1

```

```

*SET,ELSET=LAYER3,GENERATE
1,1,1
*ELSET,ELSET=CENTER,GENERATE
1,141,10
*ELSET,ELSET=BDRY,GENERATE
10,150,10
*ELSET,ELSET=FRONT,GENERATE
1,10,1
*MATERIAL
*ELASTIC
29E6,0.3
*DENSITY
0.000728
*BOUNDARY
CENTER,1
BDRY,1,2
*AMPLITUDE,TIME=D,VALUE=R,NAME=BLAST
0.0,1.0,1E-3,0.0
*STEP,NLGEOM,INC=3,AMP=STEP,CYCLE=100
*DYNAMIC,ALPHA=-0.250,PTOL=10,MTOL=4E4
.01E-3,1E-3
*LOAD,AMPLITUDE=BLAST
FRONT,P1,2500.0
*EL PRINT,ELSET=CENTER,FREQ=1
2,1,1,2,1
2,1,1,1,1,1
2,2,2
*NODE PRINT,FREQ=1
2,1,1,1,1,1,1,1
*PLOT,FREQ=1
DEFORMED SHAPE
*DISPLACED
1,,1
*DETAIL,ELSET=CENTER
*CONTOUR
1,,,1,1
*CONTOUR
2,,,1,1
*EL FILE,ELSET=CENTER,FREQ=1
2,2,2,2,2
2,2,2,2,2
2,2,2
*ENERGY FILE,FREQ=1
*NODE FILE,NSET=CENTER,FREQ=1
2,2,2,2,2
*END STEP

```

Figure 8: Listing of ABAIN.

```

ABARUN.
USER,SUMMER,GOSH.
CHARGE,26730025,ABAQUS.
SETTL,X.
****
**** INPUTS:  ABAIN
**** OUTPUTS: ABAOUT, PLOTNPF, TAPEBOL
****
PURGE,ABAOUT/NA.
PURGE,PLOTNPF/NA.
DEFINE,OUTPUT=ABAOUT.
GET,ABAIN.
COPYBF,ABAIN,TAPE5.
DEFINE,TAPEB=TAPEBOL.
ATTACH,ABAQPRE/UN=APPLLIB.
****
**** EXECUTE THE PRE PROGRAM
****
ABAQPRE,*PL=99999.
FTN5,I=TAPE28,PL,OPT=2,LO=0,B=MGO.
RETURN,TAPE20,TAPE25,TAPE26,TAPE27.
RETURN,TAPE28,TAPE29,TAPE30.
RETURN,TAPE13.
RETURN,ABAQPRE.
DEFINE,TAPE13=MAINPLT.
ATTACH,ABAQLIB/UN=APPLLIB.
****
**** EXECUTE THE MAIN PROGRAM
****
LDSET,LIB=ABAQLIB,PRESET=INDEF,MAP=N.
MGO,PL=99999.
GET,UNIPROC/UN=APPLLIB.
BEGIN,UNIPLT,UNIPROC,NE.
LIBRARY,UNIPLT.
ATTACH,ABAQPLT/UN=APPLLIB.
DEFINE,NPFIL=PLOTNPF.
****
**** EXECUTING THE PLOT CONVERSION
****
ABAQPLT,*PL=99999.
PURGE,MAINPLT.
STATUS,F.
DAYFILE.
****
EXIT.
STATUS,F.
DAYFILE.

```

Figure 9: Listing of ABARUN.


```

ABARUNP.
USER,SUMMER,GOSH.
CHARGE,26730025,ABARUS.
SETTL,*.
****
**** INPUTS:  ABAINP, TAPE80L
**** OUTPUTS:  ABAOUTP, NPFIL=RUNPNPF
****
PURGE,ABAOUTP/NA.
DEFINE,OUTPUT=ABAOUTP.
GET,ABAINP.
COPYER,ABAINP,TAPE5.
****
**** ATTACH TAPE80L FROM THE MAIN RUN
****
ATTACH,TAPE8=TAPE80L.
ATTACH,ABAQPRE/UN=APPLLIB.
****
**** EXECUTING ABAQPRE
****
ABAQPRE,PL=99999.
FTN5,I=TAPE28,OPT=2,LO=0,B=MGO.
RETURN,TAPE20,TAPE25,TAPE26,TAPE27.
RETURN,TAPE28,TAPE29,TAPE30.
RETURN,ABAQPRE.
DEFINE,TAPE13=RUNPPLT.
DEFINE,NPFIL=RUNPNPF.
ATTACH,ABAQLIB/UN=APPLLIB.
****
**** EXECUTE THE MAIN PROGRAM.
****
LDSET,LIB=ABAQLIB,PRESET=INDEF,MAP=N.
MGO,PL=99999.
****
GET,UNIPROC/UN=APPLLIB.
BEGIN,UNIPLT,UNIPROC,NE.
LIBRARY,UNIPLT.
ATTACH,ABAQPLT/UN=APPLLIB.
****
**** EXECUTING THE PLOT CONVERSION
****
ABAQPLT,*PL=99999.
PURGE,RUNPPLT.
STATUS,F.
DAYFILE.
**** EXIT ROUTINE IN CASE OF ERROR
EXIT.
STATUS,F.
DAYFILE.

```

Figure 10: Listing of ABARUNP.

```

*POST FILE
HISTORY AT ELEMENT 1 POINT 2: FINE MESH
****
*HISTORY, TIME=DYNAMIC
TIME                DISPLACEMENT:NODE 1
NODE,1,2,0,1,1.0,  VERT. DISPL.
*****
*HISTORY, TIME=DYNAMIC
TIME                SPEC STRAIN EN 1,2
ELEM,1,2,0,81,1.0,SPEC STN EN 1,2
****
*HISTORY, TIME=DYNAMIC
TIME                STRAIN ENERGY ELT 1
ELEM,1,2,0,85,1.0,STRAIN EN ELT 1
****
*HISTORY, TIME=DYNAMIC
TIME                TOTAL STRAIN ENERGY
ENER,2,,TOTAL STRAIN ENERGY
*****
*HISTORY, TIME=DYNAMIC
TIME                S(RR) AT 1,2
ELEM,1,2,0,1,1.0,S(RR) AT 1,2
****
*HISTORY, TIME=DYNAMIC
TIME                S(ZZ) AT 1,2
ELEM,1,2,0,2,1.0,S(ZZ) AT 1,2
****
*HISTORY, TIME=DYNAMIC
TIME                HOOF STR AT 1,2
ELEM,1,2,0,3,1.0,HOOF STR AT 1,2
****
*HISTORY, TIME=DYNAMIC
TIME                S(RZ) AT 1,2
ELEM,1,2,0,4,1.0,S(RZ) AT 1,2
*****

```

Figure 11: Listing of ABAINP.

SECTION VI

DISCUSSION OF THE RESULTS

The results presented here are preliminary in nature due to computer and weather problems, and further computer runs are needed to verify the observations presented.

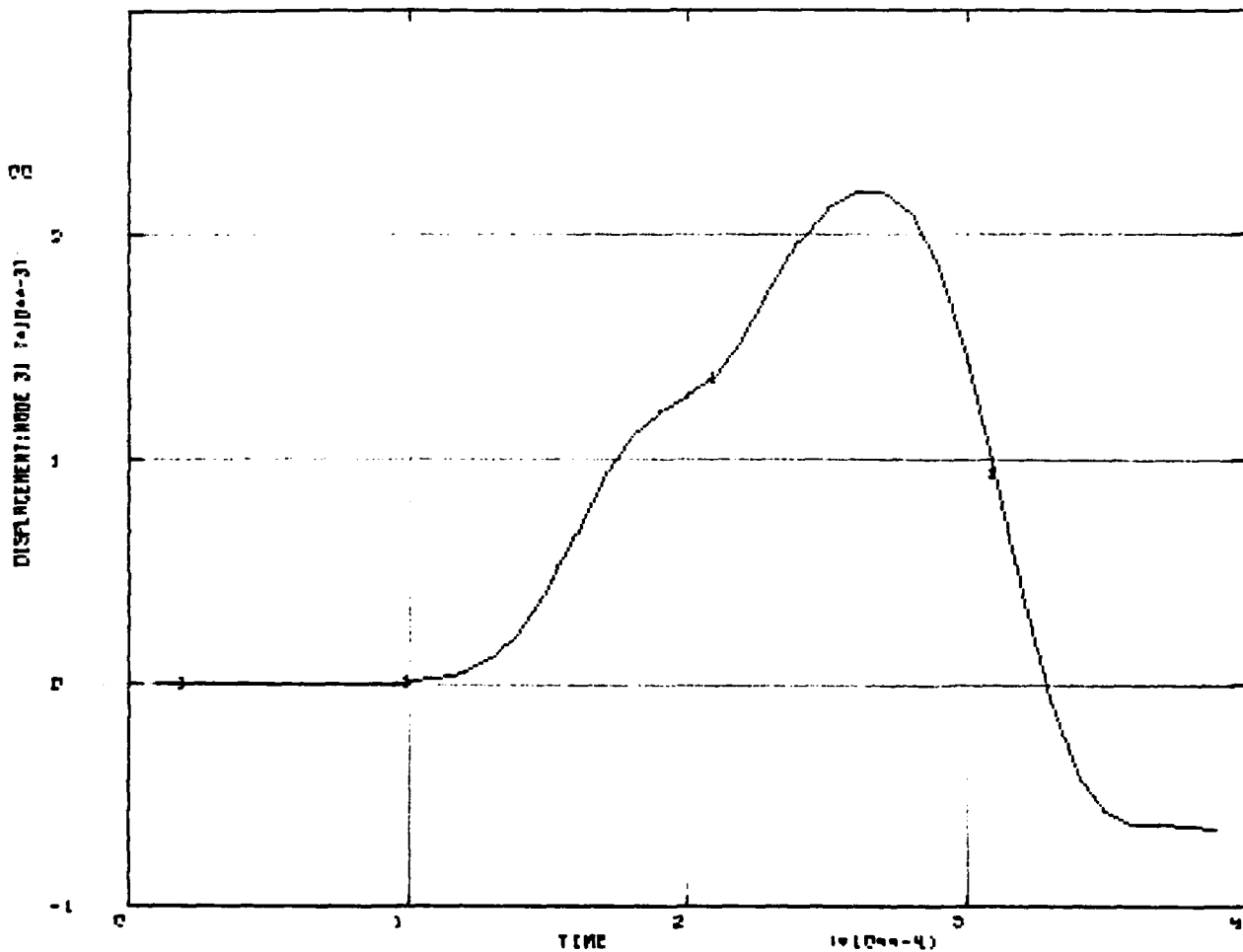


Figure 12: Deflection of node 31 in the unlayered model.

Figure 12 shows the deflection curve of the unlayered model for node 31. Note that the maximum deflection is about 0.0023 inches, and the time at which this occurs is about 0.27 msec after the blast wave impact on the exterior surface. The time delay of 0.1 msec before node 31 begins to deflect is due to the finite speed of the wave propagation in the wall. A simple calculation

shows that this speed is 7620 m/sec. This compares favorably with the experimentally determined value for steel of 5800 m/sec (Reference 2).

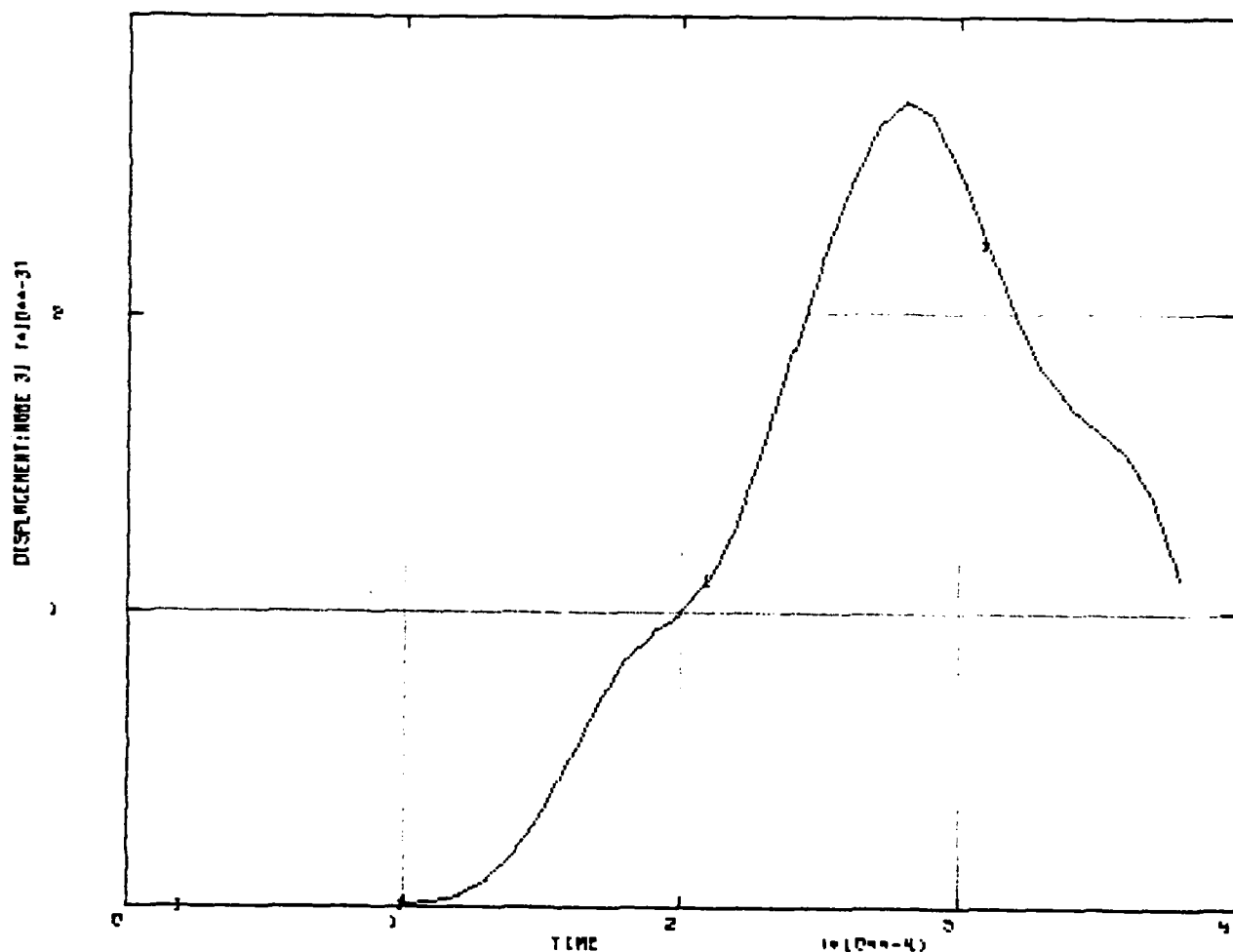


Figure 13: Deflection of node 31 in the layered model.

Figure 13 shows the deflection curve of the layered model for node 31. The time at which the maximum deflection occurs remains about 0.27 msec, however the value of this deflection is now about 0.0028 inches. This is due to the weakened material in the middle of the layered model.

Since the greatest global deflection takes place at 0.27 msec, it follows that the compressive wave front must propagate through the wall before this time. This is because the spalling phenomenon that results from the compressive wave front is local in nature and occurs before global deformation takes place.

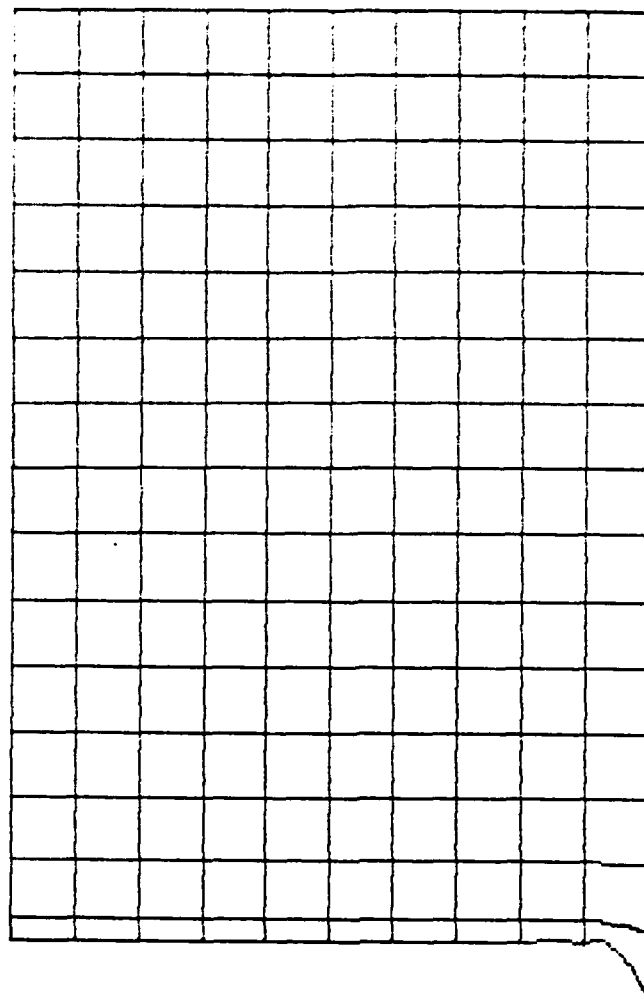


Figure 14: Model just after the blast wave is incident on the bottom (exterior) face.

Figure 14 gives a better understanding of the compressive wave caused by the blast. This figure shows the model just after the blast wave hits the exterior face. We see the compressive pulse initiating at the bottom face. This is clear from the figure since the bottom layer of elements are greatly compressed. This pulse propagates through the model by local deflection and reaches the interior face, causing the spalling phenomenon of interest in this report. Notice that no deformation of the interior nodes has occurred.

It would have been instructive to view the pressure wave at a subsequent time in its path through the wall, however, computer problems prevented getting such an output. Figures 15 and 16 show the desirable effect of the damping layer in action. Figure 15 shows the stress in the transverse (i.e. axial) direction for element 41, which is the last element of Layer 1. The compressive pulse is clearly evident and has a value of -19000 psi.

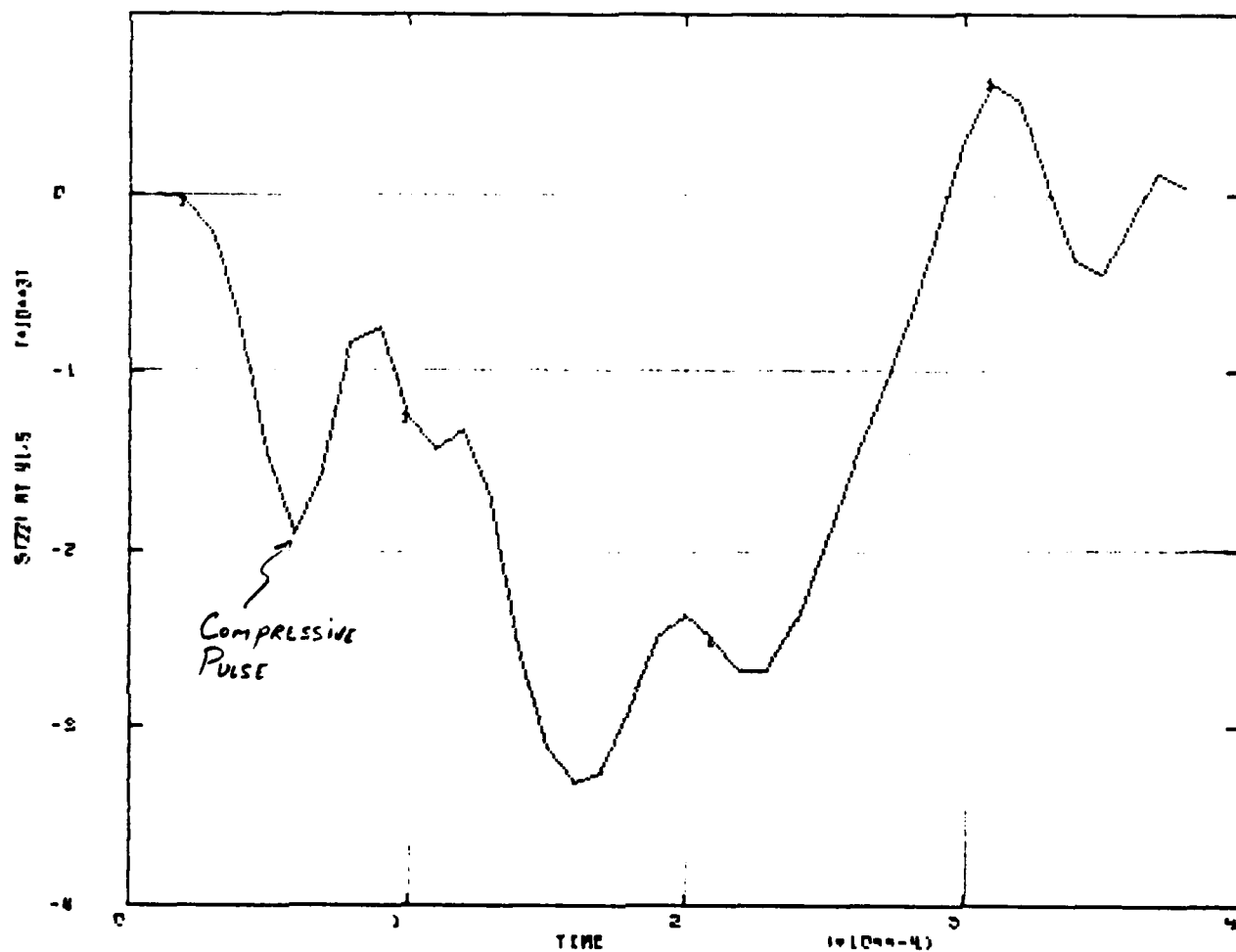


Figure 15: Axial stress for element 41 (layered model).

Figure 16 is the corresponding plot for element 51, which is the first element of Layer 2. We see that the compressive pulse has been reduced markedly to a value of about -1500 psi.

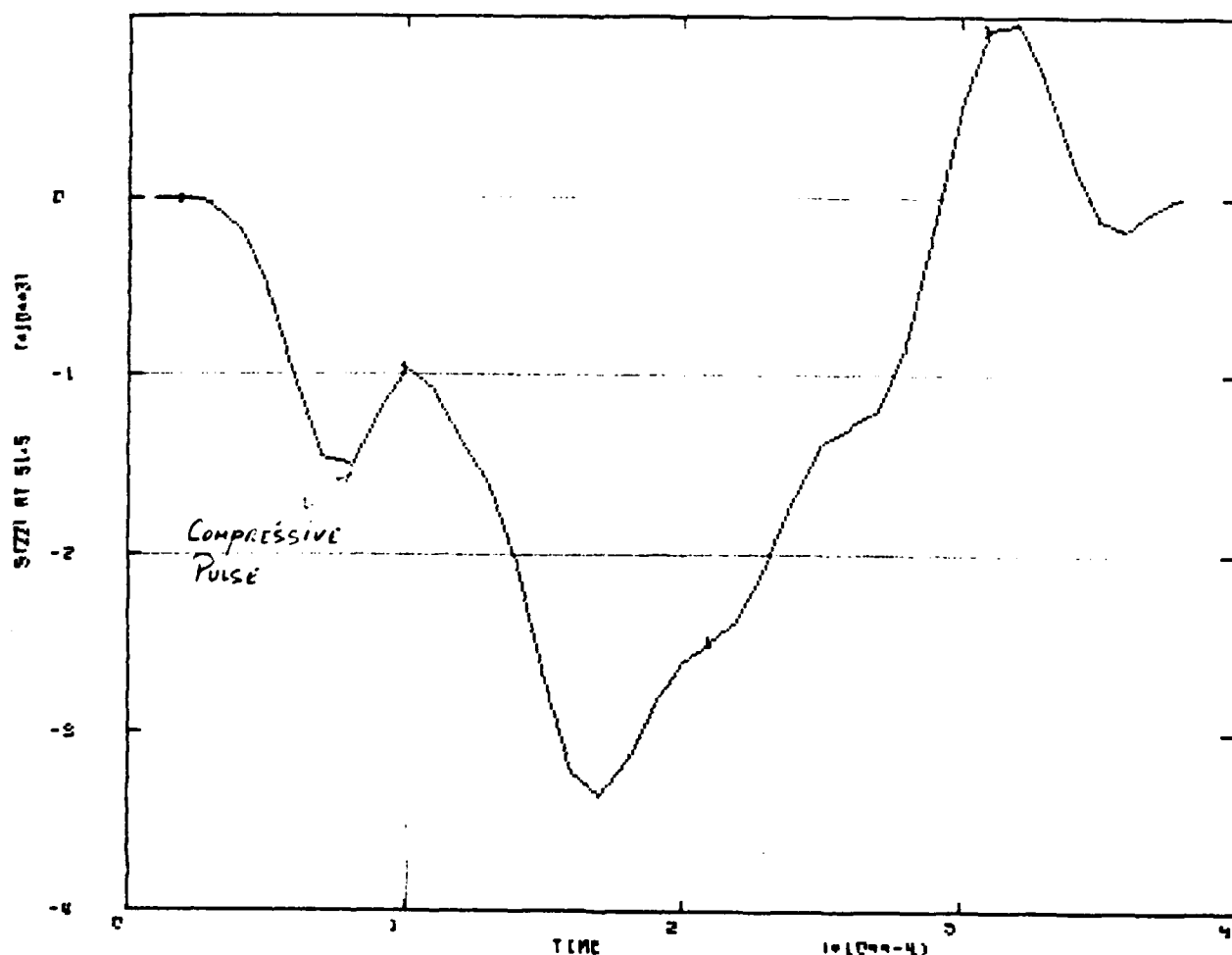


Figure 16: Axial stress for element 51 (layered model).

Figures 17 and 18 show the situation at the interior boundary, for the unlayered and layered models respectively. In both curves we see the peak marked X, which is the incoming compressive pulse, and then at a later time, we see the peak Y which is the reflected tensile pulse. A comparison between these curves shows a small reduction in both the compressive and tensile pulses for the layered structure. This is in spite of the greater deflection of the layered model.

The effect in these computer runs was not large, and further more sensitive runs need to be made to compare models of approximately the same structural strength.

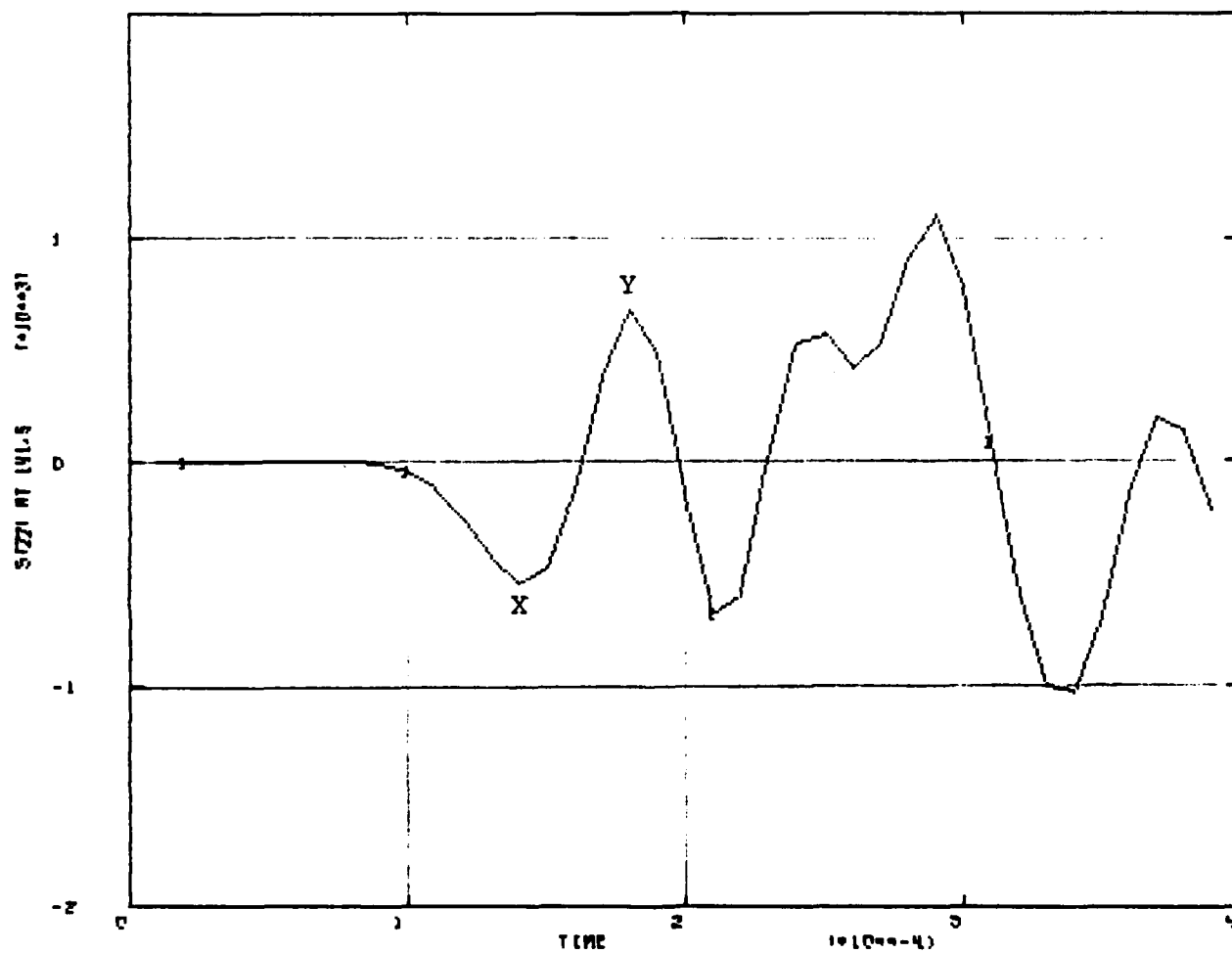


Figure 17: Axial stress at the interior boundary for the unlayered model.

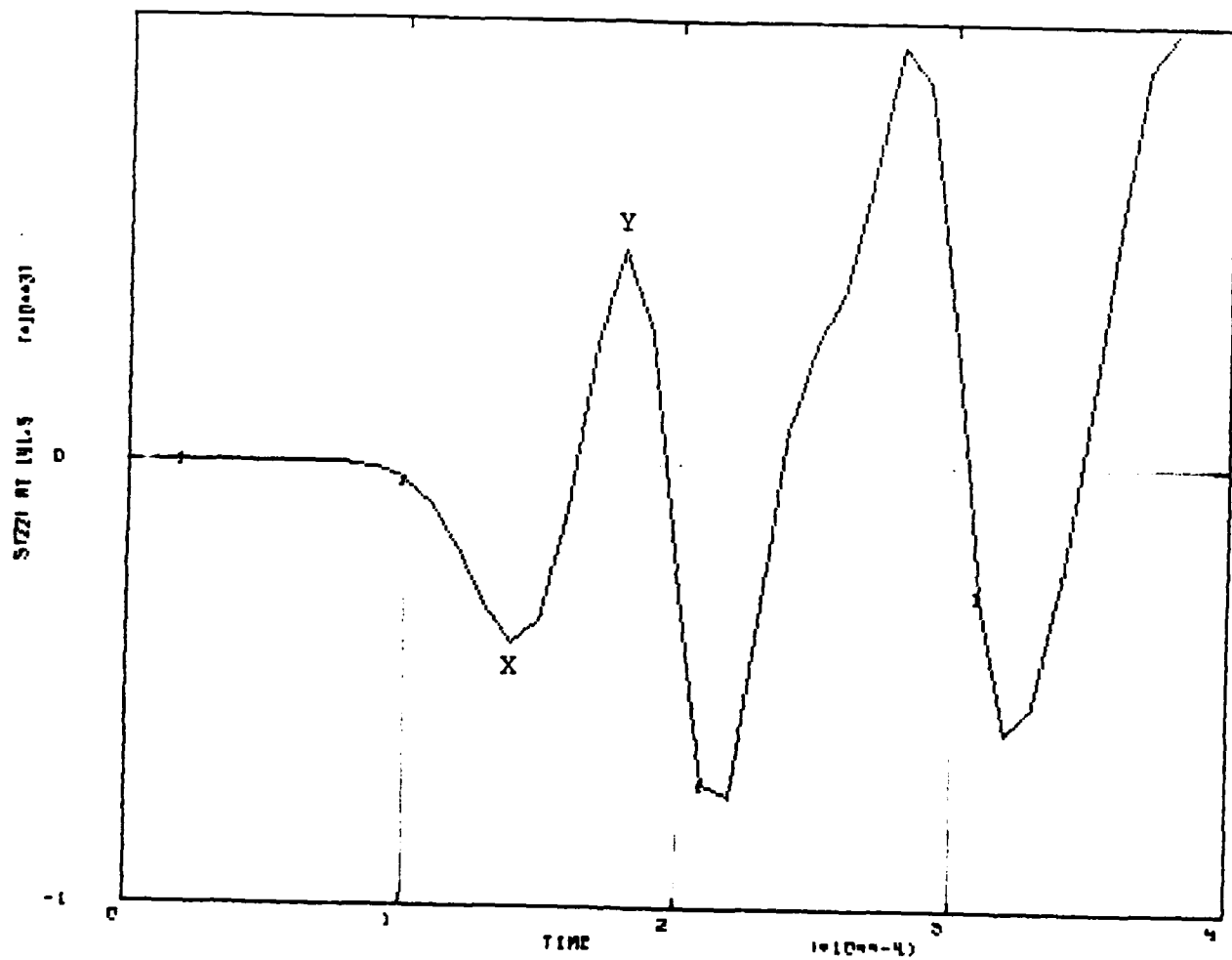


Figure 18: Axial stress at the interior boundary for the layered model.

SECTION VII

CONCLUSIONS

The beneficial predicted effects of a composite wall system discussed here seem to exist. Composite wall construction shows promise for the rapid attenuation of the pressure wave and thus an improvement of the spall resistant capabilities, while reducing the material costs. An improvement in secondary characteristics such as insulation and sound attenuation, can also be expected.

An observation on the performance of the ABAQUS code seems to be warranted at this point. In one of the first runs, a small model of 750 elements with 100 load increments was submitted. The analysis was linear and the model utilized axisymmetric elements, which made the model two dimensional in nature. The computer run took 7 hours and 10 minutes of central processor time. This is unacceptable. Such a long run time is very unusual and more efficient finite element codes are available.

The above observation needs to be balanced against the user friendly nature of ABAQUS, and the good support available from Hibbitt, Karlsson and Sorensen, Inc.

SECTION VIII

RECOMMENDATIONS

Further more sensitive computer runs should be made to study the attenuation of the pressure wave through the composite wall section. An effort should be made to compare the composite wall section with a conventional wall of similar structural strength.

Subject to the above computer results, a test program on composite wall sections may be warranted. This program should compare composite wall with conventional construction from the standpoints of spalling, pressure wave attenuation, and finally, economic criteria.

Serious consideration should be given to an adoption of an alternative finite element computer code. While ABAQUS is quite user friendly and has good support from Hibbitt, Karlsson and Sorensen, Inc., it is quite inefficient. However, when alternate codes are being considered, high priority should still be given to ease of use and customer support.

REFERENCES

1. Crawford, Robert E. et al., "Protection from Nonnuclear Weapons", AFWL-TR-70-127, Air Force Weapons Laboratory, Kirtland AFB, NM, February 1971.
2. Rinehart, John S., Stress Transients in Solids, Santa Fe, NM, Hyperdynamics, 1975.
3. "Structures to Resist the Effects of Accidental Explosions", Department of the Air Force Manual, AFM 88-22, June 1969.

1985 USAF-UES SUMMARY FACULTY RESEARCH PROGRAM/
GRADUATE STUDENT SUMMER SUPPORT PROGRAM

Sponsored by the
AIR FORCE OFFICE OF SCIENTIFIC RESEARCH

Conducted by the
UNIVERSAL ENERGY SYSTEMS, INC.

FINAL REPORT

Novel Means of Formaldehyde Analysis
Adapted to USAF Laboratory Needs

Prepared by:	Thomas Pierce, Ph.D.
Academic Rank:	Associate Professor
Department and	Department of Chemistry (Ind. Hygiene)
University:	University of North Alabama
Research Location:	USAF Occupational and Environmental Health Laboratory (USAF OEHL), Analytical Services Division, Environmental Chemistry Branch
USAF Research:	Thomas C. Thomas Chief, Laboratory Operations Branch
Date:	20 August 1985
Contract No:	F49620-85-C-0013

ABSTRACT

NOVEL MEANS OF FORMALDEHYDE ANALYSIS ADAPTED TO USAF LABORATORY NEEDS

by

Thomas Pierce, Ph.D.

The USAF OEHL must possess the means to efficiently perform the analysis of formaldehyde-in-air. The topicality and broader interest in this subject is revealed by a recent review covering only two years of papers in this area which reveals some 42 entries (1).

During this study, current advances in monitoring technology were evaluated and adapted for possible USAF OEHL use. Specifically, reported advances in liquid and ion chromatography were shown to possess needed attributes and a commercially-available kit for "field-use" colorimetric analysis was evaluated.

All experiments described here should be treated as preliminary in nature; it is estimated an additional six month-two year period is necessary to address this problem. A grant proposal is being submitted to the USAF Office of Scientific Research to continue this work.

ACKNOWLEDGEMENTS

The author is most appreciative of the opportunity provided by the Air Force Systems Command, the Air Force Office of Scientific Research, and the Universal Energy Systems. Personnel at the USAF Occupational and Environmental Health Laboratory provided research opportunities that were both professionally and personally enlightening.

Special efforts of the following individuals are especially appreciated:

Col Jerry Thomas

Mr Thomas C. Thomas

Capt Ray Nakasone

Capt Jim Boehne

Lt John Bonnin

I. INTRODUCTION: The particular abilities that led to my assignment to this project center upon my interest in environmental analytical chemistry, particularly those studies that relate to industrial hygiene and toxicology. In terms of both my academic preparation and work experience, my background is divided between chemistry and public health (industrial hygiene) activities.

In general, applied chemists may monitor fundamental developments in analytical chemistry that are potentially relevant to a variety of tasks, or they may apply the results of other environmental laboratories to particular problems of interest to them.

This study recognizes certain analytical improvements that could be made in the current USAF OEHL formaldehyde analysis procedure. Such improvements appear desirable in order to improve the sensitivity and specificity of the method, while minimizing the length of time that field occupational health personnel must wait for analytical results.

II. STATEMENT OF OBJECTIVES: Due to its early nature, the objectives of this study have been kept broad to permit flexibility in experimental design. Means for formaldehyde analysis to be considered include liquid and ion chromatography and a proprietary colorimetric reaction.

Objectives are:

- a. Prepare and analyze a coated adsorbent tube for formaldehyde analysis.
- b. Investigate a new ion chromatographic procedure for low molecular weight aldehyde analysis.
- c. Apply a colorimetric procedure, given both laboratory and field conditions, to formaldehyde analysis.

III. REVIEW OF SELECTED FORMALDEHYDE LITERATURE:

a. Applied toxicity information.

Formaldehyde is at the same time a highly studied compound and a controversial pollutant, particularly in terms of its implication in human carcinogenesis (2). Formaldehyde, at least in trace levels, is relatively ubiquitous in our air environment, often the result of fugitive emissions attending its use as an industrial chemical, or due to its fate as a by-product of incomplete combustion.

For the most part, standards in the United States are oriented toward workplace air concentrations. The American Conference of Governmental Industrial Hygienists Threshold Limit Value (reg. TM) list shows a Notice of Intended Change for formaldehyde for 1984-85 to provide a lowered time-weighted average of 1.5 mg/m^3 (1.0 ppm) and also lists formaldehyde as an industrial substance suspect of carcinogenic potential for man. The broad range of toxic effects of formaldehyde, which include irritation and immunologically-mediated sensitization, should not be overlooked on account of interest in mutagenicity or carcinogenicity (3).

A far-reaching move of note occurred in Denmark in 1978, when Danish authorities adopted quality (design-based) standards for the production of materials of construction that would ensure emitted formaldehyde concentrations $<0.1 \text{ ppm}$ (3). Various state agencies in the United States have also proposed similar manufacturing standards that limit concentrations in new conventional or mobile home-type housing (3).

A thorough review of the toxicology pertinent to formaldehyde is not addressed here. The present toxicology summary is only intended to document the topicality of interest in formaldehyde monitoring.

b. Occupational health-type monitoring.

Many of the means available for formaldehyde analysis have their roots in industrial hygiene efforts to characterize particular emissions. Commonly used methods of analysis include adsorbent tube or impinger sampling schemes, which are followed by chromatographic, colorimetric, voltammetric, or other analysis methods.

Historically, the chromotropic acid method of analysis, which utilizes a purple chromogen formed in a strongly acidic solution, has been widely applied to the analysis of formaldehyde. This method of analysis is coupled to an impingement collection technique but suffers from serious (negative) interference problems from phenol.

The pararosaniline hydrochloride reagent constitutes a related colorimetric technique used in the analysis of formaldehyde. Modifications to the technique have allowed the deletion from the procedure of a hazardous tetrachloromercurate reagent (4).

Nair and Gupta (5) determined formaldehyde concentrations by virtue of a color reaction with oxalyldihydrazide and copper (II) although their work did not include actual air measurements.

A fluorometric technique has been developed by Bisgaard et al. (6). Bisgaard's method relies upon collection of the formaldehyde in water impingers and reaction with ammonia and acetylacetone to form 3,5-diacetyl-1,4-dihydrolutidine, which is fluorescent.

Because spectrophotometric techniques inherently represent only identification and/or quantification, as opposed to separation, various chromatographic means of separation and quantification have been explored pertinent to formaldehyde analysis.

Ion chromatographic analysis of formaldehyde has historically involved the oxidation of formaldehyde to formate ion, which is then detected through conductimetric means (7,8). A more recent innovation in analysis relies upon derivatization of formaldehyde (or other carbonyl-containing) compounds as bisulfites, followed by ion chromatographic analysis (9).

Liquid chromatography relies upon the derivatization of formaldehyde as 2,4-dinitrophenylhydrazone (10,11,12,13). Formaldehyde has also been collected on 13X molecular sieves or sodium bisulfite-impregnated filters, and later analyzed using ion chromatography or colorimetry (pararosaniline hydrochloride).

While solid sorbent methods represent a means of sampling, analytical methods have been developed which match these sampling techniques. Smith et al. (14) developed a collection method based upon the use of an impregnated charcoal. Once collected, the sample is desorbed with hydrogen peroxide and analyzed using ion chromatography. These workers (15) noted problems of storage stability of the generated formate on the treated charcoal.

The reagent 2,4-dinitrophenylhydrazine has been coated on Amberlite XAD-2 resin (16), silica gel (17,18), and glass beads (19). The high-pressure liquid chromatographic analysis of the hydrazone reaction product is performed using an ultraviolet detector.

In order to provide a convenient check on the operation of the gas calibration system, a "quick-check" impinger method known as the SCAN test was used. This proprietary system relies upon the use of evacuated vials which contain pre-measured amounts of the Purpald reagent (4-amino-3-hydrazino-5-mercapto-1,4-triazole). Calibration checks of the specially-prepared adsorbent tubes were made using both generated concentrations (approximate) and the SCAN kit. Table 2 indicates the major findings relative to this portion of the study.

b. Bisulfite addition/ion chromatography.

Experiments were conducted to adapt an existing USAF OEHL sampling method to the requirements of a recently published report involving ion chromatographic analysis of formaldehyde. Only preliminary experiments were conducted which indicates the need for more work in this area.

The method of DuVal et al. (9) utilizes a bisulfite addition to formaldehyde. This might be considered a fortuitous event, considering that the USAF OEHL collection scheme for formaldehyde also relies upon a bisulfite addition.

Due to the highly specific (research) nature of equipment used by DuVal's group, suitable operating parameters had to be selected for the Dionex 2010i ion chromatographic system used in the present work. Table 3 provides a summary of these operating parameters.

After initial ion chromatographic experiments designed to ensure proper molar ratios of bisulfite to formaldehyde, and other experiments intended to optimize the choice of an eluent, an attempt was made to generate a formaldehyde concentration-dependent response curve. Figure 5 illustrates the nature of this calibration curve and highlights a plastic labware contamination problem.

IV. RESULTS: Three major means of formaldehyde analysis were investigated on a preliminary basis. The methods chosen were:

- a. 2,4-dinitrophenylhydrazine/silica gel
- b. bisulfite addition/ion chromatography
- c. field analysis of Purpald-filled impingers

Due to special formatting requirements for this report, the experimental section is included as Appendix I.

- a. 2,4-dinitrophenylhydrazine (2,4-DNPH/silica gel).

Figure 1 indicates the results of the use of the method of Beasley et al. (17) in a preliminary attempt to react the 2,4-DNPH with known amounts of formalin solution. The assumptions used in arriving at the assigned amounts of formalin are shown in Figure 2. These approximate quantities of formalin were used in both this and later experiments.

Figure 3 is a typical chromatographic tracing obtained in these experiments. The "late" peak (at ca. 10-13m) represents the formaldehyde derivative while the "early" peak (ca. 6m) is believed to occur on account of unreacted 2,4-DNPH. As the concentration of formaldehyde is increased, an increase in the size of the derivative accompanies a decrease in the size of the unreacted 2,4-DNPH peak.

It was also thought necessary to check the system using a dynamic gas calibration system. The USAF OEHL gas calibration system shown (in simplified form) in Figure 4 was used to dose the adsorbent tubes prepared according to the method of Beasley et al. (17). A vapor-phase depolymerization of trioxane was employed in order to generate known concentrations of formaldehyde vapor (20). Table 1 demonstrates the constancy of diffusion rates as determined gravimetrically during the present work.

c. Field analysis of Purpald-filled impingers. Figure 6 indicates the results of a side-by-side comparison of Purpald-filled impingers with an approximate gas concentration of formaldehyde as generated using the USAF OEHL gas calibration system previously described in Figure 4. Additionally, the monitors were used to estimate formaldehyde concentrations in the autopsy room of Wilford Hall Medical Center. Table 4 summarizes findings from the autopsy room sampling. Dosimeters were also used during this sampling exercise; dosimeter results are not reported on account of their unsatisfactory nature.

V. CONCLUSIONS:

a. 2,4-DNPH/Silica Gel. Values shown in Figure 1 indicate a reasonably linear instrument response based upon formalin concentrations when the method of Beasley et (17) was adapted to our instrument (Hewlett-Packard 1084B HPLC). It should be noted that the formalin solution was diluted by a factor of ten (37.0%-3.7%) in order for measurable microliter amounts to be delivered with a glass syringe. Hence, amounts of formaldehyde delivered are well below the current TLV.

Table 2 provides a comparison of adsorbent tube results with generated concentrations of formaldehyde. It would appear from these preliminary results that the method is applicable to the resources available in this laboratory. A complete validation of the method is found in Beasley's work (17). Table 2 also shows a result obtained using the SCAN impinger method. This method provided a quick check on the generator.

Preparation of the adsorbent tubes is likely the critical step pertinent to this means of sampling and analysis. Particular problems were encountered in drying the freshly-coated tubes using an evaporative

method. The 2,4-DNPH may be explosive when crystals are dried, thus oven-drying methods are NOT recommended. Interference studies (using propionaldehyde and acetaldehyde) have been inconclusive to date and will be performed after fresh stocks of these reagents are obtained.

b. Bisulfite addition/ion chromatography. Although this portion of the study was begun fairly late, adaptation of the ion chromatographic procedure offers the greatest potential for sensitivity of the methods presently studied. As was noted in Figure 5, judicious choice of labware is critical. It should also be noted that a much lower sodium bisulfite concentration (ca. 2 mM-not optimized) is recommended. Again, interference studies have yet to be performed.

c. Field analysis of Purpald-filled impingers. This method appears to offer good sensitivity to formaldehyde in reasonably low air concentrations. Although the procedure generally calls for the use of a hand-held portable spectrometer, accuracy may be improved by using a bench model instrument, such as the one employed here (Bausch & Lomb Model 20). The method is sensitive to formaldehyde "and other" aldehydes, making future studies necessary relative to interferences.

VI. RECOMMENDATIONS:

a. The use of 2,4-DNPH/silica gel tubes by the USAF OEHL is somewhat dependent upon the commercial availability of these tubes. In-house production of the tubes is viewed as a laborious process subject to a number of quality-control type errors. Additional work needs to be performed to ascertain the storage stability and interference characteristics of such tubes.

Particularly attractive features attending the adsorbent tube method include its adaptability to other low molecular-weight aldehydes and the preferred use of solid sampling media.

b. Plans are being made to present and publish additional findings relative to the ion chromatographic analysis adaptation previously described. This method is particularly attractive as a confirmatory test when colorimetric measurements for formaldehyde are independently made.

c. The Purpald-filled impinger technique has tremendous utility to provide quick answers in the field concerning likely levels of formaldehyde emissions. Use of the SCAN test kit should be encouraged where field personnel need quick results or in cases where shipping problems for samples requiring laboratory analysis may pose a particular difficulty. Again, interference studies are lacking and have yet to be performed.

REFERENCES

1. Melcher, R.G. and M.L. Langhorst, "Industrial Hygiene," Anal. Chem., 1985, 57, 238R-254R.
2. Hileman, B., "Formaldehyde" Assessing the Risk," Environ. Sci. Technol., 1984, 18(7), 216A-221A.
3. Bernstein, R.S., L.T. Stayner, L.J. Elliott, R. Kimbrough, H. Falk, and L. Blade, "Inhalation Exposure to Formaldehyde" an Overview of its Toxicology, Epidemiology, Monitoring and Control," Am. Ind. Hyg. Assoc. J., 1984, 45(11), 778-785.
4. Miksch, R.R., D.W. Anthon, L.Z. Fanning, C.D. Hollowell, K. Rezvan, and J. Glanville, "Modified Pararosaniline Method for the Determination of Formaldehyde in Air," Anal. Chem., 1981, 53(13), 2118-23.
5. Nair, J. and V.K. Gupta, "A New Spectrophotometric Method for the Determination of Formaldehyde in Air," Talanta, 1979, 26, 962-963.
6. Bisgaard, P., L. Moelhave, B. Rietz, and P. Wilhardt, "Quantitative Determination of Formaldehyde in Air Using the Acetylacetone Method," Anal. Lett., 1983, 16 (A17-18), 1457-68.
7. Estes, E., P. Grohse, W.F. Gutknecht, and R.K.M. Hayanty, "Laboratory Evaluation of an Impinger Collection/Ion Chromatographic Source Test Method for Formaldehyde," Avail. NTIS, Order No. PB83-225326 (1983); CA 100(4) 25531v.
8. Lorrain, J.M., C.R. Fortune, B. Dellinger, "Sampling and Ion Chromatographic Determination of Formaldehyde and Acetaldehyde," Anal. Chem., 1981, 53(8), 1302-5.
9. DuVal, D.L., M. Rogers, and J.S. Fritz, "Determination of Aldehydes and Acetone by Ion Chromatography," Anal. Chem., 1985, 57, 1583-1586.
10. Fung, K. and D. Grosjean, "Determination of Nanogram Amounts of Carbonyls as 2,4-Diphenylhydrazones by High Performance Liquid Chromatography," Anal. Chem., 1981, 53, 168-171.
11. Lowe, D.C., V.K. Schmidt, D.H. Ehkalt, C.G.B. Fricksom, and H.W. Nurnberg, "Determination of Formaldehyde in Clean Air," Environ. Sci. Technol., 1981, 15, 819-23.
12. Grosjean, D., "Formaldehyde and Other Carbonyls in Los Angeles Ambient Air," Environ. Sci. Technol., 1982, 16(5), 254-262.
13. Lowe, D.C., V. Schmidt, D.H. Ehkalt, and C.G.B. Fricksom, and H.W. Nurnberg, "Determination of Formaldehyde in Clean Air," Environ. Sci. Technol., 1981, 15, 819-23.

14. Smith, D.L., W.S. Kim, and R.C. Kupel, "Determination of Sulfur Dioxide by Adsorption on a Solid Sorbent Followed by Ion Chromatography Analysis," Am. Ind. Hyg. Assoc. J., 1980, 41(7), 485-8.
15. Smith, D.L., M. Bolyard, and E.R. Kennedy, "Instability of Formaldehyde Air Samples Collected on a Solid Sorbent," Am. Ind. Hyg. Assoc. J., 1983, 44(2), 97-9.
16. Andersson, G., K. Andersson, C.A. Nielsson, and J.D. Levin, "Chemosorption of Formaldehyde on Amberlite XAD-2 Coated with 2,4-Dinitrophenylhydrazine," Chemosphere, 1979, 10, 823-827.
17. Beasley, R.K., C.E. Hoffmann, M.L. Rueppel, and J.W. Worley, "Sampling of Formaldehyde in Air with Coated Solid Sorbent and Determination by High Performance Liquid Chromatography," Anal. Chem., 1980, 52(7), 1110-14.
18. Guenier, J.P., P. Simon, J. Delcourt, M.F. Diderjean, C. Lefevre, and J. Muller, "Air Sampling of Aldehydes - Applications to Chromatographic Determinations of Formaldehyde and Acetaldehyde," Chromatographia, 1984, 18(3), 137-44.
19. Grosjean, D. and K. Fung, "Collection Efficiencies of Cartridges and Microimpingers for Sampling of Aldehydes in Air as 2,4-Dinitrophenyl-hydrazones," Anal. Chem., 1982, 54(7), 1221-4.
20. Geisling, K.L., R.R. Miksch, and S.M. Rappaport, "Generation of Dry Formaldehyde at Trace Levels by the Vapor-Phase Depolymerization of Trioxane," Anal. Chem., 1982, 54, 140-142.

Figure 1
Reaction of 2,4-DNPH
with Known Vol's. of Formalin

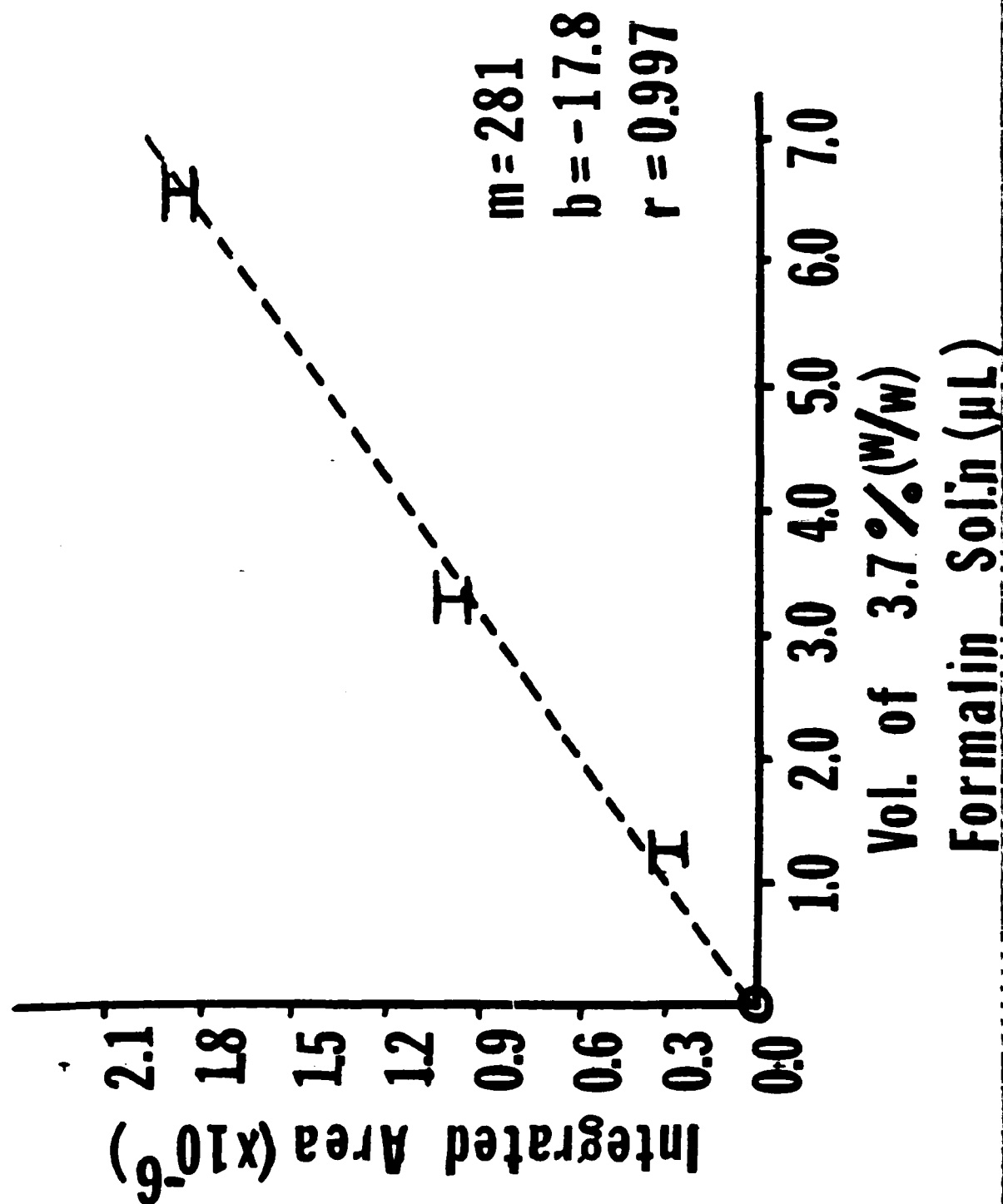


Figure 2

**Assumptions Used
in Preparing CH₂O (liq.) Standards**

**CH₂O TLV[®] 2ppm (ceiling)
 1ppm (proposed)**

**Assume 20L air sample
 @ 200 mL/m**

$$\begin{aligned}
 & (20\,000\text{ mL})(2/10^6) = 4 \times 10^{-2} \text{ mL} \\
 & (4 \times 10^{-2} \text{ mL}) \left(\frac{\text{mmole}}{24.5 \text{ mL}} \right) = 1.63 \times 10^{-3} \text{ mmole} \\
 & (1.63 \times 10^{-3} \text{ mmole})(30 \text{ mg/mmole}) \\
 & = 48.9 \times 10^{-3} \text{ mg} \\
 & = 1.32 \text{ mg} \\
 & \text{(or } \sim 1.3 \mu\text{L of 37\% Formalin)}
 \end{aligned}$$

**Figure 3
2,4-DNPH/Formaldehyde
Chromatogram (Typical)**

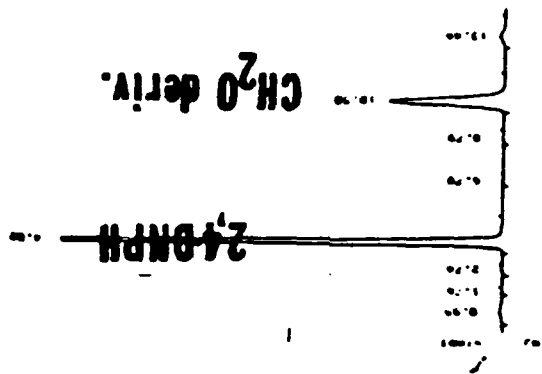


Figure 4
Dynamic Calibration System

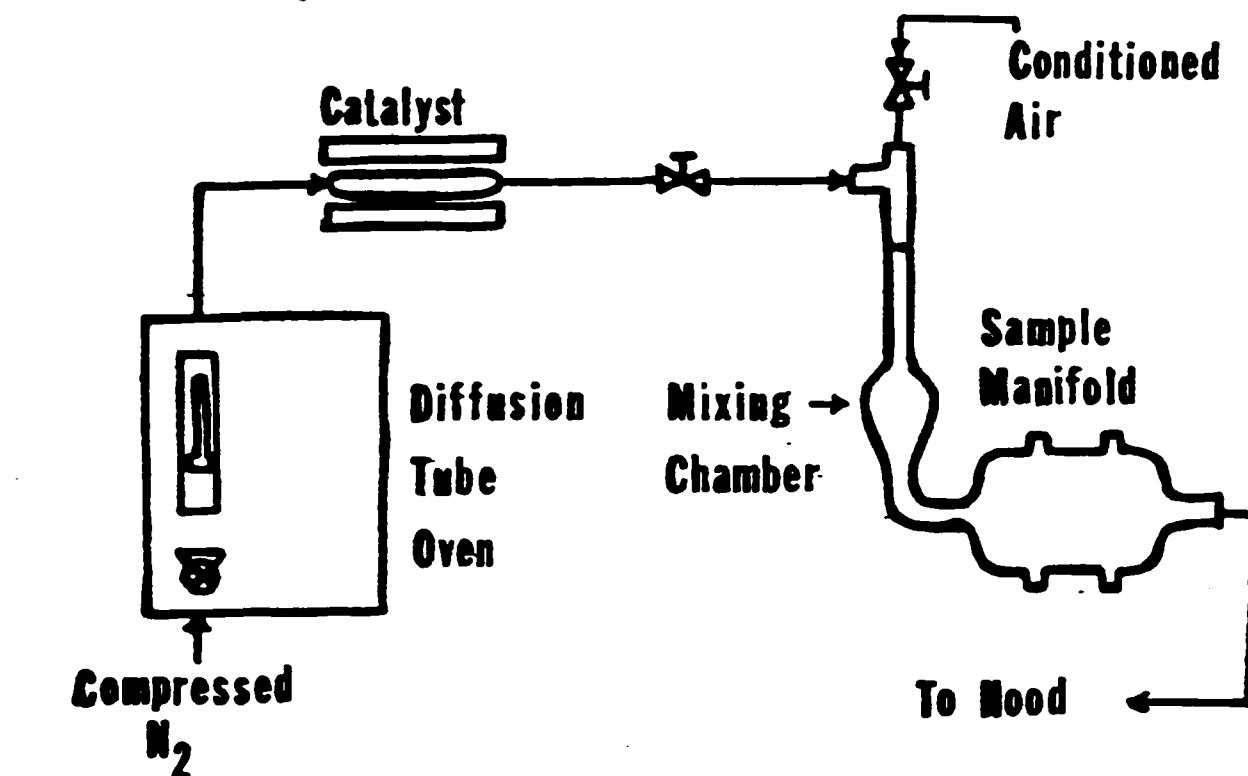


Figure 5
1C Analysis of Bisulfite
CH₂O Addition Product

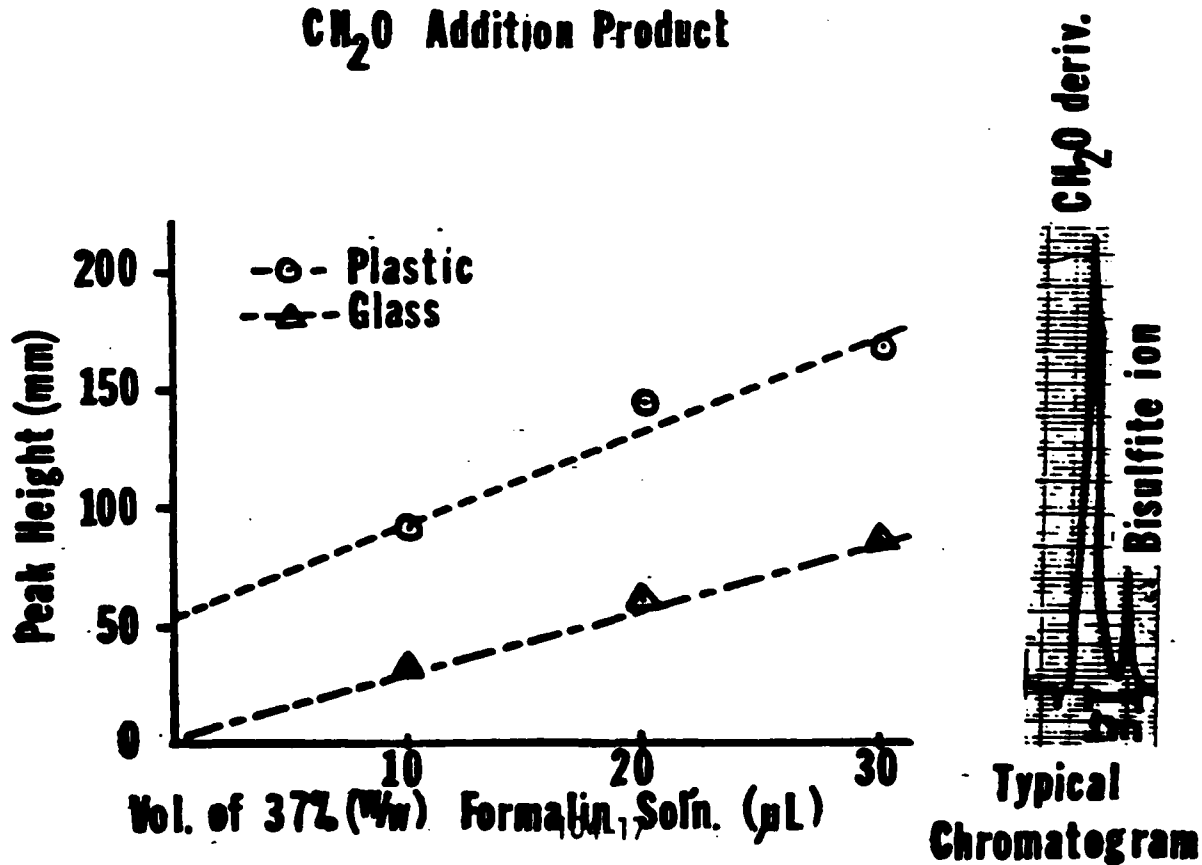


Table 1
Diffusion Tube Formaldehyde
Generation

Day Interval	Rate of Diffusion ($\mu\text{g}/\text{m}$)	Air Flow Provided (LPM)	Concentration Estimate (ppm)
1	6.80	2.3	3.0
8	7.27	4.6	1.6
10	6.86	9.4	0.8

Rel. humidity 39 %
Temperature 25°C

Table 2
Methods Comparison

Method	Principle	Concentration(ppm)
Dynamic Generator	Gravimetric	0.72
SCAN	Colorimetric	0.81 (avg.)
2,4-DNPH Tube	HPLC/UV	0.88 (avg.)

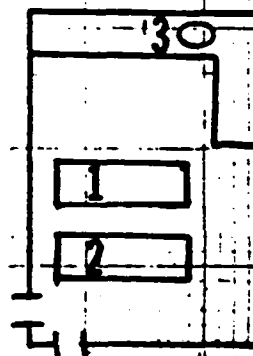
Table 3
IC Adaptation (HSO_3^- derivative)

Du Val⁽²¹⁾	Present Study
Separator Column Anion Exchange	Anion Exchange
Suppressor N/A	Anion
Detection Conductivity	Conductivity
Eluent 20mM Citric Acid	~2.5mM $\text{Na}_2\text{CO}_3 / \text{NaHCO}_3$ sol'ns.

Table 4
SCAN Sampling *
in Autopsy Room

Operation	Location	Concentration (ppm)
Histopath.	1	0.03
Prep.		
Autopsy	2	0.05
Autopsy	3	0.72
(Brain		
Perfusion)		
Autopsy (1983) [†]	-	0.39
Background	1	<0.01

**Room
Layout**



*** 30m samples**

† not SCAN

APPENDIX I

EXPERIMENTAL

a. 2,4-DNPH/silica gel. Hewlett Packard 1084B Liquid Chromatograph/79850B Terminal

b. Bisulfite addition.

Reaction conditions

10 mL of 2 mM NaHSO_3 (aq.)

Indicated volumes of formalin

Chromatographic conditions

Elvent (2.5 mM/2.5 mM $\text{NaHCO}_3/\text{Na}_2\text{CO}_3$)

Flow rate - 2 mL/m

Chart speed - 1 cm/m

Full scale - 30 μS

c. Purpald-filled impingers

30 m sampling periods

Available as Scan Test Kit K-4203

(Envirotech Services, Inc.,

547 Park Avenue,

Prairie du Sac WI 53578,

608-643-4755)

AD-A166178

UNITED STATES AIR FORCE SUMMER FACULTY RESEARCH PROGRAM

2/11

1985 TECHNICAL RE (U) UNIVERSAL ENERGY SYSTEMS INC

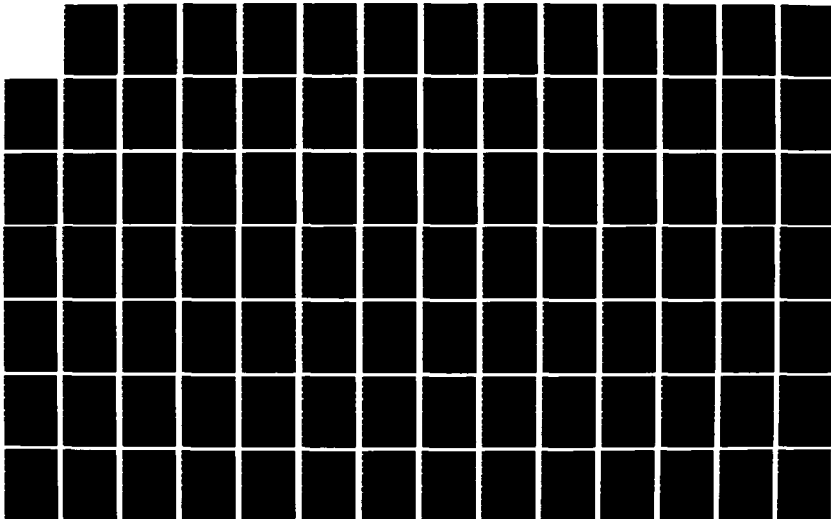
DAYTON OH R C DARRAH ET AL DEC 85 AFOSR-TR-86-0141

UNCLASSIFIED

F49620-85-C-0013

F/G 5/9

NL





MICROCOPY RESOLUTION TEST CHART
NATIONAL BUREAU OF STANDARDS-1963-A

Mr Pierce/SA/11/19 Aug 85/8-16-5/IRL/PIERCEPAP

1985 USAF-UES SUMMER FACULTY RESEARCH PROGRAM/
GRADUATE STUDENT SUMMER SUPPORT PROGRAM

Sponsored by
AIR FORCE OFFICE OF SCIENTIFIC RESEARCH

Conducted by the
UNIVERSAL ENERGY SYSTEMS, INC.

FINAL REPORT

RAMAN SPECTROSCOPY OF GLYCOSAMINOGLYCANS FROM CORNEA

Prepared by:	Dr. Boake L. Plessy and Barbara Wilson
Academic Rank:	Professor
Department and	Division of the Natural Sciences,
University:	Dillard University
Research Location:	Neurosciences Function Section, School of Aerospace Medicine, Brooks Air Force Base
USAF Research:	Dr. John Taboada
Date:	September 25, 1985
Contract No:	F49620-85-C-0013

RAMAN SPECTROSCOPY OF GLYCOSAMINOGLYCANS FROM CORNEA

by

Boake L. Plessy and Barbara Wilson

ABSTRACT

Research was continued in the development of Raman spectroscopy as a non-invasive probe to monitor structural changes in glycosaminoglycans from cornea as a function of the development, maturation, and senescence of the selected species. Keratan sulfate and chondroitin-4-sulfate extracted from bovine cornea were characterized and further fractionated by alcohol precipitation in preparation for spectroscopic examination by laser Raman techniques. Infrared spectroscopy and classical colorimetric methods indicated one relatively pure sample of each glycosaminoglycan expected. Development of a laser Raman spectrometer based on commercial Jarrell-Ash and Bausch and Lomb 0.5 meter Ebert type monochromators was initiated. Spectral bands were observed for several compounds using a single monochromator mode and stray-light was significantly reduced in a dual-monochromator mode. The results indicate that a cost effective Raman spectrometer system can be developed around commercially available optical and electronic components.

Acknowledgement

The authors would like to acknowledge and thank the Air Force Systems Command, the Air Force Office of Scientific Research, and Universal Energy Systems, Inc. for providing the opportunity for them to spend the summer engaged in meaningful and interesting research at the School of Aerospace Medicine, Brooks Air Force Base, San Antonio, Texas. They would like to thank all members of the Division for their hospitality and loan of equipment and facilities.

The authors owe a special debt of gratitude to Dr. John Taboada and Dr. Bryce Hartman of the School of Aerospace Medicine for collaboration in choosing the area of research, guidance, and sponsorship in the program. They would like to acknowledge the help of Dr. Otis McDuff and Dr. Rex Moyer of the SFRP and of Dr. Jim Mrotek of Meharry Medical College.

I. INTRODUCTION

Research has been continued into the development of laser Raman spectroscopy as a non-invasive probe to monitor structural changes in glycosaminoglycans from cornea as a function of development, maturation and senescence.

Although Raman spectroscopy has recently been applied to structural studies on biomolecules, including proteins and nucleic acids, there have been very few reports on the application of this technique to the determination of the structure of polysaccharides. Its use as a structural probe for glycosaminoglycans was suggested in the first and only reported application of this technique to these complex carbohydrates (1). Recent studies have demonstrated the feasibility of using Raman spectroscopy as a structural probe in biophysical aspects of eye research (2,3). The success achieved in the determination of sulfhydryl concentration changes along the optical axis during aging suggests its use in determining structural changes in corneal glycosaminoglycans.

Glycosaminoglycan is a coined word derived from glycosamine (amine sugar) and glycan (polysaccharide) (4). The disaccharide repeating unit of the biopolymer consists of a N-acetylated D-glucosamine or D-galactosamine bonded through o-glycosidic bonds to either D-glucuronic acid, L-iduronic acid, or D-galactose. Glycosaminoglycans are generally sulfated and are present in tissue as covalently

bonded carbohydrate sidechains of larger macromolecular proteins, proteoglycans.

Two glycosaminoglycans have been isolated from corneal tissue. Keratan sulfate has a disaccharide repeating unit consisting of N-acetylglucosamine and galactose polymerized through 1-3 -glycosidic linkages with the glucosamine moiety sulfated in the C-6 position. The repeating unit of chondroitin is D-glucuronic acid and N-acetylgalactosamine polymerized through 1-3 -glycosidic bonds. The galactosamine moiety is either non-sulfated or sulfated in the C-4 position. Keratan sulfate constitutes about 67% of the corneal glycosaminoglycans with pure or sulfated chondroitin constituting the remainder.

Recent studies have suggested that the size and organization of collagen fibres in corneoscleral tissue may be controlled by the glycosaminoglycan composition of proteoglycans in the surrounding matrix (5). It has been known for some time that precise spacing of collagen fibres is a requirement for maintaining the transparent state of the cornea (6). Further, it has been suggested that the large number of anionic charges of the acidic glycosaminoglycans makes hydration of the corneal stroma possible (7). There is ample evidence to indicate that the nature and composition of the glycosaminoglycans change on development and aging and , therefore, will affect both corneal hydration and transparency.

II. OBJECTIVES

The overall goal of the research program for the Summer, 1985 was the development of laser Raman spectroscopy as a non-invasive probe to detect physiological and age-related changes in various parts of the eye. The objectives as originally stated included:

1. Extraction, characterization, and determination of Raman spectra of glycosaminoglycans and proteoglycans from bovine cornea.
2. Development of experimental techniques for the determination of the Raman spectra on intact bovine cornea.
3. Examination of Raman spectra obtained along the optical axis of bovine lens with particular emphasis on disulfide and sulfhydryl bands.
4. Preliminary work on certain root extracts to ascertain their effect on vision.

It became apparent during the first few weeks of the program that instrumental difficulties beyond the control of the principal investigator or his USAF research colleague would preclude obtaining spectra on any samples for a period of at least several weeks. Consequently, the following objective was incorporated to supplement the preliminary objectives previously stated:

5. To develop and evaluate a Raman spectrometer based on an available 0.5 meter Ebert-type single monochromator .

III. MATERIALS AND METHODS

The glycosaminoglycans were isolated and characterized by methods which have been previously described in detail in earlier papers (8,9). Briefly, bovine eyes were obtained from the slaughterhouse less than one hour post-mortem. The cornea were immediately excised and frozen until use. Fifty-five grams of cornea were suspended in 200-ml of 0.1M phosphate buffer with EDTA and L-cysteine HCl added to a final concentration of 0.005M and adjusted to pH = 6.5. Papain was added at 13 mg/g of tissue and the cornea were proteolytically digested at 65°C until solubilized. The small residue was removed by centrifugation and discarded.

Ecteola cellulose (Sigma Chemical Co.) was prepared by washing with 1N sodium hydroxide, 1N hydrochloric acid and deionized water. A column 4 cm x 20 cm was gravity packed with an aqueous suspension of prepared Ecteola.

The solution of digested cornea was applied directly to the Ecteola column and washed with one bed volume of water. The column was eluted with two bed volumes of 0.02N hydrochloric acid, 2.5M ammonium formate, and 2M sodium chloride respectively at room temperature and a flow rate of 1.5 ml/min. The appearance of the glycosaminoglycans was monitored by layering 95% ethanol on the eluate and observing a precipitate at the interface.

Glycosaminoglycans were obtained from solution by

alcohol precipitation. The ammonium formate eluates and sodium chloride eluates were adjusted to 2.5% in sodium acetate and the precipitate obtained by addition of 5 volumes of 95% ethanol. After standing overnight, the precipitate was harvested by centrifugation, redissolved in water, and freeze-dried.

The two fractions of glycosaminoglycans were characterized by hexose determination with anthrone (10), uronic acid determination by carbazole (11), and total hexosamine content with a modified Elson-Morgan test. The samples were hydrolyzed in 6N hydrochloric acid in sealed tubes at 95°C for six hours (12). Additionally, UV and IR spectra were obtained on each sample.

Raman spectrometer systems were developed around three available single monochromators. Initially, the system was assembled using a 0.5 meter Ebert-type Jarrell-Ash monochromator. Subsequently, this was replaced by Bausch and Lomb 0.5 meter Ebert-type monochromators used singly and in tandem. The excitation source was a Spectra Physics Model 164 Argon laser equipped with a Model 265 Exciter. The laser was operated at 476.5 nm wavelength. The Raman lines were detected using a Thorn Emi Gencom Model Fact-50 MKIII photomultiplier cooled to -25°C and powered with a Emi Gencom Model 3000R power supply. The analog output from a C-10 photon counter (Thorn Emi Gencom) was recorded on a Hewlett-Packard x-y recorder when using the Jarrell-Ash

monochromator. The x input was obtained from a 5k precision potentiometer mechanically coupled to the scan control of the monochromator and powered by a variable DC voltage supply. When using the Bausch and Lomb units, scanning was done manually with digital output being recorded at appropriate wavelengths.

IV. DISCUSSION

The Ecteola chromatography of the glycosaminoglycans resulted in two fractions. The 2.5M formate fraction proved to be a mixed fraction with approximately equal amounts of keratan sulfate and chondroitin-4-sulfate. The sodium chloride fraction proved to be relatively pure keratan sulfate with chondroitin-4-sulfate contributing 7% to the total glycosaminoglycan content. These results were comparable to those previously reported (8). The formate fraction was further fractionated by alcohol precipitation (13). A portion of the fraction was dissolved in 0.5% sodium acetate solution and precipitated with exactly 1.25 volumes of absolute ethanol. Under these conditions, all keratan sulfate remains in the supernatant liquid yielding a precipitate of pure chondroitin-4-sulfate. Analysis of the precipitate indicated that the uronic acid content rose from 16% to 31% (91% of the theoretical value for "standard" material). At the same time, the uronic acid content of the supernatant dropped from 16% to 4.5%, indicating enrichment of the supernatant in keratan

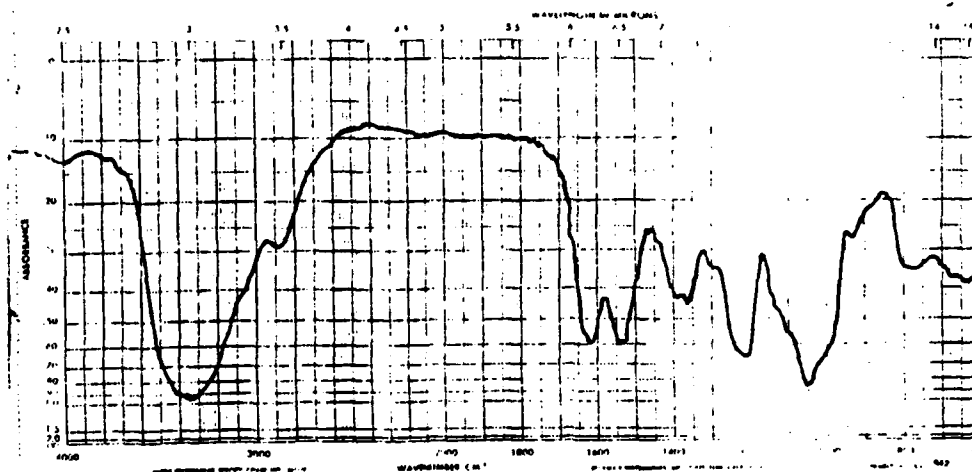


Figure 1. IR Spectra of Keratan Sulfate

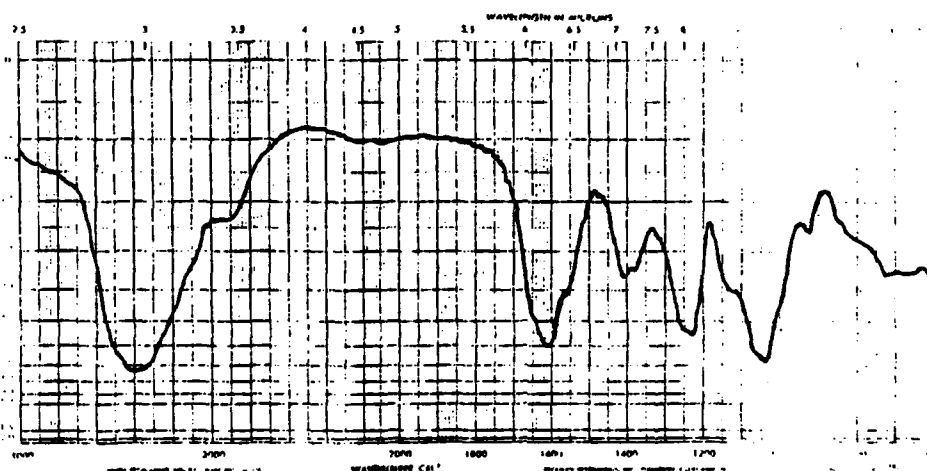


Figure 2. IR Spectra of Chondroitin-4-sulfate

sulfate. This material was precipitated using 4 volumes of absolute ethanol.

Infrared spectra of all fractions of the extracted and fractionated glycosaminoglycans were obtained using the KBr pellet technique. In all cases, the IR spectra

corroborated the findings of the analytical tests. Typical spectra of keratan sulfate and chondroitin-4-sulfate are given in Figures 1 and 2 respectively. These are comparable to spectra previously reported (8).

Previous attempts to obtain Raman spectra on aqueous solutions of glycosaminoglycans were plagued by a strong background fluorescence which was attributed to residual amino acids remaining subsequent to incomplete proteolytic digestion. In addition to this strong fluorescence, unexpected UV absorption bands were present at 260 nm and 220 nm. The recent extracts of glycosaminoglycans show no UV absorption throughout the region 200-400 nm which is consistent with their polysaccharide structure.

Raman spectrometers have generally been developed using dual monochromators because of the extremely low stray-light requirements of the instrumentation. The development and evaluation of Raman systems based on commercially available 0.5 meter single monochromators has contributed significantly to the assessment of needs in developing a simple, cost-effective Raman system for studying glycosaminoglycans and proteoglycans.

The Raman system based on the Jarrell-Ash monochromator successfully indicated selected Raman lines for water, methanol and acetone. These spectra are shown in Figures 3,4,5, and 6 which show the -OH stretching band for water in Figs. 3 and 4, the -C=O band in acetone, and

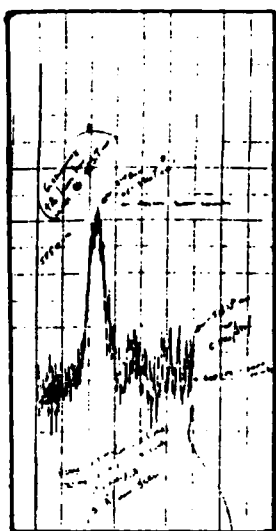


Figure 3

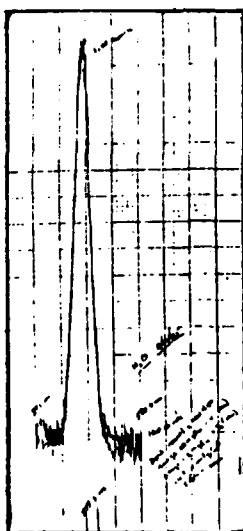


Figure 4

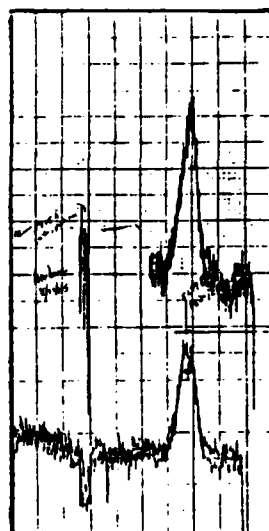


Figure 5

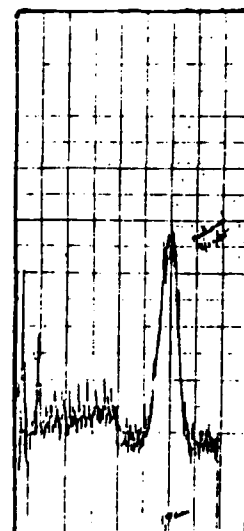


Figure 6

the OH band in methanol in Figs. 5 and 6 respectively. All spectra recorded were at relatively high wavelengths in comparison to the laser excitation line at 476.5 nm and as one approached this wavelength, the background signal became significant so as to render Raman lines undetectable. This behavior is expected under conditions of marginal stray-light rejection. Resolution of the spectra were acceptable with bandwidths being comparable to those obtained on a Cary 82 Raman spectrometer. Throughput of the monochromator was acceptable but the system was critically dependent on focusing at the entrance slit, which was obtained with a collimating lens between the sample cell and slit. Attempts to link the exit slit to the photomultiplier through fiber optics were unsuccessful and signals could only be detected when the photomultiplier

was connected directly to the monochromator through appropriate lenses.

The Bausch and Lomb monochromator was connected in a manner similar to that used with the Jarrell-Ash unit. The most significant difference in the system was the throughput which was as much as seven times greater with the Bausch and Lomb unit based on the maximum signal count for the water peak. The background count was however similarly increased. Stray-light rejection was unacceptable with the single monochromator, with background count rising from 9000 counts at 590 nm to 20500 counts at 510 nm. This latter value is comparable to that of the value at the water peak.

Two Bausch and Lomb monochromators were connected in tandem, with the exit slit of the first mating directly to the entrance slit of the second. With this arrangement, stray-light was significantly reduced with the background count registering 5400 at 590 nm and 6600 at 495 nm. The dark count of the photomultiplier was approximately 200 counts, the additional background being attributed to leakage of ambient room light. Resolution of the system in the tandem mode seemed to have decreased. It is possible that the arrangement of the monochromators produced subtractive dispersion causing this reduction in resolution. This latter point has not been investigated further. Typical water spectra for the single and tandem

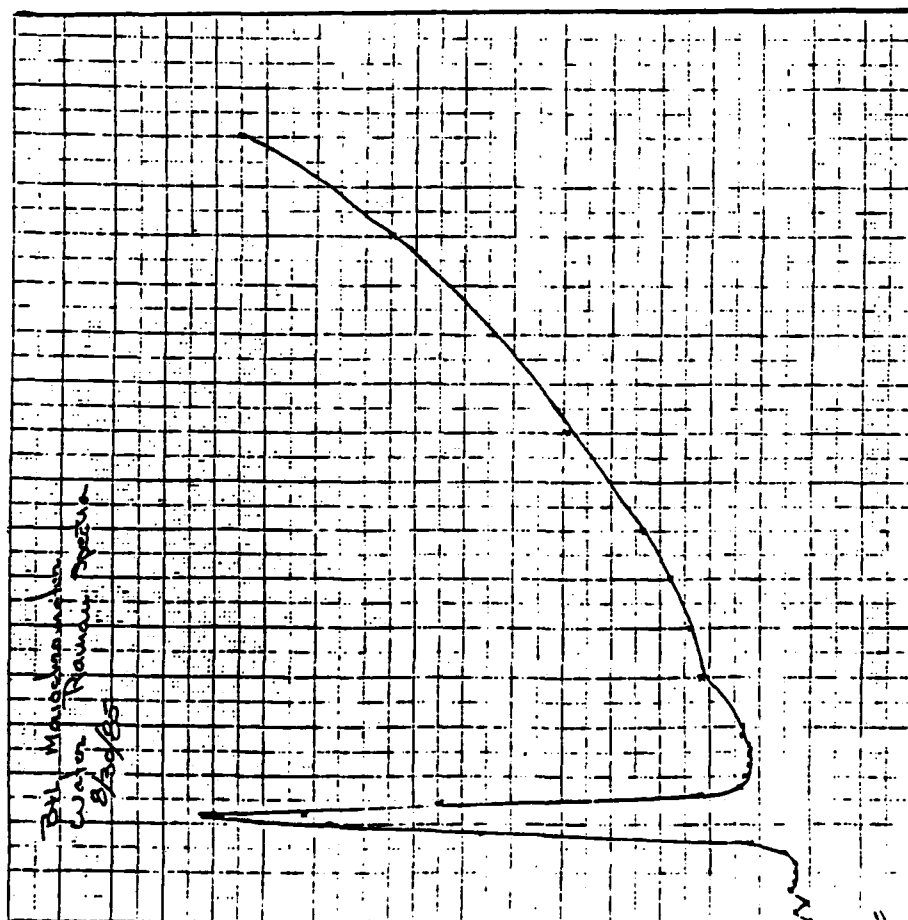


Figure 7

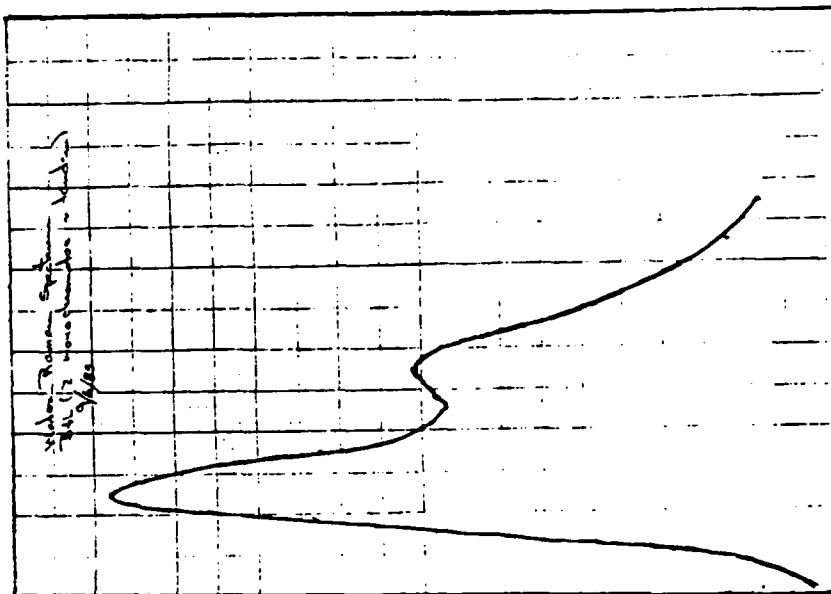


Figure 8

mode are shown in Figures 7 and 8 respectively.

V. RECOMMENDATIONS

The research to date has demonstrated the feasibility of developing a simple, cost-effective Raman spectrometer based on commercially available components. It is recommended therefore that this avenue be pursued. There are, however, several options to be investigated. Several dual monochromators are commercially available and these should be considered for use with particular attention given to their stray-light rejection and resolution. Microcomputer control of the spectrometer for both scanning and data acquisition should be considered. There have been several reports on these systems and, since both hardware and software were available for one such system (14,15), some preliminary work on adapting it has already begun. This system is written in Applesoft Basic and is completely menu driven, each item executing a specific command. Multiple scans can be made thereby enhancing the signal to noise ratio for weak signals. Finally, a companion program is available for smoothing data using the Savitsky and Golay method (16). This work should be continued.

Pure samples of glycosaminoglycans are available for Raman spectroscopy and these should be run as soon as instrumentation becomes available. Subsequently, the investigation of age-related changes of glycosaminoglycans should proceed as outlined in the preliminary objectives.

REFERENCES

1. Bansil, R., I.V. Yannas, and H.E. Stanley, "Raman Spectroscopy: A Structural Probe of Glycosaminoglycans," Biochimica et Biophysica Acta, Vol. 541, pp.535-542, 1978
2. Askren, C.C., N. T. Yu, and J. F. Kuck, "Variation of the Concentration of Sulfhydryl along the Visual Axis of Aging Lenses by Laser Raman Optical Dissection Technique," Exp. Eye Res., Vol. 29, pp. 647-654, 1979.
3. Kuck, J. F. R., N. T. Yu, and C. C. Askren, "Total Sulfhydryl by Raman Spectroscopy in the Intact lens of Several Species: Variations in the Nucleus and Along the Optical Axis During Aging," Exp. Eye Res., Vol. 34, pp. 23-27, 1982.
4. Chakrabarti, B., and J. W. Park, "Glycosaminoglycans: Structure and Interaction," CRC Reviews in Biochemistry, pp.225-313, August, 1980.
5. Borcharding, M. S., L. J. Blacik, R. A. Sittig, J. W. Bizzell, M. Breen, and H. G. Weinstein, "Proteoglycans and Collagen Fibre Organization in Human Corneoscleral Tissue," Exp. Eye Res., Vol. 21, pp. 59-70, 1975.
6. Maurice, M. B., "The Structure and Transparency of the Cornea," J. Physiol. (London), Vol. 136, pp. 263, 1957.
7. Francois, J., and V. Victoria-Troncoso, "Molecular Biology of the Cornea," in Vith Congress of the European Society of Ophthalmology. Brighton 21-25 April 1980: The Cornea in Health and Disease, edited by Patrick Trevor-Roper, (Academic Press, Inc., London), 1980.
8. Frannson, L. A., and A. Anseth, "Studies on Corneal Polysaccharides: IV. Chromatography oof Corneal Glycosaminoglycans on ECTEOLA Cellulose using Formaye Buffers as Eluting Solvents," Exp. Eye Res., Vol. 6, pp. 107-119, 1967.
9. Plessy, B. L., and F. A. Bettelheim, "Water Vapor Sorption of Keratan Sulfate," Mol. and Cell. Biochem., Vol. 6, pp. 85-91, 1975.
10. Dische, Z., in Methods of Biochemical Analysis, (Interscience Publishers, New York, 1955), Vol. 2, pp. 36

11. Bitter, T., and H. M. Muir, "A Modified Uronic Acid Carbozole Reaction," Anal. Biochem., Vol. 4, pp. 330-334, 1962.
12. Antonopoulos, C. A., "Separation of Glucosamine and Galactosamine on the Microgram Scale and Their Quantitative Determination," Arkiv. F. Kemi., Vol. 25, pp. 243-247, 1966.
13. Roden, L., J. R. Baker, J. A. Cifonelli, and M. B. Mathews, "Isolation and Characterization of Connective Tissue Polysaccharides," Methods Enzymol., Vol. 23, pp. 73-140, 1972.
14. Madison, N., and M. J. D. Low, "A Bolt-on Step Drive for Monochromators," Chem., Biomed., and Environ. Instrumentation, Vol. 10, pp. 209-220, 1980.
15. DeBellis, A. D., and M. J. D. Low, "Data Acquisition and Control of a Raman Spectrometer using an Apple Microcomputer," Analytical Instrumentation, Vol. 13, pp. 257-267, 1984-85.
16. Savitsky, A., and M. J. E. Golay, "Smoothing and Differentiation of Data by Simplified Least Squares Procedure," Anal. Chem., Vol. 36, pp. 1627, 1964.

1985 USAF-UES SUMMER FACULTY RESEARCH PROGRAM

Sponsored by the
AIR FORCE OFFICE OF SCIENTIFIC RESEARCH

Conducted by the
UNIVERSAL ENERGY SYSTEMS, INC.

FINAL REPORT

PREDICTION OF SURFACE ROUGHNESS EFFECTS ON HEAT
TRANSFER AND SKIN FRICTION

Prepared by:	Dr Arnold Polak
Academic Rank, Department and University	Professor, Department of Aerospace Engineering and Engineering Mechanics University of Cincinnati
Research Location:	Air Force Wright Aeronautical Laboratories Aero-Propulsion Laboratory Turbine Engine Division Components Branch
USAF Research Contact:	Dr. Richard B. Rivir
Date:	7 June 1985
Contract No.:	F49620-85-C-0013

PREDICTION OF SURFACE ROUGHNESS EFFECTS
ON HEAT TRANSFER AND SKIN FRICTION

by

Arnold Polak

ABSTRACT

Results are presented from a theoretical study of heat transfer and skin friction in a compressible two-dimensional turbulent boundary-layer over a rough surface. The turbulence structure of the flow is modeled with an eddy viscosity approach of Cebeci-Smith, and the roughness is represented by arrays of uniformly distributed drag force and heat source/sinks. Solution to the governing equations are obtained by a finite difference implicit numerical method. Results compare relatively well with low speed experimental data, although some discrepancy is observed when compared to a similar prediction method.

ACKNOWLEDGEMENTS

I wish to gratefully acknowledge the opportunity and support by the Air Force Systems Command, the Air Force Office of Scientific Research and the Universal Energy Systems, Inc.

A very special thanks is due to Dr. Richard B. Rivir for the enlightening council and helpful discussions during the entire course of this study.

The friendly atmosphere in the Components Branch of the Turbine Engine Division made my stay at the Aero Propulsion Laboratory very pleasant.

1. OBJECTIVES

Surface roughness can significantly increase heat transfer to gas turbine components. The STAN5 boundary flow code currently employed at the Aero Propulsion laboratory, Wright-Patterson AFB has many versatile features and is a widely used tool for predicting heat transfer levels to gas turbine blades. It does not however have the capability to account for the influence of surface roughness. The present study therefore sets as its objective to develop this additional computational capability.

A survey of literature related to the subject of surface roughness effects reveals that prediction methods can be classified basically into two categories (a) the Schlichting's equivalent sand-grain roughness method, and (b) the discrete element method. Implementation of the first method in an analysis using eddy viscosity turbulence model leads to the introduction of a modified mixing length, so as to affect a shift in the velocity profile induced by roughness. The discrete element method is a more rational approach. It accounts for the presence of the arrays of roughness elements directly in the equations for conservation of mass, momentum and energy. The roughness elements are modeled by discrete arrays of drag force and heat source/sinks. The discrete element method was pioneered by Finson [1] and later applied and extended by others (see Refs. [2] and [3]). Taylor et al [3] have made an important contribution by introducing and calibrating the heat source/sinks to model energy transport.

We have adopted the discrete element approach to accomplish our objective. We use the calibration for the local drag force coefficient and local Stanton Number of the roughness elements as presented in Ref. [3]. While method (a) could be implemented relatively easily, the method (b)

requires a significantly higher level of effort and a detailed knowledge of the algorithms build into STAN5 code. It was therefore decided that the main thrust of this research effort will be to develop a separate computer code for calculating turbulent boundary layer flow characteristics over rough surfaces. This code can be used also as a complement to the STAN5 code.

2. ANALYTICAL APPROACH

2.1 INTRODUCTION

The approach taken in this study is that classical Prandtl's boundary layer equations modified to include the effect of roughness is an appropriate set of governing equations to be used for prediction of heat transfer and skin friction in high Reynolds number compressible viscous flows over rough surfaces. The model used to represent roughness is a discrete array of force and heat source/sinks distributed over the surface. This representation allows to account in part for size, shape, and spacing of the roughness elements. The first underlying assumption in this approach is that the roughness elements are small relative to the boundary layer thickness, so that the interaction between the inviscid flow and the boundary layer is negligible. Secondly, the geometry of the roughness elements is ignored as far as the details of the flow field in the immediate vicinity of the roughness element is concerned.

2.2 THE GOVERNING EQUATIONS

The governing equations are taken to be the boundary-layer equations with inclusion of an algebraic eddy viscosity turbulence model (see Ref [4]) and a roughness discrete element model of Ref [3]. For two-dimensional compressible laminar and/or turbulent flow, the dimensionless form of these equations in terms of mean flow variables is as follows:

Continuity Equation

$$\frac{\partial}{\partial x}(B_x \rho u) + \frac{\partial}{\partial y}(B_y \rho v) = 0 \quad (2.1)$$

Momentum Equation

$$\rho(u B_x \frac{\partial u}{\partial x} + v B_y \frac{\partial u}{\partial y}) = B_x \rho_0 u_0 \frac{du_0}{dx} + \frac{\partial}{\partial y}[B_y(\mu + \mu_t \Gamma) \frac{\partial u}{\partial y}] - \frac{1}{2} \rho u^2 C_D \sqrt{R_x} \frac{D}{L_x L_y} \quad (2.2)$$

Energy Equation

$$\rho(u B_x \frac{\partial T}{\partial x} + v B_y \frac{\partial T}{\partial y}) = - \frac{\bar{R}}{\bar{C}_p} [B_x u \rho_e u_e \frac{du_e}{dx} - B_y (\mu + \mu_e \Gamma) (\frac{\partial u}{\partial y})^2] \\ + [B_y (\frac{\mu}{\bar{\rho}_e} + \frac{\mu_e}{\bar{\rho}_e}) \frac{\partial T}{\partial y}] + \frac{1}{2} \frac{\bar{R}}{\bar{C}_p} \rho \sqrt{Re} C_D \frac{D}{l_x l_z} u^3 + \pi \frac{Nu_d}{\bar{\rho}_e} \frac{\mu}{l_x l_z} (T_R - T) \quad (2.3)$$

The boundary conditions are

$$u(x, 0) = v(x, 0) = 0 ; \quad T(x, 0) = T_w , \text{ or } \frac{\partial T}{\partial y}(x, 0) = 0 \quad (2.4a)$$

and

$$u(x, \infty) = u_e(x) ; \quad T(x, \infty) = T_e(x) \quad (2.4b)$$

The temperature of the roughness element, T_R , is set here equal to T_w , the wall temperature.

The unbarred dimensionless variables were defined as follows:

$$u = \bar{u}/\bar{u}_\infty , \quad v = \bar{v}\sqrt{Re}/\bar{u}_\infty , \quad \rho = \bar{\rho}/\bar{\rho}_\infty , \quad p = \bar{p}/\bar{\rho}_\infty \bar{u}_\infty^2 ,$$

$$T = \bar{T}/\bar{u}_\infty^2/\bar{R} , \quad \mu = \bar{\mu}/\bar{\mu}(\bar{u}_\infty^2/\bar{R}) , \quad x = \bar{x}/\bar{L} , \quad y = \bar{y}\sqrt{Re}/\bar{L} ,$$

$$D = \bar{D}\sqrt{Re}/\bar{L} , \quad l_x = \bar{l}_x\sqrt{Re}/\bar{L} , \quad l_z = \bar{l}_z\sqrt{Re}/\bar{L} , \quad Re = \bar{\rho}_\infty \bar{u}_\infty \bar{L}/\bar{\mu}(\bar{u}_\infty^2/\bar{R})$$

The dimensionless parameters related to the roughness model are:

B_x, B_y = blockage parameter

C_D, Nu_d, D = local drag coefficient, Nusselt number, cross-sectional diameter at distance y from surface

l_x, l_z = spacing in x, z direction

For a given geometry of the roughness element, the local diameter $D=D(y)$ is a function of the roughness height. The local drag coefficient, C_D is a function of local Reynolds number, $Re_d=uD/\nu$ and the Nusselt number is a function of Re_d and Prandtl number, Pr . Both, C_D and Re_d are deduced from empirical data for banks of cylinders (see Ref [3]).

The examination of the governing equations will disclose that for a given body shape, free stream Mach number, Reynolds number, and wall temperature the skin friction and heat transfer will depend on the roughness size, spacing, and geometry.

It is assumed that the roughness elements have circular cross-section parallel to the surface. It can be then shown that $B_x=B_y=1-D^2/(4l_x l_z)$ (see Ref [3]).

2.3 TRANSFORMED EQUATIONS

Significant computational advantage is gained by transforming the equations (2.1) - (2.4) in terms of the Levy-Lees independent variables and

simultaneously introducing new similarity dependent variables F, Θ and V in lie of u, T and v . We have found that in form, the transformed equations resemble more closely the smooth wall case if the blockage parameter $B_x(y)$ is incorporated in the definition of η . This transformation is written as follows:

$$\xi = \int_0^x \rho_e \mu_e u_e dx, \quad \eta = \frac{u_e}{\sqrt{2\xi}} \int_0^y B_x \rho dy \quad (2.5 a, b)$$

$$F = \frac{u}{u_e}, \quad \Theta = \frac{T}{T_e} = \frac{\rho_e}{\rho} \quad (2.6 a, b)$$

and

$$B_y \rho v = \frac{d\xi}{dx} \frac{1}{\sqrt{2\xi}} V - \frac{\partial \eta}{\partial x} \sqrt{2\xi} F \quad (2.6 c)$$

The transformed governing equations are:

Transformed Continuity Equation

$$\frac{\partial V}{\partial \eta} + 2\xi \frac{\partial F}{\partial \xi} + F = 0 \quad (2.7)$$

Transformed Momentum Equation

$$\begin{aligned} \frac{\partial}{\partial \eta} (B_x B_y l \bar{\epsilon} \frac{\partial F}{\partial \eta}) - V \frac{\partial F}{\partial \eta} + \frac{2\xi}{u_e} \frac{du_e}{d\xi} (\theta - F^2) - 2\xi F \frac{\partial F}{\partial \xi} \\ - \xi \sqrt{Re} \frac{F^2 C_D D}{l_x l_z \rho_e u_e \mu B_x} = 0 \end{aligned} \quad (2.8)$$

Transformed Energy Equation

$$\begin{aligned} \frac{\partial}{\partial \eta} (B_x B_y \frac{l}{Pr} \hat{\epsilon} \frac{\partial \theta}{\partial \eta}) - V \frac{\partial \theta}{\partial \eta} + \frac{2\xi St_d Re}{\rho_e u_e l_x l_z B_x (d\xi/dx)} \theta^2 (\theta_r - \theta) \\ - 2\xi F \frac{\partial \theta}{\partial \xi} + \alpha B_x B_y l \bar{\epsilon} \left(\frac{\partial F}{\partial \eta} \right)^2 + \alpha \xi \sqrt{Re} \frac{C_D D F^3}{B_x l_x l_z (d\xi/dx)} = 0 \end{aligned} \quad (2.9)$$

where

$$l = \frac{\rho \mu}{\rho_e \mu_e}, \quad \alpha = \frac{\bar{R}}{C_p} \frac{u_e^2}{T_e}, \quad St_d = \frac{Nu_d}{Re Pr} \quad (2.10 a, b, c)$$

and , are the turbulence parameters defined as

$$\bar{\epsilon} = 1 + \frac{\mu_e}{\mu} \Gamma, \quad \hat{\epsilon} = 1 + \frac{\mu_e}{\mu} \frac{Pr}{Pr_e} \Gamma \quad (2.11 a, b)$$

We take $Pr=0.72$ and $Pr_t=0.90$ and is a longitudinal intermittency function to simulate transition from laminar to turbulent flows. The eddy viscosity, and the longitudinal transition intermittency function used here are as described by Harris [4].

The boundary conditions are

$$F(\xi, 0) = V(\xi, 0) = 0, \quad \theta(\xi, 0) = \theta_w(\xi), \quad \text{or} \quad \frac{\partial \theta}{\partial \eta}(\xi, 0) = 0 \quad (2.12 a, b, c)$$

Note that the transformed continuity equation is identical in form for both rough and smooth surface. The blockage parameters, B_x and B_y and the spacing parameters, l_x and l_z are set equal to unity, and C_D and St_D are set equal to zero over the smooth surface and also when $y \geq k_s$ where k_s = roughness height.

2.4 SKIN FRICTION AND HEAT TRANSFER COEFFICIENTS

The tangential stress at the surface is the sum of the smooth wall shear stress plus the contribution of the drag force due to the presence of the roughness elements. The heat transfer coefficient is evaluated in a similar way.

The skin friction coefficient is defined by

$$C_f = \frac{(B_y \bar{\tau})_w + \frac{1}{2} \frac{1}{l_x l_z} \int_0^{\bar{k}_s} \bar{\rho} \bar{u}^2 C_D \bar{D} d\bar{y}}{\frac{1}{2} \bar{\rho} \bar{u}_\infty^2} \quad (2.13 a)$$

The heat transfer coefficient is defined by

$$C_h = \frac{(B_y \bar{k} \frac{\partial \bar{T}}{\partial \bar{y}})_w - \frac{\pi}{l_x l_z} \int_0^{\bar{k}_s} \bar{k} Nu_d (\bar{T}_r - \bar{T}) d\bar{y}}{\bar{\rho} \bar{u}_\infty^3} \quad (2.13 b)$$

In terms of the variables of the computational plane, the dimensionless skin friction and heat transfer coefficients are written as

$$C_f = 2(B_x B_y)_w \frac{\mu_e \rho_e u_e^2}{\sqrt{2\tau}} \left(l \frac{\partial F}{\partial \eta} \right)_w / \sqrt{Re} + \frac{\sqrt{2\tau}}{L_x L_z} \int_0^{L_z} (C_D DF^2/B_x) d\eta \quad (2.14a)$$

$$C_H = (B_x B_y)_w \frac{\bar{C}_p}{R Pr} \frac{\mu_e T_e u_e \rho_e}{\sqrt{2\tau}} \left(l \frac{\partial \theta}{\partial \eta} \right)_w / \sqrt{Re} + \frac{\sqrt{2\tau}}{L_x L_z} \frac{\bar{C}_p}{R} \sqrt{Re} \pi \frac{\mu_e T_e}{u_e \rho_e} \int_0^{L_z} [St_d l \theta^2(\theta_R - \theta)/B_x] d\eta \quad (2.14b)$$

2.5 NUMERICAL METHOD

A finite difference scheme is used to obtain numerical solutions to the governing equations (2.7), (2.8) and (2.9). The momentum and energy equations are linearized. An implicit finite difference scheme transforms the linearized equations into a tridiagonal matrix form of algebraic equations. These are solved for the dependent variables F , θ and V in an iterative manner at each station η in a marching fashion. Each iterative cycle consists of the following sequence: (a) solution of the energy equation, (b) update of the properties (eddy viscosity), and (c) solution for the momentum and continuity equations in a coupled form. The iteration is terminated after the change in $(\partial F/\partial \eta)_w$ between two successive iterations is less than a prescribed small quantity, here taken as 0.0001. A variable step size in the y -direction is used, essentially a requirement for turbulent flows. In the present study, a geometric progression of the form $\Delta \eta_{j+1} = \Delta \eta_j \cdot K$; $j=1, \dots, N$ was used to define the normal mesh. For the calculations presented in this report $\Delta \eta_1 = 0.005$, $K=1.12$, and $N=76$ was taken. The solution algorithm is set up in such a way that both smooth and rough wall calculations can be performed. Merely, for the roughness height, k_s equal to zero (and also for $y \geq k_s$) the spacing and blockage parameters, l_x , l_z , B_x , and B_y become unity and the local roughness drag coefficient, C_D and the local roughness Stanton number St_d are both set equal to zero.

3. RESULTS AND DISCUSSION

The purpose of the present study was to develop a computer code for predicting heat transfer and skin friction over rough surfaces. The calibration and testing of this code was performed against the experimental results of Stanford University workers, Healzer, Pimenta and Coleman (See Refs. [5] and [3]). These are some of not too many well documented and well controlled heat transfer data available for flow over rough surfaces. The flat test surface in these experiments was fabricated by brazing together 50 mills in diameter copper balls in the most dense array.

The first test to which the computer code must be subjected is a check whether it predicts flow over a smooth surface correctly. Figure 1 shows that both the Stanton number and skin friction coefficient compare favorably with the correlation of these quantities against $Re_x^{-0.2}$ for turbulent flow over a flat plate. This calculation was performed for Healzer data with $U_\infty = 242$ fps. Figure 1 was reproduced from Ref. [5] as it summarizes Healzer experimental data. It shows that rough wall C_f and S_t do not correlate with x -Reynolds number. The data are sensitive to the free stream (edge) velocity. The skin friction is affected more than heat transfer by roughness.

For densely packed spheres the location of the base wall cannot be well defined. The recirculating flow below the equators of the spheres is blocked from the main streamwise flow in the boundary layer and does not contribute to the tangential viscous shear stress significantly. Schlichting has suggested that in the calculations the effective wall ($y = 0$) should be placed at the equator plane, i.e. taking the effective roughness height equal to the radius of the sphere. A number of workers have adopted this suggestion (See Ref. [1]). However Taylor et al [3] have found best agreement with experimental

data by taking $k_{s,eff} = 0.4R$. We have chosen to calibrate our computer program against one set of Healzer data [5], with $u_\infty = 242$ fps and found best agreement for $k_{s,eff} = 0.6R$. Figure 2 shows two calculations (dashed lines) using the present numerical model with $k_{s,eff} = 0.6R$. The full line represents calculations of Ref. [3] with $k_{s,eff} = 0.4R$. Since we have adapted the model for the roughness C_D and St_D from Ref [3] the disagreement between the two sets of calculations at $k_{s,eff} = 0.4R$ is suprising. Although our algorithm is written for high speed compressible flow with variable properties, while the algorithm in Ref [3] was set up for constant property boundary layer flow we would expect the two sets of calculations be in close agreement for these low speed flows. At this point we cannot offer an explanation for this discrepancy.

All or subsequent results shown in Figures 3-6 were calculated with $k_{s,eff} = 0.6R$. The ratio of rough to smooth values for skin friction and heat transfer are shown in Figure 3. This demonstrates that the Reynolds analogy is not applicable for flow over a rough surface. Figure 4 compares the theoretical prediction to the experimental data of Pimenta, at $u_\infty = 130$ fps. In Figures 5 and 6 comparison is made for flow over the rough flat surface under favorable pressure gradient. The predictions for the skin friction distribution show an increase in the streamwise direction, although the experimental data in Figure 5 do not show this tendency. On the other hand, experimental data of Healzer [5] show an increase in skin friction with increase in boundary layer edge velocity.

4. RECOMMENDATIONS

Based on the comparisons presented above, it is concluded that a computer code is at hand for predicting heat transfer and skin friction in two-dimensional turbulent boundary-layer flows over rough and smooth surfaces. The following suggestions are offered for further testing, improvements and extension of this code:

(1) Test the code against experimental data wherein compressibility effects are significant. Determine whether further adjustments need to be made in the modeling of roughness.

(2) Improve the efficiency of the calculations by quasi-linearization (instead of simple linearization) of the non-linear terms in the governing partial differential equations.

(3) Modify the mathematical formulation to extend the applicability to axisymmetric flows.

5. REFERENCES

1. - Finson, M. L. and Clark, A. S., "The Effect of Surface Roughness Character on Turbulent Reentry Heating," AIAA Paper 80-1459, 1980.
2. Christoph, G. H. and Pletcher, R. H., "Prediction of Rough-Wall Skin Friction and Heat Transfer," AIAA Journal, Vol. 21, No. 4, pp. 509-515, 1983.
3. Taylor, R. P., Coleman, H.W., and Hodge, B.K., "A Discrete Element Predictive Approach for Turbulent Flow Over Rough Surfaces," Report TFD-84-1, Mississippi State University, 1984.
4. Harris, J. E., "Numerical Solution of the Equations for Compressible Laminar, Transitional, and Turbulent Boundary Layers and Comparisons with Experimental Data," NASA-TR-R-368, 1971.
5. Healzer, J. M., Moffat, R. J., and Kays, W. M., "The Turbulent Boundary Layer on a Porous, Rough Plate: Experimental Heat Transfer with Uniform Blowing," AIAA/ASME Paper No. 74-680, 1974.

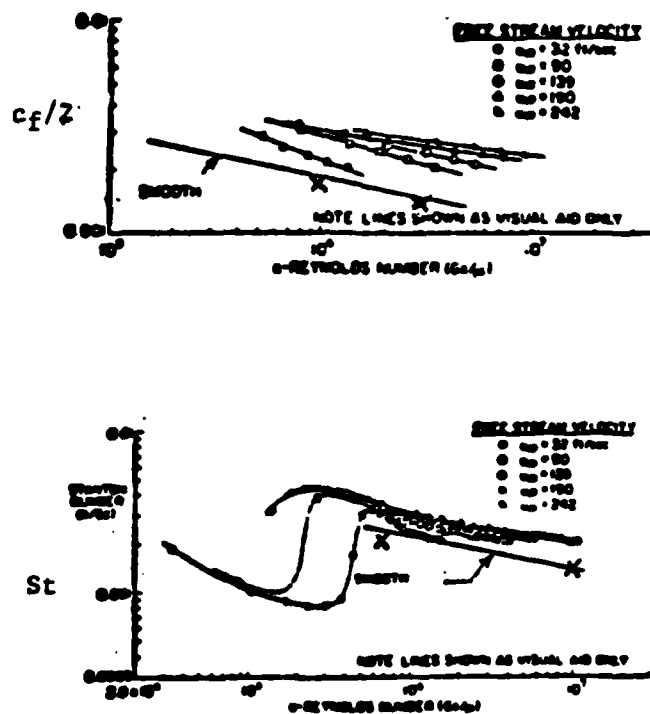


Figure 1 Skin Friction and Stanton Number Versus x-Reynolds Number ; Healzer Exper. Data (X Present Calculation, Smooth Wall)

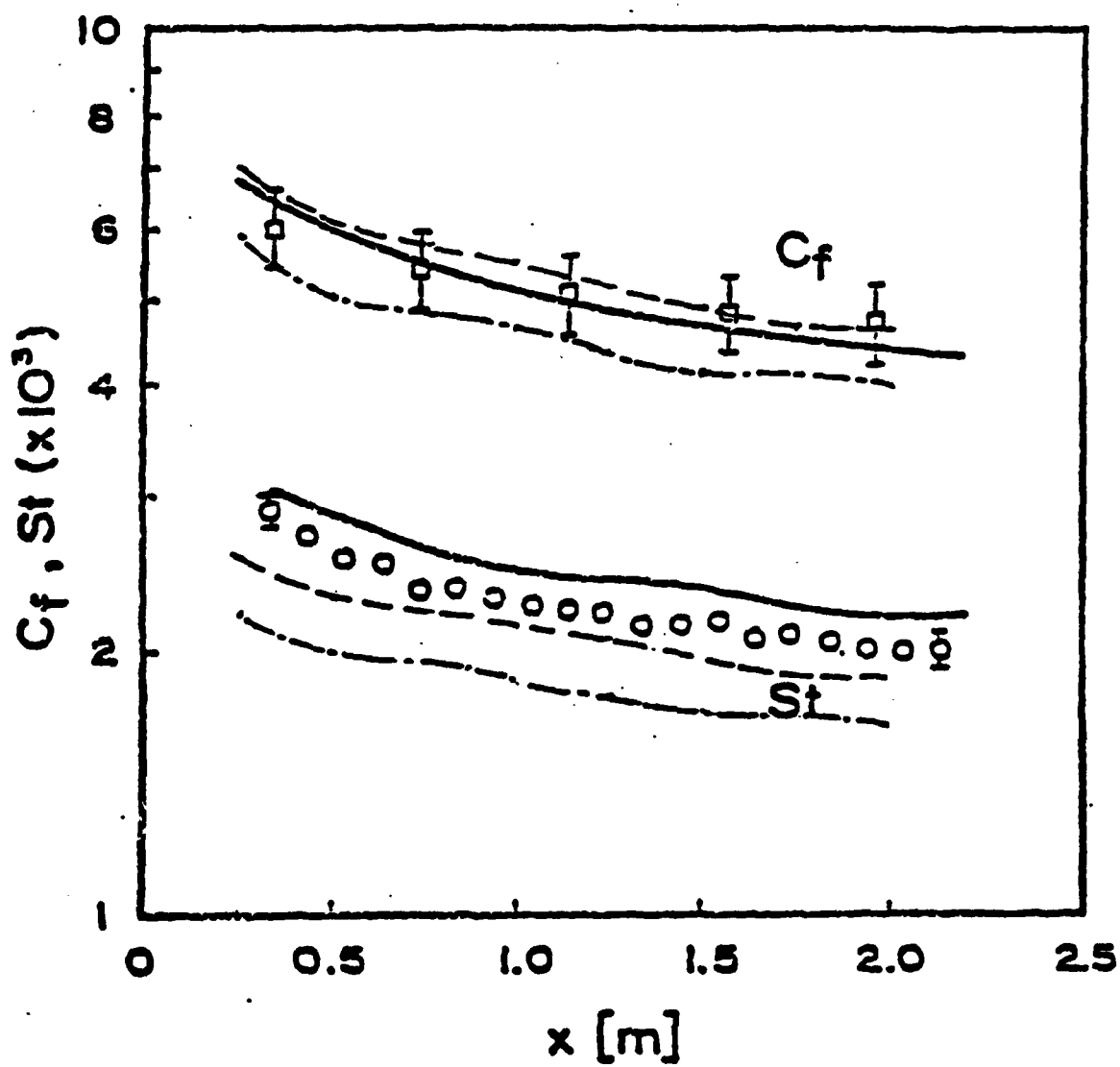


Figure 2

Comparison of Calculations with the Data of
Healzer; $U_\infty = 74$ m/s

○ □ Healzer Data; — Calculation Ref. [3];
 --- Present Calculation ; $k_s = 0.6R$
 - · - · - " 106-17 ; $k_s = 0.4R$

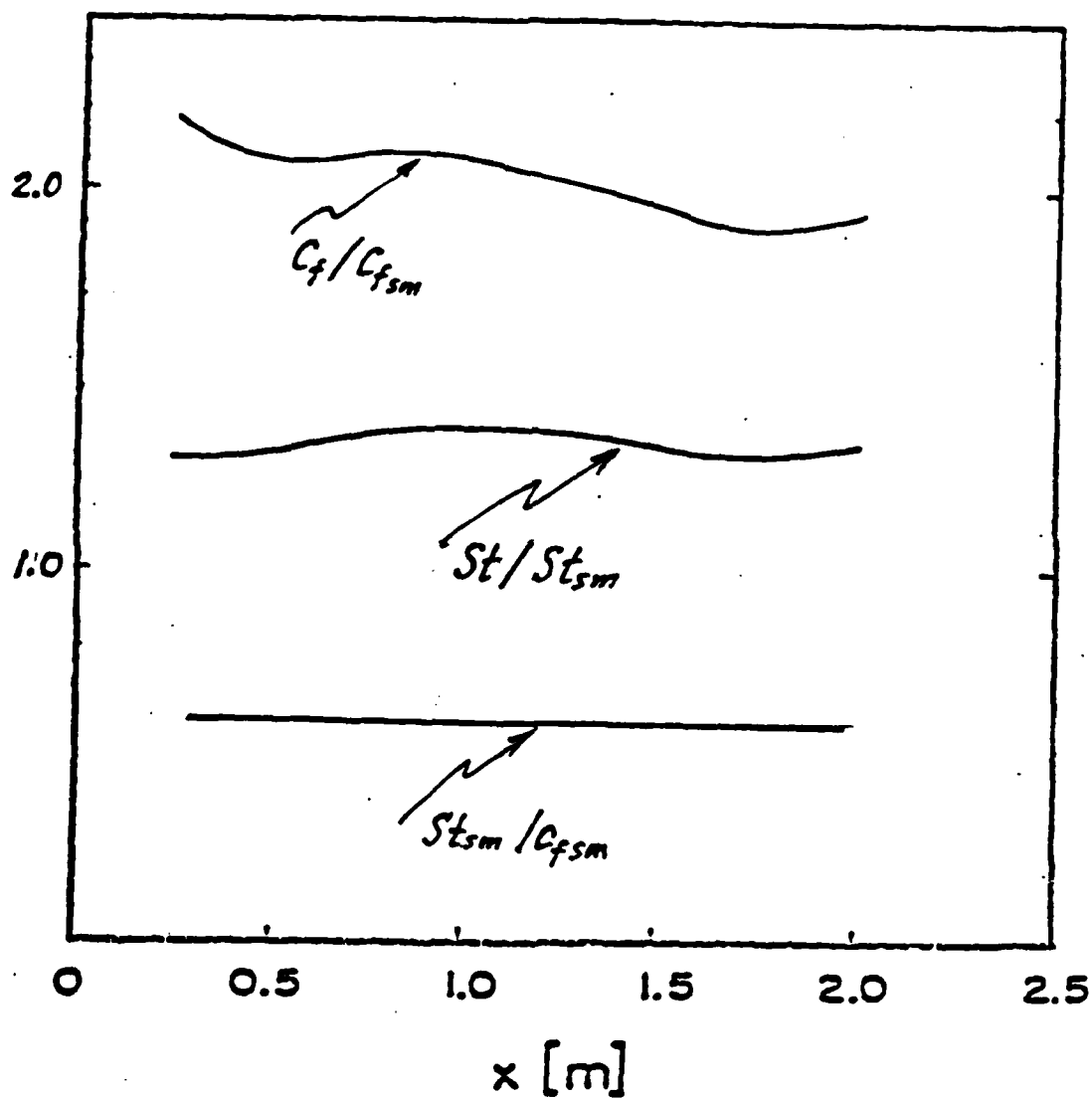


Figure 3 Present Calculation Corresponding to Healzer Data; $U = 74$ m/s . Ratio of Rough to Smooth Skin Friction and Stanton Number

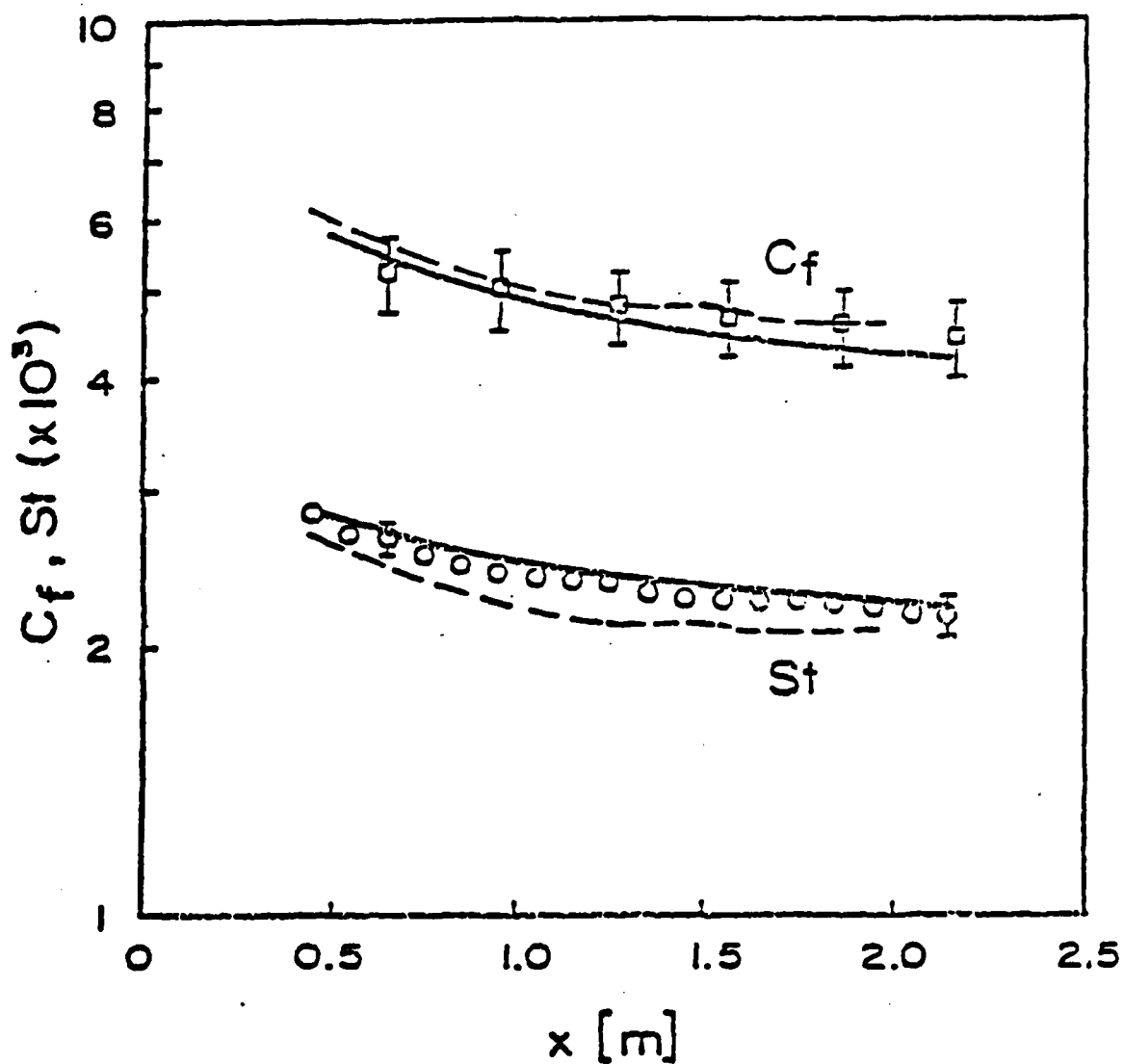


Figure 4

Comparison of Calculations with the Data of
Pimenta; $U_e = 39.6$ m/s

○ □ Pimenta Data; — Calculation Ref. [3];

--- Present Calculation

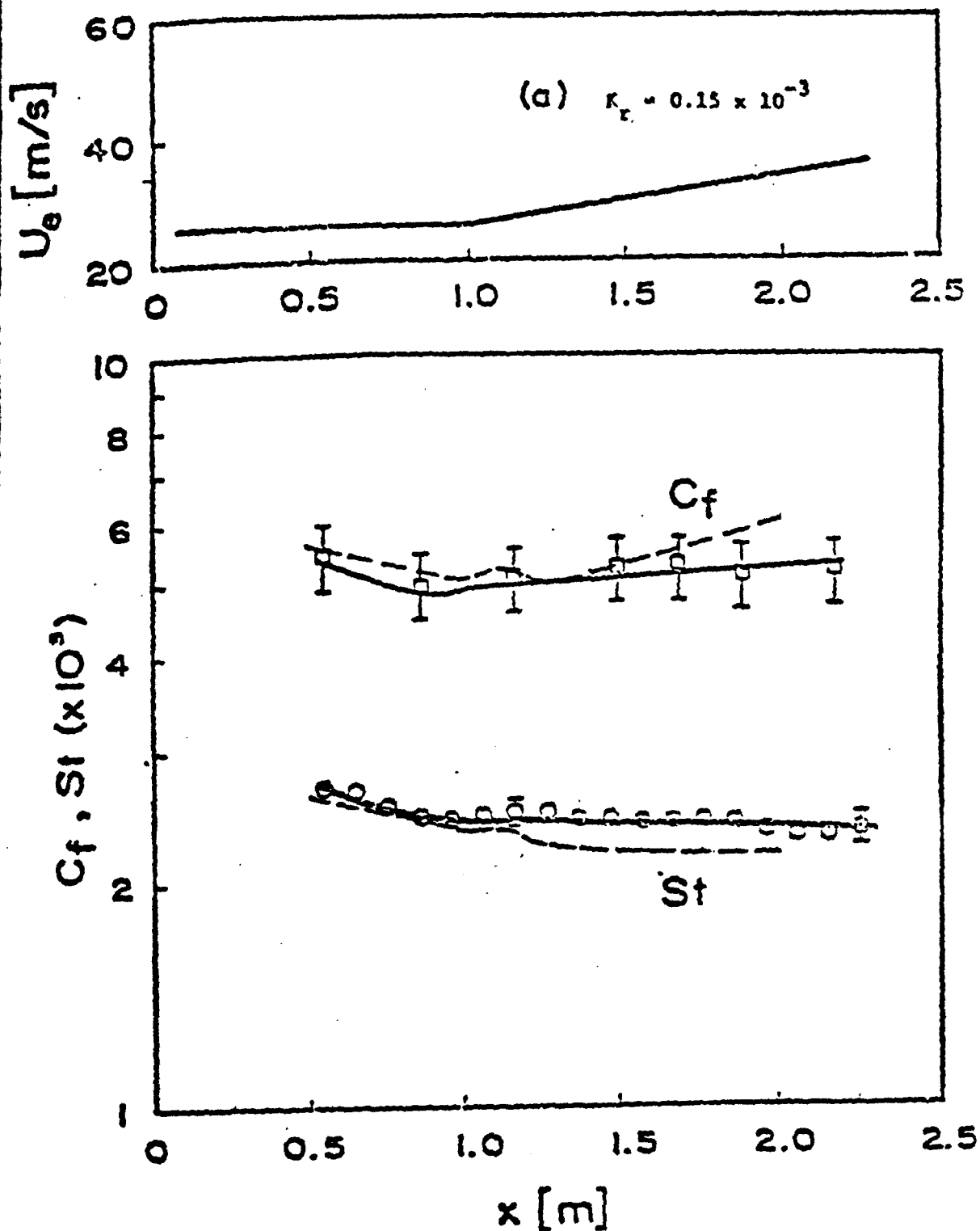


Figure 5

Comparison of Calculations with the Data of
 Coleman; $K_r = 0.15 \times 10^{-3}$; Constant Wall
 Temperature $K_r = (1/2) (\bar{\theta}/\bar{U}_e) (d\bar{U}_e/dx)$

○ Coleman Data; — Calculation Ref. [3];

--- Present Calculation

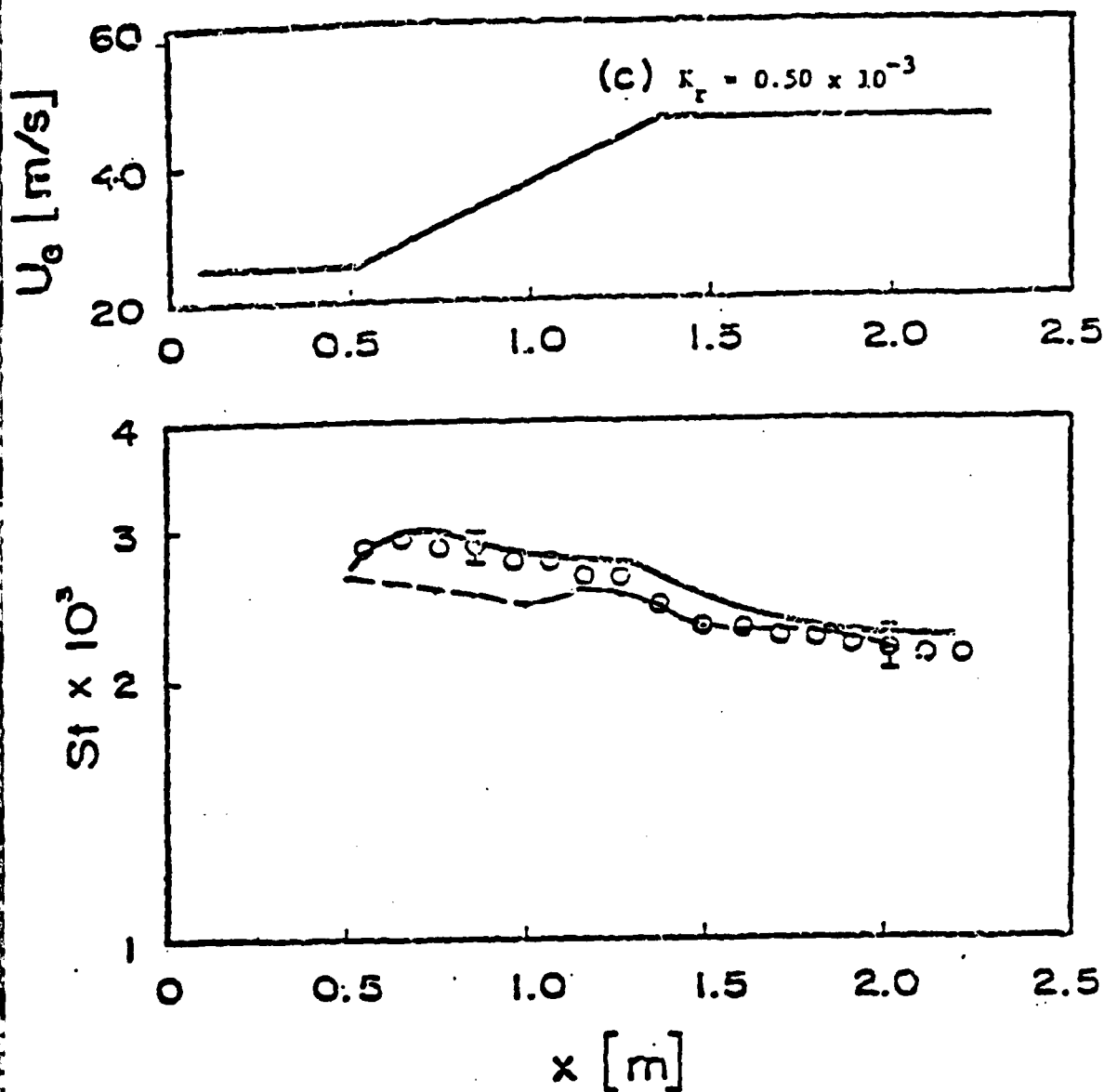


Figure 6 Comparison of Calculations with the Data of Coleman; $K_r = 0.5 \times 10^{-3}$; Constant Wall Temperature
 ○ Coleman Data; — Calculation Ref. [3] ;
 --- Present Calculation

1985 USAF-UES SUMMER FACULTY RESEARCH PROGRAM/
GRADUATE STUDENT SUMMER SUPPORT PROGRAM

Sponsored by the

AIR FORCE OFFICE OF SCIENTIFIC RESEARCH

Conducted by the

UNIVERSAL ENERGY SYSTEMS, INC

FINAL REPORT

The Influence of Condensed Water Revaporization
on Wind Tunnel Test Results

Prepared by:	Dr. Justin H. Poland
Academic Rank:	Associate Professor
Department and	Mechanical Engineering
University:	University of Maine at Orono
	Orono, Maine 04469
Research Location:	Arnold Engineering Development Center Directorate of Technology Von Karman Gas Dynamics Facility
USAF Research:	E. S. Powell
Date:	10 September 1985
Contract No:	F49620-85-C-0013

The Influence of Condensed Water Revaporization
on Wind Tunnel Test Results

by

Dr. Justin H. Poland

ABSTRACT

A study was made of the effect of evaporation of condensed water in a shock wave on the flow downstream. The describing equations for two dimensional and conical flow fields were derived and numerical results were calculated for some two-dimensional flows with complete evaporation in the shock. The evaporation of 0.7 to 1.4 percent condensed water mass fraction in flows with upstream Mach numbers of 2.1 to 3.7 respectively changed downstream flow parameters by 2 to 5 percent for normal shocks, and by 7 to 30 percent for the weakest possible oblique shocks when compared to dry flows through the same shocks. A brief survey of the state of the art in modelling the rate processes of homogeneous nucleation and droplet evaporation revealed that the present models to predict the onset of nucleation are too complex to be accommodated in anything but a one dimensional flow code. It was also found that droplet evaporation has been successfully modelled although the models have not been applied to the conditions of interest in supersonic flows of the Mach number range studied here.

NOMENCLATURE

A, B, C, D, = dimensionless constants used to simplify equations, defined where first used.

C_p = specific heat at constant pressure

E = dimensionless phase change energy parameter

h_{fg} = enthalpy change per unit mass due to phase change

ℓ = total number of chemically distinct species

\dot{m} = mass flow rate

M = molecular weight

Ma = Mach number

p = pressure

\bar{R} = universal flow rate

s_{fg} = entropy change per unit mass due to phase change

s = entropy per unit mass

T = absolute temperature

V = velocity

x = mole fraction

y = mass fraction

β = angle between oblique shock and upstream flow

γ = ratio of specific heats (c_p/c_v)

θ = angle flow is turned by an oblique shock

ρ = density

cw = condensed water

ncg = non-condensable gas

n = component normal to shock

o = isentropic stagnation state

wv = water vapor

I. INTRODUCTION:

The following describes the particular abilities of the author and the nature of the USAF research area which was assigned to him for the ten week period from 7/8/85 to 9/12/85.

Education:	B.S.M.E.	University of Maine	1968
	M.S.M.E.	Northeastern University	1970
	Ph.D.M.E.	University of Colorado	1979

Ph.D. Disseration: "Transient Phenomena in Thermal Explosion of Confined Gases"

A mathematical model was developed for the induction period of a thermal explosion in a confined, chemically reacting gas. The transient solution to the model equations was calculated using singular perturbation methods supplemented by numerical methods when necessary. The solution was advanced until the reaction rate became very rapid. To go beyond this point rationally sequencing the chemical and physical events would require more detailed and precise knowledge of the chemical kinetics' parameters than is generally available.

Experience:

1984 to present	Associate Professor of Mechanical Engineering, University of Maine at Orono, Orono, Maine Courses taught: Thermodynamics, Viscous Fluid Flow, Solar-Thermal Engineering, Thermodynamic Design of Combustion Engines, Senior Laboratory
1981	Consulting (Part-time) State of Maine Department of Transportation, Bangor, Maine, Designed solar energy system to preheat ventilation air for a

vehicle maintenance garage and advised during construction.

1978 to 1984	Assistant Professor of Mechanical Engineering
1972 to 1973	Design Engineer, Martin Marietta Corporation, Orlando, Florida, Designed missile airframes and test fixtures.
1970 to 1972	Commissioned Officer, U. S. Army Field Artillery, Served at Fort Sill, Oklahoma, and Republic of Vietnam

Professional Societies: American Society of Mechanical Engineers

Research (non-funded)

1. An investigation of the ability of the TRNSYS computer simulation program to model the performance of the ventilation air preheating solar energy system (item two under experience above.)
2. Preliminary, smoke injection trace, flow visualization experiments of natural convection in horizontally baffled enclosures are in progress. These are to establish design parameters for a well instrumented, precisely controlled apparatus suitable for accurate experimental work.

Research Undertaken for U. S. Air Force - Summer 1985

Development of procedures for calculating the effect of water sometimes present in wind tunnel airstreams on the state of the air. The energy change associated with phase change, affects changes of properties across shock waves as well as during equilibrium expansions and compressions of the airstream.

II. OBJECTIVES OF THE RESEARCH EFFORT

The following goals and objectives were initially formulated for the

research effort into influence of phase change of water on wind tunnel test results.

GOAL 1: Determine the influence of condensation and evaporation of water on test results in wind tunnels

Objective a: Relate the initial and final states of the following processes as a function of initial Mach number and composition:

Saturated expansion

Saturated compression

Condensation shock

Shock wave with evaporation

Objective b: Determine when the end states of the processes in Objective a differ from the corresponding adiabatic process by more than 2 percent.

GOAL 2: Provide a logical explanation for some existing test data for a flow containing condensation and evaporation processes.

Objective: Predict measured final states in the flow given initial states and theory for the process.

GOAL 3: Learn the current state-of-the-art in modelling homogeneous nucleation and droplet evaporation processes.

Objective: Determine if expressions exist permitting one to incorporate the rate processes of nucleation and evaporation into a macroscopic flow model.

The selection of 2 percent difference of end states as the criterion for need to consider phase changes is based upon the author's experience that careful experimentation can usually yield results accurate to $\pm 1-2\%$. Therefore, 2% deviation is the minimum deemed

necessary to insure that the deviation observed is more than experimental uncertainty.

During the project no additional goals were added but rather the above stated goals and objectives were narrowed slightly.

Evaluation of some recent past and present efforts here at AEDC [1, 2] revealed that under Objective a, the process of a shock wave with evaporation was the case most in need of treatment. Therefore effort was focused primarily on that process, however, the above mentioned efforts of others in the other three processes will be cited and briefly discussed.

The work on Goal 2 as originally conceived would require access to classified data. At about the seventh week of the ten week effort, the necessary security clearance had not been received and the results to date had raised the possibility that the results from cone pressure probes used to determine local Mach number might in some cases need to be corrected for the effects of evaporation. It was at that point decided to modify Goal 2 to address conical flows to determine when probe data needs to be corrected and by how much.

III. SHOCK WAVE WITH EVAPORATION

A. One and Two Dimensional Flows

Wegener and Mack [3] laid the foundations for the equations to be used here. They made the following assumptions:

1. Volume of the condensed phase is negligible
2. There is no slip velocity between the condensed and gaseous phases of the mixture.
3. The condensed phase remains dispersed in the gaseous phase.
4. The condensing specie behaves as an ideal gas while in the vapor or gaseous state.

These assumptions were found to be valid for the flows of interest in this investigation. The equations derived by Wegener and Mack [3] for one dimensional flow through a shock wave with phase change are

$$\rho_1 V_1 = \rho_2 V_2 \quad (1)$$

$$\rho_1 V_1^2 + P_1 = \rho_2 V_2^2 + P_2 \quad (2)$$

$$c_p T_1 - y_{cw1} h_{fg1} + V_1^2/2 = c_p T_2 - y_{cw2} h_{fg2} + V_2^2/2 \quad (3)$$

$$P = \rho(1 - y_{cw}) \bar{R} T / M_{mix} \quad (4)$$

Introducing the Mach number based on the ideal gas relationship of the speed of sound to temperature, permits the above to be rearranged to express parameter ratios across the shock in terms of Ma_1 , Ma_2 , y_{cw1} , y_{cw2} , and γ . It was found convenient [3] introduce a modified Mach number defined by

$$\bar{Ma}^2 \equiv Ma^2 / (1 - y_{cw})$$

to simplify the expressions. They are

$$P_2/P_1 = (1 + \gamma \overline{Ma}_1^2)/(1 + \gamma \overline{Ma}_2^2) \quad (5)$$

$$T_2/T_1 = (\overline{Ma}_2^2/\overline{Ma}_1^2)(P_2/P_1)(1 - \gamma_{cw1})/(1 - \gamma_{cw2}) \quad (6)$$

$$P_2/P_1 = (\overline{Ma}_1^2/\overline{Ma}_2^2)(P_1/P_2) \quad (7)$$

$$\overline{Ma}_1^2(\overline{Ma}_1^2 + 2/(\gamma-1) - E_1)/(1 + \gamma \overline{Ma}_1^2)^2 = \overline{Ma}_2^2(\overline{Ma}_2^2 + 2/(\gamma-1) - E_2)/(1 + \gamma \overline{Ma}_2^2)^2 \quad (8)$$

where

$$E_i \equiv \frac{2}{\gamma-1} \frac{\gamma_{cwi}}{(1 - \gamma_{cwi})} \left(\frac{h_{fg}(T_i)}{C_p T_i} - 1 \right) \quad (9)$$

represents the energy conversion strength of the phase change process. It is customary in flows without phase change to eliminate \overline{Ma}_2^2 from eqs (5) - (9) and have expressions for downstream flow parameters as functions of upstream parameters. For expediency in getting numerical results it was decided to use the above forms as is noting that eq (8) can be rearranged to a quadratic expression for \overline{Ma}_2^2 .

$$A \overline{Ma}_2^4 + B \overline{Ma}_2^2 + C = 0 \quad (10)$$

where

$$C = \frac{\overline{Ma}_1^2(\overline{Ma}_1^2 + 2/(\gamma-1) - E_1)}{(1 + \gamma \overline{Ma}_1^2)^2} \quad (11)$$

$$A = \gamma^2 C - 1 \quad (12)$$

$$B = \frac{2(A - \gamma C) + E_2(\gamma-1)}{\gamma-1} \quad (13)$$

Following Liepman and Roshko [4] these can be adapted to two dimensional flow through oblique shocks by replacing \overline{Ma}_1^2 by $\overline{Ma}_1^2 \sin^2 \beta$ and

\bar{Ma}_2^2 by $\bar{Ma}_2^2 \sin^2 (\beta - \theta)$ where the interpretation of β and θ is shown in Figure 1.

By introducing two new variables β and θ into the equations, with only one of them, likely to be specified in any case, another equation is needed which relates β and θ to the flow parameters. This relationship comes from the geometry shown in Fig. 1; and is

$$\frac{\tan(\beta - \theta)}{\tan \beta} = \frac{V_{n2}}{V_{n1}} = \frac{\bar{Ma}_2^2 \sin^2(\beta - \theta)(1 + \gamma \bar{Ma}_1^2 \sin^2 \beta)}{\bar{Ma}_1^2 \sin^2 \beta (1 + \gamma \bar{Ma}_2^2 \sin^2(\beta - \theta))} \quad (14)$$

where V_{n1} and V_{n2} are velocities normal to the shock.

Equation (14) can be solved for \bar{Ma}_2^2 to give

$$\bar{Ma}_2^2 = 1 / (D \sin 2(\beta - \theta) - \gamma \sin^2(\beta - \theta)) \quad (15)$$

where

$$D = (1 + \gamma \bar{Ma}_1^2 \sin^2 \beta) / \bar{Ma}_1^2 \sin 2\beta \quad (16)$$

In the case of oblique shocks the solution procedure is more complicated than for a normal shock. The procedure chosen was to step through the possible β range for a given \bar{Ma}_2^2 by guessing θ and correcting the guess iteratively until eqs (10) and (15) both gave the same value for \bar{Ma}_2 . Examining Fig 4.1 of [4] showed that by starting at $\beta = 90$ and decreasing, it would be easy to always choose an initial guess such that θ was slightly less than θ_{cr} making convergence rapid. A quick numerical check of eqs (10) and (15) revealed the following pattern.

$$\theta < \theta_{tr} \Rightarrow \bar{Ma}_2 \text{ eq (10)} < \bar{Ma}_2 \text{ eq (15)}$$

which was exploited to achieve convergence to the correct θ .

The limiting range of β is defined by the second law of thermodynamics.

For our flows this is

$$\sum_{i=1}^l \dot{m}_{i2} s_i(T_2, p_2) \geq \sum_{i=1}^l \dot{m}_{i1} s_i(T_1, p_1)$$

which can be expanded to the following more useful form.

$$c_{p m_{12}} \ln(T_2/T_1) - (\bar{R}/M_{mix}) \left(\sum_{i=1}^l x_i \ln(x_{2i}/x_{1i})_{gas} + \ln(P_2/P_1) \right) + \gamma_{cw1} s_{fg}(T_1) - \gamma_{cw2} s_{fg}(T_2) \geq 0 \quad (17)$$

Two additional quantities of interest to experimenters are stagnation pressure, p_o , and stagnation temperature, T_o . They are given by the following equations:

$$T_o = T \frac{(1-\gamma_{cw})}{(1-\gamma_{cw0})} \frac{\bar{M}a_2^2 + 2/(\gamma-1) - E}{2/(\gamma-1) - E_o} \quad (18)$$

$$p_o = p (T_o/T)^{\gamma/(\gamma-1)} \quad (19)$$

In the cases of interest here $\gamma_{cw0} = 0$ which implies $E_o = 0$ and no other equation is needed to solve for the unknowns γ_{cw0} and T_o .

Equations (5) - (19) were solved for several test flow conditions defined by $T_o, p_o, T_1, p_1, Ma_1, X_{i1}, i = 1 - l, X_{cw}$ covering the full range of possible β with the lower limit on β dictated by the requirement $S_2 - S_1 \geq 0$. This was done by programming the equations (5) - (19) including the criteria for convergence to the correct θ and the corresponding equations for a dry adiabatic flow in Basic and solving using a Zenith 89 microcomputer equipped with 64K bytes of memory.

The comparison of the geometry of the shocks as a function of Ma_1 is shown in Fig 2 for the range of test conditions of most interest. It can be seen that for any given turning angle of the flow, θ , the weak oblique shock, $Ma_2 > 1$, with evaporation is more oblique to the flow, smaller β , while the opposite is true for the strong oblique shock $Ma_2 <$

1. Also very weak oblique shocks $\beta < 17$ deg, $\epsilon < 5$ deg at $Ma_1 = 3.69$ and $\beta < 32$ deg, $\epsilon < 7.5$ deg at $Ma_2 = 2.1$ result in $s_2 - s_1 < 0$ under the assumption of complete evaporation of water by the shock. These very weak shock waves simply don't dissipate enough kinetic energy to completely evaporate the condensed water. The θ values, for which complete evaporation by the shock is not possible are smaller than the half angles of most wedges of practical interest, but the same may not be true for conical bodies which generate weaker shocks for given half angle than do wedges [4]. Table 1 presents excerpts from a computation for an upstream flow with $Ma_1 = 3.179$ $Y_{cw_1} = .01309$ which show some typical magnitudes of deviation from dry flow results caused by evaporation. First we note that the change in P_2/P_1 , T_2/T_1 , ρ_2/ρ_1 due to evaporation is consistent with the intuitive notion that evaporation cools and compacts the flow. The stagnation temperature behind the shock is always less than for a dry flow though a shock at the same β because some of the dissipated kinetic energy is absorbed as h_{fg} at constant temperature rather than as sensible enthalpy which would result in higher stagnation temperature.

Figures 3 and 4 demonstrate more clearly the effect of evaporation on parameters downstream of a shock. It is apparent that the impact of the h_{fg} energy conversion due to evaporation increases as the shock strength decreases i.e. as β decreases and less kinetic energy is dissipated. No further explanation of the patterns of variation in Figs. 3 and 4 is available at this time beyond a statement that the jump conditions are non linear.

B. Conical Flow

The equations for isentropic compressible flow over sharp pointed

cones were given by Shapiro [5]. If one is interested in complete evaporation through a conical shock then those equations apply without change to the flow field downstream of the shock. Many solutions have been tabulated [6] for dry air with $\gamma = 1.4$. Provided that this value of γ is acceptable for the mixture of gases being dealt with, one could easily determine the upstream wet flow for any of the given conical flows using the shock jump conditions derived in section III A. above. The more interesting problem is to locate the shock and define its downstream flow field given the upstream "wet" flow parameters. The equations of Shapiro [6] still apply if evaporation is completed by the shock, but now one must guess conditions at the cone surface integrate outward, and try to match both the geometric condition at the shock as defined by eqs (15) and (16) derived from eq (14) and the conservation of energy condition defined by eqs (10) - (15) with \bar{M}_a , replaced by $\bar{M}_a \sin \beta$ and \bar{M}_{a2} replaced by $\bar{M}_{a2} \sin (\beta - \theta)$. The complexity of the nonlinear ordinary differential equations for the conical flow field as well as the nonlinearity of the shock jump conditions makes selection of a convergence criteria for the iteration to correct β and V_{rs} difficult. Some numerical experimentation had led to a convergence criteria which should work; however, there was not sufficient time to implement and prove this, so numerical results for conical flow fields have not been obtained. Dry conical flows show similar shock effects to those of dry two dimensional flow but of different magnitude. The same is anticipated for the wet flows. The results obtained for two-dimensional flow with evaporation by a shock are based on the assumption of instantaneous state change to keep the system always in a state of thermodynamic equilibrium. There is some test evidence [1, 7] that

this is not always the case and it is well known that supersaturation [3] occurs in some very clean wind tunnel flows. Condensation which begins at $T = T_{sat}$ for the water vapor can be dealt with using the methods of [5] [3] for simple T_o change if one accounts for the phase change energy transformation h_{fg} at constant temp in computing T_o . These methods have been implemented [1] in a one dimensional flow code which predicts discharge conditions for nozzles which match quite well with experimental data.

Robinson, Bauer, and Nichols [2] have dealt with condensation which begins after some supersaturation by using an empirical curve derived from experimental data [3] to predict the onset of condensation. The resulting two dimensional flow code worked well for both external and internal flows with specific humidities up to .005 which are somewhat lower than those of interest here. Ultimately it would be more satisfying to model the onset of condensation based upon fundamental principles i.e. homogeneous nucleation. Also evaporation in the case when thermodynamic equilibrium isn't maintained requires the treatment of droplet evaporation.

IV. Homogeneous Nucleation and Droplet Evaporation Modelling

Wegener [8] reported that the major obstacle still to be overcome in accurately modelling homogeneous nucleation is the model of surface (or interfacial) tension associated with small clusters of condensed phase molecules. Robinson, et al, [2] in a very recent work, reported that the kinetic theory approach to modelling homogeneous nucleation at present is too complex to be effective in two and three dimensional flow field codes. They also reported that it has been applied to one dimensional flow by Stewart [9].

In droplet evaluation, most of the previous work has dealt with two widely separated flow regimes:

1. Large droplets (2 to 4 mm dia) traveling at subsonic speeds relative to their gaseous environment [10, 11]
2. Smaller drops (1 to 2000 μm dia) under supersonic conditions [12, 13]

The first regime is not pertinent to most supersonic wind tunnel testing, but the second may be depending upon shock strength and flow Mach number.

Roth and Fischer [12] compared evaporation rate calculations to experimental results for $\text{C}_{24}\text{H}_{38}\text{O}_4$ droplets of initial Knudsen number 0.1 to 0.8 (just inside the continuum flow regime) dispersed in Argon gas and impacted by relatively weak shocks with $P_2/P_1 = 2$ to 3. The evaporation rate was quite sensitive to shock pressure rise, varying from a factor of 4 decrease in radius in 1 ms at $P_2/P_1 = 3$ to very little decrease in 2 ms at $P_2/P_1 = 2$. The calculations compared very well with the experimental data when a non-continuum correction was included.

Swain et al [13] performed numerical calculations using a sophisticated model including particle dynamics as well as thermal processes. They investigated conditions in the hypersonic reentry flow regime of droplets or ice crystals ranging in size from 200 to 2800 μm in dia. The reentry vehicle was a 7 deg cone angle spherically blunted (0.75 in rad.) cone 80 in. long travelling at Mach 16 at 20,000 ft altitude. For these conditions aerodynamics mass stripping and catastrophic droplet breakup must be modelled as well. Here too both continuum and non-continuum effects must be considered as the particles decrease in size.

While not an exhaustive literature search the above references show that the process of evaporation can be modelled and there is some confirmation of the success of the models. It should therefore be possible to model the flows of present interest also, since rate coefficients are available for situations which bracket the present interest.

V. Conclusions

The study of evaporation of condensed water by shock waves in two dimensional flow fields has revealed several important features of wet flow compared to dry flows:

1. The influence on flow through normal shocks is relatively small, less than or equal to about 5 percent for all flow field properties for the combinations of upstream Mach number and condensed water mass fraction of interest.
2. The substantial variation in the total pressure field with shock angle β in a two dimensional flow field implies that a wedge probe used in a wet flow to measure both stagnation and static pressure for use in computing local Mach number will require correction for the effects of evaporation to yield accurate values of Mach number.
3. Conclusions (1) and (2) together imply that a minimum amount of correcting would be required for a probe of small enough half angle to preclude complete evaporation in the flow along its sides.
4. Matching both temperature and pressure downstream of a shock in a wet flow to those in a dry flow over three dimensional bodies will prove difficult because:

- a. Magnitude of evaporation influence changes drastically with shock angle β at low β .
- b. Relative magnitudes of influence on pressure and temperature also change drastically (see Fig 3) with shock strength.

IIV. RECOMMENDATION

The following recommendations can be made:

1. Correct wet flow wedge pressure probe data for evaporation effects unless the particular "wetness" situation or accuracy desired don't require this.
2. Obtain the magnitude of evaporation effects on conical flow fields for use in correcting cone probe pressure data.
3. Consider conclusion 4 very carefully and develop a strategy for deciding whether testing under one wet flow condition can be used to simulate a slightly different dry flow to the accuracy required. Part of this strategy will probably be extension of the principles presented here for simple flows to more sophisticated flow models.

ACKNOWLEDGEMENTS

The author gratefully acknowledges the sponsorship of the Air Force Systems Command, Air Force Office of Scientific Research, and Arnold Engineering Development Center. Timely and efficient administration by Universal Energy Systems Inc. was also appreciated. Special thanks go to Dr. E. S. Powell for consultation throughout the work to keep it on target toward information useful in the testing at AEDC.

REFERENCES

1. Private Communication from E. S. Powell
2. C. E. Robinson, R. C. Bauer, and R. H. Nichols, "Estimating Water Vapor Condensation Effects for Transonic and Supersonic Flow Fields," submitted for publication to AIAA.
3. Peter P. Wegener and Leslie M. Mack, "Condensation in Supersonic and Hypersonic Wind Tunnels" in Advances in Applied Mechanics, Vol 5 eds H. L. Dryden and Th. von Karman, New York, New York, Academic Press Inc., 1958, pp. 307-448.
4. H. W. Liepmann and A. Roshko, Elements of Gasdynamics, New York, New York, John Wiley and Sons, Inc., 1957.
5. Ascher H. Shapiro, The Dynamics and Thermodynamics of Compressible Fluid Flow, Vol 2, New York, New York, The Ronald Press Co., 1954, pp. 653-663.
6. Zdenek Kopal, Tables of Supersonic Flow Around Cones, Cambridge, Massachusetts, MIT Press, 1947.
7. H. Thomann and R. A. White, "An Experimental Investigation of the Influence of Humidity on the Recovery Temperature at Mach number 3," The Aeronautical Research Institute of Sweden (FFA), Report 89, 1961.
8. Peter P. Wegener, Nonequilibrium Flows Part I, New York, New York, Marcel Dekker, 1969, Chapter 4.
9. V. W. Stewart III, "A Kinetic Theory Approach to Computation of Supersonic Nozzle Flow with Water Vapor Condensation," Masters Thesis, University of Tennessee, August 1983.

10. H. R. Pruppacher and R. Rasmussen, "A Wind Tunnel Investigation of the Rate of Evaporation of Large Water Drops Falling at Terminal Velocity in Air," Journal of the Atmosphere Sciences 36, 1979, pp. 1255-1260.
11. K. N. Shukla, "Diffusion and Evaporation of a Liquid Droplet" AIAA Journal, 18, 1980, pp. 706-711.
12. R. Fischer and Paul Roth, "Evaporation Rates of Submicron Aerosol Droplets at High Temperatures," Journal of Aerosol Science 14, 1983, pp 376-380.
13. C. E. Swain, W. T. Webber, and H. G. Trimmer, "Particle/Shock Layer Interaction in Hypersonic Reentry," AIAA Paper 75-110 presented at 13th Aerospace Sciences Meeting, Pasadena, California, January 20-22, 1975.

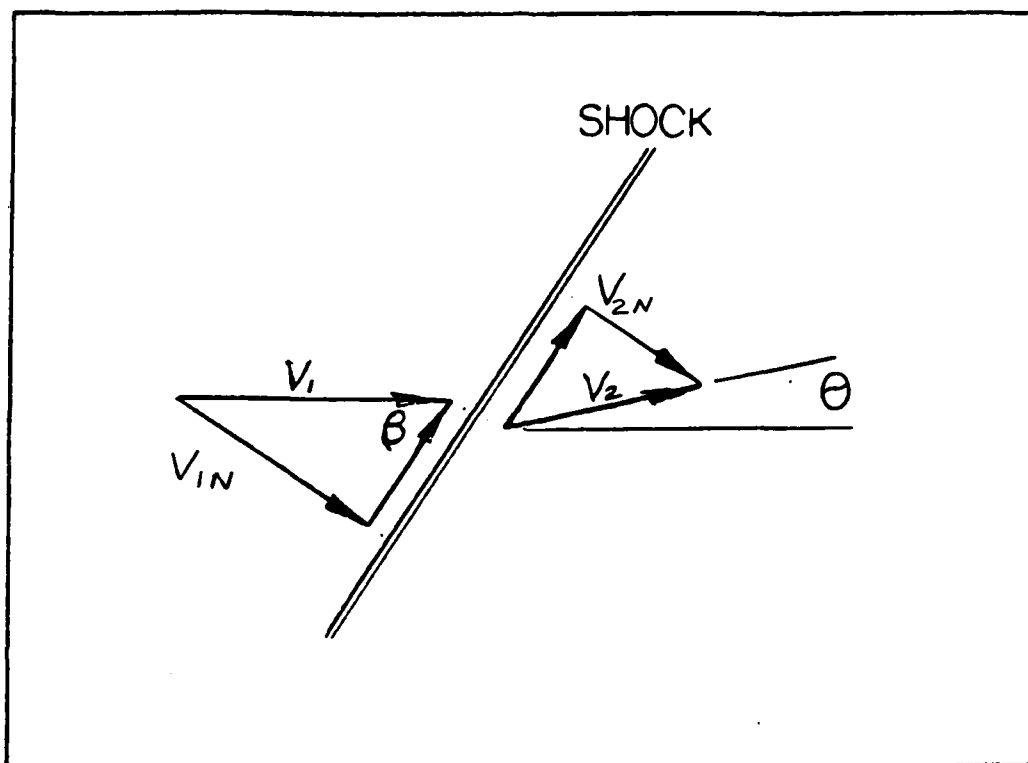


Fig 1.

Oblique shock geometry

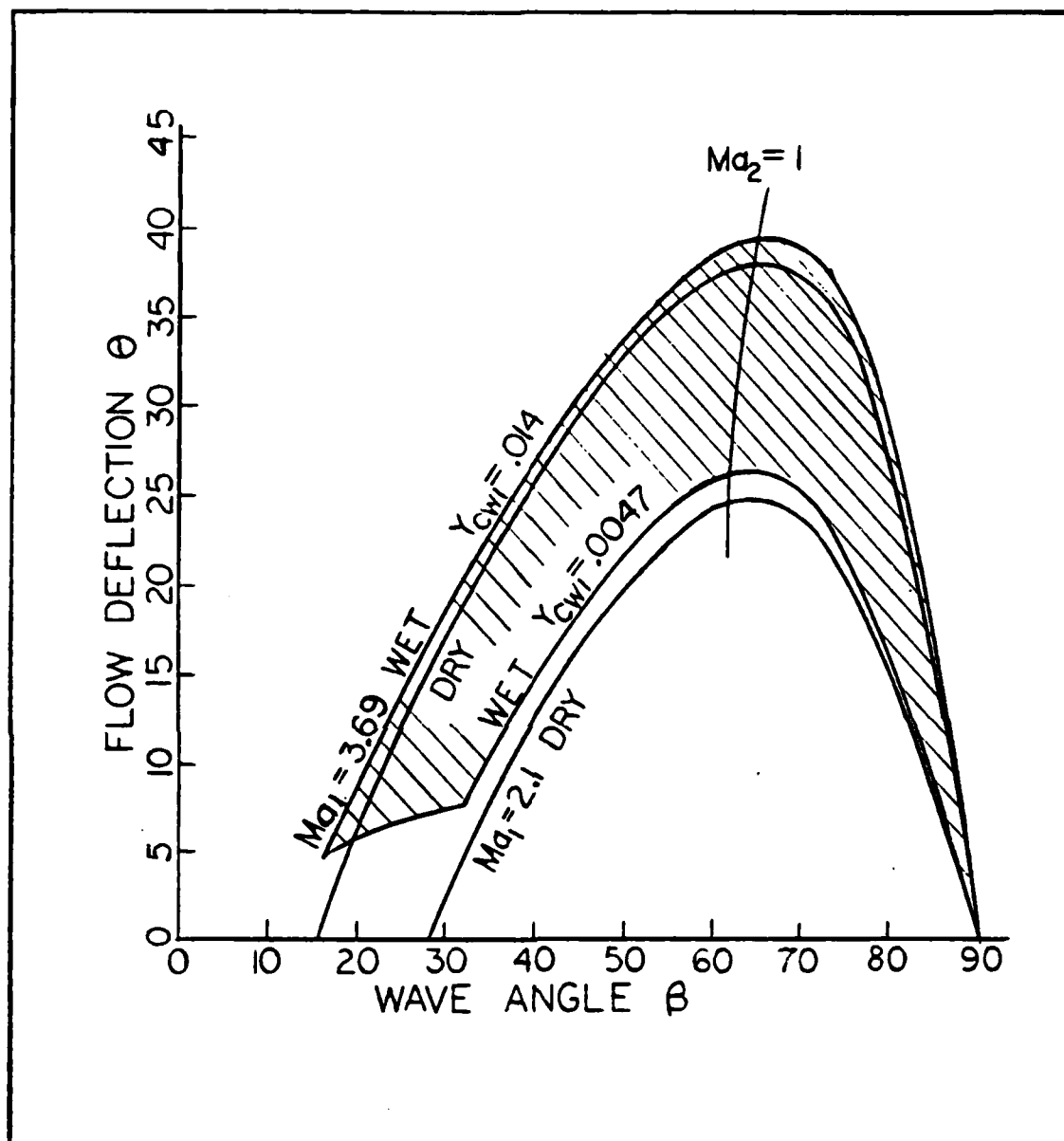


Fig 2.

Comparison of wet and dry flow shock geometry for largest y_{cw1} at two values of Ma_1 . Shaded region is possible wet flow envelope^{cw1} for largest y_{cw1} at intermediate Ma_1 values.

TABLE 1.

Effect of Evaporation on Flow Property Changes
Across Four Oblique Shock Waves

FLOW TT,PT,T1,P1,M1									
1413.2 R		195.16 <i>psia</i>		467.7 R		4.07 <i>psia</i>		3.179	
FLOW MOLE FRACTS N2,O2,H2O,CO2,AR									
.7805		.1593		.02784		.02258		9.34E-03	
GAS MOLE FRACTIONS									
.7972		.1627		6.87E-03		.02306		9.54E-03	
MOLECULAR WEIGHTS									
28.016		32		18.016		44.01		39.94	
CP (BTU/LBM-R)									
.248		.219		.445		.203		.1253	
HFG (BTU/LBM), SFG (BTU/LBM-R)									
1220		2.612							
MIXTURE CP,MW,GAMMA,XCW,YCW									
7.01093		28.8324		1.39551		.0209483		.0130896	
BETA		THETA		MACH2		P2/P1		T2/T1	
						D2/D1		S2-S1	
TT2		PT2							
EVAP		88		6.5		.449		11.9	
DRY				6.0		.469		11.5	
RATIO						1.02		.957	
						4.02		2.49	
EVAP		64		37		1.00		9.67	
DRY				35.		1.00		9.34	
RATIO						1.03		.949	
						3.08		1.04	
EVAP		40		24.		1.98		4.98	
DRY				22.		1.94		4.69	
RATIO						1.06		.931	
						1.75		.048	
EVAP		22		9.0		2.93		1.85	
DRY				5.0		2.91		1.48	
RATIO						1.25		.935	
						1.32		.012	
EVAP						1.31		.932	
DRY								1.23	
RATIO									

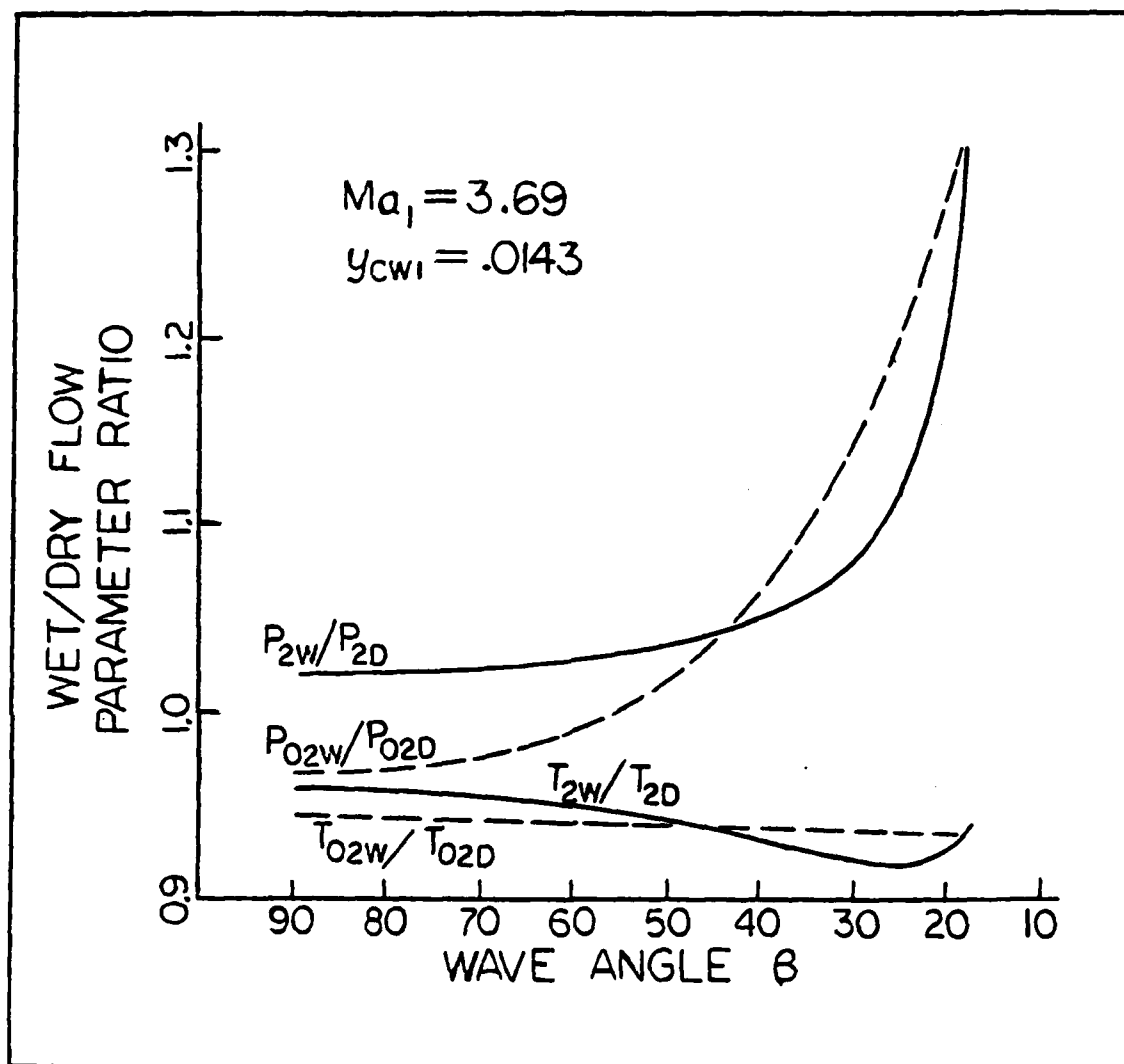


Fig 3.

Influence of evaporation on values of p , p_0 , T , and T_0 downstream of a shock wave for given upstream conditions $P_1 = 2.01$ psia, $T_1 = 472.3$ R

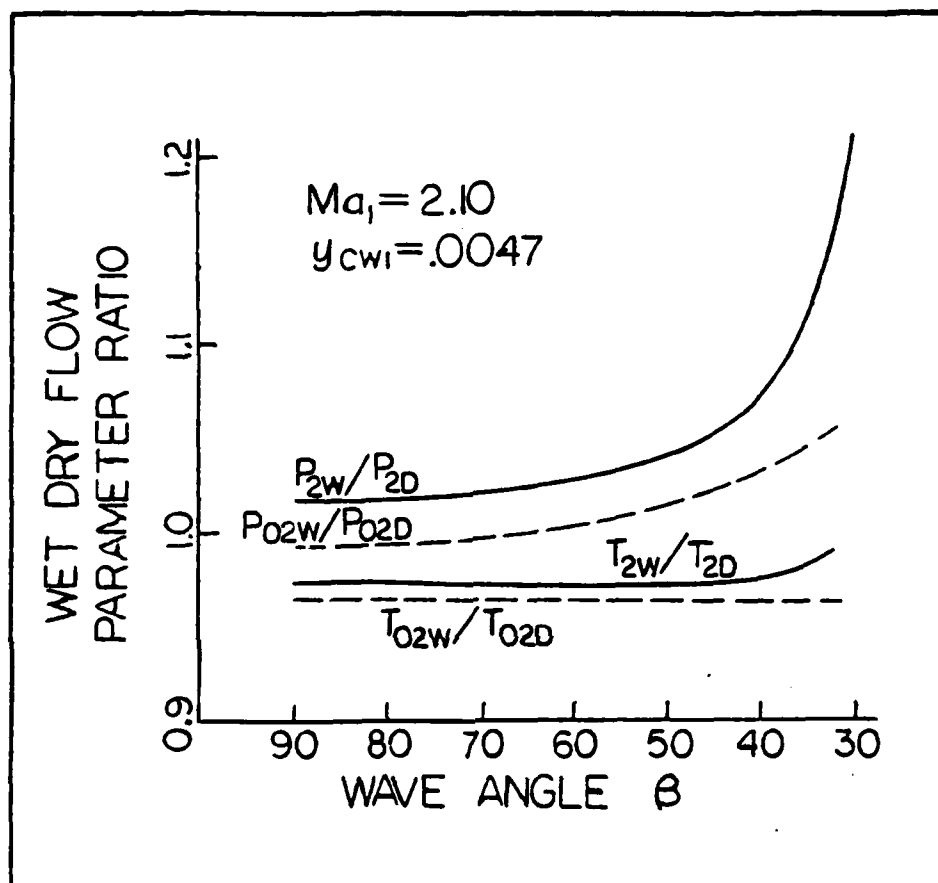


Fig 4.

Influence of evaporation on values of P , P_0 , T , and T_0 downstream of a shock wave for given upstream conditions $P_1 = 3.73$ psia, $T_1 = 423.8$ R.

1985 USAF-UES SUMMER FACULTY RESEARCH PROGRAM/

GRADUATE STUDENT SUMMER SUPPORT PROGRAM

Sponsored by the
AIR FORCE OFFICE OF SCIENTIFIC RESEARCH

Conducted by the
UNIVERSAL ENERGY SYSTEMS, INC

FINAL REPORT

STUDY OF SYSTEM IMPAIRMENT DETECTION AND
CLASSIFICATION ALGORITHM FOR UNMANNED RESEARCH VEHICLE

Prepared by: Kuldip S. Rattan
Academic Rank: Associate Professor
Department and University: Department of Electrical Systems Engineering,
Wright State University
Research Location: Air Force Wright Aeronautical Laboratories
Flight Dynamics Lab
Flight Control Division
Flight Control Development Branch
USAF Research Colleague: Phillip R. Chandler
Date: Sept. 6, 1985
Contract: F49620-85-C-0013

Distribution limited to U.S. Government agencies and their contractors (critical technology/27 Sept. 1985). Other requests for this document must be referred to AFWAL/FIGL, WPAFB, Ohio 45433-6553.

STUDY OF SYSTEM IMPAIRMENT DETECTION AND CLASSIFICATION ALGORITHM
FOR AN UNMANNED RESEARCH VEHICLE

Kuldip S. Rattan

ABSTRACT

System impairment detection and classification (SIDC) algorithm for actuator failures is studied in this effort. The objective of this research is to evaluate the SIDC algorithm of ALPHATECH, INC. which is capable of detecting, isolating and classifying control surface failure and apply this algorithm to detect and classify the actuator failures of the unmanned research vehicle (URV). This algorithm can detect the presence of stuck, floating and partially missing control surfaces and is based on decentralized residuals. Log likelihood ratio (LLR) and sequential probability ratio (SPRT) tests are used in hypothesis testing for the failure detection and isolation (FDI) algorithm. Recommendation for further research in the area is given.

ACKNOWLEDGEMENTS

The author hereby expresses his gratitude to the Air Force System Command, the Air Force office of Scientific Research and Universal Energy Systems, Inc. for providing him with the opportunity to spend a worthwhile five weeks at the Flight Dynamics Laboratory, Wright-Patterson Air Force Base, Ohio. He appreciates the hospitality and excellent working condition that the Control Systems Development Branch offered.

The author would like to thank Messrs. Phillip R. Chandler, Duane Robertus, John Perdsock, and Mark Mears for their help. He would like to acknowledge Alphatech Inc. who developed the SIDC algorithm for General Electric. Finally, he would like to express his appreciation to Mrs. Dolores Davis of the School of Engineering, Wright State University for her careful and professional typing of this report.

I. INTRODUCTION

Present aircraft which employ fly-by-wire (FBW) closed-loop flight control systems (FCS) are primarily designed with control laws that require each element of the control loop to perform properly. These control laws are not designed to exploit the resulting control power if a primary surface becomes inoperative due to combat damage or mechanical failure. Stringent safety-of-flight reliability standards imposed on FCS's have resulted in the addition of extensive redundant hardware in aircraft. The extra hardware results in considerable additional cost and reduces the mean time between maintenance actions. Most aircrafts have redundant control effectors and control power (at many flight conditions) which provide an alternative to adding redundant hardware by distributing the forces and moments of the failed surface to the remaining healthy control surfaces. The concept known as Reconfiguration utilizes the existing redundancy in producing generalized forces and moment acting on the aircraft, rather than the brute force approach of adding redundancy in actuator and servo hardware to ensure proper operation after failure and damage.

Reconfiguration of the flight control law of the URV after effector failure was studied recently using the control mixer concept [1]. The simulation results obtained from this study showed that the reconfigured aircraft was able to track the unimpaired response if another primary healthy surface is available. The scope of this study was limited to the evaluation of the control mixer which assumes the knowledge of the failed surface and its classification. For reconfiguration of FCS of the URV it is important that the reconfiguration algorithm is able to detect and classify surface failures. This study is a step in this direction and is based on the SIDC report of ALPHATECH, INC.

II. OBJECTIVES

The main objective of this research is to evaluate SIDC algorithm of ALPHATECH, INC. which is capable of detecting, isolating and classifying control surface failure. The specific objectives are

1. To develop an algorithm for the detection and classification of the actuator failures of the URV.
2. To identify directions for future research.

III. STRUCTURE OF FAILURE DETECTION AND ISOLATION ALGORITHM

All failure detection methods [2-5] can be described by the structure shown in Fig. 1

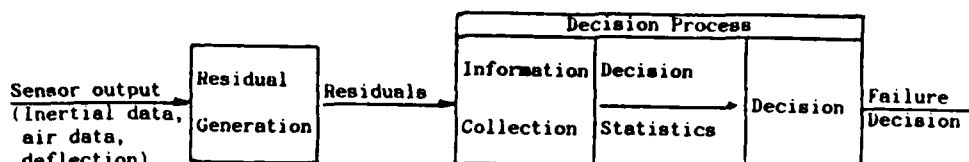


Fig. 1. General Structure of FDI

There are two fundamental parts of failure detection. The first is the generation of a set of signals called residuals whose deviation from nominal behavior (typically meaning near zero without significant trends or patterns) can be used as the basis for detecting and identifying system failures. The second component is the decision process consisting of information collection and decision-logical functions which process the residuals to make the FDI decisions.

3.1 RESIDUAL GENERATION

The residuals represent the difference between functions of the observed sensor outputs and the expected values of these functions in the normal (no-fail) mode. In the absence of a failure residuals should be unbiased, showing agreement between observed and expected normal behavior of the system.

The basis for the residual generation is redundancy, which can be divided into two general areas: direct redundancy and functional redundancy. Direct redundancy involves the direct comparison of the outputs of two or more identical sensors. Analytical redundancy uses redundant information of dissimilar sensors, and, therefore requires less hardware. Voting techniques are the most common form of direct redundancy, while analytical redundancy is characterized by real time modeling techniques involving complex software algorithm.

Once one has identified all the redundancy relations that are relevant to the failures under consideration, the next step is to specify how such relations should be used in forming residuals. The residual generations should be based on those relations that are least

specify how such relations should be used in forming residuals. The residual generations should be based on those relations that are least sensitive to parameter uncertainties and are maximally sensitive to failure. One commonly used approach is to use a large centralized Kalman filter or observer which mixes together relationships that are known very well with those that are far more uncertain. For this reason centralized approaches that are optimal when models are well known become far from optimal when model uncertainty is taken into account.

Thus in order to achieve selective sensitivity in the FDI algorithm, one must generate residuals in a decentralized manner. Individual relationships between the measurable variables can then be considered in terms of their sensitivity to specific failure modes and to various sources of model error. Since the FDI system that is produced consists of a collection of extremely simple, low-order sub-algorithms, the overall system is extremely simple to implement, verify and troubleshoot. Only the best relationships for detecting and distinguishing individual failure modes or subsets of failure modes is then used in the hypothesis test which makes up the second part of the FDI structure of Fig. 1.

3.2 DECISION PROCESS

The decision process consists of information collection and decision test block as shown in Fig. 1. The accumulation of information is necessitated due to the fact that the instantaneous value of a residual is not sufficient for accurate detection and identification and must be accumulated over time to achieve reliable decision. We can trade off decision delay with decision reliability. Processing residuals over short time periods results in increased uncertainty associated with the corresponding decision. Likewise, longer processing intervals lead to more reliable decisions. Since the severity of a failure is unknown a-priori, statistical tests whose performance is monotonically increasing with failure severity are required. Large failure should result in failure decisions which have lower probability of miss detection since these failures have large impact on FDI algorithm. The block diagram of the structure of the decision process is shown in Fig. 2.

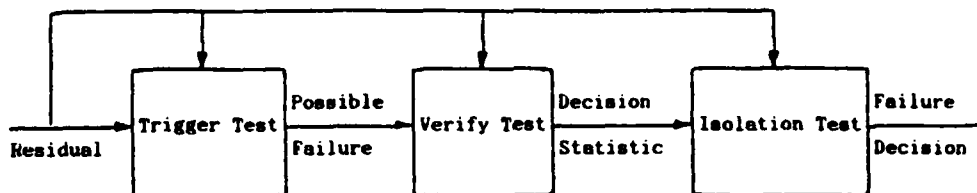


Fig. 2. Structure of Decision Process

The first part of the decision process is the trigger test which is based on quick detection and is designed to give full coverage to all failure modes and limit missed detection. Failures are declared using short interval for information accumulation and relatively low threshold. This produces very fast detection at the expense of possible false trigger rate.

The second part of the decision process is initiated by the trigger test and is somewhat longer running. This test, which makes use of the same residual, verifies that the quick response alarm was not a false start, and at the same time performs tests to isolate the failure source. Sequential Probability Ratio Test [6,7] is used as a hypothesis test which has the property that it reaches a decision in as short a time as possible given the level of uncertainty in the residual and probability of false alarm.

The last part of the decision process shown in Fig. 1 is the decision logic. The function of this block is to interpret the hypothesis test performed in the accumulation of information phase.

3.3 HYPOTHESIS TESTING

The general problem of statistical hypothesis testing can be described as follows. Consider that the observation space corresponds to a set of N observations, $y(N)$. Let the probabilistic transition mechanism generate points according to two known conditional probability densities $P(y/H_1)$ and $P(y/H_0)$ (for binary hypothesis, however, multiple hypothesis can also be considered). The object is to use this information to develop a suitable decision region D_1 which maps the

observables, y , into decision about the system status in an optimal manner. Two commonly used criterion are Bayes and Neyman-Pearson which are discussed below:

3.3.1. Bayes Criterion

A Bayes test is based on two assumptions: probability and cost assignments. Let P_1 and P_0 be a priori probability of each hypothesis and C_{00} , C_{10} , C_{11} , C_{01} are cost assigned to four different decision conditions. The total cost C is given by

$$C = \sum_{i,j} C_{ij} \cdot P(y \in D_i / H_j) \quad (1)$$

where C_{ij} is the cost of deciding that hypothesis i is true when in fact hypothesis j is true. The optimization problem, $\min_{D_1} E(C)$ gives the solution [8]

$$\Lambda(y) = \frac{P(y/H_1)}{P(y/H_0)} \underset{D_0}{\overset{D_1}{\gtrless}} \frac{P_0(C_{10}-C_{00})}{P_1(C_{01}-C_{11})} \quad (2)$$

The quantity $\Lambda(y)$ is called the likelihood ratio. Because the ratio of two functions of a random variable is a random variable, $\Lambda(y)$ is a one-dimensional variable regardless of the dimensionality of y . Thus Bayes criterion leads to a likelihood ratio (LR) or log likelihood ratio (LLR) test given by

$$\Lambda(y) \underset{D_0}{\overset{D_1}{\gtrless}} \eta \quad \text{or} \quad \ln \Lambda(y) \underset{D_0}{\overset{D_1}{\gtrless}} \ln \eta \quad (3)$$

where $\eta \triangleq \frac{P_0(C_{10}-C_{00})}{P_1(C_{01}-C_{11})}$ is called the threshold. The result in (3) enables us to build the entire processor and leave η as a variable threshold to accommodate changes in the estimate of priori probability and cost as shown in Fig. 3

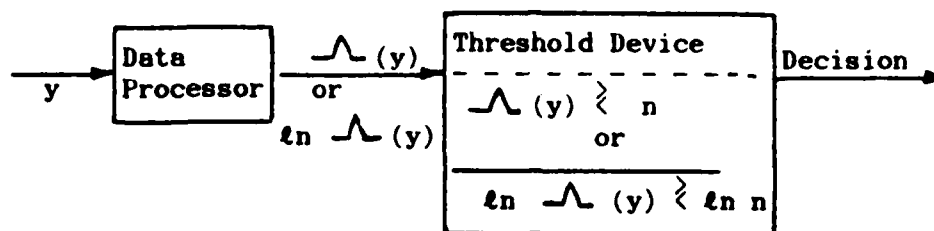


Fig. 3. Likelihood ratio processor

3.3.2. Neyman-Pearson Tests

In many physical situations it is difficult to assign realistic cost or a priori probabilities. A way to bypass this difficulty is to work with the conditional probabilities P_F , probability of incorrectly deciding that H_1 is true when H_0 is in fact true, and P_D , probability that the correct decision H_1 is made when H_1 is true. The optimization problem is then to max P_D subject to the constraint $P_F = \gamma$. The solution of this optimization (8) is

$$\frac{D_1}{D_0} \lambda(y) \underset{D_0}{\underset{D_1}{\gtrless}} t \quad (4)$$

To satisfy the constraint we choose t so that $P_F = \gamma$. In other words

$$P_F = \int_t^\infty P(\lambda/H_0) d\lambda = \gamma \quad (5)$$

Solving (5) for t gives the threshold. The LLR tests described above are known as fixed sample size. Another test which has been used extensively for FDI is the sequential probability ratio test (SPRT) [9]. Rather than basing decision on a fixed sample of data, the SPRT decides automatically when enough samples have been taken to make a reliable decision. Given P_F and P_D , the SPRT chooses one of the three following decisions:

$$\begin{aligned} \ell_k &> t^+ \longrightarrow \text{decide } H_1 \\ \ell_k &< t^- \longrightarrow \text{decide } H_0 \\ t^- &< \ell_k < t^+ \longrightarrow \text{take another sample} \end{aligned}$$

where $\ell_k = \ln \lambda(y_k)$. If we choose t^+ and t^- by

$$t^+ = \ln \left[\frac{1-\beta}{\alpha} \right]$$

$$t^- = \ln \left[\frac{\beta}{1-\alpha} \right]$$

then it has been shown [10] that $P_{FA} < \alpha$ and $P_D > 1-\beta$

IV. SIDC FOR STUCK/FLOATING SURFACES OF THE URV

The SIDC structure for the stuck/floating surface of the URV is shown in Fig. 4

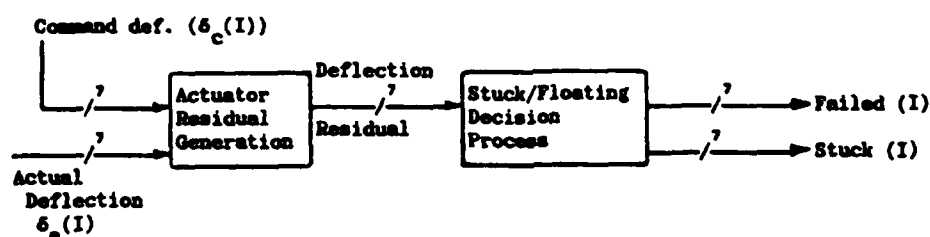


Fig. 4. SIDC Structure for Actuator Failure

The surface is considered to be stuck if the actual surface deflection is constant in time and is significantly different from the commanded deflection. The surface is assumed to be floating if the actual surface deflection varies in time, equal to some floating angle and is significantly different from the commanded deflection. The deflection of a floating surface varies when the aircraft moves. The SIDC algorithm for Stuck/Floating surfaces is organized as seven independent, parallel subsystems (one for each surface). The output of each subsystem are two logical signals which are defined as

FAILED(I) = TRUE(FALSE) Indicates ith surface has malfunctioned (operating normally)

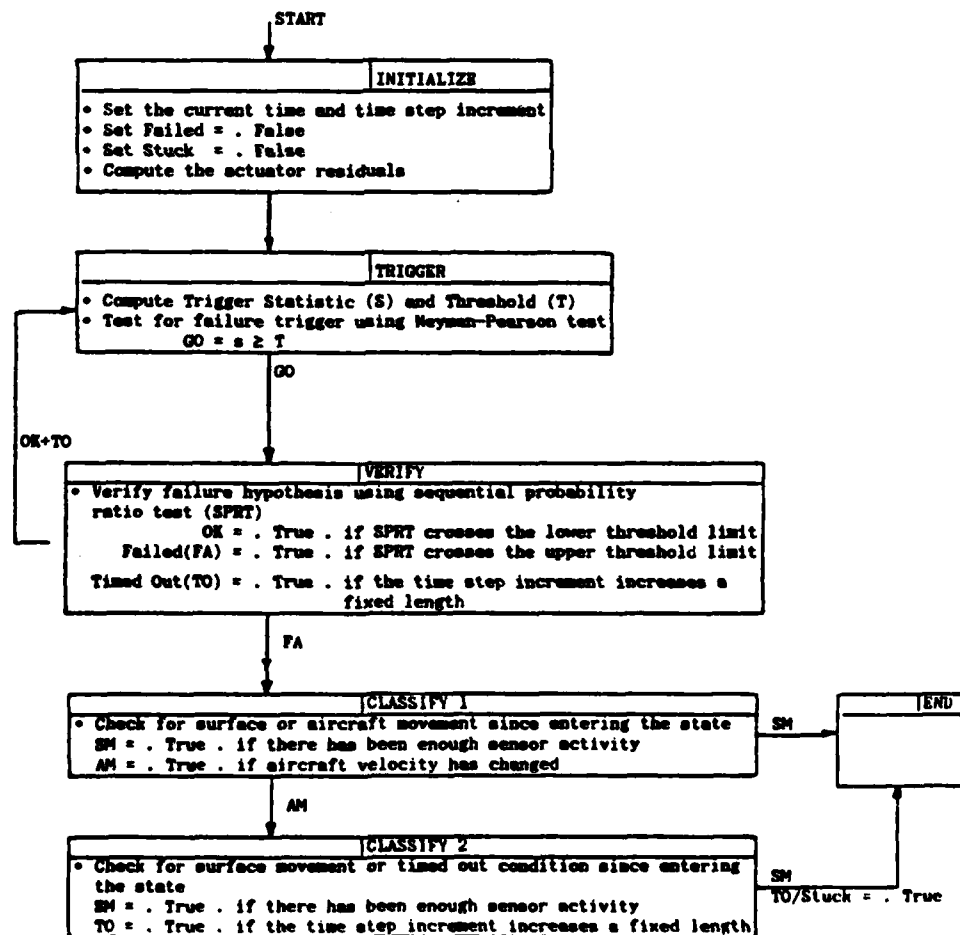
STUCK(I) = TRUE(FALSE) Indicates ith surface has been classified as stuck(floating)

The surface numbering convention is given in Table 1

TABLE 1

Surface Number	Description
1	Left Elevator
2	Right Elevator
3	Left Aileron
4	Right Aileron
5	Left Flap
6	Right Flap
7	Rudder

In this study it is assumed that the SIDC algorithm will be invoked at regular intervals of $T = 40$ msec. The results of the statistical tests for the current iteration control which test is performed next. Thus, each subsystem is a finite state machine whose flowchart is given in Fig. 5.



4.1 ACTUATOR RESIDUAL GENERATION

The transfer function of the actuator model is given by

$$\frac{\delta_E(s)}{\delta_C(s)} = \frac{364}{s^2 + 25.4s + 364} \quad (6)$$

where δ_C is the commanded deflection and δ_E is the estimated surface deflection. The z-transform of the actuator model given by (6) is represented in the difference equation form as

$$\delta_E(k) = 1.0501 \delta_E(k-1) - .362 \delta_E(k-2) + .1824 \delta_C(k-1) + .1296 \delta_C(k-2) \quad (7)$$

where k is the iteration step. The residual, γ , is the difference between the measured surface deflection, δ_A , and the estimated deflection, δ_E , and is given by

$$\gamma(k) = \delta_A(k) - \delta_E(k) \quad (8)$$

4.2 CALCULATION OF TRIGGER STATISTIC AND THRESHOLD

The trigger statistic and threshold is based on a fixed window length, N , and uses the Neyman-Pearson test. The trigger statistic is the absolute value of the residual average over the fixed window (moving window average, MWA) as shown in Fig. 6 and is given by

$$S(K) = |S_1(K)| \quad (9)$$

where

$$S_1(K) = \frac{1}{N} \sum_{i=0}^{N-1} \gamma(k-i) \quad (10)$$

Taking the z-transform of (10), we get

$$S_1(Z) = \frac{1}{N} \frac{Z^{N-1}}{Z^{N-1}(Z-1)} \gamma(Z) \quad (11)$$

Therefore

$$MWA(z) = \frac{S_1(z)}{\gamma(z)} = \frac{1}{N} \frac{z^N - 1}{z^N - z^{N-1}} \quad (12)$$

Eqn. (12) can be written in the difference equation form as

$$S_1(k) = S_1(k-1) + \frac{1}{N} (\gamma(k) - \gamma(k-N)) \quad (16)$$

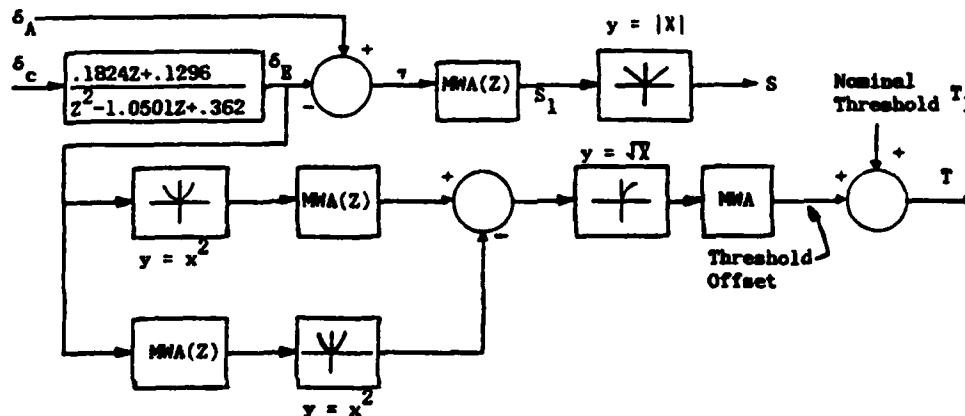


Fig. 6. Trigger State of the Stuck/Floating SDIC

The trigger threshold is computed by adding the threshold offset and nominal threshold value. The threshold offset is a measure of the error introduced in the residual due to modelling error of the actuator dynamics and is computed from the standard deviation of the estimated surface deflection as

$$\text{Standard Deviation of } \delta_E = \sqrt{E(\delta_E^2) - [E(\delta_E)]^2} \quad (17)$$

where $E(\cdot)$ means the expected value and is calculated by taking the average of the deflection over a fixed window length. The threshold offset is the average of the standard deviation over the fixed window as shown in Fig. 6. The nominal threshold is based on the following assumptions

1. The command deflection, δ_c , is noise free

2. The measured deflection, δ_A , is corrupted by an additive, white, Gaussian noise process with zero mean and standard deviation of 0.1 degree

3. The desired probability of false alarm, P_{FA} , is 10^{-4}

Using the normal distribution table [10] for $P_{FA} = 10^{-4}$, the value of the nominal threshold, T_1 , is given by

$$T_1 = 3.5 \frac{\sigma}{\sqrt{N}} = \frac{.35}{\sqrt{N}} \text{ degrees} \quad (18)$$

Therefore

$$T = T_1 + \text{Threshold offset}$$

Thus the logical GO signal for transition from trigger to verify state as shown in Fig. 5 is given by

$$GO = S \geq T$$

4.3 HYPOTHESIS TEST FOR VERIFY STATE

The statistic S_v and threshold T_v for the verify state is based on the sequential probability ratio test (SPRT) which is given by

$$\ell(k) = \sum_{i=0}^k \left(\gamma(i) - \frac{m}{2} \right) \frac{m}{\sigma^2} \begin{matrix} \text{Failed} \\ \text{OK} \end{matrix} t^1 \quad (19)$$

where

$k = 0$ is the time at which verify state is entered

$\ell(k)$ = log-likelihood ratio

m = mean of γ under failure hypothesis

σ = standard deviation of γ

$t^1 = \ln(\text{probability of detection/probability of false alarm})$

Using (19), if $T_1^v = \frac{\sigma^2}{m} t^1$, S_v is given by

$$S_v(k) = \left| \sum_{j=0}^k \tau(i) \right| - \frac{m}{2} \sum_{i=0}^k 1 \quad (20)$$

Let

$$\begin{aligned} \hat{S}_v(k) &= \sum_{i=0}^k \tau(i) \\ &= \sum_{j=0}^K \tau(k-j) \end{aligned} \quad (21)$$

Taking the z-transform of (21), we get

$$\frac{\hat{S}_v(z)}{\tau(z)} = \frac{z}{z-1} \quad (22)$$

Eqn. (22) can be written in the difference eqn. form as

$$\hat{S}_v(k) = \tau(k) + \hat{S}_v(k-1) \quad (23)$$

The nominal threshold, T_1^v , is based on the previous three assumptions alongwith the following two assumptions:

4. The desired probability of detection, P_D , is $1-10^{-4}$.
5. A surface is considered failed if the residual mean, m , is 0.1 degree.

Therefore

$$T_1^v = \frac{(0.1)^2}{0.1} \ln \left(\frac{1-10^{-4}}{10^{-4}} \right) = 0.92 \text{ degrees} \quad (24)$$

The details of the operations performed in the verify state is shown in Fig. 7

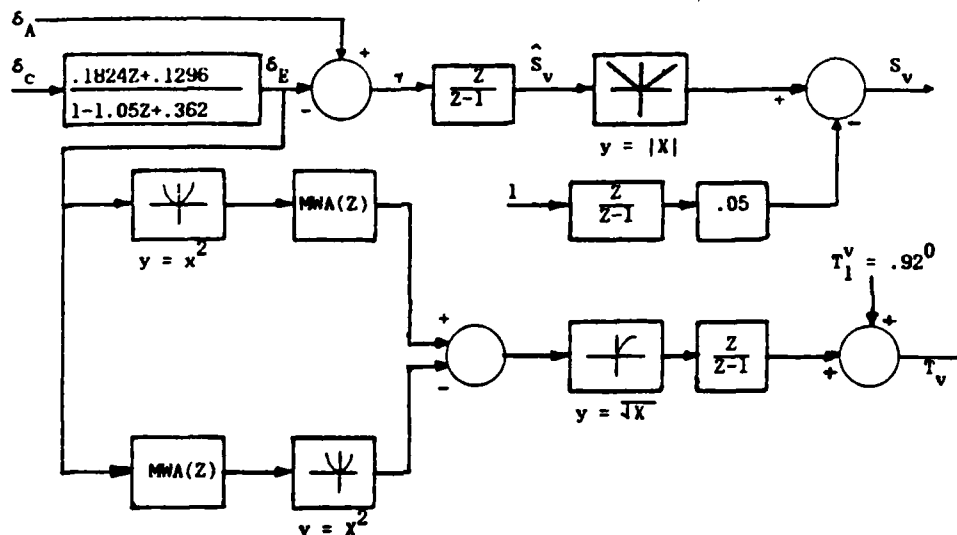


Fig. 7. Operations of VERIFY state

The decision rules for the verify state are thus given by

$$\begin{aligned} \text{OK} &= S_v \leq -T_v \\ \text{FAILED} &= S_v \geq T_v \\ \text{TIMED OUT} &= \text{Fixed Sample length} \end{aligned}$$

4.4. CLASSIFY I STATE

In this state two hypotheses, surface moved (SM) and aircraft moved (AM), are tested. The residuals $\tau_1(k)$ and $\tau_2(k)$ to test hypothesis SM and AM respectively are given by

$$\tau_1(k) = \delta_A(k) - \delta_A(0) \quad (25)$$

$$\tau_2(k) = \begin{cases} \alpha(k) - \alpha(0), & \text{for horizontal surfaces} \\ \beta(k) - \beta(0), & \text{for vertical surfaces} \end{cases} \quad (26)$$

where α is the angle of attack, β is the aircraft side slip angle and $k = 0$ is the time at which CLASSIFY I state is entered. The statistic corresponding to the two residuals are given by

$$S_1(k) = |\gamma_1(k)| \quad (27)$$

$$S_2(k) = |\gamma_2(k)|$$

The two decision rules are given by

$$SM = S_1 \geq T_1 \quad (28)$$

$$AM = S_2 \geq T_2$$

The thresholds, T_1 and T_2 , are calculated to ensure a reliable decision about the surface and aircraft movement. Since γ_1 is a Gaussian random variable with a standard deviation $\sigma_1 = 0.14$ degrees, T_1 is chosen to satisfy probability of false alarm as

$$T_1 = 3.5 \sigma_1 = 0.49 \text{ degrees} \quad (29)$$

If we make the assumption that the angle of attack, α , is corrupted by an additive, white, Gaussian noise process with zero mean and standard deviation of 0.001 radians, the standard deviation of γ_2 is given by

$$\sigma_2 = 0.0014 \text{ radians} \quad (30)$$

For reliable decision of aircraft motion, T_2 must satisfy

$$\begin{aligned} T_2 &= \max(T_1, 3.5 \sigma_2) \\ &= (.0086 \text{ radians}, .0014 \text{ radians}) \\ &= 0.0086 \text{ radians} \end{aligned} \quad (31)$$

Equations (25) and (26) are implemented as shown in Fig. 8 using z-transform as follows

$$\text{Let } \hat{\tau}_1(k) = \tau_1(k) - \tau_1(k-1) \quad (32)$$

Substituting (25) in (32), we obtain

$$\hat{\tau}_1(k) = \delta_A(k) - \delta_A(k-1) \quad (33)$$

Taking z-transform of (32) and (33), we get

$$\frac{\hat{\tau}_1(Z)}{\delta_A(Z)} = 1 - Z^{-1} = \frac{Z-1}{Z} \quad (34)$$

$$\frac{\tau_1(Z)}{\hat{\tau}_1(Z)} = \frac{1}{1-Z^{-1}} = \frac{Z}{Z-1} \quad (35)$$

Similarly

$$\frac{\hat{\tau}_2(Z)}{\text{angle}(Z)} = \frac{Z-1}{Z} \quad (36)$$

and

$$\frac{\tau_2(Z)}{\hat{\tau}_2(Z)} = \frac{Z}{Z-1} \quad (37)$$

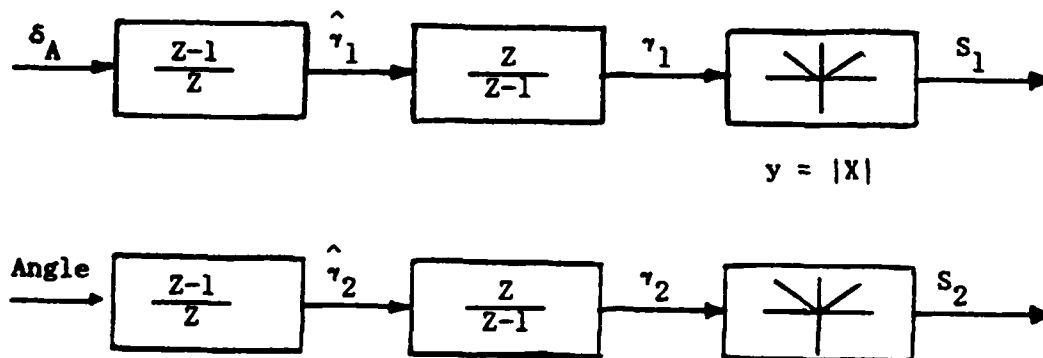


Fig. 8. Classify I State of Stuck/Floating SIDC

4.5 CLASSIFY II STATE

The algorithm for the CLASSIFY II state is similar to CLASSIFY I state and is shown in Fig. 9. The Algorithm reach CLASSIFY II state only if there has been a significant change in the aircraft velocity. The timed out (TO) condition occur if the decision rule is not satisfied in a fixed window e.g. 5. A Counter, TIME, is zeroed on entry into this state and is updated using the equation

$$\text{TIME}(K+1) = \text{TIME}(K) + 1 \quad (38)$$

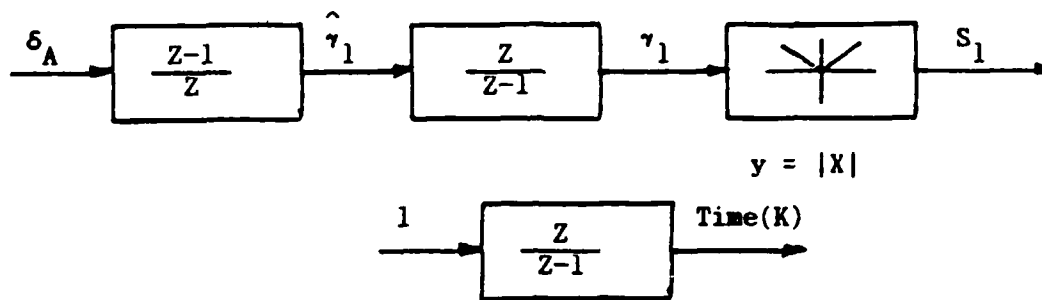


Fig. 9. CLASSIFY II State of Stuck/Floating SIDC

V. RECOMMENDATIONS

This research has focused upon the study of system impairment detection and classification algorithm of ALPHATECH, INC. which is capable of detecting, isolating and classification of control surface failures. This algorithm can detect the presence of stuck, floating and partially missing control surfaces and is based on decentralized residuals. The objective of this research was to develop an algorithm for the detection and classification of stuck and floating actuator failures of the unmanned research vehicle. This algorithm uses the log likelihood ratio and sequential probability ratio tests to test hypothesis for failure detection and isolation. A crucial step in this test is the selection of nominal threshold vlaue which is based on the model uncertainties (residual mean and standard deviation) and probabilities of detection and false alarm. The value for these parameters were arbitrarily selected in this study. For robust SIDC algorithm, a study should be made to find the effects of these parameters on the failure detection and whether it is possible to select

this threshold dynamically. In addition, the following recommendations are made for future research:

1. Program the SIDC algorithm developed in this report for URV and perform the simulation to test for stuck and floating surfaces.
2. Develop an algorithm for partially missing surfaces of the URV and perform simulation.
3. Develop an algorithm for SIDC based on hinge moment model and compare results.

REFERENCES

1. Rattan, K.S., "Study of Control Mixer Concept for Reconfigurable Flight Control System," Proceeding NAECON, May 1985, pp. 560-569.
2. Willsky, A.S., "A Survey of Design Methods for Failure Detection in Dynamic Systems," Automatica, Vol. 12, 1976, pp. 601-611.
3. Chow, E.Y. and A.S. Willsky, "Analytical Redundancy and the Design of Robust Failure Detection System, " IEEE Transaction on Automatic Control, Vol. AC-29, No. 7, July 1984, 603-614.
4. Pattipati, K.R., A.S. Willsky, J.C. Deckert, J.S. Eterno and J.L. Weiss, "A Design Methodology for Robust Failure Detection and Isolation, " 1984 American Control Conference, San Diego, CA, June 1984, pp 1755-1762.
5. Daly, K.C., E. Gai and J.V. Harrison, "Generalized Likelihood Test for FDI in Redundant Sensor Configuration," J. Guidance and Control, Vol. 2, No. 1, Jan-Feb. 1979, pp 9-17.
6. Deckert, J.C., M.N. Desai, J.J. Deyst and A.S. Willsky, "F8-DFBW Sensor Failure Identification Using Analytic Redundancy, " IEEE Transaction on Automatic Control, Vol. AC-23 No. 5, Oct. 1977, pp 795-803.
7. Van Trees, L. Harry, Detection Estimation and Modulation Theory, Part I, Wiley & Sons, Inc., 1968.
8. Wald, A., Sequential Analysis, Dover Publications, Inc., New York, 1947.
9. Craig, A.T. and R.V. Hogg, "Introduction to Mathematical Statistics", McMillian Publishing Co., New York, 1970.

1985 USAF-UES SUMMER FACULTY RESEARCH PROGRAM

Sponsored by the

AIR FORCE OFFICE OF SCIENTIFIC RESEARCH

Conducted by the

UNIVERSAL ENERGY SYSTEMS, INC.

FINAL REPORT

NONLINEAR ANALYSIS OF COMPOSITE SUPPORTS FOR ARMOR

Prepared by:	Hemen Ray
Academic Rank:	Assistant Professor
Department and University:	Mechanical Engineering Department North Carolina A&T State University
Research Location:	Flight Dynamics Laboratory/WPAFB
USAF Research:	James Hodges
Date:	31 July 1985
Contract No:	F49620-85-C-0013

NONLINEAR ANALYSIS OF COMPOSITE SUPPORTS FOR ARMOR

by

HEMEN RAY

ABSTRACT

Finite element solution for the deformed shape of the composite supports for armor indicates that the idealized single-degree-of-freedom model for the armor system is reasonable as a first approximation. In order to obtain more accurate and realistic results, the materials for the supports for armor are considered nonlinear because isolators are usually very nonlinear. The method of nonlinear analysis for composites as developed by Sandhu have been studied and will be used to analyze the problem.

ACKNOWLEDGEMENT

The author wishes to thank the United States Air Force Systems Command and the Air Force Office of Scientific Research for providing an opportunity to perform a very interesting and rewarding summer research at Wright-Patterson Air Force Base, Dayton, Ohio.

James Hodges of Flight Dynamics Laboratory provided excellent support, encouragement, and suggestions for the research work. The author is very grateful to R.S. Sandhu for help learning nonlinear response and failure analysis of composites.

I. INTRODUCTION

With the advancement of space and nuclear technology it is more likely that the conventional defense system will play a greater role than before. In this respect survivability of combat aircrafts is an important issue. Addition of armor, either integral or conventional, would improve the survivability of these aircrafts [1,2]. The conventional armor is attached to the aircrafts by appropriate supports (bracketry) [3].

Preliminary investigation [4] showed that the use of either specially designed composite or inclined bracketry would reduce the force transmitted to the aircraft. These type of bracketry allow the armor to rotate in its plane. Thus the impact energy is absorbed in the rotational direction in addition to the usual normal to the plane of the armor. Application of these type of bracketry could increase the ballistic limit, and thus improving the survivability of the combat aircrafts.

II. OBJECTIVES

The objective of the research effort is to perform nonlinear analysis for composite supports (bracketry) [see Reference 4] for the armor. Considering a single-degree-of-freedom model, and central normal impact of a projectile, analyze the composite bracketry by using nonlinear composite materials. The analysis with nonlinear composite materials will provide more realistic results.

III. LINEAR ANALYSIS

The stiffness k of each composite support (see Fig.1) in the vertical direction (z -direction) is

$$k = \frac{A}{l \bar{S}_{22}} \quad (1)$$

where A is the cross sectional area, l is the length of a composite support, \bar{S}_{22} is the transformed reduced compliance [5].

The kinetic energy of the system is given by

$$\begin{aligned} T &= \frac{1}{2} M \dot{z}^2 + \frac{1}{2} I_z \dot{\alpha}^2 \\ &= \frac{1}{2} M \left[1 + \frac{1}{3} \left(\frac{\bar{S}_{26}}{\bar{S}_{22}} \right)^2 \right] \dot{z}^2 \end{aligned} \quad (2)$$

where M is the mass of the armor, z is the displacement of armor in the vertical (z -direction) direction, I_z is the centroidal polar mass moment of inertia of the armor, α is the angular displacement of the armor in its plane (xy plane), \bar{S}_{22} and \bar{S}_{26} are the transformed reduced compliances. A dot (.) denotes derivative with respect to time t .

The potential energy U of the system is

$$\begin{aligned} U &= (4) \frac{1}{2} \int (\sigma_x \epsilon_x + \sigma_z \epsilon_z + \tau_{xz} \gamma_{xz}) dV \\ &= 2 \left[\bar{Q}_{11} n_1^2 + \bar{Q}_{66} n_2^2 + 2 \bar{Q}_{16} n_1 n_2 \right. \\ &\quad \left. + 2 \bar{Q}_{12} n_1 + 2 \bar{Q}_{26} n_2 + \bar{Q}_{22} \right] \left(\frac{z}{l} \right)^2 \end{aligned} \quad (3)$$

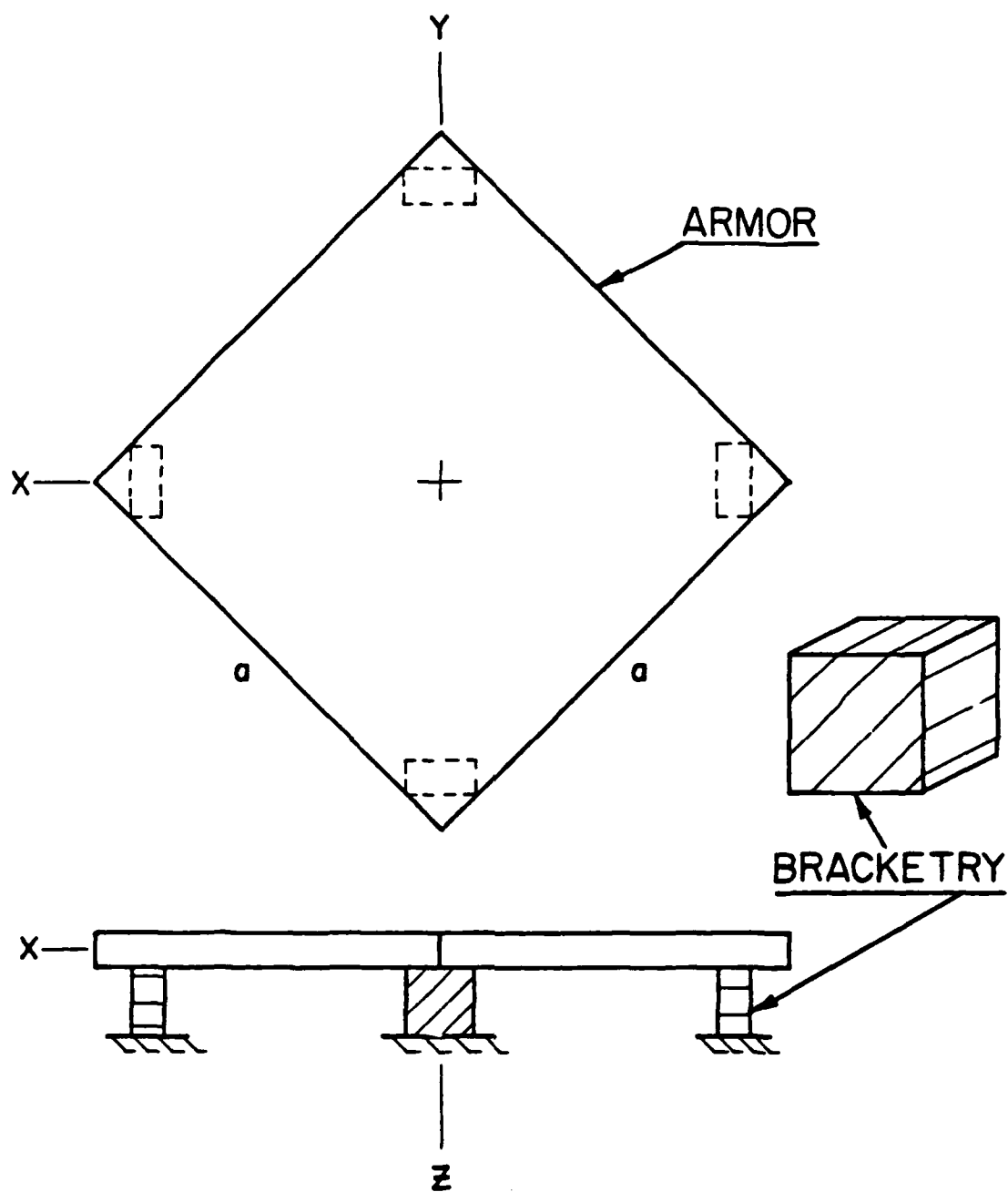


Figure 1. Composite Bracketry

where \bar{Q}_{ij} are the transformed reduced stiffnesses [5], and

$$\eta_1 = \frac{\bar{S}_{12}}{\bar{S}_{22}}, \quad \eta_2 = \frac{\bar{S}_{26}}{\bar{S}_{22}}. \quad (4)$$

Applying Lagrange's equation, and using (2) and (3) the differential equation of motion of the armor is

$$\ddot{z} + \omega^2 z = 0 \quad (5)$$

where ω is the natural frequency of the system, and is given by

$$\omega^2 = \frac{4A \left[\right]}{lM \left(1 + \frac{1}{3} \eta_2^2 \right)} \quad (6)$$

The quantity in the bracket [] is same as that in the equation (3).

By selecting appropriate value of the natural frequency (usually lower value), force transmitted to the aircraft can be reduced. Figure 2 shows the change in natural frequency with the fiber direction.

IV. FINITE ELEMENT ANALYSIS

The finite element analysis allows more realistic representation of the armor system. But an idealized single-degree-of-freedom representation of the armor system is useful to study the influence of some important parameters with

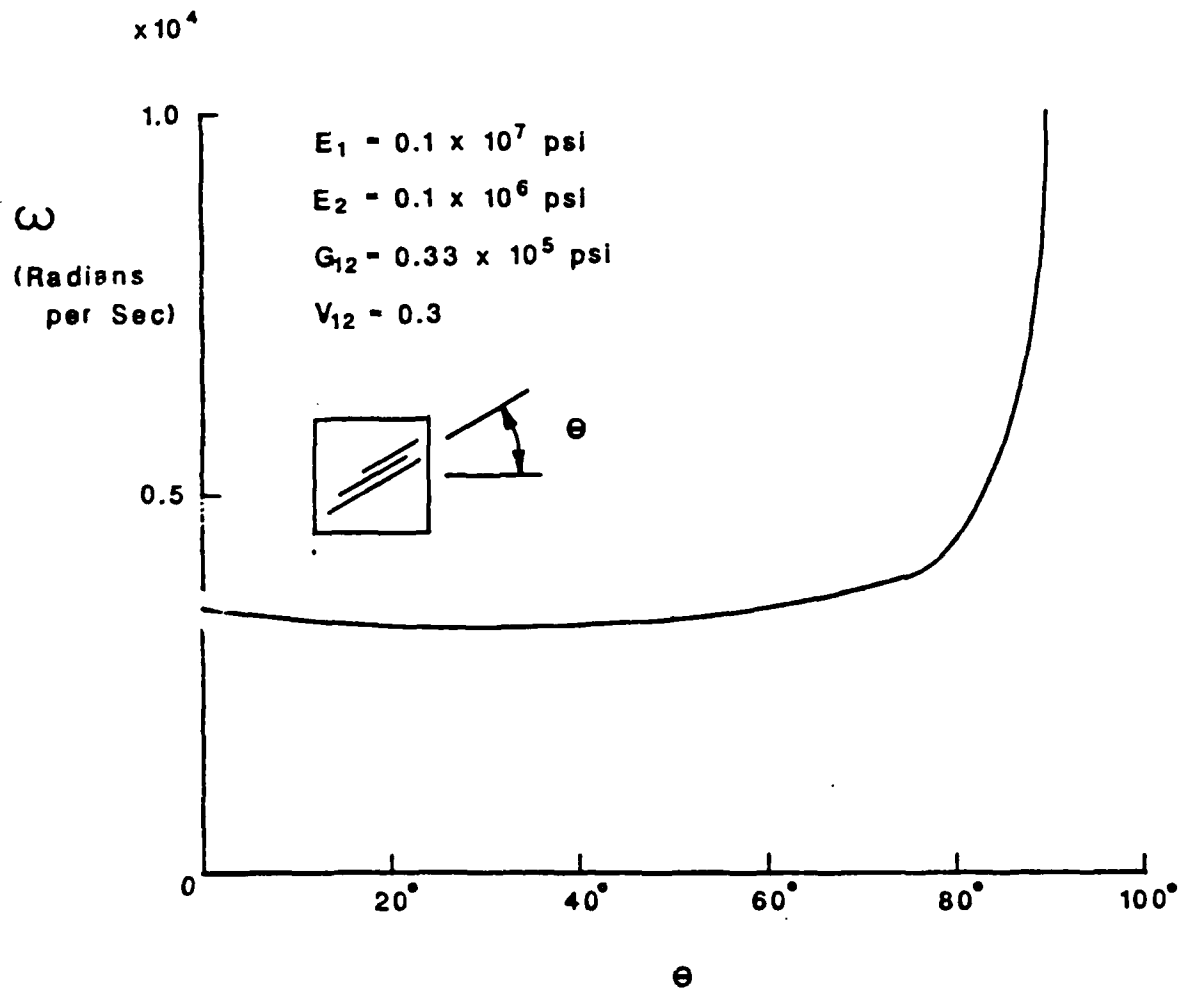


Figure 2. Natural frequency of the armor system vs. fiber direction.

simple means. In order to check the accuracy in modelling the composite supports by linear springs, a finite element program developed by Sandhu [6] is used. Figure 3 shows the deformed shape of a composite support. The ratio of the horizontal to the vertical displacements for node 65 is plotted (Figure 4). The deformation of node 65 is used to model the composite support by a linear spring. The results indicate that this type of idealization is reasonable.

V. NONLINEAR ANALYSIS

The materials for isolators (supports for armor) are usually nonlinear. Typical force-deflection curves for isolator materials [7] are shown in Figure 5. In linear analysis these curves are taken as straight lines. So to obtain more realistic solution to armor supports it is necessary to consider the nonlinearity in the materials for the supports for the armor. The analysis technique similar to that developed by Sandhu [8,9] will be utilized. The method of analysis is briefly described as follows. The incremental constitutive relations are used

$$[d\epsilon] = [S] [d\sigma] \quad (7)$$

where $[d\epsilon]$, $[d\sigma]$ are the strain and stress increments with respect to the material axes 1,2, and $[S]$ is the compliance matrix which depends on the strains $[\epsilon]$. The incremental stress-strain relation is given by

$$[d\sigma] = [Q] [d\epsilon] \quad (8)$$

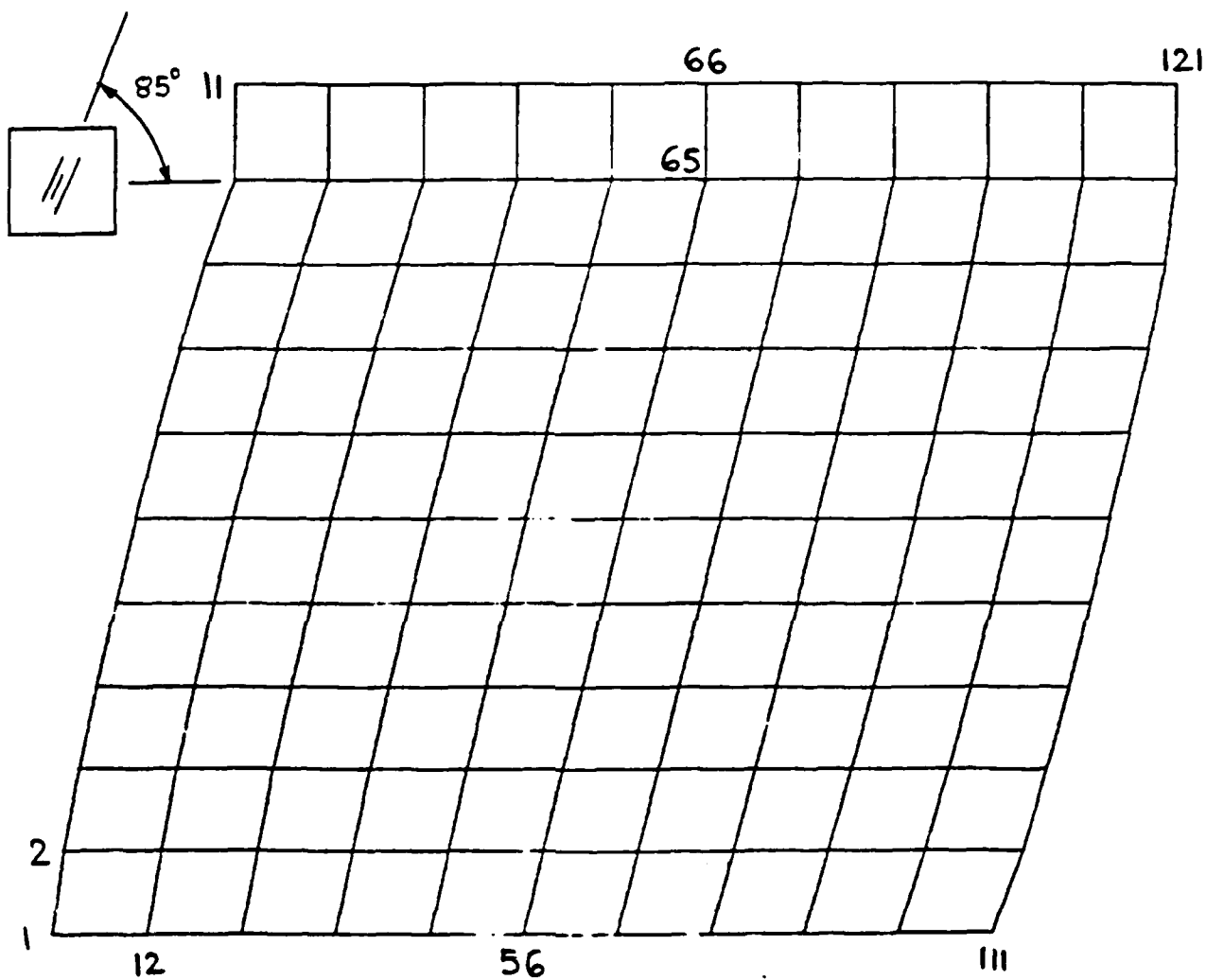


Figure 3. Deformed shape of a composite support.

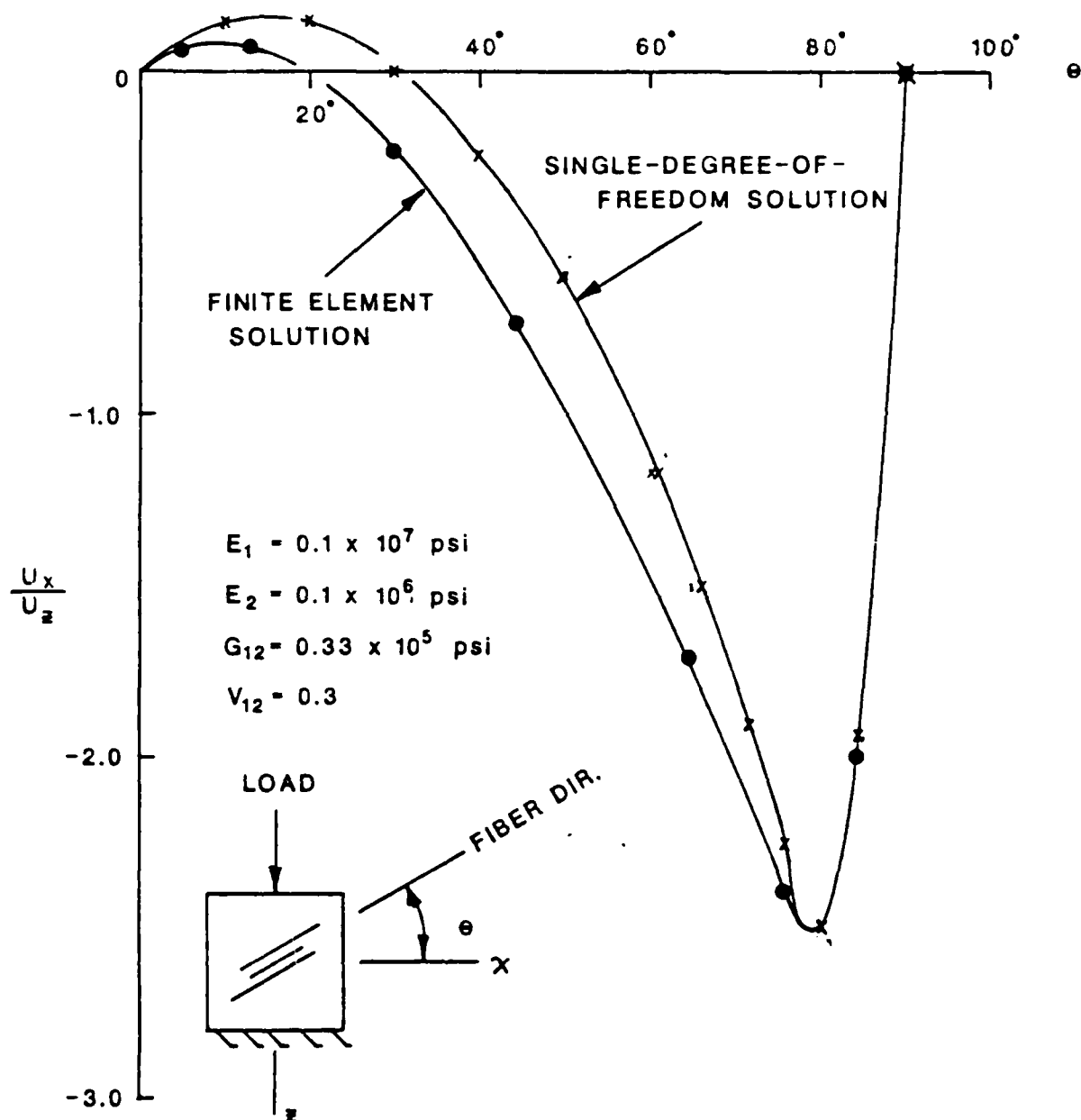


Figure 4. Ratio of the horizontal displacement (x-dir.) to vertical displacement (z-dir.) vs. fiber direction.

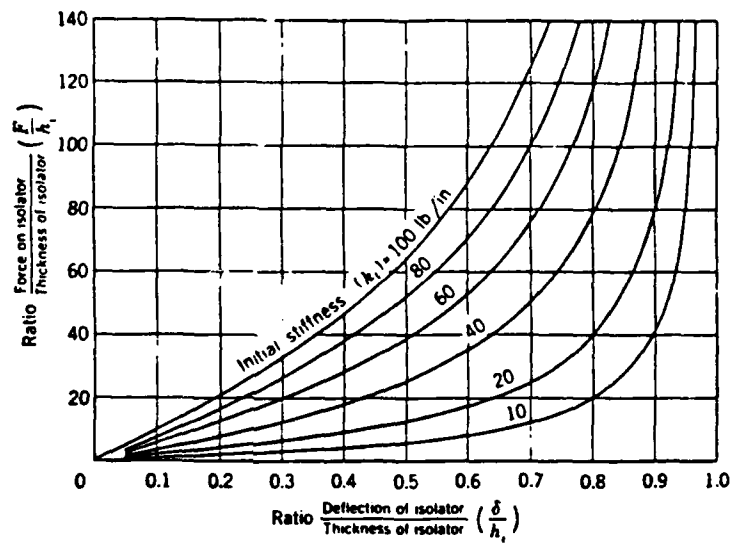


Figure 5. Typical force-deflection curves for isolators [Reference 7].

AD-A166 178

UNITED STATES AIR FORCE SUMMER FACULTY RESEARCH PROGRAM

3/11

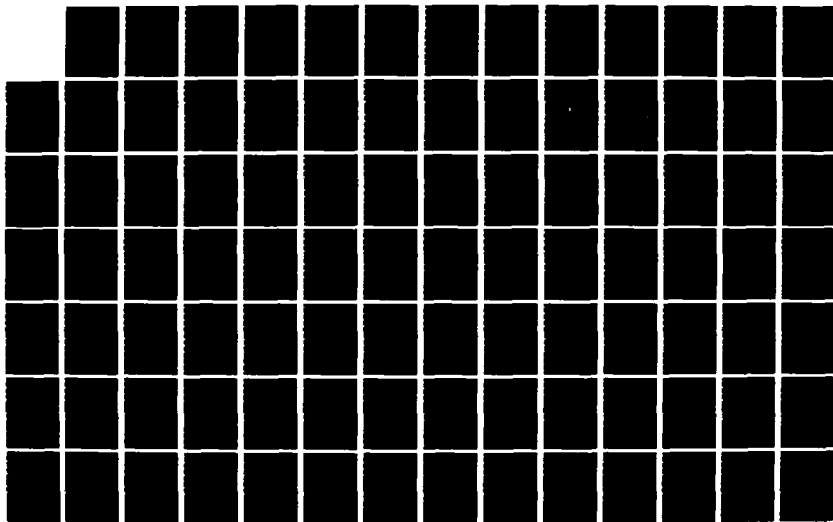
1985 TECHNICAL RE (U) UNIVERSAL ENERGY SYSTEMS INC
DAYTON OH R C DARRAH ET AL DEC 85 AFOSR-TR-86-8141

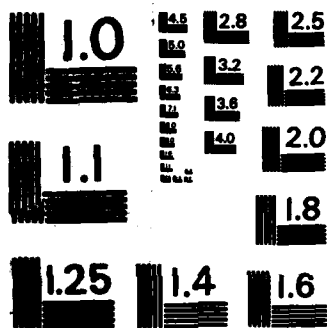
UNCLASSIFIED

F49620-85-C-0013

F/G 5/9

NL





MICROCOPY RESOLUTION TEST CHART
NATIONAL BUREAU OF STANDARDS-1963-A

where $[Q]$ is the stiffness matrix.

The stress and strain increments in two coordinate system (material coordinates 1,2, and body coordinates x,z) are related by a transformation matrix $[T]$, i.e.

$$\begin{aligned} [d\sigma] &= [T] [d\bar{\sigma}], \\ [d\epsilon] &= [T] [d\bar{\epsilon}], \end{aligned} \quad (9)$$

where $[d\bar{\sigma}]$, $[d\bar{\epsilon}]$ are the stress and strain increments with respect to the body coordinates x,z - horizontal, vertical directions.

The stress-strain data for the materials for the supports are represented by a piecewise cubic spline interpolation functions. This is used to compute the tangent moduli for the materials. In computing the moduli the equivalent strains are used to account for the effects of biaxial stresses

$$\begin{aligned} d\epsilon_1|_{eq.} &= \frac{d\epsilon_1}{1 - \nu_{12} B}, \\ d\epsilon_2|_{eq.} &= \frac{d\epsilon_2}{1 - \frac{\nu_{21}}{B}}, \end{aligned} \quad (10)$$

where ν_{12} is the major Poisson's ratio and $B = d\bar{\epsilon}_2/d\bar{\sigma}_1$.

The computational scheme is as follows:

1. For an increment of time dt , solve numerically for an increase in the vertical deflection dz from the differential equation (5).
2. Compute the average strain increment $d\bar{\epsilon}_z$ in the vertical direction (z-direction).
3. Compute the stress increments $[d\sigma]$ with respect to the body coordinates x, z .
4. Obtain the stress and strain increments $[d\sigma]$, $[d\epsilon]$ in the principal material directions 1,2 by using equation (9).
5. Add half of the strain increment obtained in step 4 to the total strain obtained before starting a set of iterations. Corresponding to this resulting strain compute the tangent moduli for the material.
6. Using the tangent moduli obtained in step 5, compute the reduced stiffnesses $[\bar{Q}]$ and compliances $[\bar{S}]$. Using these values solve for the increment in vertical deflection dz from the differential equation (5) for the same dt as in the step 1. In solving the differential equation proper initial conditions should be used.
7. Repeat the steps 1 through 6 until the difference in the values of dz in two consecutive cycles is within a specified tolerance.

VI. RECOMMENDATIONS

Since the properly designed supports (bracketry) for armor would absorb more impact energy, further research should be directed to investigate their potential application.

- * The material for the supports should be considered nonlinear which is more realistic and nonlinear analysis should be performed.
- * The armor should be considered elastic instead of rigid.
- * Finite element solution should be obtained for more realistic results.
- * The influence of duration of impact should be studied to obtain the optimum specifications for the supports for the armor.
- * Perform ballistic experiments with composite and inclined bracketry for various fiber directions and angles of inclination.

REFERENCES

1. Buxton, R., and Verette, R., "Analytical and Experimental Development of Design Techniques for the Installation of Parasitic Armor," AFFDL-TR-68-26, Vol. I, Wright-Patterson Air Force Base, Ohio, March 1968.
2. Hodges, J, and Penderson, A.H., "The Design and Test of an Integrally Armored Cockpit," MCAIR 71-019, McDonnell Aircraft Co., St. Lois, Mo, Third Aircraft Design and Operations Meeting of AIAA, 1971.
3. Hodges, J., "Design Techniques for Installing Parasitic Armor," AFFDL-TR-68-5, Wright-Patterson Air Force Base, Ohio, February 1968.
4. Ray, H., "Analysis of Armor Bracketry," 1984 USAF-SCEEE Summer Faculty Research Program, Flight Dynamics Laboratory, Wright-Patterson AFB, July 1984.
5. Jones, R.M., Mechanics of Composite Materials, McGraw-Hill, 1975.
6. Sandhu, R.S., Computer program for finite element analysis of composites under plane stress (unpublished), Flight Dynamics Laboratory, Wright-Patterson AFB, 1985.
7. Crede, C.E., Vibration and Shock Isolation, Wiley, 1951.
8. Sandhu, R.S., "On Design of Off-Axis Specimens," AFWAL-TR-84-3098, Flight Dynamics Laboratory, Wright-Patterson AFB, March 1985.
9. Sandhu, R.S., "Nonlinear Behavior of Unidirectional and Angle-Ply Laminates," Journal of Aircraft, Vol. 13, No. 2, pp.104-111, February 1976.

1985 USAF-UES SUMMER FACULTY RESEARCH PROGRAM/
GRADUATE STUDENT SUMMER SUPPORT PROGRAM

Sponsored by the
AIR FORCE OFFICE OF SCIENTIFIC RESEARCH

Conducted by the
UNIVERSAL ENERGY SYSTEMS, INC.

FINAL REPORT

DIAGNOSTICS OF SOLID PROPELLANT COMBUSTION

Prepared by:	John P. Renie* and Brian K. McMillin**
Academic Rank:	*Assistant Professor and **Graduate Research Assistant
Department and University	Mechanical and Industrial Engineering University of Illinois at Urbana/Champaign
Research Location:	Air Force Rocket Propulsion Laboratory/DYCR
USAF Research:	Mr. David P. Weaver
Date:	24 September 1985
Contract No:	F49620-85-C-0013

DIAGNOSTICS OF SOLID PROPELLANT COMBUSTION

by

John P. Renie and Brian K. McMillin

ABSTRACT

This report details the summer activities at the Air Force Rocket Propulsion Laboratory of a Summer Faculty Fellow and a Graduate Student in the field of diagnostics as applied to the study of solid propellant combustion. At the onset of the research effort, a detailed literature review of diagnostic techniques was pursued with particular emphasis placed on those methods that are optical in nature, and therefore, non-intrusive. Also, strong emphasis was directed to the laser-based techniques currently being used to determine both temperature and species concentration in a reactive system such as the combustion zone above a deflagrating solid propellant surface. Experimental investigations were conducted in the AFRPL servo-controlled combustion bomb which permits extended observation of the combustion event. A particular class of solid propellant formulations was selected for investigation - this being a series of AP/HTPB composite propellants wherein the oxidizer particle size distribution was carefully monitored. In summary, the laser-based diagnostic technique referred to as laser-induced fluorescence (LIF) is considered to be a good candidate to use to determine temperature and species data in solid propellant flames, however, continued research is warranted since the reaction zone is very complex with quantitative analysis of such data suspect at best. In addition, spectroscopic emission data for the radical species involved in the combustion reaction can easily be obtained with such data lending credence to the claim that reactions are occurring at a much larger distance from the propellant surface than theoretically modeled.

ACKNOWLEDGEMENTS

The authors would like to acknowledge the support of the Air Force Systems Command, Air Force Office of Scientific Research and Universal Energy Systems for their generous support of this summer research program. The personnel at the Air Force Rocket Propulsion Laboratory are to be commended for making the experience both enjoyable and intellectually stimulating. In particular, we would like to thank our colleagues in the Combustion Laboratory who provided us with both assistance in experimentation and lively discussions concerning the research undertaken. Included in this list are Jay Levine, Dave Weaver, Dave Campbell, Tim Edwards and Sue Hulsizer. Laboratory assistants Ish Singh and Melissa Rose are also thanked for their data analysis assistance. Finally, we would like to acknowledge Wayne Roe of AFRPL and Rodney Derrah and Sue Espy of UES for their part in managing this program.

I. INTRODUCTION

In the study of solid propellant combustion, the reaction zone above the deflagrating propellant surface is a very complex admixture of competing processes. Within this region, gases from the surface pyrolysis/decomposition reactions are continuing to react as well as diffusing together to take part in subsequent chemical reactions. In composite propellant combustion, various flames can be present corresponding to the temperatures and pressure within this zone and the continuously changing structure of the surface. Over the past couple of decades, numerous researchers [1,2] have attempted to model these processes in the mean with mixed results. At a recent workshop [3], representatives from the propulsion community attempted to present a post-mortem on solid propellant modeling with emphasis placed on non-metallized, composite solid propellants response functions - both steady and non-steady behavior. Much of the concern of this workshop dealt with the validity of the assumptions or approximations previously invoked in detailing the flame zone structure above the deflagrating surface. The thesis of the first author [4] provides an excellent example of the type of modeling that has recently been associated with composite solid propellants.

At the workshop, the general consensus from the community was that one of the major unresolved problems to date is how the composite propellant microstructure, through the populations of various oxidizer particle sizes and states - inherent in the formulation of heterogeneous propellants - is able to produce a coherent macroscopically observable response. Along with a call for a good, systematic response function data base to be used to evaluate present as well as future modeling efforts, there was the additional request for more diagnostic information involving the microstructure and the reaction zones present above the surface.

It is in this light, that an ambitious attempt to seek out existing and/or new techniques to provide such information has been embarked upon. With the advent of the high powered, continuous and pulsed laser, many new combustion diagnostic techniques have been made available to the researcher in the ultimate quest of obtaining temperature and radical species concentration data within the combustion regions. Since these techniques are optical, they have the added benefit of being non-intrusive in nature, that is, the flow is not disturbed because of the observation. Intrusive techniques such as the insertion of thermocouples or gas sampling probes have the inherent drawback that the flow is disturbed or altered in the process of sampling. It is therefore, the objective of this summer's research to investigate the possibility of using such optical techniques to obtain desired flow properties in solid propellant flames. The reason that the Air Force Rocket Propulsion Laboratory (AFRPL) was selected by the authors was that such

research is currently being conducted by colleagues employed there. Additionally, the Combustion Laboratory at AFRPL has a servo-controlled combustion bomb in which samples of solid propellant can be burned and observed for a significant portion of the burning process. Access to a pulsed-dye laser/spectroscopic analyzer system was also considered necessary along with the availability of particular solid propellant formulations. In the following sections, the efforts expended by the authors are summarized with significant results highlighted and recommendations for future research presented.

II. OBJECTIVES OF THE RESEARCH EFFORT:

It was stated above that one of the primary purposes of this summer's research activity at the Air Force Rocket Propulsion Laboratory was to assess the feasibility of using laser-based diagnostic techniques in the study of solid propellant combustion. In this light, it was our goal to accomplish the following tasks in an effort to achieve this primary objective:

- o Study the pertinent literature on classical emission/absorption spectroscopy of atomic and molecular species concentrating on radicals present within solid propellant flame systems (OH, CH, CN, etc.).
- o Survey the current literature associated with combustion diagnostics employed within laboratory flames with special emphasis on solid propellant systems.
- o Familiarization with basic laser theory and operation with special emphasis on tunable pumped dye lasers used typically in laser-based diagnostic applications.
- o Familiarization with the theory and operation of the optical multi-channel analyzer presently employed by the AFRPL Combustion Laboratory to acquire spectroscopic data from both laboratory and solid propellant flames.
- o Select propellant formulations to be analyzed in the servo-controlled combustion bomb with an analysis of the feasibility of performing emission and/or laser-induced fluorescence measurement to obtain temperature and species concentration data.

In the following sections, the activity performed by the authors to achieve the above objectives will be briefly discussed. This will be followed by recommendations of future research based on our findings.

III. BRIEF LITERATURE REVIEW:

The quantity of literature pertaining to the use of classical emission/absorption spectroscopy of atomic and molecular species in the study of combustion radical temperature and concentration determination is enormous. However, there are a few classical references that were studied [5-10] at the onset of this research effort. Among these, the references by Herzberg and Gaydon gave excellent detail into the complexity of the problem at hand. It should therefore suffice to say that within combustion systems, the molecules in the gaseous state have energy values limited to a number of possible values, that is, their energy is quantized. Therefore, the wavelengths at which molecules can emit or absorb are limited to a relatively small number of lines in the electromagnetic spectrum. Since multi-atomic molecules can possess energy in any of various forms (electronic, vibrational, or rotational) molecular spectra emitted from typical species can be attributed to various energy transitions each being quantized.

Spectra in the visible and ultra-violet regions are generally due to changes of electronic energy. That is, a transition from one configuration of electrons about the nucleus to another configuration. Such a change determines the position of the band system in the electromagnetic spectrum. With accompanied changes in vibrational energy, the position of individual bands within the band system is determined. Finally, the fine structure of the individual band is a result of small changes in rotational energies. For example, one of the major bands observed for the OH radical is in the ultraviolet centered about 3064 Angstroms [6]. This band system corresponds to transitions from the lowest level vibrational states (0,0) of the $2\Sigma^+$ excited electronic state to the 2Π electronic ground state. Since OH plays an important role in the oxidation mechanism for carbon monoxide to carbon dioxide, the emission/absorption of this radical species has been studied extensively within this band system. The OH emission from a solid propellant flame at pressure is reported in a later section of this report. Additionally, laser-induced fluorescence of the OH radical within this band system has also been quite popular recently. For fluorescence, pumping within this area of the spectra can easily be accomplished using the pumped dye laser system currently available at the AFRPL.

Five papers [11-15] provide an excellent overview of laser-based diagnostics as applied to combustion systems. The latter of these recently appeared in the Twentieth Symposium

(International) on Combustion. This paper provides summary tables showing how laser techniques have been applied for measurements of temperatures, pressures, densities, species concentration, density gradients, velocity components, particle sizes, flow visualization, and velocity-density correlations. Additionally, tables are provided that summarize the current state-of-art of available laser systems as well as photo-detector equipment. The first two references provide more technical information about different diagnostic techniques concentrating on Raman and fluorescence methods. References 13 and 14 are compilations of the numerous studies conducted by various researchers in the combustion field. These two references summarize the magnitude of the research currently being conducted in this field. The final conclusion drawn by these reviews, is that both temperature and species concentration measurements are quite feasible using laser-based diagnostic equipment within combustion systems of current interest. However, it becomes quite evident that the analysis of acquired spectroscopic data is by far the crucial limiting step in all of the studies cited. After reading these references, we decided to continue on in our effort to assess applicability of such techniques within solid propellant combustion systems.

In reviewing the solid propellant combustion spectroscopy literature, it was clear that the environment being examined was not as nice as many of the "clean flame" studies previously reviewed. In one of the earliest papers on the subject, Rekers and Villers [16] presented emission spectra for AP-based composite propellant burned in a unique combustion/positioning device that enabled detailed exposure of the flame zone throughout the complete burning time of a 72 inch length of propellant. As one can judge from the data on this reference, the field of emission spectroscopy of solid propellants is not new. However, at the present time, only the researchers at the AFRPL [17-19] are actively engaged in spectroscopic analysis of actual solid propellant burning. This has been made possible by the use of a servo-controlled combustion bomb which is described later. Only by holding the surface of the deflagrating propellant surface stationary can extended periods of observation be permitted. It should be mentioned, however, that researchers with the Army Ballistic Research Laboratory in Maryland [20,21] are conducting laser excited fluorescence (LEF) measurements within a laboratory scale $\text{CH}_4/\text{N}_2\text{O}$ flame to determine both temperature and radical species concentration profiles. Such investigations in a "clean flame" environment are being conducted to elucidate the flame chemistry taking place in nitramine-based solid propellants; however, data is only being acquired at atmospheric pressures.

Even though the multitude of laser-based diagnostic studies appearing in the literature will not be reviewed in this paper, there is one such reference that is deemed necessary to discuss because a technique referred to as planar laser-induced fluorescence (PLIF) is detailed. This

technique is currently being investigated by researchers at the AFRPL [18-19] as being an excellent diagnostic tool in the study of solid propellant combustion. In this paper, Kychakoff and his colleagues at Stanford [22], detailed the use of PLIF for simultaneous multiple-point measurements of OH in various combustion flow systems. In their study, the laser wavelength was tuned to the $Q_1(6)$ line of the $A^2\Sigma^+(v'=0) \leftarrow X^2\Pi(v''=0)$ electronic OH transition. Laser powers of 2 mJ/pulse with a bandwidth of approximately 0.4 cm^{-1} were obtained with a pulsed dye laser, pumped by a Nd:YAG laser with subsequent frequency doubling. A planar sheet of 200 μm width was imaged through various types of flames. Fluorescence radiation was collected off-axis and focused onto the front of an image-intensified camera with subsequent digitization and analysis. Their work emphasized that PLIF is especially well suited for the visualization of radical species concentrations because it is non-intrusive and highly sensitive. The radical species OH was selected for study because it plays an important role in the oxidation of many hydrocarbons. They concluded that PLIF's chief value is in its ability to visualize relative species distributions in planar cross-sections of a particular flowfield and not the ability to obtain absolute measurements. Additionally, the acquisition of simultaneous multiple-point measurements can be used to test models describing interactions between the chemistry and fluid mechanics of combustion phenomena.

In order to familiarize ourselves with basic laser theory and operation, we studied various references. Among these references, the textbook by O'Shea [23] gave a good overview of the physical theory needed to understand lasers emphasizing the devices themselves, their construction, and their applications. We focused particular interest to the theory and operation of tunable, pumped dye lasers since these devices are currently being used for laser-induced fluorescence studies of radical species in the ultraviolet region of the spectra. Furthermore, the AFRPL Combustion Laboratory employs such a laser system in their ongoing solid propellant spectroscopic studies [18,19]. In order to probe additional radical species at higher pulse power in the lower wavelength regions, the AFRPL has acquired an excimer laser system. However, this system was not operational during the summer months, but we did investigate its potential merits.

In the following section, the experimental equipment available to the authors at the AFRPL is briefly described. Such equipment was used to obtain emission/fluorescence results discussed in a subsequent section.

IV. EXPERIMENTAL INVESTIGATION

The experimental apparatus used in this research was originally designed to simulate the conditions inside a solid rocket motor as closely and accurately as possible. The apparatus is composed of a high pressure combustion bomb equipped with a servo-controlled propellant feed system along with an optical and data acquisition system. This experimental device will be briefly described herein with the reader referred to Refs. [24] and [25] for a more detailed description.

The combustion bomb employed is similar in many respects to "high pressure window bombs" used in other solid propellant combustion studies. The bomb design incorporates four 3.8 cm diameter, 2 cm thick sapphire windows to provide optical access for wavelengths between .15 and 6 microns. A variable pressure (1000 psig maximum) nitrogen purge is employed to both pressurize the test chamber and expel the combustion gases and residue smoke particles, thus minimizing optical interference of the burning propellant surface. One unusual feature of this combustor design is its ability to keep the burning surface at a fixed height relative to the optical collection volume. This feature permits an increased examination time of a specific region of the propellant flame - a crucial requirement for the proposed flame chemistry analysis. The height of the surface is maintain by pushing the propellant up as it burns by means of a piston connected to an electronically controlled stepping motor. An automatic/manual switch is incorporated to permit initial setup and also permit the bomb to function in the conventional manner; that is, with the piston fixed as the propellant burns down. The combustor and propellant feed system are illustrated in Fig. 1.

The servo-control for the propellant feed system is based on the feedback from a measured intensity ratio of a positioning laser beam and a constant intensity light source. A Spectra-Physics model 125A laser beam is focused to spot of approximately 50 micron diameter just above the propellant surface and then passes onto a photo-diode detector. The control system is designed to maintain a constant partial blockage of this positioning beam (98% in this experiment) during the automatic mode of operation. The stepping rate of the system, i.e. the propellant feed rate, is increased automatically when the tracking beam becomes greater than prescribed equilibrium intensity. Conversely, the propellant feed rate is decreased when the tracking beam intensity falls below the equilibrium point. A narrow band-pass filter (1nm centered at the 632.8 nm He-Ne laser wavelength) is located between the combustion bomb and the photo-diode detector to reduce possible interference from either room light or combustion radiation. The system includes two digital meters which provide readings of the displacement of the piston during an elapsed time interval. During operation in the automatic mode, the quotient of

these two readings indicates the measured burn rate for a particular propellant run.

The optical system consists of a pair of 25 cm focal length lenses and two mirrors which collect, collimate, and focus the radiation emitted from the flame within the combustor onto the entrance slit of a SPEX 1877 Triplemate Spectrograph. The mirrors served to turn, as well as, rotate the horizontal flame image ninety degrees for projection onto the vertical entrance slit of the spectrometer. A Hughes 5 mW He-Ne laser is used to align the optical system. The distance between the alignment beam and positioning beam defines the investigated height above the propellant surface. The ability to adjust this height provides a means of both spatial and temporal resolution of species concentration and temperature.

The spectrometer is used to isolate a fixed spectral range and resolution of the flame emission. The entrance slit chosen was 20 microns wide by 10 mm high which provides a very fine spatial resolution of emission intensity above the surface. The flame image is dispersed within the spectrometer through a selected grating with a density of 1200 grooves/mm and then projected onto an EG&G/PAR Model 1420 Reticon photo-diode array detector with 700 light sensitive elements (pixels). The Reticon is controlled by a EG&G/PAR Model 1218 solid state detector controller and data is collected and analyzed by an EG&G/PAR OMA II. The experimental apparatus including the combustor, alignment and positioning lenses, optical system and the data acquisition/analysis system is shown schematically in Fig. 2.

In the laser-induced fluorescence studies described herein and in Refs. 18 and 19, a Nd:YAG pulsed laser (DCR-1) manufactured by Quanta-Ray with an Electronic Line Narrowing (ELN-1) system retrofitted to it is employed. The laser pulse from this system is passed through a frequency doubling harmonic generator and a prism harmonic separator prior to pumping a Quanta-Ray dye laser (PDL-1) system. The output of the dye laser is then directed through a Quanta-Ray wavelength extension (WEX) system for frequency doubling/tuning prior to passing into the combustion volume. In the schematic presented by Fig. 2, the pulsed laser output is directed into the combustion bomb with subsequent fluorescence emission collected off-axis by the spectrometer/OMA II system. The pulsed dye laser system in the present configuration is capable of generating up to 6-7 mJ pulses of 10 nanosecond duration at a 10 hertz repetition rate.

The detector controller is capable of data collection with both variable signal integration time as well as a variable number of scans. For example, with the sodium emission measurements described subsequently, the controller was set to scan only 60 pixels corresponding to a 21 Angstrom bandwidth centered near 589.0 nm with the selected grating. The signal integration

time, that is, the time the signal is collected before the array is scanned, was set at 0.0339 sec/scan and 150 scans were collected sequentially in each run. The signal integration time was chosen to provide a very high signal intensity to background noise ratio without saturating the Reticon. The background noise was not subtracted from the collected emission due to the computational time involved but was typically only 5-10% of the maximum intensity of any particular run.

In the sodium emission measurements described in the next section, the propellant feed system was operated in the manual mode rather than in the automatic feed mode. This procedure allowed the Na emission intensity to be recorded as a function of height above the surface by relating the individual scan times to the respective propellant burn rate. The burn rates for these propellants, however, were determined separately by using the automatic propellant feed system and recording the displacement and duration measurements from the LED displays.

It was decided that in order for emission data collected from the combustion bomb to be significant, that a series of monodisperse oxidizer propellant formulations be investigated. Since emission collected off-axis is an average over the entire surface, the behavior of the surface should be statistically uniform in both time and space. By employing monodisperse, or all one size, oxidizer grinds, the flame information collected at various heights above the surface can be correlated to the oxidizer particle size involved. Therefore, the propellants used in this study were "academic" in nature in that they were formulated with only one characteristic variable - the oxidizer particle size distribution. The propellants selected were composite, non-aluminized, uncatalyzed, HTPB binder, ammonium perchlorate (AP)-based propellants. They were formulated with 80 percent solids (AP particles) and identical in all respects except for particle size. Three propellants were mixed by the Propellant Lab at AFRPL Area 1-30 under the supervision of David Ferguson.

The first propellant, designated CI-3, was a unimodal propellant formulated with 20 micron AP particles as delivered by the manufacturer. The second propellant, CI-4, was also unimodal being formulated with 200 micron AP particles which were sieved through 300 and 150 micron Tyler Standard Screen Scales manufactured by Van Waters and Rogers, Inc. The sieves were shaken on a CENCO-MEINZER Sieve Shaker manufactured by Central Scientific Company. The objective of sieving the oxidizer particles was to narrow the particle size distribution and make a more truly monodisperse propellant. The third propellant, CI-5, was a 20/200 micron bimodal blend propellant and was formulated with both the "as received" 20 micron and the "sieved" 200 micron AP. The purpose for studying these propellants was to verify that the 20 micron unimodal

propellant reached its maximum flame temperature closer to the surface than the 200 micron unimodal propellant and to observe any effects in the bimodal propellant which could be attributed to the oxidizer particle size combination.

The propellant strands burned in these experiments were "plugged" (approximately 6 mm in diameter) from a half gallon rectangular block of cured propellant and cut to lengths of about 3.5 cm. The strands were water washed just prior to burning to dissolve the loose AP surface particles thus preventing side burning during the test. The strands were positioned at a height of 7-8 mm above the point at which the alignment beam was just completely blocked. This position was chosen so that a few of the initial scans showed little or no sodium emission and the intensity gradient above the surface would be clearly discernible. Even in the initial scans, some sodium emission was observed but was attributed to reflections within the combustor or an artifact of hot gases swirling in the chamber from the ignition sequence.

For the sodium tests, the propellants were burned at a pressure of 100 psig with at least one minute of nitrogen purge to ensure that all air has been expelled from the combustor. The strands were ignited with an electrically heated nichrome wire (0.015 inch diameter) placed across the propellant surface. The ignition switch was thrown manually and immediately afterward the detection system was triggered manually, also.

V. RESULTS AND CONCLUSIONS

In this section, the significant experimental results of the summer research program are presented. As stated earlier in the objectives section, a large portion of the summer was dedicated to the study of pertinent literature dealing with emission/absorption spectroscopy and review of laser-based diagnostic techniques as applied to combustion system with particular emphasis on solid propellant combustion. Therefore, comments as to the results of these endeavors have been presented in a earlier section. However, it was concluded that one technique, laser-induced fluorescence spectroscopy, has an excellent possibility as a means by which temperature and radical species concentrations can be obtained in solid propellant flames. In this light, the authors assisted their colleagues in the Combustion Laboratory of the AFRPL during the summer in their continuing study of this technique. The status of this investigation is to be reported on by AFRPL personnel at subsequent technical conferences [18,19].

The OH emission from a burning solid propellant strand at a pressure of 100 psi is depicted in Fig. 3. In this figure, the collected OH emission in arbitrary intensity units from the detector

is plotted as a function of Reticon track count. A track count on this figure between 1 and 700 corresponds to a linear decay in wavelength between 316 and 304 nm with the first peak from the right side being the head of the 306.4 nm OH (0,0) band system. These data for OH corresponds to the $A^2\Sigma^+$ excited level to $X^2\Pi$ electronic ground state transition. The propellant employed in this emission spectra is a 87% AP/HTPB propellant [17] and not one of the 80% AP formulations described previously. However, spectra for reduced oxidizer propellants were found to be similar with lower intensity due to the significantly reduced flame temperatures involved.

An example of laser-induced fluorescence emission obtained for solid propellant is given in Fig. 4, again for the higher loaded oxidizer formulation. In this figure, the collected OH emission taken off-axis from a solid propellant flame after the pumping laser pulse is presented as a function of track count corresponding to the same spectral band given in the previous figure. In this test, the laser pulse was tuned to a specified group of lines near the 306.4 band head. In Fig. 4, the intensity of radiation about the pump lines is filtered to prevent over-saturation of the Reticon due to intense Rayleigh scattering and resonant fluorescence at this wavelength region. Laser-induced fluorescence emission in the lower AP loaded propellants, however, were of insufficient intensity to be recorded due to the reduced flame zone temperatures.

In assessing proposed emission/fluorescence spectroscopic studies of solid propellant flame zones, two significant problems appear. The first of these is that as the pressure is increased, control over the propellant surface is reduced due to the inability of the He-Ne tracking beam to pass through the soot laden flame zone above the surface [25]. The second problem is alluded to above and that is for lower flame temperature propellants, the intensity of laser-induced fluorescence emission is significantly reduced preventing accurate detection with the present system. An additional question that needs to be resolved is how to translate collected emission data at given heights above the surface into meaningful temperature/concentration information. One means of coming to grips with the latter two concerns is the employment of higher energy pulses, such as those obtained with excimer lasers. Higher energy pulses can lead to the saturation condition which simplifies data reduction [11-14]. Additionally, the excimer laser can probe additional ultra-violet regions of the spectra so that other radical species can be probed other than OH.

After realizing that the three "academic" propellant formulations described previously would not yield adequate fluorescence emission with the present system, it was decided to only observe the sodium D-line emission and see if some correlation with oxidizer particle size could be obtained. The strong doublet sodium D-lines at 589.0 nm and 589.6 nm were recorded with the

spectrometer/OMA II system as the respective propellants burned through the narrow observation region. In essence, the intensity of the emission as a function of time could then be correlated to height above the surface once the burning rate of the propellant was determined. It will suffice to say that for the purposes of our initial investigation, that this intensity could be related to the flame temperature, or more specifically, the extent of the combustion reaction as a function of distance above the surface. Our primary interest was in determining whether there was a difference in the extent of reaction as a function of the oxidizer particle size. Also, previous experimentation [17] has shown that the reaction zones above solid propellants at moderate pressures have been measured to be much larger than previously modeled [1,5].

Figs. 5a through 5c present the results of the sodium D-line intensity as a function of height above the propellant surface for the three propellants; CI-3, CI-4, and CI-5, representing the two unimodal formulations, 20 and 200 micron, and the 50/50 bimodal blend formulation, respectively. These figures are representative samples of many duplicate runs for each propellant formulation. Two significant results should be pointed out. First, the extent of the reaction zone indicated by the sharp intensity rise in these curves is on the order of 1000 to 2000 microns in height above the surface with the smaller oxidizer propellant (CI-3) yielding slightly smaller reaction zones. Also, the signal is much smoother with distance for this propellant over the larger oxidizer propellant (CI-4) indicating that the combustion of the smaller oxidizer formulations could have a more premixed nature. Secondly, the signal obtained with the bimodal blend (CI-5) has a significant characteristic roughness that could be attributed to large pockets of oxidizer extending well into the region zone above the surface due to the heterogeneous nature of the propellant surface. The major aspect that these figures illustrate is that the combustion reaction extends to larger distances above the surface than previous assumed.

VI. RECOMMENDATIONS

The authors recommend that laser-based diagnostic studies of solid propellant combustion phenomena should be continued. In this light, it is suggested that the higher pulse power excimer laser currently available to the Combustion Laboratory of the AFRPL be employed in conjunction with the servo-controlled combustion bomb. This will permit more sensitive measurements of the fluorescence emission, that is, more rapid sampling as well as smaller investigated flame volumes leading to the desired saturation condition. Additionally, following the lead of Kychevoff [22], the planar laser-induced fluorescence technique (PLIF) should be attempted in order to map out the 2-D temperature and radical species concentrations above the burning solid propellant. As mentioned in an earlier section, it is extremely important to use a well characterized series of

propellant formulations in order to assess the dependency of measured flowfield physio-chemical properties on propellant composition and/or propellant oxidizer size distribution. For example, a follow-on study could systematically investigate the effect of different types of energetic binders on the flame zone chemistry of AP-based composite propellants. Finally, it is deemed extremely important that once emission data is collected from discreet points above the deflagrating propellant surface, an accurate data reduction scheme be employed to determine the corresponding temperature and/or radical species concentrations. Only with such accurate flowfield data can propellant gas phase chemistry be assessed.

REFERENCES

1. Cohen, N.S., "Review of Composite Propellant Burning Rate Modeling," AIAA Journal, Vol. 18, No. 3, March 1980, pp. 277-293.
2. Ramohalli, K.N.R., "Steady-State Burning of Composite Propellants under Zero Cross-Flow Situation," Fundamentals of Solid-Propellant Combustion, Edited by K.K. Kuo and M. Summerfield, Progress in Astronautics and Aeronautics, Volume 90, 1984, pp. 409-477.
3. Cohen, N.S., "Workshop Report: Analytical Models of Combustion Response Functions", to be presented at the 22nd JANNAF Combustion Meeting, Pasadena, CA, October, 1985.
4. Renie, J.P., "Combustion Modeling of Composite Solid Propellants," Ph.D. Thesis, Purdue University, West Lafayette, IN, December 1982.
5. Herzberg, G., Molecular Spectra and Molecular Structure. I: Spectra of Diatomic Molecules, Second Edition, Van Nostrand Reinhold, New York, 1950.
6. Dieke, G.H. and Crosswhite, H.M., "Ultraviolet Bands of OH - Fundamental Data," Journal of Quantitative Spectroscopic Radiation Transfer, Vol. 2, 1961, pp. 97-199.
7. Herzberg, G., The Spectra and Structures of Simple Free Radicals: An Introduction to Molecular Spectroscopy, Cornell University Press, London, 1971.
8. Gaydon, A.G., The Spectroscopy of Flames, Second Edition, Chapman and Hall, London, 1974.
9. Gaydon, A.G. and Wolfhard, H.G., Flames: Their Structure, Radiation and Temperature, Fourth Edition, Chapman and Hall, London, 1979.
10. Incropera, F.P., Introduction to Molecular Structure and Thermodynamics, John Wiley and Sons, New York, 1974.
11. Eckbreth, A.C., Bonczyk, P.A., and Verdick, J.F., "Combustion Diagnostics by Laser Raman and Fluorescence Techniques," Progress in Energy and Combustion Science, Vol. 5, 1979, pp. 253-322.
12. Bechtel, J.H. and Chraplyvy, A.R., "Laser Diagnostics of Flames, Combustion Products, and Sprays," Proceedings of the IEEE, Vol. 70, No. 6, June 1982, pp. 658-677.
13. Crosley, D.R., Editor, Laser Probes for Combustion Chemistry, American Chemical Society Symposium Series 134, Washington, D.C., 1980.
14. McCay, T.D. and Roux, J.A., Editors, Combustion Diagnostics by Nonintrusive Methods, Progress in Astronautics and Aeronautics Series - Vol. 92, 1984.
15. Penner, S.S., Wang, C.P., and Behadori, M.Y., "Laser Diagnostics Applied to Combustion Systems," Twentieth Symposium (International) on Combustion, The Combustion Institute, 1984, pp. 1149-1176.
16. Rakers, R.G. and Villars, D.S., "Flame Zone Spectroscopy of Solid Propellants," The Review of Scientific Instruments, Vol. 25, No. 5, May 1954, pp. 424-429.

17. Edwards, T., Weaver, D.P., Campbell, D.H., and Hulsizer, S., "Investigation of High Pressure Solid Propellant Combustion Chemistry," Twenty-first JANNAF Combustion Meeting, CPIA Publication No. 412, Vol. II, October 1984, pp. 163-171.
18. Edwards, T., Weaver, D.P., Campbell, D.H., and Hulsizer, S., "Two-Dimensional Laser-Induced Fluorescence Imaging of Solid Propellant Combustion," Twenty-second JANNAF Combustion Meeting, October 1985.
19. Edwards, T., Weaver, D.P., Hulsizer, S., and Campbell, D.H., "Laser-Induced Fluorescence in High Pressure Solid Propellant Flames," Western States Section/The Combustion Institute, Fall Meeting, October 1985.
20. Anderson, W.R., Decker, L.J., and Kotlar, A.J., "Temperature Profile of a Stoichiometric $\text{CH}_4/\text{N}_2\text{O}$ Flame from Laser Excited Fluorescence Measurements on OH," Combustion and Flame, Vol. 48, 1982, pp. 163-176.
21. Anderson, W.R., Decker, L.J., and Kotlar, A.J., "Concentration Profiles of NH and OH in a Stoichiometric $\text{CH}_4/\text{N}_2\text{O}$ Flame by Laser Excited Fluorescence and Absorption," Combustion and Flame, Vol. 48, 1982, pp. 179-190.
22. Kychekoff, O., Hanson, R.K., and Howe, R.D., "Simultaneous Multiple-Point Measurements of OH in Combustion Gases Using Planar Laser-Induced Fluorescence," Twentieth Symposium (International) on Combustion, The Combustion Institute, 1984, pp. 1265-1272.
23. O'Shea, D.C., Collen, W.R., and Rhodes, W.T., Introduction to Lasers and Their Applications, Addison-Wesley Publishing Company, Reading, MA, 1977.
24. Goetz, F., "A High-Pressure Combustion Bomb for Spectroscopic Measurements of Combustion Processes," AFRPL-TR-80-79, February 1981.
25. Edwards, T., Weaver, D.P., Adams, R., Hulsizer, S., and Campbell, D.H., "A High Pressure Combustor for the Spectroscopic Study of Solid Propellant Combustion Chemistry," submitted to The Review of Scientific Instruments.

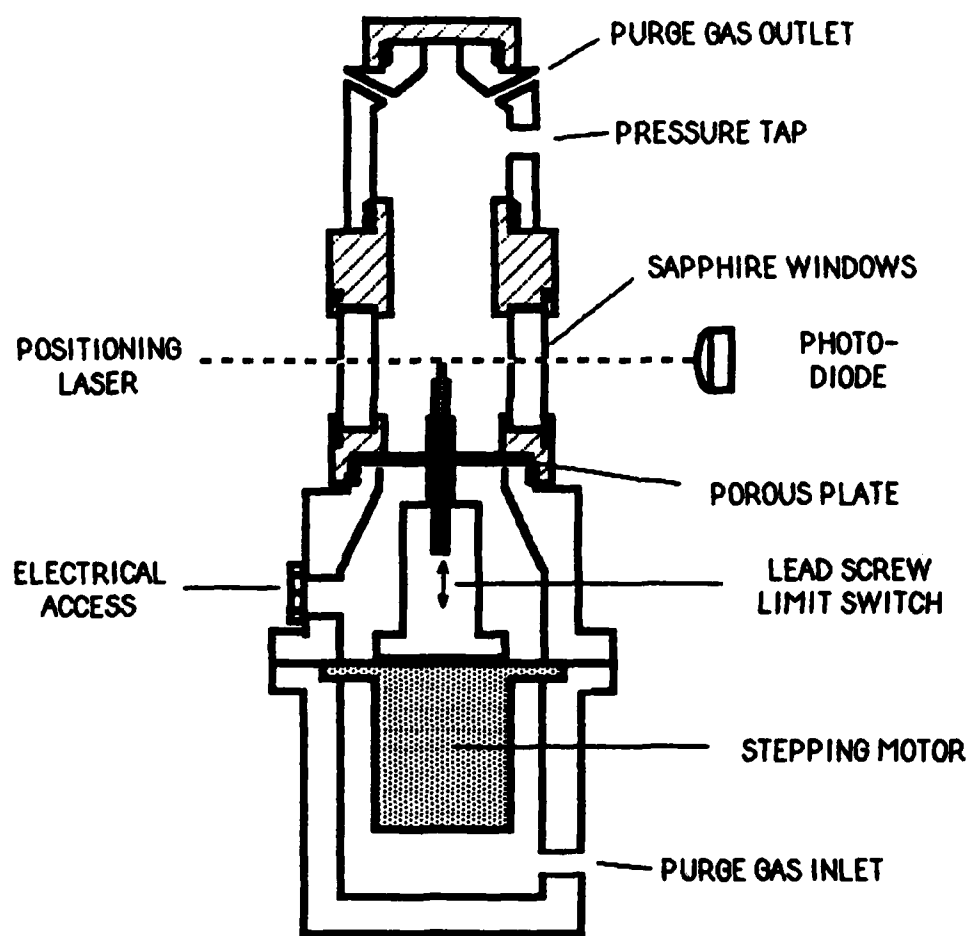


Figure 1. Schematic of the Servo-Controlled High Pressure Combustor.

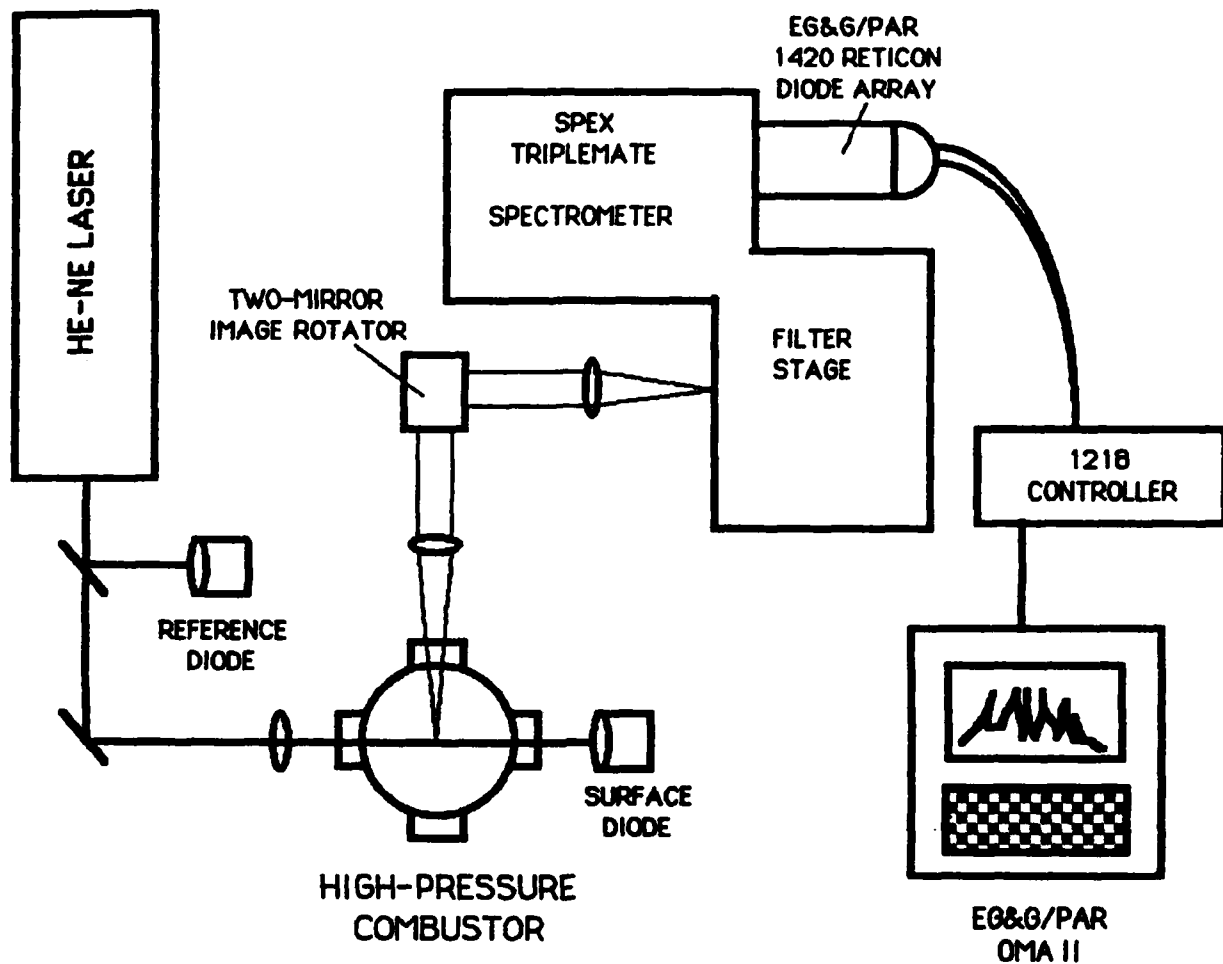


Figure 2. Experimental Optical-Detector System for Acquisition of Propellant Emission Data

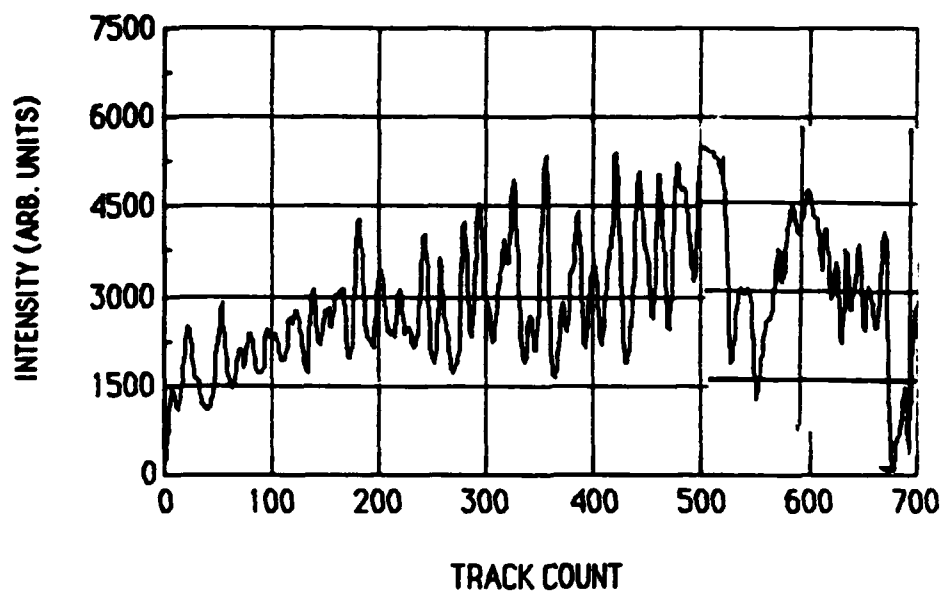


Figure 3. OH Emission Spectra for 87% AP Propellant (100 psi)

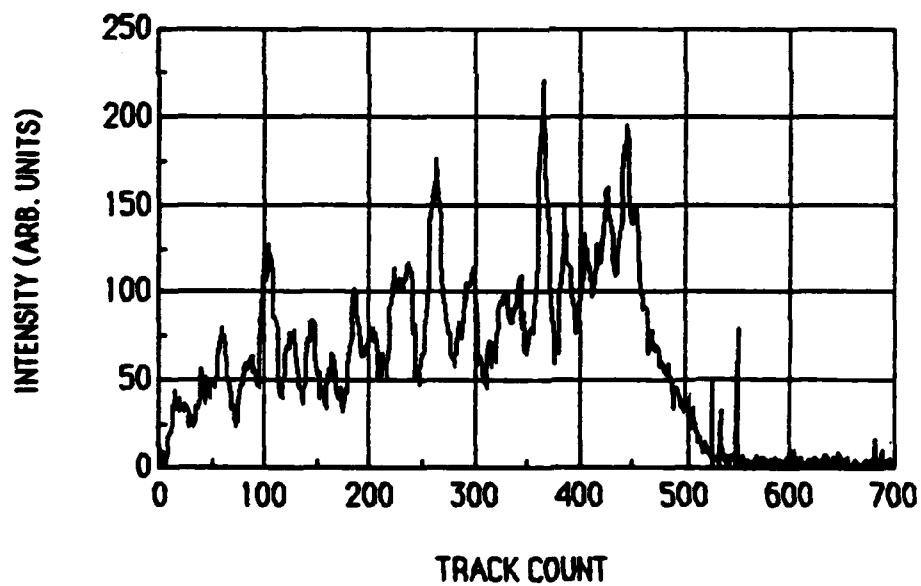


Figure 4. OH Emission Spectra in Fluorescence for 87% AP Propellant (100 psi)

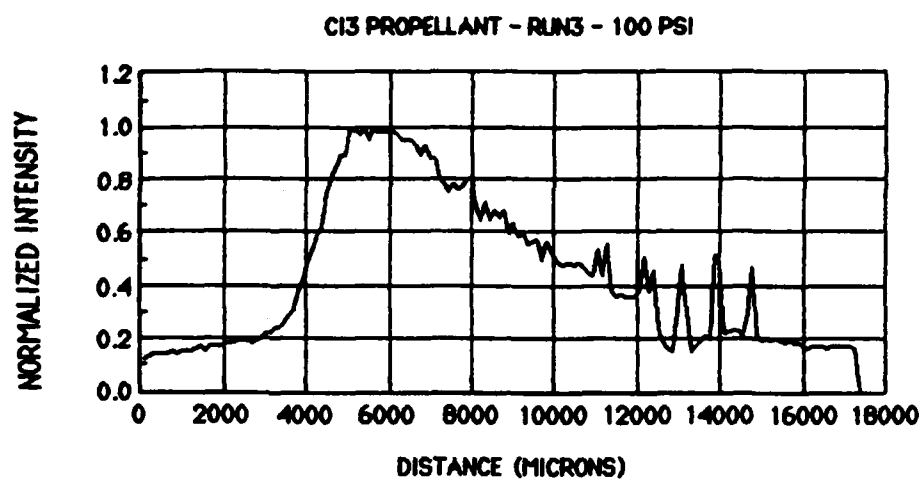


Figure 5a. Sodium D-Line Intensity for Propellant CI3 (20 micron)

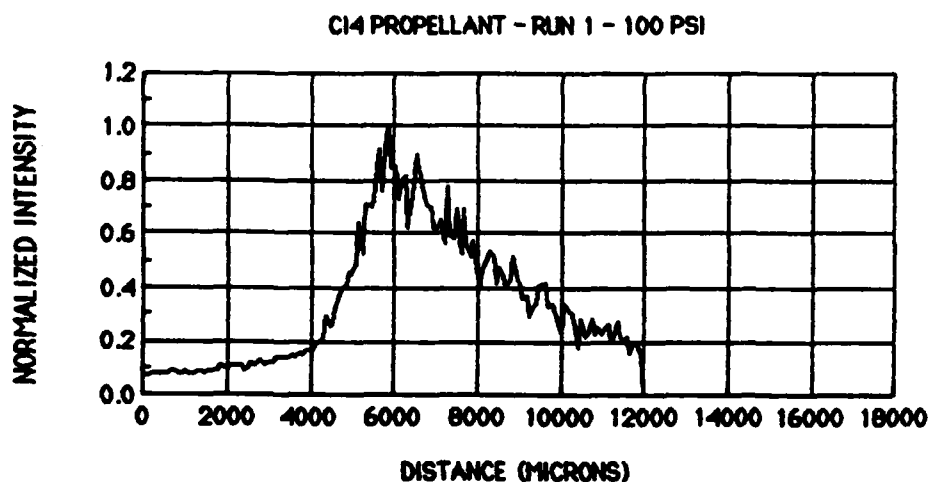


Figure 5b. Sodium D-Line Intensity for Propellant CI4 (200 micron)

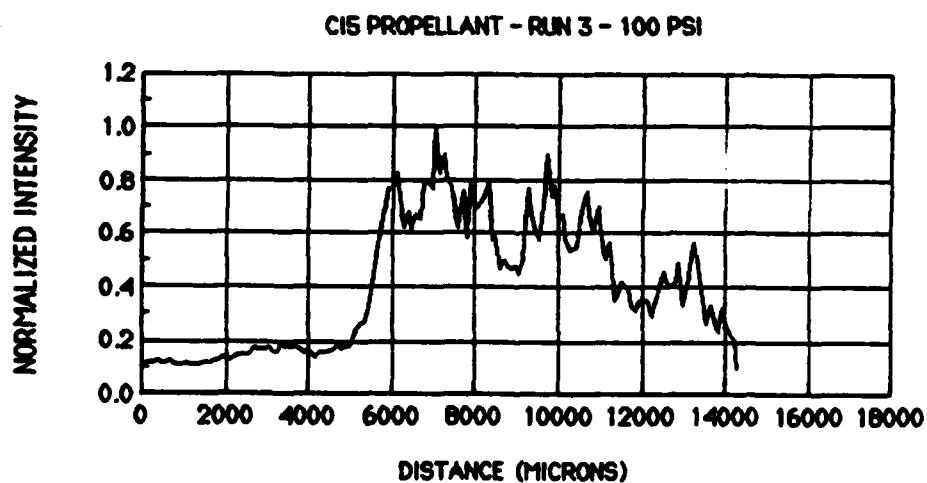


Figure 5c. Sodium D-Line Intensity for Propellant CI5 (20/200 micron blend)

1985 USAF-UES SUMMER FACULTY RESEARCH PROGRAM/
GRADUATE STUDENT SUMMER SUPPORT PROGRAM

Sponsored by the
AIR FORCE OFFICE OF SCIENTIFIC RESEARCH

Conducted by the
UNIVERSAL ENERGY SYSTEMS, INC.

FINAL REPORT

CONSTRUCTION OF APPROXIMATE FORMULAE FOR THE CALCULATION OF
CONDUCTIVITY COEFFICIENTS IN PARTIALLY IONIZED GASES

Prepared by: Michael Barry Rhodes
Academic Rank: Assistant Professor
Department and Department of Physics, Clark College
University:
Research Location: Air Force Geophysics Laboratory,
Hanscom Field
USAF Research: J. R. Jasperse
Date: 7 September, 1985
Contract No: f49620-85-C-0013

CONSTRUCTION OF APPROXIMATE FORMULAE FOR THE CALCULATION OF
CONDUCTIVITY COEFFICIENTS IN PARTIALLY IONIZED GASES

by

MICHAEL BARRY RHODES

ABSTRACT

A Green's Function method for the solution to the Boltzmann-Fokker Planck equation for a homogeneous plasma in the presence of weak field gradients is presented. Because of the difficulty associated with the numerical solution of the BFP it is desirable to have alternate slightly less accurate methods or mixture rules to calculate conductivity coefficients. As a byproduct of the Green's Function solution a method for generating mixture rules is suggested.

ACKNOWLEDGMENTS

The author wishes to thank the Air Force Systems Command, the Air Force Office of Scientific Research, the various personnel at Hanscom Field, Air Force Geophysics Laboratory and especially Dr. J. R. Jasperse for their valued support. I would also like to thank Drs. Retterer, Decker, Basu, and Wodzinski for making my stay at AFGL such a pleasant one.

I. INTRODUCTION: My previous research efforts have dealt with the construction of approximate formulas, or mixture rules, for homogeneous plasmas, (i.e. constant number densities) in the presence of weak field gradients. The mixture rules are based on the Boltzmann Fokker Planck equation, (hereafter referred to as the BFP equation), using a variational technique due to Chen^{1,2}. Basically the procedure was to consider the variation of the conductivity coefficient with respect to some properly chosen function $a(x)$ from a constant value \bar{a} . $a(x)$ is that function in the reduced BFP which contains all the various parameters on which the coefficients depend (e.g. temperature, number density, fractional ionization, and neutral particle momentum transfer cross section). If the variation of the conductivity coefficient is small enough then $a(x)$ can be replaced by \bar{a} . Once \bar{a} is found and a functional relationship is determined between \bar{a} and the coefficient, then the conductivity coefficient may be determined. Besides all the analysis involved in the variational approach the work entailed finding an "exact" numerical solution to the BFP from which to compare the mixture rules. It was because of a mutual interest in the solution to the BFP that I was assigned to AFGL to work amongst the group headed by J.R. Jasperse.

II. OBJECTIVES OF THE RESEARCH EFFORT: Because of the short time scale (10 weeks) and the difficult task of

implementing a new research problem it was felt that a reasonable goal would be to continue my past work on mixture rules. My goal then was to construct new mixture rules using a different approach based directly on the BFP. These approximate formula were to be based on a Green's Function solution to the BFP, be easily implemented, and have an maximum error of less than ten percent for a wide range of fractional ionizations and gases. Any greater accuracy is not warranted since approximations in the BFP as well as uncertainties in the momentum transfer cross sectional data have an inherent inaccuracy of at least 5-10 %³.

III. BACKGROUND THEORY: The basis for a description of a collision dominated partially ionized gas in the presence of weak external field gradients is given by the solution to the Boltzmann Fokker Planck equation given by

$$n_e \frac{\partial f}{\partial t} + n \vec{v} \cdot \nabla_x f + n \frac{\vec{E}}{m} \cdot \nabla_v f = \sum_p C_p \quad (1)$$

$$C_p = n n_p \Gamma_p \left\{ \frac{\partial}{\partial v_r} f \frac{\partial H}{\partial v_r} + \frac{1}{2} \frac{\partial^2}{\partial v_r^2 \partial v_r} (f \frac{\partial^2 G}{\partial v_r^2 \partial v_r}) \right\}$$

where the functions H, G, and Γ_p are defined as usual⁴ and where $f(v)$ is the electron velocity distribution function and the summation on the right side is over electron electron, electron ion and elastic electron neutral particle collisions. Taking the case of a plasma subjected to a weak external constant electric field and integrating out the spherically symmetric scattering angles,

equation (1) becomes after much algebra²

$$D''(x) + P(x) D'(x) + Q(x) D(x) - a(x) D(x) = R(x) + S(x) \quad (2)$$

where

$$x = \frac{\sqrt{2m}}{\sqrt{2kT}} v$$

$$f = f_M + D(x) f_M \quad \begin{cases} f_M \equiv \text{Maxwellian Distribution} \\ D(x) \equiv \text{Departures from } f_M \end{cases}$$

$$P(x) = 2x - \frac{1}{x} + \frac{1.2x^2 \Phi'}{\Delta}$$

$$Q(x) = \frac{1}{2}x^2 - \frac{1}{\Delta} \{ 1 + \Phi - 2x^2 \Phi' \}$$

$$\Phi = \text{Erf}(x)$$

$$\Phi' = \text{Erf}'(x)$$

$$\Delta = \Phi - x \Phi'$$

$$R(x) = -\frac{2x^2}{\Delta} \left(1 + \frac{K}{x} \right) I_0(x) (1.2x^2 - 1)$$

$$S(x) = \frac{K}{\Delta} \{ x I_3(x) - 1.2x I_4(x) - x^2 I_5(x) (1 - 1.2x^2) \}$$

where

$$I_n(x) = \int_0^x y^n e^{-y^2} D(y) dy ; \quad I_n(\infty) = \int_0^\infty e^{-y^2} D(y) dy$$

$$K = \frac{1.6}{\sqrt{\pi}}$$

$$a(x) = \frac{x^2}{\Delta} (2.2812 \times 10^4 T^2 Q_{en} \gamma_\alpha)$$

where

T = electron Temperature

Q_{en} = Cross Section for Momentum Transfer

α = fractional Ionization

Notice that equation (2) is a linear integro-differential equation of second order. Notice also that all the various physical parameters upon which $f(x)$ depends are lumped into the one function $a(x)$.

For $\theta_{en} = 0$ or equivalently $a(x) = 0$ equation (2) reduces to the equation for a fully ionized gas first derived by Spitzer and Harm⁵. By defining a dimensionless quantity σ as the ratio of the electrical conductivity of a partially ionized gas to that of a fully ionized gas of the same temperature and density then we can associate σ directly with moments of $f(x)$. Specifically σ is equal to I_3 defined in equation (2). It is thus the calculation of I_3 which will be the goal of the mixture rules.

IV. CONSTRUCTION OF THE MIXTURE RULE: The approach taken will be to try and generate an approximation for $D(x)$ which will be used to approximate the various moments of D , i.e. the conductivity coefficients. Rewrite equation (2) as

$$D''(x) + P(x) D'(x) + Q(x) D(x) + S(x) = R(x) + a(x) D(x) \quad (3)$$

Replace the right side of equation (3) by $\delta(x-\xi)$ and find $G(x|\xi)$ from

$$G''(x|\xi) + P(x) G'(x|\xi) + Q(x) G(x|\xi) = \delta(x-\xi) \quad (4)$$

$D(x)$ is then written in terms of G as

$$D(x) = \int_0^\infty G(x|\xi) \{ R(\xi) + a(\xi) D(\xi) \} d\xi \quad (5)$$

Notice that this is a nonlinear integral equation and can be solved by iteration (assuming the iteration converges) as

$$D_{n+1} = \int_0^{\infty} G(x|\xi) \{ R(\xi) + a(\xi) D_n(\xi) \} d\xi \quad (6)$$

The approximation is then to let D_0 be the $D(x)$ for a Lorentz Gas (a Lorentz gas is a gas of essentially electrons and neutral particles and is valid for very low degrees of ionization) for which there is a very well known simple closed form solution. Let the $I_0(\infty)$ in the $R(x)$ term be that of a fully ionized gas (Spitzer Harm⁵ result) and only iterate once. Thus

$$D_{\text{Approx}} = \int_0^{\infty} G(x|\xi) \{ R(\xi) + a(\xi) D_{\text{Lorentz}}(\xi) \} d\xi \quad (7)$$

Notice that D_{approx} is necessarily exact in the limit of a fully ionized gas. This follows from the fact that for a fully ionized gas $a(x) = 0$ and equation (6) is no longer nonlinear. Thus the first iteration is the correct answer. Equation (7) is also exact in the limit of a weakly ionized gas since in this case the initial guess D_0 is very close if not equal to the expected form of $D(x)$. Thus the approximate formula for I_3 is thus

$$\sigma_{\text{Approx}} = I_{3(\infty)} = \int_0^{\infty} D_{\text{Approx}} x^3 e^{-x^2} dx \quad (8)$$

The validity of the approximation is based on three assumptions:

- 1.) That D_{approx} will start to converge
- 2.) That the intermediate ionization range will result in a D_{approx} which is not too far from the correct D
- 3.) $G(x|f)$ exists and can be computed.

The construction of the mixture rule hinges on being able to find $G(x|f)$. The majority of my efforts have been in trying to calculate G .

V. NUMERICAL METHOD FOR FINDING $G(x|f)$: All that is required to construct a Green's Function is two linearly independent solutions to the homogeneous equation⁶. Then G can be constructed. Various attempts were made to find g_1 and g_2 which are linearly independent solutions to

$$g'' + P(x)g' + Q(x)g + S(x) = 0 \quad (9)$$

$$g(0) = 0 \quad g'(0) = 1 \quad g(0) = 0 \quad g'(0) = -1$$

g_1 was found numerically but g_2 proved difficult. Equation (9) is a "stiff" integro-differential equation which means that any error in the integration of g_1 grows as g_2 . Soon g_1 swamps g_2 and significance is lost due to roundoff error. All traces of g_2 are soon gone. A standard remedy for this type of numerical instability is to integrate backwards moving towards ever increasing values of g_2 , however singularities in the $Q(x)$ term at $x = 0$ defeated the approach.

Another method for finding g_2 is to utilize the Wronskian as in the following

$$\frac{d}{dx} \frac{g_2}{g_1} = \frac{g_2' g_1 - g_2 g_1'}{g_1^2} = \frac{W}{g_1^2} \quad (10)$$

Therefore

$$\frac{g_2}{g_1} = \int \frac{W}{g_1^2} dz \quad \text{or} \quad g_2 = g_1 \int_0^x \frac{W}{g_1^2} dz \quad (11)$$

For ordinary differential equations W is

$$W = W(x_0) \exp \left\{ - \int_{x_0}^x P(z) dz \right\} \quad (12)$$

but because of the integrals in the S term of equation (9) W is no longer a known function. W is the solution to

$$W' + PW + g_1 S[g_2] - g_2 S[g_1] = 0 \quad (13)$$

Notice that W depends on g_2 . Thus equation (13) along with equation (11) form a coupled set of equations which must be solved simultaneously. It turns out that the above equations are no easier to solve than the original equation for g_2 . It must be said that the greatest part of my time this summer was devoted to attempting to calculate G through the previous methods.

VI. Series Solution for $G(x|t)$: Another approach to obtaining G is to seek series expansions. Because of the

integrals in the S term of equation (2) it is difficult to find an expansion which will allow a term by term integration as required by $I_0(x)$, $I_3(x)$, and $I_5(x)$.

However if the transformation $D(x) = \exp(-x^2)F(x)$ is made then equation (2) becomes

$$e^{x^2} \{ F'' + 4x F' + (4x^2 + 2) F + P(2x F + F') + Q F \} + S = \delta(x-\xi) \quad (14)$$

where the integral in S are now of the form

$$I_n(x) = \int_0^x F y^n dy \quad (15)$$

Let $F = \sum_{n=-\infty}^{\infty} C_n e^{i n \pi x/L}$ where it is understood that $F = F(x/\xi)$
 $C_n = C_n(\xi)$

Then equation (14) becomes

$$F'' + P^* F' + Q^* F + e^{x^2} S = e^{x^2} \delta(x-\xi) \quad (16)$$

where

$$\begin{aligned} P^* &= P + 4x \\ Q^* &= Q + 2xP + 4x^2 + 2 \end{aligned} \quad (17)$$

After expanding $e^{x^2} \delta(x-\xi)$ in a series as well as the integrals in S and much algebra

$$C_n = \frac{1}{2L} e^{-(\xi^2 + i n \pi \xi/L)} \left\{ -\frac{n^2 \pi^2}{L^2} + (P + 4x) i \frac{n \pi}{L} + (Q + 2P x + 4x^2 + 2) + e^{-x^2} S \right\}^{-1} \quad (18)$$

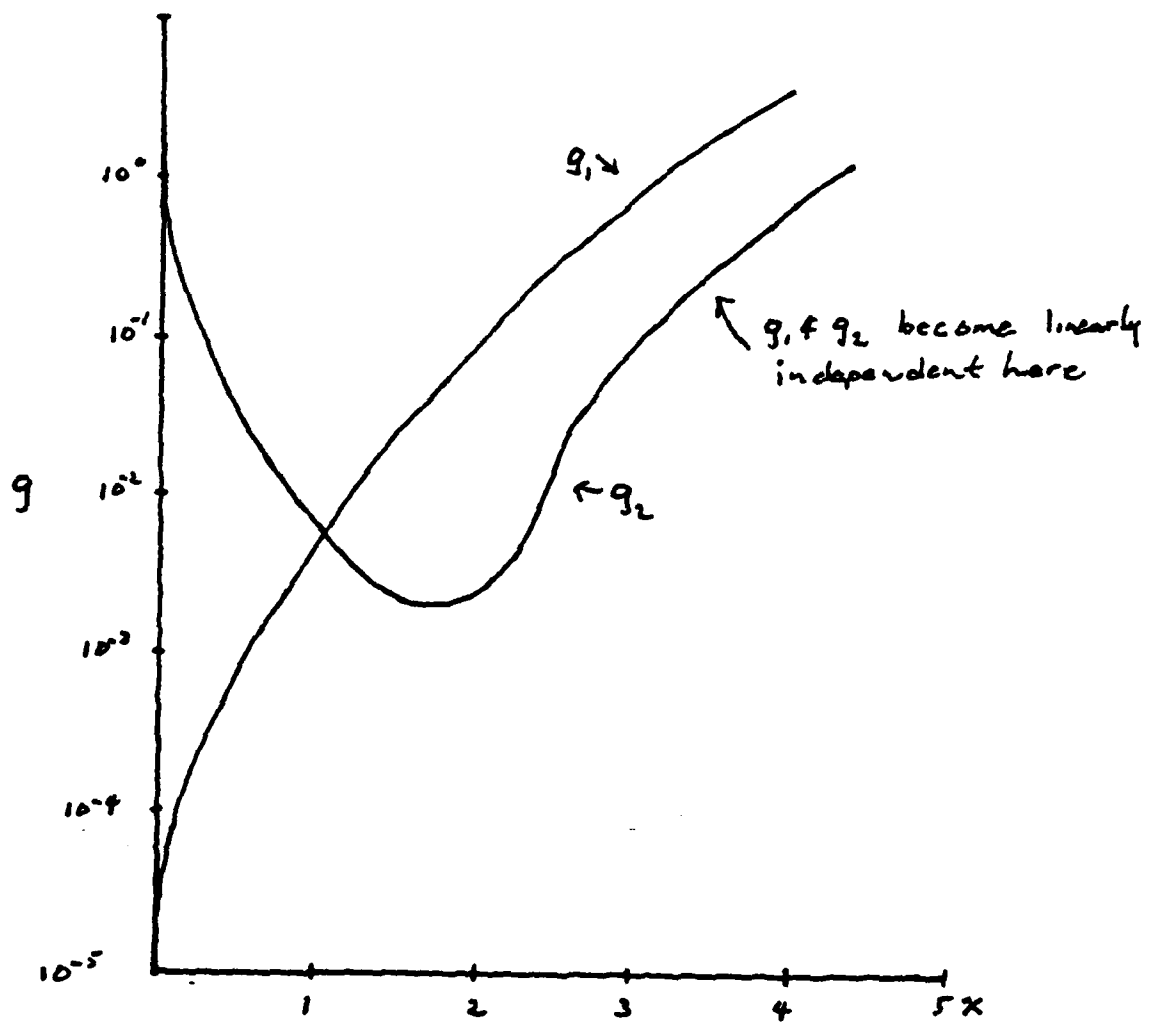
Finally G is given by

$$G(x|\xi) = e^{x\tilde{F}} = e^{x\tilde{\sum} C_n(\xi)} e^{i\pi n \eta_L} \quad (19)$$

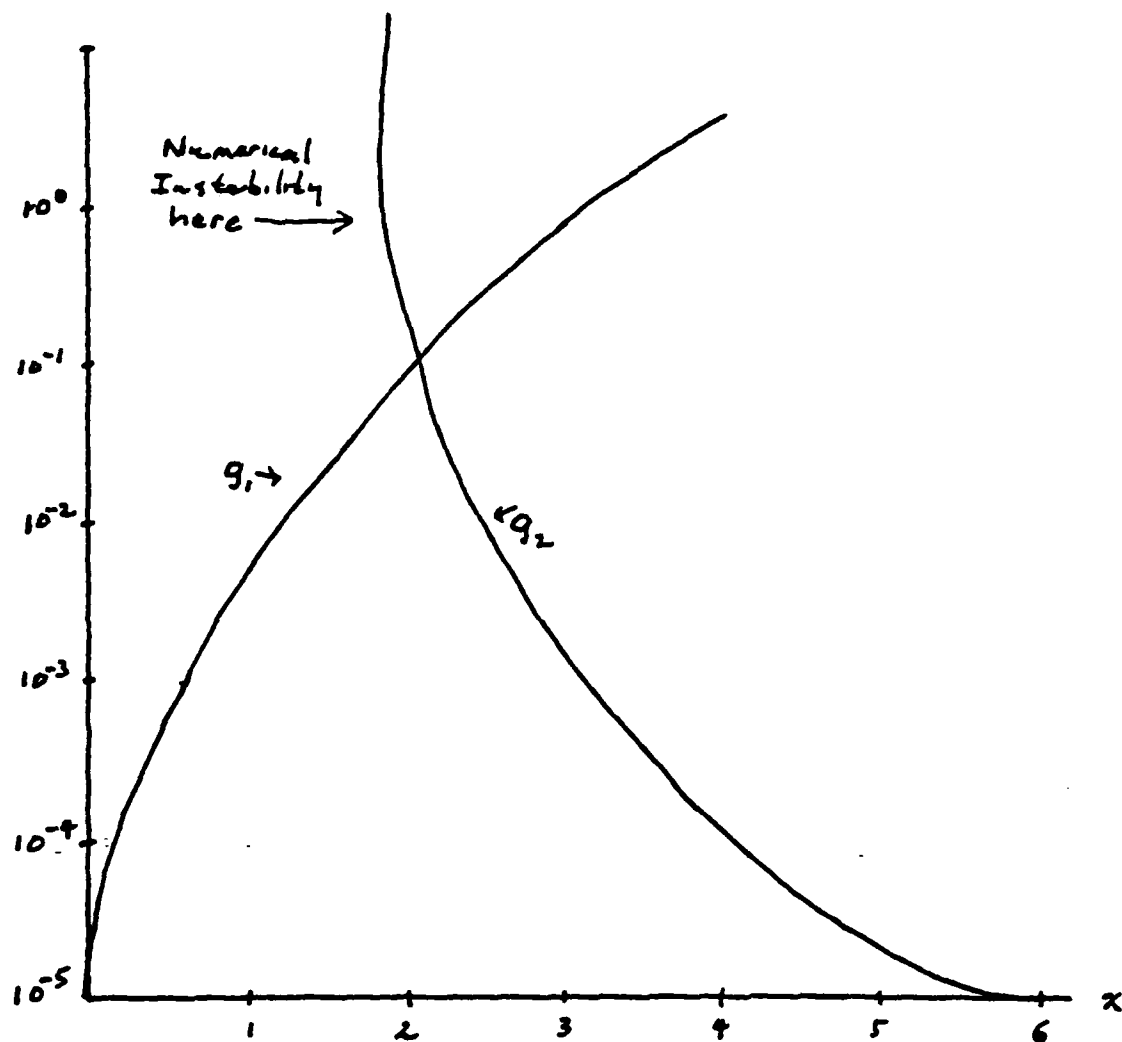
Preliminary indications are that C_n will converge although rather slowly. Note that this is not the only expansion possible. A power series is equally valid and may prove a more expedient approach to expanding G. Another possibility is to replace the Fourier expansion with a Fourier Transform since the interval is essentially infinite. This may be the most promising approach of all. Unfortunately time ran out before I had a chance to explore this approach.

VII. RECOMMENDATIONS: Much work needs to be done on the series solution approach, especially the Fourier transform idea. Much of the series approach occurred in the last week of my research appointment and thus is not very far along at this time. I do feel encouraged with the convergence of C for several values of x, however this does not guarantee convergence over the entire interval.

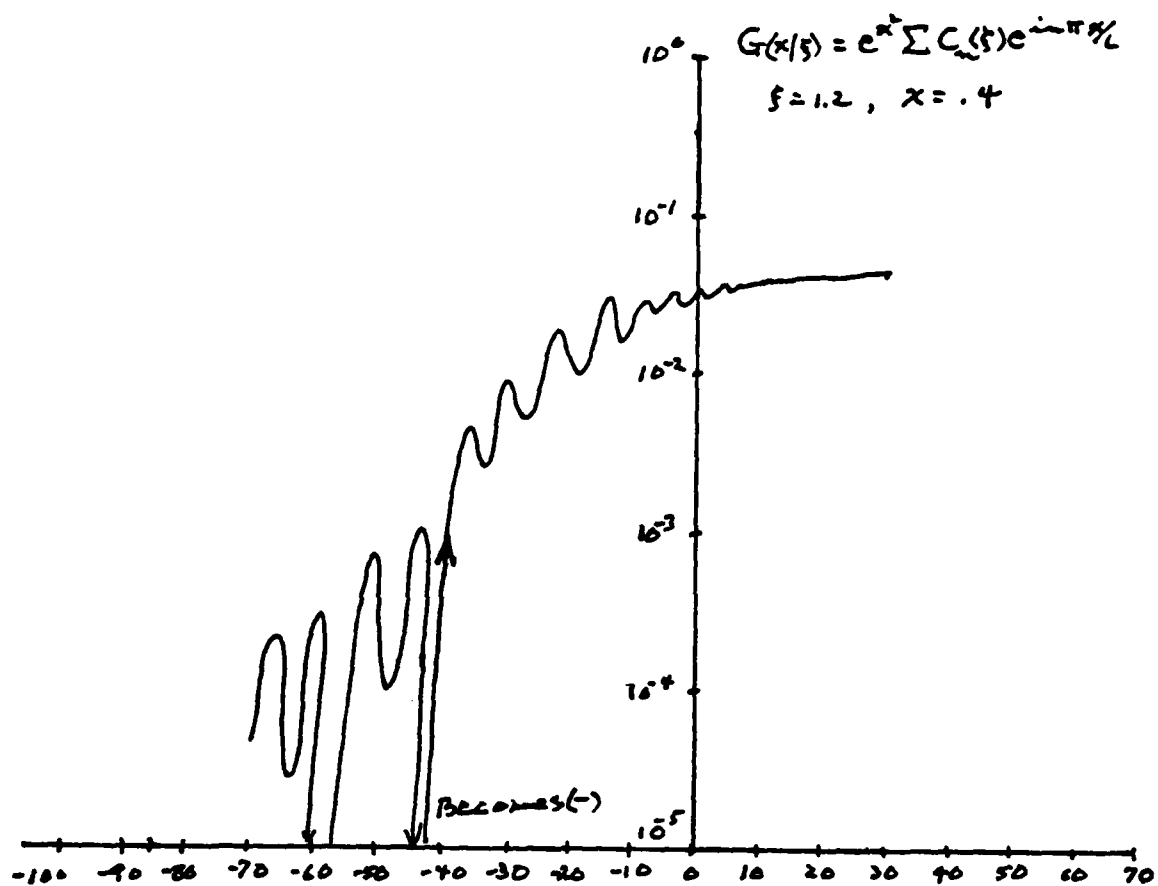
Assuming G is obtained the validity of the mixture rule needs to be investigated. This would entail applying the approximation to various "worst case" gases over a wide range of fractional ionizations. These could be compared to known values and the validity of the approximation could be checked.



Graph of g_1 and g_2 . g_2 is obtained by the Wronskian method



Graph of g_1 and g_2 . g_2 is obtained by backward integration



Graph of the convergence of C_n

REFERENCES

1. Chen, R.L.W., Plasma Physics 23, 539 (1981)
2. Rhodes, Michael Barry, Calculation of Conductivity Coefficients in Partially Ionized Gases, Unpublished Dissertation, Emory University, Atlanta Ga, (1983)
3. Frost, L.S., and A. V. Phelps, Phys. Rev. 136, A1538 (1964)
4. Mitchner, K and E.H. Kruger, Partially Ionized Gases New York, Wiley, 1975
5. Spitzer, L., and R. Harm, Phys. Rev. 89, 977 (1953)
6. Gallaher, L.J., and I.E. Perlin, " Use of Green's Functions in the Numerical Solution of Two Point Boundary Value Problems," Proceedings of the Conference on the Numerical Solution of Ordinary Differential Equations, The University of Texas at Austin, Austin Texas, Oct. 19,20 1972, pp. 374

1985 USAF-UES SUMMER FACULTY RESEARCH PROGRAM/

GRADUATE STUDENT SUMMER SUPPORT PROGRAM

Sponsored by the
AIR FORCE OFFICE OF SCIENTIFIC RESEARCH

Conducted by the
UNIVERSAL ENERGY SYSTEMS, INC.

Prepared by: Robert W. Ricci, Ph.D.
Academic Rank: Professor
Department and Chemistry Department
University: College of the Holy Cross, Worcester, MA
Research Location: UV Surveillance and Remote Sensing Branch
Ionospheric Physics Division
Geophysics Laboratory
Hanscom Air Force Base
Boston, MA

USAF Research: Robert Huffman, Ph.D.

Date: August 20, 1985

Contract No: F49620-85-C-0013

A LITERATURE SURVEY ON THE FORMATION AND LUMINESCENCE
OF NO($A^2\Sigma$) IN A HYDRAZINE/ N_2O_4 PROPELLANT SYSTEM

by

Robert W. Ricci, Ph.D.

ABSTRACT

The exhaust plume of a rocket charged with an unsymmetrical dimethylhydrazine/nitrogen tetroxide (UDMH/ N_2O_4) propellant emits considerable radiation in the ultraviolet region of the electromagnetic spectrum. Nitric oxide and to a lesser extent CO(4^+) and OH radicals are three sources of this radiation. Improved methods of missile surveillance could result from the detection of the distinctive plume signature resulting from the ultraviolet radiation emitted by these and other species present in the exhaust of rockets employing UDMH/ N_2O_4 propellants. The object of this study was the completion of a literature survey on the available technical reports and journal articles pertaining to the formation and luminescence of NO($A^2\Sigma$) in the exhausts of rockets fueled by UDMH/ N_2O_4 .

ACKNOWLEDGMENT

I would like to acknowledge my appreciation to the Air Force Systems Command, Air Force Office of Scientific Research, Mr. Robert A. Skrivanek, Director of the Ionospheric Physics Division and particularly Dr. Robert Huffman of the UV Surveillance and Remote Sensing Branch of the Geophysics Laboratory for the opportunity to be a member of the 1985 USAF Summer Faculty Research Program.

I. INTRODUCTION: I am a full professor of chemistry at the College of the Holy Cross and chairman of the department for the past six years. I received a Ph.D. in physical chemistry from the University of New Hampshire and a B.S. degree from Boston College. My research experience has been in the general area of photochemistry and photophysics. I have been particularly interested in energy-transfer mechanisms and have investigated these processes in several molecular and ionic systems. In the course of the above studies I have developed an understanding of UV-visible and fluorescence spectroscopy as well as reaction kinetics of excited states and chemiluminescence.

Publications:

"Inclusion Complexes of Indole with α -Cyclodextrin," R. Ricci, Carbohydrate Research, 129 (1984) 278-286.

"Fluorescence Quenching of Photoexcited Aromatics," Gordon Research Conference, Wolfboro, N.H. (Summer 1978).

"Singlet Quenching of Photoexcited Aromatics by Carbonyl Compounds," D. Busch, B. Siwicke, R. Ricci, Tetrahedron Letters, 51 (1977) 4489.

"Inter- and Intramolecular Quenching of Indole Fluorescence by Carbonyl Compounds," R. Ricci and J. Nesta, Journal of Physical Chemistry, 80 (1976) 974.

"Fluorescence Quenching of the Indole Ring System by Lanthanide Ions," R. Ricci and K. Killichowski, Journal of Physical Chemistry, 78 (1974) 1953.

"Interfacing a Programmable Calculator in the Physical Chemistry Laboratory," Northeast Regional American Chemical Society Meeting, Burlington, VT (Summer 1974). Co-authored with G. Vidulich.

II. OBJECTIVES: The exhaust plume of a rocket charged with UDMH/ N_2O_4 propellant emits considerable radiation in the ultraviolet region of the electromagnetic spectrum. Nitric oxide ($NO(A^2\Sigma)$) and to a lesser extent $CO(4^+)$ and OH radical are three sources of this radiation.

One of the missions of the UV-Surveillance Branch of the USAF Geophysics Laboratory at Hanscom Air Force Base is improved missile detection systems. As part of their program to meet this goal they have been reviewing the possibility of detecting ICBM's from satellites equipped with sensors attuned to the distinctive plume signature resulting from the ultraviolet radiation emitted by the chemiluminescent agents present in the rocket exhausts employing UDMH/ N_2O_4 propellants.

As a Summer Faculty Fellow attached to this group, I was given the task of conducting an exhaustive survey of the literature as it pertains to the formation and luminescence of $NO(A^2\Sigma)$ in rocket exhausts fueled by UDMH/ N_2O_4 . The following four areas were selected for study:

- A. Laboratory and field studies on rocket plume radiation from UDMH/ N_2O_4 and, when possible, aluminized solid propellant.
- B. Kinetics, mechanism and thermodynamics of the combustion of UDMH/ N_2O_4 in propellants and flames.
- C. Fundamental studies on the mechanism for the formation, emission and quenching of $NO(A^2\Sigma)$.
- D. Computer modeling of the plume chemistry responsible for emission in the ultraviolet and visible regions of the electromagnetic spectrum.

In addition to its presence in rocket exhaust plumes, nitric oxide is an important species in three other types of related problems: air pollution studies; ballistic missile re-entry phenomena and upper-atmospheric chemistry. This survey was undertaken in order to outline

what has been accomplished in these vital fields and to help define those areas which are only poorly understood and in need of further investigation.

III. SURVEY: Research for this survey was carried out at the AGL Research and Holy Cross Science Libraries. A search was made of the literature published between 1950 and 1985.

A. Laboratory and field studies on rocket plume radiation from UDMH/
N₂O₄ propellants and aluminized solid propellant.

J. W. Sutton, Laboratory Studies of Rocket Plume Radiation at Reduced Pressure.

The Boeing Company, Contract No. AF 19(604)-7439, 1961. Geophysics Research Directorate, Air Force Cambridge Research Laboratories, Office of Aerospace Research, United States Air Force, Bedford, MA.

Laboratory studies were conducted of the spatial and spectral distribution of rocket plume radiance at simulated altitudes. Motors of 150 to 200 pounds thrust were operated at sea level and at pressures equivalent to approximately 50,000 and 100,000 feet. The propellant combinations studied were gasoline/oxygen, RP 1/oxygen, JP 4/oxygen, UDMH/N₂O₄ and aluminized solid propellant.

A traversing rocket technique was employed which permitted simultaneous observation of a number of radiometric and spectrometric properties of a common area of the plume. The graphical presentations of these data are interpreted on a qualitative and semi-quantitative basis.

This report contains the most extensive set of radiance studies of laboratory motors to be found in the nonclassified literature. Spectral output for the UV (.26μ - .39μ), visible (.4μ - .7μ) and infrared (1μ - 5μ) are recorded as a function of plume geometry and external pressures. Relevant observation from this study are:

a. The maximum values of ultraviolet radiance in hydrocarbon-oxygen exhaust are found in the same zones as the maximum in infrared. The ultra-

violet radiance decreases rapidly with altitude; the maximum value near 100,000 feet was found to be 1 to 2 percent of the sea level value.

b. At sea level the spectral characteristics for the UDMH-N₂O₄ propellant combination are markedly different from those of hydrocarbon-oxygen systems. The continuum contributions do not appear. The 2.7 and 4.3 micron band radiations correspond in intensity to those in the hydrocarbon-oxygen exhaust at sea level.

c. The spectral distribution of infrared radiation from aluminized solid propellant motors is surprisingly similar to that for hydrocarbon-oxygen exhaust. The scattering properties of the alumina particles show a different wavelength dependence from that of the carbon particles in the 1 to 3 micron range.

d. The spatial distribution of radiance in the solid propellant exhaust at altitude is grossly different from the hydrocarbon-oxygen exhaust. A more nearly uniform level of infrared radiance is found for the entire length of the observed plume in the solid exhaust.

Keefer, D.R.; Phillips, W.J.; Harwell, K.E., Photographic Spectroscopic Measurement of Ultraviolet Solid Rocket Motor Plumes. University of Tennessee Space Institute, Tullahoma, Tenn. Report VTSl-GD-TR-80-1. UV spectra (250nm - 370nm) of the exhaust plume of a rocket motor containing an unspecified solid fuel were taken. A considerable portion of the spectra is due to a strong continuum. Some spectral features were identified as due to OH, PbO, NO and CHO.

Burrows, M.C., Mixing and Reaction of Hydrazine and Nitrogen Tetroxide at Elevated Pressure. AIAA Journal 5, 1700, 1967.

A jet combustor with a windowed chamber was constructed and spectra of the gases were obtained. OH bands from 2600 to 3500Å and NH bands centered at 3360 and 3370Å were the principal radiating species in the UV range. Weaker NH₂ radiation bands from 5000 to 7000Å were also recorded. The Schumann-Runge bands of O₂ were not observed. Spectral emissions were correlated with overall reaction mechanism as described by Sawyer

Zirkind, R., Radiation from Rocket-Exhaust Plumes. Eleventh Symposium
(International on Combustion, Combustion Institute, Pittsburgh, PA., 1966 p 613.

A general review on the emission of optical radiation from rocket exhaust
plumes. Discusses in a general way the chemistry, fluid mechanics and
radiation from rocket-exhaust plumes. Good general introduction into rocket
motors as a source of high temperature gases.

Jacobs, T.A. et al., Measurements of Ultraviolet Emission from Rocket Exhaust
Plumes with In Situ Determined Atmospheric Conditions.

Aerospace Corporation, Report No. TDR-469(5240-20-3) 1965 (unpublished).

Jacobs, T.A. et al., Ground-Based Measurements of Ultraviolet Emission from
Exhaust Plumes of In-Flight Missiles. Aerospace Corporation, Report No.
TDRF-169(3230-0-TN-3, 1963 (unpublished)

Above two reports cited by R. B. Lyons and C. E. Kolb at Workshop on the
Space Applications of Ultraviolet Techniques Aerospace Corp., November, 1985.
Seven inch diameter quartz element telephotometer designed to measure
312.5 nm radiation were used to track Minute Man II, Titan II, Thor-Delta,
Polaris, Atlas, Pershing and Thor-Asset Rockets at Patrick AFB from
December 1962 to October 1964.

Debell, A.G.; Simmons, F.S. and Levin, B.P., Spectral Radiances and
Emmissivities of Rocket Exhaust Plumes, Rocketdyne Report 12-3216, 1961,
(unavailable).

Balwanz, W.W., Radiation from Rocket Exhaust. Proceedings Fourth Naval
Science Symposium, Naval Problems in Electromagnetic Radiation Office of
Naval Research, Report ONR-6, 1960 (unavailable).

Bundy, F.P.; Johnson, R.H. and Strong, H.M., Final Report on Optical Studies
of Rocket Flames at Malta Test Station, G.E. Report Project Hermes No.
R50A0506, 1950 (unavailable). Study directed toward measuring the tempera-
ture of rocket flames as a function of their geometry.

Ferriso, C.C., The Emission of Hot CO_2 and H_2O in Small Rocket Exit Exhaust Gases. 8th Symposium (International) on Combustion, the Combustion Institute, Pittsburgh, PA. 1960, p. 275.

This article deals with quantitative infrared spectral data on hot gases produced by rocket motors. It contains an extensive treatment on the experimental procedures required to record spectra of a rocket exhaust.

Wolfhard, H.G. and Hinck, E., Elementary Processes in Low-Pressure Flames and Their Relation to Rocket-Exhaust Radiation. Eleventh Symposium (International) on Combustion, The Combustion Institute, Pittsburgh, PA, 1967, p. 589.

Flame characteristics are correlated with conditions occurring in rocket engines. Radiation emitted from the exhaust plume of a rocket is discussed as it relates to the following factors:

- a) Chemical composition of the propellants,
- b) Fuel-oxygen ratio of the propellant,
- c) Degree of mixing of the propellants in the motor,
- d) Expansion ratio of the nozzle,
- e) Ambient pressure of the exhaust plume.

The complete combustion of hydrocarbon fuels with oxygen leads to CO_2 + H_2O neither of which emit in the visible or UV. Contrary to these expectations, however, hydrocarbon-oxygen rocket exhaust emit light strongly due to imperfect propellant mixing leading to the formation of soot which emits a strong continuum. Excess fuel can also self-ignite in the air surrounding the plume leading to additional radiation. On the other hand, fuels such as alcohol and the amine-type will not form carbon and thus lack the continuum-type radiation.

Thomson, J.A.L. et al., High Altitude Rocket Plume Structure. General Dynamics/Convair, San Diego Report GD/COBEC5-023, Final Report on Contract NONR 4747/00, 1965.

A comprehensive review and extended analysis of the interaction of the expanding exhaust plume with the external air flow as the booster reaches the higher altitude.

Adamson, T.C., The Structure of the Rocket Exhaust Plume Without Reaction at Various Altitudes. University of Michigan, Institute of Science and Technology, (UMIST) Report 4613-45-T, 1963.

A study of the fluid-mechanical problems when an exhaust expands into the ambient environment.

Light, G.C. and Zittel, P.F., Detection of High-Altitude Missile Exhaust Plumes at Submillimeter Wavelengths. The Aerospace Corporation, Contract No. FO4701-82-C-0083, 1982, Air Force Systems Command, Los Angeles, CA. The burning of hydrogen fuels result in the formation of a large mole fraction of water vapor which cools to $\approx 50^\circ\text{K}$ during the adiabatic expansion from the rocket nozzle. The resulting cloud of cold H_2O vapor can attenuate the earth's blackbody radiation ($\sim 250^\circ\text{K}$ blackbody) at wavelengths corresponding to transitions between low-lying rotational states. On the other hand, the cloud can be a source of emission when viewed against the cold background (4°K) of space. In either case the H_2O cloud should be detected by its unique submillimeter ($\lambda = .539\text{mm}$) optical properties.

It is tentatively concluded that low-thrust plumes can be observed at high altitudes by this technique. A number of issues that require further study are presented.

Williams, W.D.; McCay, T.D.; Powell, H.M.; Weaver, D.P. et al.,
Experimental Study of the Plume Characteristics of an Aged-Monopropellant
Hydrazine Thruster. ARO, Inc., 1979, Air Force Rocket Propulsion Laboratory/PCAP, Edwards Air Force Base, California.

An experimental study of the exhaust plume of an aged (200,000 pulses), 0.44 N (0.1 lbf), hydrazine monopropellant thruster was performed with the goal of characterizing both the gas dynamic and contamination properties of the vacuum plume expansion. The thruster was operated in a high vacuum chamber over a thrust range from 0.44 to 1.10 N (0.1 to 0.25 lbf) with a nominal 0.14-sec-on/9.86-sec-off duty cycle using initial catalyst bed (Shell 405) temperatures of 376°K (200°F), and 589°K (600°F). Exhaust plume diagnostic systems employed included a mass spectrometer probe, a quartz crystal microbalance (QCM), a laser-Raman/Rayleigh scattering system, an electron beam fluorescence system, and a particle collection network. These systems determined plume species number densities and temperature, mass deposition rates, and the level of particulates in the plume; they also permitted visualization of the plume. Traditional engine performance parameters were also determined in order to relate performance and exhaust plume properties. Luminescent character of the plume was not reported.

Kummler, R.H.; Fisher, E.R.; Boynton, F.P., Substituted Hydrazine
Chemistry and Chemiluminescence in High-Altitude Plumes. Phys. Dyn.
Inc., 1973. U. S. Nat. Tech. Inform. Serv. No. 776040/8GA. (CA 81,564398).
 N_2H_4 and amino-based fuels undergo highly exothermic oxidn. reactions which can be a major source of IR energy under conditions appropriate to high altitude plume afterburning. In low pressure, high O atom environment, a single step, highly exothermic mechanism is capable of initiating

the emission of IR radiation. A specific set of reactions and energy transfer processes which characterize this potential emission are presented and an extensive review of the current literature related to amine oxidn. is included. A flow field calcn. directed toward testing the importance of chemi-excitation in amine afterburning is presented.

McGregor, W.K., On the Radiation from Small Particles. J. Quant. Spectrosc. Rad. Transf., 19, 659, 1978.

Visible-UV spectra of plume emission from solid propellant rockets reveal considerable continuum radiation similar to that of a blackbody. One source of this radiation is from particles (e.g., Al_2O_3) in the plume. This paper discusses the emissivity of particles as a function of wavelength.

Jensen, D.E. and Wilson, A.S., Prediction of Rocket Exhaust Flame Properties. Combustion and Flame, 25, 43, 1975.

Describes a general technique for predicting various properties of low-altitude rocket exhaust flame. Study is not applicable to reactions of high activation energy such as the formation of nitrogen oxides and the ionization of alkali metals.

Cavorc., M. and Feinburg, R.M., Formation of NO in Shock-Heated Air.

11th Symposium (International) on Combustion, The Combustion Institute, Pittsburgh, PA 1963, p. 137.

Chemical changes in shocked air become important in high-speed flight above Mach 6. In particular, NO becomes a significant constituent of air. Two mechanisms may be operating at these temp. ($\sim 2000^\circ\text{C}$)

a) $\text{N}_2 + \text{O}_2 \rightarrow 2\text{NO}$, or b) $\text{O}_2 + \text{M} \rightarrow 2\text{O} + \text{M}$; $\text{N}_2 + \text{O} \rightarrow \text{NO} + \text{N}$; $\text{N} + \text{O}_2 \rightarrow \text{NO} + \text{O}$). Nitric oxide is lost from the reaction $2\text{NO} \rightarrow \text{N}_2\text{O} + \text{O}$.

Heicklen, J., Gas-Phase Chemistry of Re-Entry. AIAA Journal, 5, 4, 1967.

Friction between missile and the atmosphere during re-entry results in

the electronic excitation of molecules which emit in the visible and ultraviolet portion of the spectrum. Well known examples are the second-positive bands of N_2 and $\gamma + \beta$ bands of NO.

Swenson, G.R.; Mende, S.B.; Clifton, K.S., Ram Vehicle Glow Spectrum;

Implication of Nitrogen Dioxide Recombination Continuum. (Lockheed Palo Alto Res. Lab., Palo Alto, CA. Geophys. Res. Lett. 12, 97, 1985.

The glow on the shuttle tail pod was analyzed and it was determined that the emission originates from the recombination continuum of NO_2 .

Killinger, D.K.; Menyuk, N., and Mooradian, A., Sensing of Turbine Engine Gases. Technical Report (NTIS) ESO-TR-82-014, AFESC/ESL-TR-82-016, Lincoln Lab., MIT, Lexington, MA, 1982.

This article discusses the long-range (2.7 km) sensing of hydrazine using a CO_2 laser. NO was also detected by the same laser. The method requires a "Topographic Target" to reflect the beam back to the analyzer.

B. Kinetics, Mechanism and Thermodynamics of the Combustion of UDMH/
 N_2O_4 Propellants and Flames.

Jensen, D.E., and Jones, G.A., Reaction Rate Coefficients for Flame Calculations. Propellants, Explosives and Rocket Motor Establishment, Westcott, England, PERME-TR-35; BR58144, 1977.

Report contains an extensive listing of rate constants and equilibrium constants for reactions of interest to workers in the field of flame and propellant chemistry. The rate coefficients are expressed as a function of temperature (100° - 3000°K range).

Alemasov, V.E.; Dregalin, A.F.; Tishin, A.P.; Khodyakov, V.A. and Kostin, V.N. Thermodynamic and Thermophysical Properties of Combustion Products. United States-Israel Binational Science Foundation, Report No. ISBN-0-7065-1571-4, 1976, p. 533.

Sawyer, R.F. and Glassman, I. (U. California, Berkeley), Symp. Combust. 11, 861-9, 1966.

Sawyer, R.F., The Homogeneous Gas Phase Kinetics of Reactions in the Hydrazine-Nitrogen Tetroxide Propellant System. Dept. of Aerospace and Mechanical Sciences, Princeton Univ., TR 761, AFSOR-66-0855, AD-634277, 1965.

Rates, overall activation energies, and orders of subject reactions were detd. under comparable conditions in an adiabatic flow reactor. In this app. the reaction at $\leq 1300^\circ\text{K}$ under adiabatic condition is monitored by the temp. change through the reaction zone. By varying the carrier-gas temp., flow velocity, and reactant concns. one can measure reaction rates as a function of temp. and concn. to obtain the reaction parameters noted. The reactants and carrier gases were completely mixed during flowing about 5 cm. An induction period at const. temp. and a reaction zone of rising temp. then followed. Vapor of N_2H_4 evapd. and dild. with N_2 in a vaporizer was delivered to the reactor at about 110° and injected into the oxidizer-contg. hot carrier gas. NO_2 was prepd. from heated liq. N_2O_4 . Other gases used were obtained as such. Besides the reaction of N_2H_4 with NO_2 , those with O_2 , NO , and O_2/NO mixts. in the same reactor were studied for direct comparison of the reaction parameters and for deducing the relative roles of N_2H_4 decompn. and oxidn. Reactant concn. in the carrier N_2 were $(0.3-3) \times 10^{-7}$ moles/cc. with partial pressures of 6-30 mg. Hg in a total pressure of 1 atm., at $810-1060^\circ\text{K}$. The $\text{N}_2\text{H}_4/\text{NO}_2$ reaction occurred in 2 distinct steps of greatly different reaction rates; the temp. profile shows 2 reaction traces sepd. by a const.-temp. plateau, whereas the other reactions show monotonically rising temps. through the reaction zone. Each step involves a no. of sep. reactions and would, for a stoichiometric mixt., consume half the N_2O_4 : Step 1: $\text{N}_2\text{H}_4 + \text{NO}_2 \rightarrow \frac{1}{2}\text{N}_2\text{H}_4 + \text{H}_2\text{O} + \text{NO} + \text{H}_2$ Step 2: $\frac{1}{2}\text{N}_2\text{H}_4 + \text{NO} \rightarrow \text{H}_2\text{O} + \text{N}_2$. Comparison of measured and predicted heats of reaction for both steps indicates that Step 2 is accompanied by a 15% decompn.: $\text{N}_2\text{H}_4 \rightarrow \text{NH}_3 + \frac{1}{2}\text{H}_2 + \frac{1}{2}\text{N}_2$. The $\text{NH}_3 + \frac{1}{2}\text{N}_2$. The NH_3 and H_2 did not react with NO at these

temps. Step 1 has a higher rate and a lower activation energy than the N_2H_4 decompn., and occurs not by N-N bond fracture but primarily by abstraction of H from N_2H_3 . The reaction $N_2H_4 + O_2 \rightarrow 2H_2O + N_2$ goes to completion at a single rate which is proportional to $[N_2H_4]$ but independent of $[O_2]$. Decompn. and oxidn. are concurrent. Abstraction of H by O_2 is much slower than by NO_2 . The following rate consts. are given for $N_2H_4 + NO_2$:

Step 1, $d[N_2H_4]/dt = -k_1[N_2H_4][NO_2]$, $k_1 = 10^{15.83} \exp(-26,700/RT) [cc.mole^{-1}sec.^{-1}]$,
 Step 2, $d[N_2H_4]/dt = -k_2[N_2H_4]$, $k_2 = 10^{10.17} \exp(-39,600/RT) [sec.^{-1}]$; for
 $N_2H_4 + O_2$, $d[N_2H_4]/dt = -k_3[N_2H_4]$, $k_3 = 10^{9.91} \exp(-37,200/RT) [sec.^{-1}]$; for
 $N_2H_4 + NO$ and O_2 , $d[N_2H_4]$, $k_3 = 10^{10.35} \exp(-39,100/RT) [sec.^{-1}]$; and for
 $N_2H_4 + NO$, $d[N_2H_4]/dt = k_4[N_2H_4]$, $k_4 = 10^{11.48} \exp(-45,400/RT)$. Postulated reaction mechanisms are presented in a table listing 22 separate reactions.

Saad, M.A.; Detweiler, M.B. and Sweeney, M.A., Analysis of Reaction Products of Nitrogen Tetroxide with Hydrazines under Nonignition Conditions. AIAA Journal, 10, 1073, 1972.

Products formed by reaction of nitrogen tetroxide and hydrazine or methylhydrazines at low temperatures were collected and analyzed, using mass spectroscopy, gas chromatography and infrared absorption spectroscopy. It was found that hydrazine and nitrogen tetroxide form water, nitrogen, nitric oxide, hydrazinium nitrate, and ammonia. When monomethylhydrazine is used instead of hydrazine, the products include methylamine, dimethylamine, methanol, methylnitrosamine, dimethylnitrosamine, N-methylformamide, water, methylhydrazinium nitrate, nitrogen, and dissolved oxides of carbon and nitrogen. When 1,1-dimethylhydrazine is used in place of hydrazine, the products include methylamine, dimethylamine, methanol, dimethylnitrosamine, dimethylformamide, formamide, nitrogen, water, dimethylhydrazinium nitrate, and dissolved oxides of carbon and nitrogen. Between 60% and 80% of the liquid portion of the products is dimethylnitrosamine. Based on the evidence provided by these analyses, reaction mechanisms are proposed.

Tuazon, E.C.; Carter, W.P.L.; Brown, R.V.; Winer, A.M. and Pitts, Jr., J.N.,
Gas-Phase Reaction of 1,1-Dimethylhydrazine with Nitrogen Dioxide. J. Phys.
Chem. 87, 1600, 1983.

The gas-phase reaction of part-per-million concentrations of nitrogen dioxide with 1,1-dimethylhydrazine in air and in N_2 at 298 K was investigated by in situ long-path Fourier transform infrared (FT IR) spectroscopy. In both air and N_2 , the reaction occurs with an apparent overall rate constant (defined in terms of rates of hydrazine decay) of $(2.3 \pm 0.2) \times 10^{17} \text{ cm}^3 \text{ molecule}^{-1} \text{ s}^{-1}$. The major products were nitrous acid and tetramethyltetrazene-2, with the overall reaction stoichiometry being $(CH_3)_2NNH_2 + 2NO_2 \rightarrow 2HONO + \frac{1}{2}(CH_3)_2NN=NN(CH_3)_2$, regardless of initial reactant concentration ratios or whether the reaction was carried in air or in N_2 . There was no observable reaction of NO with $(CH_3)_2NNH_2$ in N_2 . However, when NO_2 , was also present, NO participates in the reaction, causing formation of N_2O , N-nitrosodimethylamine, and significant amounts of an unidentified compound believed to be an N-nitrosohydrazine, in addition to HONO and tetramethyltetrazene-2. Probable mechanisms accounting for these observations are discussed.

Sawyer, R.F., Theoretical Effects of Nonequilibrium Combustion on $N_2H_4|N_2O_4$
Propellant Performance. J. Spacecraft 5, 116 1968.

Combustion chamber kinetics remains complex and still largely unknown for the $N_2H_4|N_2O_4$ propellant systems. Nonetheless, propellant performance can be ascertained using simplified models based on the concept of partial equilibrium combustion. The model proposes that all hydrazine in excess of stoichiometric requirements, i.e. 2:1, $2N_2H_4 + N_2O_4 \rightarrow 4H_2O + 3N_2$, will decompose to produce NH_3 , $N_2H_4 \rightarrow NH_3 + \frac{1}{2}H_2 + \frac{1}{2}N_2$. Similarly, in the N_2O_4 -rich case, N_2O_4 decomposes to give NO, $2N_2O_4 \rightarrow 2NO + O_2$. These results were confirmed in part by Burrows who obtained spectrographs of the emitting gases in the fuel rich and oxidizer rich regions of a rocket engine. The fuel rich zones showed $NH + NH_2$ emissions. These radicals are considered to be initial products in the decomposition of N_2H_4 .

Weiss, H.G., Basic Study of the Nitrogen Tetroxide-Hydrazine Reaction.

Dyn. Sci. Corp., Monrovia, Calif. NASA (Nat. Aeronaut. Space Admin.) Access.
1965, Number: NASA-CR-64338, p. 56.

Citation: Sci. Tech. Aerospace Rept. 1965, 3(19), N65-30838, Avail: CESTI Price \$3,
CA: 66(26)117536h, Technical Report.

In this report the reaction between hydrazine and nitrogen tetroxide were studied at low temperatures using IR spectra and differential thermal analysis. It was found that reaction occurs at temperatures as low as -133°C . From measurements of the gas evolved at this temperature it appears that the initial stages of the reaction involve adduct formation. A further reaction, involving heat evolution, occurs at -58°C . The products of this reaction include hydrazinium nitrate, nitrous oxide and traces of nitric oxide and N_2 .

Under actual conditions in an engine these initial reactions would occur very rapidly. They estimate that the reaction goes to completion essentially on contact. The very rapidity of the reaction requires the utilization of special injector techniques to accomplish liquid phase mixing before the gases and heat evolved, disrupt the mixing process and decrease performance. The study describes experiments using additives to either inhibit the reaction or increase the rate of miscibility of N_2O_4 /hydrazine.

Mayer, S.W.; Taylor, D. and Schieler, L., Preignition Products from Storable Propellants at Simulated High-Altitude Conditions. Aerospace Corp.

TR-0158(9210-02)-1 1967.

Report describes the mass spectrometric analysis of preignition reaction products between N_2O_4 and a variety of hydrazines. In each case nitrosamine or the corresponding methyl substituted nitrosamine was detected. IR studies revealed the presence of nitrosamines as well as hydrazinium nitrate formed from hydrazine oxidation.

Christos, T.; Miron, Y.; James, H. and Perlee, H.E., Combustion Characteristics of Condensed-Phase Hydrazine-Type Fuels with Nitrogen Tetroxide. U.S.

Dept. of the Interior, Bur. of Mines, Pittsburgh, PA. J. Spacecr. Rockets,

1967, 4, 8, pp. 122-9.

Aerazine-50 (50% H_2N_2 /50% UDMH)/ N_2O_4 mixtures were mixed with liquid N_2 and placed in a differential scanning calorimeter while still in the frozen state. The temperature initially at -80°C was raised slowly. At -60°C a highly exothermic reaction was recorded. The results were similar to Weiss. Hydrazine nitrate was found as a residue.

Ray, A.B.; Koehler, G.; Salser, G.E. and Dauerman, L., Evidence for the Formation of Azides in the $\text{N}_2\text{H}_4/\text{N}_2\text{O}_4$ Reaction. New York Univ., Bronx, N.Y. AIAA (Amer. Inst. Aeronaut Astronaut.) J., 1968, 6, 11, pp. 2186-7.

Saturated carbontetrachloride solutions of hydrazine and nitrogen tetroxide were prepared. An immediate reaction occurred upon mixing. The solid products were taken and analyzed with IR. Azides were detected.

Roux, J.A.; Wood, B.E.; Alt, R.E.; Frazine, D.F.; Smith, A.M. and Scott, H.E., Optical Properties of Bipropellant Exhaust Constituents Condensed at 77K. AEDC Div., Aro, Inc., Arnold Air Force Stn., TN. J. Spacecr. Rockets, 1979, 16, 6, pp. 373-81.

Roux, J.A. and Wood, B.E., Infrared Optical Properties of Solid Monomethyl Hydrazine, Nitrogen Tetroxide (N_2O_4), and Hydrazine (N_2H_4) at Cryogenic Temperatures. Univ. Mississippi, University, MS., J. Opt. Soc. Am., 1983, 73, 9, pp. 1181-8.

Exhaust constituents for a nitrogen tetroxide/monomethyl hydrazine propellant were condensed out at cryogenic temperatures and examined with IR. In addition to CO_2 and H_2O some unreacted N_2O_4 was detected as well as small amounts of NO.

Miyajima, H. and Sakamoto, H., Gas Phase Ignition of Hydrazine with Nitrogen Dioxide. Kakuda Branch, Natl. Aerosp. Lab., Miyagi, Japan. Combust. Sci. Technol., 1973, 8, 4 pp. 199-200.

The induction period in the gas-phase reaction between hydrazine and nitrogen

dioxide was measured as a function of temperature (70-160°) and pressure (40-90 Torr). An apparent activation energy at 9.0 KCal/mole was determined.

Lawton, E.A. and Moran, C.M., MMH-nitrate and Plume Deposits from NTO/MMH Engines. Jet Propul. Lab., California Inst. Technol., Pasadena, CA. CPIA Publ., 1983, 384, JANNAF Plume Technol. Meet., 14th, Vol. 1, pp. 1-8.

A hygroscopic white solid deposit from the plume of a methylhydrazine/ N_2O_4 rocket motor was determined to be methylhydrazine nitrate. This appears to be the same deposit found by Weiss and Christos, who studied the same reaction at cryogenic temperatures.

McCay, T.D.; Powell, H.M. and Busby, M.R., Direct Mass Spectrometric Measurements in a Highly Expanded Rocket Exhaust Plume. Aro., Inc., Arnold Air Force Station, TN. J. Spacecr. Rockets, 1978, 15, 3, pp. 133-8.

An absolute measurement of the constituency of a 11b thrust rocket engine exhaust was attempted by sampling the plume with a mass spectrometer probe. At an O/F ratio of 1.60 over forty species were detected including NO. (.0022 mole fraction). The amount of water found was always less than expected for complete combustion. Signal variations from the combustion products were measured as a function of O/F ratio. A significant increase in the NO signal was recorded for increasing O/F ratios due to the increased amount of N_2O_4 available for cracking.

Ozto, K. and Shelef, M., Studies of Surface Reactions of Nitric Oxide by Isotope Labeling. V. Reaction Between Nitric Oxide and Hydrazine at 25-125 deg. Fuel Sci. Dep., Ford Mot. Co., Dearborn, Mich. Catal., Proc. Int. Congr., 5th, Editor: Hightower, J.W., 1973, 1, pp. 305-16.

Products of the above named reaction were separated and analyzed using Mass, UV, IR + NMR techniques.

Singh, S.P. and Prasad, R.K., Analysis of the Ignition Products of Un-symmetrical Dimethyl Hydrazine with Nitric Acid and the Probable Reaction Mechanism. Dept. Chem., R.D.S. Coll., Muzaffarpur, India. J. Indian Chem. Soc., 1983, 60, 2, pp. 170-5.

Reacting NO with N_2H_4 which exists as a liquid film on a solid substrate produces N_2O , $N_2 + N_2O$, i.e., $4NO + N_2H_4 \rightarrow 2N_2O + N_2 + 2H_2O$. If one starts with $N^{15}O$ and $N_2^{14}H_4$ the products are almost exclusively (97% isotopic purity) $4N^{15}O + N_2^{14}H_4 \rightarrow 2N_2^{15}O + (N_2^{14} + N_2^{15}) + 2H_2O$.

Gray, P. and Spencer, M., Studies of the Combustion of Dimethyl Hydrazine and Related Compounds. 9th Symposium (International) on Combustion, The Combustion Inst., Pittsburgh, PA., 1961, p. 148.

The critical pressure limits of spontaneous ignition were determined for the systems: $N_2H_4 + NO$; $N_2H_4 + N_2O$; and $DMH + O_2$. Chemiluminescence was found to occur in $DMH + O_2$ mixtures in the preignition regions.

Williams, W.D.; Powell, H.M.; McGuire, R.L.; Rice, L.L.; Jones, J.H.;

Weaver, D.P. and Lewis, J.W.L., Diagnostics of Rocket Plume-Airstream Turbulent Mixing Using Laser-Raman Scattering. Aro. Inc., Arnold Air Force Station, TN. Prog. Astronaut, Aeronaut., 1978, 58, Turbul. Combust., pp. 273-89.

A $MeNHNH_2/N_2O_4$ rocket exhaust plume was entrained with a co-flowing air stream at mach 0.35-2.05 and a simulated altitude of 1.5-20 km. The temperature (900-1800°K) and species density (10^{17} - $10^{19}/cm^3$) within the plume were determined.

Bellerby, J.M., The Autooxidation of Hydrazine and Alkyl Substituted Hydrazine Vapors. Memo - propellants, Explos. 92, 1981.

Stone, D.A., Autooxidation of Hydrazine, Monomethylhydrazine and unsymmetrical dimethylhydrazine. Proc. Spie-Int. Soc. Opt. Eng. 1981, 289 (Int. Conf. Fourier Transform Infrared Spect.)

The above two articles deal with the kinetics and products in the gas phase, room temperature oxidation of hydrazines. Air oxidation of hydrazine is of concern to both the propellant and environmental chemist.

Summers, W.H. and McMullen, E.T., Combustion of the $N_2H_4-N_2O_4$ Propellant System. Edwards Air Force Base, Calif. IAA (Int. Aerosp. Abstr.) Access. 1966, Number: A66-34223, p. 11.

This technical report deals with an experimental investigation of the $N_2H_4-N_2O_4$ propellant system for the purpose of determining its reaction mechanisms at rocket chamber conditions. A mass spectrometer was used to analyze the combustion species in the rocket plume.

Lee, A. and Houseman, J., Popping Phenomena with Nitrogen Tetroxide/Hydrazine Injectors. Jet. Propul. Lab., California Inst. Technol., Pasadena, Calif. West, States Sect. Combust. Inst. (Pap.) 1970. Number: 70-25, p. 21,

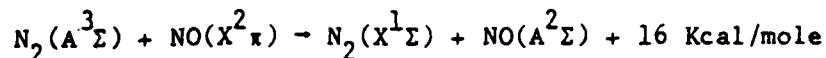
Rocket engines employing N_2O_4 /hydrazine propellants are subject to occasional hard starts which are referred to as "popping phenomena." It has been suggested (Saad, Detweiler and Sweeney) that azides formed by oxidizing hydrazine are the cause of these violent detonations. However, Bernard and Duford blame the hard starts to the decomposition of hydrazine nitrates, i.e., $RNH + HNO_3 \rightarrow RNH_2^+ NO_3^-$ - decomposition.

C. Fundamental Studies on the Mechanism for the Formation, Emission and Quenching of $NO(A^2\Sigma)$.

Becker, K.H. and Bayes, K.D., Chemiluminescence from Oxygen Atom-Hydrazine Flames. J. Phys. Chem. 71, 371, 1967.

Mixtures of gaseous hydrazine and atomic oxygen undergo a rapid chemiluminescent reaction. The emitting species include NH , NH_2 , OH and NO . A major finding of this study was that the intensity of the NO bands increased strongly by the addition of NO . This suggests that the excited NO is not formed directly in

a chemical reaction but rather acquires its electronic excitation by energy transfer from another molecule. Energetic considerations suggest strongly that the most likely source is $N_2(A^3\Sigma)$: i.e.,



Birely, J.H., Kinetics and Mechanisms of Ultraviolet Emission. Aerospace Corp. El Segundo Calif. Lab Operations, Corp. Source Codes: 009575, Report No.: TR-0074(4642)-1; SAMSO-TR-73-267, 1973, p. 27.

Contract No. F04701-73-C-0074.

Excellent review of the mechanisms for production of near-ultraviolet and vacuum-ultraviolet radiation in reactions of oxygen with C_2H_2 , C_2O_4 , C_3O_2 , C_2F_2 , N_2H_4 , and several other molecules. A copy of the report is attached. The following emitting species are discussed. 1) CO Fourth - Positive Band; 2) CO Cameron Bands; 3) N_2 Lyman-Birge-Hopfield Bands; 4) N_2 Birge-Hopfield Bands; 5) NO emissions; 6) OH emissions. With regard to NO emissions, Birely recommends that more work be done on the combustion of amine type fuels. In particular, he suggests that rate constants for the formation of various ground states and electronically excited intermediates be determined. In addition, the kinetics of emission should be characterized more fully.

Brennan, W. and Shane, E.C., Energy Transfer Mechanisms in Optical Observables.
Part I. The nitrogen afterglow and the rate of recombination of nitrogen atoms in the presence of nitrogen, argon and helium. Part II. Chemiluminescence of the atomic oxygen-hydrazine reaction. Pennsylvania Univ., Philadelphia
Dept. of Chemistry. Corp. Report No. AFOSR-Tr-71-0151, 31 Jan '71,
p. 57. Contract No. F44620-67-C-0106, AF-9739.

Shane, E.C. and Brennan, W., Chemiluminescence of the Atomic Oxygen-Hydrazine Reaction. J. Chem. Phys. 55, 1479, 1971.

Chemiluminescence from the atomic oxygen-hydrazine flame was studied. As in previous studies emission was observed from $OH(A^2\Sigma - X^2\Pi)$, $NO(A^2\Sigma - X^2\Pi)$,

$\text{NH}(\text{A}^3\text{x-X}^3\Sigma)$, $\text{NH}_2(^2\text{A}_1-^2\text{B}_1)$ and from NO_2 when the O atoms were in excess.

Quenching experiments in which NH_3 was added to the flame resulted in suppressing the NO, OH, and NH emission by equal fractions. These results are consistent with a mechanism in which NO, OH and NH are excited from their ground state by a common energetic precursor, namely $\text{N}_2(\text{A}_3\Sigma)$.

Crosley, D.R.; Smith G.P. and Golden, D.M., Laser Probes of Propellant Combustion Chemistry. SRI Int. Menlo Park, CA USA. Report Date: 1984, Number: SRI-MP-84-053, ARO-17416.9-CH, p. 201.

Laser-induced fluorescence (LIF) can be used to measure the atomic, diatomic, and triatomic free radicals that are the intermediates in combustion chemistry. Coupled with detailed models, which incorporate a sound and consistent set of reaction rate constants, such measurements can lead to an understanding of that chemistry, having predictive value for use under experimentally difficult conditions.

This report describes the development of LIF techniques, the applications of such techniques to flames and to laser pyrolysis/laser fluorescence kinetics experiments, studies of rate constant estimations and detailed modeling of combustion chemistry. The chemistry studied is that of combusting mixtures of $\text{CH}_4/\text{N}_2\text{O}$, $\text{CH}_2\text{O}/\text{N}_2\text{O}$, $\text{CH}_2\text{O}/\text{NO}_2$ and related compounds. These contain the chemical networks, individual reactions, and radical species present in the gas-phase combustion of nitramine propellants, such as HMX and RDX.

The tasks described are LIF diagnostic studies on O, N, OH, NCO, and NH_2 in flow systems and flames, rate constant estimation studies for unimolecular decomposition of CH_2O and several hydrocarbons, modelling of the $\text{CH}_2\text{O}/\text{N}_2\text{O}$ flame, and laser pyrolysis/laser fluorescence studies of $\text{CH}_4/\text{N}_2\text{O}$ and $\text{CH}_2\text{O}/\text{N}_2\text{O}$ chemistry.

Nine journal articles and 18 conference presentations are included in the report.

Slanger, T.G., Chemistry of Nitrogen Compounds in Combustion Processes. SRI International, Menlo Park, CA.

Sponsor: Army Research Office, Research Triangle Park, NC., Report NO. ARP-17561.3-CH, 2 Mar '84, p. 86. Contract No. DAAG29-81-K-0001.

The photochemistry and kinetics of nitrogenous molecules, using F_2 and KrF excimer lasers as initiating sources are described. Resonance excitation of NO by the 1576\AA laser line was observed and the spectroscopy clarified. The photophysics of $CN(A^2\Pi)$ is described.

Bernard, M.L.J. and Duford, J., On The Existence of Detonation Conditions on the Combustion of Some Nitric Acid Propellants. 8th Symposium (international) in combustion, p. 1074, 1960.

While investigating the ignition delays of hypergolic liquids in a micro-rocket with a transparent window they noticed that, under certain conditions, a build up of pressure accompanied the phenomenon of ignition. They assumed that the primary reaction of nitric acid with amine-type fuels was the formation of amine nitrates, i.e., $RNH + HNO_3 \rightarrow RNH_2^+ NO_3^-$, followed by a more or less explosive decomposition.

Moore, G.E.; Shuler, K.K.; Silverman, S. and Herman, R., Reaction of Ammonia and Hydrazine With Oxygen Atoms and Hydrogen Atoms in Atomic Flames. J. Phys. Chemistry 60, 813, 1956.

Hydrazine was reacted with O produced by a silent discharge and the emission bands of the products were determined. They were $NH_2(\alpha, \approx 4000\text{\AA})$; $NH(\approx 3360\text{\AA})$; $OH(\approx 3064\text{\AA})$ and the γ bands of NO. When the N_2H_4/O ratio is small the air afterglow from the formation of NO_2 appears strongly.

Vinogradov, I.P. and Vilesov, F.I., Study of the luminescence of Imino and Amino Radicals Formed During the Photodissociation of Ammonia, Hydrazine,

and N-N-dimethylhydrazine. ZH. FIZ. Khim. 51, 2017, 1977. CA: 87(22)175038s.

The abs. value of the quantum yield of radical luminescence of NH and NH_2 was obtained in the photodissocn. of gaseous NH_3 , N_2H_4 , and N,N-dimethylhydrazine in the spectral range from generation threshold up to 885 Å.

The velocity const. k is given for self-quenching of luminescence for NH and NH_2 radicals. The value of k is not dependent upon the exciting radiation energy.

Heicklen, J. and Cohen, N., The Role of Nitric Oxide in Photochemistry.

Advances in Photochemistry, Vol. 5, 1968. Noyes, A.W.; Hammond, G.S.; Pitts, Jr. J.M., Editors.

A review of the spectroscopy, energetics and reactions of nitric oxide.

Dagnall, R.M.; Smith, D.J.; Thompson, K.C., and West, T.S., Emission Spectra Obtained from the Combustion of Organic Compounds in Hydrogen Flames. Analyst, 94, 874, 1969 .

A study is presented of the emission spectra produced by nebulisation of organic liquids into a nitrogen-hydrogen diffusion flame burning in air. All organic nitrogen-containing compounds tested gave Cn, Nh, and NO emissions. A spectrum of 50 percent methanol-50 percent 0.88 ammonia solution U/V in the nitrogen-hydrogen diffusion flame is shown.

D. Computer Modeling of the Plume Chemistry Responsible for Emission in the Ultraviolet and Visible Regions of the Electromagnetic Spectrum.

Zhuang, Fengchen; Zhou and Jin, Steady-State Theory for Ignition Computation of Unsymmetrical Dimethylhydrazine Droplets. Gongcheng Rewuli Xuebao, 4, 85-91, 1983.

Kohl, F.J.; McBride, B.J.; Zelenznik, F.J. and Gordon, S., Use of the NASA Chemical Equilibrium Compositions Code for the Prediction of Combustion Gas Deposit Compositions. Proc. Electrochem. Soc., 83-7, 308-18, 1983.

Mitchell, R.E. and Kee, R.J., General-Purpose Computer Code for Predicting Chemical-Kinetic Behavior Behind Incident and Reflected Shocks.

Journal: Report, Date: 1982, Number: SAND-82-8205; Order No. DE82015878, Pages: 31pp., Citation: Energy Res. Abstr. 1982, 7(20), Abstr. No. 54622, Avail: NTIS.

Seigny, Rene, The Lewis Chemical Equilibrium Program with Parametric Study Capability. Location: Eng. Syst. Dep., Comput. Sci. Corp., El Segundo, CA. Journal: NASA (Contract. Rep.) CR Date: 1981, Number: NASA-CR-161811, Pages: 287 pp., Citation: Sci. Tech. Aerosp. Rep. 1981, 19(17), Abstr. No. N81-26275, Avail: NTIS.

Briscoe, F.; Curtress, N.; Farmer, C.L.; Fogg, G.F. and Vaughan, G.J., EEC-sponsored Theoretical Studies of Gas Cloud Explosion Pressure Loadings. UKAEA, Culcheth/Warrington, Engl., Journal: Comm. Eur. Communities, (Rep.) EUR, Date: 1979, Number: EUR 6119, Pages: 120 pp.

Bunn, M.M.; Broschk, J. and Manski, D., Program Listing of an Analytic Mass Model for Chemical Rocket Stages.

Chem. Raketenantriebe, Dtsch. Forsch.-Und Versuchsanst. Luft- und Raumfahrt, Lampoldshausen, Ger., Journal : Report, Date: 1976, Number: DLR-1B-456-76/2, Pages: 44pp. Coden: D9REPB, Language: German, Citation: Sci. Tech. Aerosp. Rep. 1978, 16(9), Abstr. No. N78-18125, Avail: NTIS.

Gordon, S. and McBride, B.J., Computer Program for Calculation of Complex Chemical Equilibrium Compositions, Rocket Performance, Incident and Reflected Shocks, and Chapman-Jouguet Detonations. Journal: NASA (Spec. Publ.) SP, Date: 1976, Number: NASA-SP-273, Rev. Pages: 145 pp. Citation: Sci. Tech. Aerosp. Rep. 1978, 16(8), Abstr. No. N78-17724, Avail: NTIS.

Morsi, S.E. and Ragheb, M., On the Problem of Homogeneous Simultaneous Gas Equilibriums and Flame Temperatures. 1. Explicit Equations and Numerical Solution for the Carbon, Hydrogen, Oxygen, Nitrogen Thermodynamic System. Egypt. J. Chem. 18, 823-32, 1978.

Case, P.L. and Pratt, D.T., A New Integration Algorithm for Chemical Kinetics. Univ. Utah, Salt Lake City, Utah, Journal: West. States Sect., Combust. Inst., (Pap.), Date: 1977, Number: WSS/CI 77-23, Pages: 15 pp.

Bastos-Netto, D. and Alonso, J.A.M.P., Calculation of High Temperature Ionizing Chemical Equilibrium Compositions. AIAA Pap. 75-1345, 1975.

Bittker, D.A. and Scullin, V.J., General Chemical Kinetics Computer Program for Static and Flow Reactions, with Application to Combustion and Shock-Tube Kinetics. Lewis Res. Cent., NASA, Cleveland, Ohio. Journal: NASA Tech. Note, Date: 1972, Number: NASA TN D-6586, Pages: 187.

Franciscus, L.C. and Healy, J.A., Computer Program for Determining Effects of Chemical Kinetics on Exhaust-Nozzle Performance. Lewis Res. Center, Cleveland, Ohio. Journal: NASA Tech. Note, Date: 1967, Number: No. TN D-4144, Pages: 104, Avail: CFSTI.

Gordon, S. and McBride, B.J., Computer Program for Calculation of Complex Chemical Equilibrium Compositions, Rocket Performance, Incident and Reflected Shocks, and Chapman-Jouguet Detonations. Lewis Res. Cent., NASA, Cleveland, Ohio. Journal: NASA Spec. Publ., Date: 1971, Number: NASA SP-273

Gordon, S. and McBride, B.J., Computer Program for Calculation of Complex Chemical Equilibrium Compositions, Rocket Performance, Incident and Reflected Shocks, and Chapman-Jouquet Detonations (NASA SP-273) Date: 1971, Pages: 245 pp. CODEN: BookA7, Publisher: (NTIS).

Zelevnik, F.J. and Gordon, S., A General IBM 704 and 7090 Computer Program for Computation of Chemical Equilibrium Composition, Rocket Performance, and Chapman-Jouquet Detonations. NASA TND-1454, Oct. 1962, NASA, Wash.

IV. RECOMMENDATIONS:

a) Mini Grant Request.

Conducting a survey of the literature on the formation and luminescence of nitric oxide in rocket exhausts fueled by UDMH/ N_2O_4 has afforded me the opportunity to expand my own area of expertise on fluorescence quenching mechanisms into a field which is of interest to Air Force scientists who are developing improved methods of high-altitude missile detection.

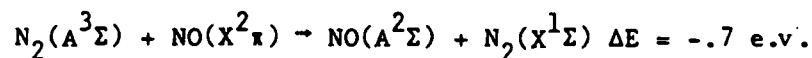
Recent discoveries have shown that it may be possible to detect ICBM's from satellites equipped with sensors attuned to the distinctive plume signature resulting from the ultraviolet radiation emitted by the chemiluminescent agents present in rocket exhausts.

The quantity of ultraviolet radiation emerging from a rocket plume will be determined by the rate of formation of the emitting species less the rate of quenching of the excited state by agents present in the plume and capable of destroying the photoexcited state before it emits. An ability to identify these quenching agents is important not only for an understanding of the mechanism of the chemical reaction between hydrazine and N_2O_4 but also for the development of computer programs

capable of modeling the photochemistry occurring in the rocket plume.

A worthwhile follow-on research project would be to (a) identify those species present in a rocket plume capable of quenching the nitric oxide fluorescence, and to (b) determine the mechanism(s) by which these substances quench the nitric oxide fluorescence. I am submitting a mini grant application describing this project and titled, "Fluorescence Quenching of $\text{NO}(\text{A}^2\Sigma)$."

b) The mechanism(s) for the formation of $\text{NO}(\text{A}^2\Sigma)$ in a $\text{UDMH}/\text{N}_2\text{O}_4$ flame lacks final scientific proof. Three mechanisms are possible. The first, population of the $\text{NO}(\text{A}^2\Sigma)$ state which is 5.4 e.v. in energy above the ground state by thermal excitation is not expected to be important even at the maximum flame temperature of $\approx 2800^\circ\text{C}$. A second mechanism would be the formation of $\text{NO}(\text{A}^2\Sigma)$ via a chemiluminescent reaction pathway. The recombination of nitrogen and oxygen has been investigated as a possible mechanism though the concentration of oxygen and nitrogen atoms in the flame is not expected to be high enough to lead to the formation of an appreciable amount of $\text{NO}(\text{A}^2\Sigma)$ by this route. The third and most probable mechanism is the formation of $\text{NO}(\text{A}^2\Sigma)$ via an energy transfer mechanism. At least two groups of workers have suggested this process and have implicated triplet N_2 as a precursor of photoexcited NO, i.e.,



has a radiative lifetime of 0.8 sec. and in the absence of competing processes should provide for the efficient production of $\text{NO}(\text{A}^2\Sigma)$.

However, no direct evidence that would substantiate the validity of this proposal currently exists. I recommend a laser experiment be performed to provide this evidence. An argon laser could be used to excite N_2 to

the triplet state. The $N_2(A^3\Sigma)$ would then be admitted to a flow system where it could mix, collide and transfer energy to NO. The photoexcited NO could then be detected through its characteristic fluorescence.

1985 USAF-UES SUMMER FACULTY RESEARCH PROGRAM/
GRADUATE STUDENT SUMMER SUPPORT PROGRAM

Sponsored by the
AIR FORCE OFFICE OF SCIENTIFIC RESEARCH
Conducted by the
UNIVERSAL ENERGY SYSTEMS, INC.

FINAL REPORT

NUMERICAL MODELING AND INVERSION OF $63\mu\text{m}$
EARTHLIMB EMISSION FROM ATOMIC OXYGEN

Prepared by:	James P. Riehl
Academic Rank:	Associate Professor
Department and	Department of Chemistry
University:	University of Missouri-St. Louis
Research Location:	Air Force Geophysics Laboratory Infra-red Technology Division Infra-red Dynamics Branch
USAF Research	Dr. Ramesh D. Sharma
Date:	August 20, 1985
Contract No:	F49620-85-C-0013

NUMERICAL MODELING AND INVERSION OF 63 μ m
EARTHLIMB EMISSION FROM ATOMIC OXYGEN

by

James P. Riehl

ABSTRACT

Simulated earthlimb radiance and spectral lineshape data for the 63 μ m (158.5 cm^{-1}) transition ($^3P_1 \rightarrow ^3P_2$) of atomic oxygen has been generated from several assumed oxygen ground state density, temperature, and pressure atmospheric profiles. The simulations have been accomplished by modification and application of a version of the NLTE computer code written at the Air Force Geophysics Laboratory. An inversion procedure has been formulated, and a computer program written, that is able to successfully recover the excited state density and temperature for a wide range of tangent heights from the model radiance data. The region successfully treated includes high tangent heights where the transition can be considered "thin", and the edge of the earthlimb where effects due to self-absorption begin to appear. Considerable progress has also been made in continuation of the inversion to lower altitudes.

ACKNOWLEDGMENTS

The author of this report would like to acknowledge the sponsorship of the Air Force Office of Scientific Research, the Air Force Systems Command, and, especially, the Air Force Geophysics Laboratory at Hanscom Air Force Base. Of special mention is the very kind hospitality received in the Infra-red Dynamics Branch of the AFGL, and, particularly, the hospitality and support of Dr. Ramesh D. Sharma.

I. INTRODUCTION

My current position is Associate Professor of Chemistry at the University of Missouri-St. Louis. My current research interests include a wide range of spectroscopic problems with special emphasis on theoretical and experimental aspects of emission spectroscopy. In addition, I have considerable experience in the application of computers in Chemistry, especially in the computer modeling of molecular dynamics and molecular energetics.

My assignment for the ten week term of the 1985 AFOSR/UES Summer Faculty Fellowship program was with the Infra-red dynamics branch of the infra-red technology division of the Air Force Geophysics Laboratory (AFGL/LSI) located at Hanscom Air Force Base in Bedford Massachusetts. My experience and interest in emission spectroscopy and computer modeling led to my association with the computer modeling group of the infra-red dynamics branch, and particularly with Dr. Ramesh D. Sharma.

II. OBJECTIVES OF THE RESEARCH EFFORT

The principal objectives of the research project that I have been involved with were to generate simulated earthlimb radiance data for the 63 μm fine-structure transition of atomic oxygen, and to investigate methods to invert this radiance data such that the oxygen atom density and temperature profiles can be recovered. This preliminary effort is concerned with analysis of artificial "infinite resolution" data, extensions of this work to mimic "real" experimental results (i.e. finite resolution, spectral noise, etc.) should allow the determination of experimental parameters necessary for the use of this kind of measurement as a sensitive measure of oxygen atom density in the upper atmosphere.

III. BACKGROUND INFORMATION

Atomic oxygen has long been known to be an important constituent in the upper atmosphere. Over thirty years ago, Bates¹ suggested that the fine structure transition $\text{O}(^3\text{P}_1) \rightarrow \text{O}(^3\text{P}_2)$ played an important part in the cooling of the thermosphere. More recently, it has been demonstrated that oxygen atoms are involved in a large number of important chemical and physical processes in the atmosphere, and it has become clear that in order to be able to fully understand the dynamics and energetics of the earth's atmosphere, accurate oxygen atom densities must be known.

Various experimental techniques have been used in attempts

to measure oxygen atom density as a function of altitude. The 5577 Å green line emission has been studied both from rockets² and satellites³, resonance fluorescence and absorption near 130 nm⁴ has been measured, and the more indirect measurements of NO luminescence⁵, silver film oxidation⁶, and hydroxyl airglow⁷ have also been used. The most often used technique has been cryo-cooled or cryo-pumped mass spectrometers.⁸⁻¹⁰ These measurements have been summarized by Offermann et al.¹¹ A large variability in the results of these various measurement techniques has been noted¹², and truly reliable results have not yet been obtained.

As mentioned above the research described in this report is concerned with the possible use of the infra-red emission from the fine structure transition of oxygen at 63 μm as a probe of oxygen atom density and temperature. This experiment was first suggested by Munch¹³, and some experimental results have been reported although the quality of this data is not very good.¹⁴ Our emphasis, as described below, is on measurements using earthlimb geometry.

IV. THEORY AND METHODOLOGY

A derivation of the radiative transfer equation appropriate for earthlimb geometry has been presented elsewhere.^{15,16} In this report we will present a brief summary of the formalism appropriate for oxygen atom emission. It is convenient to consider the atmosphere as composed of slabs of finite thickness (Δz) with each slab being associated with a constant density, temperature,

and pressure. The radiance at frequency ν , N_ν , is related to the optical depth, τ , by the following equation

$$dN_\nu/d\tau = -N_\nu + 2c\nu^2\gamma/(1-\gamma) \quad (1)$$

where c is the velocity of light, and γ is defined as

$$\gamma = g_1 n_u / g_u n_l \quad (2)$$

Integration of equation (1) over a slab of thickness Δz yields the result

$$N_\nu(z+\Delta z) = N_\nu(z)\exp(-\Delta\tau_\nu) + 2c^2[\gamma/(1-\gamma)][1-\exp(-\Delta\tau_\nu)] \quad (3)$$

The optical depth of the slab is defined as

$$\Delta\tau_\nu = [S(\nu_0, T_s)[P_1(T)/P_1(T_s)](1-\gamma)[1-\exp(-c_2\nu_0/T_s)]^{-1} \\ \times f(\nu-\nu_0)n\Delta z \quad (4)$$

In this equation $S(\nu_0, T_s)$ is the line strength of the transition; $P_1(T)$ denotes the probability that the lower state is populated at temperature T ; $c_2 = 1.4388 \text{ K/cm}^{-1}$ is the second radiation constant; n is the total density; and $f(\nu-\nu_0)$ is a normalized lineshape function.

An energy level diagram for the ground state term of atomic oxygen (p^6) is given in Figure 1. Also given in this figure are the Einstein coefficients taken from Wiese.¹⁷

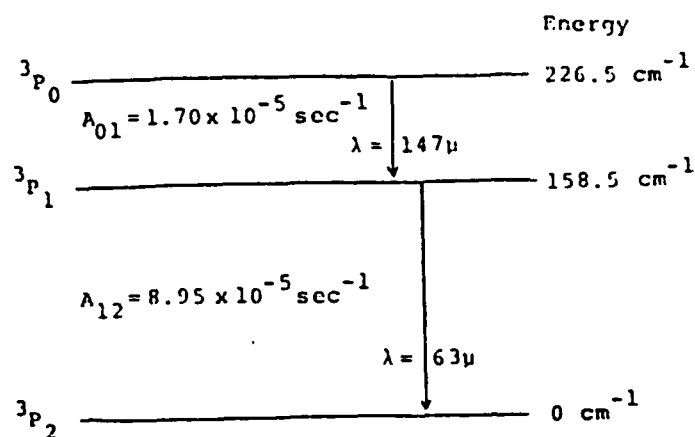


Figure 1. Approximate Energy Level Diagram and Einstein Coefficients for Oxygen Atom Ground State Term

The Einstein coefficient A_{12} along with an assumed density, temperature, and pressure atmospheric profile were input data for a modified form of the NLTE computer code developed at the Air Force Geophysics Laboratory. The modification was accomplished such that the program calculated the radiance for the 63 μm line in the earthlimb geometry for tangent heights from 80 to 180 km. The atmospheric density and temperature profiles used in this study are plotted in Figure 2. The two density profiles

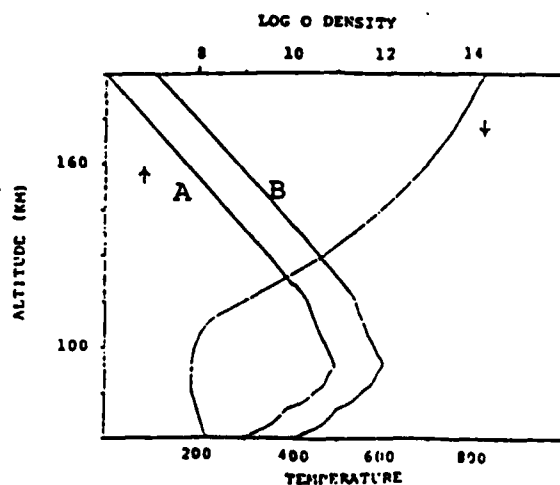


Figure 2. Atmospheric Density and Temperature Profiles Used in this Work.

(A and B) differ by a simple factor of 10. The calculated radiances [from eq. 2] versus wavelength for several tangent heights are plotted in Figures 3 and 4 appropriate for the two profiles. In these calculations it was assumed that

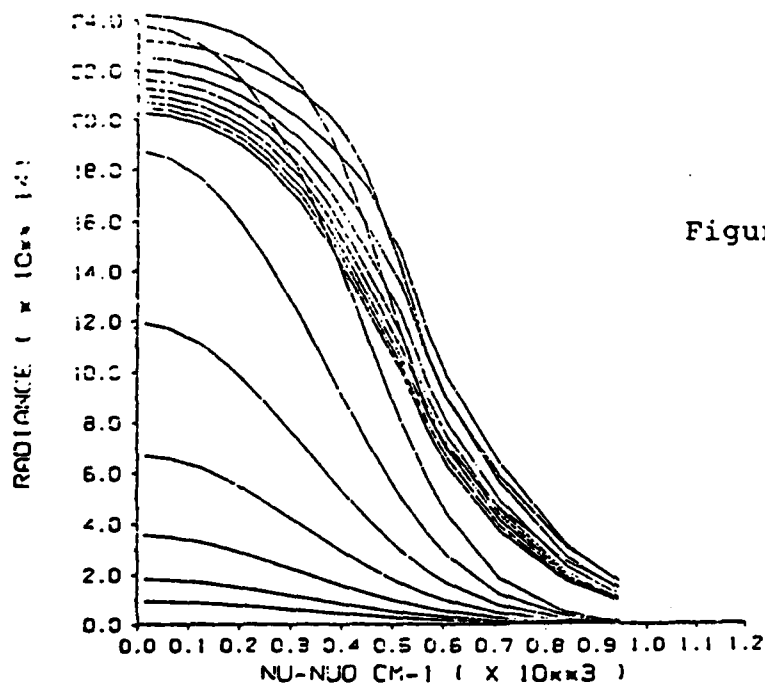


Figure 3. Calculated Radiance versus Wavelength for Oxygen Profile A.

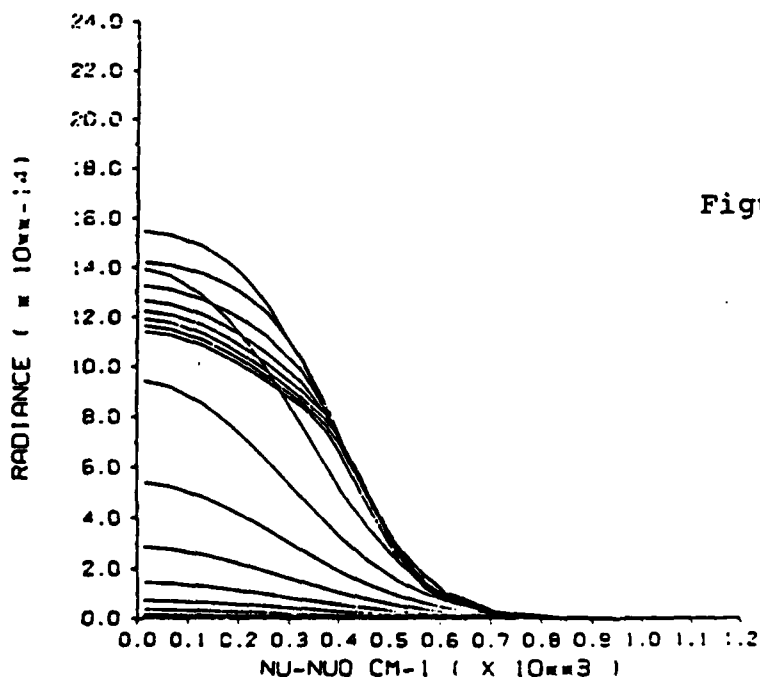


Figure 4. Calculated Radiance versus Wavelength for Oxygen Profile B.

the energy levels were in thermodynamic equilibria appropriate for the temperature specified. A voigt lineshape was assumed in all of the work reported here.

The principal aim of this work was to develop a reliable procedure for recovery of the density and temperature profiles from the "artificial" radiance data described above. For the purpose of this study it was assumed that "infinite resolution" radiance data and the total integrated radiance data for the transition were available. At the highest tangent heights considered, it was assumed that the transition was "thin". In this case, the integrated radiance, N , depends only on the excited state density profile, which is related to the ground state density through the temperature. Formally, we may write

$$N(H_T) = 1/2\pi \int \epsilon(H)W(H, H_T)dH \quad (5)$$

where $\epsilon(H)$ is the total volume emission rate at altitude H .

$$\epsilon(H) = n^*(H)A_{12} \quad (6)$$

In eq. (5) $W(H, H_T)$ is a geometrical weighting factor corresponding to earthlimb observation geometry.

The high altitude density profile has been assumed to decrease exponentially

$$n^*(H) = n^*(H_T)\exp(-kH) \quad (7)$$

Using eqs. (6) and (7) in eq. (5) we obtain the result

$$N(H_T) = (1/2\pi)n^*(H_T)A_{12} \int \exp(-kH)W(H,H_T)dH \quad (8)$$

where

$$W(H,H_T) = (R + H)[(R+H)^2 - (R + H_T)^2]^{-1/2} \quad (9)$$

R denotes the radius of the earth.

The integral in eq. (8) can be evaluated analytically with the result

$$N(H_T) = A_{12}n^*(H_T)\exp[k(R+H_T)](R + H_T)K_1[k(R+H_T)] \quad (10)$$

K_1 is the modified Bessel function. The two unknowns in this equation can be evaluated by considering the integrated radiance at the two highest tangent heights. An approximate excited state density profile for the highest altitude regions can then be constructed from eq. (7). We have made the additional assumption that the temperature in this region varies in a linear fashion, and can be approximated from known temperature profiles. These approximations appear to be reasonable, and, in fact, as long as the highest measurement is far removed from the atmospheric region of interest these values have little effect on the lower radiances.

The inversion procedure which we have developed to recover the density and temperature profiles is outlined below.

1. Beginning with the highest tangent height, guesses are made for the ground state density and temperature of the current slab.
2. The integrated radiance is calculated and compared to the "measured" value. If the values agree to within a preset error limit, the radiance at the line center is calculated, and compared to the "measured" value. If these values also agree, then the inversion proceeds downward to the next slab.
3. If the integrated radiances do not agree, then the density is incremented by a set fraction, the calculation repeated, and a next guess determined by assuming that the integrated radiance and density vary in a linear fashion. This process is repeated until the integrated radiances agree to within acceptable error limit.
4. If, after the integrated radiances are found to agree, the radiances at line centers do not agree, a correction is made to the temperature guess, in a similar manner as described above. If the temperature has been changed, the integrated radiance is rechecked, and the entire process iterated until agreement is reached.

5. If convergence is not obtained after a specified (typically 10 tries) the slab is skipped and the calculation continued.

V. RESULTS

The current status of the inversion procedure outlined in the previous section is presented in Figures 5 and 6.

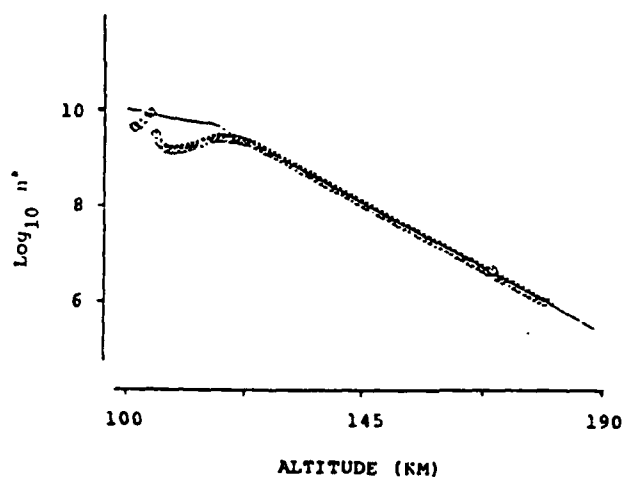


Figure 5. Oxygen Atom Excited State Density Recovered from the Inversion Procedure (\diamond). Solid Line is Actual Value for Profile A.

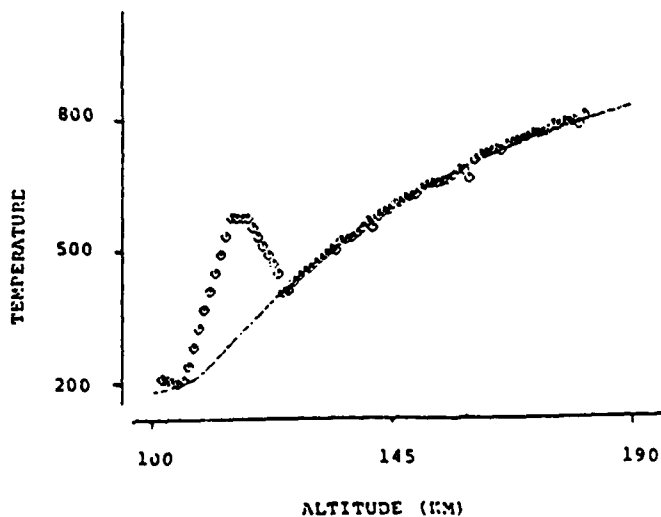


Figure 6. Oxygen Atom Temperature Recovered from the Inversion Procedure (\diamond). Solid Line is Actual Value for Profile A.

As can be seen from these figures, the inversion technique as described in the previous section, is able to recover the temperature and excited state density for altitudes greater than 125 km. This is approximately the altitude in which the density profile (B) for atomic oxygen can no longer be considered optically thin.

VI. RECOMMENDATIONS

Although the approach taken for the inversion of the atomic oxygen radiance data has been shown to be successful for the high altitude regions, continuation of the inversion to higher density lower altitude regions leads to instabilities in the numerical procedure. In all of the work reported here, only the radiance at the line center, and the total integrated radiance were used as input to the inversion program. As can be seen in the radiance data presented earlier in this report, as the altitude decreases and self-absorption becomes important, the radiance at the line center changes only slightly. The resulting small gradient is certainly one source of the observed instability.

An obvious modification to the work reported here, and something which we will explore in future work, is the use of radiance data at other positions in the line either separately, or in combination with the line-center radiance. It is anticipated that this additional data will allow the inversion to be successful for these lower altitudes.

An important consideration is the extension of the work described here to inversion of actual experimental measurements. In this regard, we also plan to examine model radiance data in which we have added noise, and in which the resolution is finite.

REFERENCES

1. Bates, D. R., Proc. Phys. Soc., 1951, 64b, 805.
2. Offerman, D., and Drescher, A., J. Geophys. Res., 1973, 78, 6690.
3. Wasser, B., and Donahue, T. M., J. Geophys. Res., 1979, 84, 1297.
4. Dickenson, P. H. G., Bain, W. C., Thomas, L., Williams, E. R., Jenkins, D. B., and Twitty, N. D., Proc. R. Soc. Lond. A, 1980, 369, 379.
5. Golomb, J. D., and Good, R. E., in Space Research, V. 12, Akademie, Berlin, pp 675-683.
6. Henderson, W. R., J. Geophys. Res., 1971, 76, 3166.
7. Good, R. E., Planet. Space Sci., 1976, 24, 389.
8. Scholz, T. G., and Offerman, D., J. Geophys. Res., 1974, 79, 307.
9. Philbrick, C. R., Faucher, G., and Trzcinsky, E., in Space Research, V. 18, Pergamon Press, Oxford, pp 139-142.
10. Arnold, F., Krankowsky, D., Marien, K. H., and Joos, W., J. Geophys. Res., 1977, 44, 125.
11. Offerman, D., Friedrich, V., Ross, P., and Von Zahn, U., Planet. Space Sci., 1981, 29, 747.
12. Sharp, W. E., Planet. Space Sci., 1985, 33, 571.
13. Munch, G., Astrophys. J., 1962, 136, 823.
14. Feldman, P. D., and McNutt, D. P., J. Geophys. Res., 1969, 74, 479.
15. Sharma, R. D., and Zachor, A. S., Appl. Opt., 1983, 22, 2665.
16. Zachor, A. S., and Sharma, R. D., J. Geophys. Res., 1985, 90, 467.
17. Wiese, W. L., Smith, M. W., and Glennon, B. M., Hydrogen Through Neon, Vol. I, Nat. Stand. Ref. Data Sys., p. 153.

Computer Science Department

Research Goals and Objectives
For Summer Fellow, Michael D. Ross
1985 USAF-UES Summer Faculty Research Program

Background

The Modeling and Analysis Branch of the Air Force Aerospace Medical Research Laboratory, Biodynamics and Bioengineering Division, at Wright-Patterson Air Force Base utilizes two computer simulation models of the human body (the Articulated Total Body Model and the Head-Spine Model) that require the entry of substantial amounts of data in fixed format form prior to execution of the simulation program.

Goals

The goals of the summer research shall be:

1. to develop user-friendly interactive data entry computer program modules to facilitate data entry for each of the two computer simulation models.
2. to explore ways to reduce the time required to enter the data by using techniques, such as preprocessing the data, to reduce the amount of data that must be entered.
3. to explore ways to assist in data development, such as using graphic image processing to assist users to convert data from graphic form into numerical form.

Date

The research is to be conducted at AFAMRL/BBD from June 24 to August 30, 1985.

Immediate Supervisor

Dr. Ints Kaleps, Chief
Modeling and Analysis Branch
AFAMRL/BBM
WPAFB, OH 45433

Effort Focal Point

Ms Patricia M. Lewandowski
AFAMRL/TSA
WPAFB, OH 45433

Local UES Representative

Mr. M. Danishek

1985 USAF-UES SUMMER FACULTY RESEARCH PROGRAM/

GRADUATE STUDENT SUMMER SUPPORT PROGRAM

Sponsored by the

AIR FORCE OFFICE OF SCIENTIFIC RESEARCH

Conducted by the

UNIVERSAL ENERGY SYSTEMS, INC.

FINAL REPORT

NONDESTRUCTIVE EVALUATION OF ADVANCED COMPOSITES BY STRAIN
FIELD ANALYSIS ACQUIRED THROUGH CORRELATION OF X-RADIOGRAPHS

Prepared by:	Samuel S. Russell
Academic Rank:	Assistant Professor
Department and	Mechanical Engineering
Univeristy:	University of South Carolina
Research Location:	WPAFB, AFWAL/MLLP

USAF Research:	Thomas J. Moran
----------------	-----------------

Date:	Sept. 25, 1985
-------	----------------

Contract No:	F49620-85-C-0013
--------------	------------------

ABSTRACT

NONDESTRUCTIVE EVALUATION OF ADVANCED COMPOSITES BY STRAIN FIELD ANALYSIS ACQUIRED THROUGH CORRELATION OF X-RADIOGRAPHS

by

Samuel S. Russell

Displacement and strain fields were determined by correlation analysis between radiographs of a specimen in unstrained and strained states for a $[90,0]_g$ glass-epoxy coupon. The error of these measurements was less than 3% when compared to an extensometer. The same coupon was then subjected to an impact in the gage length, which caused radical shifts in the strain field. When subjected to a tensile load, negative strains were measured locally in the damage zone using the X-radiograph correlation method, clearly identifying the flawed region.

ACKNOWLEDGEMENTS: The author would like to thank the Materials Laboratories at Wright-Patterson AFB and the Office of Scientific Research for a rewarding summer of research. The discussions with Dr. Thomas J. Moran and Mr. Robert T. Andrews were helpful in formulating this project. Thanks are also extended to Messrs. Ed Khostermn, Mark Ruddell, and Ed Porter for their efforts with the hardware and specimens, and Dr. W.H. Peters, Mr. Douglas Finch and Dr. M.A. Sutton for assistance with the correlation software.

I. INTRODUCTION:

The summer fellow received a Ph.D. in engineering mechanics in 1982 from Virginia Tech. His dissertation title was "An Investigation of the Excitation Frequency Dependent Behavior of Fiber Reinforced Epoxy Composites During Vibrothermographic Inspection."

Vibrothermographic inspection uses a scanning infrared video camera to map the surface temperature of a structure being vibrated mechanically. Flawed and damaged zones appear as hot spots, provided the material in the structure has low thermal conductivity. Vibrothermography has been used to nondestructively evaluate (NDE) fiber reinforced composites for damage when the composite has a low thermal conductive matrix. References 1-6 address the application of vibrothermography for inspection of polymer-matrix composites. The investigator has also used traditional NDE methods of inspection such as x-ray, radiography and ultrasonic C-scans (see Refs. 2-4 and 6).

The summer fellow was assigned to the AFWAL/MMLP group for the ten week period. This group was involved in the development of NDE techniques and in particular NDE of advanced composites.

II. OBJECTIVES OF THE RESEARCH EFFORT: Correlation between two images of an object in motion was used by Peters, et.al., Ref. 7, to determine the objects velocity and rotational speed. Poplin, et.al. Ref. 8, correlated two images of paint speckle on a composite cylinder. For one

image the cylinder was resting free of load and for the other image the cylinder was internally pressurized. From the correlation the displacement field lying parallel to the cylinders surface was determined, but any out of plane motion introduced errors. Image correlation of angiograms was used by Layrisse, Ref. 9, to characterize atherosclerotic plaque. However, all the above studies were characterized by relatively large displacements and strains.

The first objective of this study was to measure the order of the error in strain fields acquired through digital image correlation of x-rays. Strain levels were kept within the elastic range of engineering fiber-reinforced composite materials. X-ray radiographs were taken with contact film held next to test specimens by a foam rubber pad, so the correlation analysis was insensitive to out-of-image plane motions.

The second objective was to determine if strain fields acquired by image correlation analysis can be used as an indicator of damage in advanced composite materials. Several investigators, Refs. 10,11 and 12, sight relationships between the reduction of the stiffness and the damage state or residual strength of a fiber reinforced composite. With the reduction of stiffness due to damage, the average of the strain field must increase for a constant or standard applied mechanical load. Also, if the damage is localized such as with an impacted zone, the strain field should indicate the damage location as an anomaly. The second objective was to determine if strain fields measured

by image correlation of radiographs could be used to nondestructively locate impact damage in advanced composites.

III. CORRELATION METHOD FOR RADIOGRAPHS:

3.1 Digital Image Formation

The film radiographs were digitized by a Fairchild CAM3000 camera and a Datacube, Inc digital interface board. The digitization was controlled by an IBM XT personal computer, and the image was stored on a 5 1/4in floppy disk. Every picture element (pixel) intensity was stored as an eight-bit number. Each image consisted of 512 by 460 pixels, indicating rows x columns, respectively.

A light table illuminated each radiograph for digitization by the Fairchild IBM-XT system and the image was stored on disk (Figure 1). At a later time the images were read over a link to a VAX 11/780 computer. Because the number of operations required for a correlation between a pair of images is substantial, this analysis must be performed on the VAX rather than the personal computer.

3.2 Correlation Algorithm

A brief description of the digital image correlation process follows. A complete description is included in Reference 7. Each image consists of an array of 460 columns with 512 rows in each column. The values in the array represent the light intensity of the pixel array. The

correlation program divides one image, usually chosen to be the unstrained image, into subsets. The subsets usually are of ten, twenty, or thirty pixels square. Each subset must be chosen large enough so that it's light intensity pattern does not resemble any other subset, that is, it's intensity pattern must be unique. The program searches the second image, usually the strained image, for the location which most resembles the light intensities of each of the subsets in the unstrained image. The displacement field u and v is the difference between a subset's location in the unstrained image and its location in the strained image.

The identification of corresponding subsets is represented by the value of a correlation coefficient, C , defined by

$$C_i(u,v) = \frac{1}{\Delta M_i} \int \int [A(x,y) - B(x+u, y+v)]^2 dx dy \quad (1)$$

where A and B are the image intensities of the unstrained and strained images, and ΔM_i is the region occupied by the i th subset of the unstrained image. For a perfect correlation B would have the same value as A at all points, and the correlation coefficient would vanish. The program searches the second image throughout the user-specified range and selects the u and v which corresponds to the smallest value of the correlation coefficient for each subset.

A bilinear interpolation is then used to generate a continuous intensity field from the strained digital image. This allows the displacements to be accurately determined to

fractions of a pixel width. This accuracy limit was determined experimentally and will be discussed at a later time.

It should be noted that motion out of plane to u and v causes an apparent strain and may produce an unfocused image. Hence image correlation analysis is in tolerate to out-of-plane motion. Because the radiograph were converted to digital images using a fixed distance between the digital camera and the light table, and the radiographs were held flat on the table, this source of error was eliminated.

3.3 Strained x-ray Radiograph

To permit x-raying of specimens under load, a portable load frame (Figure 2) was fabricated. The strain in the specimen was monitored by a 2.54cm. (1 in.) gage length MTS extensometer, seen to the right of the load frame. The load frame consisted of two commercial grips, two 3 in. steel L's and two 1/2 in. diameter threaded rods. A pair of nuts on each threaded rod were turned equal amounts to force the grips apart. A foam rubber mat under the film forced it to remain in contact with the back surface of the specimen.

The x-ray source was a commercial machine with a spot size of 0.7mm. The source to film distance was 1.22 m (48 in). A single coated (type SR) Kodak film was used to prevent multiple image formations when the film was digitized. The exposure was for 5 min. at a tube voltage of 27.5 KV and an amperage of 5 ma.

IV. EXPERIMENTS AND RESULTS:

AD-A166 178

UNITED STATES AIR FORCE SUMMER FACULTY RESEARCH PROGRAM

4/11

1985 TECHNICAL RE (U) UNIVERSAL ENERGY SYSTEMS INC

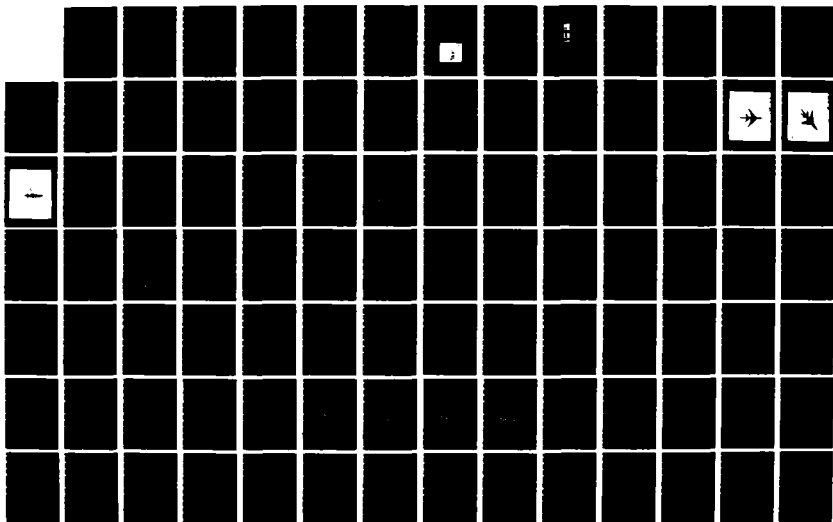
DAYTON OH R C DARRAH ET AL DEC 85 AFOSR-TR-86-8141

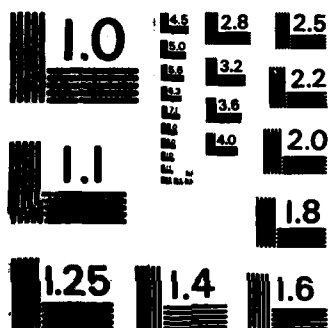
UNCLASSIFIED

F49620-85-C-0013

F/G 5/9

NL





MICROCOPY RESOLUTION TEST CHART
NATIONAL BUREAU OF STANDARDS-1963-A

4.1 Penetrant Enhanced Radiographs

A [90,0]_g Gl-Ep specimen was radiographed in both strained and unstrained states after being soaked with an X-ray absorbing penetrant, Tetrabromoethane (TBE). The correlation in this case was between naturally occurring features such as the shadows of the fibers and the enhanced cracks. However, the correlation analysis failed to produce meaningful results as the cracks and fibers were periodically spaced. To the correlation algorithm, the subsets of the image fail to appear unique, and the displacement selected were often incorrect. Hence, a surface coating was used to produce a unique intensity pattern on the x-ray film, and the surface displacements were correctly identified.

4.2 Steel Powder Surface Paint

To provide a surface with a unique X-ray shadow pattern, a mixture of metal powder was sprinkled over one side of the test coupons and then stabilized by a coat of clear paint. Two different mixtures were tried. The first mixture consisted of equal parts by volume of 300 micron Fe and 37 micron stainless steel powder stabilized by a rubber base strippable paint. A second mixture consisted of equal parts of 37, 74, and 98 micron diameter type 316 stainless steel powder stabilized by sprayed clear lacquer. In both cases, the paint kept the powder in place. Both mixtures seemed to produce an intensity texture which correlated well. However, the strippable paint tended to peel, somewhat particularly at edges of the specimen.

4.3 [90,0]_g Gl-Ep Specimen

A glass-epoxy cross-ply tensile coupon 15.2x2.54x0.18cm (6x1x0.071in.) without damage was radiographed unstrained and strained at 1.31% over a 2.54 cm gage length as measured by the extensometer. Images of the gage section were made from the radiographs with 124 pixels/cm (315 pixels/in). The correlation based on 20 X 20 pixels subset size and columns of 260 pixels, produced an average strain of 1.273%. This represents a 2.8% difference from the strain measured with the extensometer. Figure 3 graphically presents the axial displacement u as the height of the nodes. The u displacements increase monotonically except for the single peak on the top left edge of the grid. Examining the raw data this subset had a high correlation value. This high correlation value could have been due to either a hole in the paint or lifting of the strippable paint. However, with the exception of this one subset the data indicates a global tensile axial strain where, the strain is computed as the difference between u of adjacent subsets down the length, divided by the separation distance of the centers of the subsets. This same specimen was subjected to a impact in the gage length and was reexamined by the X-radiographic correlation method. The results of this test are presented in the following section.

4.4 Displacement and Strain Fields in Impact Damaged [90,0]_g Gl-Ep Coupon.

The same Gl-Ep coupon was subjected to a impact of 2.7J energy from a 190 g steel sphere on the center of the previously used gage length. The specimen was C-scanned in an immersion tank by a 25 MHz, 2 in. focus commercial ultrasonic transducer (Figure 4). The specimen was then examined by the X-ray correlation method.

The region impacted showed shifts in the displacement field as indicated by Figure 5. The displacement data shown for the impact zone is multiplied by a positive scale factor for Figure 5. The magnitude of the scale factor was different from the negative scale factor used in Figure 3. Hence, direct comparison of displacements by comparison of these figures was not possible. The longitudinal strain in the gage length prior to impact was positive everywhere except at a single subset. This single region probably was a zone where the paint probably lifted from the surface. For the correlation analysis after impact, the lacquer paint was used and hence this type of error was eliminated.

The 2.54 cm gage length was subjected to an average longitudinal tensile strain of 0.565% as measured by the extensometer. For this correlation analysis, there were 98 pixels/cm (250 pixels/in.). The section was located 0.7cm to the right of the specimen left edge and the right edge was 0.12cm to the left of the specimen edge. The longitudinal distance of the analyzed section was 2.25cm. The large displacements, and hence the large strains at the top of Figure 5, were probably caused by the epoxy strip used to hold the extensometer knife edge in place. The

increasing displacement in the transverse direction was due to a rotation between radiographs when the two images were digitized and not caused by a shear strain.

Several strains were computed and were marked between the subset centers used for computation of these strains. Large negative and positive strains occurred in the neighborhood of the zone indicated by the C-scan as damage. The average strain measured by the correlation method down the full length of the center column was 0.528% and disagrees with the extensometer by 6.5%

V. CONCLUSIONS

1. X-ray correlation acquired strains had an error of less than 7%.
2. Damage due to low energy impact of a glass fiber-reinforced composite caused a shift in the strain field, which was detected as high compressive and tensile strains by the X-ray correlation technique.

VI. RECOMMENDATIONS

1. A program must be written to process the displacement data from the correlation program into strain field data. The strain data should be presented graphically in a manner similar to the displacements.

Additional x-ray radiographs were taken at Wright-Patterson but were not analyzed during the ten-week summer program. These radiographs can be processed by the correlation technique during the minigrant period, since the digital image analysis hardware and software is located at the College of Engineering, USC, Columbia, SC. The radiographs were taken at several strain levels, providing several data points to evaluate the effectiveness of the correlation technique. Correlation analysis on the radiographs could be evaluated for the following experiments:

2. Strain fields could be acquired around a lap joint of adhesively bonded Aluminum strips.

3. The strain field could be acquired in the neighborhood of a low impact energy damaged zone in a $[0, 90_2, +45, -45]_s$ Gr-Ep coupon.

4. Strain field acquired by correlation analysis at a hole through a nylon (linear elastic homogeneous isotropic material) coupon could be compared to the closed form classical elasticity solution.

5. A statistical analysis of the error bounds on correlation generated strains for small gage lengths, 20 pixels could be performed. The previously acquired error limits were based on gage lengths of greater than 2cm, approximately 200 pixels.

VIII. FIGURES :

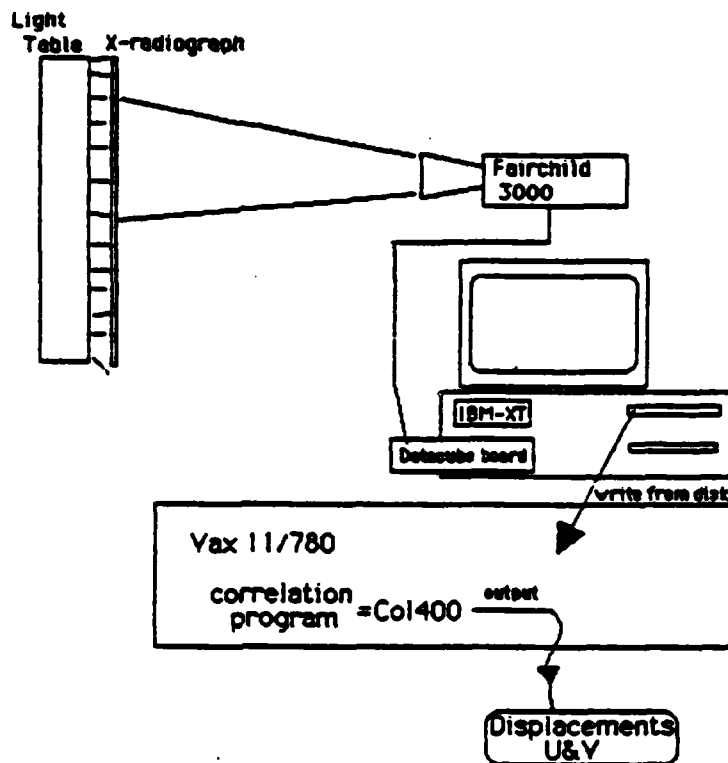


Figure 1. Schematic X-radiographic Digital Correlation

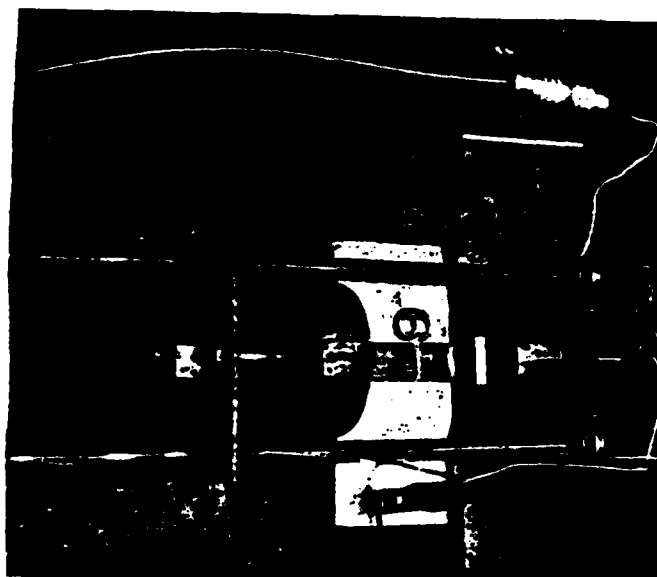


Figure 2. Portable Load Frame, X-Ray, Film and Gl-Ep Specimen in Frame.

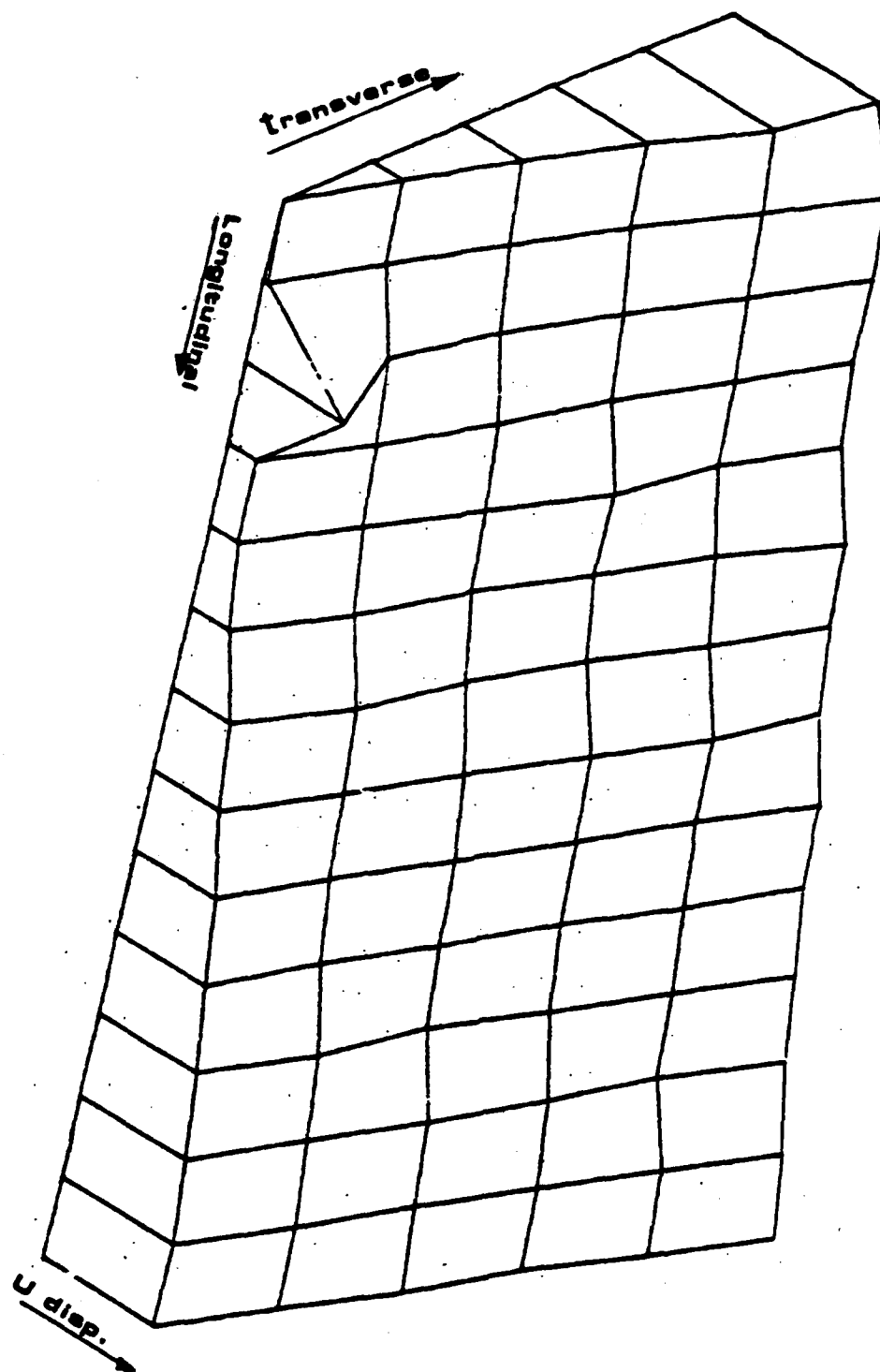


Figure 3. Longitudinal Displacement (U) within Gage Section of Extensionometer of Undamaged $[90,0]_S$ G1-Ep Coupon. Subset Size = 20 X 20 pixels, 1 cm = 124 pixels.

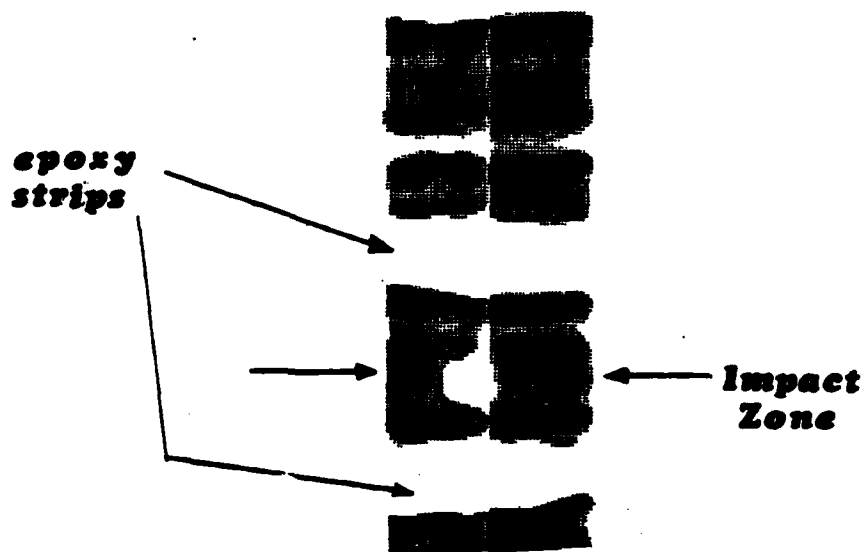


Figure 4. Ultrasonic C-Scan with 25 MHz Focus Transducer of Impact Damaged Region of $[90,0]_s$ G1-Ep Coupon. Impact Energy = 2.7 J. White and Grey Represent Poor and Fair Ultrasonic Transmission, Respectively.

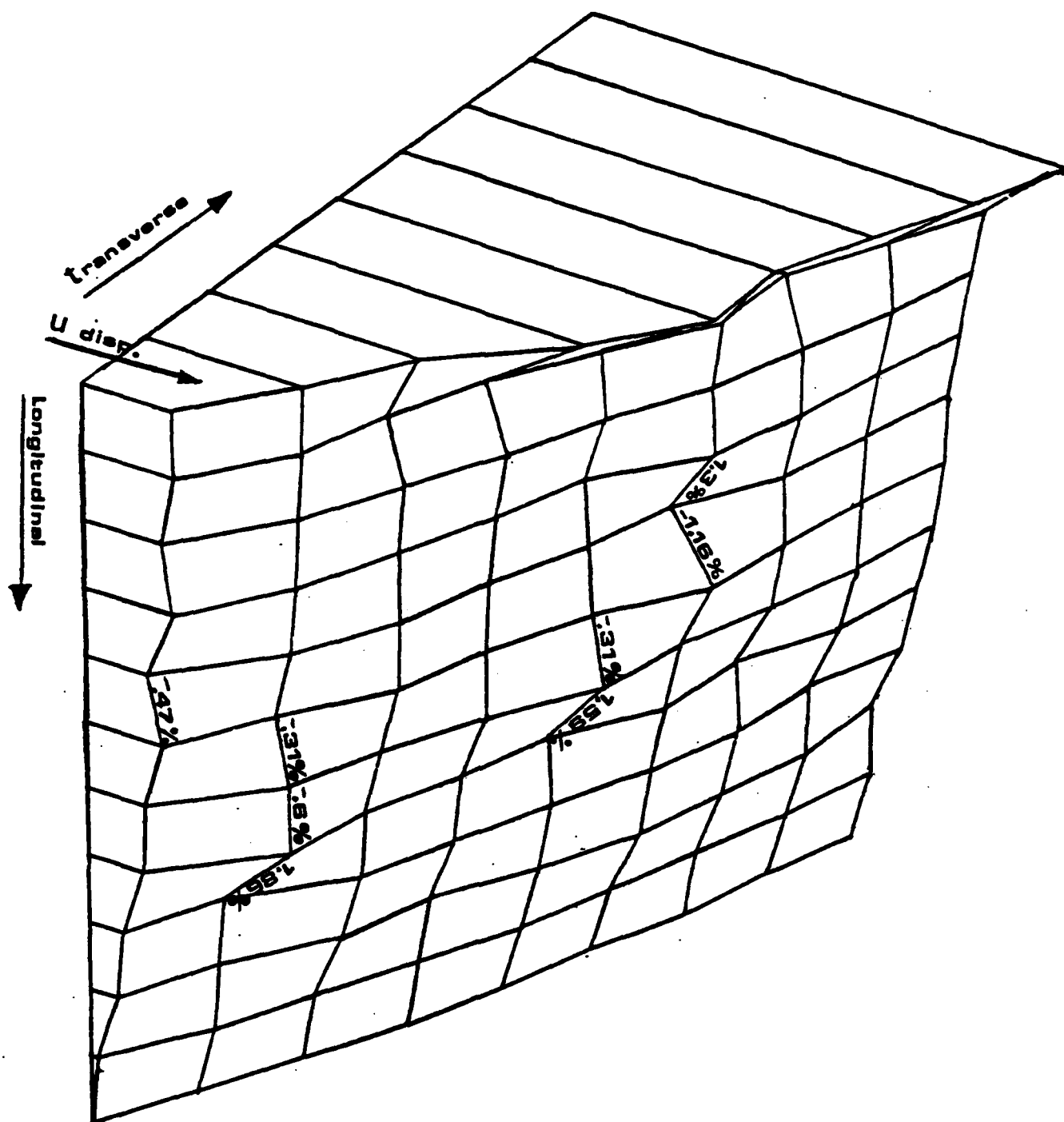


Figure 5. Longitudinal Displacement (U) in Impacted Zone of $[90,0]_g$ G1-Ep Coupon. Strains between Adjacent Subsets Indicated for High Strain Regions. Subset Size = 20 X 20 pixels, 1 cm = 98.

IX. REFERENCES

1. Russell, S.S. and Henneke, E.G., II, "Dynamic Effects During Vibrothermographic Nondestructive Evaluation of Composites", NDT International, Vol. 17, No. 1, February 1984.
2. Henneke, E.G., II, and Russell, S.S., "Impact Damage Detection and Evaluation by Active and Passive Thermography and Stereo X-Ray Radiography in Advanced Composite Panels", Proceedings of the 14th Symposium on Nondestructive Evaluation, San Antonio, TX, April 1983.
3. Duke, J.C. and Russell, S.S., "The Investigation of Imperfections in Sheet Molding Compound", Materials Evaluation, Vol. 40, No. 5, April 1982.
4. Henneke, E.G., II. and Russell, S.S., "Vibrothermographic Nondestructive Investigation of a Single Screw Gate Rotor", Proceedings of the ASNT Spring Conference 1982, Boston, MA.
5. Henneke, E.G., II, Russell, S.S., "Parameters Affecting Thermographic Inspection of Glass Fiber Reinforced Composites", Proceedings of the ASNT Fall Conference, 1982, Atlanta, GA.
6. Henneke, E.G., II, Russell, S.S. and Reifsnider, K.L., "Thermography as an Observational and Predictive Method for Dynamic Loading of Composite Structures", Proceedings

of A Critical Review:Techniques For the Characterization
of Composite Material, held in Boston, MA, June 1981.

7. Peters, W.H., Ranson, W.F., Sutton, M.A., Chu, T.C. and Anderson, J., "Application of Digital Correlation Methods to Rigid Body Mechanics", Optical Engineering, Nov/Dec 1983, Vol. 22, No. 6.
8. Poplin, W.M., Walker, D.M., Peters, W.H., Sutton, M.A. and Ranson, W.F., "Whole Field Experimental Displacement Analysis of Composite Cylinders", Submitted to Experimental Mechanics, Spring 1985.
9. Layrisse, Maria Isabel, "Atherosclerotic Plaque Characterization Utilizing Image Correlation Techniques in Angiography", University of South Carolina Masters Thesis, Aug. 1985.
10. Reifsnider, K.L. and Highsmith, A., "The Relationship of Stiffness Changes in Composite Lamintes to Fracture-Related Damage Mechanisms", Fracture of Composite Materials, 1981.
11. O'Brien, T.K. and Reifsnider, K.L., "Fatigue Damage Evaluation Through Stiffness Measurements in Boron-Epoxy Lamnates", Journal of Composite Materials, Vol. 15, Jan. 1981.
12. O'Brien, T.K., "Analysis of Local Delaminations and

their Influence on Composite Behavior", ASTM Symposia
on Delamination and Debonding of Materials, Nov. 83,
Pittsburg, PA.

1985 USAF-UES SUMMER FACULTY RESEARCH PROGRAM

Sponsored by the

AIR FORCE OFFICE OF SCIENTIFIC RESEARCH

Conducted by

UNIVERSAL ENERGY SYSTEMS, INC.

FINAL REPORT

INFRARED RADIATION TARGET MODELING SYSTEM

Prepared by:	Sally A. Sage
Academic Rank:	Assistant Professor
Department and University:	Mathematics and Computer Science Department West Georgia College
Research Location:	Air Force Armament Laboratory, Eglin AFB Division: DLM Branch: DLMI, IR Technology
USAF Research Contact:	Mr. Steve Butler
Date:	August 21, 1985
Contract No:	F49620-85-C-0013

INFRARED RADIATION TARGET MODELING SYSTEM

by

Sally A. Sage

ABSTRACT

A description is given for an infrared radiation (IR) target modeling system. The goal of the system is to generate an IR signature for the target. Initially, the target is modeled by a set of triangular facets which completely cover the outer surface of the target. The first of three tasks is to use the three-dimensional model to produce a two-dimensional image which has been processed by a hidden-line algorithm so that the image is represented by a set of pixels. Each pixel has a correspondence to a facet that is directly in the sensor's line-of-sight. The IR target signature can then be calculated by the integration of the radiance over the projected area of the target along the line-of-sight of the sensor. The second task is to develop a similar facet model for the plume of the target. The plume also makes a significant contribution to the IR signature and should be incorporated into the modeling system. The third task is to develop an interactive system to identify specific regions of the target surface, namely the facets covering the engine. The engine facets have a significantly higher temperature than the other regions of the target and these temperatures contribute to the IR signature.

Acknowledgements

I would like to express my appreciation to the Air Force Systems Command, the Air Force Office of Scientific Research, and the Air Force Armament Laboratory for the opportunity to work in the Summer Faculty Research Program at Eglin AFB, Florida. I am especially grateful to Steve Butler for his encouragement and suggestions. The advice and help of Dennis Garbo and Grady Lambert are also cordially acknowledged. A special thanks to my mathematical friends, Jennifer Davis and David Wilson, for reminding me of crucial but long forgotten mathematical truths.

I. INTRODUCTION

Aerospace manufacturing companies have turned to exotic materials and manufacturing techniques in order to reduce the visibility of future aircraft. The radar cross-section, visible contrast and infrared emissions are to be minimized. Though considerable thought and effort have been directed to radar and visible signatures, infrared signatures are little understood. To begin a detailed analysis of future and current aircraft, a suitable model for aircraft infrared radiation must be established.

To provide a suitable model, the aircraft must be measured in shape and radiation in realistic environments. The contributing sources must be identified and understood. This research effort includes the development of tools which model an aircraft's infrared radiation. This includes the creation of a multifacet model for current aircraft, the association of radiation properties to each facet, and the integration into radiant intensity vs. angle for each target model.

Sally A. Sage received the B.A. degree in Mathematics from San Francisco State University in 1977 and the M.S. degree in Computer Science from the University of Pittsburgh in 1979. Her teaching responsibilities over the past six years as a member of the Department of Mathematics and Computer Science at West Georgia College have included courses in Advanced Pascal, Assembly Language Programming, Data Structures, Programming Languages and Compiler Construction. Her main research interests are image processing, algorithms, and optimization techniques.

II. Objectives of the Research Effort

The goal of this research is to develop an infrared radiation (IR) target modeling system. A target is input to the simulator system and

the system generates an IR signature for the target as output. The target signature will be given by the integration of the radiance over the projected area of the target along the line-of-sight of the sensor. The target itself is modeled by a set of triangular facets which completely cover the outside of the target. In addition to the target model itself, other parameters which can affect the IR sensor are input to the system: power setting, speed, atmospheric conditions (relative humidity, air temperature, etc.), range of the sensor, and the viewing angles. The area is determined for the portion of the target facing the sensor. Temperature and emissivity values are assigned to each facet to determine the radiance of each facet. The sum over all the facets provides the target intensity which is the infrared signature of the target. Two other subgoals of the system involve the enhancement of the target data. An interactive system is needed to generate a plume facet model that can be attached to the target. The plume makes a significant contribution to the IR but it was not modeled as part of the original physical target. A second interactive system is needed to assign identification codes to user-selected sections of the target. The identification codes can then be assigned individual temperatures. Thus, a facet can be assigned a specific temperature through the facet's identification code.

III. Overview of the Target Modeling System

Three specific FORTRAN programs related to this system have been implemented: PLOTVIEW, PLUME, and IDCOCES. The PLOTVIEW program creates a two-dimensional image that is represented by a set of pixels where each pixel has a correspondence to a facet that is directly in the line-of-sight of the sensor. The PLUME program develops a facet model for the target plume. The IDCOCES program develops a facet identification system which assigns identifying code numbers to specific areas of the target.

IV. Details of the PLOTVIEW Program

The PLOTVIEW program generates a two-dimensional IR image of the target. Input data files containing three-dimensional models of the targets exist in a data base. The target, however, undergoes several stages of processing to determine the projected area viewed by the sensor. The target model is input to a program called SHOTGEN which converts the target description to a set of three-dimensional triangular facets which cover the target both inside and outside. The file is then modified so that only those facets which describe the exterior surface of the target are retained. This facet model is the input file to the PLOTVIEW program. PLOTVIEW requests several of the sensor viewing angles and the range of the sensor. The three-dimensional model is rotated and projected onto a two-dimensional plane. The PLOTVIEW program then performs a hidden line algorithm on the two-dimensional facet model. Any triangle which is covered by another triangle is eliminated from the facet model. Furthermore, if one triangle partially covers another, the visible area of the triangle is retained so that it can be included in the energy integration. PLOTVIEW sorts facets in the sensor viewing area from back to front. The pixels contained in each facet are generated geometrically and are then mapped to an array called COLLISION. The sorted facet order is used to map the generated pixels into COLLISION. This sorted ordering causes the back facets to be mapped into COLLISION first and the front facets to be mapped into COLLISION last; thus, any pixel left in the grid after all the pixels have been mapped into COLLISION is in the sensor line-of-sight. The line-of-sight model is converted to a color pixel map of the viewable area of the target. This color map displays every point in the line-of-sight of the sensor. A correspondence is retained between each pixel and the facet in which the pixel is contained. Thus, the intensity of each pixel in the map is dependent upon the facet's identification code.

V. Details of the PLUME Program

The PLUME program generates the X,Y,Z coordinates of a plume. The plume is described geometrically by a series of truncated cones which are covered by two disks with radii to match each end of the plume. The target file is scanned initially so that the appropriate X,Y,Z coordinates at the rear of the engine can be used to determine the correct position of the plume. The plume's X coordinate is given as input after the user examines the range of the engine's coordinates. The plume's starting radius is determined by the range of the engine's Y and Z coordinates. The plume's Y and Z coordinates are calculated from trigometric identities:

$$\text{SIN (A) = (Y / RADIUS)}$$

$$\text{COS (A) = (Z / RADIUS)}$$

where A is the angle from the the center of the unit circle.

Eight points are generated to approximate a disk. The coordinates of these points are stored in a table ordered by angle, starting with angle equal to 0 and ending with angle equal to 315. These eight points are related to a set of eight triples. Each triple consists of the vertices of a triangle. The eight triangles describe the approximated surface of the circle.

Figure 1(a) shows the circle covered by triangular facets. The facets are numbered with the original SHOTGEN-like triples. Each facet is described by ordered triples: the first facet's triples are 1,2,3; the second facet's triples are 2,3,4; thus, the Nth facet's triples are N,N+1,N+2. Eight facets, including two lines, describe the circle.

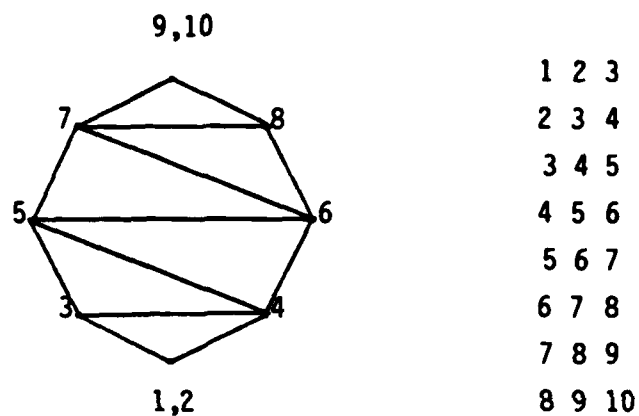


Figure 1(a) circle covered with
triangular facets

These facets are related to eight angles of the circle ordered from 0 degrees to 315 degrees. Figure 1(b) shows the angles and their assigned vertex number.

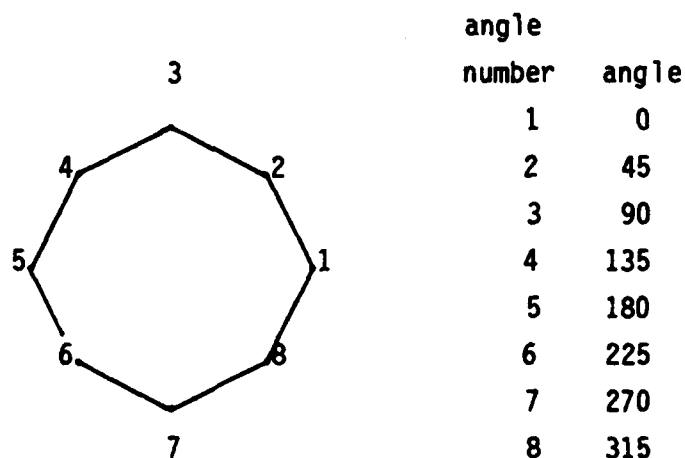
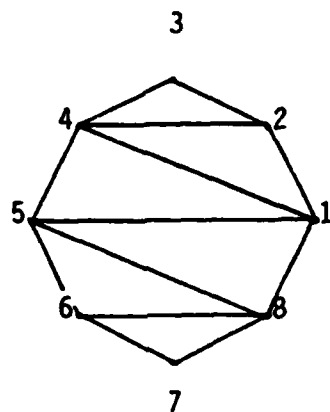


Figure 1(b) points numbered by
increasing angle

corresponding angles

Figure 1(c) shows the relationship between the original triples and the assigned angle numbers.



7 7 6
8 6 7
6 8 5
1 5 8
5 1 4
2 4 1
4 2 3
3 3 2

Figure 1(c) circle covered with
triples using angle numbers

angle number triples

A cone is generated in a similar manner by sixteen points. These points describe the circle on each end of the cone. The triples represent the vertices of the triangles which cover the surface of the cone. Figure 2(a) shows the three-dimensional cone with the original triples. Again, facets are sequentially described: 1,2,3; 2,3,4; 3,4,5; etc.

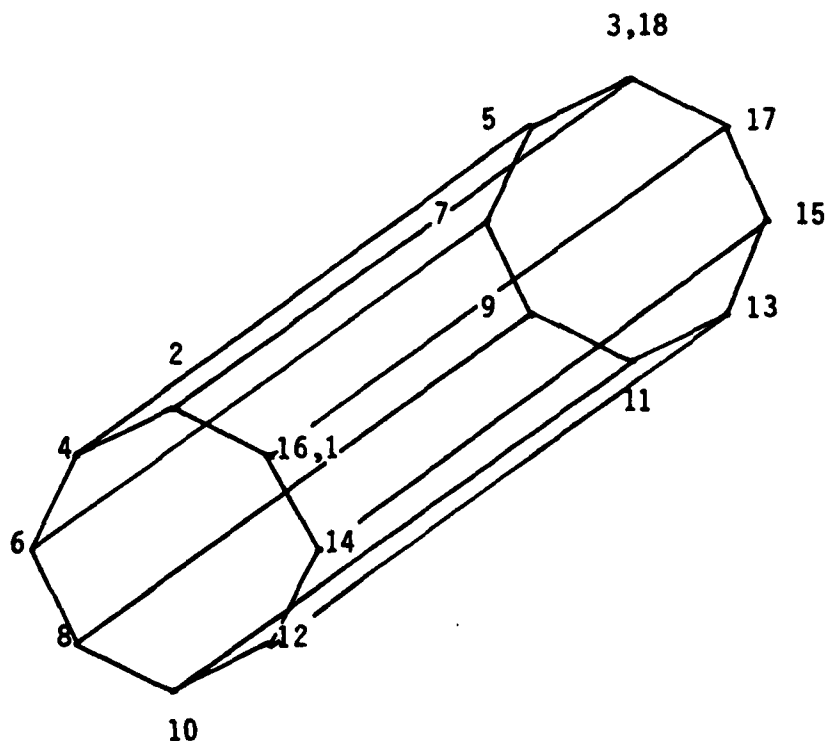


Figure 2(a) cone with original vertices

Figure 2(b) shows the facets which cover the cone's surface. The facets are labeled with the angle numbers.

angle 45 90 135 180 225 270 315 0 45

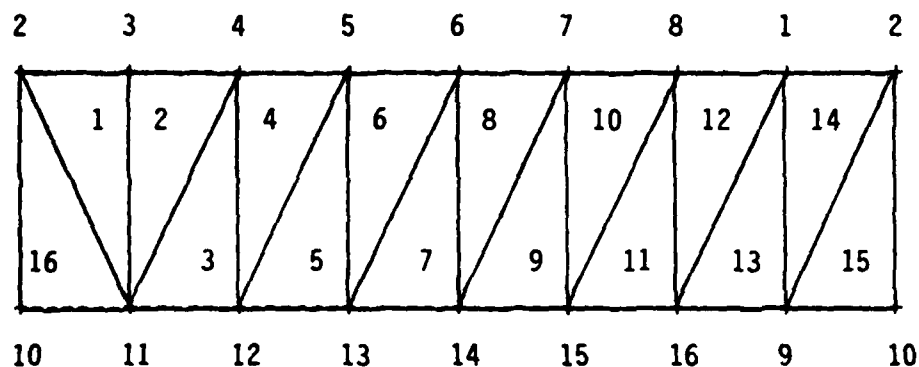


Figure 2(b) facets which cover the cone using angle numbers

VI. Details of the IDCODE Programs

The IDCODES program is divided into two separate programs. Initially in IDCODES_PART1, the target is run through a set of routines taken from the PLOTVIEW program which generate a two-dimensional image. The program is run for six cardinal views of the target. The cardinal views are listed in Table 1.

	azimuth	elevation
(1)	0	0
(2)	90	0
(3)	180	0
(4)	270	0
(5)	0	90
(6)	0	270

Table1 the six cardinal views

After IDCODE_PART1 finishes executing, print-out is made for each

cardinal view. This print-out shows the facet number which corresponds to each pixel in the line-of-sight of the sensor. During execution of IDCODES_PART2, these facet maps can be referenced by the user to aid in assigning identification codes to specific facets. Program IDCODES_PART2 creates/modifies a file called SECTIONi. This file is a list of the identification codes which correspond to the facets. There are 5000 entries in SECTIONi, one for each possible facet. Any non-zero value is the actual identification code for the corresponding facet. A value of zero indicates that no identification code has been assigned to that facet. The operations in IDCODES_PART2 include the ability to specify an identification code for a set of specific facet numbers as well as the ability to assign an identification code to a rectangle of the COLLISION array. Deletion operations are also included. Once modification of the SECTIONi file is complete, the program generates a new display image. Identification codes may be assigned individual intensity codes so the user can see a image colored by identification codes.

VII. Conclusion and Recommendations

The IR image modeling system has achieved the main objective. Several different target files have been successfully run through the programs. The plume has been attached to the engine of the target. Facets, corresponding to higher temperature areas have been assigned identification codes by the IDCODE programs and thus have a higher intensity values in the IR images. Appendix A shows some of these generated images.

The next step in the development of the IR signature model will be to assign temperature and emissivity values to each facet so the radiance can be computed. Additional parameters, such as speed and atmospheric conditions, which can affect the IR sensor must be added to the system.

Appendix A

The pictures were drawn using VADS, a collection of image processing routines supported by the VAX 11/780 for the DeAnza QV5500 display system.

The viewing angles of the pictures:

	azimuth	elevation	range	yaw	pitch	roll
(1)	0	45	250	0	0	0
(2)	45	45	250	0	0	0

Figure A.1 and A.2 are color pixel maps of the IR image. Figure A.3 shows the set of facets in the sensor's line-of-sight.

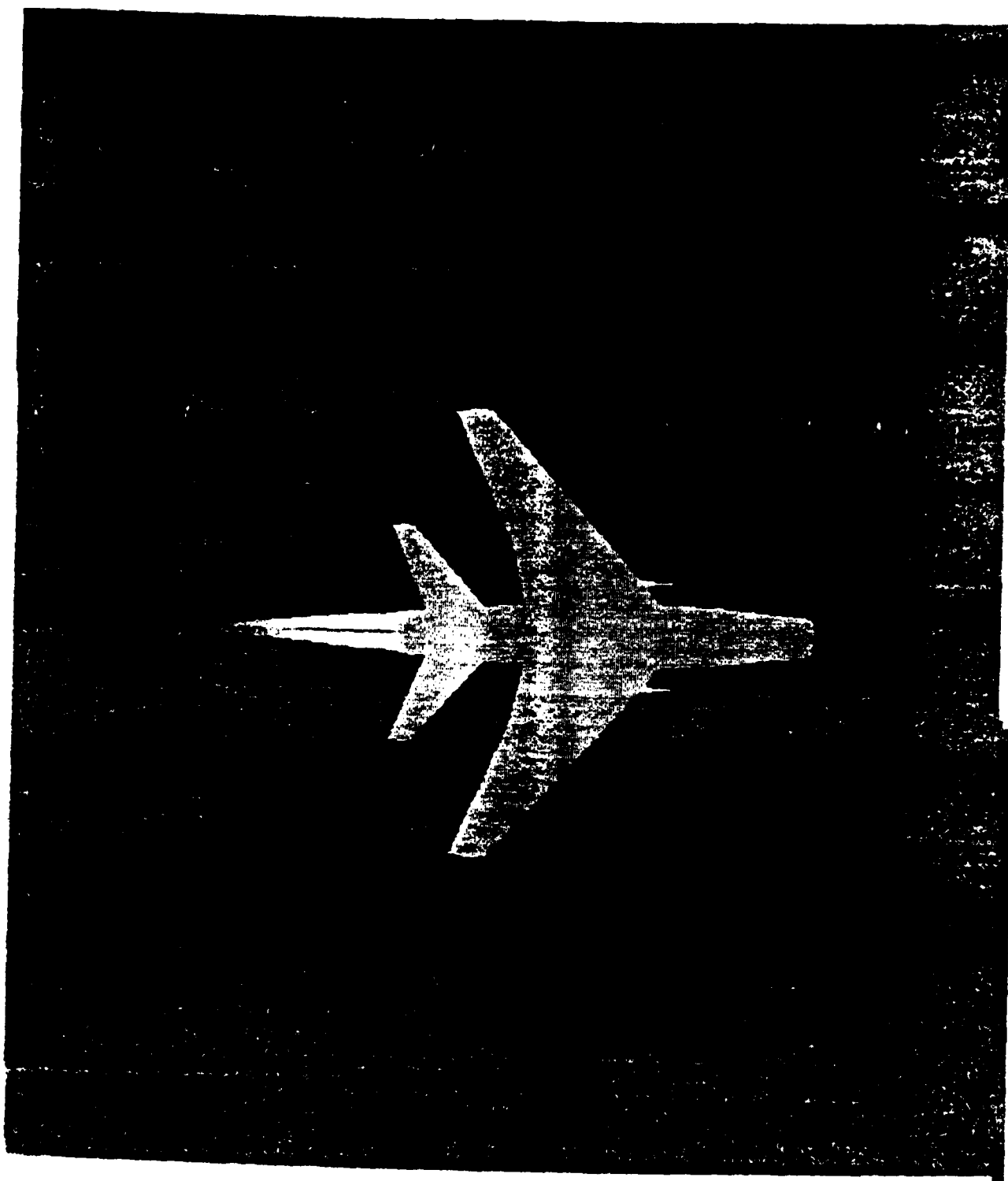


Figure A.1

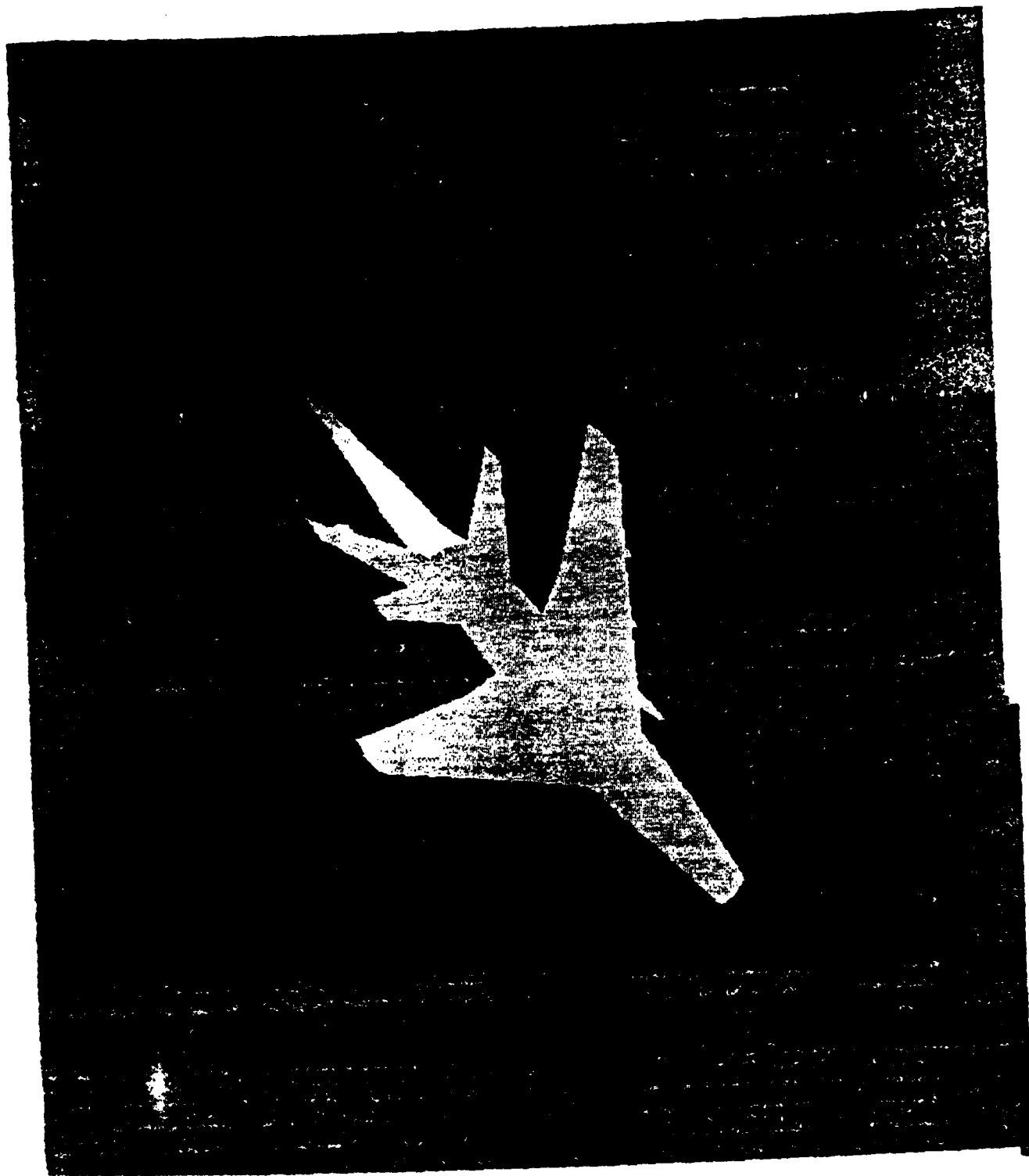


Figure A.2

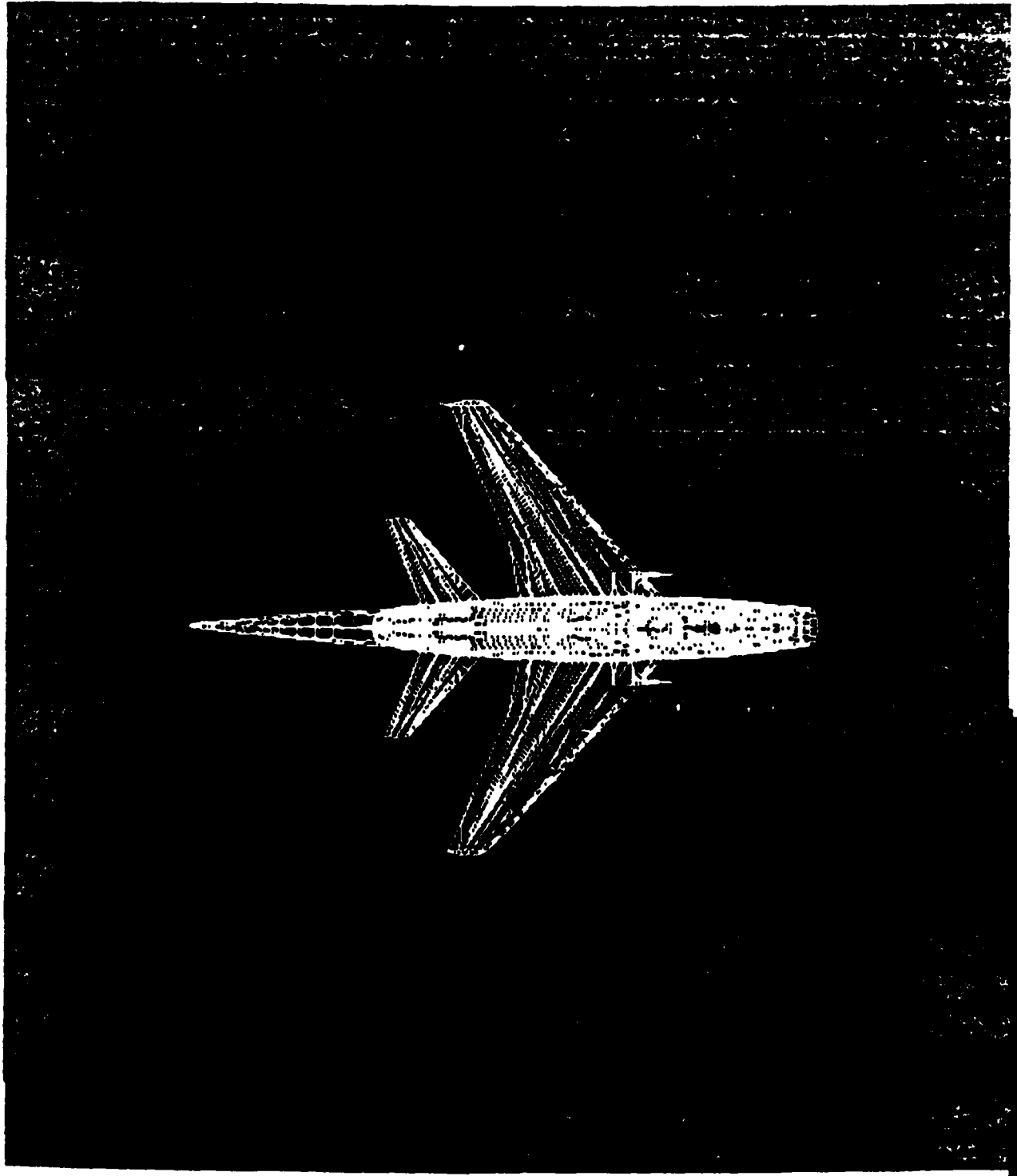


Figure A.3

1985 USAF-UES SUMMER FACULTY RESEARCH PROGRAM

**Sponsored by the
Air Force Office of Scientific Research**

**Conducted by the
Universal Energy Systems**

Final Report

MODELING OF TIRE/SOIL INTERACTION

Prepared by: Dr. Joseph E. Saliba

Academic Rank: Assistant Professor

Department and Department of Civil Engineering

University: University of Dayton

**Research Location: Wright Aeronautical Laboratory
Vehicle Equipment Division
Mechanical Subsystem Group**

USAF Research: George J. Sperry

Date: 19 July 1985

Contract No.: F49620-85-C-0013

MODELING OF TIRE/SOIL INTERACTION

BY

JOSEPH E. SALIBA

ABSTRACT

The viscoplastic finite element program for modeling Tire/Soil Interaction has been shown to be a powerful analytical tool that has a significant promise for improving the Air Force ability to predict aircraft ground operation.

A brief review of the mathematical theory of viscoplasticity and the computational procedure used in the finite element program is first presented. Next some of the capabilities of this powerful analytical tool are demonstrated. The first example considered is that of the effect of tire pressure on sinkage and rut depth produced on constant strength clay and sand soils. Then, the effect of layered soil on sinkage and rut depth is examined considering the possibility of both soft over hard as well as on hard over soft layers. This latest case is further studied investigating the effect of the variation of the top thickness layer on sinkage. In conclusion, a set of tables were shown that provided an equivalent cone index for a two layered clay soil of different strengths and thicknesses. To demonstrate the capability of the program to model contingency surfaces, the behavior of standard flexible and rigid pavements under a medium tire pressure were considered.

Finally, it is recommended that work hardening/softening models be identified and included in the routine to provide urgently needed ability for analytically modeling the tire multi-pass phenomenon.

Acknowledgement

I would like to respectfully thank the Air Force Systems Command, the Air Force Office of Scientific Research, and Universal Energy Systems for providing me with the opportunity to spend a very interesting and worthwhile ten weeks at the Air Force Wright Laboratory, Wright-Patterson AFB, Ohio. I would like to acknowledge the Laboratory, in particular the Mechanical Subsystems Group, for its hospitality and excellent working conditions.

I would like also to thank Mr. George J. Sperry for his collaboration and guidance during this project. Finally, I would like to thank Mrs. Merry Moses for typing this report.

I. INTRODUCTION

Readiness and survivability, important United States Air Force (USAF) objectives for nonstrategic forces, must be achieved in the key area of sortie generation. Critical elements in obtaining rapid and sustained sortie generation are aircraft launch and recovery where current and long-range actions are providing improvements. The effective development, optimization, and application of many of these actions depend upon reliably predicting aircraft capability to operate on various ground surfaces.

Most USAF aircraft were designed for operation on high-strength, smooth paved surfaces making these surfaces high priority wartime targets and subject to damage. Reliable prediction techniques exist for aircraft operation on conventional pavement surfaces. However, validated techniques are not yet available for predicting aircraft operation on soil, or any other contingency/austere ground surfaces.

In the past two decades the Air Force accomplished a number of research efforts resulting in computer programs which simulate the operation of aircraft on soils⁽¹⁻⁵⁾. These programs are only valid for constant strength media restricting simulation capabilities over layered soils. To remedy this problem a viscoplastic finite element program⁽⁶⁾ was developed to correlate layered soil, or other layered surfaces, to a single strength media. But such a program can be much more useful than as a correlation tool only. For example it can be applied to compute the sinkage and rut depth profiles under a tire or the variation of pressure or stress with depth.

II. OBJECTIVE

The objective of this study was to demonstrate the capabilities of the viscoplastic finite element computer program to predict sinkage and rut depth which can later be used as input data to existing routines that simulate aircraft operating on soil and other contingency/austere ground surfaces. The tasks pursued to achieve the objective were to:

- Summarize the mathematical theory of viscoplasticity and the computational procedure used in the finite element program.
- Use the program to compute sinkage and rut depth due to low, medium, and high pressure tire travel over constant strength single layer clay and silty sand type soils.
- Predict sinkage and rut depth for tire travel over layered soil and study the effect of top layer thickness.
- Compute an equivalent cone index for a two layered soil of different strength and thicknesses for an F-4 tire.
- Predict sinkage and rut depth for tire travel over flexible and rigid pavements.

III. MATHEMATICAL THEORY OF VISCOPLASTICITY⁽⁷⁾

1. GENERAL

The elasto-viscoplastic theory is based on the assumption that the total strain rate is divided into two parts,

$$\dot{\epsilon} = \dot{\epsilon}_{vp} + \dot{\epsilon}_e \quad (1)$$

where: $(\dot{})$ = differentiation with respect to time, ϵ , ϵ_e , ϵ_{vp} are the total, the elastic and the viscoplastic strain respectively.

The total stress σ can then be written as:

$$\sigma = D\epsilon_e \quad (2)$$

where D is the elasticity matrix.

The viscoplastic behavior is dictated by a scalar yield criterion:

$$F(\sigma, \epsilon_{vp}) - F_0 = 0 \quad (3)$$

in which F_0 is the uniaxial yield stress, which may itself be a function of the state of the material. With $F < F_0$, a purely elastic behavior will occur with $F > F_0$ a viscoplastic behavior is assumed.

To define the relationship between the various strain components, we borrow from the classical plasticity theory the idea of a plastic potential, denoted herein by $Q(\sigma)$.

$$\dot{\epsilon}_{vp} = \gamma \langle \dot{F} \rangle \frac{DQ}{D\sigma} \quad (4)$$

where:

$\frac{D}{D}$ is the partial derivative, γ is a fluidity parameter controlling the plastic flow rate, \dot{F} is a positive monotonically increasing function for $F > 0$ and $\langle \dot{F} \rangle$ is equal to \dot{F} for $F > 0$ or $= 0$ for $F \leq 0$

If $F = Q$, then the flow rule is of the associated kind. If $F \neq Q$, then the flow rule is said to be nonassociated.

We can rewrite Equation (4) as:

$$\dot{\epsilon}_{vp} = \gamma \langle \dot{F} \rangle a \quad (5)$$

where vector $a = \frac{DQ}{D\sigma}$

2. THE VISCOPLASTIC STRAIN INCREMENT

Kanichi, Zienkiewicz, and Owen⁽⁸⁾ suggested using a parameterized time stepping scheme to define a strain increment $\Delta \epsilon_{vp}^n$ occurring in a time interval $\Delta T_n = t_{n+1} - t_n$ as:

$$\Delta \epsilon_{vp}^n = \Delta t_n \left\{ (1 - \alpha) \dot{\epsilon}_{vp}^n + \alpha \dot{\epsilon}_{vp}^{n+1} \right\} \quad (6)$$

A fully explicit method can be obtained if α is set to zero. A fully implicit scheme results if α is set to one. An implicit trapezoidal or Crank-Nicolson rule will be obtained if $\alpha = 1/2$.

3. STRESS INCREMENTS

Using an incremental form of Equation (2), we obtain:

$$\Delta \sigma^n = D \Delta \epsilon^n = D (\Delta \epsilon^n - \Delta \epsilon_{vp}^n) \quad (7)$$

By expressing the total strain increment in terms of the displacement increment as:

$$\Delta \epsilon^n = B^n \Delta d^n \quad (8)$$

where: B = nodal strain displacement operator matrix

Δd = incremental displacement

and substituting for $\Delta \epsilon_{vp}^n$, we can write Equation (7) as:

$$\Delta \sigma^n = \hat{D}^n (B^n \Delta d^n - \epsilon_{vp}^n \Delta t_n) \quad (9)$$

where:

$$\hat{D}^n = (I + DC^n)^{-1} \quad D = (D^{-1} + C^n)^{-1} \quad (10)$$

4. EQUATIONS OF EQUILIBRIUM

The force equilibrium equation at time t_n over the complete domain is:

$$\int_{\Omega} (CB^n)^T \Delta \sigma^n d\Omega + r^n = 0 \quad (11)$$

where r^n is a vector containing applied nodal surface tractions, body forces, thermal loads, etc. During a time increment, the equilibrium equation can then be written as:

$$\int_{\Omega} (CB^n)^T \Delta \sigma^n d\Omega + \Delta r^n = 0 \quad (12)$$

where Δr^n is the change in applied nodal loads during the time interval Δt_n .

The tangential stiffness matrix can be computed by replacing the elasticity matrix D by \hat{D}^n in the regular formulation of the elastic problem; thus, we have

$$K_T^n = \int_{\Omega} CB^n)^T \hat{D}^n B^n d\Omega \quad (13)$$

Using Equations (12) and (13), we can state that:

$$\Delta d^n = K_T^n^{-1} \Delta r^n \quad (14)$$

where:

$$\Delta V^n = \int_{\Omega} [B^n]^T \Delta \epsilon^n d\Omega + \Delta r^n$$

Replacing $\Delta \epsilon^n$ by Equation (9), we obtain:

$$\Delta V^n = \int_{\Omega} [B^n]^T \hat{D}^n \dot{\epsilon}_{vp}^n \Delta t_{no} d\Omega + r^n \quad (15)$$

V^n are called the incremental pseudo-loads. Stricklin and Haisler (9) suggested computing the residual forces V as:

$$V^{n+1} = \int_{\Omega} [B^{n+1}]^T \epsilon^{n+1} d\Omega + r^{n+1} \neq 0 \quad (16)$$

This residual force is then added to the applied nodal force increment at the next time step, thus avoiding an iteration process and at the same time reducing the error propagation.

5. YIELD CRITERIA FOR SOIL

The failure of a soil mass seems to be in accordance with the tenets of the Mohr theory of failure.

The Mohr-Coulomb failure surface defined in terms of the stress invariants, $\sigma_1 = J_1$, J_2 , and the Lode angle θ_0 can be written as:

$$F = \sigma_m \sin \phi + J_2 \cos \theta_0 - \frac{J_2}{\sqrt{3}} \sin \theta_0 \sin \phi$$

$$- c \cos \phi = 0$$

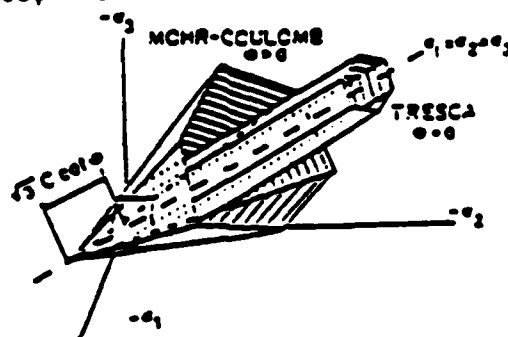


Figure 1

The yield surfaces defined in the preceding section have a serious drawback due to their angular nature in the principal stress space. Whenever stresses are such that they fall on one of the "ridges" of the yield surfaces, the directions of derivatives are not unique.

If the Mohr-Coulomb surface is to be represented by a circular cone, which one would represent the angular surface best? There are an infinite number of cones which could be chosen. One example is the Drucker-Prager which can be written as:

$$F = \frac{6 \sin \theta}{\sqrt{3} (3 - \sin \theta)} + J_2 - \frac{6 c \cos \theta}{\sqrt{3} (3 - \sin \theta)} = 0$$

which represents a cone passing through the exterior corners of the Mohr-Coulomb pyramid.

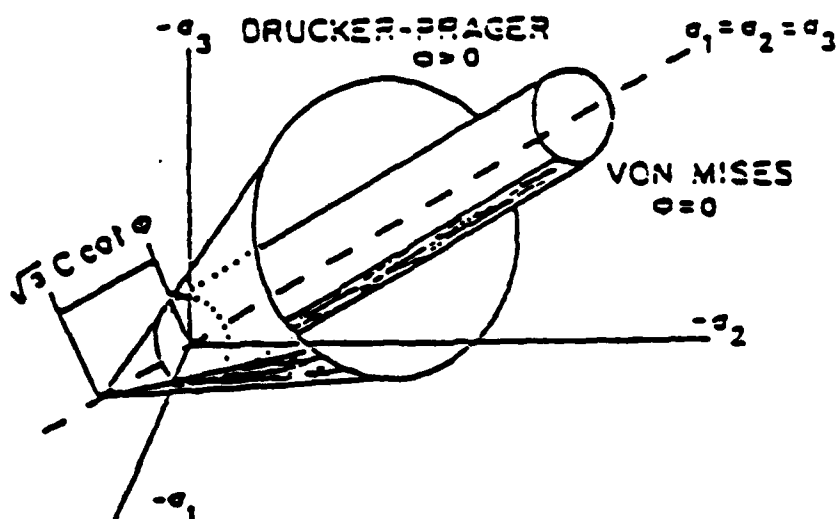


Figure 2

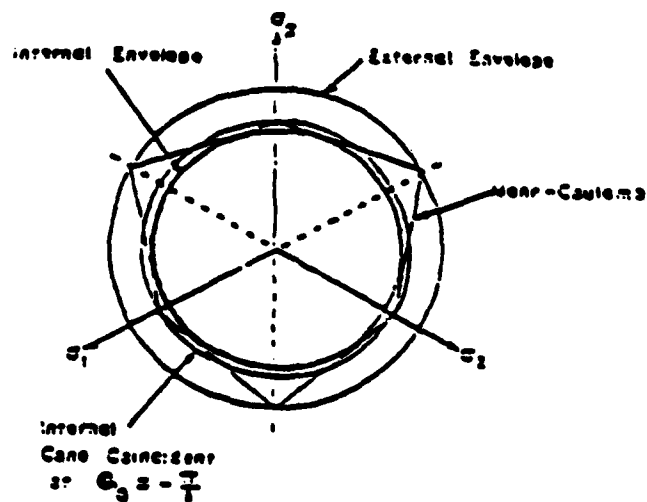


Figure 3

6. COMPUTATIONAL PROCEDURE

The computational procedure is divided into six major steps.

(1) Suppose at time $t = t_n$ we have an equilibrium situation d^n , σ^n , $\dot{\epsilon}_{vp}^n$, and f^n are known. The following quantities are computed:

- (a) $B^n = B_0 + B_{NL}(d^n)$ where $B_{NL}(d^n)$ is the nonlinear term of the strain matrix
- (b) $C^n = C^n(\sigma^n, \Delta t_n)$
- (c) $\hat{D}^n = (D^{-1} + C_n)^{-1}$
- (d) $K_T^n = \int_{\Omega} [B^n]^T \hat{D}^n B^n d\Omega$
- (e) $\dot{\epsilon}_{vp}^n = \gamma(\phi(f)) \hat{a}^n$

Once all of the above are computed, then proceed to:

(2) (a) Compute the displacement increments Δd^n from Equation 14

$$\Delta d^n = [K_T^n]^{-1} \int_{\Omega} [B^n]^T \hat{D}^n \dot{\epsilon}_{vp}^n \Delta t_n d\Omega + \Delta f^n \quad (17)$$

(b) Compute the stress increment $\Delta \sigma^n$

$$\Delta \sigma^n = \hat{D}^n (B^n \Delta d^n - \dot{\epsilon}_{vp}^n \Delta t_n)$$

(3) Compute the total displacements and stresses:

$$d^{n+1} = d^n + \Delta d^n$$

$$\sigma^{n+1} = \sigma^n + \Delta \sigma^n$$

(4) Update the viscoplastic strain rate:

$$\dot{\epsilon}_{vp}^{n+1} = \gamma(\phi(f)) \hat{a}^{n+1}$$

(5) Apply the equilibrium correction Equation (16) and add it to the incremental pseudo-loads for use in the next time step.

(6) Check if a steady state has been reached at each of the integration points in each element. If so, the solution is terminated or the next load increment is applied, or else return to step (1) and repeat for the next time step.

It has been shown⁽¹⁰⁾ that the generalized one parameter family of implicit integration schemes which apply to both associated and nonassociated flow rules and to any smooth yield function are unconditionally stable numerically for the value of that parameter larger than or equal to $1/2$.

IV. EFFECT OF TIRE PRESSURE ON CONSTANT STRENGTH SOIL SINKAGE AND RUT DEPTH

The program was used to compute tire sinkage and rut depth due to low, medium, and high pressure tires traveling over two types of constant strength single layer soils shown below:

MATERIAL PROPERTIES	CLAY	SILTY SAND
Modulus of Elasticity	5000 PSI.	15000 PSI.
Poisson's Ratio	0.3	0.3
Cohesion Factor	5.0 PSI.	1.0 PSI.
Friction Angle	0.0 DEG.	25.0 DEG.
Fluidity Parameter	0.05 1/SEC.	0.05 1/SEC.

The fluidity parameter used is arbitrary since we are interested in the steady state solution. Thus we are neglecting the effect of the load rate making this analysis valid only for very low speed (less than 5 mph.) or quasistatic cases. The strip of soil lies in a plane perpendicular to the long axis of the footprint. Only half of the strip is modeled taking advantage of the symmetry in the problem. The finite element model with all the geometry and the three different pressure distributions are shown in Figure 4.

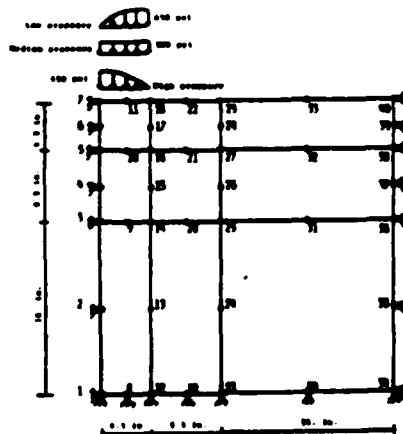


Figure 4 - CONSTANT STRENGTH FINITE ELEMENT MODEL

A state of plane strain is assumed and the Mohr-Coulomb yield function is chosen to predict yielding. Associated flow rule is assumed for clay while nonassociated flow is considered to model the viscoplastic flow rate for sand. The load is applied in increments of 0.6, 0.2, 0.2 and -1.0 times the maximum pressure thus modeling a one pass phenomenon over that strip of soil. The results of this study are shown in Figures 5 and 6 where the sinkage and the rut depth of the top surface is plotted for the three different tire pressures over the clay and sand soils

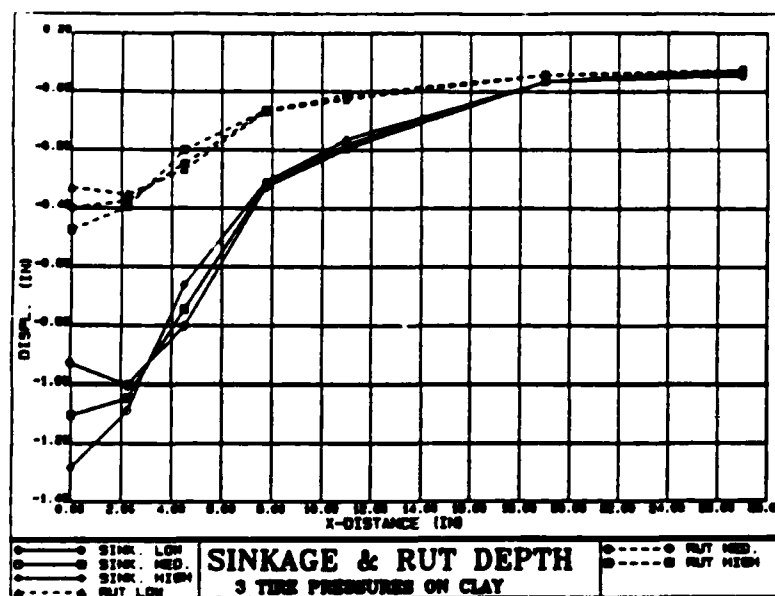


Figure 5

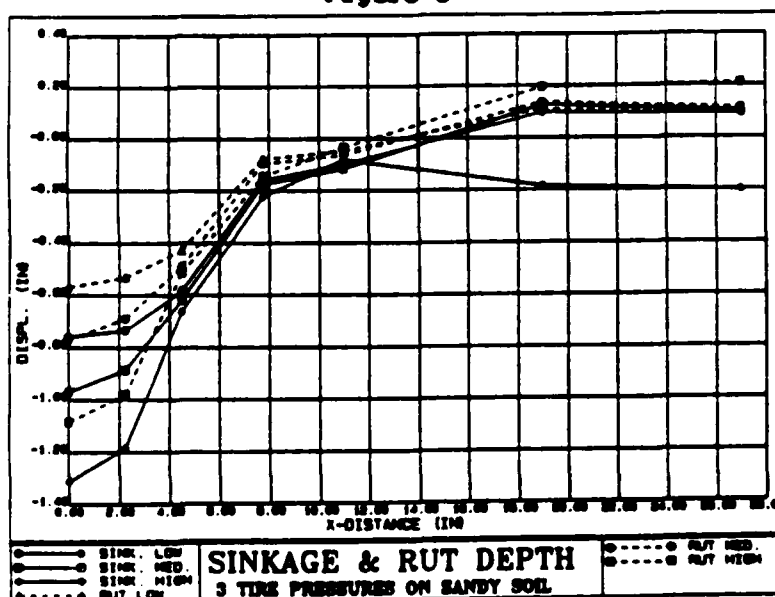


Figure 6

V. EFFECT OF LAYERED SOIL ON SINKAGE AND RUT DEPTH

The next problem attempted was to predict tire sinkage and rut depth resulting from a medium pressure tire traveling over clay and sand surfaces having two different layered strengths with the material properties shown below.

MATERIAL PROPERTIES	CLAY		SAND	
	SOFT	HARD	SOFT	HARD
Modulus of Elasticity	4500 PSI.	10000 PSI.	7000 PSI.	30000 PSI.
Poisson's Ratio	0.3	0.3	0.3	0.3
Cohesion Factor	3.0 PSI.	6.0 PSI.	0.5 PSI.	2.0 PSI.
Friction Angle	0.0 DEG.	0.0 DEG.	20.0 DEG.	20.0 DEG.
Fluidity Parameter	0.05 1/SEC.	0.05 1/SEC.	0.05 1/SEC.	0.05 1/SEC.

A medium tire pressure is assumed and the finite element model with all the geometry is shown in Figure 7. The top layer is assumed to be three inches thick while the bottom layer is taken to be thirty-seven inches. A hard over soft as well as a soft over hard layer is examined and the sinkage and rut depth for the top surface are plotted in Figure 8 for clay and Figure 9 for sand. Note that the same parameters for constant soft and hard layers of the same soil are also plotted on the same graph to better correlate the effect of layered soil.

MEDIUM PRESSURE IIII 300 PSI

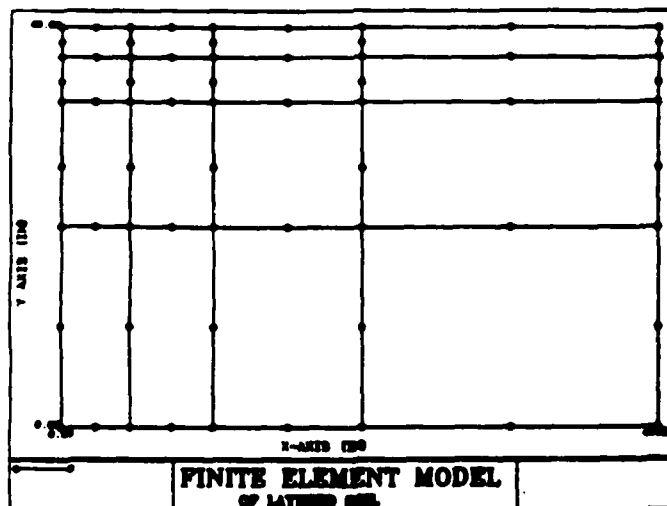


Figure 7 - LAYERED SOIL FINITE ELEMENT MODEL

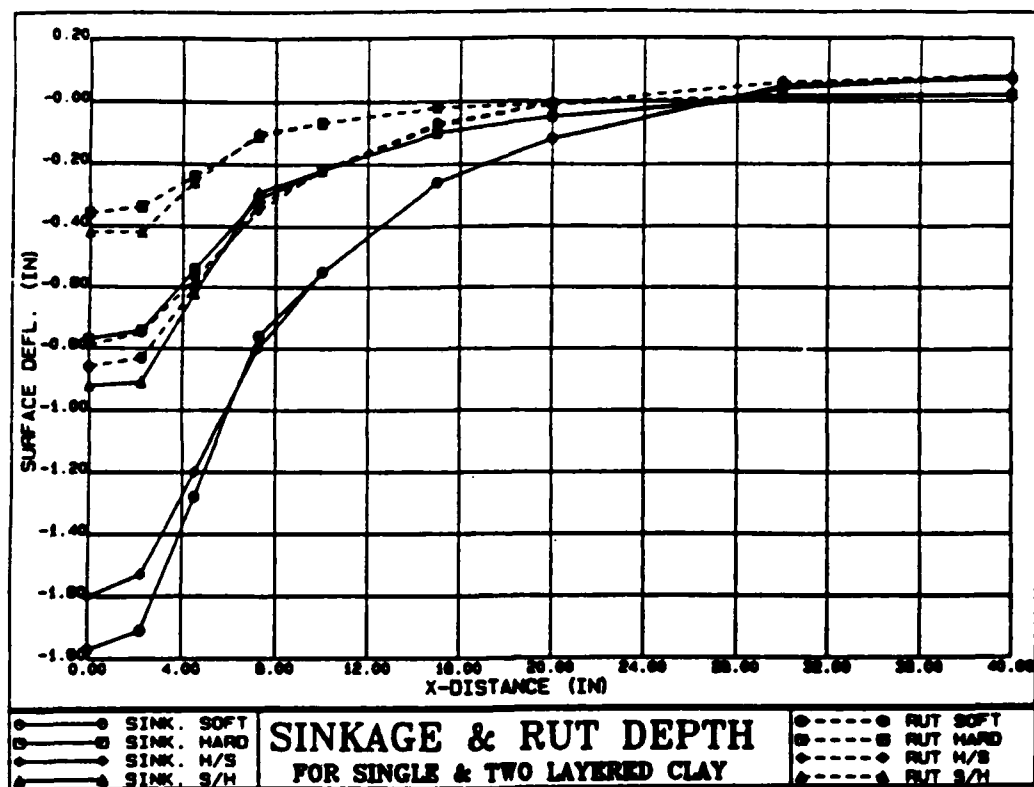


Figure 8

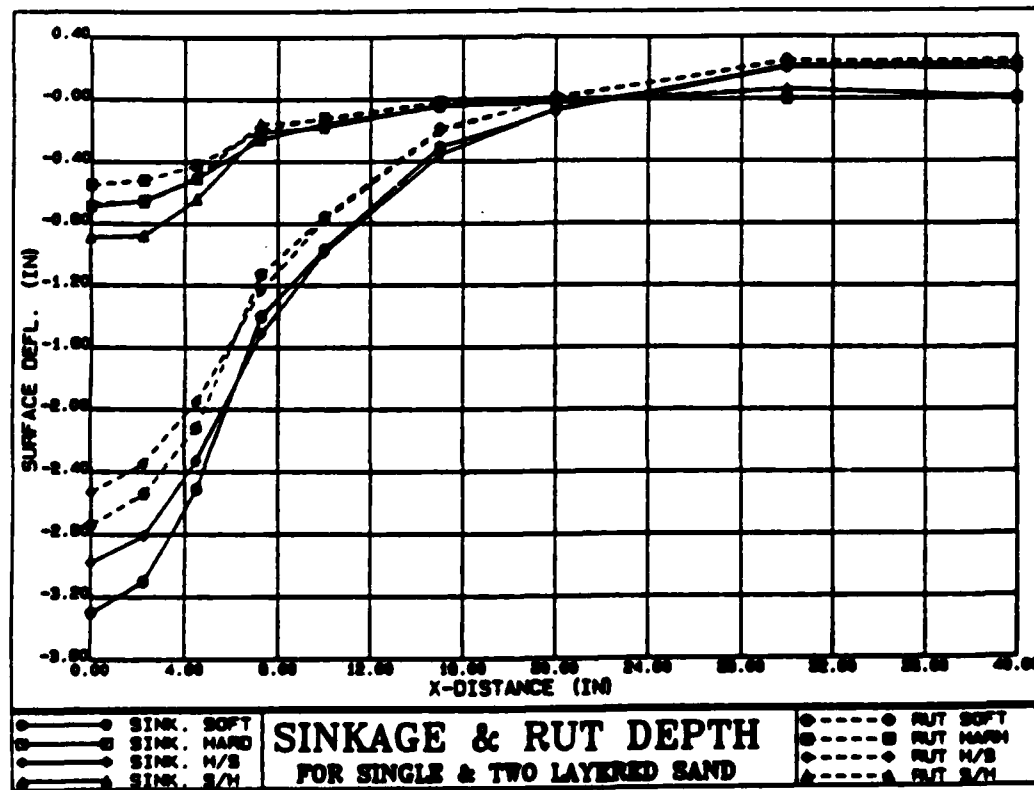


Figure 9

VI. EFFECT OF THE TOP THICKNESS LAYER ON SINKAGE

The Figure 7 Finite Element Model was used to study the effect of the top layer thickness on soil behavior. The effect of a soft layer on top of a hard one is not a problem as can be seen in the previous two graphs. In contrast, the behavior of a hard layer on top of a soft one is much more complex and more common in practice. This case was examined by varying the top thickness by making it 2, 3, 6, 9, and 20 inches thick. The resulting tire sinkages are shown for the clay soil in Figure 10 and the sandy soils in Figure 11.

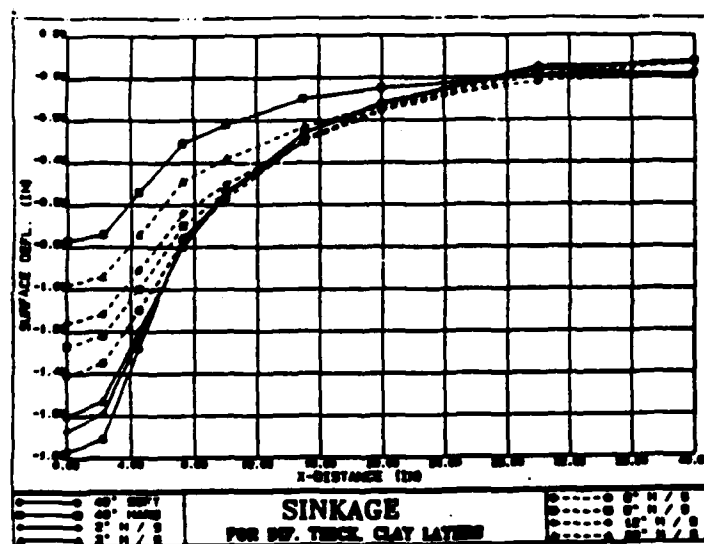


Figure 10

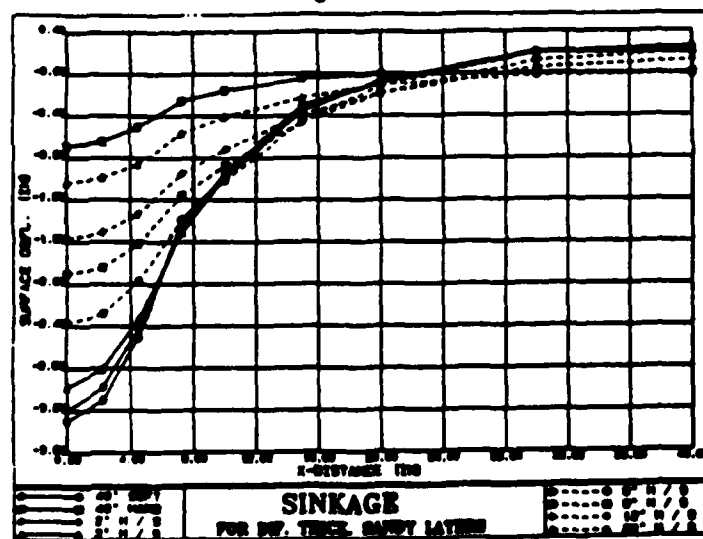


Figure 11

VII. EQUIVALENT CONE INDEX FOR AN F-4 TIRE ON CLAY

To compute an equivalent cone index for a two layered soil different strength and thickness we first picked material properties such that both sinkage and rut depth from the finite element program matched their respective experimental values for cone indexes of 240, 320, 400, 480, 560, 640, 720, and 800. Then all the possible combinations of ratios with cone index 240 were considered and the sinkage and rut depth were computed for top thicknesses of 1, 2, 3, 4, 6, 8, 10, and 12 inches keeping the total thickness constant and equal to 40 inches. Then the computed sinkages and rut depths were matched again with experimental values and an equivalent cone index was selected. This equivalent cone index was then divided by 240 and a dimensionless K constant was obtained. The summary of this study is shown in Figures 12 and 13.

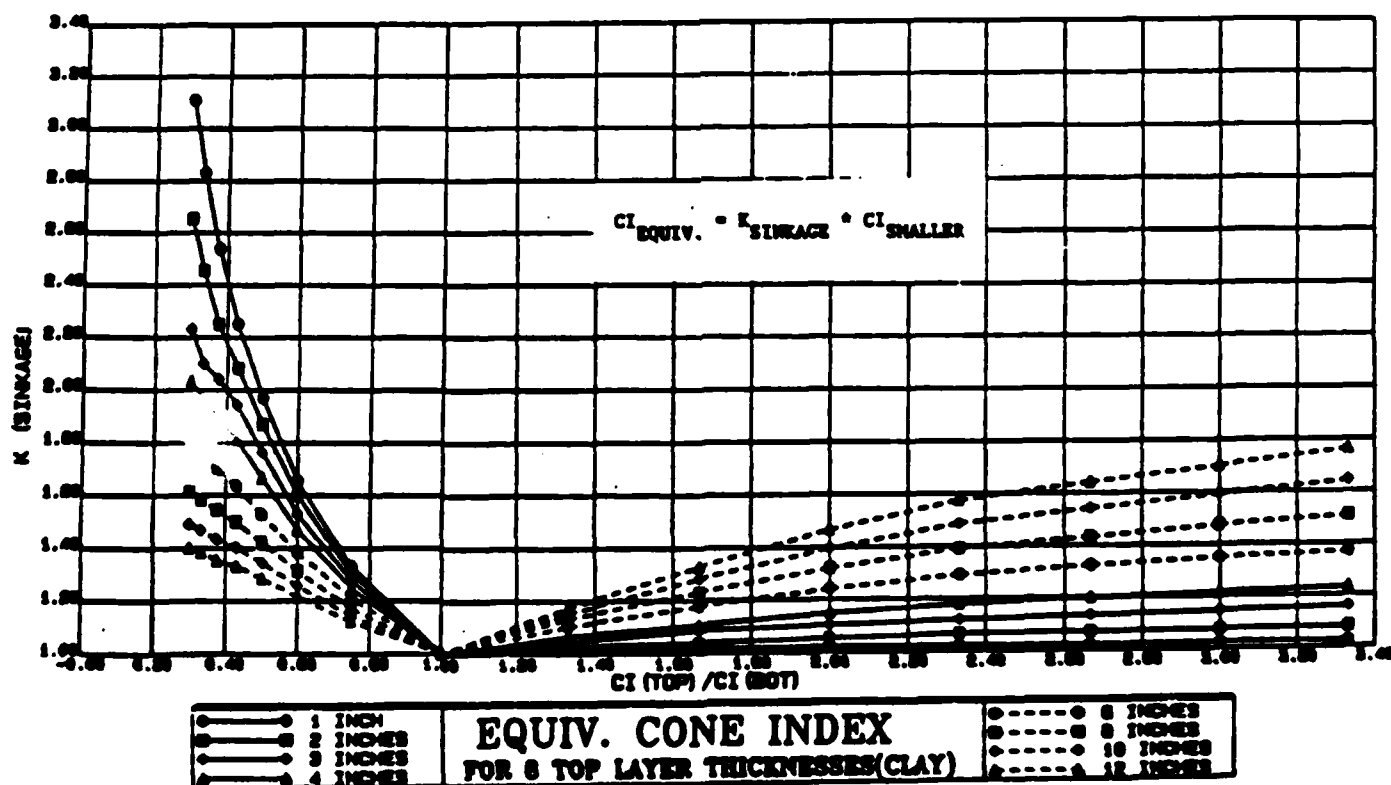


Figure 12

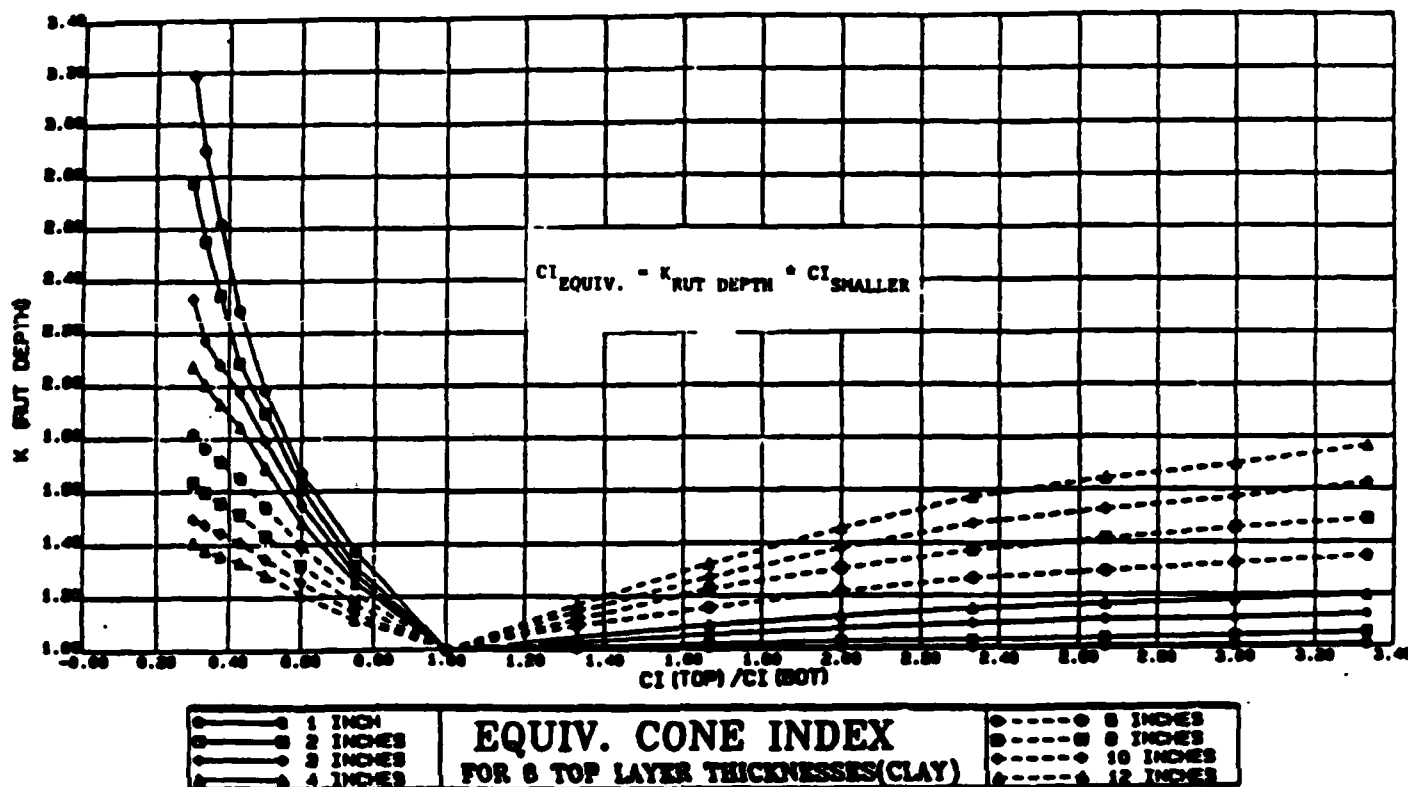


Figure 13

VIII. SINKAGE AND RUT DEPTH FOR FLEXIBLE AND RIGID PAVEMENTS

Finally a flexible and a rigid pavement under a medium pressure tire were considered. The pavement was assumed to be composed of 9-1/2 inches of a weak asphalt concrete or a Portland Cement concrete on top of 19 inches of crushed limestone on top of a layer of clay. Average published values were used to establish the material properties used which are shown below:

MATERIAL PROPERTIES	ASPHALT/PORTLAND CEMENT/CONCRETE	CRUSHED STONE	CLAY
Modulus of Elasticity	15000/340,000 PSI.	50000 PSI.	3000 PSI.
Poisson's Ratio	0.3/0.15	0.3	0.3
Cohesion Factor	10.0/990 PSI.	25.0 PSI.	3.0 PSI.
Friction Angle	0.0/0.0 DEG.	45.0 DEG.	0.0 DEG.
Fluidity Parameter	0.05/0.05 1/SEC.	0.05 1/SEC.	0.05 1/SEC.

The finite element model for this study is shown in Figure 12.

Figure 13 shows the predicted tire sinkages and rut depths.

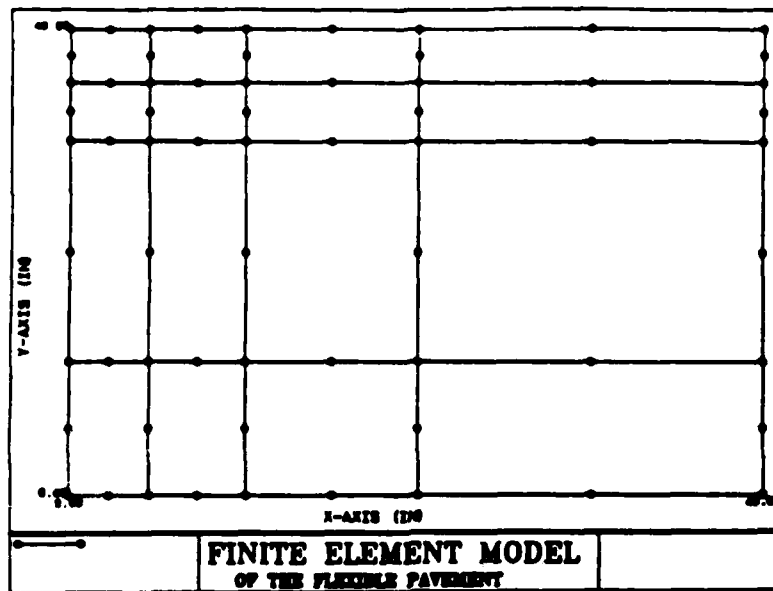


Figure 14

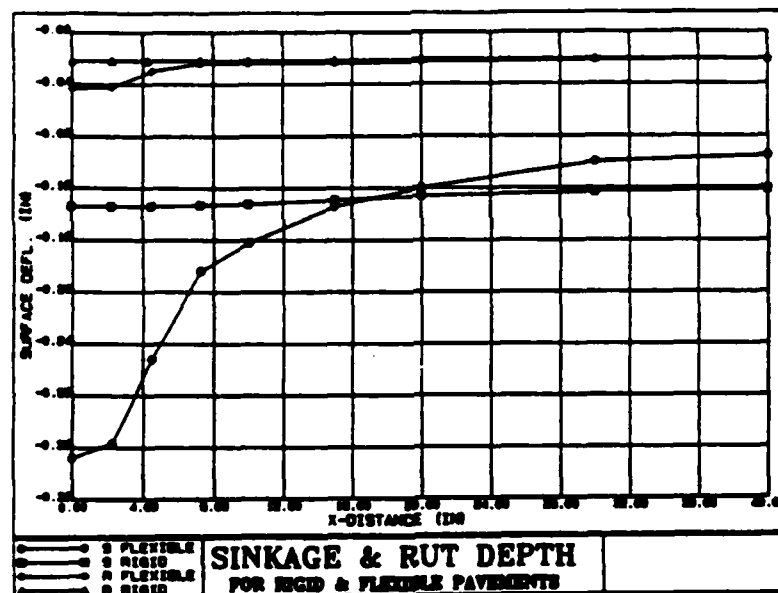


Figure 15

IX. CONCLUSION

The developed theoretical technique and the resulting finite element program provide a powerful analytical tool and holds significant promise to improve Air Force ability to predict aircraft ground operation.

This viscoplastic finite element program uses the state of the art in both constitutive relations and numerical techniques to model soil. It is capable of providing urgently needed improvements for predicting aircraft

tire sinkage and rut depth on soils or any contingency/austere surface. This study has demonstrated that the computer program can be applied to significantly improve the reliability and accuracy for predicting aircraft operation on soil surfaces having large variations in strength with depth. This study also showed that the analysis procedure can be adapted to provide a basis for predicting aircraft operation on other contingency surfaces.

X. RECOMMENDATIONS

To make the viscoplastic finite element program more suitable for potential Air Force applications, and to verify its application, feasibility and benefits, the following recommendations are proposed.

No analytical technique is currently available for examining or modeling multi-pass phenomenon. The finite element program has the ability to consider soil work hardening/softening such as caused by multiple aircraft tire passes. Thus additional research is needed to identify applicable work hardening/softening models and include them in the routine and demonstrate their capability of simulating the effect of cyclic loading obtained during multi-pass phenomena.

Because the viscoplastic finite element program uses the state of the art in constitutive relations, all the necessary tests have not been identified for determining all of the material properties needed as program input. Thus some research is urgently needed to remedy this problem.

Simulations have not been accomplished to establish the program's applicability for improving ability to predict aircraft operation on soil and other airfield contingency surfaces. Thus the finite element program should be used to compute load sinkage curves or tables which can then be used as input to existing computer prediction codes to verify the program's applicability for improving ability to predict aircraft ground operation.

REFERENCES

1. "Aircraft Surface Operation Soil Surface Correlation Study," Department of Civil Engineering Research Institute, University of Dayton, Dayton, Ohio, AFFDL-TR-70-30.
2. Luning, H., "Analytical Aircraft Landing Gear Soil Interaction Phase II, Rolling Single Wheel Analytical Sinkage Prediction Technique and Computer Program," University of Dayton, Dayton, Ohio, AFFDL-TR-70-142.
3. Kraft, D., "Multiwheel Landing Gear-Soils Interaction and Flotation Criteria, Phase III," University of Dayton, Dayton, Ohio, AFFDL-TR-71-12, Part I & II.
4. Kraft, D., "Landing Gear/STOL Interaction Development of Criteria for Aircraft Operation on Soil During Turning and Multi-Pass Operations," University of Dayton, Dayton, Ohio, AFFDL-TR-73-78.
5. Phillips, Norman S. and Saliba, Joseph E., "Landing Gear/Soil Interaction Development of Criteria for Aircraft Operation on Soil During Turning and High Speed Straight Roll Computer Programs Documentation Volume II," ESL-TR-82-29, Air Force Flight Dynamics Laboratory, Wright-Patterson Air Force Base Ohio, June 1981.
6. Saliba, Joseph E., "An Elastic-Viscoplastic Finite Element Model for Representing Layered Soils-Description Volume I," AFESC/RDCR, Air Force Engineering and Services Center, Tyndall Air Force Base, Florida, January 1984.
7. D. R. J. Owen and E. Hinton, Finite Elements in Plasticity Theory and Practice, (Swansea, U.K.: Pineridge Press Limited, 1980).
8. H. B. Kanchi, O. C. Zienkiewicz and D. R. J. Owen, "The Viscoplastic Approach to Problems of Elasticity and Creep Involving Geometric Nonlinear Effects," Int. J. Num. Meth. Engr., Vol. 12, 1978, pp. 169-181.
9. J. A. Stricklin, W. Haialer, and W. Reissmann, "Evaluation of Solution Procedures of Material and/or Geometrically Nonlinear Structural Analysis," AIAA J., Vol. 11, 1973, pp. 292-299.
10. J. E. Saliba, Numerical Stability of Implicit Integration Schemes in Nonassociated Viscoplasticity, University of Dayton, 1983.

1985 USAF-UES SUMMER FACULTY RESEARCH PROGRAM/

GRADUATE STUDENT SUMMER SUPPORT PROGRAM

Sponsored by the

AIR FORCE OFFICE OF SCIENTIFIC RESEARCH

Conducted by the

UNIVERSAL ENERGY SYSTEMS, INC.

FINAL REPORT

BACTERIOLOGIC TECHNIQUES FOR THE ISOLATION OF LEGIONELLAE
FROM AQUATIC ENVIRONMENTS

Prepared by:	Gordon D. Schrank
Academic Rank:	Associate Professor
Department and University:	Department of Biological Sciences St. Cloud State University
Research Location:	Epidemiology Division School of Aerospace Medicine Brooks Air Force Base, Texas 78235-5000
USAF Research:	Dr. Jerome P. Schmidt
Date:	August 16, 1985
Contract No.:	F49620-85-C-0013

BACTERIOLOGIC TECHNIQUES FOR THE ISOLATION OF LEGIONELLAE
FROM AQUATIC ENVIRONMENTS

by

Gordon D. Schrank

ABSTRACT

Effort was directed at defining methods for the isolation of Legionellae from aquatic environments. Organisms can be isolated from both potable and nonpotable water using selective culture media. Bacteria in samples must be concentrated by centrifugation. Neither vacuum or pressure filtration is recommended in most routine applications. Recovery of Legionellae from heavily contaminated specimens is facilitated by acid treatment of the concentrated sample before plating. Prolonged exposure of samples to low temperatures (2-10°C) is not recommended. Direct fluorescent antibody staining of specimens may be useful in final identification of organisms. However, it is not recommended for screening purposes.

More basic research is needed regarding the flagellar antigens of Legionellae. Only crude preparations have been characterized to date. Methods for isolating and propagating phage lytic for Legionellae are needed. Preliminary work was completed in both of these areas.

ACKNOWLEDGMENTS

I would like to thank the Air Force Systems Command, the Air Force Office of Scientific Research and the Universal Energy Systems, Inc., for providing this research opportunity. The personnel of the Epidemiology Division, School of Aerospace Medicine, Brooks Air Force Base, were most helpful in providing supplies and facilities for this work.

Individual acknowledgments include Dr. Jerome P. Schmidt for initiating and implementing this project. Dr. Louis E. Blouse provided many helpful suggestions. Others contributing to the completion of the work include MSgt. Joe Mokry, Sgt. Aaron Sinclair, ALC Tracy Cole, Maj. Roy Almeida, Mr. Robert Ball, Dr. Vee Davison, and Sgt. Jorge Ruiz. Special acknowledgment is given to Mr. Cliff Miller.

I. INTRODUCTION

The family Legionellaceae contains the organism responsible for Legionnaires' Disease and a number of related species. Currently 22 species of Legionella have been proposed (Brenner, et al., 1985). These organisms are phenotypically unique and contain DNA that has been found to be distinct among known bacterial species. It is likely that several other species will be described in the future. Speciation is dependent upon DNA homology studies. In addition, Legionella as the single genus within the family remains to be resolved.

Legionellae typically grow on buffered cysteine-yeast extract agar but not blood agar, have a growth requirement for cysteine, are gram negative, urease and nitrate negative, nonfermentative, and catalase positive. Legionellae will not grow on media for Francisella tularensis although the latter usually will grow on media for Legionellae. None of the currently known Legionellae react with antisera against F. tularensis. Legionellae produce a brown pigment on tyrosine-containing yeast extract agar, liquefy gelatin, and are motile. Some species hydrolyze hippurate and produce a fluorescent pigment.

In summary, Legionellae require cysteine, do not react with antisera against F. tularensis, do not grow on blood agar, and are gram negative. Speciation ultimately requires deoxyribonucleic acid (DNA) homology studies.

The Microbiology Section of the Epidemiology Division is a reference center for Air Force clinical laboratories throughout the world. Personnel in this laboratory are interested in procedures for isolation and characterization of pathogens from patient specimens or from

environmental sources. Legionellae are frequently found in aquatic environments including both potable and nonpotable water.

My experience in microbiology includes work in a clinical laboratory as well as contract work involving Brucella sp. I have been doing basic research with Legionellae for at least two years. The lack of metabolic diversity among species and the number of species makes this group of organisms very interesting subjects for basic research.

II. OBJECTIVES:

The major objective for the summer research period involved the study of sampling techniques for both potable and nonpotable water samples. Emphasis was to be placed on comparing concentration techniques and methods for reducing the growth of contaminating organisms in the particular specimen.

Historically, Legionellae have been isolated using embryonated eggs, guinea pigs, and direct inoculation of laboratory media. Direct plating has been shown to be as sensitive as other methods for recovery of organisms (Edelstein, 1981; Brenner, et al., 1985). With this basic issue resolved, more emphasis was placed on concentration and plating techniques using known media formulations. Pretreatment techniques for specimens must be considered. These involve methods designed to reduce the number of contaminating organisms in the specimens. Such pretreatment methods include exposure to heat and/or an acid buffer before plating of samples. I was fortunate to have some preliminary data from my last summer research program as well as information obtained during the last year in my own research laboratory.

Two additional objectives developed during the summer research period. Because of my experience with isolation and characterization of bacterial flagella (Yang, et al., 1977), I began the task of isolating and characterizing flagella from several Legionella species. Previous work in this area has produced only crude flagella preparations (Rogers and Laverick, 1984).

A second new objective developed regarding isolation of phage lytic for Legionellae. Such viruses could be used in phage typing procedures and genetic studies. Preliminary studies would indicate that methods for isolation and propagation of phage related to this family of organisms will prove difficult because of the slow growth rate of the host and the need for very complex growth media for the host.

III. NOMENCLATURE:

Only eight Legionella species were used in the present study. These included L. bozemanii, L. dumoffii, L. gormanii, L. micdadei, L. pneumophila, L. jordanis, L. wadsworthii, and L. longbeachae. All of these organisms were obtained from Dr. Hazel Wilkinson at the Centers for Disease Control during the summer of 1984.

IV. CONCENTRATION TECHNIQUES:

Various concentration techniques have been used for water samples. These include pressure and vacuum filtration as well as centrifugation. Combinations of filtration and centrifugation may be used under certain circumstances. Some unknown conditions do not seem to favor the growth of Legionellae in the San Antonio area. Therefore, I limited my studies

to water samples that had been seeded with Legionellae (L. micdadei, L. pneumophila, or L. bozemanii). These three species were chosen for two reasons. First, I had a commercial preparation for direct fluorescent antibody staining for each. Secondly, these three organisms do show some diversity in their growth pattern; the fluorescent pigment of L. bozemanii may be detected by exposing the colonies to ultraviolet light, for example.

The laboratory basically has choices of vacuum filtration, pressure filtration, and centrifugation. Vacuum or pressure filtration with the subsequent grinding of the filter to release organisms does not seem to be desirable except for very clear (potable) water systems. I was able to collect sample material from a cooling tower using pressure filtration; vacuum filtration is totally unacceptable under these circumstances.

The method of choice seems to be centrifugation whereby one liter samples are concentrated using Nalgene polypropylene bottles (Cat. #3120-1000) fitted with a lock-tight cap. Samples are centrifuged at 3500 rpm for 1 h (Sorvall Instruments, RC-3B Refrigerated Centrifuge). Although I was using the H-6000 head for the centrifuge (accepts six liter containers), I would recommend concentrating only two liters of water during a single centrifugation period. It might be desirable to purchase the H-4000 head for the centrifuge since it can be operated at a higher speed producing a greater relative centrifugal force.

I found that samples could be adequately concentrated by centrifugation at 20°C. Several authors have noted a decrease in viability of

Legionellae when handled and stored at 2-10°C (Wadowsky, et al., 1985). Other factors such as pH, dissolved oxygen, and chlorine concentration can affect the multiplication of Legionellae (Wadowsky, et al., 1985; Kuchta, et al., 1983).

V. TREATMENT OF SAMPLES BEFORE PLATING:

Various treatment protocols have been proposed for concentrated water samples including heat treatment (50°C for 30 min.) and acid treatment (exposure to a pH 2.2 solution for 4 min.). Both of these treatments are designed to reduce the number of contaminating organisms present in the inoculum. Acid treatment has been recommended for most specimens and I concur (Brenner, et al., 1985). I had some difficulty evaluating these treatments with laboratory adapted strains. However, for acid treatment, the concentrated specimen is diluted 1:10 in a 0.2 M HCl-KCl buffer, pH 2.2. The specimen is then mixed with a vortex-type mixture for 4 min. A 0.1 ml portion of the specimen is plated. I would also recommend neutralizing a portion of the specimen using 0.1 M KOH before plating despite the buffering action of the medium. It is important to determine the pH of the treated solution. I found that many San Antonio water samples had a high pH (pH 8-9) with a great deal of buffering capacity. The use of the acid buffer did not always bring the pH of the samples below pH 7.0. Therefore, it is important to assess the success of the acid treatment before plating.

VI. SELECTIVE MEDIA:

I concur with Fitzgeorge and Dennis (1983) that about 10^2 organisms can be detected in 10 ml of water using culture on selective media. This is particularly true of potable water samples. Selective agents

have made culture reasonable even with samples of somewhat stagnant water. On an overall basis, these selective agents reduce viability of Legionellae up to about 60%. Parenthetically, it should be noted that most Legionellae grow better when found in high concentrations (about 10^7 /ml). Therefore, near the lower detection limits, culture time may exceed the usual 48-72 h incubation period. The issue of increased CO₂ tension on primary isolation remains unresolved. Laboratory adapted strains grow very well in a candle extinction jar whereas fresh isolates may not.

I recommend the following selective media preparations:

A. GVPC Medium

Basal Medium: Buffered yeast extract agar with alpha-ketoglutarate, L-cysteine, and ferric pyrophosphate (Feeley, et al., 1979).

Prepare according to the DIFCO package insert.

Supplemental Materials:

3 mg/ml glycine

5 µg/ml vancomycin

100 U/ml polymyxin B

Reference: Joly, et al., 1984

80 µg/ml cycloheximide

B. GVP Medium

Prepare as above, omit

Reference: Joly, et al., 1984

cycloheximide

C. CVC Medium

Prepare basal medium as in (a) with the following supplements:

4 µg/ml cephalothin

0.5 µg/ml vancomycin

Reference: Brenner, et al., 1985

16 µg/ml cephalothin

NOTE: Exact expiration dates are not known for these selective media. However, six weeks has been recommended (Edelstein, 1981).

Medium A serves well to reduce growth of bacterial and fungal contaminants. The other two media are more useful when working with specimens that contain relatively low numbers of contaminants (i.e., potable water samples).

VII. DIRECT FLUORESCENT ANTIBODY STAINING:

I found the following reagents to be useful and to give minimum cross-reactivity with contaminants. I tested only a sample of the company's complete line of Legionellae reagents.

Bionetics Laboratory Products

Litton Bionetics, Inc.,

Charleston, S.C. 29405

Direct fluorescent antibody conjugates:

Legionella micdadei, serogroup 1

Legionella pneumophila, serogroup 1

Legionella bozemanii, serogroup 1

Control antigens:

Control antigens for the above conjugates.

Other controls:

Legionella negative control - FITC conjugate with rabbit globulin.

With the uncertain nomenclature and serogrouping for Legionellae,

it is difficult to make a final recommendation for selection of direct fluorescent antibody reagents. In view of the increased sensitivity of culture methods over direct fluorescent antibody staining, such reagents may not be necessary for a laboratory seeking to isolate the organisms from water samples except as an aid in identification. Complimentary DNA probes and enzyme-linked immunosorbent assay (ELISA) techniques may make direct fluorescent antibody staining obsolete.

VIII. FLAGELLAR ANTIGENS:

I initially determined the optimal culture conditions for flagella production in L. pneumophila. As noted by electron microscopy, large numbers of flagella can be produced using biphasic culture of the organism at 30°C. The standard buffered charcoal yeast extract agar is overlayed with 1.15% yeast extract broth. The organisms are cultured for five days in a 150 cm² tissue culture flask which contains the broth and solid agar.

The organisms are removed in the broth and washed once by centrifugation in 0.85% NaCl and suspended in a TRIS buffer (Yang, et al., 1977). The buffer also contains 1% Triton X-100. Flagella are removed by shearing using a Sorvall Omni-Mixer assembly (200 ml stainless steel containment cup) operated at 16,000 rpm for 30 sec. This treatment is followed by four cycles of low and high speed differential centrifugation (10,000 x g for 10 min. followed by 30,000 x g for 2 h).

Observation by electron microscopy following the differential centrifugation indicates that I was able to prepare a flagella/vesicle mixture which can be purified by density gradient centrifugation. I will complete this work in my laboratory.

This work seems particularly important in view of the crude flagellar antigen preparations made to date (Rogers and Laverick, 1984; Hebert, et al., 1980). Such information can only add to our basic knowledge of the biology of Legionellae.

IX. PHAGE ISOLATION:

Phage isolation is lacking for the Legionellae. Preliminary work during the research period has given me much information about lawn preparation and possible propagation techniques for this organism. I intend to continue this work during the next year in my own laboratory. I feel phage isolation procedures used for mycobacterial viruses may be useful in searching for viruses lytic for Legionellae. I will use some of these original protocols in future work (Redmond and Ward, 1966; Jones and Greenburg, 1978).

X. RECOMMENDATIONS:

- A. Legionella can be isolated from both potable and nonpotable water samples. Bacteria in these specimens should be concentrated by centrifugation followed by plating on selective media.
- B. Water samples should not be stored for long periods of time at 2-10°C due to the loss of viability of Legionellae at these temperatures.
- C. Treatment of samples before plating is best accomplished using brief exposure to an acid buffer (0.2 M HCl-KCl). Monitoring of the pH during this time is recommended to insure that alkaline specimens are adequately treated before plating.
- D. Three selective media are recommended. The medium containing cycloheximide was found to be very useful, particularly when working

with specimens heavily contaminated with fungi. Potency of antibiotics in the media must be considered in setting expiration dates. Currently, six weeks is recommended.

E. I would not recommend screening water samples by direct fluorescent antibody staining.

F. Two areas of research regarding the basic biology Legionellae should be pursued. These include characterization of purified flagella and characterization of phage lytic for various organisms within the group.

REFERENCES

- Brenner, D.J., et al. 1985. Ten new species of Legionella.
International Journal of Systematic Bacteriology 35:50-59.
- Edelstein, P.H. 1981. Improved semiselective medium for isolation
of Legionella pneumophila from contaminated clinical and environmental
specimens. Journal of Clinical Microbiology 14:298-303.
- Feeley, J.C., et al. 1979. Charcoal yeast extract agar: primary
isolation medium for Legionella pneumophila. Journal of Clinical
Microbiology 10:437-441.
- Fitzgeorge, R.B. and P.J. Dennis. 1983. Isolation of Legionella
pneumophila from water supplies: comparison of methods based on
the guinea-pig and culture media. Journal Hygiene (Cambridge)
91:179-187.
- Hebert, G.A., et al. 1980. The rickettsia-like organisms TATLOCK
(1943) and HEBA (1959): bacteria phenotypically similar to but
genetically distinct from Legionella pneumophila and the WIGA
bacterium. Annals of Internal Medicine 92:45-52.
- Joly, J.R., et al. 1984. Ecological distribution of Legionellaceae
in the Quebec city area. Canadian Journal of Microbiology 30:63-67.
- Jones, W.D. and J. Greenberg. Modification of methods used in
bacteriophage typing of Mycobacterium tuberculosis. Journal of
Clinical Microbiology 7:467-469.
- Kuchta, J.M. 1983. Susceptibility of Legionella pneumophila to chlorine
in tap water. Applied and Environmental Microbiology 46:1134-1139.

Redmond W.B. and D.M. Ward. 1966. Media and methods for phage-typing mycobacteria. Bulletin World Health Organization 35:563-568.

Rogers, F.G. and T. Laverick. 1984. Legionella pneumophila serogroup 1 flagellar antigen in a passive hemagglutination test to detect antibodies to other Legionella species. IN Legionella, proceedings of the 2nd international symposium. American Society for Microbiology.

Wadowsky, R.M., et al. 1985. Effect of temperature, pH, and oxygen level on the multiplication of naturally occurring Legionella pneumophila in potable water. Applied and Environmental Microbiology 49:1197-1205.

1985 USAF-UES SUMMER FACULTY RESEARCH PROGRAM/
GRADUATE STUDENT SUMMER SUPPORT PROGRAM

Sponsored by the
AIR FORCE OFFICE OF SCIENTIFIC RESEARCH

Conducted by the
UNIVERSAL ENERGY SYSTEMS, INC.

FINAL REPORT

CHEMICAL LASER RESEARCH ON THE
IODINE MONOFLUORIDE (IF) SYSTEM

Prepared by:	RONALD M. SEGA
Academic Rank:	ASSOCIATE PROFESSOR
Department and	ELECTRICAL ENGINEERING
University:	UNIVERSITY OF COLORADO, COLORADO SPRINGS
Research Location:	FJSRL/NH
	USAF ACADEMY, COLORADO
USAF Research:	MAJOR DAVID K. NEUMANN
Date:	SEPTEMBER 25, 1985
Contract No:	F49620-85-C-0013

CHEMICAL LASER RESEARCH ON THE
IODINE MONOFLUORIDE (IF) SYSTEM

by

RONALD M. SEGA

ABSTRACT

The research direction was shifted from a focus on the iodine oxide (IO) system to the iodine monofluoride (IF) system. When C_3F_7I gas was substituted for I_2 as a source of iodide, mixed with O_3 and excited by a KrF excimer laser, the resulting spectra was positively identified as IF(B). Several aspects of the experimental set-up including the O_3 generation cell, O_3 detection system, and spectroscopy system were redesigned and tested to provide increased accuracy for data acquisition. The IF system has been under investigation at the Air Force Weapons Lab for a number of years but has not been generated in this manner.

ACKNOWLEDGMENTS

Several organizations were instrumental in the success of the program including the Air Force Systems Command, Air Force Office of Scientific Research, Frank J. Seiler Research Laboratory, and the Department of Physics, United States Air Force Academy.

In particular, I wish to thank Major David Neumann, Major Albert Alexander, Major Stan Czyzak and Lieutenant Carl Sovinec for their cooperation and guidance throughout the summer research period.

I. INTRODUCTION:

The USAF research interest in the development of an efficient laser in the visible portion of the electromagnetic spectrum was the background motivation for the pursuit of this work. Major David K. Neumann of the Department of Physics, U.S. Air Force Academy had proposed a study into the iodine oxide (IO) system and was subsequently funded in this effort. The research is a joint project between faculty members of the Air Force Academy and personnel assigned to the Frank J. Seiler Research Laboratory (FJSRL), also at the Air Force Academy.

Fundamental to this effort is a knowledge of electronic transitions and diagnostic techniques for evaluating the emission from given electronic transitions. My background includes atomic physics research in L-shell ionization at Ohio State University as a Master's student (1974-1975) and over the last six years working in an applied electromagnetics area involving an infrared detection technique.

II. OBJECTIVES OF THE RESEARCH EFFORT

A. INITIAL OBJECTIVES

1. Characterize the IO (A) state by determining its molecular constants and lifetime as a function of vibrational level.
2. Undertake kinetic studies involving this state to include measurements of:
 - a. Efficiency and rate of formation.
 - b. Vibrational relaxation rate.
 - c. Rate at which it is quenched by I₂ and O₃.
3. Characterize the relevant parameters of the ground state.

B. REVISED OBJECTIVE

Analysis to be performed as in part A of the objectives on the IF(B) state.

III. APPROACHES AND RESULTS

A. INITIAL APPROACH

The research objectives and approach were aligned with the proposal by Major Neumann [1] which outlines in detail the expected reaction mechanisms and experimental set-up needed for analysis of the kinetics of the IO system.

The initial mixture of gases included O_3 from a commercial ozone generator and cooled silica gel trap combination, and I_2 vaporized from crystals, both supplied at varying pressures.

The experimental arrangement (Figure 1) for the study was in place at the beginning of the summer but had not been calibrated or optimized for detection of species present.

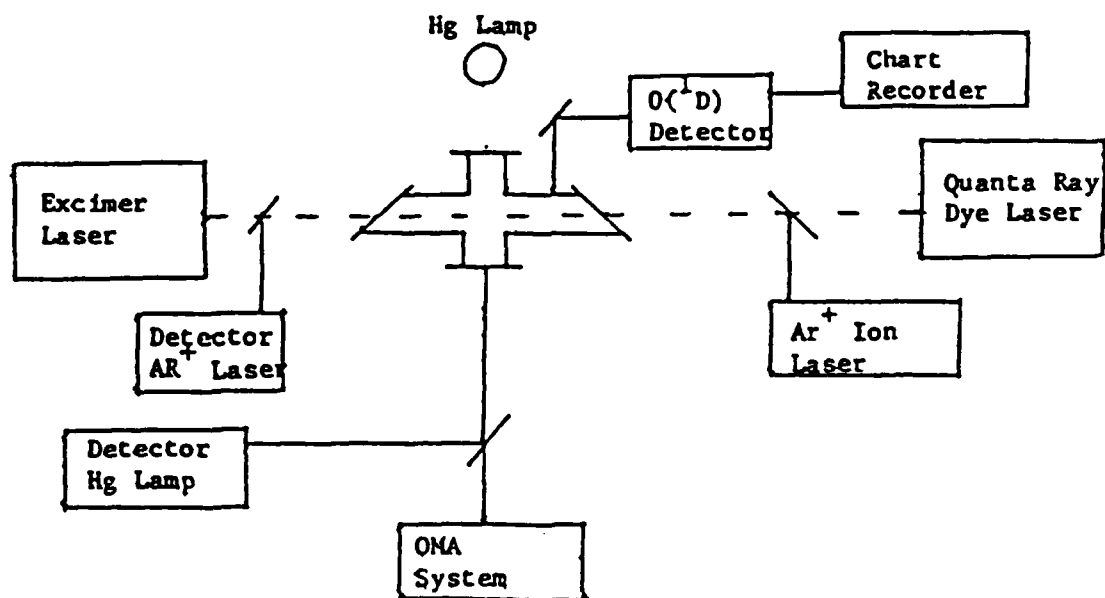


Figure 1. Static Cell Set-up

As anticipated with any new experimental effort, many problems such as vacuum leaks, lens alignment, and diagnostic calibrations consumed much of the early summer period. With the equipment functioning, the illumination with a KrF excimer laser (248nm) on the O_3/I_2 mixture produced negligible spectral results. It was hypothesized that the I_2 concentration was too low from the production technique of flowing helium (He) gas across iodine crystals in a flask. This source of iodine was replaced by a C_3F_7I gas which is readily available.

B. REVISED APPROACH AND RESULTS

Using a mixture of C_3F_7I at 0.8torr and O_3/O_2 at 0.8torr, photolysis was produced using the KrF Lambda Physik excimer laser, and a strong spectra was obtained using an OMA III Detection System. The unexpected result was the positive identification of IF rather than IO.

The spectral results are given in Figures 2 through 9 with the central wavelength located at approximately channel 512 on the horizontal axis and the channel conversion to wavelength being approximately 0.6 angstroms per channel. Mercury lines were to be used for exact calibration. Useable information from the OMA System is contained between approximately channels 180 to 900. The spectral assignments for experimental results and values obtained from the literature are given in Figure 10 which validate an IF(B) emission. The potential energy curves for IF(X), IF(A) and IF(B) are presented in Figure 11.

$$\lambda_c = 4850$$

F449 ,Memory: 1 , Cursor: 100 , & : 5025 , Magnitude: 687

Counts

X10 8

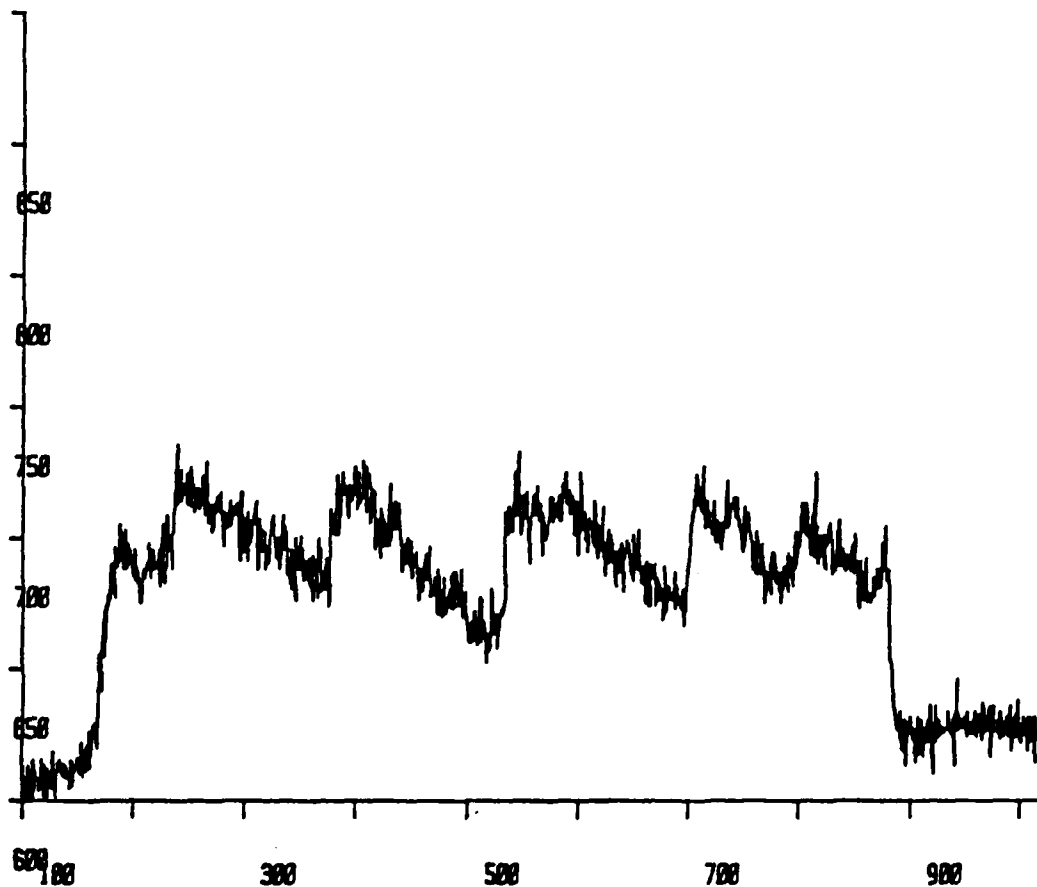


Figure 2. IF(B) Spectrum (center wavelength = 4850 angstroms)

$$\lambda_c = 5050$$

F448 Memory: 1 , Cursor: 519 , λ : 5255.5 , Magnitude: 667

Counts
X10 B

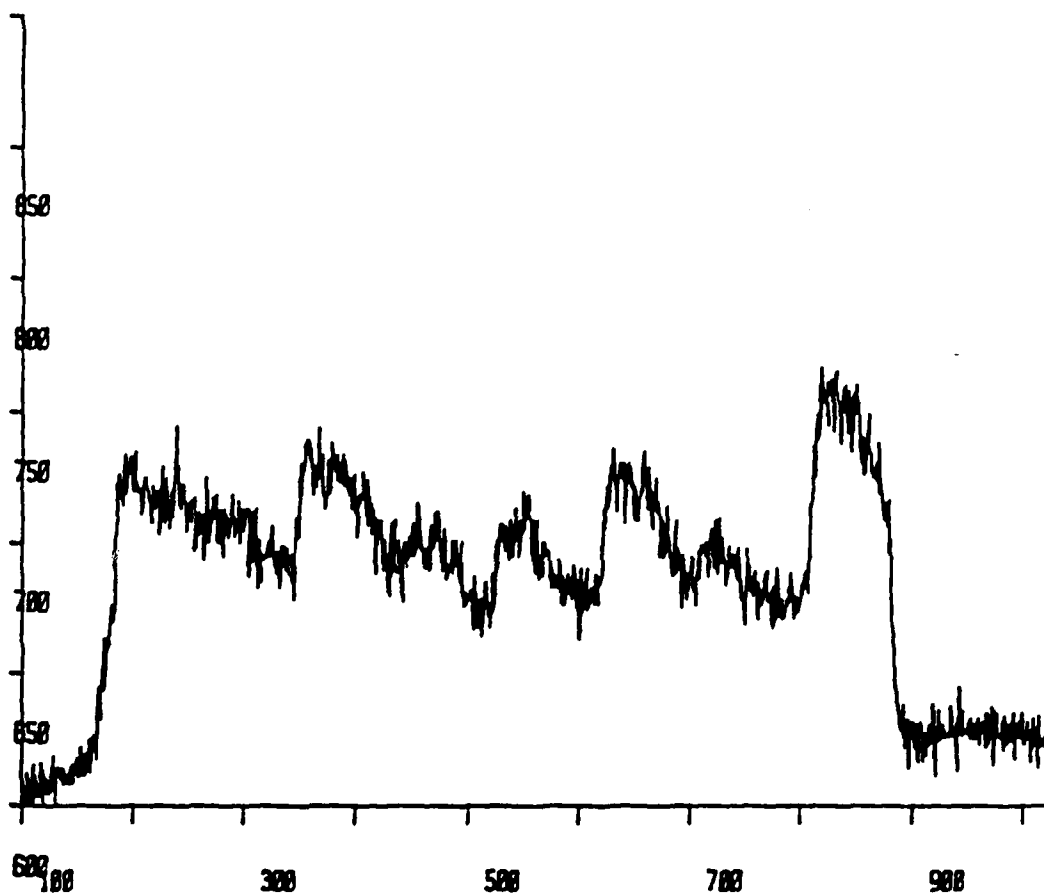


Figure 3. IF(B) Spectrum (center wavelength = 5050 angstroms)

$$\lambda_c = 5250$$

F450 , Memory: 1 , Cursor: 100 , λ : 5025 , Magnitude: 605

Counts
X10⁸

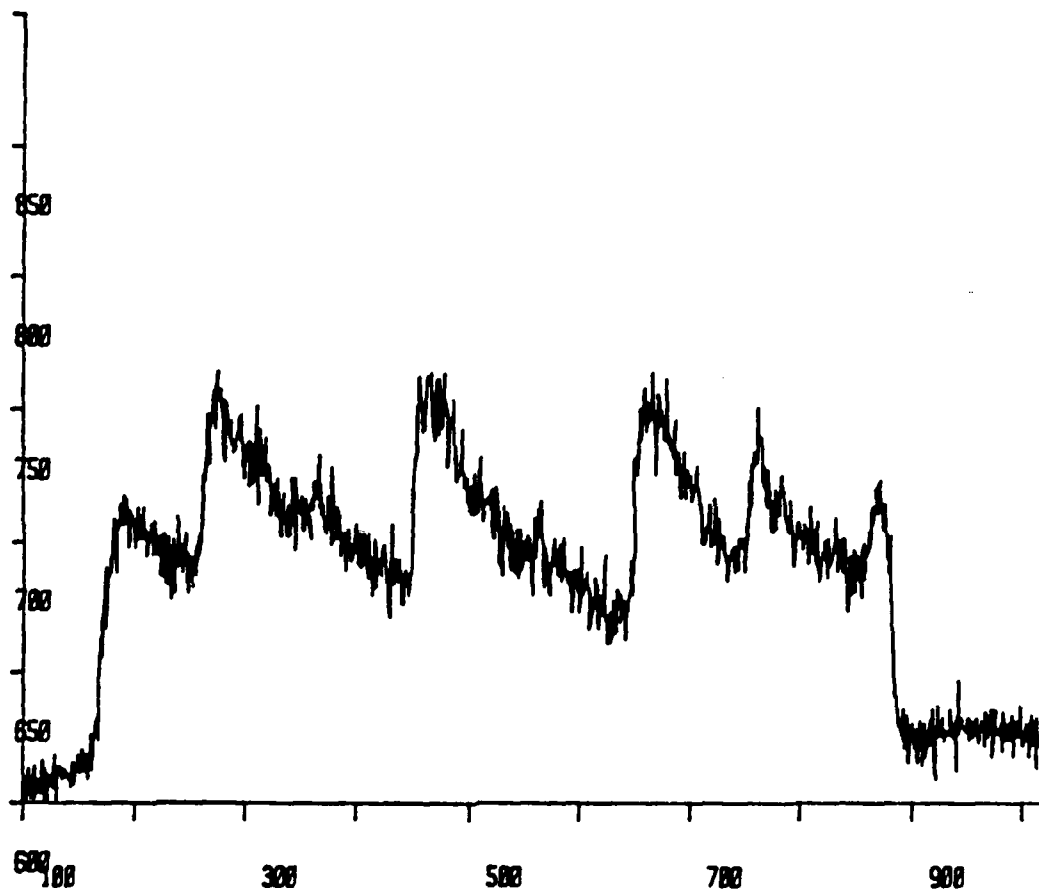


Figure 4. IF(B) Spectrum (center wavelength = 5250 angstroms)

$$\lambda_c = 5450$$

F451 ,Memory: 1 , Cursor: 100 , & : 5825 , Magnitude: 606

Counts

X10 0

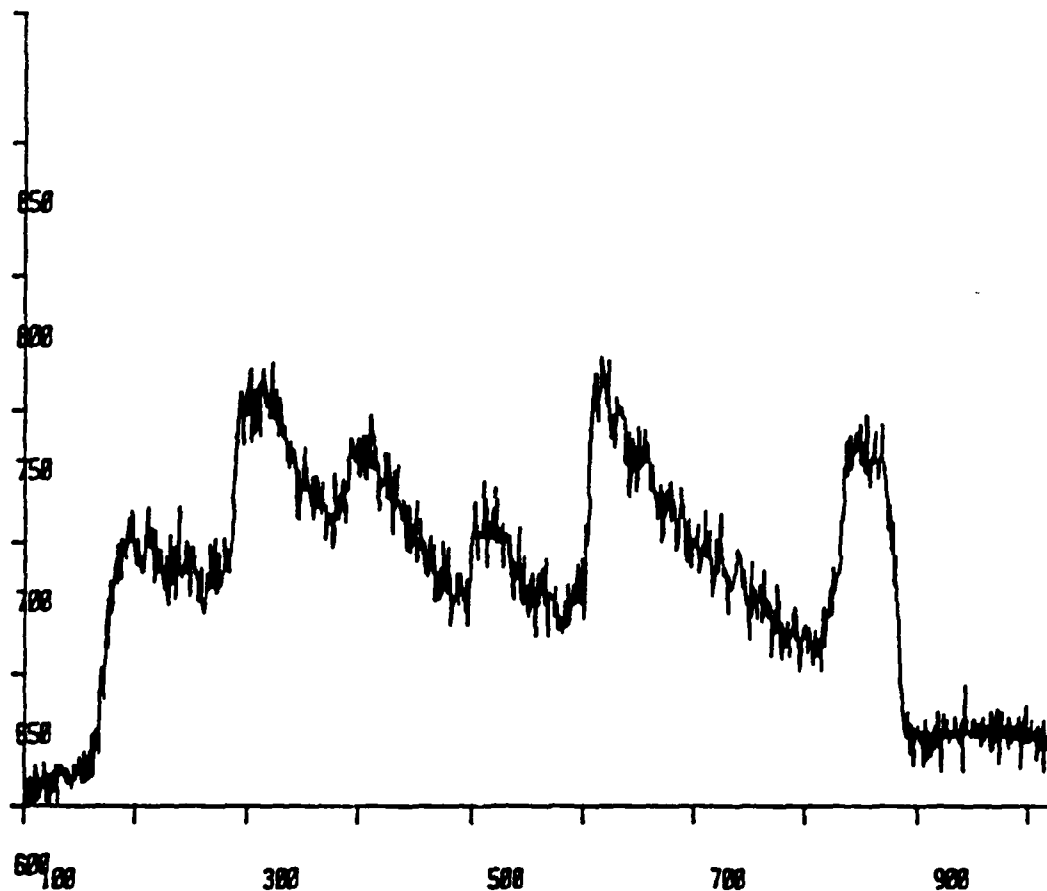


Figure 5. IF(B) Spectrum (center wavelength = 5450 angstroms)

$$\lambda_c = 5650$$

F452 ,Memory: 1 , Cursor: 188 , t : 5025 , Magnitude: 605

Counts
X10 0

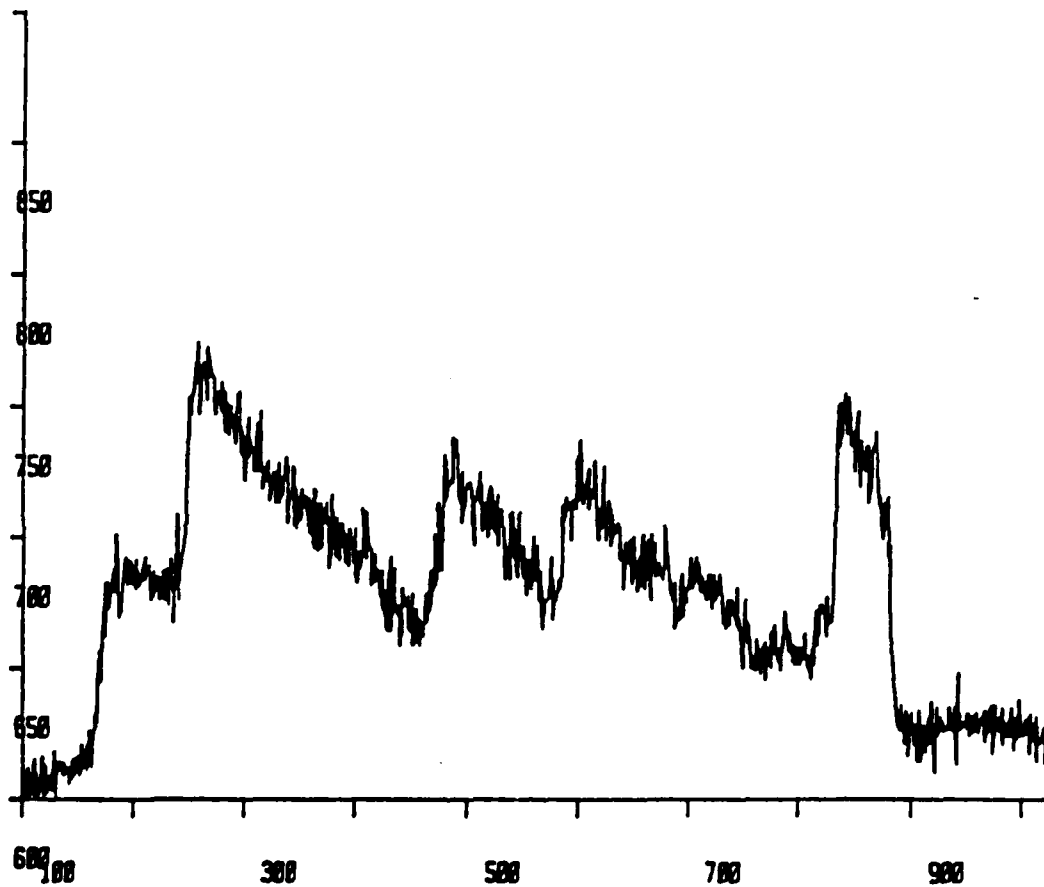


Figure 6. IF(B) Spectrum (center wavelength = 5650 angstroms)

$$\lambda_c = 5850$$

F453 , Memory: 1 , Cursor: 100 , λ : 5825 , Magnitude: 685

Counts

$\times 10^8$

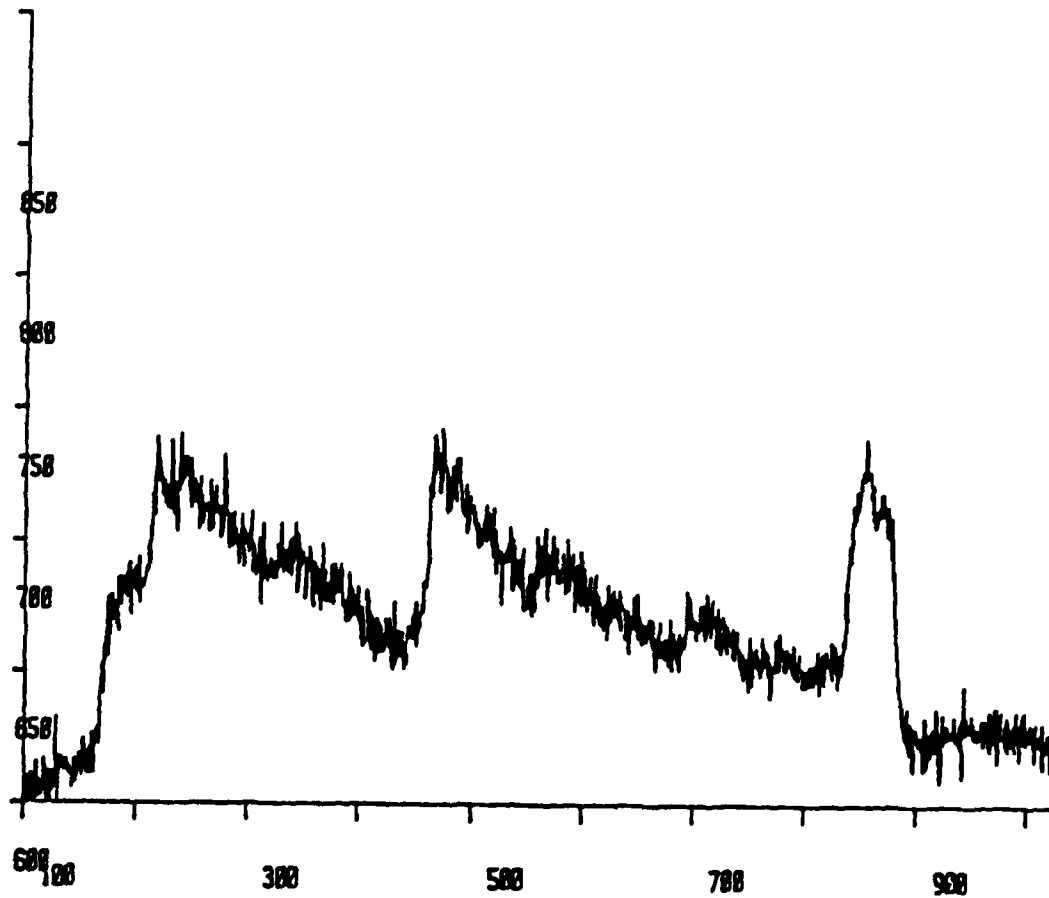


Figure 7. IF(B) Spectrum (center wavelength = 5850 angstroms)

$$\lambda_c = 6050$$

F455 , Memory: 1 , Cursor: 188 , & : 5825 , Magnitude: 684

Counts

X10 0

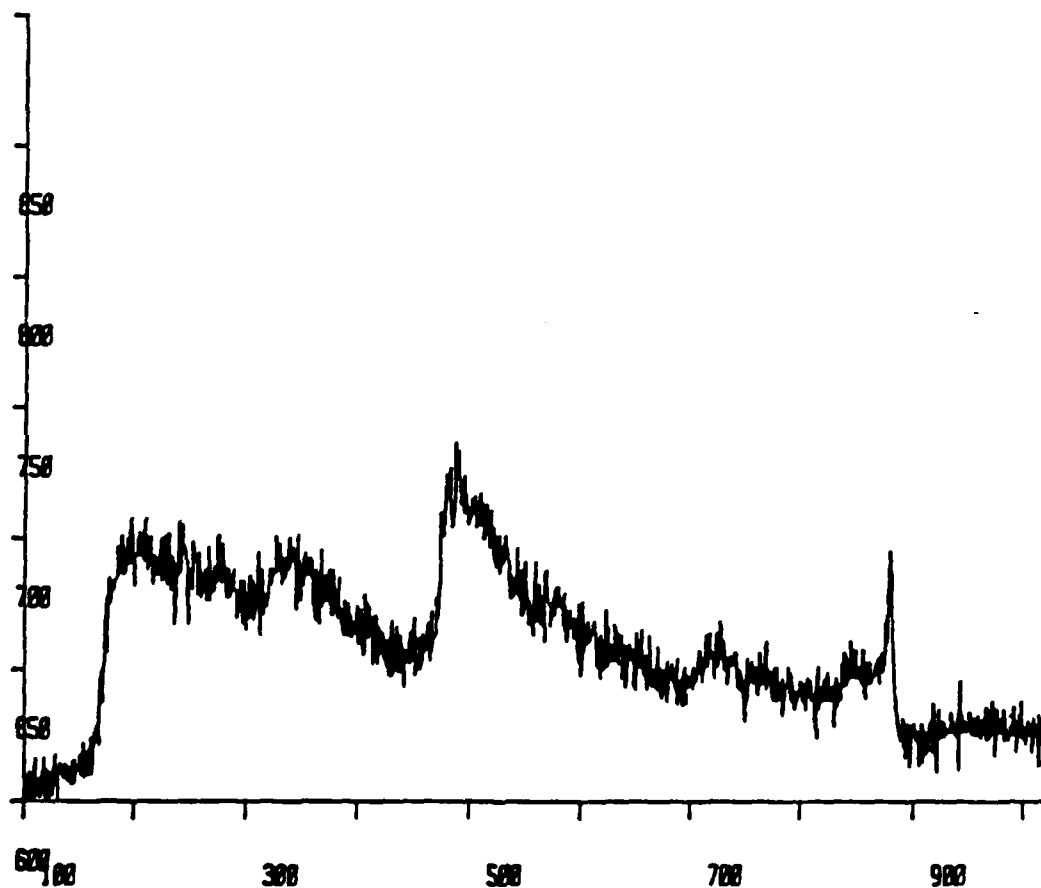


Figure 8. IF(B) Spectrum (center wavelength = 6050 angstroms)

$\lambda_c = 6250$
F456 ,Memory: 1 , Cursor: 100 , b : 5825 , Magnitude: 607
Counts
X10 8

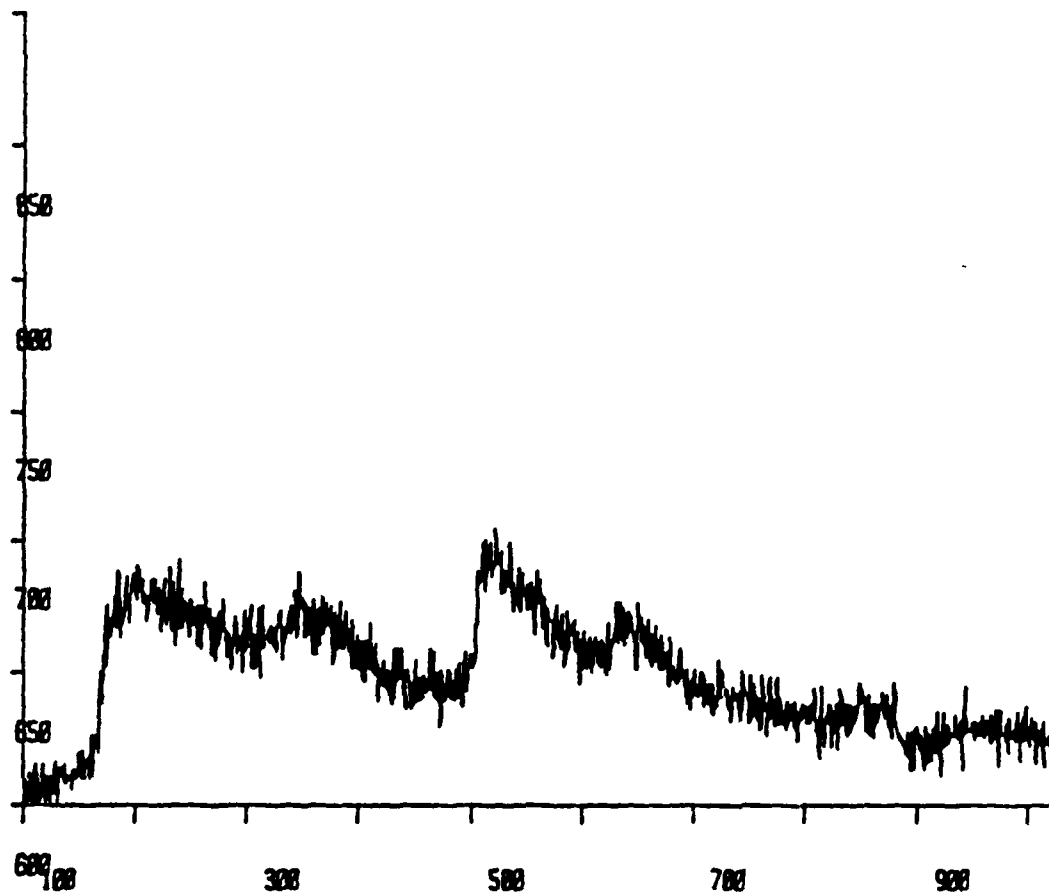


Figure 9. IF(B) Spectrum (center wavelength = 6250 angstroms)

SPECTRAL ASSIGNMENTS

TRANSITION (v', v'')	MEASURED WAVELENGTH 0 (Å)	LITERATURE VALUE 0 (Å)
(6,0)	4699	4699
(5,0)	4777	4782
(4,0)	4864	4870
(3,0)	4955	4963
(4,1)	5014	5017
(2,0)	5058	5061
(3,1)	5111	5116
(1,0)	5161	5165
(2,1)	5214	5221
(1,1); (4,3)	5329	5332, 5335
(2,2)	5386	5389
(3,3); (0,1)	5446	5448, 5449
(4,4); (1,2)	5504	5508, 5508
(3,4); (0,2)	5630	5627, 5633
(4,5); (1,3)	5689	5689, 5693
(0,3)	5824	5828
(4,6)	5876	5881
(3,7); (2,5)	5949	5947, 5952
(0,4)	6032	6033
(2,6)	6162	6162
(0,5)	6251	6252
(1,6)	6314	6318

Figure 10. IF(B) Spectral Assignments

IF POTENTIAL ENERGY CURVES

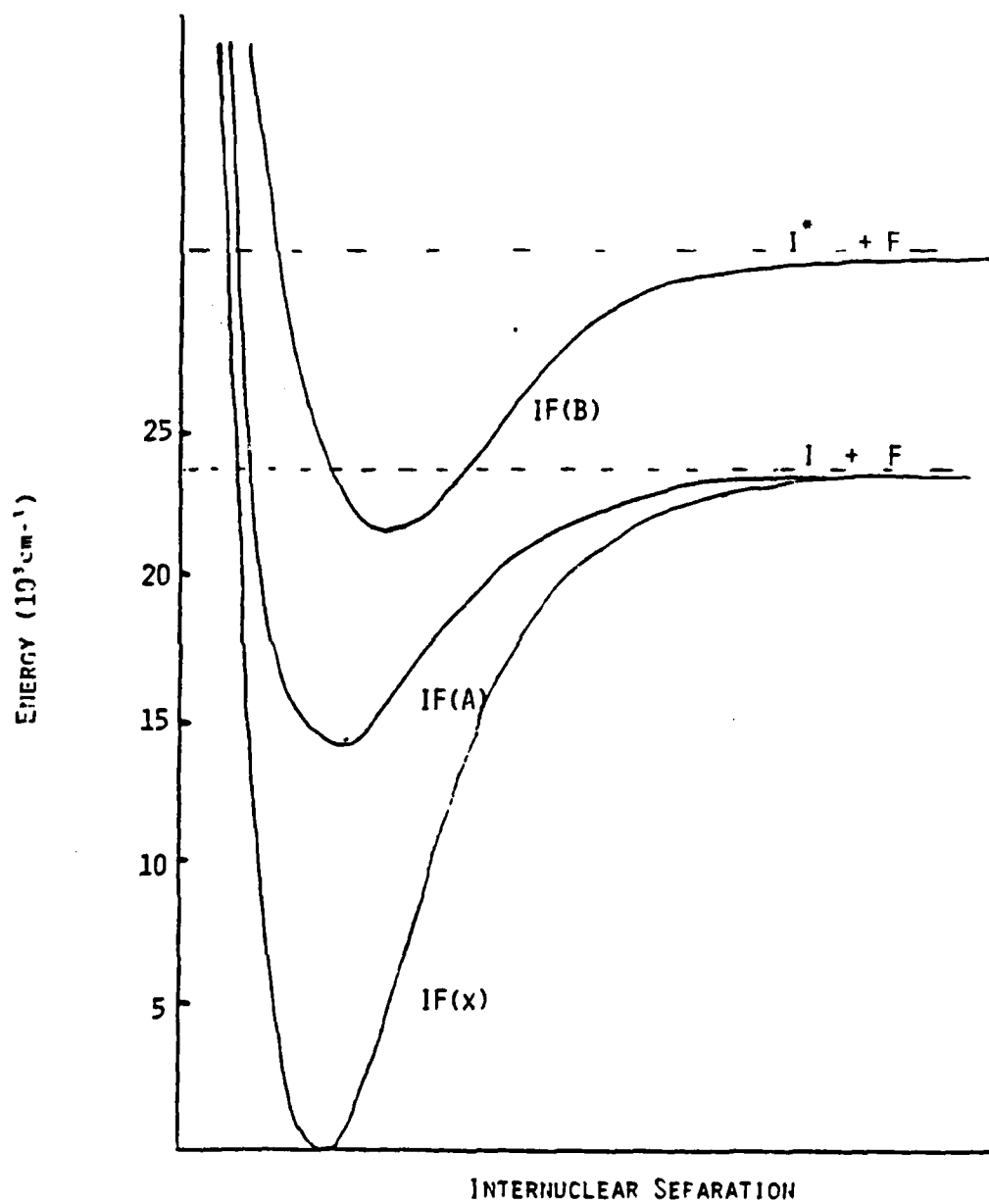


Figure 11. IF Potential Energy Curves

IV. RECOMMENDATIONS

The preliminary results of IF(B) should be thoroughly investigated through a process outlined in the initial objectives. Bonding strength information may also be confirmed from an investigation of CF₃I in addition to C₃F₇I as they react with O₃ in the static cell set-up [4,5]. This follow-on work would involve a kinetics study of the IF molecule, a demonstration of lasing, gain calculations, and an estimation of a potential system efficiency. A caution as to the volatile nature of O₃, if concentrated, must also be considered in any larger scale investigation.

REFERENCES

1. Neumann, D.K., "Proposal for Advanced Chemical Laser Research on the Iodine Oxide (IO) System".
2. Herzberg, G., Spectra of Diatomic Molecules, Van Nostrand, N.Y., 1950.
3. Davis, S., Physical Sciences, Inc., N.H. - private communication.
4. Watson, T.A., M. Addison, and C. Wittig, "Photolytic Production of $O(3p)$ in the Presence of CF_3I ," Chemical Physics, Vol. 78, 1983, pp. 57-63.
5. Trickl, T., Max Planck Institute, W. Germany - private communication during a visit to FJSRL, August 1985.

The IF molecule has been investigated by the Air Force Weapons Lab for the last several years as a possible laser candidate. IF has been lased through optical pumping and would appear to be an excellent molecular laser candidate. However, chemical production mechanisms are still under investigation. Three transitions are particularly attractive due to reasonably high probabilities for occurrence [2]. These are (2,1), (0,3) and (0,4). Possible production mechanisms of the excited B state of IF that have been suggested by Neumann and Davis [3] appear in Figure 12.

POSSIBLE PRODUCTION MECHANISMS

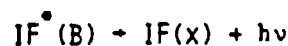
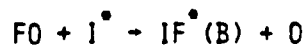
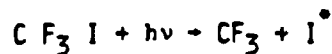
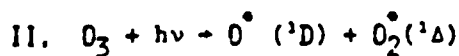
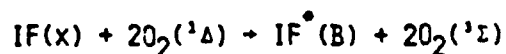
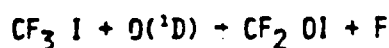
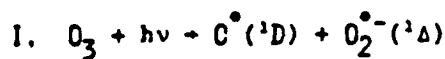


Figure 12. IF(B) Possible Production Mechanisms.

1985 USAF-UES SUMMER FACULTY RESEARCH PROGRAM/

GRADUATE STUDENT SUMMER SUPPORT PROGRAM

Sponsored by the

AIR FORCE OFFICE OF SCIENTIFIC RESEARCH

Conducted by the

UNIVERSAL ENERGY SYSTEMS, INC.

FINAL REPORT

MODELING THE TISSUE SOLUBILITIES OF HALOGENATED

METHANES, ETHANES, AND ETHYLENES

Prepared by:	Paul G. Seybold and Michael A. May
Academic Rank:	Professor of Chemistry and Chemistry Graduate Student, respectively
Department and University:	Departments of Chemistry and Biological Chemistry Wright State University, Dayton, Ohio
Research Location:	Biochemical Toxicology Branch Aerospace Medical Research Laboratory Wright-Patterson AFB, Dayton, Ohio
USAF:	Melvin E. Andersen, Ph.D.
Date:	September 11, 1985
Contract No:	F49620-85-C-0013

MODELING THE TISSUE SOLUBILITIES OF HALOGENATED
METHANES, ETHANES AND ETHYLENES

by

Paul G. Seybold, Ph.D.

and

Michael A. May

ABSTRACT

Experimental solvent:air and tissue:air partition coefficients for 25 halogenated methanes, ethanes, and ethylenes in saline solution, olive oil, and rat blood, muscle, liver, and fat tissues have been examined using theoretical molecular modeling techniques. Two graph theoretical approaches (the distance method of Wiener and the connectivity index method of Randić, Kier, and Hall) and an approach utilizing ad hoc molecular descriptors were employed. Satisfactory regression models were obtained with both the Randić-Kier-Hall approach and the ad hoc descriptors approach. The latter method revealed that fluorine substituents decrease tissue solubilities, whereas both chlorine and bromine substituents increase tissue solubilities, with the relative influence being $Cl < Br$. Tissue solubilities could also be conveniently represented in terms of contributions from oil and saline solubilities.

ACKNOWLEDGEMENTS

We wish to express our special thanks to Dr. Melvin E. Andersen and Mr. Michael L. Gargas of AFAMRL/THB for their hospitality, encouragement, and very pleasant collaboration in this work. We also gratefully acknowledge the sponsorship of the Air Force Systems Command, Air Force Office of Scientific Research, and the Biochemical Toxicology Branch, Aerospace Medical Research Laboratories.

I. INTRODUCTION

Lower molecular weight halogenated hydrocarbons are employed commercially as solvents, chemical intermediates, refrigerants, and fire retardants. However, many if not most exhibit toxic effects, and some are suspected carcinogens. The halogenated methanes, ethanes, and ethylenes - the compounds of interest in this study - are widespread in the environment, a matter of some concern because of their potential toxicities. A recent study by the Environmental Protection Agency (1) revealed that the environmental problem posed by these compounds can be especially severe in indoor settings, both because many people spend a considerable portion of their time indoors and because chemicals "offgassed" from construction and other materials cannot readily escape.

The halogenated hydrocarbons are metabolized in the body to potentially harmful intermediates and end products, and an understanding of their toxicological effects requires that their tissue distributions, metabolic pathways, and rates of metabolism be known. Over the past several years Andersen and co-workers at AFAMRL/THB have developed a physiological model for the distribution and metabolism of inhaled gases and vapors (2-5). Based on measured rates of gas uptake and tissue:air partition coefficients ("solubilities") this model can be used to assess the time-dependent distributions and Michaelis-Menten kinetic rate constants for metabolism of a variety of chemicals. An important advantage of the model is that information obtained for a chemical in one species, e.g. rats, can be extrapolated to other species, e.g. humans.

In its present form the model relies on measured values of the tissue:air partition coefficients and less-directly estimated kinetic constants. Such measurements represent a formidable effort. It was therefore of considerable interest to see if the partition coefficients and kinetic constants could be estimated in some way for halogenated hydrocarbons with reasonable reliability. If this should prove possible the model could then be used to estimate or predict the behaviors of here-to-fore untested compounds. This report describes starting attempts to estimate tissue:air partition coefficients using quantitative structure-property relations (QSPR) based on molecular structure.

II. OBJECTIVES OF THE RESEARCH EFFORT

Our objectives at the beginning of this project were three-fold: (1) to familiarize ourselves with the major features of the pharmacokinetic model developed by Andersen et al. at AFAMRL/THB and the available scientific literature related to this topic; (2) to develop and bring "on line" suitable computer programs that might be useful in carrying out QSPR studies on the halogenated hydrocarbons and (3) to develop structure-property relations for the tissue:air partition coefficients and metabolic kinetic constants.

The methods used to accomplish goal (3) above will be described in the following section. It was deemed useful first to attempt to model certain physical properties of the halogenated hydrocarbons that might be related to their tissue solubilities. Also, as the project developed it was decided to confine attention to modeling of the tissue partition coefficients, and to put off modeling of the metabolic

kinetic constants - which is expected to represent a much more complex task - for later development.

III. METHODS

Three general modeling schemes were utilized in our examination of the physical properties and tissue partition coefficients. The first two schemes, based on the approaches of Wiener (6-9) and of Randić, Kier, and Hall (10-12), are developments from chemical graph theory. The third scheme employs a collection of molecular descriptors chosen on an ad hoc basis. Due to the limited space available in this report only brief outlines of these techniques will be given, and readers are referred to more complete descriptions in the literature.

Wiener (6,7) estimated a number of physical and chemical properties of alkanes using parameters based on the distances (in terms of bonds) between atoms in molecules. Ignoring hydrogens, the Wiener index w is the sum of all unique shortest atom-atom distances in a molecule; the index p is the sum of all paths of length 3. Platt's f index (8) and the Balaban-Seybold atomic site index s (9) were also utilized within the framework of the Wiener scheme.

In the Randić scheme (10) each carbon atom in the hydrogen-suppressed graph of a molecule is assigned a "valence" δ , equal to the number of bonds to it. The "connectivity index" χ is then defined as the sum over all bonds $i-j$, as

$$\chi = \sum 1/(\delta_i \delta_j)^{1/2}. \quad (1)$$

Kier and Hall extended this concept to include higher and lower connectivity indices ${}^m\chi$, as analogous sums over atoms, bonds, and

larger structural subunits (11). Heteroatoms were included by assigning valences to these atoms in a standard way (12). This scheme has been widely used in QSPR studies (11).

Many QSPR studies rely on molecular descriptors chosen on an ad hoc basis. Such descriptors may refer to global molecular features such as molecular weights, or to more specific features such as the presence of certain atoms, functional groups or other entities. The use of such descriptors was also examined.

Rat tissue:air partition coefficients for blood, liver, muscle, and fat, as well as saline:air and olive oil:air values, were available from previous studies by Andersen and Gargas for 25 halogenated methanes, ethanes, and ethylenes. These compounds are listed in Table 1. Molecular descriptors appropriate to the above schemes were calculated for these 25 compounds. Regression analyses were carried out using the Statistical Analysis System (SAS) package (13) on the Wright State University IBM computer. A criterion of at least 5 observations per modeling parameter was imposed in most cases to assure statistical significance.

IV. RESULTS AND DISCUSSION

A. Physical Properties

Since our main interest was in the tissue solubilities, only an overview of results for the physical properties will be given. A subset of 21 halogenated hydrocarbons was examined. A major finding was that four of the physical properties - boiling points, surface tensions, heats of vaporization, and critical temperatures - were strongly inter-correlated ($r > 0.93$). These properties can be

collectively considered to be "constitutive" in nature, i.e., to depend on molecular shape, and to arise from intermolecular forces. A second finding was that the connectivity indices provided the best set of indices for modeling most of the properties examined (the four above plus molar volume). The molecular features approach was superior for modeling dielectric constants, melting points, molar refractions and water solubilities.

B. Tissue Solubilities

Following the usual custom tissue:air partition coefficients were modeled as their base-10 logarithms. Thus, SALINE, OIL, BLOOD, LIVER, MUSCLE and FAT refer to log P values for these liquids and tissues with respect to air. Because the Wiener parameters performed poorly, only the results for the connectivity and molecular features parameters will be discussed.

1. Connectivity Analysis

"Best fit" regression equations obtained for the solubilities using connectivity indices are summarized below. In these, X1V refers to the first-order valence connectivity index ${}^1\chi^v$, INVXSV to the inverse of the valence structure index χ_s^v , etc. (see Table 2). Note that r^2 , the square of the correlation coefficient, represents the fraction of the variation in the data that can be accounted for by the model. N is the number of observations and s is the root-mean-square error of the fit. Plots of calculated vs. observed values are shown in Fig. 1.

$$\text{BLOOD} = 0.828 \text{ X1V} - 0.0240 \text{ INVXSV} - 0.261 \text{ X3VC} - 0.302$$

$$N = 25$$

$$r^2 = 0.862$$

$$s = 0.225$$

$$\text{FAT} = 0.624 \text{ X1V} - 0.0282 \text{ INVXSV} - 1.28 \text{ INVCH1} - 0.814 \text{ INVX1V} \\ - 0.0862 \text{ X3VC} + 0.124 \text{ X4VPC} + 2.37$$

$$N = 25 \quad r^2 = 0.976 \quad s = 0.144$$

$$\text{LIVER} = 1.06 \text{ X1V} - 0.0207 \text{ INVXSV} - 0.471 \text{ X4VC} + 0.564 \text{ INVX1V} - 1.14$$

$$N = 25 \quad r^2 = 0.886 \quad s = 0.215$$

$$\text{MUSCLE} = 0.990 \text{ X1V} - 0.0181 \text{ INVXSV} - 0.636 \text{ X4VC} + 0.535 \text{ INVX1V} - 1.28$$

$$N = 25 \quad r^2 = 0.877 \quad s = 0.206$$

$$\text{OIL} = 0.451 \text{ X1V} - 0.0315 \text{ INVXSV} - 1.91 \text{ INVCH1} - 0.647 \text{ X4VC} \\ + 0.164 \text{ PATH} - 0.474 \text{ INVX1V}$$

$$N = 25 \quad r^2 = 0.966 \quad s = 0.169$$

$$\text{SALINE} = 2.58 \text{ X1V} - 1.70 \text{ XOV} - 0.0295 \text{ INVXSV} - 2.49 \text{ INVCH1} \\ + 0.188 \text{ PATH} + 0.246 \text{ X4VPC} + 3.13$$

$$N = 25 \quad r^2 = 0.868 \quad s = 0.242$$

Several conclusions can be drawn from these equations. First, the modeling of the partition coefficients by the connectivity indices is good, but not outstanding. The first-order valence connectivity term $^1\chi^v$ is especially important. Second, the best fits are obtained for the more lipid-rich tissues and oil, and the poorest fits for blood and saline. This most probably results because the largely isotropic van der Waals forces responsible for intermolecular forces in the lipid phases are better modeled than are the more directional polar and hydrogen-bonding forces predominant in the aqueous phases.

2. Molecular Features Analysis

Our original analysis using a large number of molecular descriptors yielded only modest fits, ranging from $r^2 = 0.677$ for BLOOD to $r^2 = 0.937$ for FAT, for the tissue solubilities. In most cases molecular weight was the best descriptor. A "second generation"

of molecular descriptors was then tested, with better results. An important addition was the "polar hydrogen" parameter Q_H , originally introduced by DiPaolo et al. in studies of anesthetics (14,15). This parameter represents the polarity of the C-H bonds as induced by halogen substituents on the same and adjacent carbon atoms (15). Also included in the second set of descriptors were representatives for the numbers of carbon (NC), fluorine (NF), chlorine (NCL), and bromine (NBR) atoms, and the numbers of trigonal (NC3) and tetrahedral carbons (NC4).

Some representative regression results are given below:

$$\text{SALINE} = 0.614Q_H - 0.372NF - 0.089 \text{ NC3} - 0.154$$

$$N = 25 \quad r^2 = 0.934 \quad s = 0.158$$

$$\text{OIL} = 0.383NC - 0.165NF + 0.570NCL + 0.946NBR + 0.310Q_H + 0.066$$

$$N = 25 \quad r^2 = 0.982 \quad s = 0.120$$

$$\text{FAT} = 0.466NC - 0.205NF + 0.561NCL + 1.021NBR + 0.272Q_H - 0.090$$

$$N = 25 \quad r^2 = 0.979 \quad s = 0.133$$

$$\text{BLOOD} = 0.152NC - 0.312NF + 0.222NCL + 0.498NBR + 0.447Q_H - 0.093$$

$$N = 25 \quad r^2 = 0.944 \quad s = 0.151$$

$$\text{LIVER} = -0.186NF + 0.363NCL + 0.579NBR + 0.348Q_H - 0.002$$

$$N = 25 \quad r^2 = 0.923 \quad s = 0.177$$

$$\text{MUSCLE} = 0.167NC - 0.198NF + 0.275NCL + 0.526NBR + 0.382Q_H - 0.430$$

$$N = 25 \quad r^2 = 0.908 \quad s = 0.183$$

It is apparent that all the partition coefficients, including SALINE and BLOOD, are reasonably well represented by the molecular descriptors.

The halogens exert a consistent influence on the solubilities: fluorine

decreases the solubility in all tissues, whereas both chlorine and bromine increase solubility, Br more than Cl. This effect is in the order of atomic polarizabilities, probably indicating increased stabilization of the halocarbon in the order $F < Cl < Br$ due to increased dispersion interactions with the tissue phase. (The effect is especially strong in oil and fat.) The polar hydrogen factor Q_H was found to consistently increase solubility, the effect being more prominent in the more aqueous tissues, saline and blood, as might be expected. Separate models obtained using composite halogen parameters for polarity (based on electronegativities) and polarizability were only slightly less successful.

3. Empirical Tissue Analysis

Sato and Nakajima (16) have demonstrated an empirical relationship between the logarithms of the blood:air, oil:air, and water:air partition coefficients:

$$\log(\text{blood/air}) = a \log(\text{oil/air}) + b \log(\text{water/air}) + c \quad (2)$$

$$N = 20 \quad r^2 = 0.935 \quad s = 0.675$$

where a, b and c are constants. (In fact, they imply that $a = b$.

(16)) It was therefore of interest to see if the blood and other partition coefficients could be equally well represented in terms of combinations of the oil:air and saline:air partition coefficients.

The results are as follows:

$$\text{BLOOD} = 0.426 \text{ OIL} + 0.515 \text{ SALINE} - 0.0703$$

$$N = 25 \quad r^2 = 0.954 \quad s = 0.128$$

$$\text{FAT} = 1.01 \text{ OIL} - 0.0916$$

$$N = 25 \quad r^2 = 0.969 \quad s = 0.144$$

$$\text{LIVER} = 0.574 \text{ OIL} + 0.302 \text{ SALINE} - 0.278$$

$$N = 25 \quad r^2 = 0.945 \quad s = 0.142$$

$$\text{MUSCLE} = 0.477 \text{ OIL} + 0.365 \text{ SALINE} - 0.374$$

$$N = 25 \quad r^2 = 0.938 \quad s = 0.139$$

The relationship is seen to hold well for all tissues. The coefficients of OIL and SALINE can be loosely considered to represent the relative lipophilic and hydrophilic characters of the various tissues.

A comparison was also made of the human blood:air partition coefficients of Sato and Nakajima (16) and the present rat blood:air values of Andersen and Gargas. For the 13 compounds common to both studies the rat values tended to be consistently about twice the human values ($r = 0.994$). Regression models for both sets of data using the connectivity indices are given below. Shown also are equations for the two measured sets of olive oil:air partition coefficients ($r = 0.981$).

Sato-Nakajima Data, 1979

$$\text{Human Blood} = -0.147 \text{ X4VPC} - 0.388 \text{ X3VC} + 1.26 \text{ X1V} - 1.26$$

$$N = 13 \quad r^2 = 0.872 \quad s = 0.191$$

$$\text{Olive Oil} = 2.36 \text{ X1V} - 0.155 \text{ X3VC} + 4.43 \text{ INVX1V} - 4.28$$

$$N = 13 \quad r^2 = 0.973 \quad s = 0.113$$

Andersen-Gargas Data, 1985

$$\text{Rat Blood} = -0.62 \text{ X4VC} + 1.53 \text{ X1V} - 0.460 \text{ XOV} + 0.121$$

$$N = 13 \quad r^2 = 0.886 \quad s = 0.157$$

$$\text{Olive Oil} = 0.832 \text{ X1V} - 0.220 \text{ X3VC} + 0.256 \text{ XOV} + 0.0168$$

$$N = 13 \quad r^2 = 0.968 \quad s = 0.109$$

V. RECOMMENDATIONS

The results presented above demonstrate the feasibility of modeling the tissue solubilities of halogenated C_1 and C_2 hydrocarbons. Both the connectivity indices and the molecular descriptors yielded adequate representations of the tissue solubilities. The representation of tissue solubilities in terms of oil:air and saline:air solubilities also has an appealing, heuristic simplicity.

It would seem desirable to continue and extend this work in several ways. The most obvious would be to search for improved molecular descriptors. Improvement of the combined halogen parameters representing polarity or polarizability effects would represent one direction worth pursuing. Another approach, not utilized above, would be to model the tissue solubilities in terms of appropriate solute molecular volumes and surface areas. Both volume and surface area have been employed with some success in other pharmacological applications. It would also be desirable to explore more elaborate molecular descriptors derived from molecular mechanics or molecular orbital calculations.

There remains, of course, the very important and possibly difficult task of modeling the Michaelis-Menten kinetic constants. It would seem reasonable now to begin that task using the successful methods illustrated above, viz. the connectivity indices and the molecular features descriptors.

REFERENCES

1. Ember, L., "Toxic chemical levels higher indoors than out," Chem. & Engr. News, June 24, 1985, pp. 21-22.
2. Andersen, M.E., "Pharmacokinetics of Inhaled Gases and Vapors," Neurobehav. Toxicol. Teratol. 3, 383-389 (1981).
3. Andersen, M.E., "A Physiologically Based Toxicokinetic Description of the Metabolism of Inhaled Gases and Vapors: Analysis at Steady State,," Toxicol. Appl. Pharmacol. 60, 509-526, (1981).
4. Ramsey, J.C. and M.E. Andersen, "A Physiologically Based Description of the Inhalation Pharmacokinetics of Styrene in Rats and Humans," Toxicol. Appl. Pharmacol. 73, 159-175 (1984).
5. Andersen, M.E., M.L. Gangas, and J.C. Ramsey, "Inhalation Pharmacokinetics: Evaluating Systemic Extraction, Total in vivo Metabolism, and the Time Course of Enzyme Induction for Inhaled Styrene in Rats Based on Arterial Blood:Inhaled Air Concentration Ratios," Toxicol. Appl. Pharmacol. 73, 176-187 (1984).
6. Wiener, H., "Structural Determination of Paraffin Boiling Points," J. Amer. Chem. Soc. 69, 17-20 (1947).
7. Wiener, H., "Relation of the Physical Properties of the Isomeric Alkanes to Molecular Structure," J. Phys. Chem. 52, 1082-1089 (1948).
8. Platt, J.R., "Prediction of Isomeric Differences in Paraffin Properties," J. Phys. Chem. 56, 328-336 (1952).
9. Seybold, P., "Topological Influences on the Carcinogenicity of Aromatic Hydrocarbons," Int. J. Quantum Chemistry, Quantum Biol. Symp. 10, 95-108 (1983).

AD-A166 178

UNITED STATES AIR FORCE SUMMER FACULTY RESEARCH PROGRAM

5/11

1985 TECHNICAL RE. (U) UNIVERSAL ENERGY SYSTEMS INC

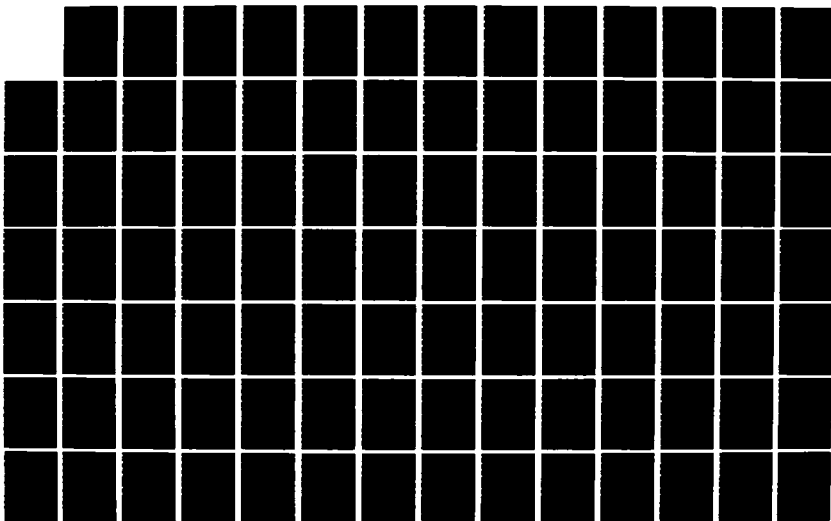
DAYTON OH R C DARRAH ET AL. DEC 85 AFOSR-TR-86-0141

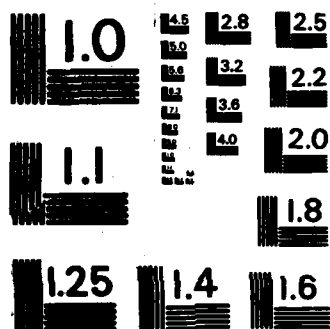
UNCLASSIFIED

F49620-85-C-0013

F/G 5/9

NL





MICROCOPY RESOLUTION TEST CHART
NATIONAL BUREAU OF STANDARDS-1963-A

10. Randic, M., "On Characterization of Molecular Branching," J. Amer. Chem. Soc. 97, 6609-6615 (1975).
11. Kier, L.B., and L.H. Hall, Molecular Connectivity in Chemistry and Drug Research, Academic Press, New York, 1976.
12. Kier, L.B. and L.H. Hall, "General Definition of Valence Delta-Values for Molecular Connectivity," J. Pharm. Sci. 72, 1170-1173 (1983).
13. SAS Institute, Inc., Box 8000, Cary, NC 27511.
14. DiPaolo, T., L.B. Kier, and L.H. Hall, "Molecular Connectivity and Structure-Activity Relationship of General Anesthetics," Molec. Pharmacol. 13, 31-37 (1977).
15. DiPaolo, T., L.B. Kier, and L.H. Hall, "Molecular Connectivity Study of Halocarbon Anesthetics" J. Pharm. Sci. 68, 39-42 (1979).
16. Sato, A., and T. Nakajima, "A Structure-Activity Relationship of Some Chlorinated Hydrocarbons," Arch. Environ. Health, March/April 1979, p. 69-75.

Table 1. Compounds and Parameter Values.

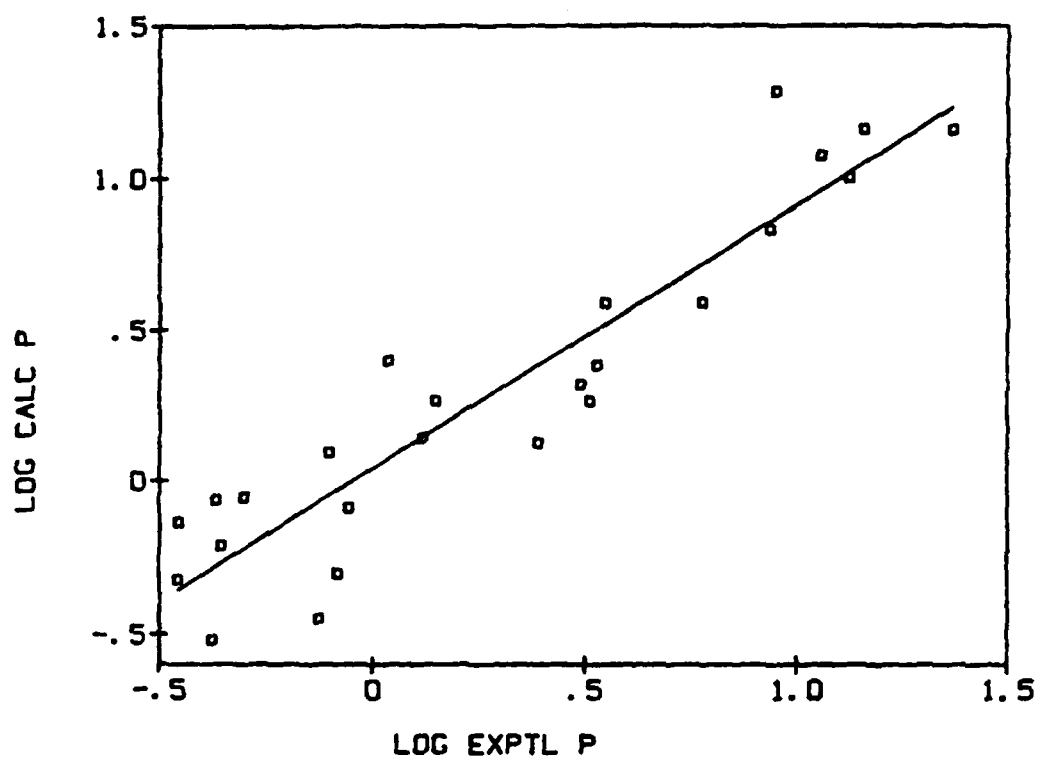
	CHI	XOV	XIV	X2V	X3VC	X4VC	X4VPC	ISV
1	CHLOROETHANE	2.13389	1.13389		0.00000	0.00000	0.00000	1.13389
2	METHYLENE CHLORIDE	2.97489	1.60357	0.90914	0.00000	0.00000	0.00000	0.90914
3	CHLOROPORN	3.97903	1.96396	2.22692	0.84170	0.00000	0.00000	0.84170
4	CARBON TETRACHLORIDE	5.03557	2.26779	3.85714	2.91572	0.00000	0.00000	0.82653
5	VINYL CHLORIDE	2.41835	1.06290	0.46291	0.00000	0.00000	0.00000	0.46291
6	1,1-DICHLOROETHENE	3.47489	1.48745	1.44464	0.45457	0.00000	0.00000	0.45457
7	CIS-1,2-DICHLOROETHENE	3.42252	1.64264	1.13389	0.00000	0.00000	0.00000	0.42857
8	TRANS-1,2-DICHLOROETHENE	3.42252	1.64264	1.13389	0.00000	0.00000	0.00000	0.42857
9	TRICHLOROETHENE	4.7903	2.07722	1.62484	0.37115	0.00000	0.42085	0.42085
10	TETRACHLOROETHENE	5.53557	2.51779	1.77675	0.64286	0.00000	1.65306	0.41327
11	CHLOROETHANE	2.84100	1.50889	0.80178	0.00000	0.00000	0.00000	0.80178
12	1,1-DICHLOROETHANE	3.84514	1.88666	1.30931	0.74231	0.00000	0.00000	0.74231
13	1,2-DICHLOROETHANE	3.68200	2.10357	1.13389	0.00000	0.00000	0.00000	0.64286
14	1,1,2-TRICHLOROETHANE	4.68614	2.51934	2.13104	0.52489	0.00000	0.59517	0.59517
15	1,1,1-TRICHLOROETHANE	4.90168	2.20084	3.62941	2.65750	0.72893	0.00000	0.72893
16	1,1,2,2-TETRACHLOROETHANE	5.69027	2.95195	2.99647	0.85714	0.00000	1.94382	0.55102
17	1,1,1,2-TETRACHLOROETHANE	5.74268	2.85618	2.88928	2.09264	0.51543	1.03086	0.58445
18	DIFLUOROETHANE	1.46304	0.53452	0.10102	0.00000	0.00000	0.00000	0.10102
19	CHLOROFLUOROETHANE	2.21896	1.06904	0.30305	0.00000	0.00000	0.00000	0.30305
20	BROMOCHLOROETHANE	3.80496	2.19051	1.57467	0.00000	0.00000	0.00000	1.57467
21	DIBROMOETHANE	4.63503	2.77746	2.72741	0.00000	0.00000	0.00000	2.72741
22	HALOTHANE	5.30910	2.64420	2.43200	0.79360	0.01560	0.98440	0.03470
23	VINYL BROMIDE	3.24840	1.54210	0.80180	0.00000	0.00000	0.00000	0.80180
24	1-BROMO-2-CHLOROETHANE	4.51210	2.69050	1.54890	0.00000	0.00000	0.00000	1.11350
25	1,1,1-TRIFLUORO-2-CHLOROETHANE	3.47490	1.72230	0.88240	0.15500	0.01910	0.11450	0.02160

TABLE 2. Identification of the Parameters used in the Models.

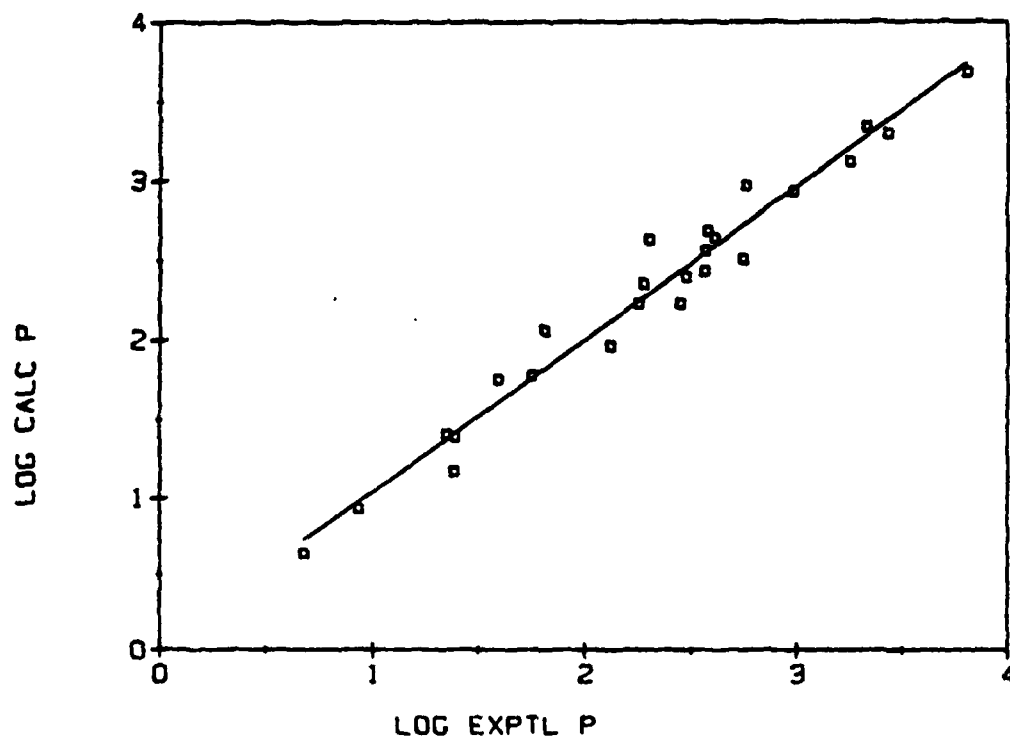
Abbreviation	Parameter
<u>Connectivity Parameters</u> (see Refs. 11, 12)	
CHI	First-order connectivity index
INVCHI	Inverse of CHI
XOV	Zeroth-order valence index
X1V	First-order valence index
INVX1V	Inverse of X1V
X3VC	Third-order valence cluster index
X4VC	Fourth-order valence cluster index
X4VPC	Fourth-order valence path-cluster index
XSV	Valence structure index
INVXSV	Inverse of XSV
PATH	Valence connectivity index for all independent halogen-halogen paths.
<u>Molecular Features Parameters</u>	
NC	Number of carbon atoms
NC3	Number of trigonal carbons
NC4	Number of tetrahedral carbons
NF	Number of fluorine atoms
NC1	Number of chlorine atoms
NBr	Number of bromine atoms
Q_H	Polar hydrogen factor (see Refs. 14, 15).

Figure 1. Plots of Calculated (Connectivity Indices) vs. Experimental Partition Coefficients.

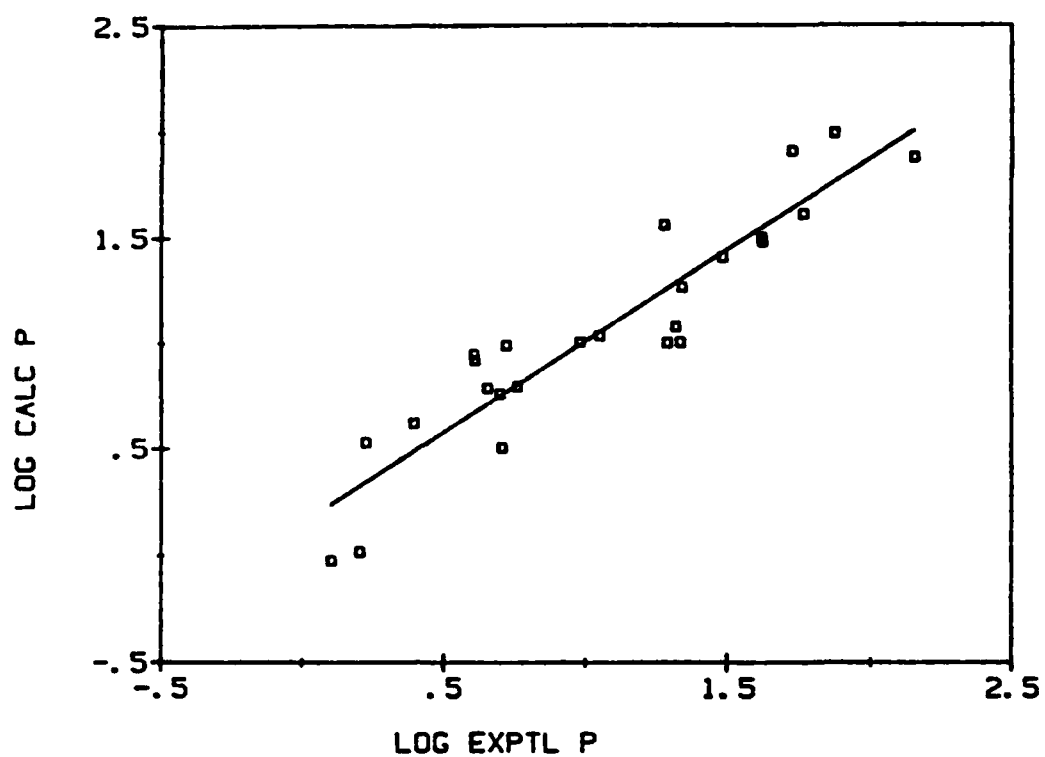
SALINE PARTITION COEFFICIENTS



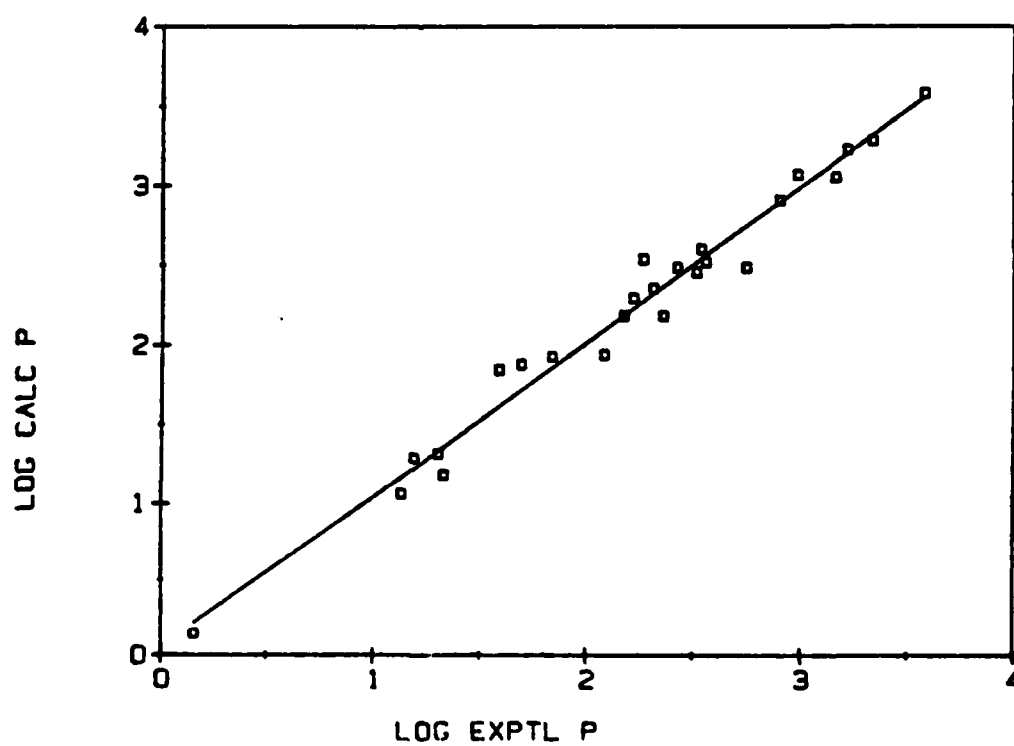
OIL PARTITION COEFFICIENTS



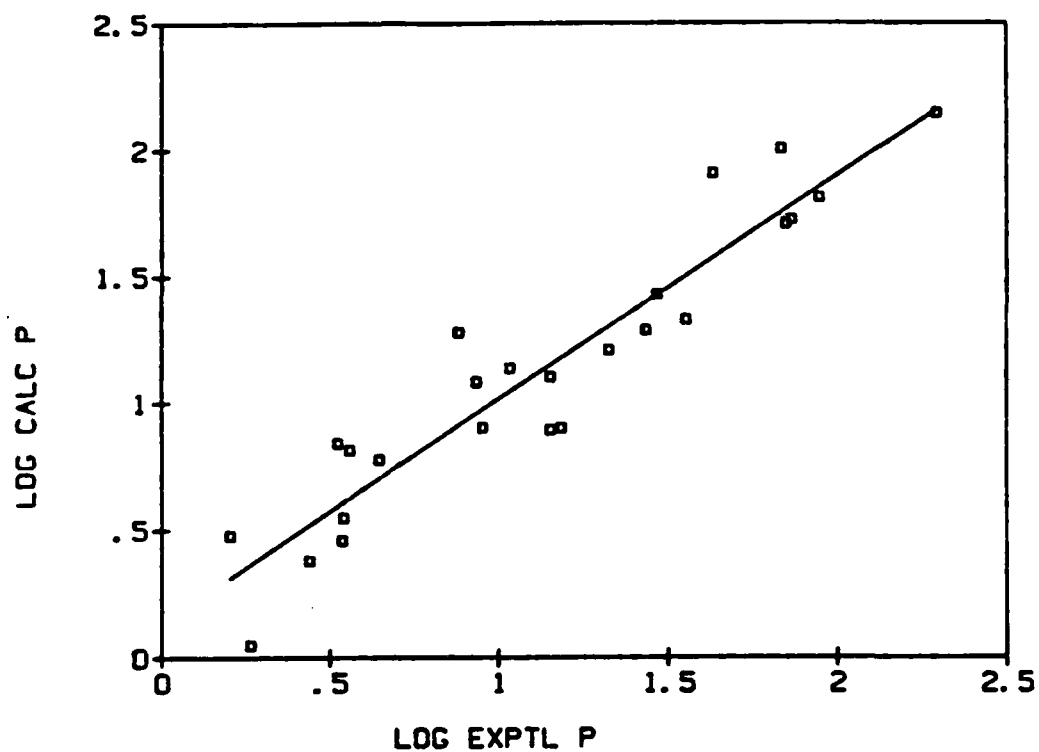
BLOOD PARTITION COEFFICIENTS



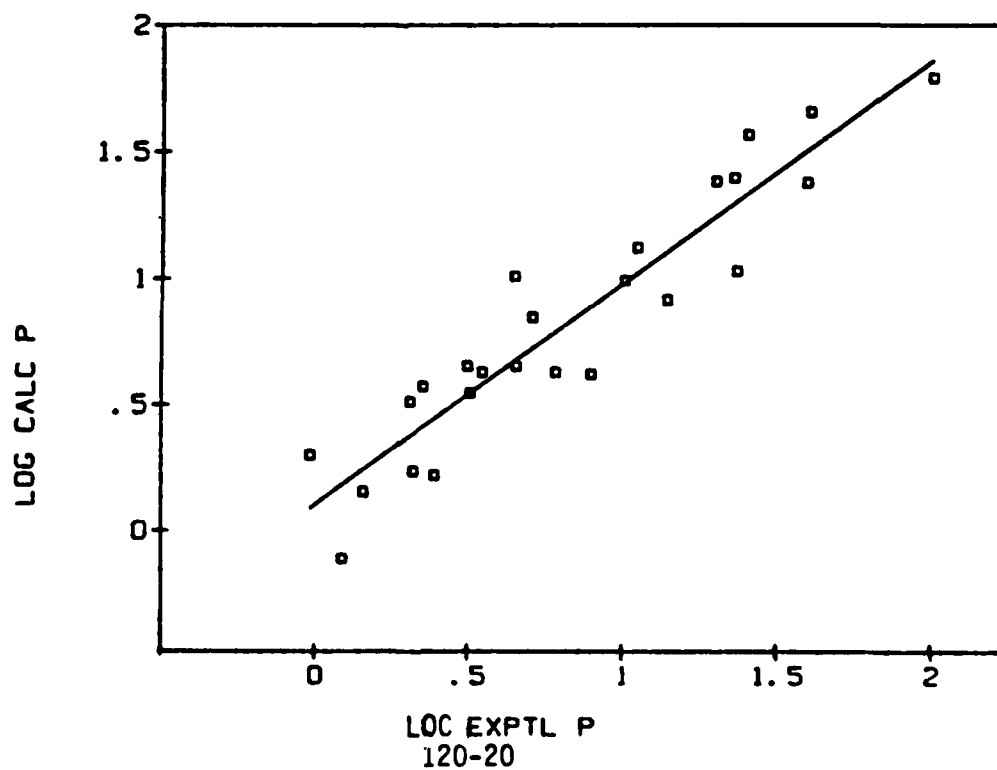
FAT PARTITION COEFFICIENTS



LIVER PARTITION COEFFICIENTS



MUSCLE PARTITION COEFFICIENTS



1985 USAF-UES SUMMER FACULTY RESEARCH PROGRAM

Sponsored by the

AIR FORCE OFFICE OF SCIENTIFIC RESEARCH

Conducted by the

UNIVERSAL ENERGY SYSTEMS, INC.

FINAL REPORT

DIGITAL SIMULATION OF SURFACE-TO-AIR MISSILES
AND SMOOTHING OF CINETHEODOLITE AND RADAR DATA

Prepared by:	Shawky E. Shamma
Academic Rank:	Professor of Mathematics/Statistics
Department:	Institute for Statistical and Mathematical Modeling
University:	University of West Florida
Research Location:	Directorate of Computer Science AD/KRB, Eglin AFB
USAF Research:	Robert Jones, Chief of Simulation Section
Date:	September 7, 1985
Contract No:	F49620-85-C-0013

DIGITAL SIMULATION OF SURFACE-TO-AIR MISSILES
AND SMOOTHING OF CINETHEODOLITE AND RADAR DATA

by

Shawky E. Shamma

Abstract

This report summarizes the activities of the participant during his SFRP.

It consisted of:

- 1 - examination of existing models which are used by the sponsor for "digital simulation for the dynamics of surface-to-air missiles" and making recommendations for implementation of more accurate methods.
- 2 - examination of the methods that are currently used by the sponsor for smoothing and analyzing cinetheodolite and radar data for missiles and bombs.
- 3 - conducting seminars for the research staff on "critical phenomena in digital signal processing" and "applied time series forecasting and control."

I. INTRODUCTION:

In a previsit to Eglin Air Force Base, the participant and the sponsor agreed on a SFRP effort consisting of three basic goals. These goals are summarized in Section II. of this report. Sections III, IV, and V contain the approaches taken in realizing each of the objectives of the effort and the results of each approach. Section VI contains suggestions for follow-on work for completion and continuation of the research effort.

II. OBJECTIVES OF THE EFFORT:

- 1 - examination of existing models which are used
by the sponsor for "digital simulation for the dynamics of
surface-to-air missiles" and making recommendations for
implementation of more accurate methods.
- 2 - examination of the methods that are currently used by the
sponsor for smoothing and analyzing cinetheodolite and radar
data for missiles and bombs.
- 3 - conducting seminars for the research staff on "critical
phenomena in digital signal processing" and "applied time
series forecasting and control."

III. DIGITAL SIMULATION FOR THE DYNAMICS OF SURFACE-TO-AIR MISSILES:

The mathematical description of the dynamical processes encountered in simulation of surface-to-air missiles requires solving a system of

ordinary differential equations subject to specified initial conditions. The sponsor uses a "modified Euler scheme" to integrate the system of governing differential equations.

Examination of the underlying theory on numerical integration of differential equations reveals that such a scheme is one of a larger class of solvers denoted in the literature as the class of one-step methods of order one:

$$\underline{y}_{n+1} - \underline{y}_n = h [(1-\theta)\underline{f}_{n+1} + \theta \underline{f}_n],$$

for solving the system $dy/dt = \underline{f}(t, \underline{y})$.

Such algorithm is stable if and only if $\theta \leq \frac{1}{2}$ and in the absence of the eigen values of the associated Jacobian matrix $|\partial \underline{f} / \partial \underline{y}|$, the optimal θ can be approximated by $\theta \approx 0.122$.

It is known that explicit numerical methods of higher order have rather small regions of absolute stability when the system is stiff due to broad varying rates of some components of the system. On the other hand, implicit methods have a somewhat larger region of stability. Recently developed methods combine the predictor - corrector schemes and implicit schemes for use when the system is stiff. In this option Adams-Moulton correctors are replaced by implicit method and direct iteration of the corrector is replaced by a form of Newton iteration. Both steplength and order are variable and the program can automatically change order as well as steplength; the strategy being such as to min-

imize the computational effort required for the Local error to be less than a stipulated bound.

Currently we are incorporating the above described method in the model for simulating the dynamics of surface-to-air missiles in order to obtain more accurate results by stipulating a prior bound on the truncation error.

IV. SMOOTHING OF CINETHEODOLITE AND RADAR DATA FOR MISSILES AND BOMBS:

Estimation and smoothing is the process of extracting information from data - data which can be used to infer the denied information and may contain errors. The sponsor uses "Moving Polynomial

Are Smoothing - MPAS" techniques in most cases and "Optimal Smoothing - OS" in selective studies.

Recent research work indicates that "smoothing by spline functions" is more preferable to moving polynomial arc smoothing because of the nature of the structure of splines with higher order differentiability and cabability of carrying the smoothing as close as needed to the end (boundary) points (Fig 1). Also modern estimation methods use known relationships about the dynamical system under study to extract optimal smoothing and estimation of the state of the system.

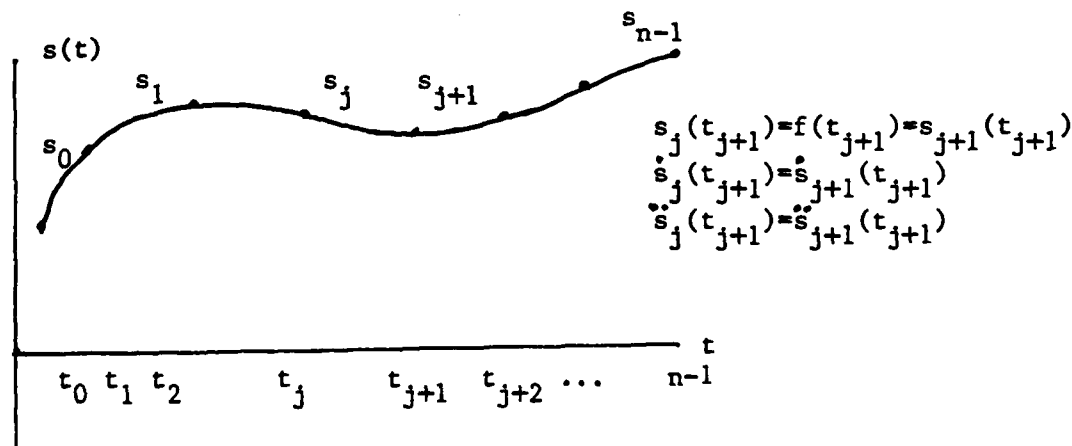


FIGURE 1

We initiated a study for developing the necessary software for a "Cubic Spline Regression Model - CSRM" that will give all pertinent statistical information about a least square estimate for estimating a cubic spline.

By way of comparison, we give here a cubic spline interpolant for a test case given by the trajectory; Fig 2:

$$y(t) = \frac{100}{2} \sin\left(\frac{10}{t}\right)$$

Such a trajectory is chosen because it resembles one of the coordinates of a maneuvering airplane. The cubic spline interpolating function is described by

$$S_j(t) = a_j + b_j (t-t_j) + c_j (t-t_j)^2 + d_j (t-t_j)^3$$

$j = 1, 2, \dots, 25$, where the interval $1 \leq t \leq 3$ is divided into 25 intervals and the velocity at $t = 1$ and $t = 3$ are taken to be $\dot{y}(1)$ and $\dot{y}(3)$ respectively.

The data used in computing the spline functions $S_j(t)$ were obtained from the function $y(t)$ and is described in table I. The resulting splines $S_j(t)$, $j = 1, 2, \dots, 25$, are given in table II. Table III gives a comparison for the velocity and acceleration as obtained from the analytic trajectory $y(t)$ and the splines $s_j(t)$. It indicates a very good approximation for velocity and acceleration through the entire interval.

Currently we are developing the software for least square spline regression and making a feasibility study of the potential use of "optimal estimation and smoothing" in various tasks of interest to the sponsor including analyzing Cinetheodolite and Radar data for Missiles and Bombs.

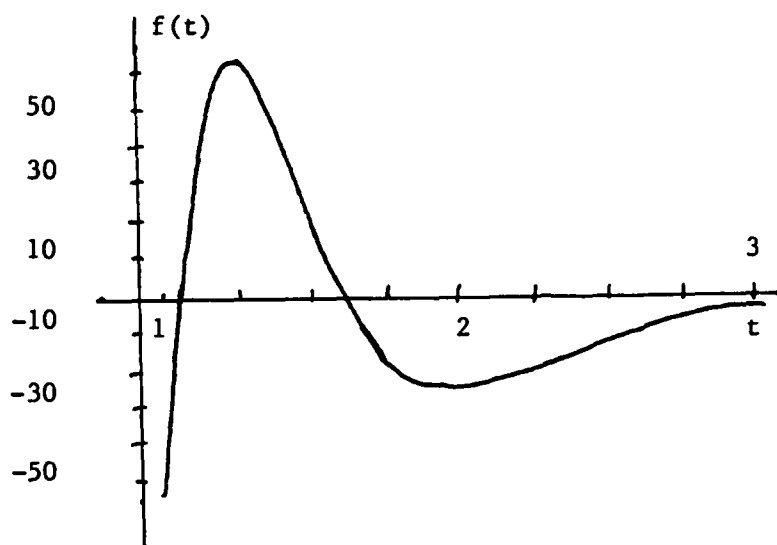


FIGURE 2 Graph of $y(t) = \frac{100}{t^2} \sin \frac{10}{t}$

TABLE 1

Input data for interpolent spline

n=	26	
$\dot{y}(1)=$	947.8757512543264	$\dot{y}(3)=13.53104669674531$
t=	1	y= -54.40211108893697
	1.08	14.12585438630988
	1.16	53.52247606128064
	1.24	63.60037423509886
	1.32	55.18507311907849
	1.4	38.65451098942449
	1.48	20.82120076056773
	1.56	5.207487186205637
	1.64	-6.861993447736568
	1.72	-15.28533213328074
	1.8	-20.52782453638341
	1.88	-23.24297838998193
	1.96	-24.07958589489283
	2.04	-23.59873639286421
	2.12	-22.24967639929587
	2.2	-20.37394162171342
	2.28	-18.22089581809409
	2.36	-15.96607650281891
	2.44	-13.72839420869567
	2.52	-11.58468859760214
	2.6	-9.581354531716319
	2.68	-7.743286282198379
	2.76	-6.080576705310711
	2.84	-4.593431000740544
	2.92	-3.275706818870399
	3	-2.117421809727613

TABLE 2

SPLINE COEFFICIENTS

<u>t</u>	<u>A</u>	<u>B</u>	<u>C</u>	<u>D</u>
+1.0000D+00	-5.440D+01	+9.479D+02	-3.478D+02	-9.915D+03
+1.0800D+00	+1.413D+01	+7.019D+02	-2.727D+03	+1.370D+03
+1.1600D+00	+5.352D+01	+2.918D+02	-2.398D+03	+4.067D+03
+1.2400D+00	+6.360D+01	-1.384D+01	-1.422D+03	+3.506D+03
+1.3200D+00	+5.519D+01	-1.741D+02	-5.810D+02	+2.180D+03
+1.4000D+00	+3.865D+01	-2.252D+02	-5.781D+01	+1.081D+03
+1.4800D+00	+2.082D+01	-2.137D+02	+2.016D+02	+3.771D+02
+1.5600D+00	+5.207D+00	-1.742D+02	+2.920D+02	-1.719D+00
+1.6400D+00	-6.862D+00	-1.275D+02	+2.916D+02	-1.711D+02
+1.7200D+00	-1.529D+01	-8.415D+01	+2.506D+02	-2.225D+02
+1.8000D+00	-2.053D+01	-4.833D+01	+1.972D+02	-2.152D+02
+1.8800D+00	-2.324D+01	-2.092D+01	+1.455D+02	-1.837D+02
+1.9600D+00	-2.408D+01	-1.169D+00	+1.014D+02	-1.459D+02
+2.0400D+00	-2.360D+01	+1.226D+01	+6.640D+01	-1.103D+02
+2.1200D+00	-2.225D+01	+2.076D+01	+3.994D+01	-8.015D+01
+2.2000D+00	-2.037D+01	+2.562D+01	+2.071D+01	-5.620D+01
+2.2800D+00	-1.822D+01	+2.785D+01	+7.220D+00	-3.792D+01
+2.3600D+00	-1.597D+01	+2.828D+01	-1.880D+00	-2.438D+01
+2.4400D+00	-1.373D+01	+2.751D+01	-7.732D+00	-1.462D+01
+2.5200D+00	-1.158D+01	+2.599D+01	-1.124D+01	-7.744D+00
+2.6000D+00	-9.581D+00	+2.404D+01	-1.310D+01	-3.023D+00
+2.6800D+00	-7.743D+00	+2.189D+01	-1.383D+01	+1.223D-01
+2.7600D+00	-6.081D+00	+1.968D+01	-1.380D+01	+2.133D+00
+2.8400D+00	-4.593D+00	+1.751D+01	-1.328D+01	+3.344D+00
+2.9200D+00	-3.276D+00	+1.545D+01	-1.248D+01	+3.987D+00
+3.0000D+00				

TABLE 3

FIRST AND SECOND DERIVATIVES AT KNOTS

t	\dot{s}	\ddot{s}	\dot{y}	\ddot{y}
+1.08D+00	+7.019D+02	-5.455D+03	+6.9883D+02	-4.9933D+03
+1.16D+00	+2.918D+02	-4.797D+03	+2.9088D+02	-4.6992D+03
+1.24D+00	-1.384D+01	-2.845D+03	-1.4187D+01	-2.8697D+03
+1.32D+00	-1.741D+02	-1.162D+03	-1.7408D+02	-1.2165D+03
+1.40D+00	-2.252D+02	-1.156D+02	-2.2512D+02	-1.5974D+02
+1.48D+00	-2.137D+02	+4.031D+02	-2.1362D+02	+3.7504D+02
+1.56D+00	-1.742D+02	+5.841D+02	-1.7417D+02	+5.6910D+02
+1.64D+00	-1.275D+02	+5.833D+02	-1.2749D+02	+5.7661D+02
+1.72D+00	-8.415D+01	+5.011D+02	-8.4135D+01	+4.9914D+02
+1.80D+00	-4.833D+01	+3.943D+02	-4.8327D+01	+3.9465D+02
+1.88D+00	-2.092D+01	+2.910D+02	-2.0919D+01	+2.9228D+02
+1.96D+00	-1.169D+00	+2.028D+02	-1.1689D+00	+2.0435D+02
+2.04D+00	+1.226D+01	+1.328D+02	+1.2256D+01	+1.3424D+02
+2.12D+00	+2.076D+01	+7.988D+01	+2.0763D+01	+8.1089D+01
+2.20D+00	+2.562D+01	+4.141D+01	+2.5615D+01	+4.2371D+01
+2.28D+00	+2.785D+01	+1.444D+01	+2.7849D+01	+1.5170D+01
+2.36D+00	+2.828D+01	-3.760D+00	+2.8277D+01	-3.2202D+00
+2.44D+00	+2.751D+01	-1.546D+01	+2.7508D+01	-1.5076D+01
+2.52D+00	+2.599D+01	-2.248D+01	+2.5990D+01	-2.2209D+01
+2.60D+00	+2.404D+01	-2.620D+01	+2.4043D+01	-2.6012D+01
+2.68D+00	+2.189D+01	-2.765D+01	+2.1889D+01	-2.7526D+01
+2.76D+00	+1.968D+01	-2.759D+01	+1.9679D+01	-2.7513D+01
+2.84D+00	+1.751D+01	-2.657D+01	+1.7513D+01	-2.6521D+01
+2.92D+00	+1.545D+01	-2.496D+01	+1.5451D+01	-2.4939D+01

V. CONDUCTING SEMINARS FOR THE RESEARCH STAFF:

I gave two summer-long seminars for the research staff. One seminar met once every week for one hour and was attended by 38 members of the staff of Freeman Mathematical Laboratory, Eglin AFB. It consisted of tutorial exposition and survey of the mathematical analysis of critical phenomena in digital signal processing. The objectives of this seminar were to outline some of the major problems that are encountered in the initial stages of time-series-analysis including data preparation and qualification, and providing guidance for updating the existing codes for times series analysis.

The second seminar met for two hours weekly and it was attended by 15 members of the research staff. The seminar covered practical aspects of Box-Jenkins methodology for forecasting stationary and nonstationary time series and methods for optimal control of discrete systems which are characterized by "multiple time series".

Lecture notes for the two seminars were distributed to participants. We give here the tables of contents of the notes:

A - table of contents of lecture notes for the seminar on "Critical Phenomena in Digital Signal Processing"

CHAPTER 1 - SUMMARY OF USEFUL CONCEPTS

- Definitions: time, series, stochastic process, stationary and non-stationary time series
- Autocorrelation function
- Spectrum
- Digital filters
- Parametric time series models

- Objectives of time series analysis: prediction, estimation, filtering and control, simulation and optimization, and generating new mathematical and physical theories.

- Frequency response studies

CHAPTER 2 - FOURIER ANALYSIS

- Classification of signals
- Fourier series
- Discrete Fourier series
- Parseval's theorem
- Fourier integrals
- Generalized functions, delta function
- Fourier transforms of signals
- Convolution and Fourier transform
- Effect of finite sample length
- Discrete Fourier transform of length N
- Sampled data and the Nyquist frequency

CHAPTER 3 - SAMPLED DATA SIGNALS

- Sampling continuous-time signal
- Pulse trains
- Impulse sampling
- Effect of data window shape and width on the measured Fourier Transform
- Aliasing
- Acquiring analog data in a digital form
- First-order filter

CHAPTER 4 - FAST FOURIER TRANSFORM

- Definition of fast Fourier transform
- Effect of adding zero data points

- Pitfalls of using discrete Fourier transform, aliasing, leakage, picket-fence effect
- Pictorial representation of the DFT
- Fast Fourier transform algorithm
- Filter algorithms
- Digital Butterworth filters

CHAPTER 5 - GENERAL CONSIDERATIONS IN DATA ACQUISITION AND PROCESSING

- Data collection
- Data recording
- Data preparation
- Data qualification
- Data analysis
- Procedures for elimination and/or minimization of effects on various problems

CHAPTER 6 - DIGITAL DATA ANALYSIS PROCEDURES AND COMPUTATION OF POWER SPECTRAL DENSITY (PSD)

- Pre-processing operations
- Digital filtering methods
- Autocorrelation functions
- Power spectral density functions
- Calculations for two records
- Effective resolution bandwidth
- Resolution limits
- Leakage
- How to compute PSD
- Tapering function - data windows
- Examples of the use of PSD functions

B - Table of contents of lecture notes for the seminar on
"Applied Time Series Forecasting and Control"

CHAPTER - 1 INTRODUCTION AND SUMMARY

- Stochastic and deterministic dynamic mathematical models: stationary and nonstationary stochastic models for forecasting and control, transfer function models, models for discrete control systems.
- Basic ideas in model building.

CHAPTER 2 - STOCHASTIC MODELS AND THEIR FORECASTING

- Autocorrelation properties of stationary models.
- Spectral properties of stationary models.

CHAPTER 3 - LINEAR STATIONARY AND NONSTATIONARY MODELS

- The general linear process.
- Autoregressive processes - AR.
- Moving average processes - MA.
- Mixed autoregressive - moving average process - ARMA.
- Autoregressive-Integrated-Moving Average models for nonstationary process - ARIMA.

CHAPTER 4 - SUMMARY OF THE BOX -- JENKINS FORECASTING MODEL

- Model identification.
- Model estimation.
- Model diagnostic.
- Forecasting.

CHAPTER 5 - MULTIPLE SERIES: OPTIMAL CONTROL AND FORECASTING
BY LEADING INDICATOR

- Transfer function and ARMAV models.
- Transfer function versus state variable approach.
- Modeling and illustrations.
- Forecasting by leading indicator.
- An illustrative example.

- Usefulness of the leading indicator.

VI RECOMMENDATIONS

Through discussions with the SFRP focal point research staff, it became apparent that there is a need for developing more accurate methods for digital simulation of surface-to-air missiles and smoothing of cinetheodolite and radar data for missiles and bombs.

The following recommendations were made and were closely coordinated with the SFRP effort focal point as a follow-on and needed research:

- 1 - Develop and apply multi-step codes, [1,2,3], with higher order accuracy for solving the differential equations simulating the dynamics of surface-to-air missiles. Developed software should have the capabilities for handling systems in regions where the governing differential equations may be "stiff", [1], due to broad varying rates of some components (solutions). It also should have variable step-size in order to achieve a prescribed minimum truncation error and largest step-size in the range of system stability, for accomplishing such accuracy.
- 2 - Develop the necessary software for a "cubic spline regression model - CSRM", that gives all pertinent statistical information about a least square estimate \hat{y} to estimate a cubic spline

$$\underline{S}_\Delta(t) = W\underline{y}$$

for ordinate vector \underline{y} where W is a known matrix from the structure of the spline on a mesh:

$$\Delta = \{t_0 \leq t_1 \leq t_2 \leq \dots \leq t_k\},$$

and two end conditions. y is treated here as the unknown population vector, to be estimated by least square procedure. The CSRM analysis, [8,9,15,16] , should be modified to fit the data observations at equally spaced time intervals.

- 3 - Develop simulation models for pre-known trajectories for testing the accuracy of CSRM versus MPAS (moving polynomial arc smoothing) techniques.
- 4 - Make a feasibility study of the potential use of "optimal estimation and smoothing - OES" [10,11,12], in various tasks with emphasis on:
 - a - Surveying existing software for "optimal estimation and smoothing" for linear and nonlinear dynamical systems and its applicability to systems simulated by the sponsor.
 - b - Comparing the accuracy and efficiency of smoothing techniques using "MPAS, CSRM and OES," on simulated test cases of interest to the sponsor for example: the tracking problem of a falling object where the range measurements are made along the line-of-sight using a discrete noisy radar.

REFERENCES

1. Shampine, L.F., and C.W. Gear, "A User's View of Solving Stiff Ordinary Differential Equations," SIAM Review, Vol 21, 1979, pp 1-17.
2. Gear, C.W., "Simultaneous Numerical Solution of Differential-Algebraic Equations," IEEE transactions on Circuit Theory, Vol CT-18, 1971.

3. Shampine, L.F., et al, "Solving non-stiff ordinary differential equations - The State of the Art," SIAM Review, Vol 18, 1976.
4. Lambert, J.D., "Computational Methods in Ordinary Difffferential Equations," Wiley, 1973.
5. Burden, R.L., and J.D. Faires, "Numerical Analysis," Third Edition, Brindle, Weber and Schmidt, 1985.
6. Dalton, O.N. and Parker, C.R. "Real-Time Flight Analysis: Fundamentals for the Generation of a Mathematical Model for a Missile in Three-Dimensional Space with Six Degrees of Freedom." Report No. 12, 1960, Flight Simulation Laboratory. White Sands Missile Range, New Mexico.
7. Nicolaides, J.D., "Free Flight Missile Dynamics," Lecture Notes, Department of Aero-Space Engineering, University of Notre, Dame, 1965.
8. Poirer, D.J., "Piecewise Regression Using Cubic Splines," Journal of the American Statistical Association, Vol 68, 1973.
9. Buse, A. and L. Lim, "Cubic Splines as a Special Case of Restricted Least Squares," Journal of the American Statistical Association, Vol 72, 1977.
10. Kaminski, P.G., and A.F. Bryson, "Discrete Square Root Smoothing," AIAA Guidance and Control Conference, 1972
11. Deyst, Jr., J.J., and Charles F. Price, "Optimal Stochastic Guidance Laws for Tactical Missiles," Journal Spacecraft, Vol 10, 1973.
12. Gelb, A., "Applied Optimal Estimation," MIT Press, 1984.

13. Davis, R.C., "Techniques for the Statistical Analysis of Cinetheodolite Data," U.S. Naval Ordnance Test Station, NAVORD Report No. 1299, 1951.
14. Sterrett, J.K., "Manual for Moving Polynomial Arc Smoothing," Ballistic Research Laboratories, Report No. 840, 1952.
15. Wold, S., "Spline Function in Data Analysis," Technometrics, Vol 16, No. 1, 1974.
16. Reinsch, C.H., "Smoothing by Spline Functions," Num. Math., Vol 10, 1967.

ACKNOWLEDGMENTS

I would like to thank the Air Force Systems Command, Air Force Office of Scientific Research, and Univeral Energy Systems Inc., for providing a worthy research program for University faculty and their students.

I would like to acknowledge Dr. Robert Braswell, Director of Computer Sciences, and Ralph Duncan, Deputy Director, for providing me with the opportunity to spend a very interesting summer at Freeman Mathematical laboratory. I would also like to express my appreciation to George Weekly, Robert Jones and Mike Hardin for providing stimulating environments and discussions. Thanks also to Marceil Caltabellota who always typed my correspondence accurately and at record speed.

To all these people I am grateful and especially to Robert (Bobby) Jones for his encouragement and invaluable assistance.

1985 USAF-UES SUMMER FACULTY RESEARCH PROGRAM/

GRADUATE STUDENT SUMMER SUPPORT PROGRAM

Sponsored by the
AIR FORCE OFFICE OF SCIENTIFIC RESEARCH

Conducted by the
UNIVERSAL ENERGY SYSTEMS, INC.

FINAL REPORT

INDOOR RADON POLLUTION

Prepared by:	Ralph W. Sheets
Academic Rank:	Professor
Department and	Department of Chemistry
University:	Southwest Missouri State University
Research Location:	USAF Occupational and Environmental Health Laboratory, Radioanalytical Services Branch Brooks AFB, Texas
USAF Research:	Maj. Edward F. Maher
Date:	August 16, 1985
Contract No:	F49620-85-C-0013

INDOOR RADON POLLUTION

by

Ralph W. Sheets

ABSTRACT

Indoor air pollution by radon-222 and its radioactive decay daughter products constitutes a significant health risk to those who live in houses or work in buildings with higher than average concentrations. Possibly hazardous sites which may be of concern to the United States Air Force include radium storage areas, missile silos, and housing built over lands suspected of having elevated concentrations of radium. This report describes apparatus and methods which were developed to give the USAF Occupational and Environmental Health Laboratory a capability for on-site monitoring of airborne radon and its daughters. Details of assembly, calibration, and testing of portable sampling kits are described, and results of field measurements made with these kits are reported. It is recommended that these kits become permanent inventory items within the Radioanalytical Services Branch of the USAF OEHL, and that they be used to determine if indoor radon decay products exposure at suspected sites are elevated to a point where they pose a health hazard to occupants.

ACKNOWLEDGMENTS

Research described in this report was sponsored by the Air Force Office of Scientific Research/AFSC, United States Air Force, under Contract F49620-85-C-0013. The author would also like to acknowledge support of the Air Force Systems Command and the USAF Occupational and Environmental Health Laboratory, Brooks AFB. Major Edward F. Maher, Chief, Radioanalytical Services Branch, USAF OEHL/RZA deserves special thanks for his guidance, assistance, and encouragement. Universal Energy Systems, Inc., people were very helpful to the author. Finally the author thanks Dr. Steven N. Rudnick, Department of Environmental Sciences and Philosophy, Harvard University, for use of his laboratory to calibrate instruments.

I. INTRODUCTION

Indoor air pollution from radon and its daughter decay products is a significant health problem for those exposed to higher than average concentrations.^{1,2,3} Radon-222 is a radioactive gas formed by decay of radium-226, and the main source of atmospheric radon is decay of radium in rocks and soils. Radon itself decays with a 3.82 day half-life to form a series of short-lived daughters which have been strongly implicated as lung carcinogens.⁴ These daughters are radioactive metal atoms which can attach themselves to particles in the air. When inhaled, they can deposit in the lungs where they irradiate the radiosensitive cells of the bronchial epithelium and pulmonary tissues. Unattached daughters preferentially deposit in the first six generations of the bronchial tree where most of the lung cancers have developed in miners exposed to airborne radon daughters.⁵ Both the radon daughter concentrations and the fraction of unattached daughters must be characterized to model lung doses to various regions of the lung.

The concentration of outdoor radon over the contiguous United States is estimated to be about 0.25 pCi/l⁶. Diffusion into buildings from soil underneath often results in indoor concentrations much higher than the outdoor levels. Typical concentrations in U.S. houses average 0.2 to 4 pCi/l³, but some indoor concentrations have been found to exceed the OSHA standard for radon in uranium mines (about 66 pCi/l)¹. Exposure of the general public to radon daughters is believed to account for a substantial number of lung cancers in the U.S. (1,000-20,000 cases per year)³.

The indoor radon pollution problem is of particular importance to the USAF Occupational and Environmental Health Laboratory. Not only

are USAF personnel around the world exposed to normal radon daughter concentrations where they live and work, but there are a number of sites that are of special concern. These include radium dial storage areas, missile silos and hardened underground installations, and housing built over lands suspected of having elevated concentrations of radium. Studies need to be carried out to determine the range and distribution of indoor radon and its daughters, and to characterize their behavior in buildings. To accomplish these ends, the USAF OEHL needs to have a capability for on-site monitoring of radon-222 and its daughters when they are present at environmentally significant concentrations.

The present investigator is Professor of Chemistry at Southwest Missouri State University where he is engaged in teaching and research in the area of environmental chemistry. He has recently become interested in indoor air pollution, especially radon pollution, and has developed plans to establish a monitoring program to determine levels of indoor radon and its daughters in southwest Missouri. A motivating force for joining the Summer Faculty Research Program was the opportunity to develop knowledge and skills needed to establish such a program.

II. OBJECTIVES OF THE RESEARCH EFFORT

The overall objective of the summer research project was to develop a capability for on-site monitoring of airborne radon-222 and its radioactive daughter decay products. This would involve assembly of portable sampling kits from off-the-shelf components; calibration of instruments; development and testing of measurement techniques to be used in the field; and performance of some actual field measurements.

Two different approaches were considered:

1. Direct measurement of airborne radon--This would require development of a portable sampling kit for collection of grab samples of air and measurement of total alpha activity using a scintillation technique. The data would permit calculation of instantaneous concentrations of airborne radon present at environmentally significant levels.
2. Measurement of radon daughter decay products--This would require development of a portable sampling kit for collection of radon daughters on filter paper and measurement of alpha activity using a scintillation technique. The data would permit calculation of the potential alpha energy concentrations (PAEC), in working level (WL). Simultaneous collection of radon daughters on a second filter with a wire mesh pre-filter would permit calculation of attached and unattached fractions of the daughters as well.

It was decided to pursue both of these approaches to accomplish the following goals:

1. Development of portable apparatus for field measurement of airborne radon-222.
2. Development of portable apparatus for field measurement of potential alpha energy concentrations (WL).
3. Calibration and testing of instruments and verification of techniques.
4. Field testing of kits with actual field measurements.

It was anticipated that the kits would become permanent inventory items within the Radioanalytical Services Branch of the USAF Occupational and Environmental Health Laboratory and would be used to determine

whether exposure to indoor radon and its decay products at USAF facilities may pose health hazards to personnel.

III. DIRECT MEASUREMENT OF AIRBORNE RADON

A. Experimental Procedures

1. Apparatus

The Lucas alpha-scintillation method⁷ was chosen for the measurement of airborne radon. A portable sampling kit was assembled from the following components: Ludlum Model 2200 battery-operated scaler; Ludlum Model 182 radon flask counter; four 100-ml Lucas-type scintillation cells (Rocky Mountain Scientific Glass Blowing Company, Aurora, Colorado). The assembled apparatus weighs approximately 20 pounds and can be hand carried in a standard USAF OEHL metal instrument case (8" X 18" X 24").

The Lucas cell is a cylindrical flask constructed from a Kovar seal. The inner surface is coated with silver-activated zinc sulfide. A quartz window with a transparent tin oxide coating on its inner surface is sealed to one end of the cell. The other end has a stopcock to permit evacuation of the air-tight cell. The cell is placed in a light-tight chamber on the window of a photomultiplier tube, and alpha scintillations produced by radon and its daughters (polonium-218 and polonium-214) are counted. The counting efficiency of such flasks is typically 0.7-0.8 (counts per minute)/(disintegration per minute).

2. Measurement Techniques

Airborne radon concentrations were calculated by the method of Jonassen and Clements⁸. This method does not require that secular equilibrium be established between radon and its daughters before

counting begins. If the initial sample of radon is free of daughter products at the time it is introduced into the counting cell, the counting period can start at any time after sampling. (If the sample initially consists of a mixture of radon and its daughters, 3-4 hours must be allowed for attainment of equilibrium before counting begins.)

The equation relating initial radon concentration to number of alpha scintillations in a given time period is:

$$Rn(pCi/l) = C / (2.22) (E) (V) (G) \quad (1)$$

where $G = 23904.80625(\text{EXP}((-0.0001259)(T_1))$

$$- \text{EXP}((-0.0001259)(T_1 + T_2)))$$

$$- 4.50748(\text{EXP}((-0.2272)(T_1))$$

$$- \text{EXP}((-0.2272)(T_1 + T_2)))$$

$$- 165.5195(\text{EXP}((-0.02586)(T_1))$$

$$- \text{EXP}((-0.02586)(T_1 + T_2)))$$

$$+ 93.65601(\text{EXP}((-0.03518)(T_1))$$

$$- \text{EXP}((-0.03518)(T_1 + T_2))) \quad (1a)$$

and T_1 is the time (minutes) between sample collection and beginning of counting; T_2 is the counting interval (minutes); C is the number of net counts in T_2 (total counts minus background counts); E is the counter efficiency (cpm/dpm); and V is the volume of the Lucas cell (liters).

These equations were programmed into a Hewlett-Packard 15C handheld calculator so that calculation of a radon concentration requires less than one minute.

The experimental procedure for the determination of airborne radon is as follows: A Lucas cell is flushed several times with helium,

evacuated, and counted in a Ludlum radon flask counter. (Typical background levels of evacuated flasks are 0.1-0.2 counts per minute.) The stopcock of the evacuated cell is opened to obtain a grab sample of air. The stopcock is closed and the time is recorded. If (as was usually the case) a filtered inlet is not used to remove radon daughters, the sample is stored for three hours to allow secular equilibrium to be reached. The cell is then counted and the initial radon concentration is calculated using a Hewlett-Packard 15C programmable calculator and Equations (1) and (1a).

3. Testing and Verification of Instruments and Methods

The radon counting apparatus was calibrated by inter-laboratory comparison. Lucas cells were filled with radon and counted at the Harvard University Public School of Health. They were then shipped to USAF OEHL where they were counted with the apparatus described above.

Several experiments were carried out to determine the sensitivity and reproducibility of the apparatus. For environmentally significant radon concentrations (down to about 1 pCi/l), the counting rate is likely to be small. As an example, for a counter efficiency of 0.7 and a Lucas cell of 100 ml volume, the number of counts produced by 1 pCi/l of radon in equilibrium with its two alpha-emitting daughters can be calculated as

$$1 \text{ pCi/l} \times 0.100 \text{ l} \times 3(2.22 \text{ dpm/pCi}) \times 0.7 \text{ cpm/dpm} = 0.47 \text{ cpm}.$$

Statistical fluctuations are large at such counting rates, although precision can be improved by using longer counting intervals. The minimum detectable activity is related to the background count and can

be estimated⁹ at the 95% confidence level by the equation

$$L_D = 2.71 + 4.65(B)^{1/2} \quad (2)$$

where L_D is the detection limit and B is the "true" background count.

Equations (1) and (2) were used to calculate representative minimum detectable concentrations of airborne radon (Table 1).

Table 1.

Calculated Minimum Detectable Concentrations of Airborne Radon

Counting Interval, min.	Background Counting Rate, cpm	Counter Efficiency, cpm/dpm	Minimum Significant Gross Counts	Corresponding Radon Concentration, pCi/l
60	0.1	0.7	20	0.52
180	0.1	0.7	40	0.28
480	0.1	0.7	83	0.16

It is seen that sensitivity is low for short counting times and increases with longer counting intervals. Reproducibility of counts is also poor at these levels. A grab sample of room air was counted for four different 60-minute intervals over a 24-hour period. Initial radon concentrations (pCi/l) as calculated by Equation (1) were $0.35 \pm 58\%$; $0.32 \pm 60\%$; $0.28 \pm 65\%$; and $0.61 \pm 44\%$. This gives a mean of 0.39 pCi/l with a standard deviation of 0.15.

Other experiments showed that for radon concentrations of 1 pCi/l or greater, 60-minute counting intervals gave calculated percent errors of 20-30%. Experiments and calculations such as these indicate that the lower limit for reliable results with this apparatus does not extend much below 0.5 pCi/l. This is not a problem, however, since indoor radon concentrations of this magnitude are of little interest.

B. Field Measurements: Results and Discussion

Measurements of indoor radon concentrations were carried out using the apparatus described above. The first series involved the building which is occupied by the USAF OEHL, Brooks AFB (Table 2). Measurements were made in the basement in two locations. In a part which has a dirt floor, radon concentration was $1.17 \text{ pCi/l} \pm 32\%$; in an adjacent area with a concrete floor, a value of $0.89 \text{ pCi/l} \pm 36\%$ was obtained. First floor laboratories had much lower concentrations. One laboratory gave a value of $0.20 \text{ pCi/l} \pm 54\%$. Measurements on two different days in another laboratory yielded values of $0.24 \pm 76\%$ and $0.28 \pm 65\%$. These concentrations are well within normal range and do not present any unusual hazards to personnel.

Table 2.

Indoor Radon Concentration, USAF OEHL Building 140

Location	Number of Measurements	Average Radon Concentration, pCi/l	Highest Value Measured pCi/l
Basement	2	1.03	1.17
Laboratory 5	1	0.20	0.20
Laboratory 25	2	0.26	0.28
Mean = 0.50 pCi/l			

A brief survey was made of some houses in the San Antonio, Texas, area occupied by USAF and USAF-associated personnel to determine the range of indoor radon concentrations. A total of 20 measurements were made on 5 different houses (Table 3). Radon concentrations ranged from about 0.1 to 2.3 pCi/l . The arithmetic mean for houses surveyed was 0.53 pCi/l ; the geometric mean was 0.36 pCi/l .

Table 3.

Indoor Radon Concentrations in Some San Antonio, Texas, Houses

House Number	Number of Measurements	Average Radon Concentration, pCi/l	Highest Value Measured, pCi/l
1	14	1.14	2.30
2	1	0.14	0.14
3	1	0.97	0.97
4	2	0.21	0.24
5	2	0.19	0.30

Arithmetic Mean = 0.53 pCi/l

Geometric Mean = 0.36 pCi/l

Only one of the houses surveyed had radon concentrations greater than 1 pCi/l. Several measurements were made on this house on different days and under various conditions of ventilation (windows open/closed; air conditioner on/off) (Table 4). All samples were taken in the

Table 4.

Indoor Radon Concentrations for House 1, San Antonio, Texas

Date	Time	Conditions	Concentration of Radon, pCi/l
6/27/85	0630	closed;A/C	1.08 + 19%
7/1/85	0630	closed;A/C	2.30 + 13%
7/22/85	1900	closed;A/C	1.47 + 28%
7/22/85	2100	closed;A/C	1.80 + 26%
7/22/85	2300	closed;A/C	1.02 + 34%
7/23/85	0630	closed;A/C	1.34 + 30%
7/23/85	1900	closed;A/C	1.47 + 28%
7/23/85	2100	closed;A/C	1.81 + 25%
7/23/85	2300	closed;A/C	1.37 + 29%
7/24/85	0630	closed;A/C	0.70 + 41%
Mean = 1.43 pCi/l			
7/24/85	1630	open	0.31 + 62%
7/25/85	0630	open	0.44 + 52%
7/28/85	0700	open	0.61 + 44%
7/29/85	0630	open	0.24 + 70%

Mean = 0.40 pCi/l

Arithmetic Mean of All Measurements = 1.14 pCi/l

Standard Deviation = 0.62

kitchen about 3 feet above the floor, which was a poured concrete slab covered with asphalt tile. Values ranged from 0.24 to 2.30 pCi/l. Highest values were recorded when windows were closed for several hours before sampling (0.70 to 2.30 pCi/l). Concentrations were significantly lower when the windows were opened for several hours (0.24 to 0.61 pCi/l).

All of the buildings reported above were of conventional construction. Several measurements were also made on a solar heated home in Knoxville, Tennessee (Table 5). Grab samples were taken in the basement, two rooms on the first floor, and one on the second. Values ranged from 2.59 to

Table 5.

Indoor Radon Concentrations of a Solar House in Knoxville, Tenn.

<u>Location</u>	<u>Radon Concentration, pCi/l</u>
Basement	7.54 + 13%
Solarium (1st floor)	5.75 + 14%
Den (1st floor)	2.59 + 21%
Bedroom (2nd floor)	2.85 + 20%

Average Concentration = 4.68 pCi/l
Standard Deviation = 2.38

7.54 pCi/l, with an average of 4.68 pCi/l. In general, concentration decreased with floor above ground, indicating that the radon is entering from the soil underneath the house. The concentrations found here are high enough to warrant further investigation.

The measurements described in this section demonstrate that the portable sampling kit allows convenient, reliable measurement of instantaneous indoor radon concentrations which are environmentally significant. It permits detection of airborne radon at concentrations well below this level.

IV. MEASUREMENT OF RADON DAUGHTER DECAY PRODUCTS

1. Apparatus

Thomas' three-interval count method^{10,11} was selected for measurement of radon daughter concentrations. A sampling kit was assembled from the following components: Ludlum 2500 scaler; Ludlum 2200 scaler; two 3-inch photomultiplier tubes with light-tight chambers; Millipore vacuum pump; Gilmont rotameter; two Gelman open-face filter holders (47 mm diameter); Millipore 0.45 millimicron cellulose ester filters; alpha phosphor-on-Mylar discs (William B. Johnson and Associates, Research Park, Montville, NJ).

2. Measurement Techniques

The method developed by Thomas for determination of the radon daughters RaA (polonium-218), RaB (lead-214), and RaC (bismuth-214) has a sensitivity of the order of 1 pCi/l for each nuclide. Air is drawn through a filter for a specified time and the total alpha disintegrations in three selected time intervals are counted. The equations relating air concentrations of the daughters to the interval counts are

$$C_2 = (0.1698G(2,5) - 0.0820G(6,20) + 0.0775G(21,30) - 0.0566R)/VE \quad (3)$$

$$C_3 = (0.0012G(2,5) - 0.0206G(6,20) + 0.0491G(21,30) - 0.1575R)/VE \quad (4)$$

$$C_4 = (-0.0225G(2,5) + 0.0332G(6,20) - 0.0377G(21,30) - 0.0576R)/VE \quad (5)$$

where C_2 is RaA concentration, pCi/l; C_3 is RaB concentration, pCi/l; C_4 is RaC concentration, pCi/l; V is sampling flow rate, l/min; E is the counter efficiency, cpm/dpm; $G(x,y)$ is the gross number of alpha counts from x to y minutes after end of sampling; R is background counting rate, cpm; and the sampling time is 5 minutes.

From these concentrations, the potential alpha energy concentration (PAEC), in working level units, may be calculated¹²:

$$\text{PAEC} = 0.0010256(C_2) + 0.0050624(C_3) + 0.0037247(C_4). \quad (6)$$

The experimental procedure for determination of radon daughter concentrations and PAEC's is as follows: A 0.45 millimicron filter is placed face down on an alpha phosphor-on-Mylar disc. This is placed on the face of a photomultiplier tube inside a light-tight box and counted with a Ludlum scaler for 30 minutes. Typical background rates are 0.02 to 0.03 cpm. The filter is connected to a Millipore vacuum pump metered with a Gilmont rotameter. Air is drawn through the filter at a constant rate for exactly 5 minutes. The filter is removed and transferred face down to the counting chamber. After 2 minutes from the end of sampling, gross alpha counts are recorded until the end of the fifth minute. Counts are subsequently recorded for the 6-20 and the 21-30 minute intervals. Concentrations of radon daughters and PAEC's are calculated using a Hewlett-Packard 15C calculator and Equations (3)-(6).

3. Testing and Verification of Instruments and Methods

Air flow rates were measured with a Gilmont rotameter. The factory calibration was verified with a soap bubble flowmeter for standard conditions. The rotameter was then calibrated with the filter in place by measuring the pressure drop across the filter and calculating a flow rate corrected to standard conditions¹³:

$$Q_{\text{STP}} = Q_a (P_a / P_{\text{STP}})^{1/2} \quad (7)$$

where Q_{STP} is the flow rate corrected to standard conditions; Q_a is the indicated flow rate; P_a is pressure inside flowmeter; and P_{STP} is the standard pressure.

The counter efficiency was determined by comparison with a Harvard University Public School of Health apparatus which had been calibrated against a Th-232 electroplated standard (NBS traceable).

Experiments were carried out to determine the sensitivity and reproducibility of the apparatus. Thomas' data¹⁰ indicate that the sensitivity of the method is in the domain of 0.005 to 0.01 WL. Most of the measurements made with the present apparatus were less than 0.005, and the results were somewhat erratic. Table 6 shows the results of

Table 6.

Radon Daughter Concentrations and PAEC's for Duplicate Samples at San Antonio House Number 1.

<u>Quantity</u>	<u>Sample 1</u>	<u>Sample 2</u>
RaA	0.719 pCi/l	0.670 pCi/l
RaB	0.222 pCi/l	0.189 pCi/l
RaC	-0.123 pCi/l	0.00645 pCi/l
PAEC	0.0017 WL + 35%	0.0017 WL + 40%

duplicate measurements made at San Antonio house number 1. Although both samples yielded the same PAEC value, there is scatter in the individual nuclide concentrations, with one of the values being a negative quantity. Other measurements of PAEC's showed that the reliable limit of measurement with the present apparatus is of the order of 0.0005 WL.

B. Field Measurements: Results and Discussion

Seven measurements of PAEC were obtained on four different days during a one-month period in Laboratory 25 of the USAF OEHL building. (Table 7). These values probably represent the limit of reliable measurement using the apparatus and method.

Measurements of PAEC were made on San Antonio House Number 1, both with windows closed and with windows open for several hours before measurement (Table 8). Values ranged from 0.00056 to 0.0034 WL. Working levels measured with windows closed were significantly higher than those with windows open (mean = 0.0033 WL vs. 0.0013 WL).

Table 7.

Potential Alpha Energy Concentrations, Laboratory 25

<u>Date</u>	<u>Time</u>	<u>PAEC, WL</u>
7/9/85	Morning	0.00032
7/9/85	Afternoon	0.00056
7/15/85	Afternoon	0.00037
7/29/85	Afternoon	0.00057
7/29/85	Afternoon	0.00024
8/9/85	Morning	0.00034
8/9/85	Morning	0.00027

Average PAEC = 0.00038 WL; Standard Deviation = 0.00013 WL

Table 8.

Potential Alpha Energy Concentrations, San Antonio House No. 1

<u>Date</u>	<u>Time</u>	<u>Windows</u>	<u>PAEC, WL</u>
7/12/85	1916	Open	0.00056
7/12/85	1954	Open	0.0017
7/12/85	2032	Open	0.0017
Mean = 0.0013 WL			
7/14/85	1650	Closed	0.0031
7/14/85	1727	Closed	0.0033
7/14/85	1803	Closed	0.0034

Mean = 0.0033 WL

Arithmetic Mean for all Measurements = 0.0023 WL

The measurements reported here indicate that the radon daughter sampling kit will yield reliable results in the field when used to measure PAEC's which are high enough to be of concern (above 0.01 WL).

V. RECOMMENDATIONS

Portable sampling kits for convenient and reliable field measurement of radon and its daughters have been developed and tested. These kits should now be used to sample suspected USAF locations to determine if indoor decay product exposures are elevated to a point where they could pose a hazard to the occupants.

Time did not permit accomplishment of one important task: modification of the filter collection systems to permit determination of the unattached fraction of daughters as well as their total concentrations. This can be done by fixing a 60-mesh wire screen to one of the filters so as to remove unattached daughters before they reach the filter. Simultaneous sampling with a modified and an unmodified filter will then allow determination of the unattached fraction of radon daughters. This modification should be made to the apparatus described above, and the apparatus should be tested in the laboratory and in the field.

Finally, since both methods described in this report are limited to grab sampling, i.e., determination of instantaneous concentrations, some thought should be given to development of techniques for continuous field monitoring. The author of this report has submitted a proposal to the MINI Grant Program describing a plan which would make use of portable, continuous-monitoring instruments to investigate the distribution, range, and characteristics of indoor air pollution due to radon-222 decay daughters. Such an approach could be used to develop a capability for continuous monitoring of suspected and hazardous sites by the USAF Occupational and Environmental Health Laboratory.

REFERENCES

1. Hillman, B., Environmental Science and Technology, Volume 17, 1983, pp. 469A-472A.
2. National Council on Radiation Protection and Measurements, Exposure From the Uranium Series With Emphasis on Radon and its Daughters, NCRP Report No. 77, Washington, D.C., National Council on Radiation Protection and Measurements, 1984.
3. Nero, A.V., "Indoor Radiation Exposure from ^{222}Rn and its Daughters: A View of the Issue," Health Physics, Volume 45, 1985, pp. 277-288.
4. Lundin, F.E., J.K. Wagoner, and V.E. Archer, Radon Daughter Exposure and Respiratory Quantitative and Temporal Aspects, Washington, D.C., United States Public Health Service, 1971.
5. Chamberlain, A.C., and E.D. Dyson, British Journal of Radiobiology, Volume 29, 1956, p. 317.
6. Gesell, T.F., "Background Atmospheric ^{222}Rn Concentrations Outdoors and Indoors: A Review," Health Physics, Volume 45, 1983, pp. 289-302.
7. Lucas, Henry F., "Improved Low-Level Alpha-Scintillation Counter for Radon," Review of Scientific Instruments, Volume 28, 1957, pp. 680-683.
8. Jonassen, Niels and W.E. Clements, "Determination of Radon-222 Concentrations by an Integrated Count Method," Health Physics, Volume 27, 1974, pp. 347-351.

9. National Council on Radiation Protection and Measurements, A Handbook of Radioactivity Measurements Procedures, NCRP Report No. 58, Washington, D.C., National Council on Radiation Protection and Measurements, 1978, p. 276.
10. Thomas, Jess W., "Measurement of Radon Daughters in Air," Health Physics, Volume 23, 1972, pp. 783-789.
11. Thomas, Jess W., "Measurement of Radon Daughters in Air by Alpha Counting of Air Filters," in H.L. Volchok and G. de Planque, EML Procedures Manual, 26th Edition, New York, N.Y., Environmental Measurements Laboratory, 1983.
12. Evans, R.D., "Engineer's Guide to the Elementary Behavior of Radon Daughters," Health Physics, Volume 17, 1969, p. 229.
13. Hinds, William C., Aerosol Technology, New York, N.Y., John Wiley and Sons, 1982, p. 32.

1985 USAF-UES SUMMER FACULTY RESEARCH PROGRAM

Sponsored by the

AIR FORCE OFFICE OF SCIENTIFIC RESEARCH

Conducted by the

UNIVERSAL ENERGY SYSTEMS, INC

FINAL REPORT

Reliability of Systems with Markov Transfer of Control

Prepared by:	Kyle Siegrist
Academic Rank:	Assistant Professor
Department and University:	Department of Mathematics and Statistics University of Alabama in Huntsville Huntsville, AL 35899
Research Location:	Rome Air Development Center Systems Reliability and Engineering Branch Reliability and Maintainability Techniques Section Griffiss AFB, NY 13441
USAF Research:	Eugene Fiorentino
Date:	August 19, 1985
Contract No:	F49620-85-C-0013

Reliability of Systems with Markov Transfer of Control

Kyle Siegrist

ABSTRACT

This report concerns systems (primarily software systems) which can be decomposed into a finite number of modules. It is assumed that control of the system is transferred among the modules according to a Markov process. Each module has an associated reliability which gives the probability that the module will operate successfully when called and will correctly transfer control when finished. The system will thus either fail or eventually complete its task successfully and enter a terminal state. The reliability of the system is studied in terms of the module reliabilities and the transition probabilities. Improved methods of predicting system reliability, allocating module reliability, and determining module sensitivity are developed. Special branching and sequential systems are studied in detail. Modeling questions are explored and recommendations made.

ACKNOWLEDGEMENTS

I am grateful to the Air Force Systems Command, the Air Force Office of Scientific Research and the Rome Air Development Center for the opportunity to participate in the 1985 Summer Faculty Research Program. I would especially like to thank my RADC effort focal point, Gene Fiorentino for his help in making the summer program a successful and rewarding experience for me and for many stimulating discussions on software reliability. Finally, I would like to thank my new friends at RADC for making the summer so enjoyable.

I Introduction

This report describes research that was conducted as a part of the 1985 AFOSR/UES Summer Faculty Research Program at Rome Air Development Center, Griffiss AFB, NY. The author is currently an assistant professor in the Department of Mathematics and Statistics at the University of Alabama in Huntsville. He received the Ph.D. degree in Applied Mathematics from the Georgia Institute of Technology in 1979. His main research areas are probability, statistics, and stochastic processes, particularly Markov processes. He has worked in the area of mathematical reliability theory since 1982. During the summers of 1982 and 1983, he participated in the NASA/ASEE Summer Faculty Fellowship Program at Marshall Space Flight Center, working on reliability growth models.

The purpose of the research was the study of certain software reliability models. It is clear that software reliability has become an essential concern. Software continues to increase in complexity and importance in both military and civilian applications as computer components are increasingly integrated with hardware components and networked with each other. The development of good mathematical and statistical models of software reliability is therefore of paramount importance and is receiving much attention. Reference [1] is a good survey of the subject.

The primary model studied here is a "modular" model first proposed by Cheung [2] and later used by Soistman and Ragsdale [3]. The model assumes that the software can be decomposed into well defined, functionally independent modules in much the same way that hardware systems can be decomposed into components. This modular approach is reasonable for large, complex computer programs which indeed usually do have a number of functionally independent parts which are usually written separately and then integrated. The model further assumes that the control of the program is transferred among the various modules according to a Markov process. This means, roughly, that given the module that is active at a particular time, the future behavior of the

program is independent of the past behavior. Also, each module has an associated reliability that gives the probability that the module will operate successfully when called and will correctly transfer control when finished. The concern of the model is the study of system reliability (the probability that the entire program will operate correctly) in terms of the module reliabilities and the probabilities that describe the transfer of control. The model will be described more precisely in section III.

II Objectives

Generally, the goal of the research was to find ways to improve and extend the model described above. It was hoped that the model could be developed to the point that it could be used early in the design stage of the software, after the modules are identified but well before final integration. In that way, system reliability could be predicted early, design changes which enhance system reliability could be made, modules which have critical importance to system reliability could be identified, and so forth. Some specific goals of the research were as follows:

(a) Predicting system reliability. The usual method of computing system reliability in this model involves the inversion of a matrix whose size is equal to the number of modules. For a large system, this method is computationally difficult and also gives little insight. It was hoped that there might be ways of improving the computation of system reliability by reducing the number of modules or by developing shortcuts that take advantage of structural properties of the particular system.

(b) Allocating module reliabilities. Another goal was to develop methods of estimating module reliabilities in order to meet a given system reliability demand (note that this is essentially the inverse of the problem discussed in (a)). A solution of this problem would be helpful in determining the extent to which the modules must be debugged or determining if the reliability demands on the modules are so severe that redesign is called for.

(c) Determining module sensitivity. The sensitivity of a module is a measure of how inaccuracies in the reliability of a module effect the reliability measure of the system. A measure of sensitivity is thus important for determining the quality of the statistical estimates discussed in (a) and (b). Indeed, if the modules are too sensitive, statistical estimates of system reliability have very little value and may even be misleading. A method of computing sensitivity was developed in [2] but it involves complicated matrix methods and gives little insight. It was hoped that a better method could be developed. It was also hoped that a measure of "inherent" sensitivity could be found which could be used to estimate module sensitivity just from the structure of the software and the transition probabilities, before the module reliabilities are estimated.

(d) Studying special structures. Early during the research effort it became apparent that certain types of software systems may be very common. It was hoped that these special software structures could be isolated and studied in detail in terms of (a), (b), and (c) above.

(e) Improving modeling methods. As with any complicated mathematical model, there were questions concerning the applicability of the model and the relationship between this model and other similar models. There were also questions about the validity of the assumptions and the robustness of the model to deviations from the assumptions. Finally there were general philosophical questions about the meaning of software reliability and the best way to measure it.

Most of the objectives have been met and the results are described in the following sections. Some goals were not completely realized so there is room for further research.

It was realized early during the research that the model might apply to systems other than just software systems. Consequently, in the following sections, somewhat abstract terminology is used ("system" instead of "software," "state" instead of "module," etc.). It should be kept in mind however that the primary application intended is the software application.

III The Markov Chain Model

Suppose that a system has a finite number of possible states. It is assumed that the system changes state in such a way that the Markov property is satisfied. This means that if the system is in a given state, then the next state of the system depends probabilistically only on the given state and is otherwise independent of the past history of the system. Thus, the successive states of the system form a Markov chain. An excellent reference on the theory of Markov chains is the book by Cinlar [4].

It is assumed that, ideally, the system will eventually finish its task and enter a terminal state. The terminal state will be denoted by T and will be an absorbing state of the Markov chain. The other (transient) states of the system will be denoted by $1, 2, \dots, n$. Usually the system will have a designated initial state which will usually be state 1 in our notation.

Mathematically, the dynamics of the ideal system are determined by the (one step) transition matrix P . That is, $P(i,j)$ is the conditional probability that the next state of the system will be j given that the current state is i . P is a stochastic matrix; the entries are nonnegative and each row sums to 1. Note that since T is absorbing, $P(T,T) = 1$. All other states eventually lead to T .

Next it is assumed that each of the transient states $1, 2, \dots, n$ is subject to failure. Specifically, it is assumed that whenever the system is in state i , it has probability $r(i)$ of not failing and successfully entering the next state as described above. Equivalently, the system has probability $1-r(i)$ of failing each time it enters state i . Mathematically, the imperfect system is modeled by adding an absorbing state F (failure) and by modifying the transition probabilities appropriately. Specifically, the imperfect system is described by a Markov chain with states $1, 2, \dots, n, T, F$ and one step transition probability matrix \hat{P} given as follows:

$$\begin{aligned}\hat{P}(i,j) &= r(i)P(i,j) \text{ for } i = 1, \dots, n \text{ and } j = 1, \dots, n, T; \\ \hat{P}(i,F) &= 1-r(i) \text{ for } i = 1, \dots, n; \\ \hat{P}(T,T) &= 1, \hat{P}(F,F) = 1.\end{aligned}$$

Thus, the dynamics of the imperfect system are completely described by the state reliability function r and the ideal transition matrix P , since this is equivalent to specifying the transition matrix \hat{P} for the imperfect system.

Indeed, a convenient way to represent the system graphically is by means of the directed transition graph of the ideal system. An edge from i to j is drawn in the graph if and only if $P(i, j) > 0$ and then this edge is labeled with the transition probability $P(i, j)$. Each node (state) i of the graph is labeled with its reliability $r(i)$. This graphical representation shows the structure of the system much more clearly than the corresponding transition matrix. This is particularly important in certain applications such as software systems in which the ideal transition graph corresponds, more or less, to the flow diagram of the system.

Note again that this model is based on two key assumptions. First, the system changes state according to a Markov process. Second, the system eventually either enters a terminal state (representing successful completion of its task) or fails. Thus, the corresponding Markov chain is eventually either absorbed into T or into F . The main quantity of interest is the probability that the chain is absorbed into T (i.e., the system reliability). The fact that the system is modeled by a discrete time Markov process (i.e., a Markov chain) means that, essentially, time has been abstracted out of the model. This is possible because the quantity of interest is the probability of success as opposed to, say, the mean time until failure or the probability that the system runs for a specified period of time.

As noted earlier, the model described here might apply to a software system where the states represent functionally independent modules of the software. The model might apply to a hardware system where the states represent components of the hardware and control is transferred among the components. The model might well apply to systems made up of both hardware and software components. The model apparently was first used in [2] in the software context. In this reference, it is assumed that states $1, \dots, n-1$ lead to state n and only state n leads directly to the terminal state. Also, transitions from a state to

itself are forbidden. While no real generality is lost by these assumptions, no benefit is gained either and indeed the model is unnecessarily complicated by them.

It is very important to realize the limitations of this model. First, if the Markov property is not satisfied then the model does not apply. The reasons are simple and profound: in the absence of the Markov property, the one step transition probabilities do not determine the dynamics of the system and the analytical methods based on the Markov property are not valid. Second, the model should not be used if the main quantity of interest is the mean time until failure or the probability that system runs for a specified length of time. The model should not be used for systems in which there is no definite terminal state corresponding to success, i.e., for systems which run more or less continuously (until they fail). For such systems, more appropriate models are those that allow a random time spent in each state in addition to the random transitions among the states. A continuous time Markov process model of this type has been considered by Laprie [5]. A more complete and versatile analysis in a semi Markov setting has been given by Littlewood [6]. Finally, this Markov model should not be confused with traditional Markov reliability models in which the states represent various configurations of working and failed components.

IV System Reliability

For each transient state $i = 1, 2, \dots, n$ let $R(i)$ denote the probability that the Markov chain for the imperfect system, starting in state i , is eventually absorbed into T (i.e., the probability that the system eventually completes its task successfully). The function R so obtained is the system reliability function.

The function R is defined in terms of absorption probabilities for a Markov chain and hence there are standard ways of computing R which can be found in any standard text on stochastic processes (for example, [4]). The most common way is as follows: Let \hat{Q} denote the restriction of the transition matrix \hat{P} of the imperfect system to the transient states $1, 2, \dots, n$. Note that $\hat{Q}(i, j) = r(i)Q(i, j)$ where Q is the restriction of the transition matrix P of the ideal system to the

transient states. The matrix

$$\sum_{k=0}^{\infty} \hat{Q}^k = (I - \hat{Q})^{-1} \quad (1)$$

is called the potential matrix of the imperfect system; its (i, j) value gives the expected number of visits to state j by the imperfect system, starting in state i . Of course, similar remarks apply to the potential matrix of the ideal system, obtained by replacing \hat{Q} with Q in (1). For each transient state i let $f(i) = \hat{P}(i, T) = r(i)P(i, T)$ denote the probability of going to the terminal state T from state i in one step for the imperfect system. Then using the notation of matrix multiplication,

$$R = (I - \hat{Q})^{-1} f = \sum_{k=0}^{\infty} \hat{Q}^k f \quad (2)$$

There are simple, intuitive arguments for these formulas. In the expression $(I - \hat{Q})^{-1} f$, the expected number of visits to a given state j (starting in a designated initial state) is multiplied by the probability of success in one step from state j . These products are then summed over all j to give system reliability. In the expression $\sum_k \hat{Q}^k f$ the probability of going to a given state j in exactly k steps (from a designated initial state) is multiplied by the probability of success in one step from state j . These products are then summed over all j and k to give system reliability. Rigorous derivations can be found in [4].

Equation (2) is the basis for computing system reliability in [2] and [3]. While this equation is conceptually very simple, it may not always be the best way to compute R . Another method for computing R is based on a system of linear equations:

$$R(i) = f(i) + \sum_{j=1}^n \hat{Q}(i, j) R(j); \quad i = 1, 2, \dots, n. \quad (3)$$

In matrix form, equation (3) is simply $R = f + \hat{Q}R$ so it is clear that (3) is equivalent to (2). However it may be easier in some cases to solve (3) directly rather than use the matrix inversion of (2). Equation (3) also points out the fact that it is important to consider quantities in a Markov chain (such as R) as functions of an arbitrary initial state even if the real world system has a designated initial state. The reason is basic to the analysis of Markov chains: as soon

as the system makes a transition, it forgets about the past and behaves just like a new system starting in the new state. Equation (3) can also be found in standard texts.

A new method of computing system reliability will now be given. Suppose that the initial state is 1. Let i be any specified transient state (i may be 1). Then

$$R(1) = A(i) + B(i)C(i)/[1-D(i)] \quad (4)$$

where $A(i)$ is the probability, starting in the initial state, of reaching the terminal state without going through state i ; $B(i)$ is the probability, starting in the initial state, of eventually reaching state i ; $C(i)$ is the probability, starting in state i , of reaching the terminal state T without returning to state i ; and $D(i)$ is the probability, starting in i , of eventually returning to state i . Each of these is defined in terms of the imperfect system. Schematically, equation (4) is represented in figure (1) below where the wavy lines indicate that these are not one step transitions. Indeed many transitions and many paths may be involved.

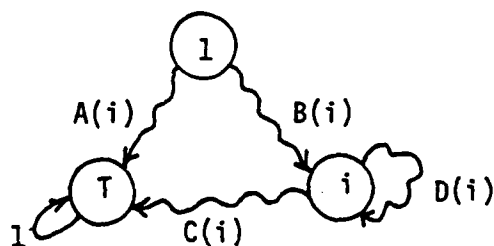


Figure 1
Schematic representation of equation (4)

The derivation of equation (4) is based on straightforward conditional probability arguments that consider the successive visits to state i . Incidentally, $B(i)/[1-D(i)]$ is the same as $(I-Q)^{-1}(1,i)$, namely the expected number of visits to state i starting in state 1 for the imperfect system.

This method of computing system reliability is important for two reasons. First, it may turn out that for some state i (such as a state which acts as a central control) the quantities $A(i)$, $B(i)$, $C(i)$, and $D(i)$ are relatively easy to compute. Thus, (4) is computationally

important. Second, of the four quantities in (4), only two, $C(i)$ and $D(i)$, depend on $r(i)$, the reliability of state i . Indeed, $C(i) = r(i)C'(i)$ and $D(i) = r(i)D'(i)$ where $C'(i)$ and $D'(i)$ do not depend on $r(i)$. Therefore (4) can be written in the form

$$R(1) = A(i) + r(i)B(i)C'(i)/[1-r(i)D'(i)] \quad (5)$$

where $A(i)$, $B(i)$, $C'(i)$, and $D'(i)$ are independent of $r(i)$. Thus, equation (5) allows us to isolate the effect of the reliability of state i on total system reliability. This fact will be crucial to the sensitivity and allocation problems to be considered later.

V Conjugate Systems

There is a slight enhancement of the method of using equation (4) to compute system reliability that is sometimes useful. Consider the graphical representation of the imperfect system described in section III. Suppose that 1 is the initial state and that some transient state i has been fixed as in the setting of equation (4). The conjugate system (relative to state i) is obtained as follows: Any edge of the form (j,i) in the original system is replaced by the edge (j,T) ; the transition probability on that edge remains the same. Conversely, any edge of the form (j,T) in the original system is replaced by the edge (j,i) ; the transition probability on that edge remains the same. All state reliabilities remain the same. Thus, given an imperfect system and a designated state i , a new imperfect system (the conjugate system) can be obtained.

In equation (4) it is clear that quantities $A(i)$ and $B(i)$ and quantities $D(i)$ and $C(i)$ have complementary meanings relative to the system and its conjugate. That is, the reliability $R^*(1)$ of the conjugate system is

$$R^*(1) = B(i) + A(i)D(i)/[1-C(i)] \quad (6)$$

Equation (6) is important because some of the quantities may be easier to compute for the original system and others for the conjugate system. Stated another way, if equation (4) is used to compute the reliability of a system, then the reliability of the conjugate system can be

obtained without any additional work. This conjugate idea will be used in sections IX and X.

VI State Reduction

Computing the system reliability using the methods of Section IV may be a difficult problem if the system has a large number of states. A natural question to ask is when can a set of states in an imperfect system be combined into a single new state in a new, reduced model. Of course, such state reduction must be done with two requirements in mind: First, the Markov property must still hold and second, the system reliability must be preserved by the state reduction.

Suppose that we have an imperfect system with transition probability matrix P as described in section III. Suppose that state 1 is designated as the initial state. Let E be a set of transient states not including state 1. The set I of initial states of set E is defined as follows: $I = \{i \in E: \hat{P}(k,i) > 0 \text{ for some } k \in E\}$. That is, I is the subset of states of E that can be reached in one step from some state not in E . For i in I and j not in E let $H(i,j)$ denote the probability that the Markov chain for the imperfect system, starting in i , first leaves E into state j .

The key assumption of this section is that $H(i,j)$ is independent of i in I ; the common value will be denoted $H(j)$.

A reduced system whose states are the states not in E , together with E as a super state, can now be defined. The transition matrix \tilde{P} of this new imperfect system is given as follows:

$$\begin{aligned}\tilde{P}(i,j) &= \hat{P}(i,j) \text{ for } i, j \text{ not in } E; \\ \tilde{P}(i,E) &= \sum_{j \in E} \hat{P}(i,j) \text{ for } i \text{ not in } E; \\ \tilde{P}(E,j) &= H(j) \text{ for } j \text{ not in } E; \\ \tilde{P}(E,E) &= 0.\end{aligned}$$

It is easy to see that \tilde{P} defined above is a legitimate transition probability matrix. Moreover, because of the key assumption, the corresponding reduced system satisfies the Markov property and has the same reliability as the original system.

Thus, to compute the system reliability by the method of state reduction, we proceed as follows: First, find a set of states E for which the key assumption is satisfied. Next compute $H(j)$ for each j not in E . Note that computing $H(j)$ is mathematically a problem which is similar to computing the reliability of a system with state space E and thus the methods of section IV (or simple modifications of them) can be used. Next, compute the transition probability matrix P of the reduced system as described above. Finally, compute the reliability of the reduced system using the methods of section IV.

The drawback to this method, of course, is the first step, namely finding a set of states E for which the key assumption is satisfied. In general, there is no simple way to find such a set or even to insure that such a set exists. There is, however, a type of set for which the key assumption is always satisfied namely a set E for which there is only one entry path in the transition graph (for then set I will consist of a single state).

The method of state reduction will be used in sections IX and X.

VII Sensitivity

Consider an imperfect system with ideal transition matrix P and state reliability function r as described in section III. Suppose that state 1 is designated as the initial state so that the system reliability is $R(1)$ which can be computed by the methods of section IV.

For any transient state i , the sensitivity of state i is defined to be $\partial R(1)/\partial r(i)$, the partial derivative of system reliability with respect to the reliability of state i . This quantity is a measure of how sensitive system reliability $R(1)$ is to small changes in the reliability $r(i)$ of state i . For example, if $\partial R(1)/\partial r(i) = 5$ then small changes in $r(i)$ are magnified approximately by a factor of 5 in $R(1)$. The result is only approximate because in general $R(1)$ will be a highly nonlinear function of $r(i)$. Note also that in general, the sensitivity $\partial R(1)/\partial r(i)$ of state i is a function of all the state reliabilities as well as, of course, the ideal transition probabilities.

In reference [2], equation (3) and various determinant expansions were used to obtain a formula for the sensitivity of a state. This method is computationally complicated and provides little insight. In this section equation (5) will be used to study sensitivity. From (5), the sensitivity of state i is

$$\partial R(1)/\partial r(i) = B(i)C'(i)/[1-r(i)D'(i)]^2 = B(i)C'(i)/[1-D(i)]^2 \quad (7)$$

where $B(i)$, $C'(i)$, $D'(i)$, and $D(i)$ are defined in section IV. Note that if equation (5) is used to compute system reliability using some specified state i , the equation (7) can be used to obtain the sensitivity of that particular state without any additional work.

The quantity $B(i)/[1-D(i)]$ is the expected number of visits to state i , starting in state 1 for the imperfect system while $1/[1-D(i)]$ is the expected number of visits to i starting in i . Therefore, if a state is visited a large number of times on average then the system reliability will be very sensitive to inaccuracies in the reliability of that state. Thus we must be very careful in our estimates of the reliability of such a state or the computed system reliability could be extremely misleading.

As noted in section IV, the terms $B(i)$, $C(i)$, and $D(i)$ will in general be complicated functions of the state reliabilities and the ideal transition probabilities. It would be very helpful to have an inherent measure of the sensitivity of the states that could be obtained from the ideal transition probabilities alone. Such a sensitivity measure could be used before the state reliabilities are measured. Since, hopefully, we anticipate that the state reliabilities will be near 1, a natural measure of the inherent sensitivity of state i is $\partial R(1)/\partial r(i)$ evaluated with $r(j) = 1$ for all transient states j . Note that when all the state reliability are set equal to 1, $B(i)$ becomes $b(i)$, $C'(i)$ becomes $c(i)$, and $D(i)$ becomes $d(i)$ where $b(i)$, $c(i)$, and $d(i)$ have the same meanings as given in section IV except relative to the ideal system rather than the imperfect system. But for the ideal system, $c(i) = 1-d(i)$ (if the ideal system does not return to state i , then it must be absorbed into the terminal state T). Therefore, substituting into (7) we see that the inherent sensitivity (denoted $S(i)$) is

$$S(i) = b(i)/[1-d(i)]. \quad (8)$$

However, the expression in (8) is merely the expected number of visits to state i , starting in the initial state, for the ideal system. Recall that this quantity can also be written $(I-Q)(1,i)$ where Q is the restriction of the ideal transition matrix P to the transient states.

In summary, the expected number of visits to state i by the ideal system is a measure of the inherent sensitivity of state i . It will be near the true sensitivity of state i for an imperfect system in which all of the state reliabilities are near 1. Moreover, it is easy to see that $B(i) \leq b(i)$, $C(i) \leq c(i)$, and $D(i) \leq d(i)$. Therefore a comparison of equations (7) and (8) shows that the true sensitivity of state i is always less than or equal to the inherent sensitivity of state i . Stated another way, the inherent sensitivity gives an upper bound on the true sensitivity. Finally, note that a ranking of the states according to inherent sensitivity will be the same as a ranking of the states according to true sensitivity if the state reliabilities are sufficiently close to 1. Examples can be constructed which show that this will not necessarily be true if the state reliabilities are not near 1.

VIII Allocation

In this section we consider the problem of how to allocate state reliabilities in order to meet a given system reliability constraint. Specifically, consider an imperfect system with ideal transition matrix P and state reliability function r . Suppose that state 1 is the initial state so that the system reliability is $R(1)$. Suppose finally that P and $R(1)$ are given. We wish to determine $r(i)$ for each transient state i .

It is clear from the analysis in section IV that the problem, as stated, does not have a unique solution. Indeed there will be infinitely many ways of allocating state reliabilities to meet a system reliability constraint. Still it would be useful to have a simple method that would give a rough estimate of the reliability $r(i)$ of a given state i that might be required for a given system reliability

$R(1)$. For example, if we want $R(1)$ to be 0.9, does the reliability of state i need to be on the order of 0.99 or 0.9999?

Consider a fixed transient state i . Solving for $r(i)$ in equation (5) gives

$$r(i) = [R(1) - A(i)] / [B(i)C'(i) + D'(i)[R(1) - A(i)]] \quad (9)$$

If the system reliability $R(1)$ is specified, if the ideal transition probabilities are known, and if the state reliabilities for the states other than i are known, then equation (9) can be used to determine the reliability of state i .

As noted above, $A(i)$, $B(i)$, $C'(i)$, and $D'(i)$ depend on the ideal transition probabilities and the reliabilities of the states other than i . If none of the state reliabilities are known, which is the primary case we want to consider, then the reliabilities of the states other than i can be set equal to 1 in equation (9) to give a rough estimate of the reliability needed for state i . Then $A(i)$ would become $a(i)$, $B(i)$ would become $b(i)$, $C'(i)$ would become $c(i)$, and $D'(i)$ would become $d(i)$ where we recall that $a(i)$, $b(i)$, $c(i)$, and $d(i)$ have the meanings given in section IV except for the ideal system rather than the imperfect system. But $b(i) = 1 - a(i)$ and $d(i) = 1 - c(i)$. Therefore substituting into (9) gives

$$r(i) = [R(1) - a(i)] / \{ [1 - a(i)]c(i) + [1 - c(i)][R(1) - a(i)] \} \quad (10)$$

Thus equation (10) can be used to determine the reliability $r(i)$ needed for a given state i in order to achieve a given system reliability $R(1)$ assuming that the other states are perfect (i.e., have reliability 1). Since, of course, the other states will not in general be perfect, equation (10) should be viewed as a rough estimate only. The true reliability needed for state i will be somewhat higher.

IX Branching Systems

In this and the following section, two special types of systems will be considered. These systems not only provide examples for the methods of sections IV-VIII but also are of sufficient generality and

richness of structure to be interesting in their own right.

In this section, a general branching system is studied which has the ideal transition graph given below:

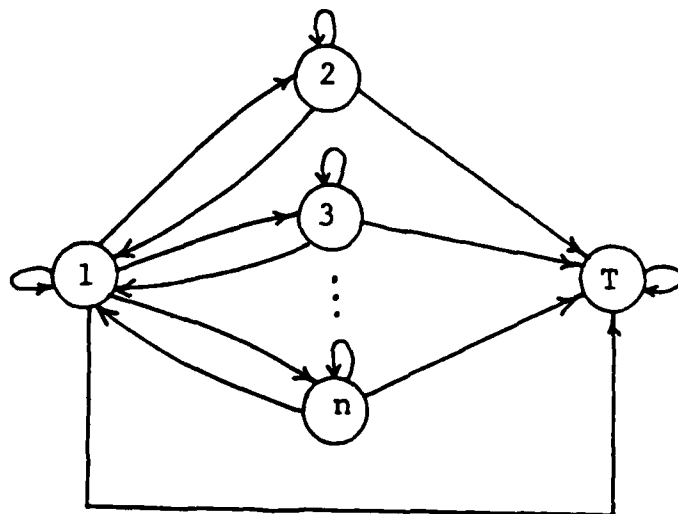


Figure 2
Branching System

In this system, state 1 acts a central controller which may pass control to any of the states 2, ..., n or back to itself or to the terminal state. Each of the branch states 2, ..., n can pass control back to itself, back to the control state 1, or to the terminal state. We assume that the ideal transition matrix P and the state reliability function r are given; they have not been shown in figure 2 in order to keep the graph uncluttered. State 1 is designated as the initial state.

Equation (4), with $i = 1$, will be used to compute the system reliability $R(1)$ explicitly. The conjugate system method of section V will also be used. Note first that since $i = 1$, $A(1) = 0$ and $B(1) = 1$. On the other hand, in order to reach T from state 1 without returning to state 1, the system must either go directly to T or to some branch state j , stay at the branch state for some k steps and then go to T . It therefore follows that

$$\begin{aligned}
 C(1) &= r(1)P(1,T) + \sum_{j=2}^n r(1)P(1,j) \sum_{k=0}^{\infty} [r(j)P(j,j)]^k [r(j)P(j,T)] \\
 &= r(1)P(1,T) + \sum_{j=2}^n r(1)P(1,j)r(j)P(j,T)/[1-r(j)P(j,j)] \quad (11)
 \end{aligned}$$

Next note that the conjugate system (relative to state 1) has exactly the same structure as the original system. The only difference between the original system and the conjugate system is that the roles of $P(j,1)$ and $P(j,T)$ are reversed. It therefore follows, without any additional work, that

$$D(1) = r(1)P(1,1) + \sum_{j=2}^n r(1)P(1,j)r(j)P(j,1)/[1-r(j)P(j,j)] \quad (12)$$

Therefore, substituting into (5), the system reliability is

$$R(1) = C(1)/[1-D(1)] \quad (13)$$

where $C(1)$ and $D(1)$ are given in equations (11) and (12) respectively. It seems unlikely that the matrix inversion technique of equation (2) could produce this explicit result.

Note that the general system includes a number of important special cases, obtained by eliminating certain paths in the general graph of figure 2. Examples are simple branching systems with no cycles ($P(i,i) = 0$ and $P(i,1) = 0$ for each i), branching systems with no one step cycles ($P(i,i) = 0$ for each i), etc.

A special example motivated by an "assault breaker" software system discussed in [3] will now be considered. The ideal transition graph is given in figure 3. State 1 is the initial state, state 2 is an executive control state, state 3 is an autopilot state, and states 4 through 9 perform such functions as flight control, dispensing munitions, etc.

Note that the system does not exactly fit the general branching system of figure 2. However states 3 through 9 form a simple branching system and therefore we can use the results above together with the state reduction technique in section VI to obtain an explicit formula for system reliability. Let $E = \{3, 4, 5, 6, 7, 8, 9\}$. Note that the key assumption in section VI is satisfied since state 3 has only one entry path. The reduced system has the ideal transition graph given in figure 4.

Using the results for branching systems above and the formulas in section VI, the transition probabilities for the reduced imperfect

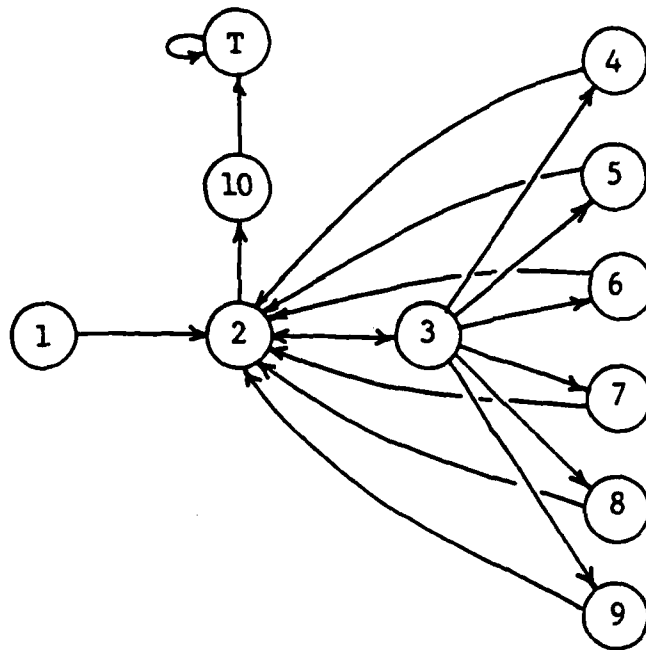


Figure 3
Assault Breaker System

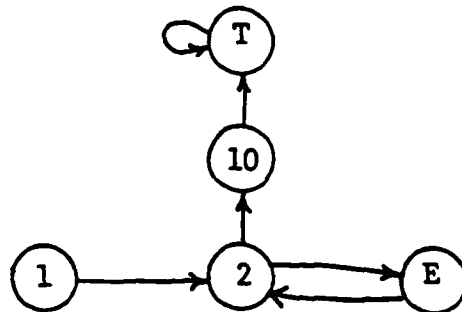


Figure 4
Reduced System

system are

$$\tilde{P}(1,2) = r(1), \quad \tilde{P}(2,E) = r(2)P(2,3), \quad \tilde{P}(2,10) = r(2)P(2,10),$$

$$\tilde{P}(E,2) = r(3) \sum_{j=4}^9 P(3,j)r(j).$$

Since the reduced system is so simple, its reliability can be computed easily. Moreover, the reliability of the reduced system is the same as the reliability of the original system. The result is

$$R(1) = r(1)r(2)P(2,10)r(10)/[1 - r(2)P(2,3)r(3) \sum_{j=4}^9 P(3,j)r(j)] \quad (14)$$

In [3], the parameter values given are $r(1) = 0.999$, $r(2) = 0.996$, $r(3) = 0.990$, $r(4) = 0.987$, $r(5) = 0.998$, $r(6) = 0.982$, $r(7) = 0.992$, $r(8) = 0.999$, $r(9) = 0.992$, $r(10) = 0.999$, $P(2,3) = 0.8$, $P(2,10) = 0.2$, $P(3,4) = 0.35$, $P(3,5) = 0.15$, $P(3,6) = 0.05$, $P(3,7) = 0.15$, $P(3,8) =$

0.05, $P(3,9) = 0.25$. Substituting into (14) gives a system reliability $R(1) = 0.911$ as was obtained in [3].

The sensitivity analysis of section VII will now be applied to the assault breaker system. Recall that the inherent sensitivity $S(i)$ of state i is the expected number of visits to state i by the ideal system and can be computed using equation (8). Alternately, $S(i)$ is the partial derivative of $R(1)$ with respect to $r(i)$ evaluated with each state reliability set equal to 1. Hence $S(i)$ can be computed using (14) and standard calculus. The results are

$$S(1) = 1, S(2) = 1/[1-P(2,3)], S(3) = P(2,3)/[1-P(2,3)],$$

$$S(j) = P(2,3)P(3,j)/[1-P(2,3)] \text{ for } j = 4, \dots, 9.$$

Thus, it is clear that state 2 is the most sensitive, regardless of the parameter values. Similarly, state 3 is more sensitive than states 4 through 9. The sensitivity rankings of the other states depend on the parameter values. For the parameter values given above, $S(1) = 1$, $S(2) = 5$, $S(3) = 4$, $S(4) = 1.4$, $S(5) = 0.6$, $S(6) = 0.2$, $S(7) = 0.6$, $S(8) = 0.2$, $S(9) = 1$, $s(10) = 1$.

On the other hand, the true sensitivity of state i , $\partial R(1)/\partial r(i)$, can be computed using (7) or using (14) and standard calculus. The explicit results are straightforward but messy and will not be presented here. However, by way of example, using the parameter values given above yields $\partial R(1)/\partial r(1) = 0.912$ and $\partial R(1)/\partial r(2) = 4.190$. As noted in section VII, the inherent sensitivities are always greater than or equal to the true ones.

The sensitivity analysis shows that system reliability will be very sensitive to changes in the reliability of state 2. For example, if $r(2)$ is decreased from 0.996 to 0.950 (all other parameter values the same), then using (14), $R(1)$ decreases from 0.911 to 0.745.

The use of this Markov chain model for the assault breaker system in [3] can be criticized on several counts. First, state 10 and the terminal state have no physical meaning but were merely added in an ad hoc manner apparently because the real system has no natural terminal state. In [3] it is stated that the creation of this fictitious path

will have a negligible effect on the analysis because the path is executed only once. This is simply not true. Indeed a slight change in the placement of the terminal state in the transition graph or of the transition probabilities assigned to it, can have a devastating, orders-of-magnitude effect on system reliability. Moreover, system reliability in this model is defined as the probability of reaching the terminal state without failing. If the terminal state has no real meaning, then system reliability defined in terms of it has no meaning. Finally, the Markov assumption which is central to the model was not discussed in [3]. The Markov property would imply, for example, that each time the system is in the autopilot state, then the system will go into the munitions dispensing state with probability 0.05, regardless of the past history of the system. It is hard to believe that this could be true.

X Sequential Systems

In this section, a general sequential type of system will be studied which has the ideal transition graph given below:

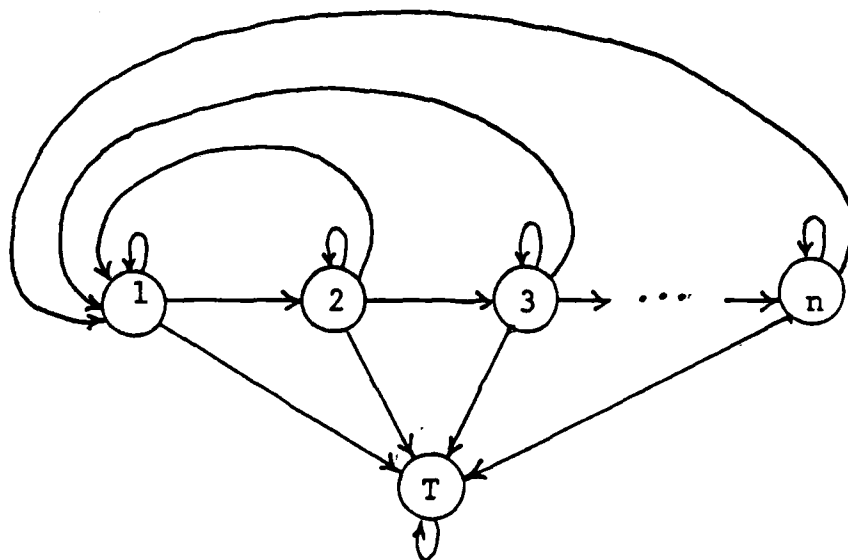


Figure 5
Sequential System

State 1 is designated as the initial state and we assume that the ideal transition matrix P and the state reliability function r are

given. Note that control tends to pass sequentially from state 1 to state 2, etc. except that, in each state, control can return to that state, to state 1 or go to the terminal state.

The system reliability $R(1)$ can be computed explicitly using the methods of sections IV, V, and VI, just as was done for branching systems in the last section. The details will be omitted. The result is

$$R(1) = C(1)/[1-D(1)] \text{ where} \quad (15)$$

$$C(1) = \sum_{k=1}^n \left\{ \prod_{j=1}^{k-1} r(j)P(j, j+1)/[1-r(j)P(j, j)] \right\} r(k)P(k, T)/[1-r(k)P(k, k)],$$

$$D(1) = \sum_{k=1}^n \left\{ \prod_{j=1}^{k-1} r(j)P(j, j+1)/[1-r(j)P(j, j)] \right\} r(k)P(k, 1)/[1-r(k)P(k, k)].$$

Once again, a number of important special cases can be obtained by eliminating certain paths from the general graph. These include simple sequential systems with no cycles, sequential systems with no one-step cycles, sequential systems in which only state n returns to state 1, etc.

A special example motivated by a "detect and warning" software system discussed in [3] will now be considered. The ideal transition graph is given in figure 6 below. States 1 through 5 are search, acquire, track, warning, and maintenance states, respectively. State 1 is the initial state and we assume that the ideal transition matrix and state reliability functions are given. The system is a slight variation of a special case of the general sequential system considered above. The system reliability is

$$R(1) = C(1)/[1-D(1)] \text{ where} \quad (16)$$

$$C(1) = r(1)P(1,5)r(5)$$

$$D(1) = r(1)P(1,1) + r(1)P(1,2)r(2)P(2,1)/[1-r(2)P(2,2)]$$

$$+ r(1)P(1,2)r(2)P(2,3)r(3)P(3,1)/\{[1-r(2)P(2,2)][1-r(3)P(3,3)]\}$$

$$+ r(1)P(1,2)r(2)P(2,3)r(3)P(3,4)r(4)/\{[1-r(2)P(2,2)][1-r(3)P(3,3)]\}$$

In [3] the parameter values are $r(1) = 0.98$, $r(2) = 0.97$, $r(3) = 0.96$, $r(4) = 0.95$, $r(5) = 0.999$, $P(1,1) = 0.855$, $P(1,2) = 0.095$, $P(1,5)$

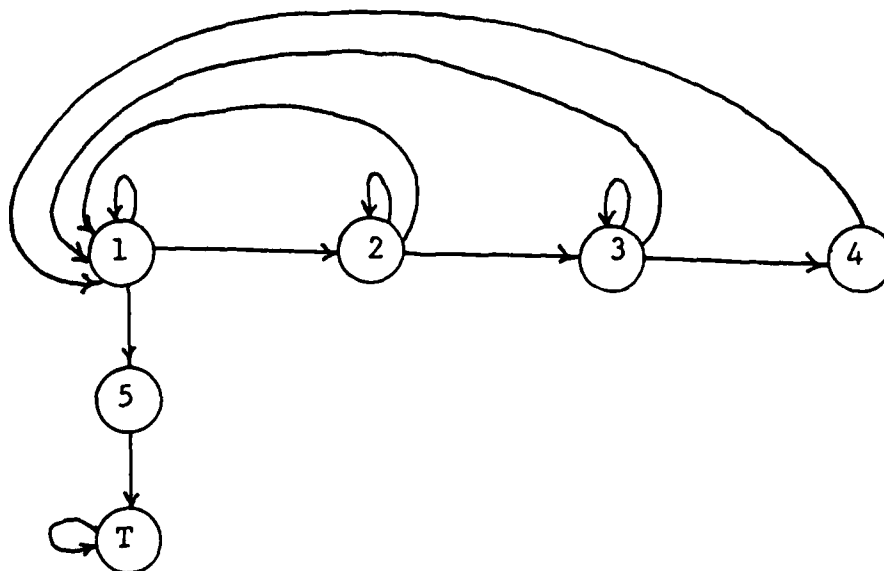


Figure 6
Detect and Warning System

$= 0.05$, $P(2,1) = 0.45$, $P(2,2) = 0.45$, $P(2,3) = 0.1$, $P(3,1) = 0.45$, $P(3,3) = 0.45$, $P(3,4) = 0.1$. Substituting into (16) gives $R(1) = 0.651$ as was obtained in [3].

A sensitivity analysis can be performed using the methods of section VII. Explicit formulas for the inherent and true sensitivities, as functions of the parameters, can be obtained using equations (7) and (8) or directly using (16). Recall that the advantage of the inherent sensitivity is that it can be computed from the ideal transition probabilities alone, before the state reliabilities are known. The analysis in this case is straightforward but notationally complicated and will not be given in detail. By way of example, using (8), the inherent sensitivity of state 1 is

$$S(1) = 1/[1-d(1)] \text{ where}$$

$$\begin{aligned} d(1) = & P(1,1) + P(1,2)P(2,1)/[1-P(2,2)] \\ & + P(1,2)P(2,3)P(3,1)/\{[1-P(2,2)][1-P(3,3)]\} \\ & + P(1,2)P(2,3)P(3,4)/\{[1-P(2,2)][1-P(3,3)]\}. \end{aligned}$$

Substituting the parameter values above gives $S(1) = 20$. Thus, the system reliability is enormously sensitive to changes in the reliability of state 1. Suppose that $r(1)$ is changed from 0.98 to 0.90 (all other parameter values the same). Then $R(1)$ decreases from 0.651 to 0.298!

The use of this model for the detect and warning system in [3] can be criticized. First, the use of the maintenance state as the terminal state seems rather artificial. Moreover, the inclusion of this state almost surely violates the Markov assumption. The Markov property would imply that whenever the system enters the search state, then with probability 0.05, the next state entered will be the maintenance state, regardless of the past history of the system. For what realistic maintenance policy could this possibly be true?

The detect and warning system will now be modified by removing the maintenance state and adding a terminal state after state 4 (the warning state). The ideal transition graph is given in figure 7.

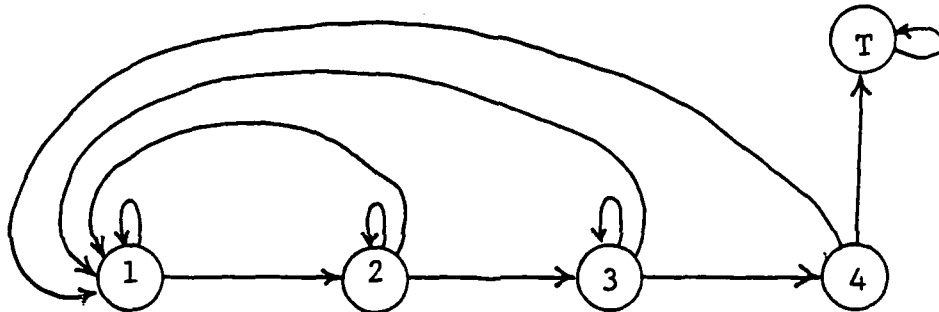


Figure 7
Modified Detect and Warning System

The modified system is a special case of the general sequential system. The system reliability is

$$R(1) = C(1)/[1-D(1)] \quad \text{where} \quad (17)$$

$$C(1) = r(1)P(1,2)r(2)P(2,3)r(3)P(3,4)r(4)/\{[1-r(2)P(2,2)][1-r(3)P(3,3)]\}$$

$$D(1) = r(1)P(1,1) + r(1)P(1,2)r(2)P(2,1)/[1-r(2)P(2,2)] \\ + r(1)P(1,2)r(2)P(2,3)r(3)P(3,1)/\{[1-r(2)P(2,2)][1-r(3)P(3,3)]\}$$

The parameter values given in [3] are changed slightly to accommodate the fact that the maintenance state no longer exists. Specifically, $P(1,1)$ is changed from 0.855 to 0.9 and $P(1,2)$ is changed from 0.095 to 0.1. Note that with this change, the transition

probabilities of state 1 are the same as those of states 2 and 3. Substituting the values into (17) gives $R(1) = 0.093$. This incredibly low system reliability shows that what may seem like minor changes in the structure of the transition graph can have enormous effects.

The system reliability value given above for the modified detect and warning system is obviously unsatisfactory. The allocation scheme of section VIII will be used. Note that for this system, $a(i) = 0$ for each i . Moreover,

$$c(1) = P(1,2)P(2,3)P(3,4)/\{[1-P(2,2)][1-P(3,3)]\},$$

$$c(2) = P(2,3)P(3,4)/[1-P(3,3)], \quad c(3) = P(3,4), \quad c(4) = 1.$$

Suppose that we want a system reliability of $R(1) = 0.9$. Substituting the parameter values and using equation (10) gives $r(1) = 0.9996$, $r(2) = 0.998$, $r(3) = 0.990$, and $r(4) = 0.9$. Recall that, for each i , the value of $r(i)$ given by the allocation scheme is the reliability needed by state i to achieve $R(1) = 0.9$, assuming that the other states are perfect. Thus we need to increase the state reliabilities somewhat for simultaneous allocation. Let $r(1) = 0.9999$, $r(2) = 0.999$, $r(3) = 0.999$, $r(4) = 0.99$. Substituting into (17) gives $R(1) = 0.9035$.

XI Recommendations

This report concerns a model for system reliability which was first used in [2] for software systems. The main assumptions of the model are the assumption of Markov transfer of control and the assumption that the system has a well defined terminal state corresponding to success. The main problem is to analyze system reliability in terms of the reliabilities of the states and the ideal transition probabilities.

A fairly deep analysis of the model has been carried out in this report. A method has been developed for computing system reliability which in many cases is better than the standard matrix inversion technique. This method can lead to explicit representations of system reliability as a function of the parameters. Moreover the method can be used to isolate the effect of the reliability of a given state on system reliability. This in turn leads to methods of evaluating the

sensitivity of system reliability with respect to the reliability of a given state and to methods of allocating state reliabilities to meet a given system reliability demand. These methods have been applied to quite general branching systems and sequential systems.

Therefore the model can be a very useful analytical tool. The methods developed here can be used very early in the design process (as soon as the ideal transition graph and some measure of the transition probabilities are known). The model can provide quantitative measures of the importance of the various states to overall system reliability; it can provide information about how the structure of the system effects the reliability. Based on this information the system can perhaps be redesigned to reduce the impact of very critical states.

On the other hand, as a statistical tool, the model probably has less value. Any statistical method which relies for its success on the simultaneous estimation of many (perhaps hundreds) of parameters, is very sensitive to inaccuracies in those estimates, and is probably very dependent on certain assumptions (the Markov property), should be used very cautiously.

As noted several times, the Markov assumption is fundamental to the model. However, it seems that some users of the model have been rather casual in regard to this assumption. The problems of determining when the Markov assumption is valid and determining the quality of the results when it is not are, by far, the most important problems for future research in this area. This is true not just of the model considered here, but other models ([5], [6]) as well. One point of view considers many systems (such as software systems) as being essentially deterministic systems driven by a random input process. In this setting, the problem can be stated as follows: For what types of systems and what types of input processes is the state process Markovian? A preliminary analysis indicates that the only situation in which the answer is obviously affirmative is when the inputs are independent and identically distributed. However in many realistic situations (such as the systems in [3] discussed in sections IX and X) the inputs will be highly correlated. Research needs to be conducted to determine to what extent correlated inputs will cause the loss of the Markov property.

The other key assumption of the model, namely that the system has a terminal state corresponding to success, also seems to have been abused somewhat in practice. For many systems (such as those in [3] discussed in sections IX and X) there is no natural terminal state; the systems run more or less continuously or for a fixed period of time). For such systems, a better model might be the semi-Markov model in [6] with mean time to failure or failure rate as a measure of reliability. The drawback to this model is its complexity, although there are reasonably simple asymptotic results. Another possibility is to consider a Markov chain model just like the one studied in this report except without a terminal state corresponding to success. The expected number of transitions until failure would be the natural measure of reliability. This would seem to be particularly appropriate for systems for which the state transitions correspond to inputs received at regular time intervals (for then the expected number of transitions until failure could be converted to expected time until failure). The advantage of this model over [5] and [6] would be its simplicity. Almost certainly an analysis similar to the one in this report could be carried out for Markov chains with mean number of transitions until failure as the measure of reliability.

In summary, the model studied in this report is a valuable analytical tool which can be used early in the design stage of a system. However, care must be taken to use the model appropriately. Moreover, further research is needed in the directions indicated above.

REFERENCES

1. Goel, A. L., "A Guidebook for Software Reliability Assessment," RADC Contract Report TR-83-176, August, 1983.
2. Cheung, R. C., "A User-Oriented Software Reliability Model," IEEE Trans. on Software Engineering, Vol. SE-6, No. 2, March 1980.
3. Soistman, E. C. and Ragsdale, K. B., "Combined Hardware/Software Reliability Production Methodology," Vol. II, RADC Contract Report OR-18-173, December, 1984.
4. Cinlar, E., Introduction to Stochastic Processes, Englewood Cliffs, NJ, Prentice Hall, Inc. 1975.
5. Laprie, J. C., "Dependability Evaluation of Software Systems in Operation," IEEE Trans. on Software Engineering, Vol. SE-10, No. 6, November, 1984.
6. Littlewood, B., "Software Reliability Model for Modular Program Structure," IEEE Trans. on Reliability, Vol. R-28, No. 3, August, 1979.

ACKNOWLEDGMENT

The author thanks the Air Force Systems Command, the Air Force Office of Scientific Research, and the Universal Energy Systems Inc., for the opportunity to explore the feasibility of the project objectives at the Air Force Rocket Propulsion Laboratory, Edwards Air Force Base, California.

The author is especially grateful to Dr. Robert D. Chapman for the inception of the project and for much advice, guidance and collegiality. Thanks are also due to the personnel in the Chemistry and Materials Branch of the Liquid Rocket Division for their hospitality, assistance and friendship and especially to Lt. John Andreshak whose technical expertise made much of the work described here possible within the time frame of one summer.

I. INTRODUCTION

Polyfunctional organic isocyanates are commonly used for preparing urethanes which serve as binders and plasticizers in the formulation of solid propellants. The reaction of such compounds with medium chain aliphatic diols results in polyurethanes with the kind of crosslinking which confers desirable binding and elastic properties to the solid propellant.

Studies have been made to determine the kinds of structural features necessary in both the diol and the isocyanate which maximize these properties¹. In the case of the former, α - ω aliphatic diols of moderate chain length appear to be optimal. The synthesis of such compounds in the laboratory and on a large scale presents no real difficulties. On the other hand, the isocyanates which have been found to be useful are not nearly as accessible. Generally these isocyanates need to incorporate three isocyanate residues in close proximity to each other. This structural requirement is needed to generate the crosslinking which optimizes adhesive properties and the structural integrity of the solid propellant.

In this work attention was focussed on the development of new and more efficient ways to obtain the desired isocyanates. At the outset it was decided to limit our attention to two particular carbon systems identified as 1 and 2 since these had already been shown to lead to polyurethanes with desirable properties.

1985 USAF-UES SUMMER FACULTY RESEARCH PROGRAM

Sponsored by the
AIR FORCE OFFICE OF SCIENTIFIC RESEARCH

Conducted by the
UNIVERSAL ENERGY SYSTEMS, INC.

FINAL REPORT

THE SYNTHESIS OF REACTIVE INTERMEDIATES

Prepared by :	Ricardo A. Silva
Academic Rank:	Professor of Chemistry
Department and	Department of Chemistry
University:	California State University, Northridge
Research Location:	Rocket Propulsion Laboratory Edwards Air Force Base, CA.
USAF Research:	Dr. Robert Chapman
Date:	30 September, 1985
Contract No:	F 49620-85-C-0013

THE SYNTHESIS OF REACTIVE INTERMEDIATES

by

Dr. Ricardo A. Silva

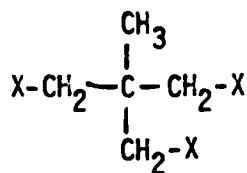
ABSTRACT

This report describes progress in the application of new synthetic methodologies leading to the transformation of readily available materials into new reactive intermediates capable of further conversion to compounds which have been shown to be useful in the formulation of solid propellants.

The report describes the successful synthesis and characterization of a number of such new reactive intermediates including two new tristriflates from 2-methyl-1,2,3-propanetriol and 1,3,5-pentane-triol; one new ditriflate from 4-trifluoroacetoxy-1,5-pentanediol; one new trifluoroacetate from 4-hydroxytetrahydropyran; and a new trispyridinium salt, 1,2,3-trispyridiniumpentane tritriplate.

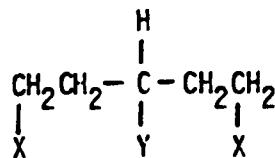
The attempted transformation of some of these reactive intermediates into propellant ingredients is described. However, the limited tenure of this work precluded completion of this part of the project. This is an area that warrants continued study.

Recommendations regarding culmination of the objectives of this project are discussed as are logical extensions of this work to include the synthesis of more energetic materials for incorporation into propellant formulation.



1

- a. X = OH
- b. X = Br
- c. X = NH₂
- d. X = OSO₂CF₃
- e. X = NCO



2

- a. X = Y = OH
- b. X = Y = Br
- c. X = Y = NH₂
- d. X = Y = OSO₂CF₃
- e. X = OSO₂CF₃
Y = OCOCF₃
- f. X = Y = NCO

The synthesis of alkyl isocyanates from amino compounds through reaction with phosgene is well documented as is the formation of such compounds from acid derivatives via the Curtius, Hoffman or Lossen Rearrangements².

The reaction of amines with trichloroacetyl chloride is limited to aromatic amines, presumably because of the higher basicity of aliphatic amines³.

Examination of the existing methodology reveals the need to develop alternate routes to isocyanates. Though the phosgene reaction is extensively employed on a large scale industrially, the toxicity of the reagents presents unique hazards (Bhopal, India, December 1984) and requires specialized handling and detection systems.

On the other hand the rearrangement of acid derivatives requires high temperatures for the final step and viable strategy for the synthesis of suitable carboxylic acid substrates. Since it was recognized that the polyol, 1a, was available commercially and that a suitable precursor for structures similar to 2 was also at hand as 4-hydroxytetrahydropyran, 3a, our efforts were directed toward the study of the conversion of derivatives of 1a and 2a to the corresponding compounds, 1e and 2f. It should be mentioned that compound 2f had already been obtained through high temperature rearrangement of the type discussed earlier¹.

It is apparent that the substrates 1a and 2a incorporate primary alcohol functions at all but one of the reaction centers, suggesting that derivatization of these groups would make them particularly vulnerable to bimolecular substitution for introduction of the isocyanate residues.

II. OBJECTIVES

The first objective of this work was to synthesize from 1a and 2a (or its equivalent) derivatives containing good leaving groups which would be subject to nucleophilic displacement. A number of these kinds of derivatives were prepared as part of a parallel scheme⁴ to arrive at the same chemical goals 1e and 2f.

The remarkable rates observed for solvolysis of triflate esters and the superior Leaving Group Ability of the trifluoromethanesulfonyl

group immediately suggested these derivatives as suitable substrates (Table 1.). The AFRPL had also been engaged in the synthesis of other kinds of triflates in the immediate past⁵ and this enhanced the attractiveness of these esters since there was on site a vast amount of experimental expertise on which to draw.

TABLE 1⁶

Relative Reactivities

Solvolysis Rates

Leaving Group Ability

$\begin{array}{c} \text{CH}_3 \\ \\ \text{C}_6\text{H}_5-\text{CH}-\text{X} \end{array}$		
X	k_{rel}	
CH ₃ COO-	1.4×10^{-6}	
CF ₃ COO-	2.5	
Br -	1.4×10	
CH ₃ SO ₂ O-	3.0×10^4	1.0
p-CH ₃ -C ₆ H ₄ SO ₂ O-	3.7×10^4	0.70
CF ₃ SO ₂ O-	1.4×10^8	5.6×10^4

The accepted mechanism for substitution reactions of triflates involves cleavage of the C-O bond, a process which is more favorable for primary alcohols than for secondary or tertiary alcohols under bimolecular substitution conditions. As mentioned earlier the substrates 1a and 2a contain primary alcohol functions at all but one of the reaction centers.

The second objective of this work was to study the parameters necessary to effect bimolecular substitution of the triflates synthesized. Initially it was intended to examine the reactions with potassium, sodium or silver isocyanate in organic solvents with or without the addition of phase transfer catalysts or macrocyclic polyethers. Alternately, quarternary ammonium isocyanates might be attempted since these materials are much more soluble in organic solvents. Finally, the use of complex metal carbonyls would be examined⁷.

III. RESULTS AND DISCUSSION

The di- and tris(triflates) described in this work are all thermally labile and analytical samples could not be obtained. The structures postulated for all new compounds were completely consistent with spectroscopic data which included infrared and nuclear magnetic resonance (^1H , ^{19}F & ^{13}C) measurements. Spectroscopic data are listed in Table 5.


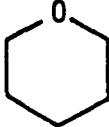
Synthesis of the tris(triflate) of 2-methyl-1,2,3-propanetriol, 1d.

A dichloromethane solution of the polyol, 1a cooled to -20°C was treated with triflic anhydride in the presence of three equivalents of dry pyridine. Reaction proceeded smoothly and purification of the previously undescribed tris(triflate) was accomplished by filtration and chromatography. The tris(triflate), 1d, was obtained in 63% yield as a slightly yellow oil which could be induced to crystallize to an off-white solid, mp $28-30^\circ\text{C}$. The identity of this material was secured by spectroscopic analysis.

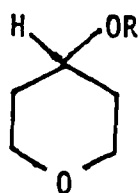
Synthesis of the trisulfate of 1,3,5-pentanetriol, 2d.

Since the triol, 2a, is not readily available commercially, it was decided to exploit the ring cleavage of cyclic ethers to generate the desired functionality at the ends of the carbon chain. Table 2 lists similar systems which have been cleaved successfully.

TABLE 2

System	Product	Ref.
	$\begin{array}{c} \text{TfO}-\text{CH}_2 \qquad \text{CH}_2-\text{OTf} \\ \qquad \qquad \\ \text{CH}_2 - \text{CH}_2 \end{array}$	8
	$\begin{array}{c} \text{TfO}-\text{CH}_2 \qquad \text{CH}_2-\text{OTf} \\ \qquad \qquad \\ \text{CH}_2 - \text{CH}_2 - \text{CH}_2 \end{array}$	9

Accordingly a dichloromethane solution of 4-hydroxytetrahydropyran, 3a was allowed to react at -60°C with triflic anhydride with an excess of pyridine.

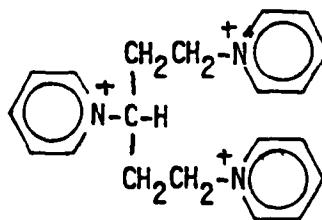


3

a. R = H

b. R = COCF_3

c. R = SO_2CF_3



4

$3\text{CF}_3\text{SO}_2\text{O}^-$

When this reaction mixture was allowed to warm to room temperature much decomposition was noted (formation of intense dark color and deposition of intractable black oils) and chromatography of the solution yielded the trispyridinium salt, 4, as the only isolable product in 28 % yield. This was recrystallized from acetone to a yellow crystalline solid, m.p. 175-80°C (decomposition). The identity of this material was established by spectral data (Table 5). The N-alkylation of pyridine derivatives by triflates had been noted earlier¹⁰.

The lability of triflates, particularly those derived from secondary or tertiary alcohols⁶ dictated careful workup, isolation and identification procedures. It was therefore decided to clearly establish methods of spectroscopic analysis so that it would be possible to follow the course of reactions either by sampling aliquots or by performing reactions in sample tubes for direct observation. Nuclear Magnetic Resonance (NMR) was chosen as a suitable analytic tool since potentially three different kinds of resonance signals (¹H, ¹⁹F & ¹³C) could be observed and analyzed. A series of small scale experiments was designed and conducted to ascertain precisely the kinds of changes in the NMR spectra which would be of value. Some experiments were done completely in NMR sample tubes with either CDCl₃ or CD₂Cl₂ as solvent. Variable temperature studies were also conducted. Since it was found that many of the attempted reactions went to completion only over a number of days, the sample tubes were maintained in a freezer and removed only for observation. Table 3 lists the kinds of changes observable in the NMR spectra.

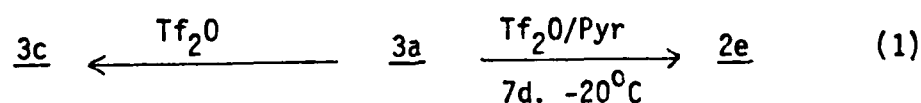
TABLE 3
Multiplicities of Relevant NMR Signals

Compound:	3a	3b	3c	2d	2e
Nucleus					
H ₂ & H ₆	m,m	m,m	m	t	t
H ₃ & H ₅	m	m	m	m	m
H ₄	t	m(syn)	m	m	m
¹⁹ F					
C-CF ₃	--	s	--	--	s
S-CF ₃	--	--	s	s,s	s
¹³ C					
CF ₃	--	q	q	q,q	q,q
C=O	--	q	--	--	q

It is clear that NMR is a powerful tool for the study of these reactions since changes in the multiplicities and the chemical shifts of relevant signals are unambiguous and assignable.

The reaction of 3a with triflic anhydride in dichloromethane at -20°C in the absence of any pyridine produced compound 3c without there being any evidence of ring ether cleavage even after two weeks. In contrast, under identical conditions we observed that ring cleavage of tetrahydropyran occurred almost immediately and was complete in a few hours. We do not have any simple explanation for this other than that the acid produced in the triflation of the alcohol group protonates the ether oxygen and thus prevents cleavage.

The addition of one mole equivalent of dry pyridine to the hydroxytetrahydropyran/triflic anhydride mixture resulted in rapid reaction with the hydroxyl group and a slower reaction with the cyclic ether as shown in Equation 1.



Since the earlier reaction with pyridine produced the alkylated compound 4, a parallel reaction was performed with the non-nucleophilic base, 2,6-di-tert-butylpyridine, 5. Compounds of this type have been employed in other work¹¹. Here again, reaction with the hydroxyl group was rapid and complete in a few minutes but ring cleavage took a number of days. Attempts to isolate the tristriflate 2e were frustrated by its thermal sensitivity. Solutions of 2e free of reactants and side-products (as determined by NMR analysis) could be obtained provided all operations were performed at low temperature. Most of the impurities formed in this reaction could be removed by filtration through silica gel and/or low temperature flash chromatography. Table 5 lists the relevant spectral data for compound 2e.

In an attempt to obtain a less labile substrate for the next reaction planned, ie. nucleophilic substitution, it was decided to find a different leaving group for the secondary alcohol in 2a.

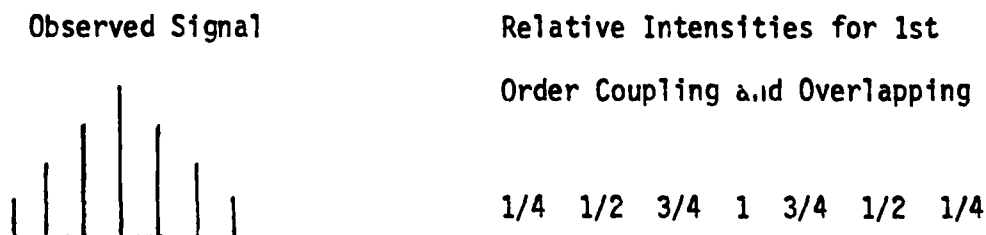
Synthesis of 4-acetoxytetrahydropyran, 3b.

The trifluoroacetyl group is a fairly good substrate for displacement reactions. This together with the fact that the presence of the CF₃

group which would be amenable to ^{19}F NMR observation made us decide to synthesize compound 3b.

When a solution of 3a in dichloromethane was treated with trifluoroacetic anhydride/pyridine at 0°C , a white voluminous material precipitated out of solution. This was filtered off after two hours and identified as pyridinium trifluoroacetate. The filtrate was passed through a short column of silica gel and removal of the solvent followed by distillation yielded 3b in 80% yield as a colorless oil, bp₇₆₀ $162-65^{\circ}\text{C}$. The identity of 3b was established from spectroscopic data as listed in Table 5.

The proton NMR spectrum of compound 3b was particularly intriguing in the area ascribable to the tertiary H at C-4. This proton produces a symmetrical seven line signal reproduced below which remained invariant over a fairly large temperature range (ambient to 110°C). Since the multiplicity of the signal can be rationalized on the basis of first order coupling and overlapping of a triplet of triplets, the invariance of the signal implies that the dihedral angle of the coupled protons does not change over this temperature range. The reason for this strong conformational preference is not immediately apparent and warrants further study.



Synthesis of 3-acetoxy-1,5-ditriflyloxy-pentane, 2e.

The conversion of 3b to 2e was accomplished in dichloromethane solution at -20°C with one mole equivalent of triflic anhydride. Again the ether cleavage reaction was found to be sluggish in comparison with unsubstituted cyclic ethers but went to completion in seven days. Conversion to the ditriflate was essentially quantitative (by NMR analysis) but the product was also thermally labile and could not be isolated. The structure of 2e is completely consistent with the spectral data (Table 5).

It is interesting to note the significant reduction in the rate of cleavage of the substituted cyclic ethers studied in this work as compared to tetrahydrofuran and tetrahydropyran. At the present time we have no way to account for these differences on the basis of a substituent group which is far removed from the reaction center. This problem should be addressed in further studies since it would provide information which would be extremely valuable in this area. Table 4 lists some of the comparative reaction times for these substituted derivatives.

Nucleophilic Substitution Reactions.

The second objective of this work was to effect the nucleophilic substitution of the triflates and other derivatives synthesized to lead to the target molecules, 1e and 2f. A large number of reagents and a vast array of reaction conditions are available to attempt these transformations. Due to the limited time available, it was decided to direct our attention to homogenous reactions since these are more

amenable to in situ spectroscopic analysis. The availability of organic isocyanates which are readily soluble in organic solvents made them the reagents of choice.

The reaction of the tristriflate, 1d, with tetraethylammonium isocyanate in dichloromethane at 0°C was attempted but no product isocyanate could be discerned in the reaction solution. The only products which could be isolated contained a carbonyl band in the IR spectrum which could not be assigned to an NCO group but rather to an amide or urea carbonyl. Further investigation revealed water contamination of the reagent tetraethylammonium isocyanate which is not surprising since this material is extremely hygroscopic. The failure to isolate isocyanate could be due to the reaction of water with the product. It is clear that this reaction should be reinvestigated under rigorously anhydrous conditions. Alternately, metal isocyanates such as those from Na, K or Ag could be used with or without macrocyclic ethers as complexing agents.

Certainly the experimental parameters required to effect this chemical change would be of obvious importance for culmination of this project.

TABLE 4.
Relative Reaction Times

Reaction	Time for 90% Reaction ^a
<u>1a</u> <u>1d</u> (Pyr)	120 mins.
<u>3a</u> <u>3c</u> (Pyr)	100 mins
<u>3a</u> <u>2d</u> (Pyr)	8 days
<u>3a</u> <u>2d</u> (di-t-Bu-Pyr)	8 days
<u>3b</u> <u>2e</u>	7 days

^aExtent of reaction determined by NMR integration of ¹H signals and of ¹⁹F signals where relevant.

TABLE 5.
Spectroscopic Data

Compound	IR (cm ⁻¹)	NMR ()				
<u>1d</u>	1426	¹ H	1.26	s	1H	
	1234-1202		4.47	s	2H	
	1141	¹⁹ F	78.4			
	957		74.5			
		¹³ C	15.5			
			40.5			
			74.4			
			118.6	q	J = 320 Hz	
<u>3b</u>	1783	¹ H	1.92	m	J = 4 Hz	4H
			3.76	m	J = 4 Hz	4H
			5.17	m	J = 4 Hz	1H
		¹⁹ F	75.8			

TABLE 5 (cont.)

3b

^{13}C	31.6			
	65.2			
	74.9			
	115.2	q	J = 286 Hz	
	157.2	q	J = 43 Hz	

3c

^1H	2.04	m	4H	
	3.70	m	4H	
	5.18	m	1H	
^{19}F	76.2			
^{13}C	32.7			
	64.5			
	85.7			
	118.5	q	J = 319 Hz	

2d

^1H	2.44	q	J = 6 Hz	4H
	4.70	t	J = 6 Hz	4H
	5.20	m		1H
^{19}F	74.9			
	75.1			

2e

^1H	2.30	q	J = 5.9 Hz	4H
	4.63	t	J = 5.9 Hz	4H
	5.35	m		1H

TABLE 5 (continued)

<u>2e</u>	¹⁹ F	75.0
		75.4

All proton chemical shifts were measured relative to tetramethylsilane. Fluorine chemical shifts were measured from CFC1₃ as internal standard.

IV. RECOMMENDATIONS

This study has shown that reactive chemical intermediates which represent the first set of compounds in a synthetic sequence can be prepared in good yield. The successful synthesis of three of these compounds makes possible the subsequent conversion to the target molecules. This latter phase of the project objectives was not completed due to the limited time available, therefore the primary recommendation of this report is that further studies be continued which would result in culmination of the project.

In the recommended study it will be necessary to establish the optimum experimental parameters for the bimolecular substitution reaction of the newly synthesized triflates. Initially, it is suggested that homogenous reaction media be examined. These would be most amenable to monitoring by NMR and IR. The data compiled in the present study would allow for establishment of a sound analytical base for such monitoring. Different solvent systems which

of necessity must be non-protic and relatively inert, as well as various organic isocyanates must be examined. Careful monitoring would provide information about reaction rates and any undesirable side reactions can be minimized by alteration of experimental conditions, eg. solvent, temperature, concentration, nature of the isocyanate counter-ion and the time for reaction. It would also be useful to study non-homogenous reaction media since this would allow the use of inorganic metal isocyanates. The use of crown ethers would be useful here since these are known to accelerate the rate of substitution reactions by separating ion-pairs through complexation.

A second recommendation is to continue to pursue the more traditional route to the target molecules by employing less reactive intermediates such as 1b, 1c, 2b and 2c; some of which have already been prepared as part of a parallel study to this project⁴. The successful synthesis of target molecules, 1e and 2f would represent a significant advance in the application of newer methods of organic chemistry for the preparation of reactive substances and it logically suggest a third recommendation.

The third recommendation is to exploit the chemistry and techniques developed in this work in order to synthesize new monomeric species for incorporation into solid propellants. These might include energetic compounds such as nitro analogues of systems 1 and 2. Such materials promise to be even more useful as binders and plasticizers. Suitable starting materials can be found in the literature¹².

REFERENCES

1. R. D. Chapman, AFRPL, Edwards AFB, private communication.
2. J. H. Saunders and R. J. Slocombe, "The Chemistry of Organic Isocyanates", Chem. Rev., 1948, 43, 203.
3. K. Kurita, T. Matsumura and Y. Iwakura, J. Org. Chem., 1976, 41, 2070.
4. S. Dimock, AFOSR 1985 Summer Graduate Fellow, AFRPL, Edwards AFB.
5. S. Shackelford, R. D. Chapman, G. Anderson and J. Andreshak, AFRPL, Edwards AFB.
6. P. J. Stang, M. Hanack and L. R. Subramanian, "Perfluoroalkane Sulfonic Esters: Methods of Preparation and Applications in Organic Chemistry", Synthesis, 1982, 85.
7. J. P. Collman, M. Kubota, J-Y. Sun and F. Vastine, J. Amer. Chem. Soc., 1967, 89, 169.
8. J. Burdon and V. C. R. McLoughlin, Tetrahedron, 1965, 21, 1.
9. E. Lindner, G. von Au and H. J. Eberle, Chem. Ber., 1981, 114, 810.
10. R. W. Alder, Chem. Ind. (London), 1973, 983.
11. H. C. Brown and B. Kanner, J. Amer. Chem. Soc., 1953, 75, 3965; 1966, 88, 986; P. J. Stang and W. Treptow, Synthesis, 1980, 283.
12. P. T. Berkowitz and K. Baum, J. Org. Chem., 1980, 45, 4853.

1985 USAF-UES SUMMER FACULTY RESEARCH PROGRAM/
GRADUATE STUDENT SUMMER SUPPORT PROGRAM

Sponsored by the
AIR FORCE OFFICE OF SCIENTIFIC RESEARCH

Conducted by the
UNIVERSAL ENERGY SYSTEMS, INC.

FINAL REPORT

POSSIBLE TARGETS FOR TESTING THE NEUTRAL PARTICLE BEAM
AT LOW ENERGIES IN THE MARK I AEROSPACE CHAMBER

Prepared by:	DR. S. BALLOU SKINNER
Academic Rank:	PROFESSOR OF PHYSICS
Department and University:	PHYSICS DEPARTMENT, UNIVERSITY OF SOUTH CAROLINA, COASTAL CAROLINA COLLEGE
Research Location:	ARNOLD ENGINEERING DEVELOPMENT CENTER ARNOLD AFS TULLAHOMA, TENNESSEE
USAF Research:	MR. W. G. KIRBY
Date:	JULY 10, 1985
Contract No:	F49620-85-C-0013

POSSIBLE TARGETS FOR TESTING THE NEUTRAL PARTICLE BEAM
AT LOW ENERGIES IN THE MARK I AEROSPACE CHAMBER

by

Dr. S. Ballou Skinner

ABSTRACT

Carbon, aluminum, silicon, liquid helium, ice, iron, platinum, and lead were examined as possible targets for testing the neutral particle beam at low energies in the MARK I Aerospace Chamber in an effort to select a target which would give the fewest nuclear reactions and therefore the smallest radiation hazards to the chamber and the personnel. The first test will probably use a neutral particle beam of approximately 1 Mev. Subsequent testings may use beams of higher energies up to approximately 20 Mev. For each target the following were calculated or literature researched: coulomb barrier, threshold energies for (p, α) and (p,n) reactions, reaction cross sections, radioactivity of the residual nucleus, stopping range, and heat properties. For carbon and aluminum, gamma yields and shielding estimates were made. For energies above the (p,n) threshold, the danger of neutron activation is acknowledged. A calculation is made for neutron activation in aluminum. For the first test using 1 Mev protons, aluminum or carbon will probably be used as a target for the neutral particle beam.

ACKNOWLEDGEMENTS

This research was supported by the U.S. Air Force Systems Command, Air Force Office of Scientific Research, Arnold Engineering Development Center, Arnold Air Force Station, Tullahoma, Tennessee. I appreciate having the opportunity of working with Mr. Bill Kirby, the advisor of this research. I further appreciate the assistance of Mr. Marshall Kingery, the Effort Focal Point, and Mrs. Della Burch of the AEDC Library. A special thanks goes to Mrs. Twyla Harrington for typing this report.

I. INTRODUCTION: The U.S. Air Force is interested in testing the neutral particle beam at low energies (1-20 Mev) in the MARK I Aerospace Chamber at the Arnold Engineering Development Center, Tullahoma, Tennessee. The target to be chosen for the beam testing should be one which has as few proton induced reactions as possible. For the $(p,p'\gamma)$ and the (p,γ) reactions, the gamma shielding must be sufficient to prevent any radiation hazards to the chamber and the personnel. If we have any (p,n) reactions, the neutrons must be captured near the target, thereby eliminating any chance for neutron activation in the chamber via (n,γ) reactions.

My background is in neutron activation analysis. For this problem I first examined the proton induced reactions in the targets. From the (p,γ) cross sections, I could calculate gamma yields. For energies above the (p,n) threshold, and from the (p,n) cross-section, I can likewise calculate neutron yields. From the neutron yields it is possible to make some calculations of neutron activation via (n,γ) reactions.

II. OBJECTIVES OF THE RESEARCH EFFORT: The preliminary goal of this research effort was to find a suitable target for testing the neutral particle beam at low energies (1-20 Mev) in the MARK I Aerospace Chamber in an effort to select a target which would give the smallest radiation hazards to the chamber and the personnel. My USAF Research Colleague and I knew this would be a difficult assignment because it is very difficult to find nuclear cross sections for proton induced reactions $[(p,\gamma)$ and (p,n) at low energies] since these cross sections are a function of energy and very little research has been done in calculating nuclear cross sections for proton induced reactions at low energies. To the contrary, finding nuclear cross sections for neutron induced reactions $[(n,\gamma)$ reaction] presented no problem because this information has been compiled by the National Neutron Cross Section Center of the Brookhaven National

AD-A166 178

UNITED STATES AIR FORCE SUMMER FACULTY RESEARCH PROGRAM

6/11

1985 TECHNICAL RE (U) UNIVERSAL ENERGY SYSTEMS INC

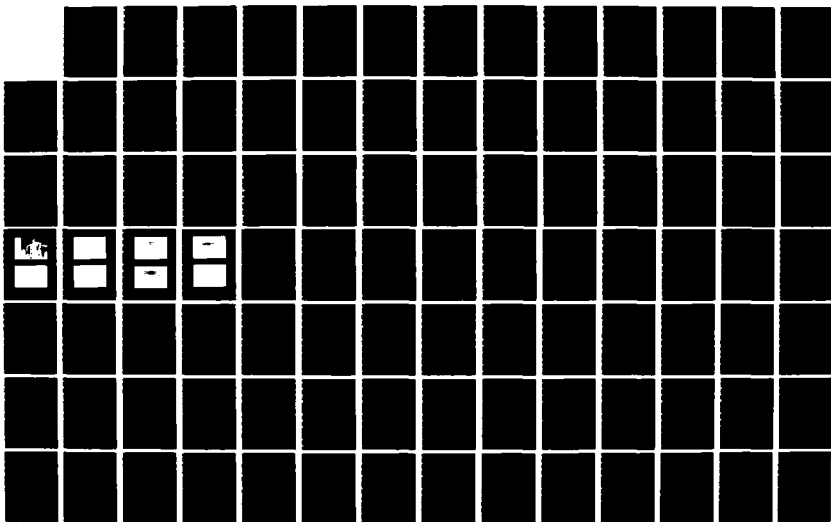
DAYTON OH R C DARRAH ET AL DEC 85 AFOSR-TR-86-0141

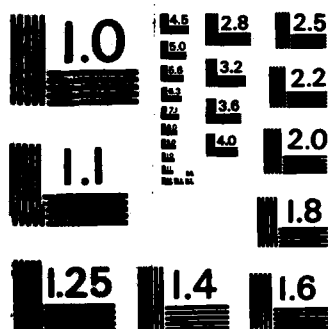
UNCLASSIFIED

F49620-85-C-0013

F/G 5/9

NL





MICROCOPY RESOLUTION TEST CHART
NATIONAL BUREAU OF STANDARDS - 1963 - A

Laboratory.

III. REPORT: Table I that follows gives a comparison of the threshold energies for proton induced reactions in carbon, aluminum, silicon, liquid helium, ice, iron, platinum and lead. The threshold of a reaction is defined to be the minimum kinetic energy of an impinging particle such that the reaction is energetically possible. Thus a nonzero threshold exists only if the Q-value of the reaction is negative and all exoergic reactions have zero thresholds. Endoergic reactions have positive threshold numbers. If no experimental mass for the residual nucleus was available, dashes are entered in Table I. The relationship between the threshold energy and the Q-value is:

$$E_T = -Q \left(\frac{M_a + M_x}{M_x} \right) \quad (\text{Eq. 1})$$

where M_a is the mass of the bombarding particle and M_x is the mass of the target (at rest in the lab system).

The coulomb barriers for the eight possible target materials as seen by a proton are given in Table II, calculated by the coulomb barrier equation:

$$E_C = \frac{1.44 \text{ Mev fm}}{1.4 \text{ fm}} \left(\frac{Z}{A^{1/2} + 1} \right) \quad (\text{Eq. 2})$$

where Z is the atomic number and A is the mass number.

TABLE II

TARGET	<u>C</u>	<u>AL</u>	<u>Si</u>	<u>Li</u>	<u>He</u>	<u>O</u>	<u>Fe</u>	<u>Pt</u>	<u>Pb</u>
Coulomb Barrier (Mev)	1.88	3.35	3.57	1.59	2.28	5.55	11.83	12.20	

If the threshold energy is much greater than the coulomb barrier, the reaction will occur with a large probability at the threshold energy. If

TABLE 1

THRESHOLD ENERGIES FOR PROTON INDUCED REACTIONS¹

TARGET	(p, α)	(p,n)	(p,2n)	(p,2p)	(p,np)	(p,d)	(p,nd)	(p,t)	(p,nt)	(p,He ³)	(p,nHe ³)	(p,He ⁴)	(p,nHe ⁴)
CARBON													
99.89% C ¹²	-1.94	19.64	-----	17.29	20.28	17.87	32.09	25.31	48.36	21.34	30.47	8.18	28.31
1.11% C ¹³	-7.55	3.23	24.85	18.88	5.33	2.93	23.09	16.35	30.49	14.20	26.54	4.38	13.46
ALUMINUM													
100% Al ²⁷	-11.59	5.80	19.60	8.58	13.54	11.23	23.02	16.53	34.10	12.08	19.68	-1.60	15.48
SILICON													
92.21% Si ²⁸	-2.75	15.66	-----	12.00	17.79	15.49	29.27	22.79	-----	17.53	29.30	7.99	25.53
4.70% Si ²⁹	-5.60	5.92	24.41	12.76	8.77	6.46	24.23	17.76	31.53	12.77	26.27	4.99	16.75
3.09% Si ³⁰	-7.30	5.18	16.88	13.96	10.96	8.66	17.42	10.95	28.70	15.73	23.71	2.45	15.94
HELIUM													
100% He ⁴	2.46	29.36	-----	24.77	25.72	22.94	-----	-----	-----	22.94	25.72	-0.00	-----
ICE													
NO REACTIONS													
99.985% H ¹	-5.49	-----	-----	-----	3.34	-0.00	-----	-----	-----	-----	-----	-----	-----
0.015% H ²	-0.60	17.23	-----	12.89	-6.65	14.28	28.33	21.68	46.30	16.20	27.41	5.54	26.87
99.759% O ¹⁶	-5.61	3.75	21.55	14.59	4.39	2.03	18.62	12.00	25.99	9.05	20.53	-1.19	9.91
0.037% O ¹⁷	-7.99	2.57	12.23	16.83	8.49	6.15	10.52	3.91	20.45	14.89	17.52	-3.98	7.23
0.204% O ¹⁸	-----	-----	-----	-----	-----	-----	-----	-----	-----	-----	-----	-----	-----
IRON													
5.82% Fe ⁵⁴	-5.05	9.20	-----	9.02	13.63	11.36	22.24	15.87	-----	13.43	24.17	3.21	17.15
91.66% Fe ⁵⁶	-6.03	5.45	15.72	10.37	11.40	9.14	18.60	12.23	25.85	12.92	22.02	1.08	13.34
2.19% Fe ⁵⁷	-6.95	1.65	13.22	10.75	7.78	5.52	16.91	10.55	20.01	10.29	20.70	-0.24	8.86
0.33% Fe ⁵⁸	-7.37	3.14	11.86	12.03	10.22	7.95	15.73	9.37	20.76	13.11	20.50	-0.42	9.90
PLATINUM													
0.78% Pt ¹⁹²	-----	4.32	-----	6.91	-----	-----	12.95	6.66	-----	7.32	-----	-7.00	1.20
32.9% Pt ¹⁹⁴	-5.06	3.31	-----	7.56	8.41	6.18	12.51	6.22	-----	7.66	13.89	-6.76	1.37
33.8% Pt ¹⁹⁵	-5.66	1.02	9.41	7.57	6.10	3.87	12.28	5.99	12.32	5.91	13.77	-6.88	-0.68
25.3% Pt ¹⁹⁶	-5.82	2.28	8.98	8.18	7.96	5.73	11.83	5.54	13.95	7.77	13.87	-6.78	1.04
7.21% Pt ¹⁹⁸	-6.48	1.09	7.64	8.83	7.60	5.37	11.25	4.96	12.92	8.13	13.91	-6.74	0.57
LEAD													
1.48% Pb ²⁰⁴	-3.25	-----	12.43	6.67	8.44	6.21	13.03	6.74	-----	6.67	13.64	-7.01	1.27
23.6% Pb ²⁰⁶	-3.55	4.45	11.62	7.29	8.12	5.88	12.65	6.36	14.80	7.11	13.80	-6.85	0.88
22.6% Pb ²⁰⁷	-3.72	3.20	11.23	7.53	6.77	4.54	12.66	6.37	13.14	6.31	13.88	-6.76	-0.10
52.3% Pb ²⁰⁸	-3.80	3.67	10.61	8.06	7.40	5.17	11.94	5.65	13.77	7.18	13.71	-6.93	0.61

the threshold energy is much less than the coulomb barrier, the reaction will hardly ever occur at the threshold energy. For any element with an atomic number greater than 50, it takes at least a 10 Mev proton to penetrate the coulomb barrier of the nucleus. If the threshold barrier is a little less than the coulomb barrier, some reactions will occur at the threshold energy by coulomb barrier tunneling.

A target material should be chosen for the first test (1 Mev) which would give as few (p, γ) reactions as possible and no (p, n) reactions. The gamma rays can be shielded with concrete or lead. Neutrons are not wanted because of neutron activation via (n, γ) reactions in the aerospace chamber. If we increase the neutral particle beam above the threshold energy for a (p, n) reactions it will then be necessary to shield the target material with boron or lithium doped paraffin bricks to absorb or capture the neutrons.

Prompt γ -rays can originate from a number of different types of nuclear reaction, commonest being $(p, p' \gamma)$, $(p, \alpha \gamma)$, (p, n) and (p, γ) . Where an element naturally contains more than one isotope, γ -rays may be produced from reactions in each of the isotopes. At incident proton energies of a few Mev, the coulomb barrier inhibits the reaction rate, particularly for heavy element targets. Cross sections for (p, γ) reactions are generally low and inelastic scattering cross sections are higher. The energy and intensity of the prompt γ -rays emitted depend on the level spacing of the final nucleus.

Gamma rays intensities go down with increasing atomic number (same energy proton) due to the coulomb barrier. There are almost no prompt γ -rays for elements with a Z number over 50 that are bombarded with protons up to 10 Mev.

The γ -ray yield is very dependent on angle and on proton yield. Maximum yield is when the beam's angle is at 90° to the target.²

(p,n) reactions are more common with the lighter than with the heavier elements, since higher energies are necessary for the nuclei of the latter to be penetrated by the protons. According to the statistical theory in its simplest form, the capture cross section for protons should fall continuously with increasing energy as ever more reactions compete for their share of the reaction cross section.

If the incident proton has an energy in excess of about 20 Mev, the compound nucleus has sufficient excitation energy to permit the expulsion of two or more nucleons.³

In order to select a suitable target material as a dump for the neutral particle beam, the following additional information is helpful: (1) the reaction cross section as a function of proton energy in order to calculate yields, (2) identification of the residual nucleus and its decay scheme (if it is radioactive), (3) thermal neutron cross sections for (n, γ) [if (p,n) reactions take place] in order to make yield calculations, (4) proton stopping ranges, and (5) heat properties.

In the remainder of Section III each target material is listed in Table III with (p, γ) and (p,n) reactions. If the residual nucleus is radioactive, the decay scheme is shown. Thermal neutron cross sections, proton stopping ranges, densities, and melting points are given. References 1 through 21, plus computations found in my lab notebook, were used in compiling Table III.

Since the most likely target for the first 1 Mev test will be aluminum or carbon, heating effects, prompt gamma yields, and shielding estimates are listed for these elements in Table III. If the beam's energy exceeds the (p,n) threshold, gamma yields via neutron activation

can be made. Such a calculation, using 10 Mev protons, is made for aluminum.

TABLE III

A. TARGET MATERIAL: Aluminum

DENSITY: 2.699 gm/cm³

MELTING POINT: 660°C

STOPPING RANGE FOR 1 MEV AND 5 MEV PROTON: 14.6 x 10⁻³ mm and 0.19 mm

(p, γ) REACTIONS: AL²⁷ (p, γ) Si²⁸ (See 1 below)

(p,n) REACTIONS: AL²⁷ (p,n) Si²⁷ (See 2 below)

RESIDUAL NUCLEUS DECAY SCHEME:

Si²⁸ is stable

Si²⁷ \rightarrow β^+ + Al²⁷ $t_{1/2} = 4.2s$ $E^+ = 3.85$ Mev MAX.

$\gamma = 0.511$ (200% γ^+)

OTHER PERTINENT INFORMATION:

Specific Heat = 0.215 cal/gm°C

Al²⁷(p, γ) cross section = 15.73 mb at 1 Mev; 321.5 mb at 5 Mev

Al²⁷(p,n) yield, i.e. $\frac{n}{p} = 10^{-4}$ with a 10 Mev proton

Al²⁷(n, γ) thermal cross section = 0.230b

(1) Prompt Gamma yield during one testing for 5 Mev protons = 1.04
curies

(1) Prompt Gamma yield during one testing for 1 Mev protons = .023
curies

Energies of the prompt gammas = 0.17, 0.843, 1.013, 1.368,
1.778 and 2.836 Mev

Shielding for prompt gammas: 2.83 inches of Pb or 15.2 inches of
concrete will give 0.123 mR per testing to control room personnel.

(2) Neutron Activation in a 10 cm by 10 cm by 2 cm with 10 Mev protons during a 2 minute testing = 4.68×10^4 curies

Above activity after cooling for 1 hour = 0.00066 curies

Heat flux will cause extreme erosion in the target material.

Cooling of the target is necessary.

B. TARGET MATERIAL: Carbon

DENSITY: 2.25 gm/cm^3

MELTING POINT: 3652° C

STOPPING RANGE FOR 1 MEV AND 5 MEV PROTON: $12.4 \times 10^{-3} \text{ mm}$ and 0.18 mm

(p, γ) REACTIONS: $\text{C}^{12}(\text{p}, \gamma) \text{N}^{13}$ (See 1 below)

$\text{C}^{13}(\text{p}, \gamma) \text{N}^{14}$

(p, n) REACTIONS: $\text{C}^{12}(\text{p}, \text{n}) \text{N}^{12}$

$\text{C}^{13}(\text{p}, \text{n}) \text{N}^{13}$

RESIDUAL NUCLEUS DECAY SCHEME:

$\text{N}^{12} \rightarrow \text{B}^+ + \text{C}^{12}$ $t_{1/2} = 10.35 \text{ ms}$ $\text{B}^+ = 16.4 \text{ Mev MAX.}$

$\text{N}^{13} \rightarrow \text{B}^+ + \text{C}^{13}$ $t_{1/2} = 9.96 \text{ m}$ $\text{B}^+ = 1.19 \text{ Mev (See 2 below)}$

N^{14} is stable

OTHER PERTINENT INFORMATION:

Specific Heat = $0.170 \text{ cal/gm}^\circ \text{ K}$

$\text{C}^{12}(\text{p}, \gamma)$ cross section = 31.5 mb at 1 Mev ; 421.4 mb at 5 Mev

$\text{C}^{12}(\text{p}, \text{n})$ cross section = 330 mb at 20 Mev

$\text{C}^{12}(\text{n}, \gamma)$ thermal cross section = 3.4 mb

(1) Prompt Gamma yield during one testing for 5 Mev protons = 3.30×10^{17} gammas

Energies of the prompt gammas = 4.5 Mev , 12.8 Mev , 15.1 Mev

Shielding for prompt gammas: 8.8 inches of Pb or 9 feet of concrete will give 8.5 mR per testing to control room personnel.

Heat flux will cause extreme erosion in the target material. Cooling of the target is necessary.

(2) Beta yield after one testing for 1 Mev proton = 1 curie

Above beta activity after cooling for 1 hour = 0.015 curie

(2) Beta yield after one testing for 5 Mev proton = 189 curies

Above beta activity after cooling for 1 hour = 0.29 curie

C. TARGET MATERIAL: Silicon

DENSITY: 2.33 gm/cm³

MELTING POINT: 1410° C

STOPPING RANGE FOR 1 MEV AND 5 MEV PROTON: 16.5 x 10⁻³mm and 0.218 mm

(p, γ) REACTIONS: Si²⁸(p, γ)p²⁹

Si²⁹(p, γ)p³⁰

Si³⁰(p, γ)p³¹

(p,n) REACTIONS: Si²⁸(p,n)p²⁸

Si²⁹(p,n)p²⁹

Si³⁰(p,n)p³⁰

RESIDUAL NUCLEUS DECAY SCHEME:

				MeV
p ²⁹ → β ⁺ + Si ²⁹	t _{1/2} = 4.4s	E ⁺ = 3.95max	γ = 0.511, 1.28, 2.43	
p ²⁸ → β ⁺ + Si ²⁸	t _{1/2} = 0.28s	E ⁺ = 11.0max	γ = 0.511, 1.78, 2.6 4.44, 4.9, 6.1, 6.7, 7.0, 7.6	
p ³⁰ → β ⁺ + Si ³⁰	t _{1/2} = 2.5m	E ⁺ = 3.24max	γ = 0.511, 2.23	
p ³¹ is stable				

OTHER PERTINENT INFORMATION:

Specific Heat = 0.168 cal/gm⁰C

Si²⁸(p,n)p²⁸ cross section = 637mb for 10 Mev proton

D. TARGET MATERIAL: Liquid Helium

DENSITY: 7.62 lb/ft³

(p, γ) REACTIONS: He⁴(p, γ)Li⁵

(p,n) REACTIONS: He⁴(p,n)Li⁴

RESIDUAL NUCLEUS DECAY SCHEME:

Li⁵ is a proton and alpha emitter with $t_{1/2} \approx 10^{-21}$ s

Li⁴ has not been detected

OTHER PERTINENT INFORMATION:

Specific Heat = 1.24 cal/gm⁰C

Helium is a stable, non-reactive gas or liquid having a negligibly small capture cross section for (p, γ), (p,n), and (n, γ) reactions.

It would take 20 diffusion pumps to take off the Helium gas that evaporated due to a 2 minute testing with 5 Mev protons.

It would take 80 diffusion pumps to take off the helium gas that evaporated due to a 2 minute testing with 20 Mev protons.

E. TARGET MATERIAL: Ice

DENSITY: 0.917 gm/cm³

MELTING POINT: 0⁰C at 1 atm

STOPPING RANGE FOR 1 MEV AND 5 MEV PROTON: 24.0 x 10⁻³mm and 0.368 mm

(p, γ) REACTIONS: O¹⁶(p, γ)F¹⁷

$^{17}\text{O}(\text{p}, \gamma) ^{18}\text{F}$

$^{18}\text{O}(\text{p}, \gamma) ^{19}\text{F}$

$^1\text{H}(\text{p}, \text{p}' \gamma) ^1\text{H}$

(p,n) REACTIONS: $^{16}\text{O}(\text{p}, \text{n}) ^{16}\text{F}$

$^{17}\text{O}(\text{p}, \text{n}) ^{17}\text{F}$

$^{18}\text{O}(\text{p}, \text{n}) ^{18}\text{F}$

No (p,n) reaction for ^1H

RESIDUAL NUCLEUS DECAY SCHEME:

^{16}F has a half-life of $\sim 10^{-19}\text{s}$

$^{17}\text{F} \rightarrow \beta^+ + ^{17}\text{O}$ $t_{1/2} = 66.6\text{s}$ $Q^+ = 1.74\text{ MeV Max}$, $\gamma = 0.511\text{ MeV}$

$^{18}\text{F} \rightarrow \beta^+ + ^{18}\text{O}$ $t_{1/2} = 109.7\text{m}$ $Q^+ = 0.635\text{ MeV Max}$, $\gamma = 0.511\text{ MeV}$

^{19}F is stable

OTHER PERTINENT INFORMATION:

Specific Heat = $0.146\text{ cal/gm}^\circ\text{C}$

One diffusion pump would take off the steam that evaporated due to a 2 minute testing with 5 MeV protons.

Evaporation would not be a problem because the vapor could be solidified on the baffles in the 20°K chamber.

Thermal Cross Sections: $^{16}\text{O}(\text{n}, \gamma) = 0.178\text{ mb}$; $^{17}\text{O}(\text{n}, \gamma) = 0.235\text{ mb}$; $^{18}\text{O}(\text{n}, \gamma) = 0.160\text{ mb}$

F. TARGET MATERIAL: Lead

DENSITY: 11.35 gm/cm^3

MELTING POINT: 327.5°C

STOPPING RANGE FOR 1 MEV AND 5 MEV PROTON: $9.10 \times 10^{-3}\text{mm}$ and 0.100 mm

(p, γ) REACTIONS: $^{208}\text{Pb}(\text{p}, \gamma) ^{209}\text{Bi}$

$^{206}\text{Pb}(\text{p}, \gamma) ^{207}\text{Bi}$

$^{207}\text{Pb}(\text{p}, \gamma) ^{208}\text{Bi}$

$Pb^{204}(p, \gamma)Bi^{205}$
 (p,n) REACTIONS: $Pb^{208}(p,n)Bi^{208}$
 $Pb^{206}(p,n)Bi^{206}$
 $Pb^{207}(p,n)Bi^{207}$
 $Pb^{204}(p,n)Bi^{204}$

RESIDUAL NUCLEUS DECAY SCHEME:

Bi^{209} is stable

Bi^{207} $t_{1/2} = 30.2y$ X-rays (0.57, 1.063, 1.771) e^{-} (0.482, 0.975, 1.048)

Bi^{208} $t_{1/2} = 3.68 \times 10^5y$ X-ray (2.614)

Bi^{205} $t_{1/2} = 15.3d$ $\beta^{+} = 0.98Max$, e^{-} and X-rays

OTHER PERTINENT INFORMATION:

Specific Heat: 0.038 cal/gm⁰C

Coulomb Barrier: 12.2 Mev

G. TARGET MATERIAL: Platinum

DENSITY: 21.45 gm/cm³

MELTING POINT: 1772⁰C

STOPPING RANGE FOR 1 MEV AND 5 MEV PROTON: $4.95 \times 10^{-3}mm$ and 0.053mm

(p, γ) REACTIONS: $Pt^{194}(p, \gamma)Au^{195}$ $Pt^{198}(p, \gamma)Au^{199}$

$Pt^{195}(p, \gamma)Au^{196}$ $Pt^{192}(p, \gamma)Au^{193}$

$Pt^{196}(p, \gamma)Au^{197}$ $Pt^{190}(p, \gamma)Au^{191}$

(p,n) REACTIONS: $Pt^{194}(p,n)Au^{194}$ $Pt^{198}(p,n)Au^{198}$

$Pt^{195}(p,n)Au^{195}$ $Pt^{192}(p,n)Au^{192}$

$Pt^{196}(p,n)Au^{196}$ $Pt^{196}(p,n)Au^{196}$

RESIDUAL NUCLEUS DECAY SCHEME:

<u>Residual</u>	<u>$t_{1/2}$</u>	<u>Emittance</u>	<u>Residual</u>	<u>$t_{1/2}$</u>	<u>Emittance</u>
Au^{194}	39.5h	e^{-}, β^{+}, γ	Au^{198}	2.7d	e^{-}, β^{-}, γ

Au ¹⁹⁵	183d	e ⁻ , γ	Au ¹⁹⁹	3.15h	e ⁻ , β^- , γ
Au ¹⁹⁶	6.18d	e ⁻ , β^- , γ	Au ¹⁹²	4.1h	e ⁻ , β^+ , γ
Au ¹⁹⁷	Stable		Au ¹⁹³	15.8h	e ⁻ , γ

OTHER PERTINENT INFORMATION:

Specific Heat: 0.0317 cal/gm°C

Coulomb Barrier: 11.83 Mev

Thermal Cross Section for (n, γ): Pt¹⁹⁴ = 1.2b

Pt¹⁹⁵ = 27b

Pt¹⁹⁶ = 0.74b

Pt¹⁹⁸ = 3.7b

Pt¹⁹² = 14b

Pt¹⁹⁰ = 150b

H. TARGET MATERIAL: Iron

DENSITY: 7.874 gm/cm³

MELTING POINT: 1535°C

STOPPING RANGE FOR 1 MEV AND 5 MEV PROTON: 6.51 x 10⁻³mm and 0.081mm

(p, γ) REACTIONS: Fe⁵⁶(p, γ)Co⁵⁷

Fe⁵⁴(p, γ)Co⁵⁵

Fe⁵⁷(p, γ)Co⁵⁸

Fe⁵⁸(p, γ)Co⁵⁹

(p,n) REACTIONS: Fe⁵⁶(p,n)Co⁵⁶

Fe⁵⁴(p,n)Co⁵⁴

Fe⁵⁷(p,n)Co⁵⁷

Fe⁵⁸(p,n)Co⁵⁸

RESIDUAL NUCLEUS DECAY SCHEME:

<u>Residual</u>	<u>t_{1/2}</u>	<u>Emittance</u>
Co ⁵⁷	270d	X-rays, e ⁻
Co ⁵⁵	18.2h	X-rays, γ , β^+
Co ⁵⁸	71.3d	X-rays, γ
Co ^{58m}	9.2h	X-rays, β^+
Co ⁵⁹	STABLE	

OTHER PERTINENT INFORMATION:

Specific Heat: 0.106 cal/gm°C

Coulomb Barrier: 5.55 Mev

Prompt Gammas: 0.354, 0.847, 1.266, 1.379, 1.760, 1.922 Mev

IV. RECOMMENDATIONS: For testing the neutral particle beam at the 1 Mev level, any one of the eight targets would be acceptable. There will be gammas from (p, p' γ) and (p, γ) reactions but these can be shielded by lead or concrete, thereby preventing any personnel from receiving a gamma radiation dosage in excess of the maximum permissible dose. All nuclides of all eight targets have (p,n) threshold energies in excess of 5 Mev [except C¹³ with a 3.23 Mev (only 1.1% isotopic abundance) and Pt and Pb]. Both Pt and Pb would be good targets for energies up to 10 Mev because any element with a mass number Z greater than 50 has a coulomb barrier of 10 Mev for a proton; therefore, giving zero or negligibly small capture cross section for (p, γ) and (p,n) reactions.

Up to 3 Mev s, Carbon would be a suitable target while aluminum would make an acceptable target up to 5 Mev . Iron would be acceptable up to 5 Mev if it were not for Fe⁵⁷'s low 1.65 Mev (p,n) threshold energy (2.19% isotopic abundance). Iron also has large thermal neutron cross sections,

making it unattractive if neutrons are produced.

Ice would be a good target because protons do not react with H' (99.985% isotopic abundance) and O^{16} has a threshold energy of 17.23 Mev for (p,n). Oxygen-17, which has a 5.61 Mev (p,n) threshold, is only 0.037% isotopic abundant and O^{16} , which has a 7.99 Mev (p,n) threshold, is only 0.204% isotopic abundant. Ice would have to be highly purified by distillation.

Silicon would make a good target up to 5 Mev if it were not for its cost of purified silicon and the limited size of silicon grown crystals.

From a reaction viewpoint, probably the most suitable target for the neutral particle beam is liquid helium, because of its high (p,n) threshold of 29.36 Mev and its zero nonelastic nuclear interaction probability up to 20 Mev. However, calculations show that the liquid helium that evaporates by absorbing the beam energy is too large a volume per unit time for the diffusion vacuum pumps to handle. If the liquid helium is incased, problems arise because there is no material thin enough to allow passage of the low energy protons and at the same time strong enough to withstand the gas pressure resulting from high energy protons.

Other factors to be considered in addition to selecting a target are the target design, the cooling of the target, the cost, the shielding of gamma rays with lead or concrete, and the capture of neutrons, if any are produced via (p,n) reactions, in the $LiCO_3$ or BF_3 paraffin shielding bricks. These factors were discussed with other scientists and the consultations are reported in my lab notebook.¹²

REFERENCES

1. Howerton, R. J., An Integrated System For Production of Neutronics and Photonics Computational Constants, Vol. 9, Lawrence Radiation Laboratory, University of California, Livermore, California, September, 1970.
2. Kenny, N. J., J. R. Bird, and E. Clayton, "Proton Induced X-Ray Yields", Nuclear Instruments and Methods, Vol. 168, 1980, pp. 115-120.
3. Meyerhof, W. E., Elements of Nuclear Physics, New York, N. Y., McGraw-Hill Book Company, 1967.
4. Janni, J. F., "Proton Range-Energy Tables, 1 Kev-10Gev", Atomic Data and Nuclear Data Tables, Vol. 27, No. 4/5, New York, Academic Press, 1982.
5. Radiological Health Handbook, U. S. Department of Health, Education, and Welfare, Washington, D. C., 1970.
6. Kunz, W. and J. Schintlmeister, Nuclear Tables, Part II, Nuclear Reactions, New York, Pergamon Press, 1965.
7. Maghabghab, S. F. and D. I. Garber, Neutron Cross Sections, Vol. 1. Resonance Parameters, National Neutron Cross Section Center, Brookhaven National Laboratory, Upton, N. Y., 1973.
8. Lederer, C. M. and V. S. Shirley (Eds.), Table of Isotopes, 7th ed., Wiley-Interscience, New York, 1978.
9. McGowan, F. K., W. T. Milner, and H. J. Kim, "Nuclear Cross Sections for Charged-Particle Induced Reactions", Vol. ORNL-CPX-1, Cross-Section Center, Oak Ridge National Laboratory, Oak Ridge, TN., 1964.
10. Barbier, M., Induced Radioactivity, London, North-Holland Publishing Co., 1969.
11. Hine, G. J., and G. L. Bronwell, Radiation Dosimetry, New York, Academic Press, 1956.
12. Consultation with the following people at Oak Ridge National Lab: R. T. Santoro (shielding and Dose Rate), C. H. Johnson (cross sections and platinum target), W. Stirling and C. C. Tsai (Target Design), and M. Hyder (Silicon Target and Detectors).
13. Particle Beam Test Configuration, Internal Document, Arnold Engineering Development Center, Arnold AFS, Tennessee, 1984.
14. Glasstone, S., Sourcebook on Atomic Energy, 3rd Ed., Princeton, N. J., D. Van Nostrand Co., 1967.
15. Lyon, W. S., Guide To Activation Analysis, Princeton, N. J., D. Van Nostrand Co., 1964.
16. McGowan, F. K. and W. T. Milner, "Reaction List for Charged-Particle Induced Nuclear Reactions", Atomic Data and Nuclear Data Tables, New York, Academic Press, Vol. 18, No. 1, 1976; Vol. 15, No. 3, 1975; Vol. 12, No. 6, 1973; Vol. 11, No. 1, 1972; Vol. 9, No. 6, 1971.
17. McGowan, F. K. and W. T. Milner, "Charged-Particle Reaction List 1948-1971", Atomic and Nuclear Data Reprints, New York, Academic Press, Vol. 2, 1973.
18. Chilton, A. B., J. K. Shultis, and R. E. Faw, Principles of Radiation Shielding, Englewood Cliffs, N. J., Prentice-Hall, 1984.
19. Shapiro, M., "Cross Sections for the Formation of the Compound Nucleus by Charged Particles", Phys. Rev., Vol. 90, p. 171 (1953).
20. Elwyn, A., A. Marinov, and J. Schiffer, "Proton Reaction Cross Sections and Strength Functions", Phys. Rev., Vol. 145, p. 957 (1966)
21. Wallace, R. and C. Sondhans, Techniques Used in Shielding Calculations for High Energy Accelerators: Application to Space Shielding, UCRL-10439, Lawrence Radiation Laboratory, Berkeley, Cal., 1962.

1985 USAF-UES SUMMER FACULTY RESEARCH PROGRAM/
GRADUATE STUDENT SUMMER SUPPORT PROGRAM

Sponsored by the
AIR FORCE OFFICE OF SCIENTIFIC RESEARCH

Conducted by the
UNIVERSAL ENERGY SYSTEMS, INC.

FINAL REPORT

Prepared by:	Terrill D. Smith
Academic Rank:	Professor
Department and University:	Central State University Edmond, OK
Research Location:	Air Force Wright Aeronautical Laboratory
USAF Research	Dr. Christ Tamborski
Date:	29 July 1985
Contract No.	F49620-85-C-0013

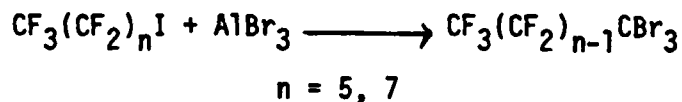
Preparation of Non-flammable

Model Compounds

Abstract

Terrill Smith

The reaction between perfluoroalkyl iodides and excess anhydrous aluminum bromide proceeds spontaneously at room temperature and results primarily in the corresponding 1,1,1-tribromoperfluoro alkane, according to the equation:



Control of the reaction is greatly facilitated by dissolving the aluminum bromide in methylene bromide solution. Yields ranged from 38% to 77%. The reaction between aluminum bromide and perfluoroalkyl bromides is not spontaneous at room temperature.

A mixture of perfluoroalkyl iodides was converted to the corresponding perfluoroalkyl bromides by reaction with bromine. Pure samples of $\text{C}_6\text{F}_{13}\text{Br}$, $\text{C}_8\text{F}_{17}\text{Br}$, and $\text{C}_{10}\text{F}_{21}\text{Br}$ were isolated by means of precision distillation and crystallization.

Several exploratory and/or confirmatory experiments were carried out to establish the generality of reactions of perfluoroalkyl halides with metal halides.

Acknowledgements

The author wishes to express his gratitude to the Air Force Systems Command, the Air Force Office of Scientific Research, and to the non-structural materials branch of AFWAL for the sponsorship and encouragement of this program. Thanks also go to the administration at Central State University for allowing me to change my summer plans from teaching to research.

The personnel in the laboratories of Building 450 are hereby recognized for their cooperation and help in learning the routine activities there, with a special word for Dr. K. C. Eapen who freely shared his laboratory, his knowledge, and his friendship.

I. Introduction

The non-structural materials branch of the non-metallic division of the Air Force Wright Aeronautical Laboratory (AFWAL) is charged with the responsibility of maintaining research programs on materials suitable for use in high performance aircraft, missile, and space systems. Such systems may encounter extremes of temperature, pressure, and mechanical stress and may also involve unusual materials at construction. Included in these systems are materials which serve as lubricants, heat-transfer agents, and hydraulic fluids. Fire-resistant hydraulic fluids are now being phased into many Air Force aircraft and higher system pressures are also contemplated, with a concomitant higher risk of fire.

The ultimate goal of a fireproof aircraft hydraulic fluid is being pursued at AFWAL. Only a few classes of organic compounds are potential candidates; among them are perfluoro compounds and other halogen-containing perfluoro compounds.

As an industrial research chemist, the writer gained considerable experience in the synthesis, formulation, manufacture, and testing of a commercial fire-resistant aircraft hydraulic fluid. I also had previously worked for an airframe manufacturer and was thus somewhat familiar with the problems and requirements which are unique to that industry. In addition I had also become acquainted with organic fluorine compounds and had prepared a number of them by various means. I assume it is because of this combination of factors which qualified me for the Summer Research Program at AFWAL.

II. Objectives at the Research Effort

- A. To prepare and characterize model compounds possessing desirable physical properties.
- B. To determine the optimum conditions under which a particular model compound can be made.
- C. To investigate alternate routes to a particular model compound.
- D. To determine the scope and limitations of a particular synthetic procedure.

III. Details and Results

A. Perfluoroalkyl iodide reaction with aluminum bromide

Perfluoroalkyl iodides will react with aluminum halides to yield 1,1,1-tribromoperfluorooctane according to the equation (1)



X = Cl or Br

n (in this work) - 5 or 7

The fate of aluminum in this reaction is unknown. However, in the procedure below the aluminum compounds present are removed as water-soluble salts. To prepare 1,1,1-tribromoperfluorooctane a general procedure is as follows: A calculated amount of perfluoroalkyl iodide ($\text{R}_\text{F}\text{I}$) is added to a stirred solution of anhydrous aluminum bromide (2 x moles of $\text{R}_\text{F}\text{I}$) in methylene bromide (2) keeping the temperature of the reaction mixture below 30° during the addition. The mixture is

allowed to stir for an additional six hours, then heated to 70-80° for 1 hour. After cooling to room temperature the mixture is poured into ice-water containing an excess of sodium thiosulfate to react with elemental iodine. The two-phase mixture is filtered, the layers are separated, and the organic layer is washed with water. The organic layer is dried, cooled in ice-water, and the product removed by filtration.

The results of experiments involving perfluorohexyl iodide (1) and perfluorooctyl iodide (2) with aluminum bromide (AlBr_3) are shown in Table I.

TABLE I
Reaction of Perfluoroalkyl Iodides ($R_F I$) with $AlBr_3$

$R_F I(a)$	Moles $R_F I/AlBr_3$	Conditions	Results
1	1/3	No solvent, heated to 50°	Vigorous exothermic reaction. $C_5F_{11}CBr_3$ product identified by GC-MS.
1	1/3	No solvent, heated to 42°. Reflux with Freon 113(b) after initial heating	Product mixed with rearrangement and replacement products from Freon
1	1/3	Heptane added as solvent, heated to 50°	No $C_5F_{11}CBr_3$ present in mixture.
1	1/3	No solvent, heated 3 hr. @ 35° then heated to 75°	Some reaction visible at 75°. Product evaporated along with acetone solvent.
1	1/3	No solvent. After $R_F I$ added @ 45°, heated to 75°.	Product formation followed by GC.
1	1/3	$AlBr_3$ dissolved in CH_2Br_2 , temp held below 30° during $R_F I$ addition	38% yield (c)
1	1/1.5	$AlBr_3$ dissolved in CH_2Br_2 , temp held below 27°	40% yield (c). Impurity identified as $CF_3(CF_2)_4CHBr_2$ present (0.4%)
2	1/3	No solvent, room temperature	46% yield (d). M.p. of purified product 45-6(e)
2	1/2	$AlBr_3$ dissolved in $CH_2Br_2(f)$, added to $R_F I$ below 28°	57% yield (d)
2	1/2	$AlBr_3$ solution added below 30°, mixture steam distilled	77% yield (d). Impurity identified as $CF_3(CF_2)_6CHBr_2$ present (1%)
2	1/2	Identical with previous run except not steam distilled	57% yield(d)
2	1/2	Room temperature, stirred for 18 hours	58% yield (d)
2	1/2	Inverse addition of $AlBr_3$ solution, steam distilled	46% yield (d)
2	1/2	Mixture diluted with ether before hydrolysis.	25% yield(c)

(a) $C_6F_{13}I(1)$, $C_8F_{17}I(2)$

(c) By gas chromatographic analysis of mixture

(e) Prepared and characterized by Dr. K. C. Eapen (AFWAL) 126-7

(b) 1,1,2-trifluoro-1,2,2-trichloroethane

(d) Isolated

(f) All subsequent experiments involving $C_8F_{17}I$ made use of CH_2Br_2 as solvent for $AlBr_3$

B. Miscellaneous Experiments

In any research effort it is usually necessary to carry out a variety of experiments to determine what will work and what will not. While these may not be part of the primary investigation they may establish the limits of a particular reaction or the source of unexpected products. Table II contains information on such experiments.

Table II.

Miscellaneous Experiments Related to the Reaction of R_fI with $AlBr_3$

<u>Reactants</u>	<u>Conditions</u>	<u>Purpose</u>	<u>Results</u>
$C_6F_{13}I$, $FeCl_3$	No solvent, heated to 75°	Determine whether a less active (than $AlBr_3$) metal halide would work.	$C_6F_{13}I$ lost by evaporation
$C_6F_{13}I$, $FeCl_3$	No solvent, heated in bomb at 130°	Same as above	White solid mp $107-9^\circ$. No further analysis
Freon 113, $AlBr_3$	Reflux 3 hours	Verify literature reference (3)	White solid, mp $208-210^\circ$ (dec) No further analysis
$C_6F_{13}I$, CBr_4 , Zn	Reflux 3 hours in dioxane solvent	Determine reactivity of mixture toward coupling	Unknown product, MW 404 by GC-MS
$CF_3(CF_2)_6CBr_3$, $AlBr_3$	Conditions for reaction of R_fI with $AlBr_3$	Determine if product could be the source of the impurity, $CF_3(CF_2)_6CBr_2H$	No apparent reaction under condition used
$C_8F_{17}Br$, $AlBr_3$	Conditions for reaction of R_fI with $AlBr_3$	Determine the reactivity of R_fBr	No apparent reaction under condition used
$C_8F_{17}Br$, $AlBr_3$	90° for 4 hours	Same as above	Product appeared after 2 hours; unreacted $C_8F_{17}Br$ present after 4 hours.

IV Recommendations

The discovery that aluminum bromide (AlBr_3) is soluble in methylene bromide has made the use of that reagent much more controllable and convenient. Because of this it is recommended that other perfluoroiodo compounds be investigated for reactivity with AlBr_3 .

This research was concentrated on establishing the optimum conditions for the reaction of perfluorooctyl iodide with AlBr_3 to produce 1,1,1-tribromoperfluorooctane which is a solid at room temperature. Since solids have little applicability it is recommended that the reaction between perfluorohexyl iodide and aluminum bromide be investigated further because the expected product would probably be liquid.

It is also recommended that a search for a solvent for aluminum chloride be continued so that a heterogeneous reaction system can be avoided.

Since only one example of a metal halide other than the aluminum halides has been tried, it is further recommended that an exploratory study be undertaken to determine if other metal or non-metal halides might be effective. Examples of possible candidates are FeCl_3 , FeBr_3 , GaCl_3 , BCl_3 , BBr_3 , ZnCl_2 , ZnBr_2 , and SnBr_4 , just to name a few.

References

1. Bissell, E.R., J. Org. Chem. 29, 252 (1964)
2. Karpov, V.M., Mezhenkova, T.V., Platanov, V.E., and Yakobson, G.G., J. Fluor. Chem. 28, 115 (1985)
3. Miller, W.T., Jr., Fager, E.W., Griswald, P.H., J. Am. Chem. Soc. 72, 705 (1950)

1985 USAF-UES SUMMER FACULTY RESEARCH PROGRAM/

GRADUATE STUDENT SUMMER SUPPORT PROGRAM

Sponsored by the

AIR FORCE OFFICE OF SCIENTIFIC RESEARCH

Conducted by the

UNIVERSAL ENERGY SYSTEMS, INC.

FINAL REPORT

STUDIES ON COMBUSTION OF LIQUID FUEL SPRAYS

IN STAGNATION FLOWS

Prepared by:	Siavash H. Sohrab
Academic Rank:	Assistant Professor
Department and	Mechanical and Nuclear Engineering
University:	Northwestern University
Research Location:	Air Force Rocket Propulsion Laboratory, Liquid Rocket Division
USAF Research:	Mr. Michael Powell
Date:	September 19, 1985
Contract No.:	F49620-85-C-0013

STUDIES ON COMBUSTION OF LIQUID FUEL

SPRAYS IN STAGNATION FLOWS

by

S. H. SOHRAB

Department of Mechanical and Nuclear Engineering
Northwestern University

ABSTRACT

The report introduces studies on steady combustion of polydispersed sprays of liquid kerosene, heptane, octane and ethyl-alcohol in the stagnation-point flows. The burner assembly is designed to produce polydispersed sprays of the fuels within the background gaseous methane/air mixtures. Thus, steady combustion of these fuels within a planar flame adjacent to the boundary layer near a quartz plate can be studied. Using the laser sheet lighting for photography, the flow field as well as droplet size and distribution throughout the pre and post flame regions are investigated. Photographs of burning kerosene droplets as they pass through planar lean methane/air flames are presented. Also, preliminary results on combustion of heptane, octane and ethyl-alcohol sprays in lean methane/air mixtures are discussed. The potential implication of the experimental model to future study of the structure, extinction and stability of poly and monodispersed spray combustion is emphasized.

ACKNOWLEDGEMENTS

This research was sponsored by The Air Force Office of Scientific Research/AFSC, United States Air Force, under contract F49620-85-C-0013. The work was performed at Air Force Rocket Propulsion Laboratory (AFRPL) under Universal Energy Systems Summer Faculty Research Program.

The author expresses his deep appreciation to Mr. Michael Powell of AFRPL for his help and support. Also, the assistance of Mr. Ranney Adams of the Combustion Research Laboratory of AFRPL is kindly appreciated. The hospitality of the personnel at the AFRPL is greatly appreciated.

I. INTRODUCTION

Combustion processes in sprays of liquid hydrocarbon fuels are of central significance to the understanding of gas turbine engines and liquid rockets. In addition, spray combustion has diverse application in industrial boilers, furnaces, diesel engines, and fuel-injected spark ignition engines. Although problems of solid propellant rockets have been extensively studied, liquid rockets and the associated stability problems remain to be resolved. In view of the significant advantages of liquid rockets in terms of their shut-off and re-ignition capabilities, progress in this area of combustion science is needed. Here, the simultaneous presence of the two phases complicate the homogeneous chemically reacting flow and the resulting interactions between flow/flame/droplet greatly enrich the physical phenomena.

Most studies of spray phenomena have been concerned with combustion of free or suspended single droplets. Even though such studies are significant for fundamental understanding of droplet burning they are only partly helpful in description of spray combustion. Because of the complex interaction between droplets, the results of tests on single droplet or those considering an array of droplets cannot be readily extended to the turbulent spray combustion which often involve dense sprays. In spite of their wide applications, relatively few studies on spray combustion have been reported. Early theoretical study of sprays was initiated by Williams [1,2] who introduced statistical formulation of the spray problem. More recently, the application of large activation energy matched asymptotic technique to spray combustion has been initiated [3].

Early experimental works on sprays were primarily of qualitative

nature providing some rudimentary understanding [4]. More recently, combustion of monodispersed sprays was investigated in Wilson-cloud chamber type apparatus [5,6]. Here, by sudden expansion of the saturated vapor of the fuel, a cloud of small droplets were generated. The spherical propagation of flame through such drops were thus studied. Also, propagation of flames in bunsen type inverted cone flames have been reported [7,8]. Here, by measuring the cone angle the flame propagation speed could be approximately deduced. The propagation of planar flames in sprays passing through tubes have also been studied [9]. These works on spray have greatly contributed to our knowledge of spray combustion. Among other observations, the thicker reaction zones with either smooth or corrugated flame surfaces have been observed. Also, the propagation speed of the flame front through such poly or mono-dispersed sprays have been determined [5-9].

Although the above mentioned studies have provided much needed insight into spray combustion, the complete modeling of actual spray has not been fully possible in these models. This is primarily caused by either the absence of flow nonuniformity or the unsteady nature of such studies. For example, spherical propagation of flame in the cloud chamber [5,6] is basically unsteady and one-dimensional. Also, the inverted cone studies [8] involve complex fluid mechanics of entrainment and the associated lack of control of the mixing shear layers. Finally, the planar flame propagation is one dimensional. It is well established however that in actual turbulent spray combustion fields, flames always encounter velocity gradients and therefore are under stretching or compression as discussed by Karlovitz [10].

II. OBJECTIVES OF THE RESEARCH EFFORT

What motivated the present investigation is to include this important factor relevant to flame stretching in the modeling of spray combustion. In view of the fact that the spray combustion in liquid rockets is fully turbulent, inclusion of this stretch is quite significant. Therefore, in the present investigation, the spray of liquid hydrocarbon fuels will be studied within the stagnation flow configuration, where the rate of stretch can be systematically controlled. Application of stagnation flow configuration to the study of flame extinction has a relatively long history [11]. More recent works, among others, have considered the application of stagnation point [12] and counterflow [13,14] configurations to the study of combustion of gaseous fuels. However, to the author's knowledge, the present study represents the first application of the stagnation flow configuration to the study of liquid fuel sprays.

In this experimental work, the feasibility of the proposed model will be first established. This will be followed by the discussion of the subsequent application of the model to the investigation of a variety of problems related to spray combustion. Among others, problems related to theoretical and experimental investigation of flame interaction initiated by Sohrab et al. [15,16] will be extended to spray burning. Moreover, the problem of flame stability [17,18] in sprays will be addressed within the framework of this new model. For this preliminary study, we will consider kerosene, heptane, octane and ethyl-alcohol as representative hydrocarbon fuels. The choice is motivated by the relevance to liquid rocket fuels as well as the ease of comparison of flame speeds with existing data obtained by previous studies with other techniques mentioned earlier.

III. EXPERIMENTAL

The burner system is composed of a contoured nozzle, a flat quartz plate and a high pressure liquid fuel atomizer. In Fig. 1 the schematic of the stagnation flow spray burner assembly is shown. Air and gaseous fuel are metered by conventional rotameter and premixed in the lower chamber of the burner before passage through a series of mesh screens as shown in Fig. 1. The combustible mixture enters the 4" diameter extension tube containing glass beads producing uniform velocity profile within the tube.

A high pressure liquid fuel atomizer is situated in the center of the extension tube as show in Fig. 1. The atomizer nozzle is enclosed within an outer tube jacket which drains the excess unatomized liquid. Liquid fuel is introduced into the atomizer from a 3 liter storage tank pressurized by high pressure nitrogen using a pressure regulator. At this preliminary stage, a conventional atomizer designed to operate at 100 psig under a constant flow rate of 0.85 gallon/hour was used. Thus, changing the liquid fuel flow rate was only possible through reducing liquid pressure. However, this would require operation of the atomizer outside of its designed pressure range thus causing irregular and nonuniform atomization. Moreover, the rated capacity of 0.85 GPH is an order of magnitude in excess of the required flow rate of the fuels being considered. Therefore, the atomizer was functional for the purpose of providing the feasibility study reported herein. However, the need for an improved atomizer is of central importance to this project as will be discussed later.

The atomized droplets are in part entrained by the methane/air mixture. In passing through the contoured nozzle a uniform velocity

polydispersed spray is formed at the exit plane of the nozzle. This flow subsequently impinges on a flat quartz plate located 1" above the nozzle rim. As shown in Fig. 1, a ring of cooling water with small water jets surrounds the nozzle for cooling the rim as well as the exhaust system. Another drain pipe is provided for droplets which may accumulate within the glass bead region. A photograph of the burner assembly with the supporting instrumentation is shown in Fig. 2.

In Fig. 3, a photograph of a typical lean methane/air flame obtained within the burner is shown. Here, the outer peripheries of the flame bend downward due to the surrounding exhaust suction (see Fig. 1). The quartz plate provides for the observation and photography of the spray from the top. Since some drops can survive through reaction zone and will impinge on the hot quartz plate, the thermal shock property of silica is essential. The observations through the transparent window allows for better monitoring of droplet motion, evaporation and combustion after the reaction zone. The system is capable of providing a stable flat flame of any gaseous fuel with the simultaneous possibility of introducing droplets of any other liquid fuel into the flow field.

For observation and evaluation of size of the droplets a sheet of Argon-ion laser beam is produced. Here, the beam is passed through a cylindrical lens producing a sheet of light about 2 mm in thickness. The sheet can be oriented parallel or perpendicular to the axis of the spray jet. This will allow for observation of droplet streamlines and diameter variations, respectively, at any axial and radial location within the flow field.

IV. RESULTS AND DISCUSSION

In these preliminary studies, combustion of polydispersed droplets of kerosene, heptane, octane and ethyl-alcohol within the background of lean methane/air mixture have been considered. The experiments involve the establishment of a homogeneous lean methane/air flame such as shown in Fig. 3. Next, droplets of the above fuels are introduced into the flow field and burn as they enter the planar methane flame. Therefore, the methane flame acts as an ignition source for the sprays. The fuel droplets are made visible by the laser light scattering.

Basically, two distinguishable burning modes were observed depending on the volatility of the liquid fuels. For less volatile fuels with large heat of vaporization, such as kerosene or ethyl-alcohol, droplets remain intact until they closely approached the methane flame. Here, the evaporation and combustion is primarily near and downstream of the methane flame. For volatile fuels such as heptane and octane, on the other hand, droplet evaporation occurs immediately after atomization. Thus, these fuels produce appreciable vapor which subsequently burns within the methane flame.

A series of photographs showing various stages as increasingly more droplets of kerosene are added to the methane/air mixture are shown in Figs. 4-9. First, the planar methane flame of Fig. 4 changes and anchors on the nozzle rim as shown in Fig. 5 as a result of the change in mixture composition and the approach towards stoichiometric condition. A trace of yellow color due to formation of soot follows the individual kerosene drops as they burn downstream of the methane flame. For large quantities of droplets, the soot formation is quite large, see Figs. 8-9, as expected for these exceedingly rich burning

conditions.

Another observation in Figs. 4-9 is the gradual thickening of the reaction zone as kerosene is added to CH_4/air mixture. This agrees with the earlier observations [5,6] of the reaction zones in sprays as compared to homogeneous gaseous mixtures. Also, variation of the flame position with respect to the stagnation plane is detected which is an indication of the change in the flame propagation speed. Indeed, the value of the axial velocity at the upstream edge of the preheat zone is defined as the flame propagation speed conditions. Evaluation of the propagation velocity of sprays is one of the main objectives of the present investigation. It is also noted that as more droplets of kerosene are added, the methane flow rate can be substantially reduced while maintaining steady burning. The characteristics of ethyl-alcohol droplets burning in methane/air were similar to those of kerosene. Photographs of ethyl-alcohol flames are as yet not available.

For heptane and octane sprays, the flames were found to be highly corrugated and unstable. As mentioned earlier, this is caused by the rapid evaporation of the droplets and the consequent mixture composition nonuniformity. Moreover, the flames of these sprays showed highly cellular structures under chaotic motion. This is expected for rich mixtures of these fuels and is the manifestation of the diffusional-thermal instability predicted by Sivashinsky [17]. It is believed that the generation of uniform droplets by the atomizer is essential to obtaining flat, but not necessarily smooth, flames of these fuels. This further emphasizes the importance of the low flow rate atomizer to the future success of the present investigation.

V. CONCLUDING REMARKS AND RECOMMENDATIONS

The present report represents the first investigation of the combustion of liquid fuel sprays in the stagnation flow configuration. The complete description of all of the implications of the present experimental model is quite extensive and will encompass almost every aspect of the field of spray combustion. In what follows certain general and immediate application of the experimental system will be outlined and their relevance to the broad topic of turbulent spray combustion will be emphasized. The objective of the studies described herein is to help in closer modeling and improved understanding of the combustion processes within turbulent sprays such as in liquid rocket engines.

To begin with, the position of flames within the stagnation flow will provide for immediate evaluation of the flame propagation speed of poly or mono-dispersed sprays under varying rates of stretch. The extrapolation to zero rate of stretch will then give the precise value of the laminar flame propagation speed in the spray. Here, the flame propagation speed is defined as the value of the axial velocity at the upstream edge of the preheat zone. It is noted that since flame surfaces within turbulent sprays always undergo stretching, the provision for systematic variation of the stretch rate by the model is significant.

Another important feature of the present model is that it provides a steady and planar flame within the spray, thus allowing for accurate diagnostic evaluation of the flame structure. Therefore, both pre and post-flame processes can be investigated. Furthermore, the phenomena of flame extinction due to variations in droplet size, droplet number

density or rate of stretch can be studied. The knowledge of flame extinction is important since it determines whether or not a flame sheet will undergo local extinction within the turbulent spray. Also, determination of the temperature profile across the planar flame will provide much needed information concerning the structure of the reaction zone.

Since the fuel droplets scatter laser light, determination of the droplet velocity with laser doppler velocimetry is readily accomplished without the need for seeding the flow field with particulates. Also, using the laser sheet lighting, the trajectory, size and distribution of droplets can be determined through photography and cinematography. Therefore, the actual history of evaporation and combustion of the droplets can be studied. Since velocities after the planar flame increase by many folds due to sudden expansion, the motion of droplets are expected to be accelerated. Knowledge of the droplet history and possible break-up through such severe velocity and temperature gradients is important to the understanding of spray combustion.

In addition, the experimental model can be used to evaluate the burning characteristics of sprays under systematic variation in the phase of the fuel. Using a liquid vaporizer, the fuel can be introduced either as droplet or as vapor premixed with air. Since the reaction zone is governed by gas phase combustion, depending on the overall fuel/air ratio, an optimum burning regime can thus be identified. Also, combustion of any liquid fuel within the background of another gaseous fuel and oxidizer mixture can be analyzed. Indeed, the results presented herein on combustion of kerosene droplets within lean methane/air mixture represents such situation. The potential

implication of an optimization procedure when the characteristics of the liquid and gaseous fuels are judiciously chosen could be far reaching and in need of further exploration.

As was mentioned earlier, in rich sprays of heptane and octane, the flame surfaces were observed to assume cellular structure. Thus, the present model is an excellent vehicle for the study of the well known flame instability phenomena in turbulent spray combustion. The understanding of the methods for suppression or judicious enhancement of such instabilities [18] is also relevant to the understanding of liquid rocket combustion. Finally, the study of counterflow diffusion flames of two sprays can be performed. Here, the structure of a diffusion flame supported by counterflowing sprays of oxidizer and fuel within the background gaseous nitrogen will be considered. Studies on interactive combustion of premixed flames introduced earlier [15,16] can also be extended to sprays in the counterflow configuration.

In view of the above considerations, the diverse and significant applications of the proposed model to the study of spray combustion is apparent. The present preliminary efforts thus far successfully established the feasibility of the model. Although the above mentioned topics are quite diverse in nature, they can all be viewed within a global framework aimed at modelling turbulent spray combustion. Various aspects of the studies outlined above will be pursued by the author at Northwestern University.

REFERENCES

1. Williams, F. A., 8th Symposium (International) on Combustion, Williams and Wilkins Co., Baltimore, MD, 1962.
2. Williams, F. A., Combustion Theory, Addison Wesley, Reading, MA, 1965.
3. T. H. (David) Lin, "An Asymptotic Analysis of Flame Propagation in Dilute Sprays," Master's Thesis, Northwestern University (1984).
4. Wolfhard, H. G. and Parker, W. G., "Evaporation Processes in a Burning Spray," J. Inst. Petrol., 35, 118 (1949).
5. Hayashi, S. and Kumagai, S., "Flame Propagation in Fuel Droplet-Vapor-Air Mixtures," 15th Symposium (International) on Combustion, The Combustion Institute, 1974, pp. 445-452.
6. Hayashi, S., Kumagai, S. and Sakai, T., "Propagation Velocity and Structure of Flames in Droplet-Vapor-Air Mixtures," Combust. Sci. Tech. 15, pp. 169-177 (1976).
7. Mizutani, Y. and Nakajima, A., "Combustion of Fuel Vapor-Drop-Air Systems: Part I - Open Burner Flames," Combust. Flame 21, 343 (1973).
8. Polymeropoulos, C. E. and Das, S., "The Effect of Droplet Size on the Burning Velocity of Kerosene-Air Sprays," Combust. Flame 25, 247 (1975).
9. Ballal, R. D. and Lefebvre, A. H., "Flame Propagation in Heterogeneous Mixtures of Fuel Droplets, Fuel Vapor and Air," 18th Symposium (International) on Combustion, The Combustion Institute, 1981, pp. 321-328.
10. Karlovitz, B., Denniston, D. W., Knapschaefer, D. H. and Wells, F. E., "Studies in Turbulent Flames," 4th Symposium (International) on Combustion, Williams and Wilkins, Baltimore, MD, 1953, pp. 613-620.
11. Potter, A. E., Jr., Heimerl, S. and Butler, J. N., 8th Symposium (International) on Combustion, Williams and Wilkins Co., Baltimore, MD, 1962, p. 1027.
12. Sohrab, S. H. and Williams, F. A., "Extinction of Diffusion Flames Adjacent to Flat Surfaces of Burning Polymers," J. of Polymer Science, Polymer Chemistry Edition, 19, pp. 2955-2976 (1981).
13. Tsuji, H. and Yamaoka, I., First Specialist Meeting (Int.) of The Combustion Institute, Tome I, Bordeaux 1981, p. 111.
14. Tsuji, H. and Yamaoka, I., 19th Symposium (International) on Combustion, The Combustion Institute, 1982, p. 1533.

15. Sohrab, S. H., Ye, Z. Y. and Law, C. K., "An Experimental Investigation on Flame Interaction and the Existence of Negative Flame Speeds," 20th Symposium (International) on Combustion, The Combustion Institute, 1984.
16. Sohrab, S. H., Ye, Z. Y. and Law, C. K., "Theory of Interactive Combustion of Counterflow Premixed Flames," Combust. Sci. Tech. 45, pp. 27-45 (1985).
17. Sivashinsky, G. I., "On a Distorted Flame as a Hydrodynamic Discontinuity," Acta Astronautica 3, p. 889 (1976).
18. Sohrab, S. H. and Chao, B. H., "Influences of Upstream Versus Downstream Heat Loss/Gain on Stability of Premixed Flames," Combust. Sci. Tech. 38, p. 245 (1984).

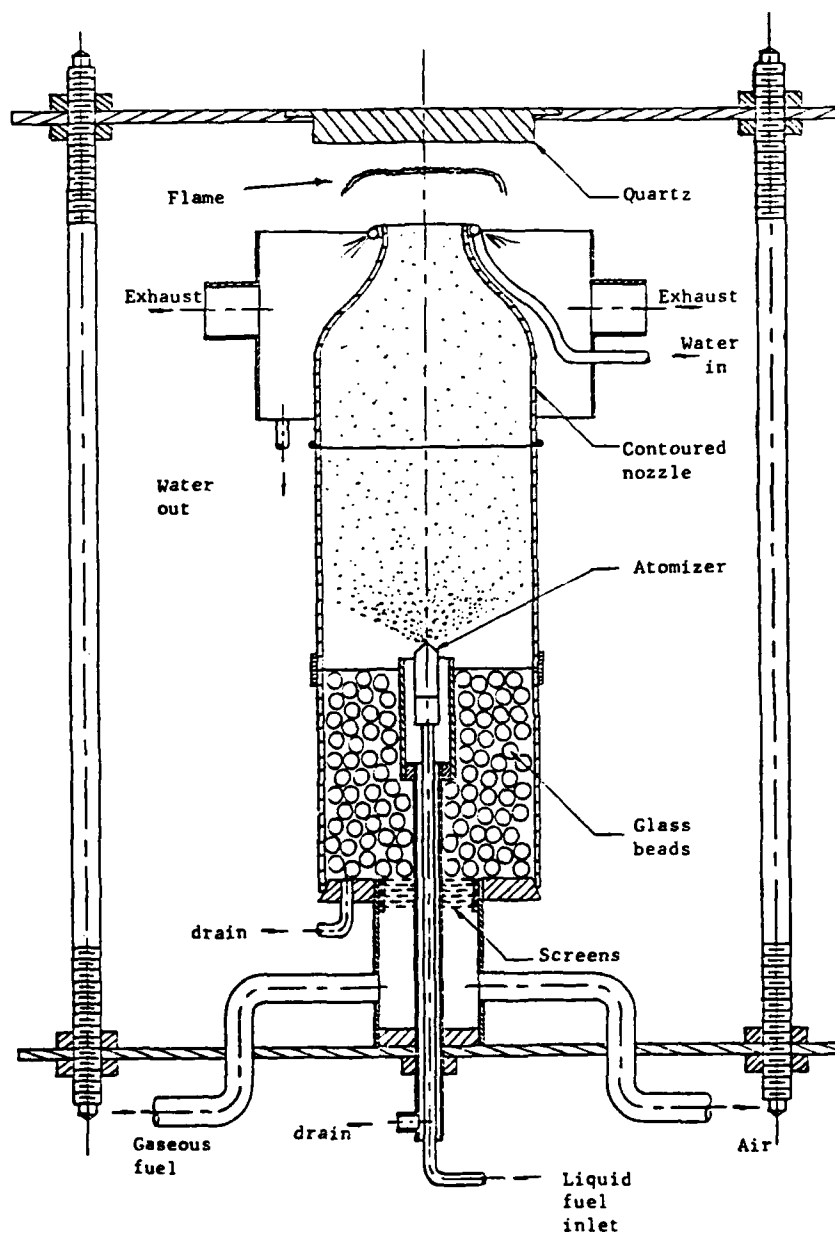


Fig. 1. Schematic of the stagnation flow spray burner.

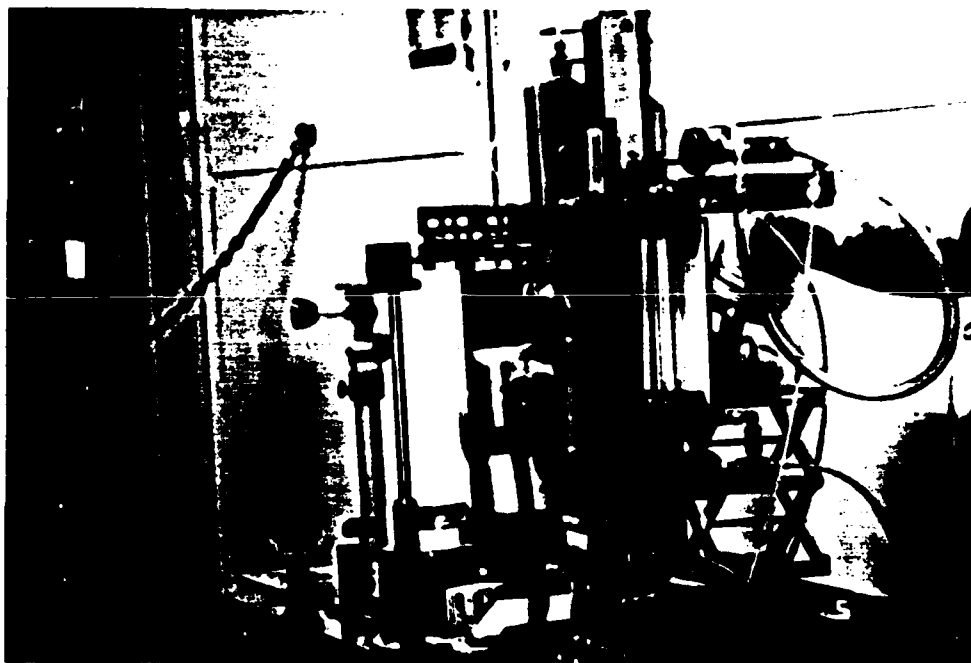


Fig. 2. Photograph of spray burner system.

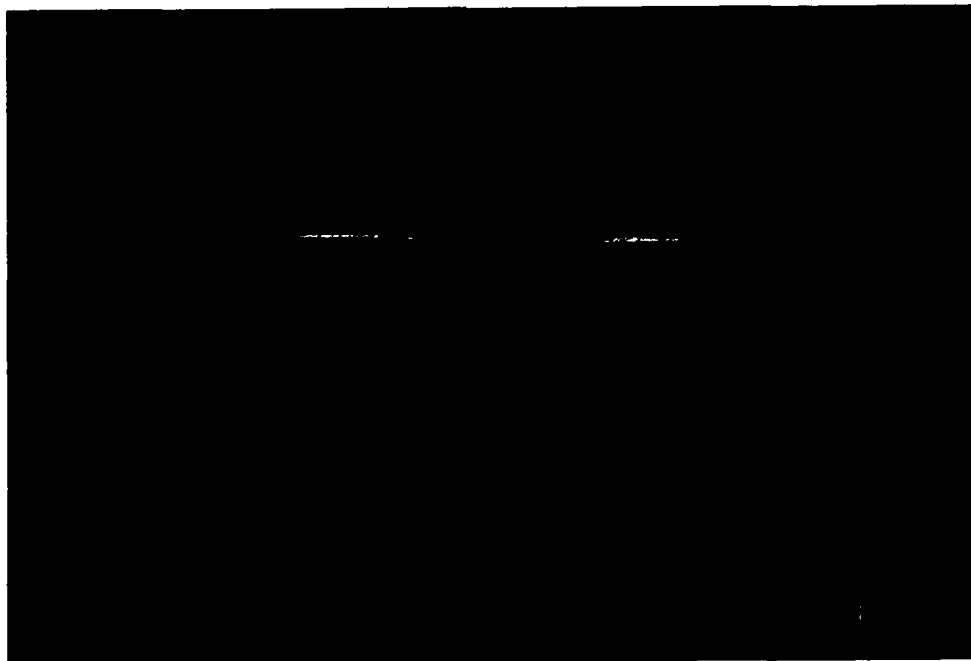


Fig. 3. Flat lean methane/air flame.

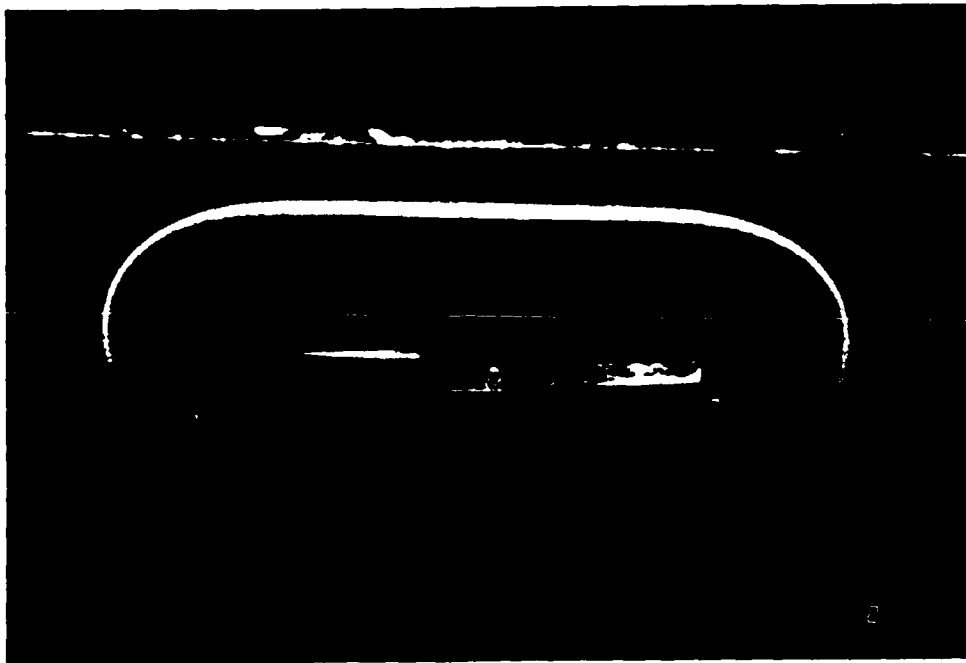


Fig. 4. Lean methane/air flame.

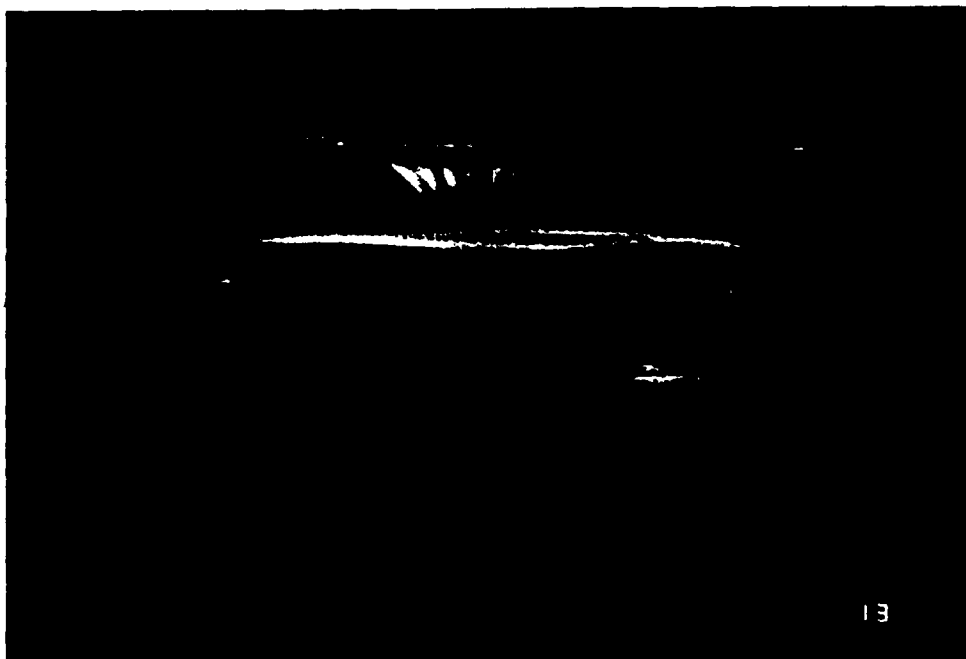


Fig. 5. Kerosene drops burning in methane/air mixture.



Fig. 6. Kerosene drops burning in methane/air mixture.



Fig. 7. Kerosene drops burning in methane/air mixtures.



Fig. 8. Kerosene drops burning in methane/air mixture.



Fig. 9. Kerosene drops burning in methane/air mixture.

1985 USAF-UES SUMMER FACULTY RESEARCH PROGRAM

Sponsored by the
AIR FORCE OFFICE OF SCIENTIFIC RESEARCH

Conducted by the
UNIVERSAL ENERGY SYSTEMS, INC.

FINAL REPORT

MONITORING ENVIRONMENTAL QUALITY BY METABOLITE ANALYSIS

Prepared by: Richard Stebbins, Ph. D.
Academic Rank: Associate Professor
Department and University: Department of Chemistry
University of Southern Maine
Research Location: Occupational and Environmental Health Laboratory,
Branch: Consultant Services Division, Environmental Quality
USAF Research: Maj Thomas Doane, USAF, BSC
Date: September 10, 1985
Contract No: F49620-85-C-0013

Monitoring Environmental Quality by Metabolite Analysis

by

Richard G. Stebbins

ABSTRACT

The USAF has an interest in determining the extent of its culpability for environmental damage caused by its more heavily used products such as JP-4 jet fuel, insecticides, and plane deicer. The transient nature of the toxic components of some products in the environment makes specific chemical monitoring of suspected spills problematic. Bluegills were separately exposed to the insecticide malathion and JP-4 jet fuel and their livers and gut analyzed for the toxic components and metabolites of these components. The analyses and the feasibility of using such analyses to monitor environmental quality is discussed.

ACKNOWLEDGMENTS

This author is most appreciative of the opportunity provided by the Air Force Systems Command, The Air Force Office of Scientific Research, and Universal Energy Systems. The time spent at the Occupational and Environmental Health Laboratory, Brooks Air Force Base, Texas was productive and professionally enlightening. The personnel at OEHL provided an excellent working environment and were always supportive.

More specifically, I would like to thank Maj Thomas Doane, Chief, Ecology Function, for initiating and providing direction for this project. I would also like to thank all the individuals in the Sample Analysis Section for their cooperation. A complete list of those aiding the project is too long to cite, but special thanks goes to Al Nishioka, Charles Martin, Adrain Sanchez, Dennis Mark and Lt Diana Bell.

INTRODUCTION:

The USAF has an interest in determining the extent of its culpability for environmental damage caused by its activities, and in complying with EPA, NIOSH, OSHA and other governmental regulations. Some of the more widely used Air Force materials with pollution potential include jet fuel, deicer, different pesticides and Aqueous Fire Fighting Foam (AFFF). Spills and leakage of these materials are detrimental to the aquatic environment as evidenced by fish kills and other stress to the aquatic ecosystem. Such problems can result in major regulatory, financial and public relations problems for the Air Force.

One method of confirming a spill in an aquatic environment is chemical analysis of the water or fish tissue for the specific chemical. For chemicals which rapidly decompose or for spills into fast moving waters, detection of the primary pollutant can be extremely difficult. One approach to this problem is analysis for metabolites associated with each pollutant rather than the primary pollutant itself. Detection of specific metabolites or elevated levels of other metabolites would constitute proof of the presence of the primary pollutant.

Much work has been done in the last 25 years to trace the metabolic pathways of different species. A large percentage of this work has been done on mammals in an effort to more fully understand the metabolism of the human body. Work on non-mammalian species is much less voluminous while work on aquatic species is spotty. Some work has been done on the hydrolytic and metabolic products of malathion (1,2,3,4). Work by Cook and Moore (5,6) on marine fish gave at least a starting point for a method of separation and detection of possible metabolites. Work on JP-4 and other jet fuels has led to the recognition that monocyclic aromatic hydrocarbons such as benzene, toluene and xylene are toxic in aquatic systems (7,8,9,10). A number of metabolic products have been identified in mammalian species (1) including phenols, carboxylic acids, alcohols and derivatives of these groups. No references concerning metabolic pathways of aquatic species for JP-4 or any of its individual

constituents have been found. Further, there has been no work done on the use of metabolite analysis as an index of the parent pollutant.

Dr Stebbins received his Ph. D. in Physical Chemistry from Texas A & M University in 1970. In 1977 he became interested in the analysis of environmentally important compounds through electron capture gas chromatography (ECD). Summer work with Grimsrud's group at Montana State University (3 summers) led to several publications in this area. His current work in this area led to the presentation of two papers in April and May of 1985. Since the most sensitive method for detection of metabolites involves gas chromatography, and the most selective involves GC-MS, Dr Stebbins was a logical candidate for the project.

OBJECTIVES:

The main objective of this project was to detect and identify at least one metabolite of each primary pollutant that could be useful in monitoring the exposure of freshwater aquatic species to heavily-used Air Force materials such as JP-4, the pesticide Malathion, plane deicer and AFFF foam. The strategy was to expose blue gills (Lepomis macrochirus) to measured amounts of each material, sacrifice the fish after a specific time and analyze the liver and other internal organs for metabolites of the primary pollutants.

In particular, the objectives were:

- 1) To obtain an analysis of each material.
- 2) To determine the active component of each material and the possible metabolites of each by a literature survey.
- 3) To analyze our water for these chemicals (baseline data).
- 4) To determine the residence time of each component in test aquaria.
- 5) To analyze fish liver after exposure to each primary pollutant.
- 6) To compare the data of part 5 with data for an unexposed population of fish.

EXPERIMENTAL:

Materials: Boron trifluoride 14%, in methanol (Regis), copper sulfate pentahydrate (Mallinckrodt analytical grade) and formalin (Mallinckrodt analyzed reagent) were used without further purification. Solvents hexane, methanol, diethylether, toluene, acetonitrile and ethyl acetate were all Baker resi-analyzed solvents. Sodium sulfate and Florosil (Floridin Co.) both met the specifications described in EPA method 608. Sodium thiosulfate (Baker analyzed), HCl and Tenex met the specifications found in EPA method 602. Malathion (95%) was obtained from the Pest Control Center at Brooks AFB. JP-4 jet fuel was obtained by OEHL at Brooks AFB. Analytical standards of benzoic acid, methyl benzoate and benzyl alcohol were obtained from Chem Services, West Chester, PA.

Instrumentation: All chromatograms were obtained using a Perkin-Elmer 2 gas chromatograph with a ^{63}Ni electron capture detector and a $6' \times 2\text{mm}$ id column packed with 1.95% QF-1/1.5% OV-17 on 80/100 mesh Gas Chrom Q. The temperature of the injector port, column and detector were 210°F , 178°F and 300°F respectively. The carrier gas was 5% methane in argon with a flow rate of 30 cc/min.

GC-mass spectrograms of malathion, malathion derivatives, pure JP-4 jet fuel and extracts thought to contain their metabolites were obtained on an HP 5840A/HP 5987-MS/HP 100-DS system with a 25 meter SE-54 capillary column. The carrier gas was helium flowing at 1cc/min. Ionizing voltage was 70 ev in the electron impact mode with the source temperature at 200°F . Runs were temperature programed from 35°F - 290°F at 6°F per minute. Occasionally an HP 3760 A-gc/5970 A mass selective detector/HP 9825 B data collector was used under basically the same conditions as noted above.

Volatile organics dissolved in water were analyzed using a purge and trap technique with a Tracor 4606 C gas chromatograph and an LSC-2 P and T sample concentrator. A PID detector and a 5% SP-1200/1.75% Bentone 34

on 100/120 Supelcoport was employed. The runs were temperature programmed with the initial temperature of 50⁰F, the final temperature of 62⁰F and a programmed rate of 6⁰F/min.

Analytical Methods: Analysis of malathion in water was performed by triplicate analysis of 500 cc samples collected and stored in glass bottles with teflon-coated screw tops. The samples were refrigerated and processed within 24 hours of collection. All glassware used in the analysis, including the collection bottles, was cleaned in accordance with EPA Method 608 and rinsed three times with resi-analyzed hexane. Each sample was acidified with 1 ml of HCl and extracted three times with 50, 25 and 25 ml portions of 15% diethylether/hexane v/v. The extracts were combined and concentrated to 5 ml by evaporation. This volume was dried over anhydrous sodium sulfate until ready for gc analysis.

Analysis of malathion in tissue was performed by duplicate analysis of freshly sacrificed bluegill tissue. At sacrifice, the appropriate tissue was immediately collected (within 20 minutes) and ground for 15 minutes with a 5 ml portion of 15% diethylether/hexane in an all glass tissue grinder (Lurex Mfg Co). The extract was poured into a glass collection tube and a second 5 ml portion of solvent ground for an additional ten minutes. This extract was combined with the first, refrigerated and dried over anhydrous sodium sulfate until analysis. Each sample was air evaporated to .3 ml and placed on a Florosil column prepared according to EPA micro method for the determination of chlorinated pesticides in animal tissue. The sample was eluted with 12 ml of hexane and 12 ml of 1% methanol/hexane v/v. The eluate was discarded and further elution with a second 12 ml portion of 1% methanol-hexane was performed. This eluate was air evaporated to 1 ml and stored over sodium sulfate until gc analysis.

Analysis of the metabolic products of malathion, specifically the monocarboxylic acids (MCA) of malathion, and the dicarboxylic acid (DCA) of malathion in tissue was performed by a modification of the method of

Cook and Moore (5). After grinding, refrigeration and storage as above, the samples were air evaporated to dryness. Each tube was washed with several portions of 5% Na_2CO_3 in water, and the washings placed in a separatory funnel. Na_2CO_3 solution was added to the funnel until a total of 100 ml of solution was in the funnel. This aqueous phase was extracted with two 25 ml portions of hexane to remove malathion, and the extract discarded. The aqueous phase was then adjusted to a pH of 1-2 by addition of 6 N HCl. Saturated NaCl was added and the aqueous phase extracted 3 times with 25 ml portions of ethyl acetate. The extracts were combined and concentrated by evaporation until about 5 ml remained. The extract was transferred to a derivatization flask and air evaporated to dryness. One half ml of 14% BF_3 in methanol was added to the flask and heated for 1 hour at 80°F in a water bath. Upon cooling, a 2 ml portions of saturated Na_2SO_4 was added to the flask and the aqueous phase extracted twice with 2 ml portions of ethyl acetate. The extracts were combined, evaporated to dryness and redissolved in .3 ml 15% ether/hexane. The samples were placed at the top of a Florosil column prepared as above and eluted in the same manner. The last 12 ml fraction was collected, evaporated and stored over Na_2SO_4 until analysis.

Analysis of the water soluble fraction of JP-4 for benzene, toluene and the xylenes was accomplished by duplicated analysis of 50 ml samples according to EPA method 602. It was important that sample vials with no available head space were used. Gc-ms standards of benzyl alcohol and methyl benzoate were weighed into a volumetric flask, diluted to the mark with toluene and then further diluted to a final concentration of about 30 ppm in each.

Analysis of tissue for metabolites of benzene, toluene and the xylenes was performed by triplicate analysis of freshly sacrificed bluegill liver. At sacrifice, the liver was collected (within 20 minutes), ground and processed as in the malathion analysis except acetonitrile was used as a solvent. After refrigeration and storage the sample was split into two halves. The first half was air evaporated to

.3 ml, placed on a Florosil column and eluted with 10 ml hexane and 5 ml of 1% methanol/hexane. This eluate was discarded. Further elution with an additional 15 ml of the methanol/hexane mixture resulted in a fraction which would, if present, contain benzyl alcohol and related alcohol species. The second half was air evaporated to dryness, placed in a derivatization flask and derivatized by adding .5 ml of BF_3 -methanol (14%) to the flask and heating for 1 hour. Two ml of 2% Na_2SO_4 were added, plus enough NaCl to saturate the system. The aqueous phase was extracted with three 2 ml portions of toluene and the extracts combined. The combined extracts were air evaporated to 1 ml and stored over Na_2SO_4 until GC-mass spec analysis.

Fish: Four groups of bluegills (Lepomis macrochirus) were obtained: the first from a commercial hatchery in Poteet, Texas and the the last three from a commercial hatchery in LaVernia, Texas. The fish were prophylactically treated for 2 hours with 1 ppm copper sulfate and 100 ppm formalin and then acclimatized for at least one week in a 130 gal tank with a water flow of .5 l/min and a water circulator.

For exposure to malathion three bluegills each comprised the control and exposure group. Each group of three was housed in a 20 l glass aquarium containing 14 l of dechlorinated, gently aerated water at $76^0 - 78^0$ F and pH = 7.2. For the exposure group, malathion was added prior to introduction of the fish such that the initial concentration of malathion was 110 ppb (a first attempt at 2.1 ppm was attempted but the fish died within three hours). Because malathion hydrolyzes in water, additional malathion was added once a day to return the concentration to its original value. This static exposure was continued for 96 hours. At that time, both groups of fish were sacrificed and their livers and gut immediately removed. Any fish dying before 96 hours were removed and processed as above as soon after death as possible.

Fish were handled the same way for the JP-4 jet fuel exposure studies. The exposed group of fish were placed in 14 l of a water soluble fraction/JP-4 water mixture at one-fourth of the 96 hour LC_{50} (5 ppm). The water soluble fraction/JP-4 mixture was prepared by gently

stirring a 95:5 v/v ration of water to JP-4 with a magnetic stirrer in a stoppered glass container for 24 hours. The mixture was allowed to stand for 4 hours, the water layer separated from the insoluble JP-4 and then diluted with dechlorinated water to the required 14 l. Since the volatile constituents of JP-4 evaporate rapidly (16), the static exposure was renewed every day by preparing a new mix of JP-4 as above and transferring the fish to a new tank. The control group was transferred also. The exposure was continued for 96 hours and the fish sacrificed as above.

Results:

A literature search resulted in the following information concerning the materials of interest:

Malathion: This compound has a 96 Hour LC_{50} range of 10-less than 1 ppm for a variety of aquatic species. It has hydrolytic and metabolic products (6). Compounds III, IV and V of Fig 1 are the predominant metabolites in marine pinfish (6).

JP-4: The water soluble fraction has a 96 hour LC_{50} of 20-25 ppm for bluegills (7,11). Possible metabolites of single ring aromatics are shown in Fig. 2 (12). Further reaction of these metabolites by sulfate and glucuronide conjugation is also possible (12).

Deicer: The active component, ethylene glycol, has a 96 hour LC_{50} of 1000-100 ppm for a variety of aquatic species (13). Metabolic products can include oxalate, glycoaldehyde and glycolic acid (12).

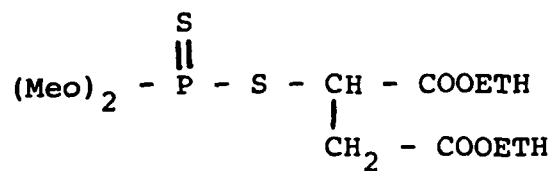
AFFF Foam: The active component, diethylene glycol monobutylether has a 96 hour LC_{50} of 100-10 ppm for a variety of aquatic species (13). Butoxy acetic acid is a possible metabolite in mammals (12).

Table 1 gives data for the analysis of malathion in water as a function of time. The half-life of malathion in this system at $pH=7.2$, $t=24^{\circ}F$ is 1.6 days. This compares with literature values of 11 days at $pH=7.4$ and $T=20^{\circ}F$ and 14,51,14 and 7 days at $pH=7.0$ and $T=20.0^{\circ}F$ (14). In general, the more basic the water, the faster the hydrolysis. Table 2 gives

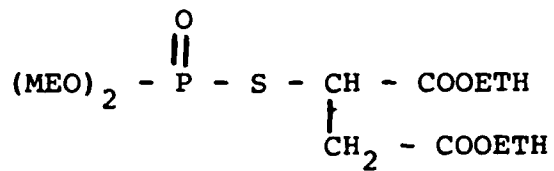
results for the exposure of bluegills to 2.08 ppm malathion for 2.5 hours while Table 3 gives results for the exposure of bluegills to malathion at 100 ppb for 96 hours. Malathion was detected in the liver ($\bar{x}=2.7 \times 10^2$ ng/g) for the shorter exposure (it was not sought in the larger exposure). Unidentified metabolites were observed in the gut of fish exposed at 100 ppb, but none were observed in the liver for either exposure. Due to lack of pure samples of each metabolite the identification of these metabolites remains unsolved.

Analysis of pure JP-4 showed an aromatic content of about 11% (15). GC-MS analysis of a pure sample revealed that the xylenes and toluene were two major components of JP-4 but little benzene was found. Because the single ring aromatic compounds of interest are volatile, the rate of loss of benzene, toluene and the xylenes from the water soluble fraction of JP-4 water system was calculated from the results of Table 4. Each of the compounds was reduced to at least 1/10 of their original value after two days time.

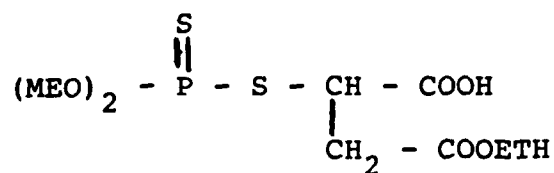
Table 5 gives data for the analysis of liver and gut of fish exposed to 25% of LC_{50} (total hydrocarbon) for 96 hours. The liver of exposed fish contained traces of an unidentified metabolite having mass fragments of 71, 93, 43, 111, 86. The gut of exposed fish contained a series of the expected fatty acids (C_{11} and C_{18}) and increased concentrations of naphthalene and the two isomers of methyl-naphthalene. Naphthalene was observed in the exposed fish while none was observed in the control. The methyl-naphthalenes increased by a factor of 40 in exposed fish relative to the control group.



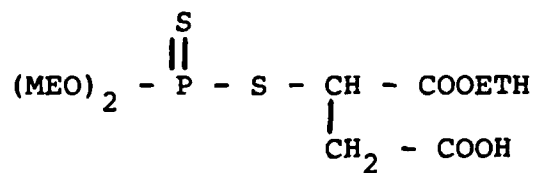
MALATHION (I)



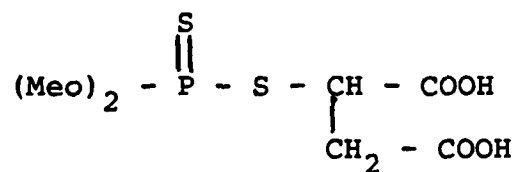
MALAOXON (II)



- MCA (III)



- MCA (IV)



DCA (V)

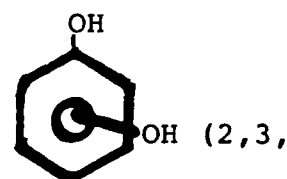
Figure 1. The structure of malathion and some of its metabolic and hydrolytic products.



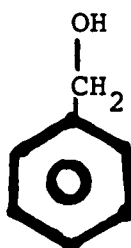
Benzene (VI)



Phenol (VII)



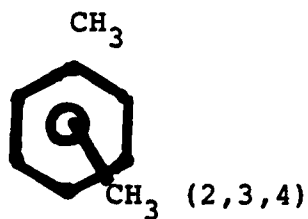
Toluene (VIII)



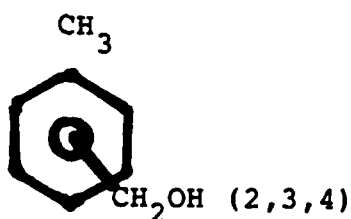
Benzyl alcohol (IX)



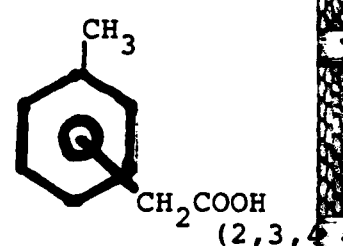
Benzoic acid (X)



Xylenes



Methylbenzylalcohols



Methylbenzoic acids

Figure 2. Aromatic volatiles of JP-4 and some of the possible metabolites.

Recommendations

Recommendations are classified under two categories, logistic and chemical.

Logistic:

There were several problems encountered that lowered efficiency:

1) Although the conceptual framework of the project was clear (through discussions with Major Doane on my pre-work visit), none of the specifics were known to either of us prior to my arrival. Although literature searches were instituted by Major Doane during the pre-work visit and by myself prior to arrival the full extent of the project was not clear until the 3rd week of the project. After deciding on the most probable metabolites in each case it became apparent that in order to make progress pure samples of each metabolite were necessary. Although the OEHL Analytical Division (SA) is a large division, they are primarily a production facility using specific EPA methods on a well defined list of priority pollutants. They do not have the wide range of chemical needed in a research facility (nor should they) nor do they have a mechanism for ordering needed chemicals within the time frame available for these projects. In other words, if you don't have it when you arrive, you won't have it when you leave. I recommend that as part of the SRFP program, a fund of \$500-\$1,000 be set up for each participant, from which that participant can order necessary supplies during the project. This would greatly increase the flexibility of the projects and aid in completion.

2) Not having a dedicated chromatograph and an assigned lab space in the sample analysis section slowed my work considerably. Although every member of the SA lab with whom I worked was helpful, not having your own space and supplies makes you dependent on the work schedules and good will of those in the lab. Submission of samples for analysis was followed by time lags, sometimes short and sometimes very long. Since the next step in analysis is often dependent on the result of the previous step, this leads to many delays. Access to a dedicated

instrument along with a defined space and set of supplies, could speed progress considerably. One must keep in mind however that this lab is primarily a production facility with their own schedules and pressures. Supplying a dedicated instrument is probably not in the best interest of the lab.

Chemical:

Because of the supply problems cited above and because the specifics of the project were not defined until the second project week, standard samples of possible metabolites were not available. Thus preliminary work on the separation and detection of each of these metabolites, except in the case of benzyl alcohol and benzoic acid, could not be done. Therefore, there is much work to be done on the specifics of separation and detection of many other possible metabolites. This is especially true in the cases of JP-4, deicer and AFFF where the literature references are few. Even in the more clearly defined case of malathion only three metabolites were pursued (III, IV and V). However there are many other possible metabolites (1,5) with separation and detection schemes needed for each.

Table 4

Evaporation of Aromatic Volatiles

Sample	Time (hours)	Benzene (ppm)	Toluene (ppm)	Xylenes (ppm)
1	0.0	5.40	8.00	4.3
2	24.0	2.30	2.90	less than 1.0
3	48.0	.16	less than .1	.4

Table 5^a

JP-4 Exposure

Sample	Liver Mass (mg)	gut mass (mg)	Metabolites	^b Other
1	14.9		+	
2	10.7		+	
3	25.2		+	
4	99.6		-	
5	55.0		-	
6		.6004	-	+
7		.4546	-	+
8		.6862	-	+
9		.5504	-	-
10		1.2312	-	-

^a 96 hour exposure at 5 ppm (total hydrocarbon) for 96 hours
 1,2,3,6,7,8 are exposed groups
 4,5,8,9 are control groups

^b + means detected
 - means not detected

Table 1
Malathion in Water Analysis

Samples	Malathion (PPM)	Time (Hours)
1,2,3	$1.25 \pm .35$	0.0
4,5,6	$0.10 \pm .04$	44
7,8,9	0.00	Blank

Table 2
Malathion Exposure 1^a

Sample	Liver Mass (mg)	Malathion (Ng)	Ng/g	Metabolites (Ng) ^b
1 ^c	8.0	1.31	1.6×10^2	ND
2	23.1	8.69	3.8×10^2	ND
3	7.9	ND		ND
4	7.2	ND		ND

^a 1 and 2 are the exposed group, 3 and 4 the control group. Exposure for 2.5 hours at 2.08 ppm.

^b Metabolites include -MCA, -MCA and DCA

^c Fish 1 died prior to liver removal

Table 3
Malathion Exposure 2^a

Sample	gut mass (g)	Metabolites detected
1	.6004	+
2	.4546	+
3	.6862	+
4	.5504	-
5	1.2018	-
6	1.2312	-

^a 96 hour exposure at 110 ppb (renewed)

1,2,3 are exposed group

4,5,6 are control group

References

- (1) Bradway, D. E. and Shafik, T. M., J. Agric. Food Chemistry, 25, 1342-1344 (1977).
- (2) Kadoum, A. M., J. Agric. Food Chemistry, 17, 1178-1180 (1969).
- (3) Wolfe, N. L., Cox, R. H. and Gordon, J. A., J. Agric. Food Chemistry, 23, 1212-1215 (1975).
- (4) Lores, E. M. and Bradway, D. E., J. Agric. Food Chemistry, 25, 75-79 (1977).
- (5) Cook, G. H. and Moore, J. C., J. Agric. Food Chemistry, 24, 631-634 (1976).
- (6) Cook, G. H., Moore, J. C. and Coppage, D. L., Bull. Environ. Contam. Toxicol., 16, 283-290 (1976).
- (7) Cairns, J., et. al., Technical Report AFOSR-TR-84-0118, "Sublethal Effects of JP-4 on Aquatic Organisms and Communities", Jan, 1984.
- (8) Bramer, J. D. and Puyear, R. L., Technical Report AFOSR-83-0513, "Identification and Quantification of the Water Soluble Components of JP-4 and a Determination of their Biological Effects Upon Selected Freshwater Organisms", Dec, 1982.
- (9) Klein, S. A. and Jenkins, D., Water Res., 17, 1213-1220 (1983).
- (10) Jenkins, D., Klein, S. A. and Cooper, R. C., Water Res., 11, 1059-1067 (1977).
- (11) Latendresse, J. R. and Fisher, J. W., Bull. Environ. Contam. Toxicol., 30, 536-543 (1983).
- (12) Casarett and Doull: Toxicology, 2nd Ed Macmillan Pub Co., Inc., NY, 1980.
- (13) Sax, N. J., Dangerous Properties of Industrial Materials, 6th Ed, Van Nostrand Reinhold Co., New York, NY, 1984.
- (14) Rogers, William, OEHL, personal communication.
- (15) Heitkamp, B. A., Technical Report AFAPL-79-2040, "Physical and Chemical Properties of JP-4 Fuel for 1978", April, 1979.
- (16) Cooper, R. C., et. al., Technical Report AFAMRL-TR-82-64, "Environmental Quality Research - Fate of Toxic Jet Fuel Components in Aquatic Systems," October 1982.

1985 USAF-UES SUMMER FACULTY RESEARCH PROGRAM/

GRADUATE STUDENT SUMMER SUPPORT PROGRAM

Sponsored by the

AIR FORCE OFFICE OF SCIENTIFIC RESEARCH

Conducted by the

UNIVERSAL ENERGY SYSTEMS, INC.

FINAL REPORT

ANALYSIS OF GEOMETRIC ATTENUATION IN GROUND MOTION TESTING

Prepared by:	Dr. B.W. Stewart
Academic Rank:	Assistant Professor
Department and	Department of Mechanical and Industrial Engineering
University:	University of Cincinnati
Research Location:	Air Force Weapons Laboratory/NTED Kirtland AFB
USAF Research:	Lt. W.A. Kitch
Date:	September 4, 1985
Contract No:	F49620-85-C-0013

ANALYSIS OF GEOMETRIC ATTENUATION IN GROUND MOTION TESTING

by

Dr. B.W. Stewart

ABSTRACT

A simple analytical method was used to investigate geometric attenuation effects in explosive soil testing. Dispersion, nonlinearity, and media attenuation were not examined. The method was used to arrive at several conclusions concerning explosive source array characterization and the definition of various scaling regions.

ACKNOWLEDGMENTS

I would like to acknowledge the assistance of Lt. W.A. Kitch of the AFWL/NTED Division at Kirtland AFB for aiding in preliminary research and also for beneficial discussions as the work progressed. Mr. Jeff Fischer of the University of Cincinnati also provided excellent support in handling the numerical computations involved. Finally, the sponsorship of the Air Force Systems Command, Air Force Office of Scientific Research, and the Air Force Weapons Laboratory is greatly appreciated.

I. INTRODUCTION:

The AFWL (Air Force Weapons Laboratory) has contracts with several outside research organizations. Although there exists some variation in each of these organizations' approach to a particular task in shock-wave propagation testing, the fundamental approach is identical: numerical computations involving previously obtained empirical relations.

I believe that my background (Ph.D, theoretical physics; M.S., mechanical engineering) enabled me to employ other, more theoretical approaches to attack some basic but still important questions in the soil shock-wave propagation testing area. My background in electromagnetic theory and applied mathematics gave me the analytical tools required, while my engineering background enabled me to keep the realities and practicalities of the application in the forefront.

II. OBJECTIVES OF THE RESEARCH EFFORT:

Initially, my research goals included an in-depth examination of the efficiency factor relating cylindrical source arrays to continuous planar arrays using the electrodynamic analogy and the examination of the nuclear explosive to high explosive equivalency factor. Unfortunately insufficient data in the hydrodynamic region existed in order to address the latter problem. (Data in the hydrodynamic region was required in order that uncertainties in media modeling wouldn't interfere with the computation.) Midway through the research period, it was determined that the approach could also be used to examine the validity of certain scaling region criteria. These criteria were previously determined by a trial and error approach and may not have had a wide area of validity even though their use was widespread.

III. APPROACH:

The major focus of the research is on geometric (multidimensional) effects. We therefore want to keep media effects such as frequency dispersion and medium attenuation to a minimum. In this spirit, we treat the medium as a homogeneous, isotropic, linearly, elastic, infinite body. An experienced researcher in this area may shutter at this seeming oversimplification. We justify it thusly: The peak of a stress wave will be attenuated as the wave propagates through a given medium. This peak attenuation arises from three separate causes: 1) frequency dispersion - the longer wavelength components of the initial pulse travel faster than the short wavelength components and the pulse flattens. This mechanism is energy conservative. 2) material attenuation - energy from the pulse is absorbed by the medium through various mechanisms (spalling, hysteresis, etc.). 3) geometric attenuation - an example of which is the well-known result that the stress wave amplitude varies as $1/R^2$ for a spherically source near the source, and as $1/R$ far from the source. This mechanism is also energy conservative. Most of the current effort in this field has been expended in examination of material attenuation for various soil types. However if the peak attenuation due to both frequency dispersion and geometric attenuation isn't "filtered" from the data, it will inevitably be attributed, erroneously, to material attenuation. Resultant soil mechanical models will then be invalid. Then, within the scope of the present effort, the use of the elastic soil model is very appropriate.

III. APPROACH: (Continued)

Given the above medium properties and assuming a harmonically time-dependent source (this causes no difficulty as any time dependence can be formed by an appropriate Fourier analysis) the governing wave equations are (1):

$$(\nabla^2 + k_1^2) \phi = f(\vec{x}') \quad (1)$$

$$(\nabla^2 + k_2^2) \psi = g(\vec{x}') \quad (2)$$

where: ϕ, ψ are the dilatational and shear potentials, respectively.

k_1, k_2 are the wave numbers for the dilatational and shear waves.

In this form dispersion effects can be incorporated.

$f(\vec{x}'), g(\vec{x}')$ are the source geometry factors.

The shear and dilatational potentials are related to the displacements u_r, u_z in cylindrical co-ordinates by

$$u_z = \frac{\partial \phi}{\partial z} - \frac{\partial^2 \psi}{\partial r^2} - \frac{1}{r} \frac{\partial \psi}{\partial r} \quad (3)$$

$$u_r = \frac{\partial \phi}{\partial r} + \frac{\partial^2 \psi}{\partial z \partial r} \quad (4)$$

We are concerned with the radial displacement at the midline ($z=0$) of the array. By symmetry:

$$u_r(z=0) = \frac{\partial \phi}{\partial r} \quad (5)$$

III. APPROACH: (Continued)

Thus the quantity of interest will be $\frac{\partial \Phi}{\partial r}$.

The solution to equation (1) is well-known to be⁽²⁾:

$$\Phi = \iiint dx' dy' dz' \frac{f(x', y', z') \exp [i k \{ (x' - x)^2 + (y' - y)^2 + (z' - z)^2 \}^{1/2}]}{[(x' - x)^2 + (y' - y)^2 + (z' - z)^2]^{1/2}} \quad (6)$$

Where ' refers to the source co-ordinate. Unprimed quantities are observation point co-ordinates.

Our problem then is to integrate eqn. (6) either analytically or numerically for various source geometries, i.e. for various $f(\vec{r}')$.

IV. RESULTS:

We examined the efficiency factor⁽³⁾ as a function of source spacing, source size, and aspect ratio. We found efficiencies of 99% (as compared to the experimentally found values of 60-70%) in every case. This was a clear indication that the mechanism behind the efficiency factor was not entirely geometric but was more strongly dependent upon medium properties. This knowledge will be very beneficial in examination of medium effects upon the efficiency factor, a study that is to be included in the follow on research proposal. Thus although we didn't find a way to completely characterize the efficiency factor theoretically, we do know more about its causes than was previously known.

We were more fortunate in our other studies. We examined even and odd arrays (see figure 1) in attempt to determine the distance from the array at which the resultant wavefront becomes planar in character. Our governing criteria was a difference of less than one percent. The results are given in Table 1.

We examined recently proposed scaling region criteria. These criteria were obtained by trial and error. We sought to either validate or modify the scaling regions as needed. Our results are given in Table 2. Our work uncovered new scaling regions, not determined by the work previously done probably due to the lack of data in these regions.

IV. RESULTS: (Continued)

In addition, we verified the outer scaling regions analytically. This is in effect a validation of our approach, as well, since the data closely fits our results as well. It also would seem to strengthen support for use of the Drake⁽⁴⁾ regions over those advanced previously by Higgins.

In summary, the major results of the research were in: a) indicating that the physical mechanisms behind the relative efficiency factor for source arrays were highly medium dependent, as well as pointing the direction for further research into these mechanisms; b) validating empirically obtained scaling region criteria by a totally independent, analytical method; c) establishing the usefulness and appropriateness of the analytical approach when dealing with geometric questions in this field of research. It may be applied quickly and accurately to future, unaddressed problems in test design instead of, or in conjunction with, the numerical procedures currently employed.

V. RECOMMENDATIONS:

When examining data in both of the planar and cylindrical regions, care must be taken that the short wavelength components have undergone significant attenuation before either the criteria of Drake or the new region criteria are used. In most cases this should not be a problem as all the wavelength components undergo a material attenuation proportional to

$$\exp \left[- \frac{br}{\lambda^2} \right]$$

λ = wavelength

r = distance from array centerline

b = positive material constant

in the hydrodynamic region. The presence of the material constant b implies no universal "cut-off" distance. Each test medium will need to be considered separately.

Further related research might include examination of the efficiency factor using a simple material model or even a thermodynamic approach. Frequency dispersion should be examined from a fundamental micro-mechanical viewpoint. This phenomenon may be even more important to the survivability of protective structures than material attenuation, but seemingly receives little attention. A properly done study could eliminate the need for further soil models as each model has a region in strain and strain-rate space of high accuracy. A dispersion study could help classify the existing models into physical regions of applicability using the peak stress and slope of the stress pulse as

V. RECOMMENDATIONS: (Continued)

guidance for various distances from the source. This study will be the object of a mini grant research proposal.

REFERENCES

1. Lee, T.M., "Surface Vibration of a Semi-Infinite Viscoelastic Medium," Proc. Int. Symposium on Wave Propagation and Dynamic Properties of Earth Materials, Univ. of New Mexico, Albuquerque, New Mexico, August 1967, pp. 123-138.
2. Jackson, J.D., Classical Electrodynamics, New York, New York, John Wiley & Sons, Inc., 1975.
3. Thomsen, J., and Wu, E., "Progress on DIHEST Source Characterization and DDT-1 Test Predictions", Technical Report No. CRTN584-01PM, California Research and Technology, Inc., Dublin, CA, May 1984.
4. Drake, J.L., "Consistent Scaling of DIHEST Ground Motions," Applied Research Associates, Inc., Albuquerque, New Mexico, August 1984.

TABLE 1

Distance at which odd arrays become planar in character:

$$R/\delta = .5 + .3/\beta$$

Distance at which even arrays become planar in character:

$$R/\delta = .7 + .5/\beta$$

Distance at which even arrays approach odd arrays in character:

$$R/\delta = .5 + .4/\beta$$

$$\beta = \delta/s \quad ; \quad s/2 = \text{source width} \quad ; \quad \delta/2 = \text{source spacing}$$



FIGURE 1

TABLE 2

Odd Arrays

$R < S/2$	Planar scaling
$S/2 \leq R < \frac{S+2S}{4}$	Cylindrical scaling
$\frac{S+2S}{4} \leq R < m$	Planar scaling
$m \leq R < l$	Cylindrical scaling
$l \leq R$	Spherical scaling

Even Arrays

$R < \frac{S+S}{4\pi}$	Planar scaling
$\frac{S+S}{4\pi} \leq R < S/4$	Cylindrical scaling
$S/4 \leq R < m$	Planar scaling
$m \leq R < l$	Cylindrical scaling
$l \leq R$	Spherical scaling

$2l$ = array length

$2m$ = array height

1985 USAF-UES SUMMER FACULTY RESEARCH PROGRAM/
GRADUATE STUDENT SUMMER SUPPORT PROGRAM

Sponsored by the
AIR FORCE OFFICE OF SCIENTIFIC RESEARCH

Conducted by the
UNIVERSAL ENERGY SYSTEMS, INC.

FINAL REPORT

Competition Guide for
Base-Level Buyers 1985

Prepared by: Lowell E. Stockstill
Academic Rank: Associate Professor
Department and Department of Business Administration
University: Wittenberg University
Research Location: Business Research Management Center
AFBRMC/RDCB, Area B, Bldg. 125, Rm. 2063
Wright-Patterson AFB, OH 45433

USAF Research

Focal Point: Lt. Col. Robert Skipp
Date: August 30, 1985
Contract No.: F49620-85-C-0013

Competition Guide for
Base-Level Buyers 1985

by

Lowell E. Stockstill

ABSTRACT

Competition Guide for Base-Level Buyers 1985 is in keeping with the COPPER 90 goal of providing on-the-job learning. The Competition in Contracting Act of 1984 (CICA) trigger this specific project.

This publication provides the base-level buyer with a quick reference to competition. It gives an overview of the new law, highlights some of the specific features, and provides a source list for competition.

The "Guide" is written in "cookbook" style. It is general enough to include all sizes, branches, and experience levels in base-level contract. It has all of the advantages and disadvantages of this approach.

Although the emphasis of the publication is competition the desired end is to assist the base-level buyer lower the cost of government procurement.

ACKNOWLEDGMENTS

Support by the Systems Command and the Office of Scientific Research are gratefully acknowledged. More specifically, the staff of the Business Research Management Center, Col. Ronald Deep, Lt. Col. Robert Skipp, Linda McLaughlin, and Eileen Thurmon, were invaluable in supplying me with information, materials and introductions. Also Capt. Jerry Ferguson and SMSGT John Chapman at the Logistics Management Center provided useful insights into the publications format.

A special word of appreciation must be expressed to the Commanders who granted me access to their Directorates or Divisions and the supervisors and employees who sacrificed their time despite the beckoning fiscal year end.

At Wright-Patterson Contracting Center, Ohio: Dexter Martin, Marty Spahr, Claud Crabtree, Sue Strickland, Joann Webb, Edith Lewis, Linda Jones, Joanne Harvey, Dottie Speakman, Chris Leonard, Fran Thaman, Ruth Terry, Mark Kellerman.

At San Antonio Contracting Center, Texas: Col. Edgar Green, Maj. Bob Tepfler, Robert Koenig, Diana Martinez, Lorraine Griffin, Zule Kahn.

At San Antonio Air Logistics Center, Texas: Robert Blocker, Col. Orsine, Richard Justus, Hugh Robichaux, Tommy Jordan, Barbara Robichaux, Fred Perryman, Steve Bennett, Edgar Zepeda.

None of the above, however, share any blame for errors or matters omitted because of space limitations.

I. INTRODUCTION

My professional background includes graduate degrees in both law and finance. For the past decade I have taught Business law which strongly emphasizes contracts and Small Business Management, a research interest. Currently I am a tenured Associate Professor at Wittenberg University, Springfield, Ohio, and a member of the Ohio Bar.

The Air Force Business Management Research Center (BRMC) located at Wright-Patterson AFB, Ohio, is part of the Directorate of Contracting and Manufacturing Policy, Headquarters USAF. BRMC is an Air Force focal point for acquisition research studies. It defines five acquisitions practices and further sub-divides them into 19 research areas. BRMC's professional staff enlists faculty and students from the Air Force Institute of Technology (AFIT), Professional Military Education (PME) and civilian sources to acquire specialized research expertise.

A combination of factors led to my introduction to BRMC: (1) knowledge of contract law; (2) background with legal research; (3) experience with interview techniques; (4) publication ranging from theoretical to "how to;" (5) enactment of the Competition in Contracting Act of 1984 (CICA); (6) implementation difficulties with CICA; (7) request from Headquarters USAF to prepare a series of "cookbook" competition manuals.

My skills and aptitudes apparently matched BRMC's needs, and I was assigned to a Summer Faculty Research position to pursue the research objectives that follow.

II. OBJECTIVES OF THE RESEARCH EFFORT

The Competition in Contracting Act of 1984 (CICA) requires executive agencies to obtain full and open competition. This legislation made major changes to the Federal Government's acquisition process for goods and services. These changes affect all procurement and are the most comprehensive revisions since the original procurement statutes in the late 1940s.

It is the objective of this research to convert the statutory requirements of CICA into implementable procedures for buyers, contracting officers, and administrators. This result will be facilitated by the preparation of a competition manual for base-level contracting.

Although CICA applies to all levels of contracting, the starting point will be base-level contracting. There are multiple sources available for many of the goods and services procured by this function. Consequently, it provides an expedient scope to derive a basic implementation model. Once the basic model is created and refined, it then can be applied to the more complex requirements of logistics and systems contracting in a subsequent study.

The sequential steps of the research will be as follows:

- A. Identification of changes in the Federal Acquisition Regulation System as applied to base-level contracting.
- B. Familiarization with base-level contracting procedures.
- C. Synthesis of the new legislation and existing

base-level contracting practice.

- D. Preparation of a competition manual for implementation of CICA for base-level contracting Purchasing Agents and Contract Negotiators.

III. METHODOLOGY

Although I had multiple research objectives they all led to one end, i.e., the preparation of a competition manual for base-level contracting.

The alternative methodologies available were survey techniques, interview techniques, or a combination of both. I chose to avoid all survey techniques because the 10-week period simply did not allow time for distribution of the instrument, analysis of the data, and preparation of a report. Also the analysis of empirical data with standard statistical packages would not lend itself understandable to the target readership, i.e., base-level Purchasing Agents and Contract Negotiators.

Instead I chose an in-depth interview technique. Interviews ranged from 40-90 minutes with a typical session around one hour. Interviews were conducted with the entire strata of base-level personnel, lowest level Purchasing Agents to Directorate Commanders. Experience levels ranged from less than 2 years to over 25 years. All base-level branches or divisions were represented as well as support personnel such as Competition Advocates, Small Business Specialists, and Contracting Committee Members, at Wright-Patterson Contracting Center, Ohio, and San Antonio Contracting Center, Texas.

Also, interviews were conducted at San Antonio Air Logistics Center. Although not a base-level contracting facility, its magnitude of procurements provided a wealth of insights and applications. In all, 28 persons were interviewed.

IV. LIMITATIONS

In-depth interviews by their very nature limit the size of the sample. Cognizance of this problem led to purposely selecting a mix of interviewees with diverse perspectives. Also depth of interviews offset some lack of breadth. Despite best efforts, however, some individual bias exists.

Another limit is that large only contracting centers were used. These provided the greatest number and variety of interviewees within the research time period. Although many respondents indicated work at a small base-level contracting organization some time during their careers, some bias exists toward large base-level contracting operations.

V. COMPETITION MANUAL

The overall objective of this research project was to prepare a competition manual for base-level Purchasing Agents and Contract Negotiators. This section includes a draft of that manual in its entirety.

FROM THE DIRECTOR

The Competition Guide for Base-Level Buyers is written to enhance your understanding. I believe that it provides a foundation for applying some of the intricacies of the Competition and Contracting Act of 1984. It heightens your awareness of the competition process with information and suggestions. Although it can help you and increase support of your mission, it is not meant to solve all problems. Please consult your supervisor, base contracting officer, or competition advocate to obtain additional details and advice concerning competition issues.

Bernard L. Weiss
Maj. Gen. HC/USAF
Director, Contracting and
Manufacturing Policies

COMPETITION GUIDE

for

BASE-LEVEL BUYERS

1985

ACKNOWLEDGMENTS

Outstanding contributions were made by Logistics Management Center, San Antonio Contracting Center, San Antonio Air Logistics Center, and Wright-Patterson Contracting Center. The individual commitment from new buyers to veteran commanders alike is gratefully acknowledged.

Published by:

Business Research Management Center
Wright-Patterson AFB, OH 45433

Author:

Lowell F. Stocks-III
Mittlerberg University

Editor:

Lt. Col. Robert Skipp
Def. Director, AFMOC PACI

Approved by:

Maj. Gen. Bernard L. Weiss
Director, AFMOC

TABLE OF CONTENTS

	Page
ACKNOWLEDGMENTS
TABLE OF CONTENTS
LIST OF ILLUSTRATIONS
PREFACE
CHAPTER I
COMPETITION LEGISLATION
CHAPTER II
SMALL BUSINESS
SOCIO-ECONOMIC PROGRAMS
OTHER PROGRAMS
CHAPTER III
FULL AND OPEN COMPETITION
COMPETITIVE PROCEDURES
EXCEPTIONS TO F&OC
CHAPTER IV
SYNOPSIS
TYPES OF SYNOPSIS
SPECIFICATIONS CHECKLIST
MINIMUM TIME REQUIREMENTS
CHAPTER V
GENERAL CONTENT
JUSTIFICATION AND APPROVAL
EFFORTS TO FIND SOURCES
FAIR AND REASONABLE PRICE
CHAPTER VI
SMALL PURCHASES PRICING
CHAPTER VII
COMPETITION ADVOCACY
RESPONSIBILITIES
SOURCE DEVELOPMENT
CHAPTER VIII
SOURCES OF COMPETITION
GOVERNMENT SOURCES
RESOURCE PERSONS
NATIONAL DIRECTORIES
LOCAL DIRECTORIES
MISCELLANEOUS SOURCES
CHAPTER IX
PROTESTS
CHAPTER X
OTHER CONTRACTING TOPICS
APPENDIX
APPENDIX 1
APPENDIX 2
APPENDIX 3
THE LIST OF ILLUSTRATIONS
FIGURE 1
FIGURE 2
FIGURE 3

PREFACE

One of the goals of COPPER 90 is to provide "on-the-job" learning for base contracting for a series of how-to manuals. The competition guide for Base-Level Buyers falls in this category. The topic was triggered by the Competition in Contracting Act of 1984 (CICA). This "Guide" tries to incorporate the relevant sections of the Act and applies them to base-level contracting.

The purpose of this publication is to provide the base-level buyer with a quick reference to competition. The "Guide" gives you an overview of the law, highlights some of the specific sections and provides a source list for competition. It is hoped that this information is relevant to you and perhaps can jog your memory on some CICA topics.

Any publication of this nature has some inherent limitations. It must be general enough to cover base contracting operations from the smallest remote site to the largest contracting center. Also, there are various branches in each of these activities. In addition, a wide variety of experience level exists among base-level buyers. As a consequence, not everything in this "Guide" will apply directly to your job. Some specific problems will have to be referred to your supervisor or researched in the regulations. On the other hand though, if this "Guide" can provide you one additional source of competition it has done its job.

Although all the emphasis in this publication is placed on competition, it is merely a means. The desired ends of competition is lower cost in government procurement. You will sometimes be required to weigh the implications of administrative cost versus the cost of competition. In these cases no law, regulation or "Guide" can substitute for the buyer's good judgment and common sense.

CHAPTER

COMPETITION LEGISLATION

The central theme of competition legislation is to promote competitive procurement. Although not a cure-all for all procurement problems, both studies and actual experience show that competition contracting saves from 10% to 50% of the contract price. In addition to savings, competition promotes innovation, technical improvements and, most importantly, enhances "fairness" in the procurement process. Although commonly referred to as "CICA," competition in contracting includes major revisions through three separate pieces of legislation.

Competition in Contracting Act of 1984 (CICA)

CICA promotes the use of competitive procurement procedures and limits the use of sole source buying. The Act sets a standard of "full and open" competition. It establishes in absolute preference for competition by placing competitive negotiation on a par with sealed bids (formal advertising). Also, it streamlines the procurement process, promotes the use of commercial products and requires the use of functional specifications.

Small Business and Federal Competition Enhancement Act of 1984

This Act promotes full and open competition by eliminating barriers in procurement. It targets small businesses in general and specifically those owned and operated by socially and economically disadvantaged individuals. The Act invites contracting participation in the competitive procurement process and expands the industrial base by providing contracting opportunities.

Defense Procurement Reform Act of 1984

This Act arises from concerns over the procurement of spare parts. It tries to eliminate excessive pricing of spare parts and to recover unjustified payments. It also concentrates on assuring fair and reasonable prices, using standard or commercially available spares, and protecting developer's technical data.

CHAPTER

SOCIO-ECONOMIC PROGRAMS

SMALL BUSINESS

For a number of years the government has helped small businesses obtain federal contracts in order to expand the U.S. industrial base and enhance competition. The Small Business Act of 1958 and its implementing regulations establish programs and procedures which provide preferences to qualifying small businesses.

Small Business Act

This Act provides government aid and assistance to small businesses. It requires that a "fair proportion" of the federal government's purchases of property and services are placed with small businesses.

Small Business Awards Program

Every contracting officer has the responsibility to contract with small business. To help you identify set-asides and avoid sole source requests, the Small and Disadvantaged Business Specialist (SADBUS) has ongoing small business programs.

Small Business Set-Asides

When a contract is a small business "set-aside," the government reserves it exclusively. For purchases under \$10,000, total set-asides are required unless the buyer is unable to obtain reasonable offers from at least two small businesses. Partial set-asides are required on contracts that exceed \$10,000 when the contract can be broken down into smaller parts, or at least one small business has the capacity to perform.

Small Business 8(a) Awards

The purpose of Section 8(a) of the Small Business Act is to assist minority and disadvantaged businesses to become self-sufficient and competitive. The Small Business Administration (SBA) certifies the competency of the firm and the Air Force then negotiates directly with the SBA.

Women-Owned Small Business

Although there are no specific set-asides for women-owned businesses, all small and disadvantaged business programs discussed above are also available to them by Executive Order 1238.

OTHER PROGRAMS

Many other socio-economic programs affect Air Force contracting. These programs allow disadvantaged classes of individuals and businesses to gain equal opportunity in the government contracting process. Some promote national objectives such as environmental protection or occupational safety. The following are key programs that you will need to be familiar with in base-level contracting.

Buy American Act

This Act gives preference to American-made goods unless they are unavailable or too costly. DOD waives this restriction for NATO and certain other countries.

Clean Air Act

Public law prohibits contracting with any company that has a criminal conviction for violating pollution standards.

Davis-Bacon Act

All contracts of more than \$2,000 are covered by this Act. It requires minimum wage, fringe benefit and working condition standards prescribed by DOL.

Equal Employment Opportunity

You must incorporate an "equal opportunity" clause in all contracts, prime or sub, over \$10,000. The Act prohibits discriminating against any employee or applicant by government contractors.

Labor Surplus Area (LSA)

DOL can set aside contracts to geographical areas with high unemployment. However, competitive procedures must be followed by LSA concerns and DOD is prohibited from paying higher prices than it can obtain from other contractors.

Service Contract Act

This law describes wages, fringes, and working conditions for services contracts in excess of \$2,500. You must submit notice to DOL 10 days prior to solicitation. It, in turn, will issue wage determinations for each class of employee expected to be hired by the contractor.

Walsh-Healey Act

This Act establishes government labor standards for prime supply contractors in excess of \$10,000. It also requires that the contractor is a regular dealer or manufacturer to prevent extra cost when no value is added.

CHAPTER _____

FULL AND OPEN COMPETITION (F&OC)

All responsible sources deserve the opportunity to compete for government contracts. First, solicitation must be made in a competitive environment. It is necessary to have at least two truly competitive sources. For example, a manufacturer and one of its distributors is ineffective competition. Secondly, synopsis requirements must be met. (See Chapter _____, Synopses.) Finally, potential sources must be given the opportunity to qualify.

COMPETITIVE PROCEDURES

Sealed Bids

When sealed bids are used, price becomes the only determining factor. The solicitation requests bids which are all open at a designated time and place. The award is then made to the lowest conforming bidder.

Competitive Proposals

This method allows factors other than price to enter into the decision-making process. Buyers can conduct discussions with offerors and negotiate the best package of terms for the government.

Combined Procedures

If neither of the preceding are appropriate, two-step sealed bidding is available. Specification or terms are discussed to better focus the solicitation and then a regular request for bids is issued.

Other Procedures

Other competitive procedures are available for J&E, R&D, and multiple award schedule orders. Specific regulations outline the procedures for each of these situations.

After Exclusions

Agencies may establish or maintain alternative sources and set-aside contracts for small businesses or labor surplus areas. Each situation has its own policies and procedures that provide for F&OC after excluding sources.

EXCEPTIONS TO F&OC

Only Responsible Source

This applies when unique suppliers or services are available from only one source. It also includes situations when only one supplier has unique capabilities.

Unusual and Compelling Urgency

The test here is whether the government is seriously injured unless the agency is permitted to limit the sources from which it solicits. The injury may be financial or other.

Industrial Mobilization

In case of national emergency or industrial mobilization, full and open competition is unnecessary. Experimental development or research work is also covered by this exception.

International Agreement

If an agreement or treaty with a foreign government specifies a particular source of supplies or services, the acquisition may be limited to that source. Written directions for reimbursing the procuring agency are usually included.

Authorized by Statute

Competition is not required when a statute expressly authorizes or requires the acquisition through a specified agency or source. Utility Services usually trigger this exception.

National Security

When disclosure of the agency's needs compromise national security, it is permitted to limit the number of sources from which it solicits.

Public Interest

If agency heads determine that it is not in the public interest to compete an acquisition, they may seek exception with permission from the Secretary of the Air Force.

SPECIFICATIONS CHECK LIST

General Description

Name of supply/service
Size or dimensions
Predominant material
Relevant tolerances included
Quantity, initial and optional
Unit of issue

Salient

Characteristics

Yes No

This synopsis publicly announces all awards exceeding \$25,000 that are likely to result in the award of subcontracts. Sometimes smaller awards are publicized when it is advantageous to the government or industry.

Pre-solicitation notices (and conferences) identify sources and aid prospective contractors to later submit proposals without undue effort. Publication of these notices are required for construction contracts in excess of \$10,000 and other complex acquisitions. Regular synopsizing is still required prior to any solicitation.

Does not restrict competitors
Will accept "or equal" model

MINIMUM TIME REQUIREMENTS

CHAPTER JUSTIFICATION AND APPROVAL (J&A)

Anytime there is a request for an exception to full and open competition, a J&A must be submitted. A "justification" necessitates the sharing of responsibility between the acquiring activity and the contracting activity. The user describes the reason why there is other than full and open competition, and the buyer determines price reasonableness, describes efforts taken to find additional sources, and certifies the information is accurate and complete. A Justification Review Document (JRD) provides the "approval." It is merely a cover letter that includes the authority, estimated dollar amount, coordinations, and the required signature levels.

GENERAL COMMENT

AWARD

24 February

RESPONSE TIME FOR BID/PROPOSAL

25 January

15 days

Threshold Amount

Small purchases are exempt. Therefore, justification and approval requirements apply only to acquisitions over \$25,000.

PUBLICATION IN CBD

Specific Authority

Each contract that is an exception to full and open competition needs to have a *specific* reference to the authority under which it was awarded.

10 January

10 days (6 days if electronically transmitted)

Invalid Justifications

The requiring activity's lack of advance planning or concern that funds will expire are not bases for exceptions from full and open competition.

TRANSMITTAL TO CBD

Maximum Practical Competition

Even when exception from full and open competition is justified, the buyer needs to solicit offers from as many potential sources as possible under the circumstances.

31 December

Determined by complexity and completeness of purchase requisition

PPE-SOLICITATION

1 October

90 days

USER PLANNING

EFFORTS TO FIND SOURCES

Past Actions

This effort is not limited to the sources you solicited. It involves all of your past actions that you have taken to make the item competitively procurable. List all past attempts to develop sources. (See Chapter ____, Source Development.)

Commercial Manuals

Commercial manuals and directories are good potential sources for procurement. Identify which ones you reviewed in your attempt to achieve competition.

Source Qualification File

Establish source qualification requirements, then create a file so that they are available to all potential sources.

Expressed Interest

List any sources that have expressed in writing an interest in the acquisition. These inquiries may be unsolicited or generated from a pre-solicitation notice or sources-sought synopsis.

Purchase Description

It may be necessary to re-examine your purchase description. If in the past your name brand or equal item has been rejected, additional information or source development may be necessary.

FAIR AND REASONABLE PRICE*

Price Competition

Even without full and open competition, there may be partial competition that allows a basis for price comparison.

Law or Regulation

Statutory and regulatory prices are presumed to be reasonable.

Market Price

Catalogs and other price listings provide an indication of price reasonableness and may often serve that purpose.

Previous Price

If you have reason to believe that a previous price was reasonable, the same price or a slight increase that includes an adjustment for inflation is likewise reasonable.

Government Estimates

A market survey or some other government estimate usually contains the information necessary to provide a basis for price reasonableness.

Value or Cost Analysis

Pricing analysts accomplish both of these techniques. Their conclusions are usually considered to be fair and reasonable prices.

None of the Proceeding

If you cannot make a fair and reasonable price determination from any of the preceding, contact your contracting officer for assistance.

*See also Chapter ____, Small Purchases Pricing.

CHAPTER —

SMALL PURCHASES PRICING

As with larger purchases, small purchase prices must be fair and reasonable. However, the pricing techniques for small purchases reflect a lesser investment of administrative time in price determinations. For purchases of less than \$1,000, prices are considered reasonable unless the buyer believes otherwise. Although competition is not required at this dollar level, buyers still have an opportunity to rotate their source selection. From purchase requests from \$1,000 to \$5,000, competition is required, although usually restricted to three sources. In general, if the offer is responsive to the solicitation, the offers are acting independently, and the prices are not too far apart, quotes are considered fair and reasonable.

Commercial Supplies

Law or regulation creates a presumption of price reasonableness. Other indicators are catalog prices and previous prices paid. When using these comparisons, you should be aware of any quantity differences, nonrecurring costs and delivery requirements.

General Services

It is more likely with services that no catalog or previous contract prices will exist. Some of the major factors that determine service prices are time, material, and travel. The Department of Labor publishes labor rates for many occupations. If you cannot locate the rate for the exact service, perhaps you can find the rate in the same line of business for comparison.

Repair Services

Repair contracts are especially troublesome because the contractor usually cannot quote until after disassembly. You can place limits on unpriced quotes with a "not to exceed" price. Tear-down and quote contracts divide the repair into two separate aspects. Usually it must be a high dollar contract to justify separating the disassembly and repair. Because of this problem, it is a good idea to rotate your tear-down awards.

CHAPTER —

COMPETITION ADVOCACY

The competition advocate position was created by CICA. It may be part of an existing position so long as the duties are not in conflict or it may be a separate individual or organization. It is the competition advocate's job to promote competition and procurement. At most base-level contracting facilities, the main tasks of the competition advocate are JSA approvals and source development. However, in larger operations the scope of the position increases in order to promote full and open competition in the procurement activity.

RESPONSIBILITIES

Resource Management

This duty refers to the resources necessary to promote competition and procurement. It includes a combination of coordinating work flow, promoting competition programs and managing resources such as employees, funds, and facilities.

Engineering Data Management

This responsibility includes the technical evaluation of products the government procures. It is a valuable asset to buyers when they have a specification or technical engineering problem.

Price Appraisal

The price appraisal responsibility covers all aspects of value analysis. It includes everything from providing pricing data to buyers in procuring activities to answering inquiries on fraud, waste, and abuse.

Source Development

This responsibility creates competition by promoting acquisition planning, advocating the use of competition, and identifying impediments to competition. In addition, JSA reviews fall within the scope of this area.

SOURCE DEVELOPMENT

Develop Own Data

One option is to create your own data. This may be done internally on a limited basis by engineering branches or divisions. More commonly, however, data development comes through the use of research development contracts.

Buy or License Data

Both of these methods give the government control of proprietary data. The only difference is the degree of actual control. When you buy data, it gives the government ownership and the discretion to control the data. On the other hand, licensing agreements only give the government use of the data and are far less desirable. Either term can be negotiated with the contract.

Challenging Proprietary Data

When the original contract proposal is submitted, often virtually everything is stamped "proprietary data." When the government feels that data is not really proprietary, it can challenge the classification. When the challenge is won, you can then compete the components.

Component Break-Out

Even though there is only one source for the prime contract, usually you can "break out" many of the component parts and solicit them competitively. The government can identify break-out items through: requesting lists of break-out items; dealing directly with subcontractors; and administrative data services identifying where the contractor adds little or no value.

Reverse Engineering

In incidences where no patents or proprietary rights exist, the government engineers may take a finished part and determine what specifications are necessary to manufacture it. Once the specifications are determined, you can competitively solicit the item.

Market Survey

These surveys merely ask the market what is available. They attempt to determine whether qualified sources exist and whether they are capable of satisfying the government's needs. Market surveys include the use of formal announcements, consulting experts and recent market tests.

CHAPTER

SOURCES OF COMPETITION

With the vast majority of purchase requisitions, many sources of competition are available. It is the difficult or the non-recurring request, however, that this chapter targets. Its purpose is to either jog your memory or perhaps provide you with a new source of competition. Since this "Guide" covers base contracting operations of all sizes and a variety of purchases within them, not all sources will apply specifically to you. On the other hand, if you get one good idea when you need it from this chapter, it has done its job. Mandatory sources such as Federal Prison Industries, National Industries for the Blind or General Services Administration (for some classes), etc., are not included.

GOVERNMENT SOURCES

Quotation History

With smaller purchases, you can refer to the past quotes or the Systems Management Branch or Division may provide you with multiple sources on a "trailer" with the purchase request package.

Prior Contracts

With larger requests that require synthesizing, prior proposals are on file. Both successful and unsuccessful contractors may provide sources of competition for future solicitations.

Bidders' Mailing List

Each Base anticipates its needs for commodities and services yearly. Potential contractors are catalogued by their 6-digit source codes and become part of the mailing list for future solicitations.

Master Vendors' File

This government-wide file consists of a computer listing in both alphabetical and vendor code sequence. In addition, there is the Master Source Listing which organizes entries by PCS with suffixes and also by vendor codes.

Procurement Automated Source System (PASS)

PASS allows potential bidders to list their capabilities via an on-line data base. The SPA avails this system to government contracting agencies and corporations that subcontract.

RESOURCE PERSONS

Requesting Activities

The users themselves are excellent sources of information for specific requests. Routinely they suggest at least one source of supply. Because of their technical expertise, however, they usually know competing sources as well.

Other Buyers

Some buyers have bought virtually everything at one time or another. More than likely in your branch or division someone will have a suggested source for most procurements. If that doesn't work, try calling another base contracting division or branch that buys the same class codes as you and talk with their buyers. Perhaps they or their co-workers can provide you with an additional source of competition.

Contracting Supervisors

Most supervisors have worked their way up through the ranks and have acquired considerable experience along the way. Even inexperienced supervisors often have good ideas because of their contact with experienced buyers and training. Even if your supervisors don't know of a source immediately, they may be able to direct you to someone who does.

Small & Disadvantaged Business Specialists (SADBUS)

This individual has access to a variety of small business directories, trade organizations, and other disadvantaged firms. The SADBUS can be very helpful with suggested sources for small purchases and other set-asides.

Manufacturers' or Distributors' Representatives

Naturally these people are trying to sell you something. On the other hand, they are knowledgeable of competing lines as well and may provide you with additional sources. Also, they may help you with information of noncompeting lines within their industry.

NATIONAL DIRECTORIES

Thomas' Register/Thomcat

This publication is the most widely available directory of company profiles for American manufacturing. In addition, it lists products and services for each company. Also catalog listings are available for many entries. Thomas' Register is very comprehensive for products, but service listings do not have the same breadth.

U.S. Industrial Directory

The U.S. Industrial Directory is another product suppliers' directory. Although not as comprehensive, its 2-volume format allows convenient use and some additional listings.

National Directory of Minority and Women-Owned Business Firms

Minority-owned businesses are targeted in this directory. Entries are well screened. You can scan specific SIC Codes and/or geographic areas of interest to meet your specific purchasing requirements.

Encyclopedia of Business Information Sources

It is impossible to anticipate (or list) all directory requirements. While it is not a directory itself, it lists directories as well as organizations, on-line data bases, etc., for industries and activities. Some typical entries are the National Tooling and Machine Power's Guide, Louisiana Construction Directory and the Nationwide Directory for Major Mass Market Merchandisers. This encyclopedia is available at most local or university libraries.

LOCAL DIRECTORIES

Business-to-Business
Yellow Pages

Since you live on the telephone anyway, the advantages of using the Yellow Pages are availability and convenience. Although the Consumer Yellow Pages are useful, the Business-to-Business version better targets manufacturers and distributors.

Chambers of Commerce

Virtually every city has a Chamber of Commerce. Generally each one publishes a company profile of each member. These Directories are usually available upon request for little or no cost.

States and Regions

Often a state or region will form an economic consortium and compile a directory. These publications are usually similar to a Chamber of Commerce Directory except for covering a larger geographic area.

Loose-Leaf Notebooks

There are internal directories which can be compiled within a branch or division. All that is needed is a three-ring binder and some standard lined forms. Then record whatever contractor information you feel is useful. For an example see Appendix _____. There is one warning, however. Unless someone is responsible for the upkeep of the book, it may become rapidly outdated and thus valueless.

MISCELLANEOUS SOURCES

Retail Catalogs

Sometimes simplest is best when it comes to source selection. Manufacturers usually sell at suggested retail prices to the government. Often distributors for large retail outlets, for example, Sears, Wards, or Penney's, can afford to sell at significant discounts because of their large quantity purchases.

Trade Materials

Trade journals, brochures, or catalogs, such as the National Mechanical Contractor Estimator, provide specific information about numerous products. Also, manufacturer representatives are always eager to supply you with more literature than you have space to file.

Newspaper Ads

Classified advertisements in daily newspapers remain one of the most popular media for selling in America. The current practice of including inserts for distribution along with the paper also provides additional sources.

Bid Boards

These are merely bulletin boards for solicitations. Depending on the size of your operation, several clipboards posted in a public lobby may be enough. Some large base contracting facilities in metropolitan areas are even experimenting with cable TV stations to publicize their requirements.

Superintendent
of Documents

The U.S. Government Printing Office publishes catalogs of "New Books" throughout the year. The Department of Commerce lists many economic publications for states, regions and industries within this catalog. It is easy to obtain subscription for the catalog, and most books listed are very inexpensive.

AD-A166 178

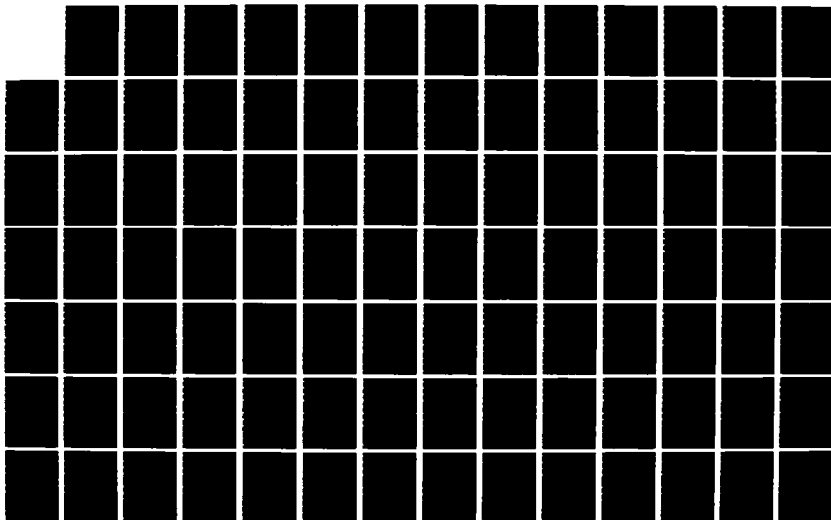
UNITED STATES AIR FORCE SUMMER FACULTY RESEARCH PROGRAM
1985 TECHNICAL RE (U) UNIVERSAL ENERGY SYSTEMS INC
DAYTON OH R C DARRAH ET AL DEC 85 AFOSR-TR-86-0141
F49628-85-C-0013

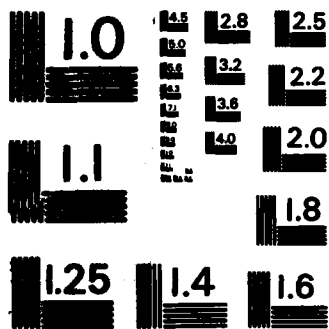
7/11

UNCLASSIFIED

F/G 5/9

NL





MICROCOPY RESOLUTION TEST CHART
NATIONAL BUREAU OF STANDARDS-1963-A

CHAPTER _____

PROTESTS

CICA has a new statutory procurement protest system concerning any alleged violation of a procurement statute or regulation. The only protests precluded by this chapter are of Automatic Data Processing (ADP) matters previously protested to the General Services Board of Contract Appeals (GSBCA). Non-statutory protests still will be considered by the General Accounting Office (GAO).

Time Frames

Normally an agency has 25 work days to present its case after the receipt of notice of a protest. With an expressed option, however, only 10 work days are available to respond to a protest. The GAO determines whether the expressed option can be used or not.

FAR Coverage

CICA moves protest coverage to Part 33 of the Federal Acquisition Regulation (FAR). Some legal uncertainty presently exists regarding stays prior to and after awards. The FAR is silent on the issues of bid-proposal and protest cost. You should consult your most recent FAR and supervisor if problems in this area occur.

Additional Forums

The GAO and Federal District Courts are still available for contracting protests. Additional forums include the United States Court of Claims and the GSBCA. Contact your supervisor and contracting legal counsel if you have any questions.

Protest Prevention

Since the initial number of protests have increased under CICA, prevention is the best medicine. Some activities that may prove useful include: pre-proposal conferences; bid opening extensions; counseling sessions with bidders to persuade initiation of protest on the local level rather than the GAO level.

CHAPTER _____

OTHER CONTRACTING TOPICS

This chapter includes a potpourri of other important contracting topics. All have relevance to full and open competition and some have new implications since implementations CICA.

Disclosure of Pricing Estimates

Pricing and cost estimates must be treated as confidential information. If you reveal these estimates to a potential contractor, it puts the government at a competitive disadvantage. Also, it is unfair to other potential contractors who do not have equal access to the data.

Proprietary Information

Often a contractor will submit an unsolicited proposal in hopes that the government will like the idea and enter into a contract. To protect a unique proposal's trade secrets or other innovations, it is necessary to maintain strict confidentiality with all proprietary data.

End-of-Year Buying

Hurry--if buying at the end of the fiscal year is expensive and often limits competition. The base contracting office should notify users of standard lead times and cut-off dates for submissions of fiscal year-end requisitions. Naturally these policies do not affect walk-throughs.

Contracting Out

A long-standing policy is that the Air Force should do only what is "inherently governmental in nature" and should not compete with industry. "Contracting out" identifies in-house work using government facilities and employees and gives private industry an opportunity to bid on these product or service contracts.

Unsatisfactory Contractors

It is one of the contracting officer's responsibilities to monitor the performance of all contractors. If a problem arises, normally you can conduct a discussion to resolve the discrepancy. If the problem persists, additional recourses are available in the form of cure notices, show cause notices, and ultimately determinations for default.

APPENDIX

T80197 FILM PROCESSING SERVICE

GROUP 7 PHOTOGRAPHIC, MAPPING,
PRINTING AND PUBLICATION SERVICES

APPENDIX
CICA REGULATIONS

CONTRACTOR NAME	ADDRESS	PHONE #	MINORITY SB/LB WOMAN	Regulations	Subject
1 ALPHA TECHNICAL SERVICES, INC.	622 DAYTON ST. HAMILTON, OH 45012	513-846-1564	SB		
2 HEW-ES-CO-INC	494 WYTHE CREEK RD. POQUDSOON, VA 23662	F.G. HEWES 804-868-6839	WOMH1895	FAC 84-5	Competition
3 URBAN LABORATORIES, INC.	950 PACIFIC AVE. SUITE 1005 TACOMA, WA 98402	GERALD BURKE 206-372-6382	SB	FAC 84-6	Protests
4 MALSEED BUSINESS SERVICE	16283 FESTIAN FRASER, MI 48026	E.R. MALSEED 313-791-8310	00042785 SB	DAC 84-10	CICA
5 TECH GRAPHICS	9222 CHESAPEAKE DR. SAN DIEGO, CA. 92123	NANCY LUTICK 714-560-0035	00078795 SB	AFFARS Change 2	Protests
6 MULTI MEDIA FILM LAB, INC.	333K S. W. 9TH ST. DES MOINES, IA 50309	R. CHERKAS 515-288-3456	00040075 SB		
7				AFARS Change 3	CICA
8					
9				AFAC 85-1	Protests
10					
11				AFAC FAR Supplement Change 1	CICA
12					
13					
14					
15					

FIGURE —
UNITED STATES AIR FORCE
TYPICAL BASE CONTRACTING DIVISION
ORGANIZATION AND PLACEMENT

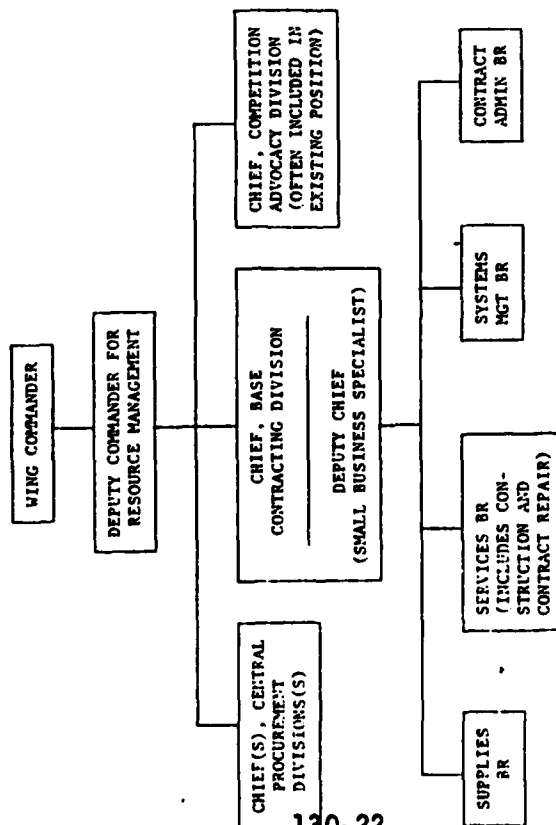


FIGURE
CICA AT-A-GLANCE
COMPETITION IN CONTRACTING 1984
FULL & OPEN COMPETITION (F&OC)

[Exclusions]		[Exemptions]	
Establish Alternate Sources w/D&F (1.7) (6.202) Set-Asides for Small Business & (19.5) Labor Surplus Area (20.2) (6.203)	Small Purchases (Part 13)	Only Responsible Source (6.302-1) Unusual Urgency (6.302-2) Industrial Mobilization (6.302-3) International Agreement (6.302-4) Authorized by Statute (6.302-5) National Security (6.302-6) Public Interest (6.302-7)	MAXIMUM EXTENT PRACTICAL COMPETITION
	8(a) Programs (19.8)		
FULL & OPEN COMPETITION			
Sealed Bids (Part 14)	Competitive Negotiation (Part 15)	Two-Step Bid Combinations (Part 14.5)	Other: A&E (Part 16.6) F&D (Part 35) GSA (Part 8.4)

VI. RECOMMENDATIONS

This competition manual for base-level contracting has Air Force-wide application. Since it can become outdated during any Congressional session, it should be edited, published, and distributed at the earliest opportunity.

There are several implications for further research in this area. If a competition manual is relevant at the base-level, then additional manuals may likewise be relevant at the logistics level or even the systems level.

The complexities and sophistications associated with the logistics or systems level will, however, require additional resources and a broader experiential base.

Another related problem that surfaced during the course of my interviews was the need for education of the requesting activities that rely on base-level contracting for their procurement needs. Users, both infrequent and frequent, are experiencing dissonance over the implementation of CICA. A "Customer's Guide to Base-Level Contracting" would be a timely and valuable reference for user organizations. Although some such guides have been prepared by individual Air Force bases, they predate CICA and are generally written in a style that inhibits use.

REFERENCES

Books and Periodicals:

1. Gansler, Jacques, The Defense Industry. Cambridge, MA: MIT Press, 1980.
2. Montalto, W. B. and Szervo, P. eds., Competition in Contracting, Seminar at Washington, D. C. and San Francisco, CA, New York: Harcourt Brace Jovanovich, 1985.
3. Lesson Book for Defense Small Purchases Correspondence Course, Ft. Lee, VA: U. S. Army Logistics Management Center, 1982.
4. The State of Small Business, A Report to the President, May 1984.
5. The State of Small Business, A Report to the President, March 1985.
6. Legal Times, various issues, Mar. 26, 1984 - Jan. 14, 1985.

Research Studies and Pamphlets:

1. "Assessment of Contractor/In-House Performance of Base Support Functions," AFLMC Gunter AFS, AL, July 1984.
2. "Base-Level Incentive Contracts," AFLMC Gunter AFS, AL, December 1984.
3. "Commander's Guide to Air Force Base-Level Contracting," AFLMC Gunter AFS, AL, 1985.
4. "COPPER '90, a Plan for Air Force Base-Level Contracting for the 1990's," AFLMC Gunter AFS, AL, December 1980.
5. "COPPER" Small Purchase Incentives," AFLMC Gunter AFS, AL, November 1984.
6. "Guide to Pre-Award Surveys," AFLMC Gunter AFS, AL, 1984.
7. "Selling to the U. S. Government," U. S. Small Business Administration, Washington, D. C., 1978.
8. "Small Purchases Pricing Guide," rev. Air Training Command, Randolph AFB, TX, March 1983.
9. "The Source Selection Process," Aeronautical Systems Division Command, WPAFB, OH, July 1981.
10. "What is a Certificate of Competency?," U. S. Small Business Administration, Washington, D. C., 1978.

Federal Laws, Statutes, and Hearings:

1. Competition in Contracting Act of 1984, Title VII of PL 98-369, (1984).
2. Defense Procurement Reform Act of 1984, Title XII of PL 98-525, (1984).
3. Small Business and Federal Procurement Competition Enhancement Act of 1984, PL 98-577, (1984).
4. Armed Services Procurement Act of 1947, 10 USC secs. 2301-2316, (1982).
5. Federal Property and Administrative Services Act of 1949, 41 USC sec. 53 et seq, (1982).
6. Davis-Bacon Act, 40 USC secs. 276A-276A-5, (1982).
7. Walsh-Healey Act, 41 USC secs. 35-45, (1982).
8. Wagner-O'Day Act, 41 USC secs. 4-6, (1982).
9. Contract Disputes Act 41 USC secs. 608, (1982).
10. Small Business Act 15 USC secs. 637-647, (1982).
11. Senate Hearings on S. 338, (1983).
12. Conference Committee Report, excerpts for H.R. 4170 H.Rpt. 98-861, (July 1984).

Federal and Air Force Regulations:

1. Federal Acquisitions Register, FAR various Parts, (1984).
2. DOD FAR Supplement, various Parts, (1984).
3. AF FAR Supplement, various Parts, (1984).
4. Federal Acquisition Circulars, FAC 874-1, 84-5, 84-6, 84-10, (1984).
5. Defense Acquisition Circulars, DAC 84-6, 84-10, (1984).
6. Department of Defense Directive 4245.9, (August 1984).
7. Office of Management and Budget, OMB 85-7, (1985).

1985 USAF-UES SUMMER FACULTY RESEARCH PROGRAM/

GRADUATE STUDENT SUMMER SUPPORT PROGRAM

Sponsored by the

AIR FORCE OFFICE OF SCIENTIFIC RESEARCH

Conducted by the

UNIVERSAL ENERGY SYSTEMS, INC.

FINAL REPORT

THE ROLE OF ANTIOXIDANTS IN
HYPERBARIC OXYGEN TOXICITY TO THE RETINA

Prepared by: William L. Stone, Ph.D.
Academic Rank: Assistant Professor
Department and Departments of Pediatrics and
University: Biomedical Sciences, Meharry Medical
College, Nashville, TN
Research Location: Brooks AFB, School of Aerospace
Medicine, Division of Hyperbaric
Medicine
USAF Research: Col. Richard Henderson, M.D., Chief of
Clinical Investigations and Acting
Chief, Hyperbaric Medicine Division

Hyperbaric oxygen treatment was found to adversely affect the electrophysiological response of the retina to light in rats fed a basal diet deficient in both vitamin E and selenium (the B diet). Both vitamin E and selenium are micronutrients that play essential roles in preventing in vivo lipid peroxidation. After 4 weeks of hyperbaric oxygen treatment (3.0 ATA of 100 % oxygen, 1.5 hrs per day, 5 day/week) rats fed the B diet deficient in vitamin E and selenium showed decreased ($p < 0.005$) in a-wave amplitudes (83 ± 13 uV, $N=8$) and b-wave amplitudes (255 ± 30 uvolts) compared with a-wave amplitudes (151 ± 12 uV, $N=17$) and b-wave amplitudes (369 ± 29 uvolts) for rats fed an identical B diet but not treated with hyperbaric oxygen. Rats fed a basal diet supplemented with both vitamin E and selenium (the B+E+Se diet) or with vitamin E alone (the B+E diet) showed fairly constant a- and b- wave amplitudes that did not decrease after 4 weeks of hyperbaric oxygen treatment. Dietary antioxidants appear to provide protection from hyperbaric oxygen damage to the retina.

ACKNOWLEDGEMENTS

The authors would like to thank the Air Force System Command, the Air Force Office of Scientific Research and Universal Energy Systems, Inc. for the honor and opportunity of contributing our scientific expertise. We thank the School of Aerospace Medicine, and particularly the Division of Hyperbaric Medicine at Brooks AFB, for their hospitality and assistance in our experimental endeavors.

Finally, we would like to thank Col. Richard A. Henderson for his detailed collaborative efforts in all aspects of this project. We also acknowledge the collaborative efforts of Dr. Howard Davis Dr.W. Butcher in the Veterinary Pathology Division at Brooks AFB. Maj. Fanton in the Veterinary Services Division is also acknowledged for his role as a consultant in this project.

REFERENCES:

- 1) Clark JM, and Fisher AB, Oxygen toxicity and extension of tolerance in oxygen therapy. In: Davis, JC, and Hunt, TK, eds Hyperbaric Oxygen Therapy. Bethesda: Undersea Medical Society, 1979, :61-77.
- 2) Small, A, New perspectives on hyperoxic pulmonary toxicity-a review. Undersea Biomed Res 1984; 11;1-24.
- 3) Kappus, K, Sies, H, Toxic drug effects associated with oxygen metabolism: redox cycling and lipid peroxidation. Experientia 1981; 37; 1233-1241.
- 4) Gable, WD, Townsend, FM (1962) Aerospace Med. 33, 1344.
- 5) Farnsworth, CC, Stone, WL, and Dratz, EA. (1978) Biochim. Biophys. Acta, 552, 281-293.
- 6) Stone, WL, Katz, ML, Lurie, M, Marmor, MF and Dratz, EA (1979) Photochem. Photobiol., 29, 725-730.

I. INTRODUCTION:

Hyperbaric oxygen therapy is currently being utilized at the School of Aerospace Medicine to enhance wound healing and to treat a variety of clinical disorders. These clinical disorders include radiation necrosis, gas gangrene, gas embolism, decompression sickness, osteomyelitis, carbon monoxide and acute cyanide poisoning. Hyperbaric oxygen therapy has also been used on an experimental basis to treat sickle cell crisis, hydrogen sulfide poisoning and carbon tetrachloride poisoning and to promote fracture healing.

The therapeutic benefits of long term hyperbaric oxygen treatment are potentially limited by the adverse clinical and pathological effects of high oxygen concentration upon the retina and the lung (1,2) and by adverse interactions with prooxidant drugs (3). Gable and Townsend (4) have observed pulmonary lesions in victims of fatal military aircraft accidents "possibly attributable to prolonged intermittent supplemental oxygen, stressing the potential hazard of oxygen toxicity for aviators". Oxygen toxicity to retinal and pulmonary tissues most likely involves free radical damage to biological membranes.

The retina is more sensitive to toxic and environmental disorders than most other tissues. The retina is particularly predisposed to the toxic effects of lipid peroxidation

initiated by oxy-radicals. This is because the retina has: a) a very high content of polyunsaturated fatty acids (about 30% 22:6n3) which are very susceptible to lipid peroxidation (5); b) a very high consumption of oxygen, about seven times more per g of tissue than the brain; c) the presence of pigments (e.g. retinal) capable of inducing photosensitized oxidation reactions (6).

In some animal models hyperbaric oxygen causes severe retinal pathology and, in humans, causes loss of visual fields and visual definition (7). The ability of the retina to resist oxidative damage is very dependent upon the functioning of both enzymatic and chemical antioxidant mechanisms (8,9). Vitamin E and selenium are micronutrients that play a central role in physiological antioxidant mechanisms. Vitamin E effectively quenches free radicals generated by lipid peroxidation. Selenium is a cofactor for glutathione peroxidase which detoxifies lipid hydroperoxides. Dietary deficiency of vitamin E and/or selenium cause in vivo lipid peroxidation (10).

We have previously found that retinas from rats fed a standard Purina diet have significant levels of vitamin E and the selenoenzyme glutathione peroxidase. Retinal levels of vitamin E and glutathione peroxidase are decreased to very low levels by nutritional deficiency of vitamin E and selenium, respectively (9,11).

Rats fed a diet deficient in both vitamin E and selenium (the B diet) for 20 weeks or longer show retinal damage as indicated by decreased a- and b-wave electroretinogram (ERG) amplitudes (6). The retinal pigment epithelium of rats fed the B diet also show a large accumulation of lipofuscin pigment as well as major ultrastructural alterations (11,12). Lipofuscin pigment is thought to be a by-product of in vivo lipid peroxidation. Recent in vitro studies of Armstrong, et al. (13), have shown that intravitreal injections of synthetic lipid hydroperoxides into rabbit eyes causes a marked decrease in the amplitude of the a-, b- and c-waves of the ERG.

II. OBJECTIVES OF RESEARCH EFFORT:

The research outlined in this preproposal is a direct continuation and follow-up of the pilot research project initiated at the USAF School of Aerospace Medicine (Brooks AFB) during the Summer of 1984. The objectives of the current research effort were to:

- i) Investigate the toxic effects of long term hyperbaric oxygen on rats fed diets deficient in antioxidant nutrients. The toxicity of hyperbaric oxygen was measured by recording electroretinograms, weight, weight gain, and food consumption.
- ii) Determine if short term hyperbaric oxygen treatment will cause retinal damage in rats previously fed an antioxidant deficient diet for 6

weeks.

iii) Investigate the possible protective effects of antioxidants nutrients on hyperbaric oxygen damage to the retina.

iv) Determine if hyperbaric oxygen treatment results in decreased levels of plasma vitamin E or plasma and glutathione peroxidase

III. EXPERIMENTAL DESIGN:

The project was divided into two phases. In phase I , weanling rats were fed the B or B+E+Se diets. After two weeks on this dietary regimen, HBO treatment was given to half the rats in each dietary group for five days a weeks for a total of four weeks. ERG measurements were made in all groups after two and four weeks of HBO treatment. During phase I, rats in B+HBO group were being depleted of vitamin E and selenium and continuously treated with HBO. It is reasonable, therefore, to ask whether any observed retinal damage in the phase I B+HBO rats actually required long term HBO treatment. An alternative hypothesis is that a critical level of vitamin E and glutathione peroxidase exists below which retinal damage will be produced even with short short term HBO treatment. This alternative hypothesis was tested in phase II of the project by treating rats fed the B diet for 6 weeks with a short term (3 days) treatment with HBO and then recording the ERG amplitudes. In this experiment the rats would already be

depleted of vitamin E and selenium at the time of HBO treatment. The detailed methodology for phase I and phase II of the project are detailed below.

Animals and Diets

Male, 30 g, inbred Fischer-344 (CDF) rats from Charles River Breeding Laboratory were housed in suspended stainless steel, wire-bottomed cages and maintained at 25 ± 2 C and 50% relative humidity. Lighting was on a 6:00 AM to 6:00 PM light period and a 6:00 PM to 6:00 AM dark period. Upon arrival at Brooks AFB the rats were fed a normal Purina laboratory chow (Rodent Laboratory Chow 5001, Ralston Purina Co., St. Louis, MO) and water ad libitum for one week while under quarantine. The rats were then randomly divided into the two dietary groups. One group (24 rats) was fed a basal diet deficient in both vitamin E and selenium (the B diet) and the other group (24 rats) was fed an identical diet but supplemented with both these micronutrients (the B+E+Se diet). The basal diet, although deficient in vitamin E and Se, has adequate levels of all other nutrients as proposed by the National Research Council for the Laboratory Rat (14). The B+E+Se diet was supplemented with 50 mg vitamin E per kg of diet (1.1 IU per mg of DL-alpha-tocopherol) and 0.4 ppm Se (added as sodium selenite).

All dietary supplies were purchased from U.S. Biochemical Co, Cleveland, OH. Diets were frequently prepared in small batches by slowly mixing the constituents to avoid heating,

and stored at 2 C. Glass and stainless steel feeders (Hazelton Systems, Aberdeen, MD) were filled every 2 days and any uneaten food discarded to minimize rancidity. Rats in all the dietary groups were provided with deionized water to which 3 ppm chromium (as CrCl_3) was added. Both diet and drinking water were provided ad libitum. The composition of the B diet is given in Table 1.

Phase I-Hyperbaric Oxygen Treatment

After being fed the B or B+E+Se diets for two weeks, eight rats in each dietary group were exposed to 3.0 ATA of 100 % oxygen for 1.5 hr/day, five days per week on a Monday to Friday schedule. The hyperbaric chamber was installed in the animal care room and oxygen was directly vented to the outside. Eight rats in each dietary group were not treated with HBO. These nonHBO rats served as controls to monitor retinal damage that might be due to antioxidant deficiency alone. The electroretinograms in the set of 32 phase I rats was measured every two weeks. When the rats in the B+HBO group showed diminished ERG a- and b-wave amplitudes they were euthanized under halothane anesthetic and tissue samples collected for future structural and biochemical studies. The remaining rats in the phase I study were also euthanized for future studies.

Phase II-Short term HBO Exposure.

Eight rats in each dietary group were not exposed to either HBO treatment nor did they have ERGs recorded in phase-I of

the experiment. These phase II rats were used for a "short-term" HBO treatment experiment. When the B+HBO rats showed ERG deterioration (about 4 weeks of HBO treatment) then the 8 phase-II rats in each dietary group were treated with HBO for 3 days and ERGs recorded. If ERGs in the phase-II B+HBO rats decreased as a result of this short-term HBO treatment, it would indicate that dietary deficiencies of vitamin E and Se are more important than 4 weeks of chronic HBO exposure. From our previous pilot experiment, we know that rats fed the B diet for 6 weeks, and not placed in the HBO chamber, do not suffer ERG amplitude decreases.

Electroretinograms

The electroretinograms (ERGs) were recorded in biweekly intervals. ERG measurements were made using an aluminized mylar plastic positive electrode placed on the cornea. This electrode effectively eliminates the possibility of corneal damage. The ground electrode was attached to the ear lobe and a negative pin electrode inserted under the scalp. We used a ganzfeld (whole field) flash, a Grass photostimulator and a Tektronic model 6512 recording oscilloscope with a 5A22N differential amplifier and a 5B10N time base amplifier. Animals were placed in a dark room for at least 1 hr before measuring ERGs. About 10 min before recording an ERG, each rat was anesthetized (IM injection) with 0.1 ml of ketamine (50 mg/ml). At least six a- and b-wave amplitude measurements were made for each eye in each rat.

Vitamin E and Glutathione Peroxidase Activities.

Four rats from each group were evaluated for plasma vitamin E, plasma glutathione peroxidase (GSHPX), and red blood cell GSHPX on a biweekly basis. GSHPX is a selenoenzyme and its activity in plasma and red blood cells (RBCs) is a good measure of selenium status. Blood was obtained from each rat after cutting (under methoxyfluorane anesthetization) off a small section from the end of the tail. This process is relatively untraumatic and can easily be done on the same rat on a biweekly basis. Blood was separated into plasma and washed RBCs. The plasma vitamin E and GSHPX assays on plasma and RBCs were done at Meharry Medical College by the P.I.

Statistics

Student's t-test and analysis of variance (ANOVA) were used to establish statistically significant differences (i.e. a $P < 0.05$) in the a- and b-wave ERG amplitudes of rats in the various dietary groups.

IV RESULTS:

Phase I-Effects of antioxidant nutrients and long term hyperbaric oxygen treatment on electroretinograms.

Table 2 shows the a- and b-wave amplitudes recorded for the B and B+E+Se groups either treated or not treated with HBO for 2 or 4 weeks. After 2 weeks, we found the ERG amplitudes to be very similar in both the B and B+E+Se dietary groups and unaffected by HBO treatment. Two-way analysis of variance with unequal subsamples confirmed that the mean a-waves (or

b-waves) were indistinguishable in the four treatment groups at week 2.

After 4 weeks of HBO treatment there was a marked decrease in the a-wave ($p < 0.005$) and b-wave ($p < 0.05$) ERG amplitudes of rats in the B+HBO group compared to rats in the B+nonHBO group. Rats supplemented with both vitamin E and Se showed no decreases in a- or b-wave ERG amplitudes after 4 weeks of HBO treatment. Furthermore, the ERG amplitudes of the B+E+Se group (both HBO and nonHBO) were similar at both 2 and 4 weeks after the start of HBO treatment.

Phase II- The effects of short term HBO on rats deficient in both vitamin E and Se.

In phase II, we examined the effects of a 3-day treatment with HBO (3.0 ATA of 100% oxygen for 1.5 hr/day) on six rats previously fed the B diet for eight weeks but not treated with HBO. A control group of four B rats were not treated with HBO. The a-wave amplitudes for this B+HBO group was 130 ± 12 microvolts, which was very similar to that observed for the control nonHBO B rats and similar to that previously observed for B+E+Se rats (HBO or nonHBO). These data indicate that prolonged HBO treatment, as well as vitamin E and selenium deficiency are required for a decrease in a-wave amplitudes.

The b-wave amplitudes in the phase II B+HBO and B+nonHBO were 262 ± 61 and 273 ± 59 microvolts, respectively. The fact that the b-wave amplitudes were similar indicates that short term HBO

treatment did not cause any decrease in retinal function. The b-wave amplitudes for the B rats was , however, somewhat lower after 8 weeks of B diet than after 6 weeks. This could indicate that prolonged antioxidant deficiency can cause retinal damage independent of HBO treatment.

Plasma vitamin E and selenium-glutathione peroxidase levels

Table 3 provides the plasma vitamin E levels and the plasma Se-glutathione peroxidase activities for rats in all treatment groups at both 2 and 4 weeks after start of HBO. Rats fed the vitamin E and Se deficient diet had significantly lower ($p < 0.005$) plasma vitamin E and plasma glutathione peroxidase than rats fed the diet supplemented with these micronutrients. This was true at both 2 and 4 weeks.

It is important to note that the levels of vitamin E and the the activity of glutathione peroxidase were not influenced by 4 weeks of hyperbaric oxygen treatment. This result is somewhat surprising. We anticipated that hyperbaric oxygen would increase vitamin E utilization and therefore increase vitamin E depletion in rats fed the B diet and treated with HBO.

Weight, weight gain and food consumption.

The weights, weight gains and food consumption of rats in all dietary groups at both 2 and 4 weeks of HBO treatment are given in Table 4. These data indicate that neither diet or HBO treatment has any significant effects on the weights,

weight gains or food consumption of rats in the experimental protocol. From our previous pilot experiment, we know that rats fed the B diet and treated with HBO will have a decreased weight gain compared to nonHBO B rats soon after 4 weeks of HBO treatment.

V RECOMMENDATIONS:

Dietary deficiencies of both vitamin E and selenium were found to adversely effect the electrophysiological response of the retina to light in rats treated with hyperbaric oxygen for 4 weeks. Decreased a-wave and b-wave ERG amplitudes as a result of hyperbaric oxygen treatment were apparent only in rats deficient in both vitamin E and selenium. Hafeman and Hoekstra (10) have shown that dietary deficiency of both vitamin E and selenium is much more effective in promoting in vivo lipid peroxidation than dietary deficiency of either vitamin E or selenium alone.

Rats are generally considered a species very resistant to oxidative damage. Rats have enzymatic antioxidant mechanisms that can be induced in response to oxidative stress (8,9,15). The degree to which an organism can induce these enzymatic antioxidant mechanisms may be an important parameter in determining an organism's susceptibility to oxygen toxicity. For example, glutathione-S-transferase activity in the rat lung increases in response to hyperoxia (15). A number of glutathione-S-transferase isozymes have a "nonselenium glutathione peroxidase" activity that may protect against

damaging in vivo lipid peroxidation reactions. These potential enzymatic responses to HBO treatment in rats must be characterized before the relevancy of our results to humans can be understood.

Our results suggest that nutritional supplementation of patients with antioxidant nutrients could diminish the oxygen toxicity problems associated with HBO therapy. Hyperbaric oxygen therapy has been experimentally used in the treatment of sickle cell crisis episodes. We and other investigators have found that sickle cell disease patients have a profound deficiency of vitamin E. We would therefore recommend that the vitamin E status of sickle cell patients be carefully considered before any treatment with hyperbaric oxygen. Precautions in using HBO therapy would also be indicated in any disease states in which antioxidant mechanisms could be impaired.

Four animals in the B, B+HBO, B+E+Se and the B+E+Se+HBO groups were euthanized at week 6 and samples of lung, liver, and retina tissue were stored at -70 C for biochemical analyses. Four rats were also perfused with Karnofsky's fixative. Retinal tissues were embedded in Epon for future analyses by fluorescent microscopy, phase contrast microscopy, and electron microscopy. We recommended follow-on biochemical studies of lung, liver and retinal tissues and detailed light/electron microscopy studies of retinal tissues, be pursued as detailed in the RESEARCH INITIATION PROPOSAL.

- 7) Nichols, C.W. and Lambertson, C.J. (1969)
New Engl. J. Med., 281, 25-30.
- 8) Stone, W.L. and Dratz, E.A. (1982) Exp. Eye Res.,
35, 405-412.
- 9) Stone, WL, and Dratz, EA. Increased glutathione
s-transferase activity in antioxidant-deficient rats.
Biochim Biophys Acta 1980; 631; 503-506.
- 10) Hafeman, DG and Hoekstra, WG. Lipid peroxidation in vivo
during vitamin E and selenium deficiency in the rat as
monitored by ethane evolution.
J Nutr 1977; 107; 666-672.
- 11) Katz, ML, Stone, WL, and Dratz, EA. Fluorescent pigment
accumulation in retinal pigment epithelium of
antioxidant-deficient rats. Invest Ophthalmol 1978; 17;
1049-1058.
- 12) Katz, M.L., Parker, K.R., Handelman, G.J., Bramel, T.L.
- 13) Armstrong, D, Hiramitsu, T, Gutteridge, J, and
Nilsson, SE. Studies on experimentally induced retinal
degeneration. 1. Effects of lipid peroxides on
electroretinographic activity in the albino rabbit.
Exp Eye Res 1982; 35; 157-171.
Dratz, E.A. (1982) Exp. Eye Res., 34, 339-369.
- 14) National Research Council Publication on Nutrient
Requirements of Laboratory Animals, No. 10, p 56,
Washington, DC, Nat Acad Sci, 1978.
- 15) Jenkinson, SG, Lawrence, RA, Burk, RF and Gregory, PE,
Non-selenium-dependent glutathione peroxidase activity
in rat lung associated with lung
glutathione s-transferase activity and effects of
hyperoxia. Toxicol and Applied Pharmacol; 1983; 68;
399-404

Table 1. Composition of basal diet.

Ingredient	g/100g
<hr/>	
Tourla yeast	36.00
Sucrose	43.05
Corn oil, tocopherol stripped	14.50
Vitamin mix 1	2.20
Mineral mix Draper 2	4.00
L-Methionine	0.25

1. The vitamin mixture provided: (in mg/100 g of diet) ascorbic acid, 99; inositol, 11; choline chloride, 16.5; p-aminobenzoic acid, 11; niacin, 9.9; riboflavin, 2.2; pyridoxine-HCl, 2.2; thiamin HCl, 2.2; calcium pantothenate, 6.6; biotin, 0.05; folic acid, 0.2; vitamin B-12, 0.003. In addition the vitamin mixture contains: (in units /100 g of diet) vitamin A acetate, 1980; calciferol (D3), 220.2.

2. The salt mix provided (in mg/100 g of diet): CaCO_3 , 654; $\text{CuSO}_4 \cdot 5\text{H}_2\text{O}$, 0.72; $\text{Ca}_3(\text{PO}_4)_2$, 1422; Ferric citrate $\cdot 3\text{H}_2\text{O}$, 64; $\text{MnSO}_4 \cdot \text{H}_2\text{O}$, 5.5; potassium citrate $\cdot \text{H}_2\text{O}$, 946; KI, 0.16; K_2HPO_4 , 309; NaCl, 432; ZnCO_3 , 1.8; and MgCO_3 , 164.

Table 2

The effects of hyperbaric oxygen (HBO) on a- and b-wave electroretinogram (ERG) amplitudes for rats fed diets either deficient or supplemented with vitamin E and selenium. Each entry is mean \pm SEM and the number of animals is indicated in parentheses.

time weeks	treatment	diet	a-wave microvolts	b-wave
2	HBO (8)	B	148 \pm 20	332 \pm 61
	nonHBO (8)	B	139 \pm 14	320 \pm 31
2	HBO (8)	B+E+Se	148 \pm 10	359 \pm 23
2	nonHBO (7)	B+E+Se	140 \pm 14	320 \pm 31
4	HBO (8)	B	83 \pm 13*	255 \pm 30**
4	nonHBO (17)	B	151 \pm 12	369 \pm 29
4	HBO (6)	B+E+Se	139 \pm 17	360 \pm 38
4	nonHBO (18)	B+E+Se	135 \pm 9	326 \pm 22

* $p < 0.005$ ** $p < 0.05$ vs. nonHBO

Table 3

Antioxidant levels (mean \pm SEM) in rats fed diets supplemented (B+E+Se) or deficient (B) in vitamin E and selenium and with or without hyperbaric oxygen (HBO) treatment.

time	treatment	vitamin E ug/ml of plasma	glutathione peroxidase milli e.u./ul of plasma
2	B+HBO	1.6 \pm 0.1*	4.0 \pm 0.2*
2	B	2.0 \pm 0.1*	4.2 \pm 0.6*
2	B+E+Se+HBO	5.5 \pm 0.6	11.0 \pm 1.0
2	B+E+Se	6.1 \pm 0.4	8.9 \pm 1.2
4	B+HBO	0.8 \pm 0.1*	2.2 \pm 1.0*
4	B	0.8 \pm 0.1*	2.1 \pm 0.5*
4	B+E+Se+HBO	5.0 \pm 0.8	8.2 \pm 1.4
	B+E+Se	4.3 \pm 0.5	9.8 \pm 2.8

1. Rats were on the indicated diets for 2 weeks longer than the time indicated in the table. Four rats were used in each table entry. Milli e.u. for glutathione peroxidase activity is nanomoles of NADPH oxidized per min.

* indicates a $p < 0.005$ vs. the B+E+Se groups.

Table 4

Weight (g), weight gain/day (g/day) and food consumption (g/day) for rats fed diets either deficient (B diet) or supplemented (B+E+Se) with vitamin E and selenium. Rats in both dietary groups were either treated (HBO) or not treated with hyperbaric oxygen (nonHBO).

treatment group	time on diets (weeks)			
	0	2	4	6
B(20)+nonHBO				
weight	94.2 \pm 0.2	131.0 \pm 1.8	168.2 \pm 6.8	186.0 \pm 10.7
wt.gain/day	-	2.6	2.7	1.3
food/day	-	-	11.1	11.4
B+HBO(8)				
weight	92.1 \pm 2.0	126.8 \pm 3.3	161.0 \pm 4.2	183.0 \pm 6.3
wt.gain/day	-	2.5	2.5	1.6
food/day	-	-	10.8	10.2
B+E+Se+nonHBO(20)				
weight	93.3 \pm 1.9	128.9 \pm 3.0	176.1 \pm 3.2	200.0 \pm 3.2
wt.gain/day	-	2.5	3.4	1.7
food/day	-	-	10.9	12.3
B+E+Se+HBO(8)				
weight	94.0 \pm 3.0	127.5 \pm 3.2	161.0 \pm 4.2	178.0 \pm 4.9
wt.gain/day	-	2.4	2.4	1.2
food/day	-	-	11.2	10.4

The number of rats is given in parentheses. Each data entry is mean \pm SEM

1985 USAF-UES SUMMER FACULTY RESEARCH PROGRAM/

GRADUATE STUDENT SUMMER SUPPORT PROGRAM

Sponsored by the

AIR FORCE OFFICE OF SCIENTIFIC RESEARCH

Conducted by the

UNIVERSAL ENERGY SYSTEMS, INC.

FINAL REPORT

ASSESSMENT OF MAXIMUM ENTROPY METHOD SOFTWARE

FOR TREATMENT OF DATA FROM THE AFGL LABCEDE FACILITY

Prepared by:	James E. Sturm
Academic Rank:	Professor
Department and	Department of Chemistry
University:	Lehigh University
Research Location:	Air Force Geophysics Laboratory
	Hanscom Air Force Base, MA
	Infrared Technology Division
	Infrared Dynamics Branch
USAF Research:	Dr. William A. M. Blumberg
Date:	September 27, 1985
Contract No:	FL9620-85-C-0013

ASSESSMENT OF MAXIMUM ENTROPY METHOD SOFTWARE
FOR TREATMENT OF DATA FROM THE AFGL LABCEDE FACILITY

by

James E. Sturm

ABSTRACT

Software available for reduction of interferometric data by the maximum entropy method (MEM) was used to study the effectiveness of this method in presenting emission spectra from high level Rydberg states of atomic oxygen excited in the AFGL LABCEDE facility. The MEM treatment at higher orders generated fine structure which was not ascribable to known transitions of oxygen atoms.

Interferograms representing model spectra, one without and one with added noise, were fabricated for use with the software. Results of both fast Fourier transform (FFT) and MEM treatments are compared. While the FFT operation reproduced the model spectrum in each case, the MEM treatment tended to overemphasize major peaks. It also produced narrower and spurious peaks, especially in the absence of noise and at higher orders. It is recommended that the code be tested for fidelity to the MEM algorithm.

I. INTRODUCTION -

A. Application and Appointment - The author's graduate training and subsequent research both relate to the characterixation of elementary processes especially those of excited species in the gas phase. When the 1985 AFOSR-SFRP program announcement appeared, the author responded with an application and requested consideration for those projects which overlapped with his background and interests. Notice of favorable action on that application was received early in March. Assignment was made to the Aif Force Geophysical Laboratory, Hanscom AFB, MA for work in the Infrared Technology Division, specifically in the Infrared Dynamics Branch, designated AFGL/LSI.

B. Choice of Project - By far the most convenient time for the author to make a pre-summer site visit was a break period in mid-March. During the visit he was cordially introduced to the staff members. Each member described potential projects within the scope of his research activity so as to provide a view of their relation to the mission of the Laboratory.

Consideration of these project ideas proceeded in a general way during April and May. The author described, in a letter to the Branch Chief, his research interests in relation to the theme of work at AFGL/LSI. He also suggested a particular study in the remote possibility that facilities might be assignable to it. In turn, members of the AFGL/LSI staff considered the suggestion along with their own goals. As the time approached for submission to UES of a goals statement, realistic perspective suggested taking up one of several projects which the AFGL/LSI staff had either tabled temporarily or which constituted

nearly-finished projects having some promise of completion during the ten-week SFRP period. It was agreed to consult with Dr. W. A. M. Blumberg of the AFGL/LSI staff for focus onto a particular project.

Work at AFGL/LSI began on 3 June, 1985. The first week or more was used in reading published papers, reports and parts of some monographs related to the following suggested projects:

1. Mechanism of production of excited infrared-emitting states of O_2^+ in the AFGL LABCEDE facility
 2. Quenching of vibrationally excited states of NH in N_2-H_2 mixtures excited by electron beams in the AFGL LABCEDE facility
 3. Mechanistic interpretation of the emission observed on electron irradiation of N_2-CO_2 mixtures in the AFGL LABCEDE facility
 4. Assessment of the maximum entropy method (MEM) of spectral analysis of interferometric data obtained in the AFGL LABCEDE facility.
- A decision was made to embrace project #4 of those listed above.

C. LABCEDE Facility - Since all of the projects suggested relate to this facility, a brief description of its characteristics and capabilities is given here. In LABCEDE, a high pumping rate gas handling system is provided to allow flow of gas at constant pressure past a collimated electron beam of energy adjustable between 2 and 6 keV with currents up to 20 mA. Infrared radiation produced by interaction of the electrons with the gas is viewed at right angles to the electron beam by a Michelson interferometer whose operation allows computer collection and storage of 2-dimensional arrays of intensity data. These intensities correspond to sets representing at least 2048 mirror positions at one of various times before, during, and after arrival of repetitive

electron pulses at the viewed sample volume of gas.

II. OBJECTIVES OF THE RESEARCH EFFORT -

A. General Principles of Data Analysis - The sets of data collected during an experiment on the LARCEDE facility need to be reduced or summarized in a manner which allows effective description of the processes involved. This data reduction can proceed by several avenues each of which usually carries with it a limited perspective on the manner of approximation and degree of completeness of a model to describe phenomena responsible for the observations. One of the desirable, but not always exercised, stages in a data treatment is the explicit identification of assumptions made and of critical features of the model.

Abels(1) states what he calls the First Principle of Data Reduction:

"The result of any transformation imposed on experimental data shall incorporate and be consistent with all relevant data and be maximally non-committal with regard to unavailable data."

Perhaps some explanation is warranted on why this report would include philosophizing on one of the tenets of the scientific method. Prior to 1965 most spectroscopic instruments were designed around analog electronic processing of signals. The link between raw measurements and their digestion or display was then rather short and direct. About 1965, Cooley and Tukey (2) noted that Fourier transforms could be made tractable even by computers of that generation. Exploitation (3) of their algorithm, the so-called fast Fourier transform (FFT), has brought about extensive and revolutionary conversion of manufactured spectroscopic instrumentation to designs having advantages of sensitivity and resolution over the earlier analog instruments.

Implementation of this algorithmic breakthrough has had its price, however. A Fourier transform is defined as an integral over an infinite range of one variable (4):

$$F(\sigma) = \lim_{x' \rightarrow \infty} \int_{-x'}^{x'} f(x) \exp(-i2\pi\sigma x) dx \quad [1]$$

Data collected by an instrument are necessarily finite in extent and often are limited by other constraints. Integration of [1] over a finite range destroys the uniqueness of the correspondence between $f(x)$ and $F(\sigma)$. Sometimes the range of integration, still finite, is extended by assigning values beyond the range of measured values (5). When zeros are assigned, side lobes are found in the resulting $F(\sigma)$ even for single-line spectral transitions (1). Often a compromise procedure is adopted to apodize the experimental values gradually towards zero at the extremes. It is difficult to defend a priori these extensions beyond the range of measurement and also these alterations of valid data; both constitute violations of the First Principle cited above (1).

B. Maximum Entropy Method (MEM) - While there are arguments (6) presented to defend the apodization algorithms, there is room for consideration of alternative approaches hopefully having a firm conceptual foundation. Soon after the introduction (7) of concepts on information theory, radio engineers began to pursue the related statistical definition of entropy in their search for methods to extract signals from a noisy background. Frequent reference is made to the work of Burg (8) who presented a formulation appropriate to spectral determination and also described a method for computing related parameters. This

so-called maximum entropy method (MEM) has been cited by Abels (1) as being more nearly in accord with the First Principle than the FFT. Both the FFT and MEM begin with a set of data points, e.g., a finite interferogram of measured intensities $I(x_i)$, $i = 1, \dots, n$. In the MEM, the spectrum is defined as that function $F(\sigma)$ having the property that the integral J given by

$$J = \int_{-\infty}^{\infty} \ln F(\sigma) d\sigma \quad [2]$$

is a maximum subject to the constraints below which relate $F(\sigma)$ to the measured intensities:

$$I(x_i) = \int_{-\infty}^{\infty} F(\sigma) \exp(i2\pi\sigma x_i) d\sigma, \quad i = 1, \dots, n \quad [3]$$

The limits of [3] need not be infinite if $F(\sigma)$ is zero outside of a spectral range of significance. Of the many papers discussing MEM theory, one (9) presents a FORTRAN code for implementing the method. It is also noteworthy that this voluminous literature on spectral analysis has so far been devoted mostly to the audio- and radiofrequency ranges. Very few applications to spectroscopy of atomic, ionic or molecular systems have been reported (10 - 12). In two of the cases just cited, the data taken were in the time domain following pulse excitation of NMR (12) or of ions in a cyclotron mass spectrometer (11). More closely related to the present study is the work of Minami, et al. (10) who compared FFT and MEM data reduction of interferograms.

The main achievements of the MEM shown in these few papers are

striking improvements in spectral resolution when compared to that achieved by the FFT reduction of the same data. No alteration analogous to apodization was imposed. Also demonstrated are cases in which improved resolution was achieved with raw data sets strikingly smaller than those needed to achieve the same or similar resolution by the FFT method. One might infer from these studies that the MEM promises to offer another leap in capability similar to that experienced with the appearance of the FFT algorithm.

C. Statement of Research Objective - With all of its promise, superresolution capabilities of the MEM must nevertheless have their own limitations which at this stage are not clearly identified. The present study was suggested in hopes of pursuing such limitations. Below is a statement of the objectives of this research effort in the context of the background ideas described above:

OBJECTIVE: to study application of the maximum entropy method (MEM) of data reduction to interferograms representing infrared emission spectra having some structure but sufficiently characterized so as to pursue assessment of the limitations of the MEM.

Some ancillary questions are:

- Is the MEM superresolution an overspecification which may generate artifacts (such as spurious structure)?
- How do the intensities in the power spectrum derived from the MEM relate to otherwise known intensities?
- Are the precise locations of peaks in the intensity (power) spectrum correct?
- If very high resolution is achieved, can one discern

hyperfine structure details in data sets from experiments on the LABCEDE facility in cases in which emission spectra should not have been collision broadened?

III. APPROACHES TOWARD MEETING OBJECTIVE -

A. Facilities Available - This study was an application of computers to a scientific question. To this end, the following hardware and software facilities were available at AFGL/LSI:

- a network of three Apollo computers, disk storage, and a hard copy printer-plotter
- compiled versions of two programs, principally, originally written in FORTRAN and for which source listings were available:
 - 'mem_tst_v1' intended for MEM data reduction
 - 'labcede_sturm' which included the FFT algorithm
- several tens of two-dimensional data files from experiments on the LABCEDE facility. From one of these sets, file 'data_hdl9d', an interferogram file containing 2048 intensities at 2048 mirror positions was extracted for use with 'mem_tst_v1' or 'labcede_sturm'. This interferogram represented emission following electron irradiation of oxygen.

B. Approaches Taken - In the context of the background material discussed above, and with the available computing facilities, effort towards increased understanding of the MEM took the following main avenues:

1. generation, by 'mem_tst_v1' operating on the experimental interferogram, of a series of intensity (power) spectra over selected frequency regions. Each member of the series represented a chosen

value of the number of 'lag' coefficients to be described later under details of the MEM. These spectra were then compared with the spectrum generated by an FFT operation on the same experimental interferogram.

2. fabrication of an interferogram corresponding to a chosen idealized intensity spectrum of known range and structure.

3. operation as in (1.) above on this fabricated interferogram. Included in the plan under (2.) and (3.) above is addition of noise to the fabricated spectrum. The mathematical and computational procedures used are described in detail later in this report.

IV. PROCEDURES AND RESULTS -

In this section are described details of how the steps towards the stated objectives were implemented. Salient features of the results of those efforts are then presented in their respective contexts.

A. MEM Algorithm - Description of the MEM computations requires some amplification of that outlined earlier. As can be seen, for example, in the paper by Ulrych and Bishop (9), it is difficult to summarise the MEM algorithm. That summary by Kawata et al. (10) is adapted here. One begins with a set of interferometric data, either from an experiment or fabricated as in (b.) of the previous section. These data are symbolized by the intensities I_k , $k = 1, \dots, n$, for the mirror positions x_k . A set of $2M$ ($M < n$) autocorrelation functions $R(m)$ can be defined in terms of these data:

$$R(m) = \frac{1}{m} \sum_{\text{over all products}} I_k I_{k+m} \quad , \quad m = -M, (-M+1), \dots, -1, 0, 1, \dots, (M-1), M$$

Next, a set of coefficients, called 'lags', a_m , $m = 1, 2, \dots, M$, is

defined along with a prediction-error power term P_M of order M in terms of the corresponding values of these quantities for the previous order $M-1$. At each order the coefficients a_m and P_M are made to satisfy the condition that

$$P_M = \frac{1}{M} \sum f_k f_k + \frac{1}{M} \sum b_k b_k \quad [4]$$

is minimized where

$$f_k = I_k + \sum_1^M a_m I_{k-m} \quad \text{and} \quad b_k = \sum_0^{M-1} a_{M-m} I_{k-m} + I_{k-M}$$

An important consequence of imposing this condition is that P_M and the coefficients a_m are solutions of the matrix equation

$$\begin{bmatrix} R(0) & R(-1) & \dots & R(1-M) & R(M) \\ R(1) & R(0) & \dots & R(2-M) & R(1-M) \\ & & \ddots & & \\ & & & & \\ R(M) & R(M-1) & \dots & R(1) & R(0) \end{bmatrix} \begin{bmatrix} 1 \\ a_1 \\ \vdots \\ a_M \end{bmatrix} = \begin{bmatrix} P_M \\ 0 \\ \vdots \\ 0 \end{bmatrix} \quad [5]$$

Having P_M and the coefficients a_m , the final step in a given MEM calculation is the generation of the intensity (power) spectrum for the order M :

$$I(\sigma) = \frac{P_M \Delta x}{\left| 1 + \sum_1^M a_m \exp(-2\pi i \sigma m \Delta x) \right|^2} \quad [6]$$

Implementation of the MEM was through the program 'mem_tst_v1' which had already been written prior to the summer project. This program

included the subroutine 'MEMPR' adapted from that given by Ulrych and Bishop (9). In the context of the expressions above, 'mem_tst_v1' offers the user to choose values of the following parameters:

1. the order $M (= n_{\text{lags}})$ of the MEM treatment. Provision is made to store P_M and the a_m as a lagfile.
2. the range $\sigma_{\text{low}} \rightarrow \sigma_{\text{high}}$ to be covered in calculation of $I(\sigma)$ by means of [6].
3. the step size $\Delta\sigma$ in generating a set of $I(\sigma)$ values for plotting. Up to 1024 values can be computed.

Provision was also made in 'mem_tst_v1' to integrate between any pair of σ values with the user's choice of $\Delta\sigma$. The simple trapezoidal integration scheme was used.

B. Known Spectral Transitions - The experimental interferogram derived from LABCEDE data set 'data_4dl9d', as described under facilities, was designed to cover the spectral range 2000 - 14000 cm^{-1} with a resolution of about 6 cm^{-1} . Figure 1a shows a spectral plot over this range following a FFT of this interferogram. Running time and program limitations forced restriction of further data treatment to the range 3000 - 5000 cm^{-1} which is depicted on Figure 1b. Three peaks show above the noise level and they correspond to the following emission processes with oxygen atoms (13):

$4p^3P$	$4s^3S_1$	(near 3456 cm^{-1})
$4p^5P$	$4s^5S$	(near 3617 cm^{-1})
$4d^5D$	$4p^5P$	(near 3772 cm^{-1})

Figure 2 shows the relevant part of a Grotrian diagram for oxygen atoms. Listed on the diagram are hyperfine positions of the transitions which

correspond to $\Delta J = 0 (J \neq 0), \pm 1$. This hyperfine structure is far from resolved in the FFT spectrum. The design resolution of the interferogram, about 6 cm^{-1} , grossly masks the required resolution of about 0.1 cm^{-1} . It is hard to see how the MEM would be able to extract hyperfine structural details from a data set not meeting design criteria for the required resolution. One source (14) has noted that the MEM can generate spurious spikes in some cases. The conditions for appearance of such artifacts are not clearly identified.

C. MEM on Experimental Interferogram - Several options are available on the program 'mem_tst_v1' even when operating on a given interferogram. The space limitations of this report allow presentation of only a few of the results obtained. Those chosen will hopefully help to manifest the salient conclusions to be drawn from the study.

Runs using 'mem_tst_v1' on the experimental interferogram were carried out to generate several lag files of order M from 100 to 2000. On Figure 3 are shown plots of the corresponding intensity (power) spectra. Peaks become not only sharpened as M is increased, but they also split into multiplets. The spacings between adjacent sharp peaks at large M values do not correspond to the known transitions described earlier.

Many integrations were also run to determine areas under the peaks. The value of these runs to the study is questionable since the integration algorithm in 'mem_tst_v1' provided for insufficient detail. Further work on this aspect may be warranted.

D. Fabrication of Interferograms - Appearance of increasingly fine-structured details in operation of 'mem_tst_v1' on the experimental

interferogram left one with a question of the amount of detail which this interferogram should represent. An alternative approach was suggested as more decisive: fabricate an interferogram to represent a well-defined model spectrum and then carry out both FFT and MEM operations on this fabricated interferogram. If the data treatment is valid, it should regenerate the original model spectrum.

Fabrication of an interferogram from a frequency spectrum is the inverse process of a Fourier transform. Choice of the model spectrum, then was made by picking an analytical form for which the Fourier transform is also of a known analytical form. The form chosen was a pair of triangle-shaped peaks of equal width but of decidedly unequal intensities as illustrated in Figure 4. The figure contains the mirrored peaks at negative frequencies so as to eliminate imaginary terms in the transformation. With respect to the labels on the four peaks in the figure, the total intensity $I(\sigma) = I_1 + I_2 + I_{-1} + I_{-2}$. The corresponding interferogram $f(x) = \text{FT}[I(\sigma)]$ and by the superposition theorem

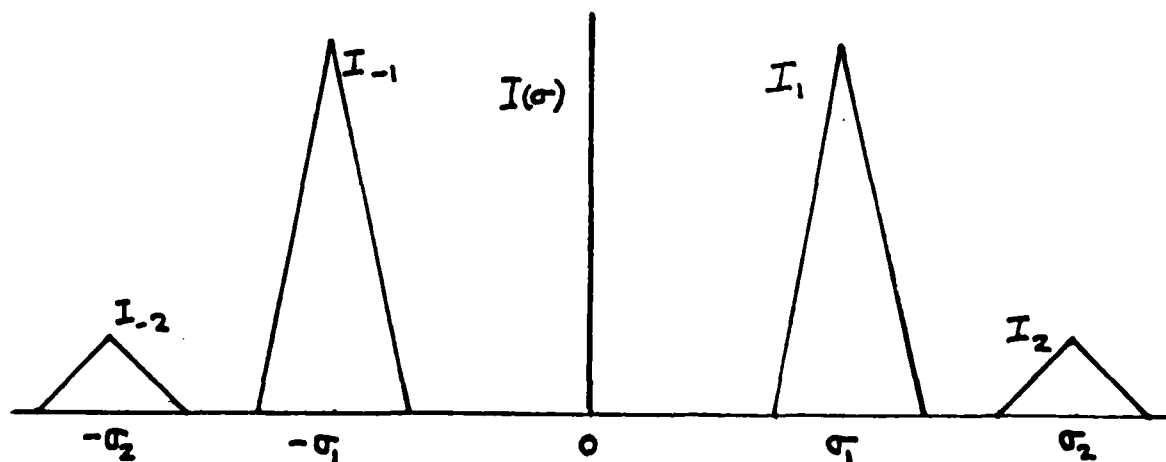


Figure 4. Model Spectrum for Fabricated Interferogram.

$$(4), \quad f(x) = \text{FT}[I_1] + \text{FT}[I_2] + \text{FT}[I_{-1}] + \text{FT}[I_{-2}] \\ = f_1 + f_2 + f_{-1} + f_{-2} \quad [7]$$

For example, one can view I_1 as $I_1(\sigma + \sigma_1)$; i.e., a triangle function $\Lambda(\sigma)$ shifted by σ_1 from the origin. By the shift theorem (4),

$$f_1(x) = \text{FT}[I_1(\sigma + \sigma_1)] = \exp(i2\pi \sigma_1 x) \text{FT } I_1(\sigma) \quad [8]$$

in which $I_1(\sigma)$ is a triangle function at the origin. Now

$$\text{FT}[\Lambda(\sigma)] = \text{sinc}^2(x) \quad \text{where} \quad \text{sinc}(x) = \sin(\pi x)/\pi x.$$

Similar transformations on the other terms in $f(x)$ lead to cancellation of the imaginary terms and one has

$$f(x) = 2 \left[\cos(2\pi \sigma_1 x) + \frac{1}{5} \cos(2\pi \sigma_2 x) \right] \text{sinc}^2(x) \quad [9]$$

One modification remains to be made in order for the fabricated interferogram correspond to Figure 4. The function $\text{sinc}^2(x)$ as it stands has a unit width but should correspond to the model spectral width. The argument x was replaced by $x' = \pi w x$ where w is a width parameter ('dsig' in the FORTRAN code). It was then possible, after trials on parameter choices, to generate a function $f(x)$ and interferogram whose FFT, shown on Figure 5, approximated the model spectrum, the positive part of Figure 4. The data file was labeled 'fab6a_if.dat'. It was then used as the 'raw_if.dat' file on which 'mem_tst_v1' operated. As with the experimental data set, several lag files and corresponding spectral plots were generated. These plots, shown also on Figure 5 for some orders M , show that the model spectrum of Figure 4 was not reliably reconstructed in any case. At low $M = 100$ there is already jagged structure to the spectrum and relative intensities do not correspond to those of the model. At high $M = 750$ the spectrum is made up almost entirely of sharp spikes whose intensities appear to be random.

An additional consideration was made. Minami et al. (14) and others note that effectiveness of the MEM is dependent on the presence of noise in the data set; the signal filtered out is that which maximizes the entropy of the remaining signal. The last step in the summer project, then was to add noise to the interferogram 'fab6a_if.dat'. A treatment similar to that leading to 9 was used to generate an interferogram representing the band-limited white spectrum shown on Figure 6.

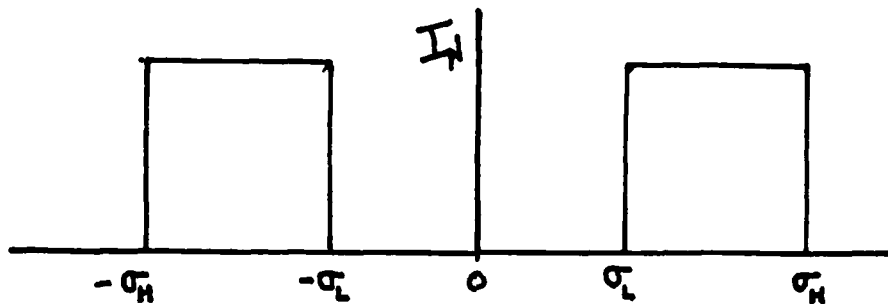


Figure 6. Model for Band-limited White Noise.

Here one has the $\text{rect}(\sigma)$ function whose Fourier transform is $\text{sinc}(x)$. Again a shift from the origin and a scale change were required; the re-interferogram $f_N(x)$ was obtained:

$$f_N(x) = \frac{2}{a} \cos(2\pi\sigma_{\text{mean}}x/a) \text{sinc}(\Delta\sigma x/a) \quad [10]$$

Addition of $f_N(x)$ to $f(x)$ had to be done in a random fashion in order to represent noise. Three random numbers were used to choose the following:

1. the position integer k on the interferogram, randomly chosen in the range $1 \leq k \leq 2048$.
2. the magnitude of the increment, chosen randomly but weighted to a Gaussian intensity distribution. A factor g was used as defined by

$$g = \exp\left[-\frac{(r^{-1} - b)^2}{2s^2}\right] \quad [11]$$

where r = random number $\leq 1.$, b = background noise level parameter, and s = standard deviation of the noise level parameter. A data set of 2048 intensities was generated from 10000 increments using these three random numbers for each increment and following values of the parameters:

$\sigma_{\text{mean}} = 3000 \text{ cm}^{-1}$, $\Delta\sigma = 1000 \text{ cm}^{-1}$, $b = 2$, $a = 0.52404$, $s = 1.$, and $w = 30.864$. This noise file, called 'fab4_if.dat', was added to the file 'fab6_if.dat' with a weighting factor of unity; the combined interferogram file was called 'n10k100.dat'. Figure 7, which is a plot of the FFT spectrum from this file, shows noise along with the peaks of the model spectrum.

Finally, this 'n10k100.dat' file was copied as 'raw_if.dat' for use with 'mem_tst_v1' to generate lag files and corresponding spectral plots which are also illustrated on Figure 7. These plots show that inclusion of noise smooths the jaggedness of a spectrum as compared to one without added noise for the same order M . While locations of the major and minor peaks are the same as those from the FFT spectra, peak widths and intensities still do not match. The tendency persists for the major peak to be overweighted.

VI. RECOMMENDATIONS -

In the interest of drawing a conclusion from the results of the effort reported here, one must note that the computations on both the FFT and MEM made use of existing software at AFGL/LSI. The program 'labcede_sturm' used the identical FFT algorithm which has been in use at AFGL in several projects. No indication exists of errors in this code. On the other hand, the failure of 'mem_tst_v1' to reproduce the model spectrum leaves one with a question about the fidelity of the code

in representing the MEM algorithm. It is therefore recommended that the source code for this program be examined carefully to insure correspondence between it and the MEM algorithm, specifically the subroutine MEMPR (9). Because of the greatly recursive nature of MEMPR, criteria for faithful coding need to be developed. An appropriate route for test of the code seems to be comparison of results at intermediate stages on both 'mem_tst_v1' and some code which has been demonstrated to reproduce a model spectrum via MEMPR.

ACKNOWLEDGEMENTS

The author wishes to express his gratitude to the Air Force System Command, Air Force Office of Scientific Research for sponsorship of the SFRP Program and to the Air Force Geophysics Laboratory, Infrared Technology Division, Infrared Dynamics Branch, for cordial accommodation. He is grateful for the support of his application by Professor G. Doyle Daves of Lehigh University. Special thanks are due Dr. William A. M. Blumberg for suggesting projects and for guidance during critical stages of the effort. Dr. Precila Ip was very helpful in familiarization with the Apollo computer system as was Ann Lozier in adapting software to the needs of the project. Stimulating discussions were held with Dr. Alfred Rahbee of AFGL and Professor James Baird of Brown University. Help by Dr. Agnes Bain in listing possible living quarters is appreciated.

REFERENCES

1. Abels, J. G., "Maximum Entropy Spectral Analysis," in Childers, D. G., ed., Modern Spectrum Analysis, New York, IEEE Press, 1978.
2. Cooley, J. W., and J. W. Tukey, "An Algorithm for the Machine Calculation of Complex Fourier Series," Math. Computation, 19, 297 (1965).
3. Connes, J., "Computing Problems in Fourier Spectroscopy," Chap. 6 in Vanasse, G. A., A. T. Stair, Jr. and D. J. Baker, eds., Aspen International Conference on Fourier Spectroscopy, 1970, Air Force Systems Command, AF CRL-71-0019, 5 Jan. 1971, Sp. Rep. No. 114.
4. Bracewell, R., "The Fourier Transform and its Applications", New York, McGraw-Hill, 1965.
5. Haykin, S., ed., Nonlinear Methods in Spectral Analysis, Springer-Verlag, 1979.
6. Jonsson, P. A., ed., Deconvolution, Academic Press, 1984.
7. For example, Brillouin, L., Science and Information Theory, Academic Press, 1956.
8. Burg, J. P., "Maximum Entropy Spectral Analysis," paper presented at the 37th Annual International Meeting, Society of Exploratory Geophysics, Oklahoma City, Oct. 31, 1967.
9. Ulrych, T. J. and T. N. Bishop, "Maximum Entropy Spectral Analysis and Autoregressive Decomposition," in D. G. Childers, ed., Modern Spectrum Analysis, New York, IEEE Press, 1978.
10. Kawata, S., K. Minami and S. Minami, "Superresolution of Fourier Transfer Spectroscopy Data by the Maximum Entropy Method." Applied Optics, 24(2), 162 (1985).

11. Rahbee, A., "Application of Maximum Entropy Spectral Analysis to Fourier Transform Mass Spectrometry," Chem. Phys. Lett., 117(4), 352 (1985).
12. Sibisi, S., J. Skilling, R. Brereton, E. D. Laue and J. Staunton, "Maximum Entropy Signal Processing in Practical NMR Spectroscopy," Nature, 311, 446 (4 Oct., 1984).
13. Bashkin, S., and J. O. Stoner, Atomic Energy Levels and Grotrian Diagrams I. H(I) - P(XV)," North Holland/American Elsevier, 1975.
14. Minami, K., S. Kawata and S. Minami, "Superresolution of Fourier transform spectra by autoregressive model fitting with singular value decomposition," Applied Optics, 24(2), 162 (1985).

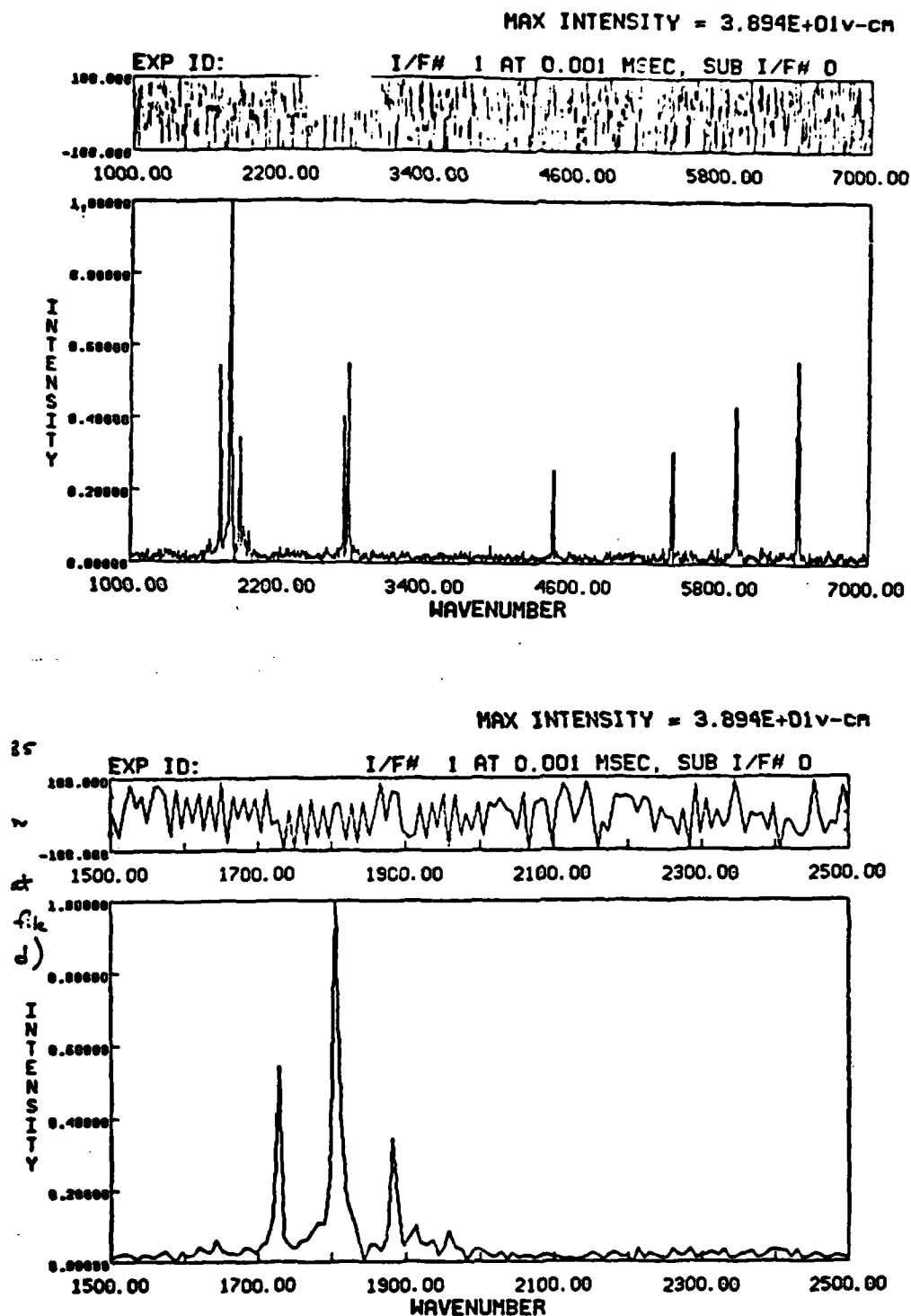


Figure 1. FFT-generated spectra from experimental interferogram.

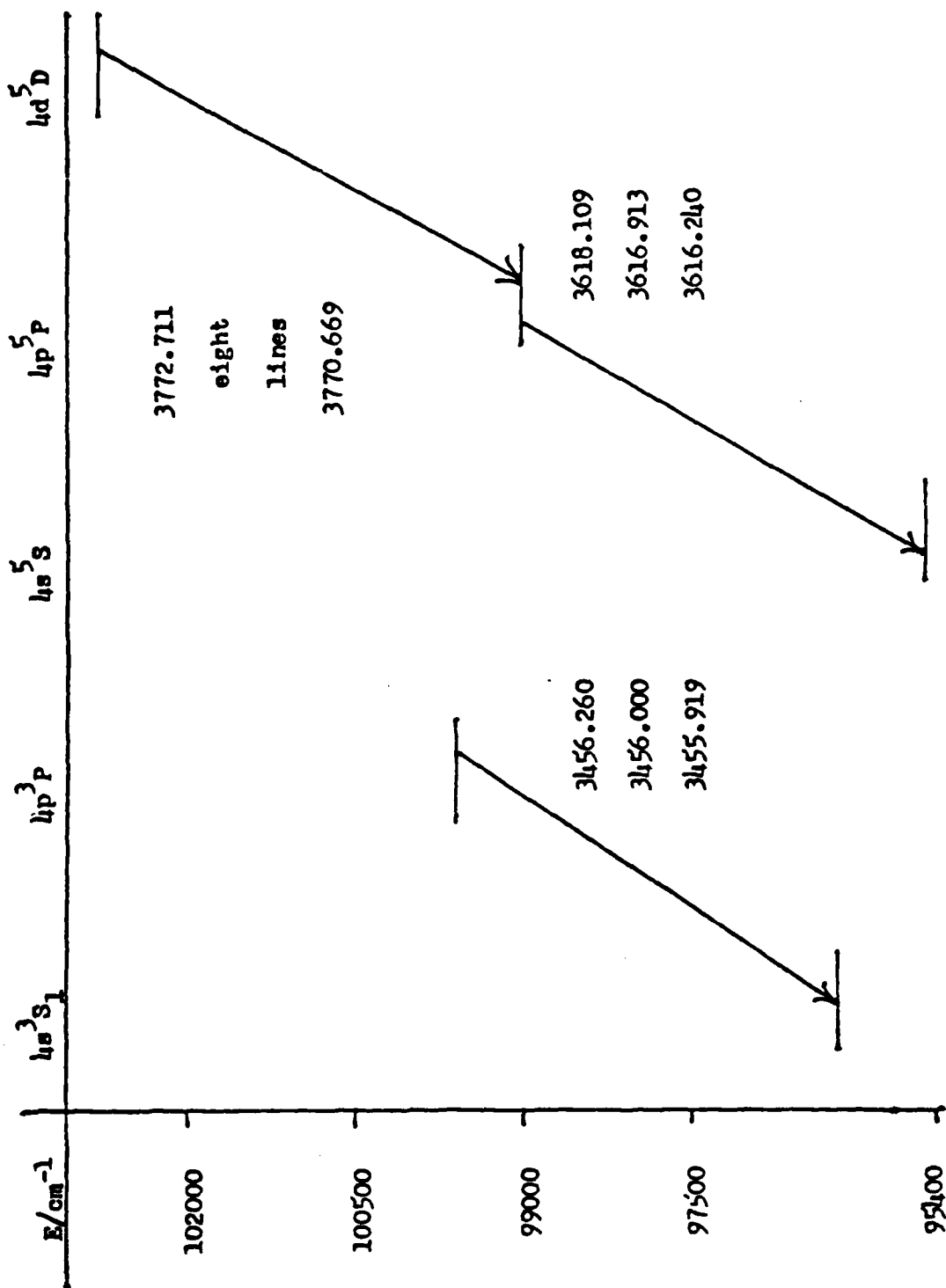


Figure 2. Partial Grotrian Diagram for Oxygen Atoms (from Ref. 13).

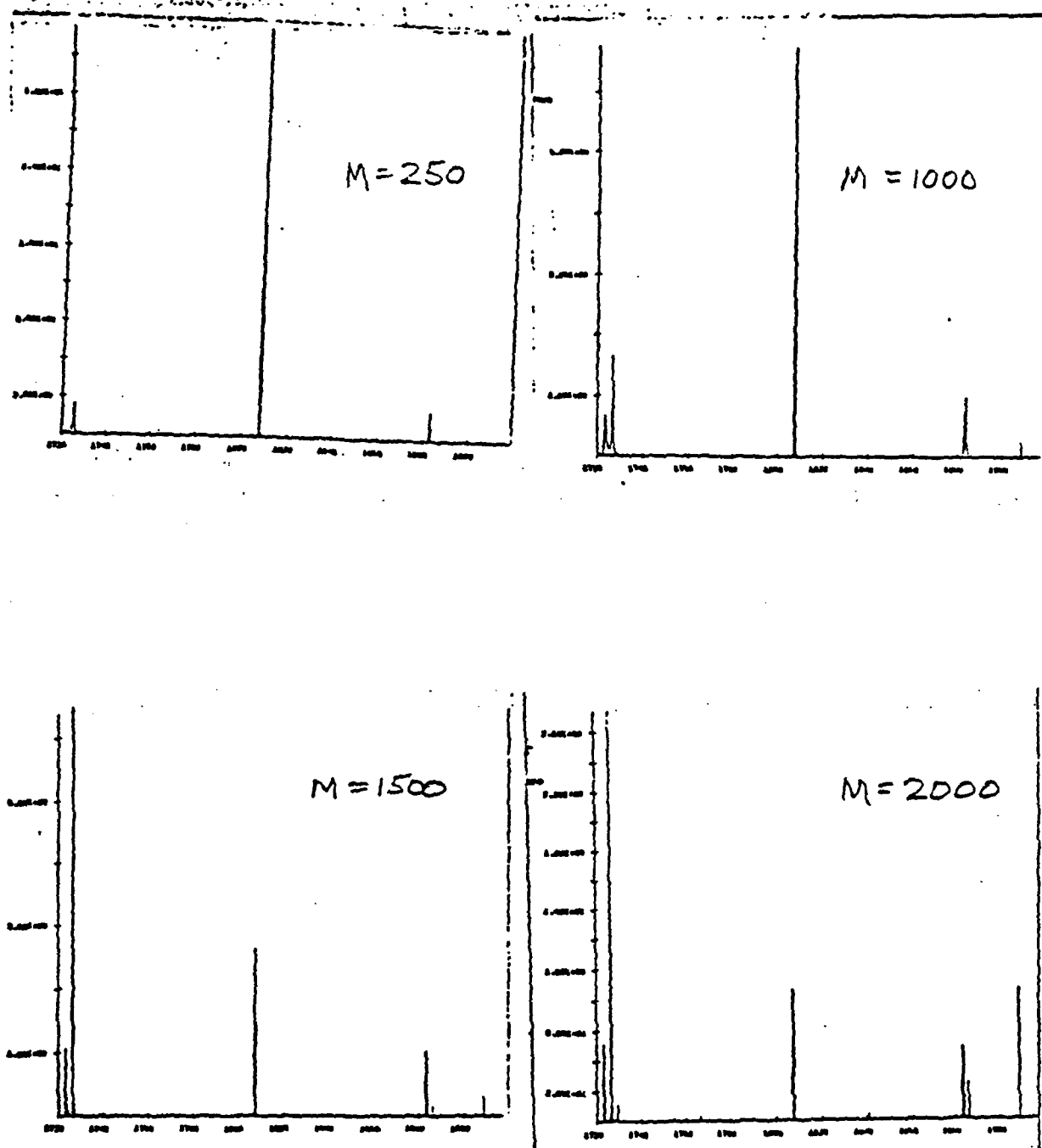


Figure 3. Spectra from MEM treatment on experimental interferogram.

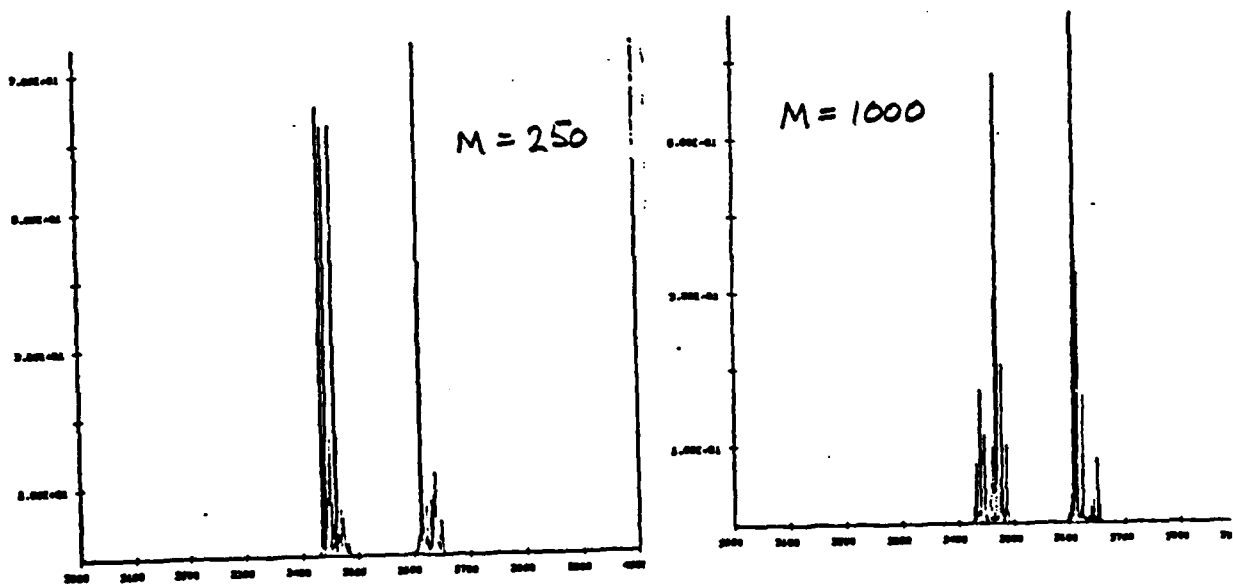
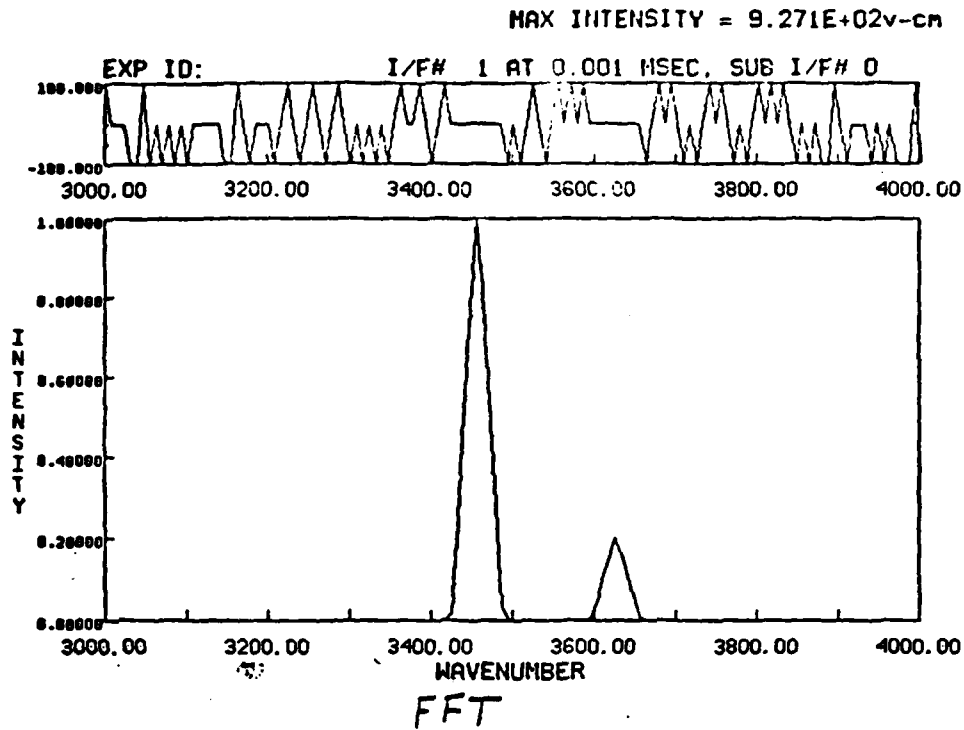


Figure 5. FFT and MEM spectra on model fabricated interferogram.

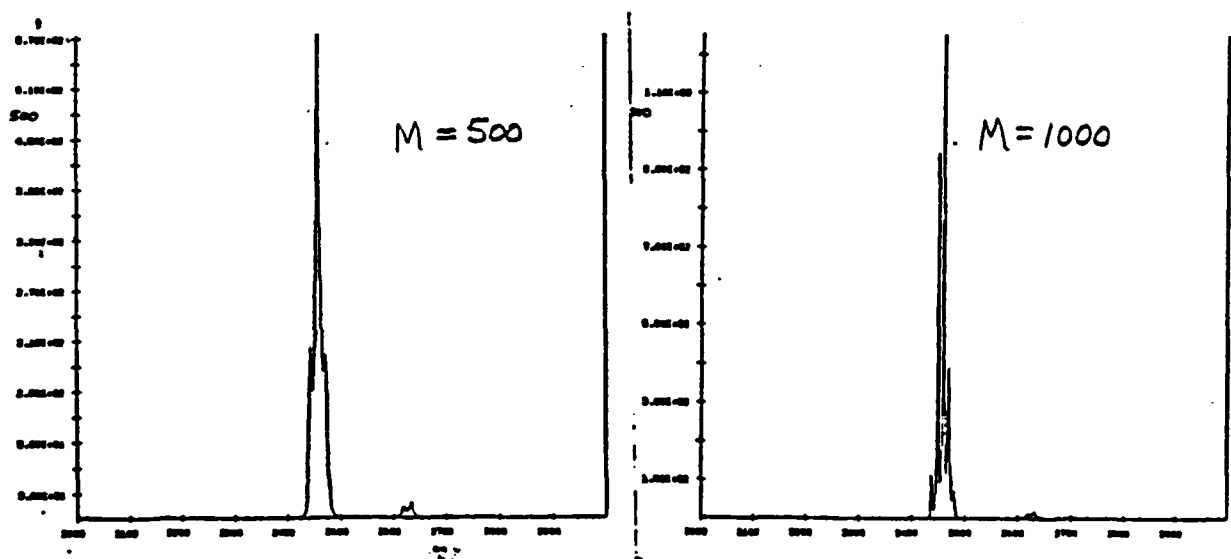
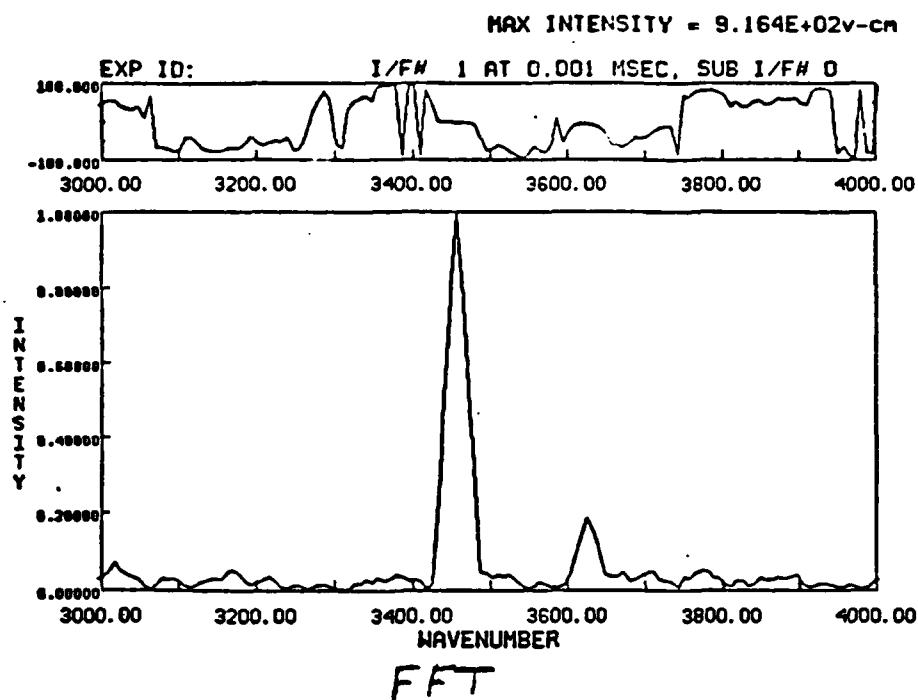


Figure 7. FFT and MEM spectra on fabricated interferogram with noise.

1985 USAF-UES SUMMER FACULTY RESEARCH PROGRAM/
GRADUATE STUDENT SUMMER SUPPORT PROGRAM

Sponsored by the
AIR FORCE OFFICE OF SCIENTIFIC RESEARCH

Conducted by the
UNIVERSAL ENERGY SYSTEMS, INC.

FINAL REPORT

Inference Propagation in Emitter, System Hierarchies

Prepared by:	Thomas A. Sudkamp
Academic Rank:	Assistant Professor
Department and	Computer Science
University:	Wright State University
Research Location:	AFWAL Avionics Laboratory
	Electronic Warfare Division
	AAWP-1
USAF Research:	Rudy L. Shaw
Date:	16 August 1985
Contract No:	F49620-85-C-0013

Inference Propagation in Emitter, System Hierarchies

by

Thomas A. Sudkamp

ABSTRACT

Passive sensors receive signals and generate evidential structures which represent a hypothesis of the type of emitter which produced the signal. The evidence is inexact due to environmental constraints, limitations of the sensors and the lack of knowledge of the emitter characteristics. Emitters are combined to form threat systems producing a hierarchy through which the evidence must flow. A representation for the evidential structure, methods for combining evidence and inference mechanisms for propagating support through the hierarchy must be established as a basis for an expert system which identifies threats in a hostile area. The applicability of the Dempster-Shafer theory and inference networks as representations of emitter/system hierarchies are examined. It is shown that the inference mechanism should be restricted to the hierarchical levels with an independent transfer of information from level to level.

ACKNOWLEDGEMENTS

This work was funded by the Air Force Systems Command under the auspices of the Air Force Office of Scientific Research. I wish to thank them for their support. I would also like to express my appreciation to the members of the ESM Technology Group, AAWP-1, at the AFWAL Avionics Laboratory for the cooperation, consideration and camaraderie.

I. INTRODUCTION. This work was completed at the Air Force Wright Aeronautical Laboratory Avionics Laboratory at Wright Patterson Air Force Base with the Electronic Support Measures Technology group, AAWP-1. The report represents some preliminary research towards the development of an intelligent system for the identification of threats in a hostile environment. This project is being undertaken at the laboratory under the direction of Mr. Rudy Shaw.

A project of this type combines many of the active research areas of artificial intelligence (AI). The development of an architecture for modeling the threat systems and the interpretation of sensor data requires the knowledge of the electronic warfare (EW) domain as well as AI data representations. There are several distinct methods for dealing with inexact and possibly contradictory data in AI systems, one of which must be determined to be the most applicable to threat identification. I was assigned to this group because of my background and interest in the theoretical aspects of AI. Due to the complexity of this problem I was able to apply my background in AI system architectures, data representations and inference mechanisms.

II. OBJECTIVES OF THE RESEARCH. The two major goals of this research are interrelated and provide a necessary theoretical basis for the development of an expert system for the identification of emitter types and threat systems in a hostile environment. The objectives are to establish a

representation for sensor data and an inference technique for pooling multiple pieces of evidence. The inference technique is dependent upon the choice of the evidential representation and propagation assumptions.

The term sensor is used to represent the combination of a passive receiver and processor. The action of the sensor is to receive a signal and establish a structure which represents evidence to be used in determining the type of radar which produced the signal. Systems using probabilistic representation and Bayesian updating suffer from the lack of flexibility necessary to represent uncertainty in the acquisition of data. Two alternative, non-probabilistic measures are examined as possible evidence structures.

Sensors repeatedly receive signals and construct additional evidence. The new evidence may increase support for a previously determined hypothesis or may contradict the current state of belief. An apparent inconsistency may be the result of erroneous sensor information, an incorrect hypothesis or even intentional deception. An inference scheme which has the capability of pooling evidence and resolving inconsistencies is the central component in a threat identification system. Methods which combine evidence at the emitter level will be analyzed. A recommendation will be made concerning propagation techniques appropriate for the sensor, emitter and threat system hierarchy.

III. SENSORS, EMITTERS AND SYSTEMS. The hierarchy consists

of three distinct entities: sensors, emitters and systems. An emitter is an object which generates the data which is received by the sensors. The goal of the expert system is to determine the type of the emitter. The sensor has three distinct purposes, acquiring the data from the emitter, processing it and interpreting the results to construct an evidential structure. The transformation of data to evidence is accomplished by using the sensor knowledge base. The knowledge base is static and contains the discrimination capabilities of the sensors and the emitter type characteristics. The resulting evidence is a set of emitter types which are consistent with the data and a measure of the likelihood of each type.

When sensors receive data they process it and transmit the results to the emitter level of the architecture. This level consists of two components, emitter data structures and an inference mechanism. Emitter characteristics, provided by the sensors, are accumulated in an emitter data structure. The inference mechanism must then pool all the evidence relating to a given emitter to obtain a hypothesis of the type of the emitter based on all the acquired data.

Systems consist of combinations of and relationships between emitters. Just as sensors provide evidence for the determination of emitters, emitter hypotheses provide evidence for the determination of systems. The system level knowledge base must contain the relationships between emitters as well as an inference mechanism to utilize the

emitter hypotheses.

The inference techniques must be able to receive evidence at any level. Although all direct data will be received by the sensors, information may be obtained from interactions with other systems which posit additional evidence at any level.

The sensor and emitter representation has a broad range of applications. The emitter may be an object which creates a noise and the sensor a combination of the human ear and brain. The emitter might be a three-dimensional object and the sensor a television camera and processor which creates a digitized map for the object identification. The application central to this work has the emitter being a radar and the sensor a passive receiver which uses the properties of the signal to develop information necessary for the identification of the radar type. Systems consist of co-located radars which comprise a threat system. It is important to reiterate that the objects to be determined are types. The goal is to hypothesize the existence of a given emitter type and system at a certain location.

Throughout this paper we let Θ be the set of emitter types. Small Latin letters e , f and g will be used to indicate individual types. When evidence is accumulated it is used to hypothesize the type of an unknown emitter. We use letters x , y and z to represent emitters, $\text{hyp}(x)$ denotes the hypothesis of the type of emitter x .

Systems will be represented by conjunctions of emitters.

One consequence of the use of conjunctions is the capability of postulating only a single emitter of a given type at a site. If there are two or more co-located emitters of the same type the conjunction will represent them as a single conjunct. This, however, is exactly the conclusion the inference mechanism should yield. If a site contains two radars emitting signals with the same characteristics the sensor will assign the evidence generated by signals from either one to the same object. Since the goal is to determine the presence of types multiple evidence sources may contribute to identification process.

Using the radar example, Θ is the set of all possible radar types which might be encountered. Included in Θ are the Pathand, Straightflush, Landroll, etc. The sensor level knowledge base will contain the characteristics of the signals generated by each radar type. A set of co-located radars acting in unison to perform a task is a system.

The conjunction representation induces a natural partial ordering on the set S of systems. Let S_1 and S_2 be two systems. We say S_1 is stronger than S_2 , $S_1 \leq S_2$, if the set of emitters in S_2 is a subset of those in S_1 . The graph in Figure 1 shows the relationships of the sample systems with directed arcs representing \leq .

As hypotheses are developed for the emitters at a site this information must be utilized to determine the system. This raises questions concerning the hierarchical properties of evidence. Sensor data directly generates evidence for

EMITTERS

$\Theta = \{e_1, e_2, f_1, f_2, g_1\}$

SYSTEMS

$$S_1 = e_1 \wedge f_1 \wedge g_1$$

$$S_2 = e_1 \wedge f_1$$

$$S_3 = e_1 \wedge g_1$$

$$S_4 = e_1$$

$$S_5 = e_1 \wedge f_2 \wedge g_1$$

$$S_6 = e_2 \wedge f_2$$

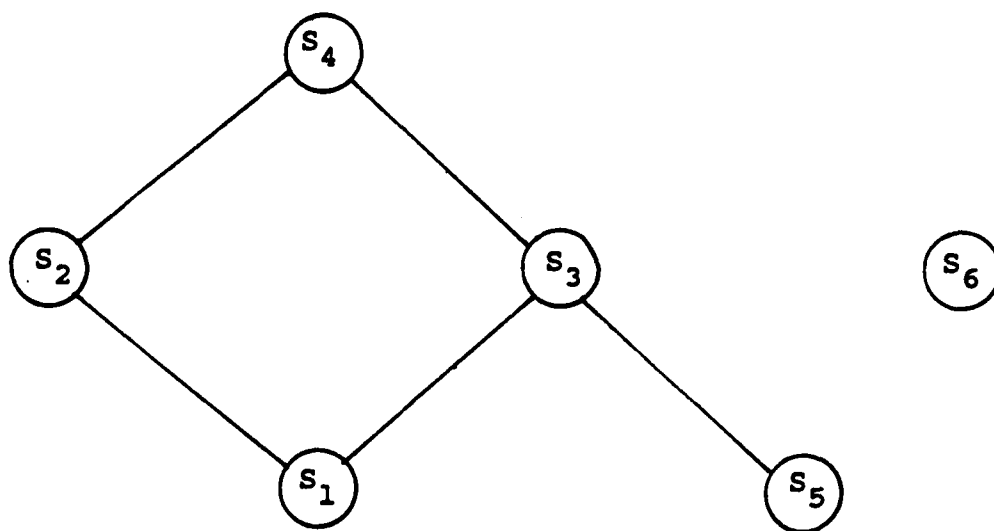


Figure 1. Emitter and system hierarchy.

emitters. Is this direct evidence for hypotheses or must it be processed further to be applicable to the system level inference mechanism? If it is direct evidence it should be used immediately to hypothesize systems. Indirect evidence must be processed to make it amenable to the higher level needs.

IV. EVIDENTIAL REASONING AND HIERARCHIES. In the theory of evidential reasoning evidence is obtained and accumulated concerning an exhaustive, mutually exclusive set of possibilities. This set is known as the frame of discernment. The objective is to combine evidence to hypothesize which of the alternatives is the most likely. A brief description of the primary features of this theory will be given and its suitability as an inference mechanism for a emitter/system hierarchy is examined. A complete exposition is given in Shafer [12]. Gordon and Shortliffe [5] give a short, readable summary and compare evidential reasoning to the combination of certainty factors and propagation techniques applied in the medical diagnosis expert system MYCIN.

On the emitter/sensor level the frame of discernment is the set of emitter types. The hypotheses consist of all combinations of emitter types which can be supported by evidence. With the frame of discernment being the set Θ of emitter types, the set of hypotheses H is simply the power set of Θ , $P(\Theta)$.

Another standard representation of the frame of discernment is that of a set of propositions, exactly one of which is true. The set of hypotheses consists of disjunctions of propositions. It is easy to see that these representations are equivalent. If the frame of discernment consists of a set of types e_i then the corresponding proposition is "the object is of type e_i ". The set operations of union and intersection correspond to disjunction and conjunction of propositions. Although both interpretations will be utilized, the standard set representation will be used in the presentation of the theory.

Evidential reasoning is a positive support technique. Evidence gives support to a subset of the frame of discernment and is represented by a basic probability assignment which is a function $m: H \rightarrow [0,1]$ satisfying

- i) $m(\emptyset) = 0$
- ii) $\sum_{A \in H} m(A) = 1.$

$m(A)$ represents the total amount of support committed exactly to the belief that the object is of a type contained in A . This belief cannot be distributed to subset of A , nor does it include belief attributed to the proper subsets of A . The assigning of support to sets differs from the probabilistic approach which would employ a "principle of indifference" to distribute the support to singletons, although the evidence may not favor any of the individual elements.

The positive nature of this formulation can be seen by considering evidence which solely supports the set A with strength $k < 1$. The remainder of the belief is not constrained to support the complement of A as a Bayesian model dictates, but is assigned to support the set \emptyset . This indicates that a portion of this evidence does not favor any of the possibilities. A basic probability assignment is represented by a vector containing each set $A \in H$ which receives support, followed by the amount of the support. Such a set is called a focal element of the probability assignment. The evidence whose only effect is to support A with strength k is denoted $[A, k; \emptyset, 1-k]$.

Each basic probability assignment generates a belief function over the set of hypotheses. This function has the form $BEL: H \rightarrow [0, 1]$ and represents the total support for an object being in a given set of types. The belief function is defined by

$$BEL(A) = \sum_{B \subseteq A} m(B).$$

For a set A , $m(A)$ represents support for A which cannot be further subdivided into support for subsets while $BEL(A)$ represents the total support of all the elements of A .

The belief function is used to construct the evidential interval, the structure used for evaluating hypotheses. The evidential interval is a two-valued system used to represent the support for and the plausibility of a hypothesis. The plausibility of a hypothesis A , $PLS(A)$, is defined by 1 -

$BEL(C(A))$, where $C(A)$ is the complement of A . In a positive support framework a hypothesis is denied only by obtaining support for its alternatives. The plausibility of A is then the measure of the evidence which does not support the refutation of A . The evidential interval is defined as $[BEL(A), PLS(A)]$. $PLS(A) - BEL(A)$ represents the lack of information concerning A in the evidence. When the evidence is conclusive $BEL(A) = PLS(A)$ and the interval shrinks to a point. No evidence concerning A or its complement results in the vacuous interval $[0, 1]$.

When two pieces of evidence are obtained they must be combined to yield a basic probability assignment which represents the pooling of the information. This is accomplished by using Dempster's rule of combination. Let m_1 and m_2 be a basic probability assignments which support A_1, A_2, \dots, A_n and B_1, B_2, \dots, B_k respectively. If $A_i \cap B_j = \emptyset$ then the evidence supporting these two sets is incompatible. We measure the amount of incompatibility of two probability assignments by determining the total support for empty set. Let $K = \sum m_1(A_i) \cdot m_2(B_j)$ where the sum is taken over all the combinations of incompatible focal elements. If m_1 and m_2 are not completely incompatible then $K < 1$ and a new basic probability function $m = m_1 \oplus m_2$, the orthogonal sum of m_1 and m_2 , is defined by

- i) $m(\emptyset) = 0$
- ii) $m(A) = \sum_{A_i \cap B_j = A} (m_1(A_i) \cdot m_2(B_j)) / (1-K).$

m_2	$\theta, .5$	$\{f, g\}, .25$	$\theta, .25$
	$\{e, f\}, .3$	$\{f\}, .15$	$\{e, f\}, .15$
	$\{e\}, .2$	$\emptyset, .1$	$\{e\}, .1$
		$\{f, g\}, .5$	$\theta, .5$
		m_1	

$K = .1$	$\{e, f\} <- .17$
$\{e\} <- .11$	$\{f, g\} <- .28$
$\{f\} <- .17$	$\theta <- .28$

Figure 2. Calculation of orthogonal sum.

The calculation of the pooled evidence using Dempster's rule can be best illustrated by a tableau method. Let $\Theta = \{e, f, g\}$ $m_1 = [\{f, g\}, .5; \Theta, .5]$ and $m_2 = [\{e\}, .2; \{e, f\}, .3; \Theta, .5]$. Build a 1 by 1 grid and proportion the sides according to the support given by m_1 and m_2 (Figure 2). These divisions split the grid into rectangles and each rectangle represents the support for the intersection of the sets which generate it. The amount attributed to the empty set is assigned 0 and the remaining support is scaled to bring the total to 1.

One of the features of Dempster's rule is the ability to dilute the effect of a piece of evidence which seems inconsistent with the other accumulated data. This property is necessary when combining sensor generated evidence which, by its nature, is inexact. If a basic probability assignment $[A, .9; \Theta, .1]$ has been established and new evidence $[C(A), .2; \Theta, .8]$ is obtained the orthogonal sum produces $[A, .88; C(A), .02; \Theta, .1]$. This indicates continued strong support for A while minimizing the support for the C(A).

The Dempster-Shafer theory is designed to determine the type of a single object from a set of possibilities. Our goal is both emitter and system identification. Systems consist of combinations of emitters, hence are elements of $P(\Theta)$. To determine systems in a straightforward manner using this method would entail having the frame of discernment be $P(P(\Theta))$. The explosion of possibilities, distribution of evidence among them and the work needed to combine evidence

makes this representation unfeasible. When evidence or systems have special properties, this formulation of directly obtaining and combining evidence over $P(P(\theta))$ may be possible. Barnett [1] shows that when evidence supports only singleton sets or their complements that Dempster's rule can be computed in polynomial time. Gordon and Shortliffe [6] present a variant of combination rule which can be used when the system relationships form a tree. When neither of these conditions are met another approach must be employed to produce evidential support for systems.

Garvey et. al. [3], [4] present techniques to determine system hypotheses using evidential reasoning. The essential feature of thier formulation which bypasses the combinatorial explosion is the creation of a separation between emitter/sensor reasoning and system reasoning. To obtain this split a transformation must be made which generates system evidence from combinations of emitter evidence. The system level evidence can then be pooled using Dempster's rule, or some other method, to form system level hypotheses.

To illustrate this procedure we consider a system with e emitters, x, y, and z. The objective is to use the sensor generated evidence to construct hypotheses for both emitters and systems. When the sensors develop a piece of evidence it is first attributed to an emitter. This can be accomplished by utilizing the previous evidence to find the most likely candidate. If this does not resolve the issue, Garvey and Lowrance [4] suggest that the choice may be made by assigning

this to the emitter which yields the smallest measure K of incompatibility when combined with the previous evidence. If the evidence does not appear to be referring to any of the previously determined emitters, a new emitter is recorded and an emitter data structure is created for the accumulation of the sensor generated data.

The i^{th} piece of evidence generated by the sensors will be denoted by EVD_i and by $EVD_i(x)$ when assigned to emitter x . All the evidence attributed to an emitter is combined to form the hypothesis for x , $hyp(x)$. This process simultaneously creates and updates hypotheses for each emitter which has been sensed. Figure 3 shows the flow of data from the sensor to the emitter hypothesis.

This process of evidence assignment removes one of the theoretical difficulties associated with Dempster's rule, that of partially dependent evidence. This occurs when the combination of evidence forms a directed graph rather than a tree. If EVD_i is pooled with both EVD_j and EVD_k and the results are combined then the resulting sum will be doubly influenced by EVD_i . The hierarchical structure depicted in Figure 3 shows that this cannot occur because the evidence combination is done linearly at the emitter level. Since no piece of evidence is assigned to more than one emitter, the dependency problem is avoided.

In [3] and [4] systems are considered disjunctions of emitters. The systems S_4 , S_3 and S_1 in Figure 1 would be represented by e_1 , $e_1 \vee g_1$ and $e_1 \vee g_1 \vee f_1$ respectively. This

$$\text{hyp}(S) = \text{EVD}_x \oplus \text{EVD}_y \oplus \text{EVD}_z$$

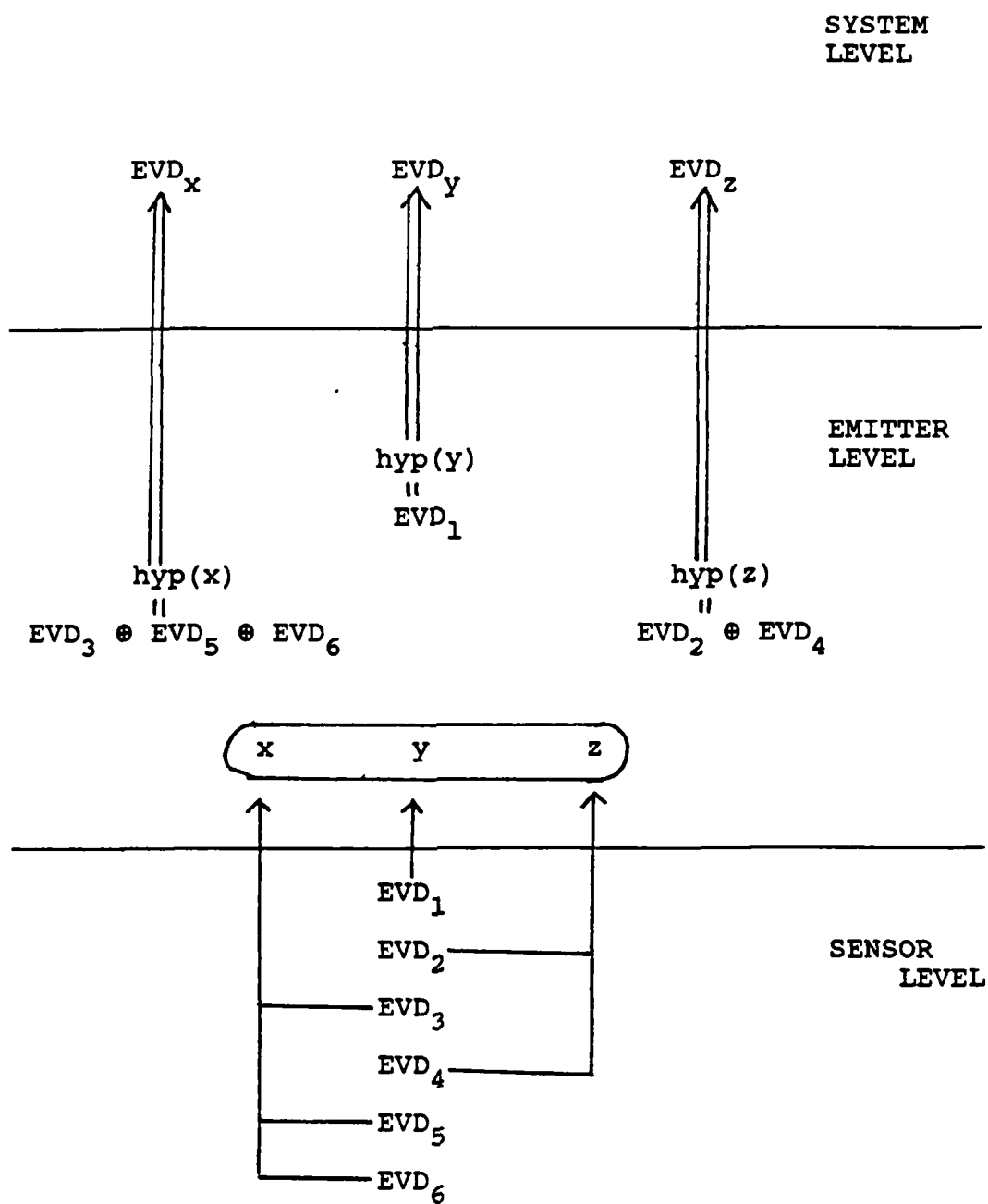


Figure 3. Flow of evidence in emitter/system architecture.

does not allow the distinction to be made if each component is necessary in a system. When a system is represented by a disjunction support for one of the elements is attributed to the entire system. Admitting that disjunctions are not a precise representation of systems, Garvey and Lowrance argue that the inference mechanism is "equally effective regardless of the source of error", be it the sensor generated evidence or the relations in the system knowledge base.

The transfer of emitter evidence to system evidence is done in a direct manner. The hypothesis for each emitter is interpreted as a single piece of evidence at the system level. This is accomplished by defining the projection of an emitter type. Let $\text{hyp}(x)$ be the hypothesis for emitter x with associated probability assignment $m_x: H \rightarrow [0,1]$ and let A be a focal element of m_x . We must determine to which systems the support for A will be assigned. For an emitter type $e \in \Theta$ define the projection of $\{e\}$ to the system level by

$$\text{proj}(\{e\}) = \{S_i: e \text{ is a disjunct of } S_i\}.$$

The definition can then be extended to H by

$$\text{proj}(A) = \bigcup_{e_i \in A} \text{proj}(\{e_i\}).$$

The support for a focal element A of an emitter hypothesis is assigned to $\text{proj}(A)$. Projecting each focal element of $\text{hyp}(x)$ yields the system evidence generated by $\text{hyp}(x)$, denoted EVD_x .

The use of disjunctions and direct transformations have implications on the type of systems represented. The inference techniques resulting from this combination yield a

pessimistic system. Using the systems in Figure 1 the determination of the existence of emitter type e_1 equally distributes support to all the systems except S_6 , even if there is no evidence to support a system stronger than S_4 . For this reason the direct evidence transfer systems do not represent nested systems, only the systems which are minimal (strongest) according to the partial ordering \leq are hypothesized.

V. INFERENCE NETS. The evidential reasoning hierarchy representation imposes a distinction between emitters and systems and passes information from the emitter level to the system level. Another technique is to represent both emitter types and systems as nodes in a graph and relationships as arcs. Such systems are known as inference nets [7] or dependency graphs [8]. Each node in the net has a measure which indicates the belief in the proposition represented by that node. These measures may be probabilities [9], evidential intervals or other techniques used to indicate possibility.

Quinlan [10], [11] developed an inference propagation scheme, called INFERNO, which makes minimal assumptions concerning the evidence and systems when propagating information through the graph. The measure of belief used is an evidential interval. This technique will be used as a model for examining inference nets as representations of emitter/system hierarchies.

Each node A is assigned two values, $t(A)$ and $f(A)$. $t(A)$ is the measure of the support for A determined by the evidence while $f(A)$ is the measure of evidence refuting A . Initially both of these values are set to 0. As evidence is accumulated $t(A)$ and $f(A)$ can increase, but never decrease. Unlike the Dempster-Shafer theory, INFERNO allows negative evidence to be obtained for a proposition. The existence of new evidence denying a proposition does not effect previously obtained support, it simply increases the f value. The evidential interval is represented by $[t(A), 1-f(A)]$. The evidence yields an inconsistency if $f(A) + t(A) > 1$ for any node A in the graph.

Nodes are connected by arcs which signify the hierarchical relationships. Each arc has an associated set of support transferring rules. The propagation rules necessary for the emitter/system hierarchy are given in Table 1. Whenever a node is assigned a new f or t value it implements the rules which transfer information to adjacent nodes. The rules consist of comparing the current value of an adjacent node to a value which incorporates the new evidence. When any value in the expression in the right-hand side of a rule is changed, that expression is evaluated. The maximum of the two values is assigned to the left-hand side, yielding the non-decreasing nature of support. New evidence is added in an identical manner, the values are compared to the current t and f values and the maximums are retained.

Figure 4 shows an example of the INFERNO inference

A enables S with strength X:

$$t(S) \leftarrow \max(t(S), t(A) \cdot X)$$

$$f(A) \leftarrow \max(f(A), 1 - (1 - f(S)) / X)$$

A negates S:

$$t(A) \leftarrow \max(t(A), f(S))$$

$$f(A) \leftarrow \max(f(A), t(S))$$

A conjoins $\{S_1, \dots, S_n\}$

$$t(A) \leftarrow \max(t(A), 1 - \sum_i (1 - t(S_i)))$$

$$f(A) \leftarrow \max(f(A), f(S_i))$$

$$t(S_i) \leftarrow \max(t(S_i), t(A))$$

$$f(S_i) \leftarrow \max(f(S_i), f(A) - \sum_{i \neq j} (1 - t(S_j)))$$

A disjoins exclusive $\{S_1, \dots, S_n\}$

$$t(A) \leftarrow \max(t(A), \sum_i t(S_i))$$

$$f(A) \leftarrow \max(f(A), 1 - \sum_i (1 - f(S_i)))$$

$$t(S_i) \leftarrow \max(t(S_i), t(A) - \sum_{i \neq j} (1 - f(S_j)))$$

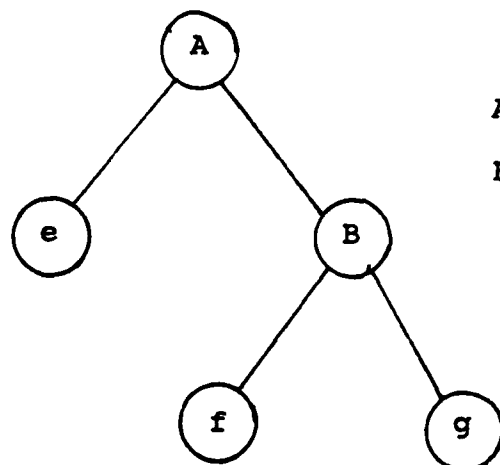
$$f(S_i) \leftarrow \max(t(S_i), f(A) + \sum_{i \neq j} t(S_j))$$

S implies A:

$$t(A) \leftarrow \max(t(A), t(S))$$

$$f(A) \leftarrow \max(f(A), f(S))$$

Table 1. INFERNO propagation rules.



A conjoins {e, B}

B disjoins exclusive {f, g}

Evidence

Values

	A	B	e	f	g
t(f) <- .3	t: 0	.3	0	.3	0
	f: 0	0	0	0	.3
f(f) <- .4	t: 0	.3	0	.3	0
	f: 0	0	0	.4	.3
t(e) <- .2	t: 0	.3	.2	.3	0
	f: 0	0	0	.4	.3
t(A) <- .7	t: .7	.7	.7	.3	.1
	f: 0	0	0	.4	.3

Figure 4. Evidence flow in an inference net.

technique. Initially all nodes have t and f values 0. The left column represents the evidence and the right the resulting belief values. When evidence supporting f is obtained it transfers support to the disjunction node B. Since B is exclusive this "ripples" negative evidence to g. Although f and g are not adjacent, changes in the value of one may ripple to alter the other.

An important feature of the minimal assumption propagation scheme can be seen by the effect of evidence which establishes $t(e)$ to be .2. Both of the conjuncts of A have support, but this yields no support for the conjunction. In a system which assumes propositional independence A would receive support. Similarly both disjuncts of B have evidence supporting their denial, but this does not propagate to $f(B)$.

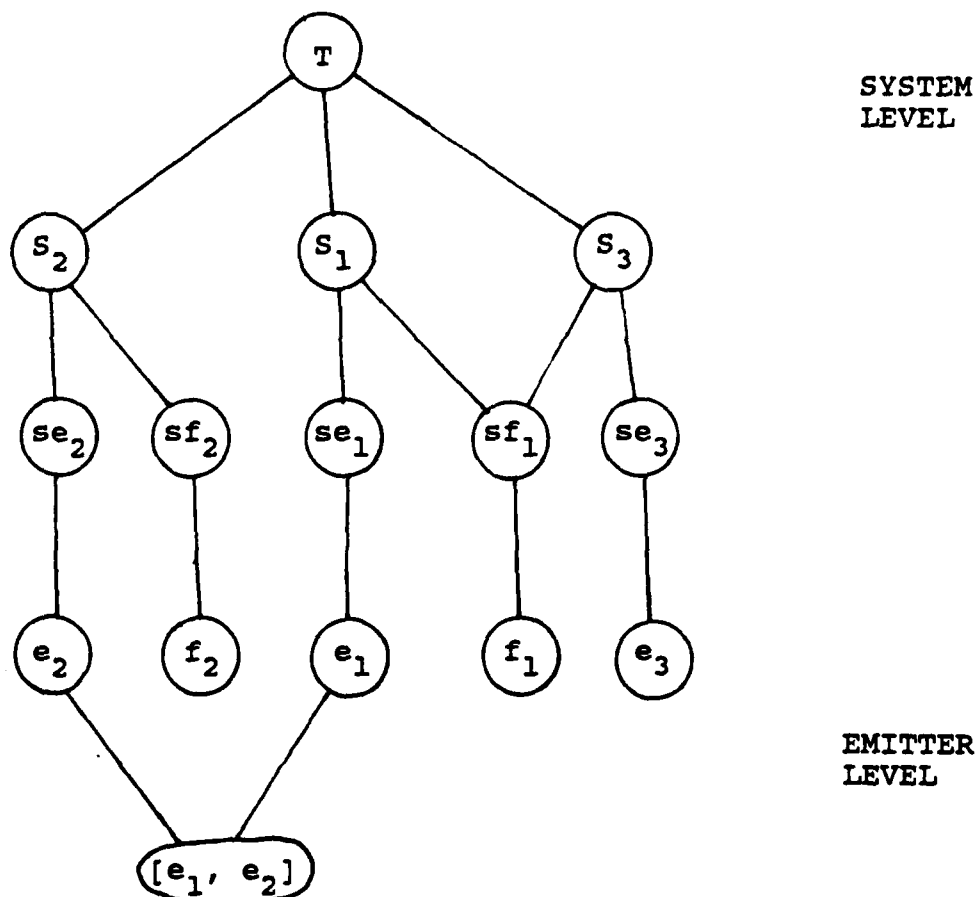
In an inference net, evidence may be assigned to any node. When $t(A)$ receives support of .7 this ripples down the hierarchy to the constituents of the conjunction. When implementing an emitter/system hierarchy this bidirectional flow may compromise the integrity of the sensor data. In the example, considering e, f, and g to be emitters, $f(g)$ is .3 although there has been no sensor evidence obtained concerning g. The hierarchical relationships combined with evidence for other emitters to form the f and t values. If the evidence obtained results in an inconsistency it does not permit one to determine whether the error was in the data or the relationships. INFERNO assumes the data to be correct and attempts to resolve inconsistencies by altering the

propagation rules. This is the opposite of the assumption which should be made in the emitter/system hierarchy where it is expected that evidence will be inexact.

To maintain the integrity of the sensor data the inference net must be divided into two levels, in a manner similar to the evidential reasoning hierarchy. On the emitter level the sensor evidence is assigned and propagated. Evidence for single emitters can then be transferred to the system level. To accomplish this two nodes must be constructed for each emitter, one on the emitter level and one on the system level. The emitter level node collects all the information which refers to that emitter type. The transfer of values should be unidirectional, maintaining the sensor data while making it available to the system relationships. A new propagation rule, implies, is added to Quinlan's list to accommodate this. Figure 5 shows the inference net representation of an emitter/system hierarchy with nodes e_i for each emitter type and se_i for its system level copy. The difference of the values of e_i and se_i gives a measure of the incompatibility of the sensor data and the system relationships.

The node labelled by T is the condition that the threat to be determined is exactly one of the systems represented. When the first evidence is obtained $t(T)$ is set to 1, signifying the existence of a system.

The nodes on each level of the inference have a specific form and purpose. The emitter level nodes are sets of



Relations: T disjoins exclusive $\{S_1, S_2, S_3\}$
 e_i implies se_i
 f_i implies sf_i
 $[e_1, e_2]$ disjoins exclusive $\{e_1, e_2\}$
 S_1 conjoins $\{se_1, sf_1\}$
 S_2 conjoins $\{se_2, sf_2\}$
 S_3 conjoins $\{se_3, sf_1\}$

Figure 5. Inference net hierarchy.

emitter types which collect and distribute evidence generated by the sensors. When information is obtained for a single emitter, either directly or from the relationships on the emitter level, it is immediately transmitted to the system level. On the system level this data is propagated to all the nodes. This representation has emitter and system hypotheses being generated simultaneously in the network.

The assignment and pooling of evidence in a inference net has several difficulties. The net is a static structure, all of which must be created when a single piece of evidence is obtained. The rippling effect of evidence does not allow the construction of only those nodes which have directly received evidence.

When evidence is obtained it must be assigned to nodes in the graph. Evidence, however, may not be directly attributable to an individual emitter type but rather to a set of types. This necessitates having nodes for each set of emitter types which may possibly receive support or denial. In the worst case this will force the existence of a node for each set in $P(\Theta)$. The number of containment relationships would make the size of this net prohibitive. Figure 5 has a node on the emitter level for the set $\{e_1, e_2\}$ signifying that this set may receive evidential information.

The non-decreasing nature of the combination and propagation of evidence does not allow independent evidence to be pooled to strengthen the hypothesis. Both the incorporation of new evidence and the propagation rules

simply choose the maximum of the current value and the new support. This has the effect that independent pieces of evidence do not combine to give more support than the maximum of either.

The strict separation of the t and f values does not permit the pooling process to dilute the effect of erroneous information. If evidence has been accumulated, by either method, to obtain an evidential interval $[\cdot.9, 1]$ for a hypothesis A and additional evidence is $[C(A), \cdot.4; \theta, \cdot.6]$ is combined using Dempster's rule the result will be the basic probability assignment $[C(A), \cdot.06; A, \cdot.84; \theta, \cdot.1]$. The conflicting data is simply subsumed by the overwhelming support for A. The result in the inference net will be an interval $[\cdot.9, \cdot.4]$ for A, indicating inconsistency. This inability to degrade the importance of seemingly inaccurate data, especially in a sensor driven identification process, makes the total separation of support and refutation an undesirable feature. It is this feature which makes certainty factors, the evidence structure of the MYCIN family of expert systems [2], unsuitable for the hierarchy applications.

Another drawback of the inference net is the inability of support to reach the system level. This was exhibited in Figure 4 where both the conjuncts were supported but none of this caused a propagation of support to the system level. To further illustrate this we examine the propagation of evidence in the hierarchy represented in Figure 5. Two

pieces of evidence are obtained, $EVD_1(x) = [(e_1, e_2), 1]$ and $EVD_2(y) = [(f_1), 1]$. In the evidential reasoning architecture, emitter hypotheses $EVD_x = [(S_1, S_2), 1]$ and $EVD_y = [(S_1), 1]$ are constructed. When combined using Dempster's rule S_1 is asserted with certainty.

When the same evidence is accumulated and propagated in the inference net, the sensor support cannot be distributed to either emitter. S_1 does not receive support since conjunctions receive support only when each conjunct does. Even if some "principle of indifference" were utilized to distribute the support for (e_1, e_2) , the result would still be less than confirmation for S_1 .

VI. INDIRECT TRANSFER. The techniques examined preserve the integrity of information on each level, that is, a change in the higher levels does not alter the hypotheses on lower levels. This feature requires the hierarchical representation to be segmented with information being transferred from the lower to the higher levels. In each of the methods examined the transfer has been direct. The hypotheses have been transferred to the higher level without additional processing, either by the function $proj$ or by the propagation rule $implies$. An indirect method of transferring the data will now be presented. The evidential reasoning paradigm will be used and an additional level will be incorporated to accomplish the transition. This refinement will produce added flexibility and an improved capability for

representing systems.

A major weakness of the evidential reasoning architecture outlined earlier was the representation of systems as disjunctions of emitters. To be able to represent systems as conjunctions the emitter hypotheses should be combined prior to the transfer to the system level. This can be accomplished by combining the hypotheses, using Dempster's rule, considering the frame of discernment to be the set of conjunctions of emitter types. With this interpretation, each focal element of an emitter hypothesis is a set of propositions. The combination constructs conjunctions from these propositions. Letting A and B be focal elements of $\text{hyp}(x)$ and $\text{hyp}(y)$ respectively, the combination $A \wedge B = \{ a \wedge b: a \in A, b \in B \}$ is assigned the support $m_x(A) \cdot m_y(B)$.

A sample hierarchy is given in Figure 6. The hypotheses for emitters x and y have been established and are combined using Dempster's rule over the conjunction frame of discernment. The result of this pooling is given in the transition level.

A partial ordering \leq can be defined on the set of conjunctions in the same manner as it was for the set of systems. When a conjunction receives support, this support must be attributed to a system. This assignment is made to the weakest systems which contain the conjunction. For a proposition x we define a greatest lower bound of x to be a system y which is stronger than x , with no systems $z \neq y$

satisfying $y \leq z \leq x$. For the systems in Figure 1 the greatest lower bounds of f_2 are S_5 and S_6 . A transfer function, trans , is defined as follows:

$$\text{trans}(\{x\}) = \{y : y \text{ is a greatest lower bound of } x\}.$$

This can be extended to sets of propositions by

$$\text{trans}(A) = \bigcup_{x \in A} \text{trans}(\{x\}).$$

If $\text{trans}(\{x\}) = \emptyset$ then this combination yields support which is not consistent with any system. Following Dempster's rule, the support for \emptyset is set to 0 and the remaining values are scaled to total 1.

The transfer function allows the immediate assignment of support to sets of systems, generating a system hypothesis. If A is a set of conjunctions with support k , then the system level hypothesis assigns support k to $\text{trans}(A)$. The possible combinatorial explosion has been avoided by utilizing the partial ordering to assign support only to systems.

The sensor/emitter relationships in the indirect architecture is identical to that outlined in the direct method. Figure 6 illustrates the emitter, transition and system levels for the indirect transfer. The conjunctions $e_1 \wedge f_2$, $e_2 \wedge f_1$ and $f_1 \wedge f_2$ do not transfer to a system and the support of the sets which contain them is attributed to legitimate combinations. In this manner the transfer function can be used as an indication of the uncertainty of the evidence. Support for non-transferable functions can only be obtained by the inexactness in the emitter hypotheses.

SYSTEM LEVEL		
	$\{e_1 \wedge f_1\}$.55
hyp(S) =	$\{e_1 \wedge f_1, f_1\}$.36
	$\{e_2 \wedge f_2\}$.09
<hr/>		
TRANSITION LEVEL		
	$\{e_1 \wedge f_1\} \rightarrow$.48
hyp(x) \oplus hyp(y) =	$\{e_1 \wedge f_1, e_2 \wedge f_1, f_1, f_1 \wedge f_2\} \rightarrow$.32
	$\{e_1 \wedge f_2\} \rightarrow$.12
	$\{e_1 \wedge f_2, e_2 \wedge f_2, f_2, f_1 \wedge f_2\} \rightarrow$.08
<hr/>		
EMITTER LEVEL		
hyp(x) = [$\{e_1\}$, .6; $\{e_1, f_1, f_2\}$, .4]		
hyp(y) = [$\{f_1\}$, .8; $\{f_2\}$, .2]		
Emitters	Systems	
$\{e_1, f_1, f_2\}$	$S_1 = e_1$ $S_2 = e_1 \wedge f_1$ $S_3 = f_1$ $S_4 = e_2$ $S_5 = e_2 \wedge f_2$	

Figure 6. Indirect transmission of evidence.

The transfer function also allows a sharper assignment to systems. Evidence supporting an emitter type will be transferred only to the weakest systems containing that emitter type. This improves the direct transfer method which attributes that support to all systems containing the emitter type, avoiding the pessimistic assignment of that method.

VII. RECOMMENDATIONS. The architecture needed to construct an expert system for threat identification needs flexibility in both its representation of evidence and propagation technique. The use of a segmented architecture with unidirectional flow of evidence avoids the combinatorial problems which can occur when moving to the system level while maintaining the integrity of evidence on each level. The evidential structure should combine both supporting and refuting evidence to be able to cope with the inexactness of data which is inherent in sensor systems. The Dempster-Shafer theory of evidential reasoning is shown to give a feasible evidence pooling technique on each level.

Evidence is transferred up the hierarchy. While maintaining the integrity of the evidence of each level, the identification system should allow information to flow in both directions between levels. The flow from the emitter level to the sensor should consist of requests for certain types of data which will combine with the existing evidence to refine the hypothesis. The system level should be able to request data on the existence of other emitters to see if all

the components of hypothesized systems are present.

To achieve this bidirectional flow the architectures must be examined for the ease in which both of these flows of information can occur. This requires the incorporation of discrimination data in the knowledge bases at each level as well as efficient methods to determine the most beneficial next acquisition. A study of the additional requirements to a emitter/system hierarchy is the next step in designing the framework for a threat identification expert system.

REFERENCES

1. Barnett, J. A., "Computational methods for a mathematical theory of evidence", Proc. 7th IJCAI, Vancouver, 1981, pp. 868-875.
2. Buchanan, B. G., and Shortliffe, E. H., Rule-based Expert Systems: The MYCIN experiments of the Stanford Heuristic Programming Project, Addison-Wesley, 1984.
3. Garvey, T. A., Lowrance, J. D. and Fischler, M. A., "An inference technique for integrating knowledge from disparate sources", Proc. 7th IJCAI, 1981, pp. 319-325.
4. Garvey, T. A. and Lowrance, J. D., Machine Intelligence for Electronic Warfare Applications, AFWAL Technical Report, 83-1168.

5. Gordon, J. and Shortliffe, E. H., "The Dempster-Shafer theory of evidence and its relevance to expert systems", in [2], pp. 272-292.
6. Gordon, J. and Shortliffe, E. H., "A method for managing evidential reasoning in a hierarchical hypothesis space", Artificial Intelligence, Vol. 26, July 1985, pp. 323-357.
7. Hayes-Roth, F. A., Waterman, D. A. and Lenat, D. B., Pattern-Directed Inference Systems, Academic Press, 1978.
8. Lowrance, J. D., Dependency-Graph Models of Evidential Support, COINS Technical Report 87-26, University of Massachusetts at Amherst.
9. Pearl, J., Fusion, Propagation and Structuring in Bayesian Networks, Cognitive Systems Laboratory, UCLA Technical Report, CSL-850022, 1985.
10. Quinlan, J. R., "INFERNO: A cautious approach to uncertain inference", The Computer Journal, Vol. 26, No. 3, 1983, pp. 255-269.
11. Quinlan, J. R., "Internal consistency in plausible reasoning systems", New Generation Computing, Vol. 3, 1985, pp. 157-180.
12. Shafer, G., A Mathematical Theory of Evidence, Princeton University Press, 1976.

1985 USAF-UES SUMMER FACULTY RESEARCH PROGRAM/
GRADUATE STUDENT SUMMER SUPPORT PROGRAM

Sponsored by the
AIR FORCE OFFICE OF SCIENTIFIC RESEARCH

Conducted by the
UNIVERSAL ENERGY SYSTEMS, INC.

FINAL REPORT

PARTICLE SCATTERING IN PLUMES

Prepared by:	William Holt Sutton
Academic Rank:	Assistant Professor
Department and University:	School of Aerospace, Mechanical, and and Nuclear Engineering University of Oklahoma
Research Location:	Arnold Engineering Development Center Sverdrup Technology, Inc. Propulsion Diagnostics/EL-3, MS 930 Arnold AFS Tullahoma, Tennessee 37389
USAF Research Colleagues:	Effort Focal Point: M. K. Kingery Sverdrup: R. A. Reed, W. K. McGregor T. L. Daugherty
Date:	31 July 1985
Contract No:	F49620-85-C-0013

PARTICLE SCATTERING IN PLUMES

by

WILLIAM HOLT SUTTON

ABSTRACT

The modelling of radiation heat transfer within the exhaust plumes of aluminized solid fuel rocket motors was the subject of this research effort. This work is very important in analyzing near field infrared test results and in benchmarking simpler models in the JANNAF SIRRM code. The problem of base heating of the rocket nozzle and adjacent components is also within the realm of the current research.

A finite, conformal-cylindrically symmetric, variable property, anisotropically scattering model subject nozzle heating conditions was formulated. A discrete ordinates numerical solution was generated for this problem. The model is currently being tested against simpler one dimensional cylindrical solutions.

ACKNOWLEDGEMENTS

The author of this report would like to express his appreciation to the Air Force Systems Command, Air Force Office of Scientific Research for the opportunity of participating in the Summer Faculty Research Program. The author would especially like to thank the people at Arnold Center for their assistance and excellent hospitality during his stay.

I. INTRODUCTION

William H. Sutton, the author of this report, is an Assistant Professor of Aerospace, Mechanical and Nuclear Engineering at the University of Oklahoma. In that capacity, he has taught graduate courses in Conduction, Convection, Radiation, and Advanced Radiation Heat Transfer. His current research interests lie in participating multidimensional radiation transport, experimental determination of radiative properties, combined modes of heat and mass transfer, and numerical solution methods in heat transfer applications.

Dr. Sutton has 6 refereed publications, 13 national or international conference papers, and many regional presentations - to his credit with nearly all of them relating in some way to radiative transport.

Dr. Sutton is also a member of the Thermophysics Technical Committee of the American Institute for Aerospace and Astronautics (AIAA). It was during his service on the committee that he learned of the reputation Arnold Engineering and Development Center (AEDC) had for rocket testing and the leading edge of technology work in experimental methods related to plume measurements. Additionally, with the sophistication level of testing rapidly growing, the personnel at AEDC were also rapidly acquiring a reputation for rocket plume modelling.

The JANNAF rocket plume computer codes have been very successful in modelling rocket performance. So much so, that they show considerable potential for diagnostic modelling of rocket plumes. Recently, test results of rockets related to the space shuttle have yielded data inconsistent with the codes. In an effort to examine more closely the physics of the plumes, a team was

assembled composed of 4 Summer Fellows (2 Faculty and 2 Students), several Sverdrup Technology people, and an outside consultant. The author's portion of the problem was to look at problems in the radiation modelling in the JANNAF code SIRR, however ample opportunity was given to be exposed to other portions of the problem. Particularly, in the author's case, the discussions with the test engineers relating to the measurements, review of filmed tests, and discussions with the analysts were very enlightening. First hand observation of an instrumented rocket engine just prior to testing was very helpful in understanding the many parts of the problem.

II. OBJECTIVES OF THE CURRENT RESEARCH EFFORT

The radiative transfer modelling in the JANNAF rocket plume computer codes is known to be rather poor in certain situations when used in a diagnostic sense. The codes perform well when performance is the required result. However, when near field information concerning structure of the plume, chemistry, or particle physics is needed such as in a test environment, the input data must usually be massaged to match the performance. These problems seemed insignificant until failure of several of the space shuttle Inertial Upper Stage (IUS) solid fuel rockets in space. Careful examination of previous tests and additional work indicated that the particles in the core of the rocket plume were radiating much more strongly than the SIRRM code predicted. The problem has many implications, including loss of performance and increased base heating to the rocket nozzle and adjacent satellite components. The Payload Assist Module (PAM) would appear to have similar characteristics except with more fuel and higher particulate loading, the radiation is likely to be more pronounced. One possible cause of the higher radiation could be that solids were remaining molten beyond the exit plane of the nozzle; a Graduate Summer Fellow under my direction, David W. Young, worked on this problem. Another possibility was that scattering was producing effects beyond the capabilities modelled in SIRRM. SIRRM uses either the Two-Flux or Six-Flux radiation models for the particulates overlaid onto gaseous modelling. Conceptually these models can be traced back to Joule [1] for a gas dynamics problem. The beauty of the Two-Flux

and the Six-Flux methods lies in computer speed and ability to model scattering. Unfortunately, the models appear to give erroneous results for highly scattering media or near edges of multidimensional regions. They are also poor for application to media with significant spatial distribution of properties.

In some instances the Two-Flux model in SRRM is superior to the Six-Flux model of the same problem compared to the test data. The objective of the current research is to provide both an efficient benchmark of the Flux methods and a usable alternative to available Monte Carlo schemes. The current research uses a discrete ordinates [2] approach to allow for variable properties and anisotropic scatter in a "conformal" cylindrically symmetric region. The method can be loosely tied to Multi-Flux models except that the angles represent Gaussian quadrature and there is no tie to adding and doubling schemes. These features allow a smoother representation of the scattering phase function and avoid tying the spatial grid to uniform optically thin distortion. Errors of the method tend to be minor systematic roundoff with solutions approaching the exact results as the grid spacing approaches zero as opposed to the statistical and targeting problems associated with Monte Carlo solutions.

III. FORMULATION OF THE PROBLEM

The current formulation of a solution to the Radiative Transfer Equation using a discrete ordinates or S_N method follows roughly that given by Fiveland [3] for a cylindrically symmetric medium with uniform properties and linearly anisotropic scatter. The discrete ordinate method is generally described as a finite difference method spatially with discrete angular directions represented by quadrature points for later angular integration. The right hand side of the Radiative Transfer Equation, which is referred to here as the Source Function, is iterated through the solution until converged.

There are several significant deviations here from Fiveland's work. In his paper the grid resolution is fairly coarse (6×10 , radial to axial). The angular definition used a symmetric area weighted quadrature for S_N , where the number of angles is stated as $N(N+2)$. The author's previous work in slab geometry [4] indicates that at least 17 spatial nodes are required to produce benchmark accuracy up to an optical thickness of 5. For three dimensional work [5], 9 nodes in each direction will give benchmark accuracy for optical thicknesses less than 2. Computer core space usually limits one to no greater resolution in three dimensional problems. Although Fiveland states that S_4 (24 solid angle directions) gives sufficient accuracy, no angular quantities were stated. Hence, one goal of this work is to determine the quality of resolution required or possible within the limits of limits of the facility. At least the resolution of a six-flux

model should be greatly improved at the expense of computer space and run time.

The Radiative Transfer Equation in a cylindrically symmetric medium is expressed in terms of spectral radiative intensity, I , (or radiance per standard military usage) as

$$\frac{\cos \phi \sin \theta}{r} \frac{\partial}{\partial r} (rI) + \cos \theta \frac{\partial}{\partial z} (I) - \frac{1}{r} \frac{\partial}{\partial \phi} (\sin \phi \sin \theta I) + \beta I = S \quad (1)$$

where the source function is defined as

$$S = (\beta - \tau) B + \frac{\tau}{4\pi} \int_{\phi'=0}^{\pi} \int_{\theta'=0}^{\pi} P^*(\theta, \phi, \theta', \phi') I \sin \theta' d\theta' d\phi'$$

The symmetric scattering phase distribution function is given by

$$P^*(\theta, \phi, \theta', \phi') = P(\theta, \phi, \theta', \phi') + P(\theta, \phi, \theta', -\phi')$$

where

$$P(\theta, \phi, \theta', \phi') = \sum_{n=0}^N A_n P_n(\cos \theta_0)$$

and

$$\cos \theta_0 = \sin \theta \sin \theta' \cos(\phi - \phi') + \cos \theta \cos \theta'$$

The intensity is next split into 4 quadrants based on symmetry,

$$\begin{aligned} I(r, z, \phi, \theta) &= A^1(r, z, \phi, \theta); \quad 0 \leq \phi \leq \frac{\pi}{2}, \quad 0 \leq \theta \leq \frac{\pi}{2} \\ &= A^2(r, z, \phi, \pi - \theta); \quad 0 \leq \phi \leq \frac{\pi}{2}, \quad \frac{\pi}{2} \leq \theta \leq \pi \\ &= A^3(r, z, \pi - \phi, \pi - \theta); \quad \frac{\pi}{2} \leq \phi \leq \pi, \quad \frac{\pi}{2} \leq \theta \leq \pi \\ &= A^4(r, z, \pi - \phi, \theta); \quad \frac{\pi}{2} \leq \phi \leq \pi, \quad 0 \leq \theta \leq \frac{\pi}{2} \end{aligned}$$

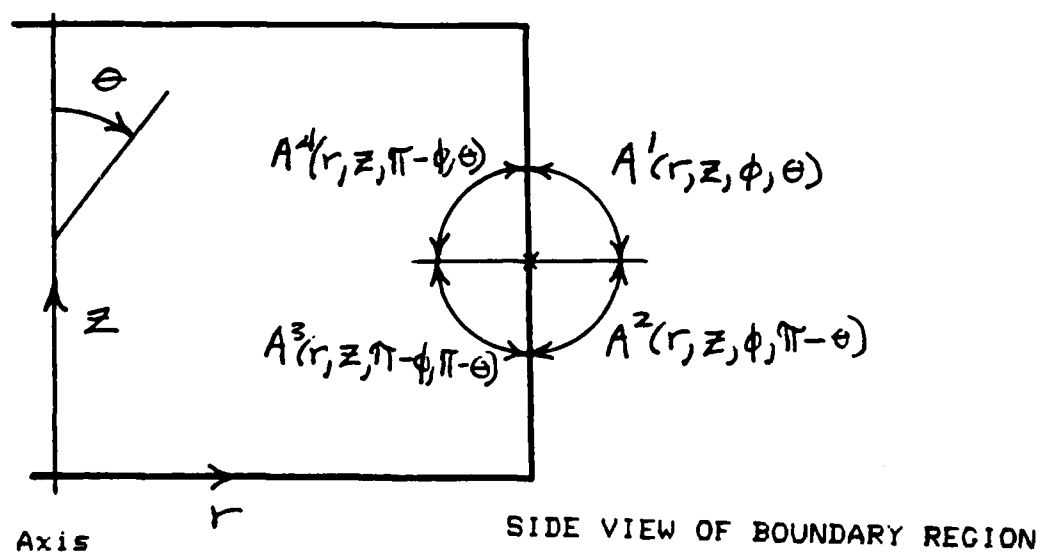
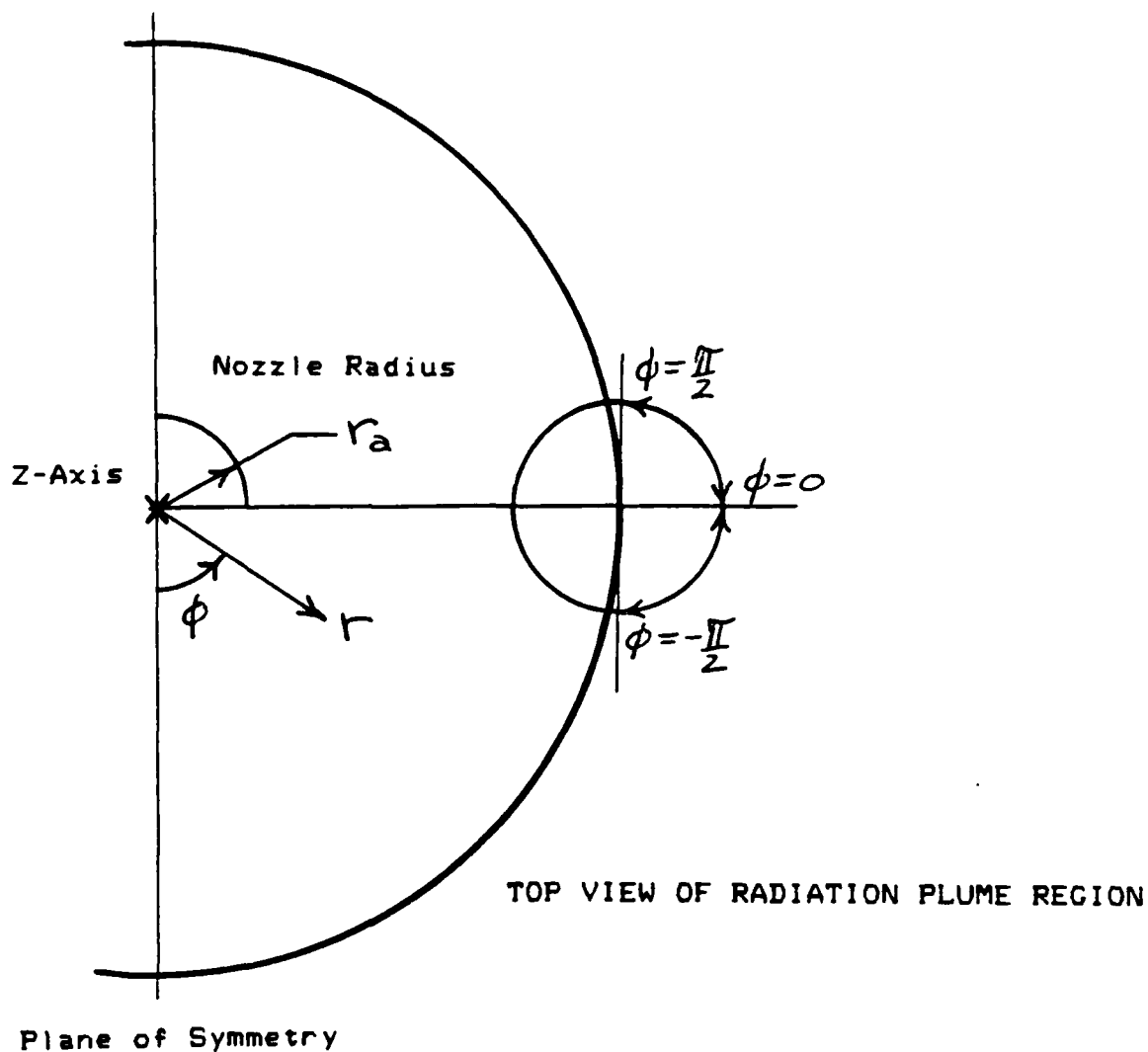


FIGURE 1. CYLINDRICAL GEOMETRY

AD-A166 178

UNITED STATES AIR FORCE SUMMER FACULTY RESEARCH PROGRAM

8/11

1985 TECHNICAL RE (U) UNIVERSAL ENERGY SYSTEMS INC

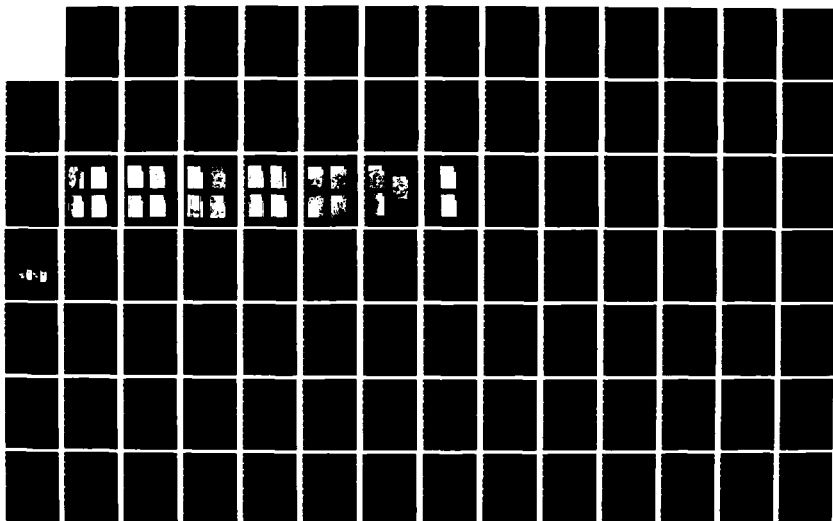
DAYTON OH R C DARRAH ET AL DEC 85 AFOSR-TR-86-0141

UNCLASSIFIED

F49620-85-C-0013

F/G 5/9

NL





MICROCOPY RESOLUTION TEST CHART
NATIONAL BUREAU OF STANDARDS-1963-A

The geometry of the model is sketched in Figure 1. The plume may take on any finite non-singular cylindrically symmetric shape within the radiation boundaries and the model will remain well posed. Clearly the choice of a finite cylindrical geometry will greatly aid the rocket base heating analysis because the model extends radially beyond the nozzle. However, care should be at the upper finite boundary since optical thickness plus shear length of the plume will force the problem to be semi-infinite.

The Radiative Transfer Equation is now recast for the split intensities transformed to the angular range $0 \leq \theta \leq \frac{\pi}{2}$, $0 \leq \phi \leq \frac{\pi}{2}$

$$\frac{\sin \theta \cos \phi}{r} \frac{\partial}{\partial r} (r A^1) + \cos \theta \frac{\partial}{\partial z} (A^1)$$

$$- \frac{1}{r} \frac{\partial}{\partial \phi} (\sin \theta \sin \phi A^1) + \beta A^1 = S^1$$

$$\frac{\sin \theta \cos \phi}{r} \frac{\partial}{\partial r} (r A^2) - \cos \theta \frac{\partial}{\partial z} (A^2)$$

$$- \frac{1}{r} \frac{\partial}{\partial \phi} (\sin \theta \sin \phi A^2) + \beta A^2 = S^2$$

$$- \frac{\sin \theta \cos \phi}{r} \frac{\partial}{\partial r} (r A^3) - \cos \theta \frac{\partial}{\partial z} (A^3)$$

$$- \frac{1}{r} \frac{\partial}{\partial \phi} (\sin \theta \sin \phi A^3) + \beta A^3 = S^3$$

$$- \frac{\sin \theta \cos \phi}{r} \frac{\partial}{\partial r} (r A^4) + \cos \theta \frac{\partial}{\partial z} (A^4)$$

$$- \frac{1}{r} \frac{\partial}{\partial \phi} (\sin \theta \sin \phi A^4) + \beta A^4 = S^4$$

The Source Function is also recast in terms of these intensities as

$$\begin{aligned}
 S = & (\beta - \sigma) B + \\
 & \frac{\sigma}{4\pi} \int_0^{\pi} \int_0^{\pi} \left(\rho^*(\theta, \phi, \theta', \phi') A^1(r, z, \phi', \theta') \right. \\
 & + \rho^*(\theta, \phi, \pi - \theta', \phi') A^2(r, z, \phi', \theta') \\
 & + \rho^*(\theta, \phi, \pi - \theta', \pi - \phi') A^3(r, z, \phi', \theta') \\
 & \left. + \rho^*(\theta, \phi, \theta', \pi - \phi') A^4(r, z, \phi', \theta') \right) \sin \theta' d\theta' d\phi'
 \end{aligned}$$

where successively,

$$\begin{aligned}
 S^1(r, z, \phi, \theta) &= S(r, z, \phi, \theta) \\
 S^2(r, z, \phi, \theta) &= S(r, z, \phi, \pi - \theta) \\
 S^3(r, z, \phi, \theta) &= S(r, z, \pi - \phi, \pi - \theta) \\
 S^4(r, z, \phi, \theta) &= S(r, z, \pi - \phi, \theta)
 \end{aligned}$$

The finite difference solution of these equations will start with known boundaries (or symmetry) and march away from them assuming the source function is known. The boundaries at the top and bottom, respectively, of the model are given by

$$z = 0,$$

$$\begin{aligned} A^1(r, 0, \phi, \theta) &= I_0(r, \phi, \theta) & ; & 0 \leq r < r_a \\ &= 0 & ; & r > r_a \\ A^4(r, 0, \phi, \theta) &= I_0(r, \pi - \phi, \theta) & ; & 0 \leq r < r_a \\ &= 0 & ; & r > r_a \end{aligned}$$

$$z = z_0,$$

$$\begin{aligned} A^2(r, z_0, \phi, \theta) &= 0 & ; & r \leq r_0 \\ A^3(r, z_0, \phi, \theta) &= 0 & ; & r \leq r_0 \end{aligned}$$

Here, $I_0(r, \phi, \theta)$ represents a specified (or calculated) nozzle exit radiance at the lower boundary. The upper boundary is taken as having negligible re-entrant radiance at this stage of the model development; this can be easily to reflect a semi-infinite condition. Radial boundary conditions represent symmetry and a free boundary for the plume axis and radial edge respectively as,

$$r = 0,$$

$$A^1(0, z, \phi, \theta) = A^4(0, z, \phi, \theta) ; 0 \leq z \leq z_0$$

$$A^2(0, z, \phi, \theta) = A^3(0, z, \phi, \theta) ; 0 \leq z \leq z_0$$

$$r = r_0,$$

$$A^4(r_0, z, \phi, \theta) = 0 ; 0 \leq z \leq z_0$$

$$A^3(r_0, z, \phi, \theta) = 0 ; 0 \leq z \leq z_0$$

No boundary condition exists for the ϕ -derivative. The implied symmetry of the special angle $\phi=0$, yields a Radiative Transfer Equation free of the ϕ -derivative. This solution then starts by differencing from $\phi=0$ to $\phi=\frac{\pi}{2}$ in the transformed angular range.

Representing each term in the split intensities as

$$[I] \equiv \frac{\sin \theta \cos \phi}{r} \frac{\partial}{\partial r} (r A^{\alpha})$$

$$[II] \equiv \cos \theta \frac{\partial}{\partial z} (A^{\alpha})$$

$$[III] \equiv -\frac{1}{r} \frac{\partial}{\partial \phi} (\sin \theta \sin \phi A^{\alpha})$$

the terms are operated on with

$$\int_{\Delta V} dV \int_{\Delta \phi} d\phi = \int_{\Delta z} \int_{\Delta r} 2\pi r dr dz \int_{\Delta \phi} d\phi$$

The subscripts represent either forward or backward differencing in a given direction. For example,

$$[I]_{br} \equiv \int_{r_{\lambda-1}}^{r_{\lambda}} 2\pi r \int_{\Delta z} \int_{\Delta \phi} [I] d\phi dz dr$$

$$[I]_{fr} \equiv \int_{r_{\lambda}}^{r_{\lambda+1}} 2\pi r \int_{\Delta z} \int_{\Delta \phi} [I] d\phi dz dr$$

will be used respectively for inward and outward directions based on known starting conditions. In summary the resultant terms based on integration where possible and the mean value theorem otherwise [2] are

$$[I]_{br} = 2\pi \sin \theta_l \overline{\cos \phi_k} \Delta \phi_k \Delta z (r_i A_{i,j,k,l}^\alpha - r_{i-1} A_{i-1,j,k,l}^\alpha)$$

$$[I]_{fr} = 2\pi \sin \theta_l \overline{\cos \phi_k} \Delta \phi_k \Delta z (r_{i+1} A_{i+1,j,k,l}^\alpha - r_i A_{i,j,k,l}^\alpha)$$

$$[II]_{bz} = 2\pi \cos \theta_l \Delta \phi_k \bar{r}_i \Delta r (A_{j,k,l}^\alpha - A_{j-1,k,l}^\alpha)$$

$$[II]_{fz} = 2\pi \cos \theta_l \Delta \phi_k \bar{r}_i \Delta r (A_{j+1,k,l}^\alpha - A_{j,k,l}^\alpha)$$

$$[III]_{b\phi} = 2\pi \Delta r \Delta z (\sin \phi_k A_{i,j,k,l}^\alpha - \sin \phi_{k-1} A_{i,j,k-1,l}^\alpha) \sin \theta_l$$

Applied to each equation, the difference forms yield the following symbolic set

$$[I]_{br} + [II]_{bz} + [III]_{b\phi} + \bar{\beta}_{i,j}^1 V_{i,j} \bar{A}_{i,j,k,l}^1 \Delta \phi_k = \bar{\beta}_{i,j,k,l}^1 V_{i,j} \Delta \phi_k$$

$$[I]_{br} - [II]_{fz} + [III]_{b\phi} + \bar{\beta}_{i,j}^2 V_{i,j} \bar{A}_{i,j,k,l}^2 \Delta \phi_k = \bar{\beta}_{i,j,k,l}^2 V_{i,j} \Delta \phi_k$$

$$-[I]_{fr} - [II]_{fz} + [III]_{b\phi} + \bar{\beta}_{i,j}^3 V_{i,j} \bar{A}_{i,j,k,l}^3 \Delta \phi_k = \bar{\beta}_{i,j,k,l}^3 V_{i,j} \Delta \phi_k$$

$$-[I]_{fr} + [II]_{bz} + [III]_{b\phi} + \bar{\beta}_{i,j}^4 V_{i,j} \bar{A}_{i,j,k,l}^4 \Delta \phi_k = \bar{\beta}_{i,j,k,l}^4 V_{i,j} \Delta \phi_k$$

The barred quantities represent finite difference cell-averaged terms.

Dividing each equation by $2\pi \Delta r \Delta z \Delta \phi$

and collecting terms gives a similar form for each equation.

For example the expression for $A'_{i,j,k,l}$ where subscripts denote differencing as

$$\begin{aligned} i &\rightarrow r \\ j &\rightarrow z \\ k &\rightarrow \phi \end{aligned}$$

is given by

$$\begin{aligned} A'_{i,j,k,l} = & \left\{ \bar{r}_i \bar{\beta}'_{i,j,k,l} + (A_{11} \bar{r}_{i-1} - A_{14}) A'_{i-1,j,k,l} \right. \\ & + (A_{12} - A_{14}) A'_{i,j-1,k,l} + (A_{13} \sin \phi_{k-1} - A_{14}) A'_{i,j,k-1,l} \\ & - A_{14} (A'_{i,j-1,k-1,l} + A'_{i-1,j,k-1,l} + A'_{i-1,j-1,k,l} \\ & \left. + A'_{i-1,j-1,k-1,l}) \right\} \left\{ A_{11} \bar{r}_i + A_{12} + A_{13} \sin \phi_k + A_{14} \right\}^{-1} \end{aligned}$$

where

$$A_{11} \equiv \frac{\sin \theta_l \cos \phi_k}{\Delta r}$$

$$A_{12} \equiv \frac{\bar{r}_i \cos \theta_l}{\Delta z}$$

$$A_{13} \equiv \frac{\sin \theta_l}{\Delta \phi_k}$$

$$A_{14} \equiv \frac{\bar{r}_i \bar{\beta}'_{i,j}}{8}$$

The numerical procedure, in order, is to start with $A^4(r, z, \phi, \theta)$ at the base edge of the plume and simultaneously difference inward, upward and away from $\phi = 0$. Then $A^3(r, z, \phi, \theta)$ is differenced from the top edge inward downward and away from $\phi = 0$. Symmetry then specifies A^1 and A^2 at $r = 0$. The differencing now proceeds in an outward direction for these two intensities. Next, the source function is calculated. Finally, iterative convergence of the source function is obtained.

Access to the AEDC mainframe computer was finally obtained at the beginning of the eighth week of the ten week summer program due to the site requirement of a secret or higher clearance. Under these circumstances, completion of the research was not possible despite the author's best efforts. Preliminary results indicate that the computer model developed is giving reasonable results for radiance distribution. However, heat flux results appear unstable in some cases indicating either further debugging or a finer grid resolution is needed.

IV. RECOMMENDATIONS

Since only minimal results are available at this time, the author would recommend completion of the testing of the numerical code. The benefits of such a diagnostic tool at AEDC would be very high. The base heating problem has become more critical as solid fuel rockets have become "hotter" due to increased performance requirements. To save weight and to add to effective fuel capacity the motors are increasingly compact with the motor of IUS and PAM being near the center of the devices. Additionally, more aluminum is added to the fuel to save weight and to enhance the combustion. These combined effects increasingly make codes such as SIRRM out of date. In the near field of the test chamber, chamber effects such as the downstream diffuser and limited wall cooling increasingly affect test results. The one dimensional multi-flux modelling in SIRRM is simply not designed to see three dimensional effects. These effects show up in signature, base heating, and performance.

The author intends to prepare a detailed proposal for continuation of the current research and a close collaboration with AEDC on specifics in making the model useful for plume diagnostics.

REFERENCES

1. S. Chandrasekhar, Radiative Transfer, Dover Publications, New York, 1960.
2. N. M. Shaeffer, Reactor Shielding for Nuclear Engineers, U. S. Atomic Energy Commission, Technical Information Center U. S. Department of Energy, NTIS TID-25951, 1973.
3. W. A. Fiveland, "A Discrete Ordinates Method for Predicting Radiative Heat Transfer in Axisymmetric Enclosures", ASME Paper 82-HT-20, The American Society for Mechanical Engineers 1982.
4. W. H. Sutton and M. N. Ozisik, "An Iterative Solution for Anisotropic Radiative Transfer in a Slab", ASME J. of Heat Transfer, Vol. 101, 695-698, November, 1981.
5. R. Kamath, "A Numerical Study of Multilayer Radiative Heat Transfer in a Three-Dimensional Participating Medium", M. S. Thesis, University of Oklahoma, 1985.

1985 USAF-UES SUMMER FACULTY RESEARCH PROGRAM/

GRADUATE STUDENT SUMMER SUPPORT PROGRAM

Sponsored by the
AIR FORCE OFFICE OF SCIENTIFIC RESEARCH

Conducted by the
UNIVERSAL ENERGY SYSTEMS, INC.

FINAL REPORT

Thermal Stability of Aluminum-Iron-Cerium Alloys

Prepared by: Robert E. Swanson
Academic Rank: Assistant Professor
Department and
University: Materials Engineering Department
Virginia Polytechnic Institute
and State University
Research Location: Air Force Wright Aeronautical
Laboratories, Materials Laboratory
Structural Metals Branch
USAF Research: Dr. F.H. Froes and Dr. Y-W Kim
Date: 20 September 1985
Contract No.: F49620-85-C-0013

Thermal Stability of Al-Fe-Ce Alloys

by

Robert E. Swanson

Abstract

Two Al-Fe-Ce alloys produced by the melt-spinning rapid solidification processing technique have been annealed and characterized in terms of thermal stability. Various means have been used to characterize microstructure, including scanning electron and transmission electron microscopy, differential thermal analysis, and electron microprobe. Microhardness measurements of two distinct solidification zones were also used to assess thermal stability. Microstructural differences included cruciform-shaped particles in the as-cast quaternary alloy and acicular particles in the quaternary alloy annealed at 1000°F for 2 hours. Two exothermic reactions were found for the ternary alloy; only one for the quaternary alloy. The lower overall hardness of the quaternary alloy was related to decreased cooling rate via poorer wetting of the melt-spin wheel. Additional work is recommended for both systems.

I. Introduction

Conventional precipitation hardened aluminum alloys of the 2000 and 7000 series have useful operating strengths up to temperatures of about 180°C (356°F). Alloying elements which contribute to solid solution strengthening and precipitation hardening diffuse at these temperatures, forming large noncoherent particles which lead to decreased strength. Dispersion hardening effects in conventional ingot metallurgy processing are usually limited to a relatively low volume fraction of an inhomogeneous distribution of coarse dispersoids. Rapid solidification processing (RSP) offers a means to extend the solid solubility of elements which otherwise show negligible equilibrium solid solubility in aluminum. Strength can thus be increased by this added solid solution strengthening as well as by the formation of a very fine, and uniform, dispersion of metastable eutectic phases. Subsequent thermomechanical processing of these alloys can lead to substantial volume fractions of fine, thermally stable aluminide dispersoids. The elevated temperature strength of these alloys therefore depends not only on the volume fraction of these dispersoids but also on their rate of coarsening. The Al-Fe system, with additions of Mo, V, Zr, Ce, or Y, has been investigated for elevated temperature stability, relying on low diffusivities and low misfit interfacial energies to decrease the rate of coarsening (1).

This study concentrated on Al-Fe-Ce and Al-Fe-Ce-W. The main goal was to investigate the effect of alloy composition on thermal stability, as measured by changes in microstructure and microhardness.

II. Experimental

Two cigar-shaped ingots were provided. One had a nominal composition of Al-8 Fe-8 Ce (designated the ternary alloy) and the other Al-8 Fe-5

Ce-0.7 W (designated the quaternary alloy).

The melt spinning technique (2) was employed, in air, to produce rapidly solidified ribbons 3 mm wide and about 70-100 μm thick. A quartz crucible, with a 1 mm wide slot, was used with a 2 psi pressure. The solid copper casting wheel, operating at a peripheral velocity of 20.75 ms^{-1} , was placed 0.8 mm from the crucible.

Samples of the ribbon were vacuum encapsulated and heat treated between $93\text{-}538^{\circ}\text{C}$ ($200\text{-}1000^{\circ}\text{F}$) for 2 hours. Sections of both as-cast and heat treated ribbons were metallographically prepared for examination. This procedure is very important in achieving good edge retention. Sections of ribbon about 40 mm long were bent into v-shapes and ultrasonically cleaned in acetone for 1-2 min., followed by a methanol rinse. They were then mounted in Epomet compound (product of A-B Buehler, Ltd., 41 Waukegan Rd., P.O. Box 1, Lake Bluff, Illinois, 60044) which had been autogenously milled in a v-blender. The v-shape of the ribbons allows for cross-sectional examination without the use of mounting clips. This in turn provides better edge retention and eliminates a galvanic corrosion effect during subsequent preparation. These mounts were wet ground in 240, 320, 400, and 600 grit silicon carbide papers, followed by grinding with 15 μm diamond paste on a card, and 3 μm diamond solution on a nylon wheel. A 1 μm alumina polishing step was followed by a 0.005 μm silicon carbide polish on microcloth. The above procedure produced a polished surface free of disturbed metal. Specimens were etched with Keller's reagent for 5-10 sec.

Metallographic examination of these mounted specimens included both optical and scanning electron microscopy (SEM). Depth-of-field advantages of the SEM, a JEOL Model 35, provided more microstructural detail than optical microscopy. Microhardness tests, using a Buehler Micromet with 10

gram load and 15 second dwell time, and a Knoop indenter were also conducted on these mounted ribbons.

Additional characterization included transmission electron microscopy (TEM), using a JEOL Model 100cx, of thin foil specimens prepared by electrochemical jet polishing 3 mm diameter discs extracted from the ribbons. A solution of methanol and 30% (volume) nitric acid at -20°C produced acceptable thin foils. TEM foils were prepared from both alloys in the following conditions: as-cast, 600°F , and 800°F .

Sections of ribbon were reduced to powder form via a rotating knife apparatus. These powders, as well as ribbon samples, were evaluated for phase transformations via differential thermal analysis (DTA) (3) using a DuPont 990 analyzer. A heating rate of 20°C per minute was used from room temperature 550°C (1022°F). Oxygen-free nitrogen was passed continuously through the specimen holder to minimize oxidation of the sample and reference disc.

III. Results

A. Chemistry and DTA Results

Chemical analysis showed that the ternary alloy contained Al-8.4% Fe-8.4%Ce and the quaternary contained Al-7.8%Fe-4.6%Ce-0.7%W. Vacuum heat treating to temperatures of 1000°F for 2 hours did not alter these compositions, indicating that any microstructural changes with heating were associated with solid state transformations and not evaporation or volatilization.

The results obtained from the DTA technique showed exothermic solid state reactions at about 260°C and about 440°C for the ternary alloy. An exothermic solid state reaction was indicated at about 230°C for the quaternary alloy. These results suggest possible precipitation reactions,

rather than dissolution, coarsening, reversion, or incipient melting. The temperature range for a solid state reaction on a DTA curve depends not only on the specific reaction, but also on the thermal capacities of both the sample and the reference material as well as the heating rate (4). Thus, several reference materials and heating rates were used to confirm these results. These exothermic reactions suggest that the as-cast ternary alloy shows precipitation reactions near 260°C (500°F) and near 440°C (824°F) while the quaternary alloy shows a precipitation reaction near 230°C (446°F).

B. SEM Results

As stated previously, the examination of metallographic sections by SEM gave results superior to the optical microscopy, in large part due to the high magnifications needed to discern the microstructural features of interest. For that reason, only SEM results are covered here.

Figure 1 shows a typical longitudinal section of the as-cast ternary alloy. (All photomicrographs of metallographic cross sections in this report represent longitudinal sections with the ribbon side, which was in contact with the melt-spin wheel, facing down). At least three solidification zones are evident. The wheel side of the ribbon shows a featureless chill zone about 12 μm wide, followed by a zone of columnar grains, about 9 μm wide. The side opposite the wheel (air side) has a zone of equiaxed grains, about 8 μm wide. An oxide layer, about 1 μm thick, covers this equiaxed region. Figure 2 shows these three solidification zones in more detail. As shown in Figure 3, the equiaxed zone has porosity, or more likely, particles which were removed during metallographic preparation, associated with the central regions of the equiaxed dendrites. This suggests that spherical constituent particles,

about 0.5 μm in diameter, acted as heterogenous sites for solidification in this region. Figure 4 shows fine spherical particles, less than 0.1 μm in diameter, in the transition region between the chill and columnar zones. Electron microprobe analysis showed that some particles tended to be rich in iron while others tended to be rich in cerium, with no apparent differences in morphology or size distinguishing the two. Figure 4 also shows the transition region between the chill and columnar regions with these fine particles tending to outline the heat flow pattern.

The microstructures for the ribbons annealed at 200°F, 400°F and 600°F appeared similar to the as-cast ternary microstructure, as examined by optical microscopy and SEM. Annealing of 800°F for 2 hours led to a coarse particulate structure in the chill zone, as shown in Figure 5. These particles tend to be equiaxed in this region and about 0.2 μm in diameter, as shown in Figure 6. Annealing at 1000°F for 2 hours produced a similar particulate structure in all regions of the ribbon, as shown in Figure 7. The particles in the columnar region (about 0.2 μm in diameter) tend to be aligned with the direction of heat flow, as shown in Figure 8. This suggests that they precipitated heterogeneously along dendrites and coarsened during the subsequent heat treatment.

The as-cast structure of the quaternary alloy has three distinct regions as does the ternary alloy. These are shown in Figure 9. The chill region, adjacent to the wheel, was about 10 μm wide, followed by a columnar region about 20 μm wide. The air side of the ribbon has an equiaxed structure about 5 μm wide with an oxide layer about 1 μm wide. These dimensions are nearly the same as corresponding dimensions for the ternary alloy, except that the columnar zone is nearly twice as wide for the quaternary. The chill zone for the as-cast quaternary was relatively featureless, as shown in Figure 10, with a fine dispersion of spherical

particles about 0.1 μm in diameter. The white particles in the equiaxed zone tend to have a cruciform shape, up to 3 μm in size, as shown in Figure 11. The smaller, round, white particles may be cross sections of cruciform arms. Preliminary electron microprobe analysis showed no compositional differences between the cruciform particles and adjacent dendrites. Figure 12 shows a cruciform particle with 4-fold symmetry, as well as more of the round particles which may be sections of cruciforms. Specimens annealed at 200°F for 2 hours showed microstructures similar to the as-solidified specimens. Annealing at 400°F, however, produced substantial changes in both the columnar and the equiaxed zones, as shown in Figure 13. Figure 14 shows that the 400°F anneal has obliterated dendrite features, forming more spherical pores. Annealing at 1000°F tended to homogenize the ribbon, as shown in Figure 15, with particles on the order of 1 μm diameter in all regions. Figure 16 shows equiaxed as well as acicular (or perhaps sections of lenticular particles) particles in the chill zone. Similar microstructures are present in the equiaxed and columnar regions. These acicular particles are about 0.1 μm wide and up to 2 μm long.

C. TEM Results

Figure 17 shows a transmission electron micrograph of the as-cast ternary alloy. The high density of fine (0.02-0.1 μm) particles is at least partially due to the foil thickness. This micrograph represents the chill zone and these particles are similar to those found to be rich in iron and/or cerium via electron microprobe analysis. While diffraction patterns and dark field images were obtained in this investigation, the many reflections precluded the characterization of particle structure and composition in the time available. Acicular particles are shown in Figure 18 from another region of the as-cast ternary ribbon. These acicular particles are about 0.02 μm wide and 0.2 μm long. It is unclear which

region they represent since no acicular particles were found in mounted cross-sections of the ternary alloy ribbons. (Acicular particles were observed in the quaternary alloy heat treated at 1000°F, as shown in Figure 16).

Figure 19 shows precipitates (about 0.04 μm diameter) aligned with dendrite boundaries. In another investigation, (5), a similar structure was found in the relatively featureless region (of air-atomized Al-Fe-Ce powders) corresponding to the chill zone in the present study. The dendritic structure revealed by the precipitates in Figure 19 is much finer than the columnar region of Figure 2. It appears that the structure shown in Figure 19 represents the chill-columnar transition region, as shown in Figure 4. It is significant to note that the structure in Figure 19 is from the ternary alloy exposed to 800°F for 2 hours and that similar structures were found for specimens having the less severe heat treatments. Another region from the ternary alloy heat treated at 800°F is shown in Figure 20. This structure is similar to that shown in the as-cast chill zone structure of Figure 17, except that the 800°F structure of Figure 20 shows a high density of large (about 0.2 μm) equiaxed particles. The structure revealed by TEM in Figure 20 appears to correspond with that revealed by SEM in Figure 5.

The as-cast structure of the quaternary alloy, shown in Figure 21, has a high density of fine (0.02–0.04 μm) diameter particles. It is not clear which zone Figure 21 represents, but the particle size and shape suggest this is the chill zone, and this corresponds to the chill zone structure shown in Figure 10. Figure 22 shows large (0.2 μm diameter) equiaxed particles as well as smaller, elongated particles (about 0.04 μm wide and 0.15 μm long). The ends of these elongated particles are rounded, compared with the pointed ends of the larger (0.06 μm wide and 0.4 μm long) acicular

particles in the quaternary alloy heat treated to 800°F, and shown in Figure 23. The change in tip radius is likely due to decreasing interface coherency with increasing particle size.

D. SEM-Wetting

During the melt-spinning process, the molten alloys did not completely wet the wheel surface. This lack of contact led to pores or depressions in the ribbon surface where the cooling rate is expected to be substantially less than in the regions where good contact was achieved. Figure 24 shows a typical wheel-side surface for the ternary alloy. The corresponding surface for the quaternary alloy is shown in Figure 25, which has at least three times the surface area fraction of depressions shown for the ternary alloy. It follows that the average cooling rate for the quaternary alloy was less than for the ternary alloy. It is the opinion of the author that an increased magnitude of superheat can be expected to decrease wetting, although this is not documented in the literature. In the case of these two alloys, both had initial temperatures of 930°C prior to melt-spin solidification. The differences in alloy composition (quaternary has 0.7% W but lower Fe and Ce than the ternary) are expected to lead to differences in liquidus temperatures and thus in a difference in the amount of superheat.

Examination of available binary (6, 7, 8) and ternary (9) phase diagrams provides insufficient evidence to state whether a shift in equilibrium cooling liquidus temperature can account for the difference in wetting for these two alloys.

E. Microhardness

In order to assess the effect of elevated temperature on microstructural stability, microhardness (Knoop) tests were conducted on the chill (Zone A) and equiaxed (Zone B) regions of polished and etched

cross sections of ribbons for each condition. The designations Zone A and Zone B are taken from work on aluminum-iron alloys (10). The microhardness results for the ternary alloy are shown in Figure 26, with the quaternary results in Figure 27. Each plotted value represents at least thirty indentations and measurements. The bar on each plotted point shows the measured range of values, after evaluation for outliers via the r test and treatment using the Anscombe rule (11, 12). This assured a coefficient of variation (ratio of standard deviation to mean value) less than 10%. In Figure 26, the as-cast microhardness values are shown to be about 196 and 117 for Zone A and the microhardness values Zone B, respectively. The values for both zones increase between about 400 and 450°F, reaching maxima at around 600°F, then falling sharply at increased annealing temperatures. The exothermic reaction detected by DTA around 500°F may increase the hardness via precipitation. The exothermic reaction noted around 824°F does not seem to correspond to changes in the microhardness data, although a precipitation reaction in the columnar zone may have occurred. Microhardness tests were not conducted for the columnar region. The precipitation of particles shown in the columnar region of Figure 8 may have resulted in this exothermic indication.

Figure 27 shows that the microhardness values for the as-cast quaternary alloy are about 152 and 123 for Zone A and Zone B, respectively. Thus, the Zone B values are about the same for the quaternary and the ternary, with the Zone A value for the ternary being higher than the corresponding value for the quaternary. The quaternary hardness values remain essentially constant with respect to temperature to about 800°F. The exothermic reaction detected via DTA is apparently not represented in the microhardness data and again may result from precipitation in the columnar region. The changes in the columnar structure around 400°F, shown

in Figures 13 and 14, may correspond to the exothermic reaction at 446°F.

IV. Discussion

The as-cast alloys have at least three distinct zones, chill (Zone A), columnar, and equiaxed (Zone B), with an oxide film covering the air side of the ribbons. The zone thicknesses are comparable, with the ternary alloy having a somewhat thicker equiaxed zone and the quaternary alloy having a thicker columnar zone.

The increased columnar zone thickness tends to coincide with the decreased wetting observed for the quaternary alloy, resulting in a decreased rate of cooling.

The chill zones of both alloys contain spherical particles about 0.1 μm in diameter. The equiaxed zone of the ternary alloy has pores, perhaps resulting from particle removal during specimen preparation, about 0.5 μm in diameter. The quaternary alloy equiaxed zone, however, has larger (1-3 μm), criciform-shaped particles. The TEM examination showed acicular particles in the as-cast ternary alloy which were not observed in the as-cast quaternary alloy.

The observation that the average microhardness values for the equiaxed regions (Zone B) in both alloys are about the same suggests that the cruciform particles are not present in high enough density to provide a significant strengthening effect. The higher hardness in the chill region (Zone A) of the ternary alloy compared with the quaternary may result from a higher volume fraction of fine (0.1 μm) particles, although this was not confirmed in the present study.

The DTA technique and microhardness test results provide a means of following the microstructural changes during elevated temperature exposure. The ternary alloy showed two exothermic peaks in the DTA tests.

An exothermic peak typically corresponds to precipitation from supersaturated solid solution, as would be expected in the rapid solidification process. However, one might expect G-P zone formation and, perhaps, dissolution prior to the precipitation. G-P zone formation would tend to be an exothermic reaction and might be interpreted as corresponding to the 260°C (500°F) peak. However, this temperature is extremely high and likely corresponds to a precipitation reaction, although no specific microstructural evidence was found. The exothermic reaction found at 440°C (824°F) in the ternary alloy may result from the formation of the 0.2 μ m particles shown in Figures 6 and 20. This higher temperature exothermic peak appears with no evidence of an intermediate endothermic reaction (for coarsening or dissolution). Again, this exothermic reaction suggests a precipitation, but such a reaction would be expected to lead to an increase in strength and thus hardness. This is not the case as the microhardness values tend to decrease in this temperature range, as shown in Figure 26. The lower temperature exothermic reaction, at 500°F, does tend to coincide with the increased microhardness values between 400 and 600°F in Figure 26.

The quaternary alloy revealed a single exothermic peak near 230°C (446°F) in DTA testing. No TEM evidence was found to correspond with this reaction, but the difficulty of preparing electron transparent regions of interest in these ribbons may mean that such a precipitation existed but was missed. The microhardness values showed no significant change for Zone A (chill) or Zone B (equiaxed) near this temperature, but the exothermic reaction may correspond to a precipitation within the columnar region.

The absence of endothermic DTA peaks for either the ternary or the quaternary alloy up to 550°C (1022°F) means that both alloys are very resistant to particle dissolution or coarsening. The DTA technique is extremely useful for the wide temperature range studied here, but further

examination of the alloys is recommended via the more sensitive technique of differential scanning calorimetry (DSC), especially to check for evidence of such coarsening or dissolution above 600°F.

The decreased microhardness values for the quaternary alloy in all conditions and in both zones appears related to a decreased solidification cooling rate from decreased wetting of the melt-spin wheel. This may be related to differences in superheat or viscosity between the two alloys.

V. Conclusions

A. As measured by microhardness, both alloys show excellent high temperature stability, the ternary to 600°F and the quaternary to 800°F.

B. The lower temperature stability of the ternary may result from the high temperature (824°F) exothermic reaction found for the ternary, but absent in the quaternary.

C. The lower overall microhardness of the quaternary appears related to decreased wetting of the melt-spin wheel, giving less solid solution strengthening in the as-cast condition.

D. Microstructural features are similar for both alloys. The primary differences include cruciform-shaped particles in the as-cast quaternary and acicular particles in all regions of the quaternary alloy after 1000°F annealing for 2 hours.

E. Results have shown importance of changes in the intermediate, columnar zone.

VI. Recommendations

A. Perform DSC tests on both alloys, especially above 600°F, to seek evidence of endothermic reactions to correspond with decreased microhardness.

B. Examine effect of superheat on wetting during rapid solidification.

C. Continue work to identify phases present in Al-Fe-Ce system.

Acknowledgements

This work was performed at the Air Force Materials Laboratory, Wright-Patterson AFB under the sponsorship of the Air Force Systems Command, Air Force Office of Scientific Research. The author wishes to express appreciation for technical discussions with Drs. F.H. Froes and Y-W Kim.

VII. References

1. C.M. Adam: Rapidly Solidified Amorphous and Crystalline Alloys, B.H. Kear, B.C. Giessen and M. Cohen, eds, Elsevier, New York, 1982, p. 411.
2. S.J. Savage and F.H. Froes; Journal of Metals, vol. 36, No. 4, 1984, pp. 20-33.
3. M.I. Pope and M.D. Judd: Differential Thermal Analysis, Heyden, Bellmawr, N.J., 1977, p.p. 44-52.
4. D.J. Skinner, R. Ker, M.J. Koczak and A. Lawley: Modern Developments in Powder Metallurgy, H.H. Hausner, H.W. Antes, and G.D. Smith, eds., MPIF and APMI, Princeton, 1981, pp. 483-99.
5. M.G. Chu, R.J. Rioja, G.J. Hildeman, and D.K. Denzer: Proceedings of the 43rd Annual Meeting of the Electron Microscopy Society of America, G.W. Bailey, ed., San Francisco Press, San Francisco, 1985, pp. 32-33.
6. M. Hansen, and K. Anderko: Constitution of Binary Alloys, 2nd ed., New York, McGraw-Hill, 1958.
7. R.P. Elliott: Constitution of Binary Alloys - First Supplement, New York, McGraw-Hill, 1965.
8. F.A. Shunk: Constitution of Binary Alloys - Second Supplement, New York, McGraw-Hill, 1969.
9. O.S. Zarechnyuk, M.G. Mysik, and V.R. Ryabov: Russian Metallurgy, No. 2, 1969, p. 133.
10. M.H. Burden and H. Jones: Metallography, 3, 1970, pp. 307-326.
11. B.W. Lindgren: Statistical Theory, MacMillan, New York, 1968.

12. W.J. Beggs: Bettis Reactor Engineering School Statistics,
Westinghouse Bettis Atomic Power Laboratory, West Mifflin, PA,
1978, pp. III-59 to III-60.

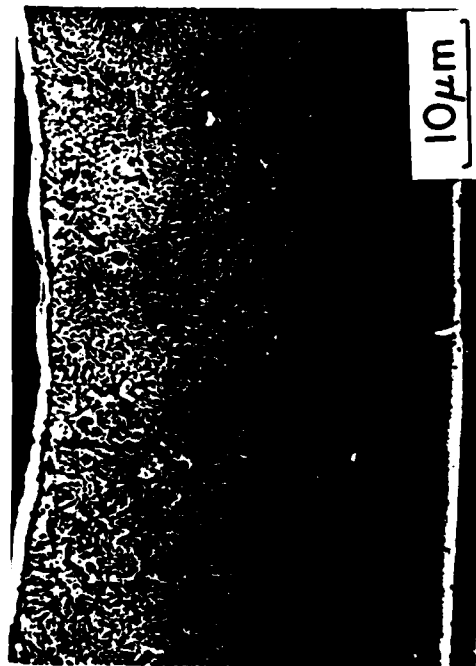


Fig. 1: SEM of longitudinal section of as-cast ternary alloy. Shows oxide, equiaxed, columnar, and chill zones (top to bottom).



Fig. 3: SEM of equiaxed zone in ternary alloy. Holes may result from particle removal during etching.

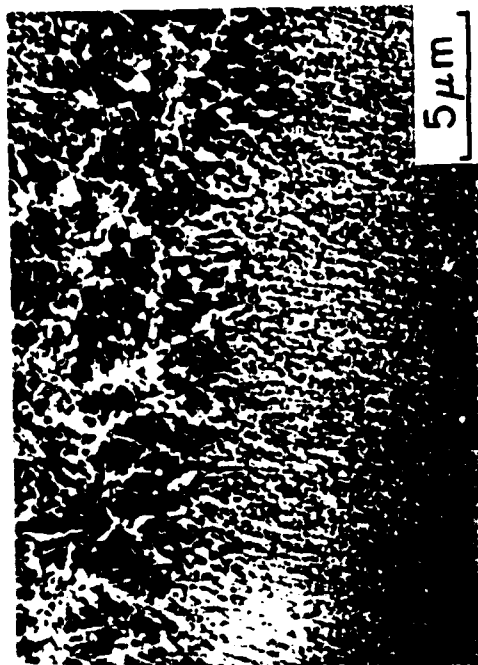


Fig. 2: SEM of ternary alloy showing three distinct zones: equiaxed, columnar, chill (top to bottom).



Fig. 4: SEM of transition region between chill (bottom) and equiaxed (top) zones in ternary alloy.



Fig. 5: SEM of longitudinal section of ternary alloy annealed at 800°F-2 hr.

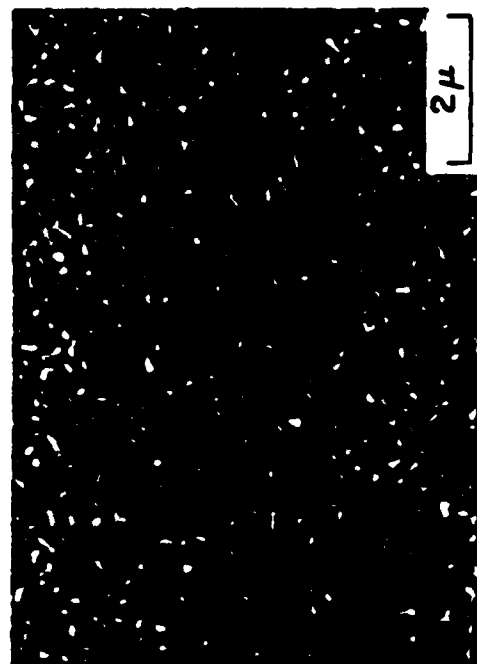


Fig. 6: SEM of equiaxed region of ternary alloy after annealing at 800°F-2 hr.

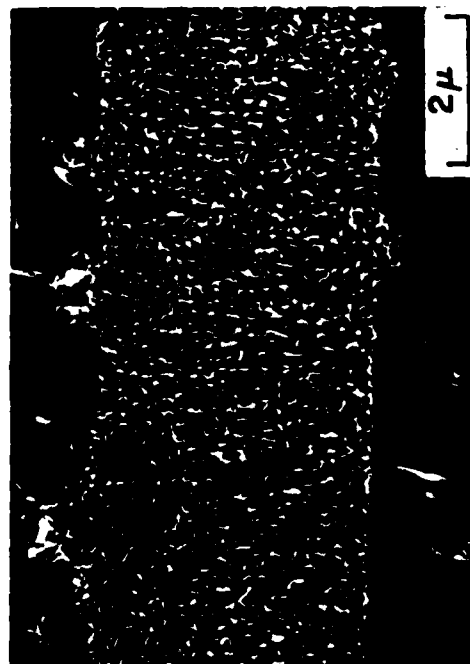


Fig. 7: SEM of ternary alloy after annealing at 1000°F-2 hr. Similar particulate structure in all regions.

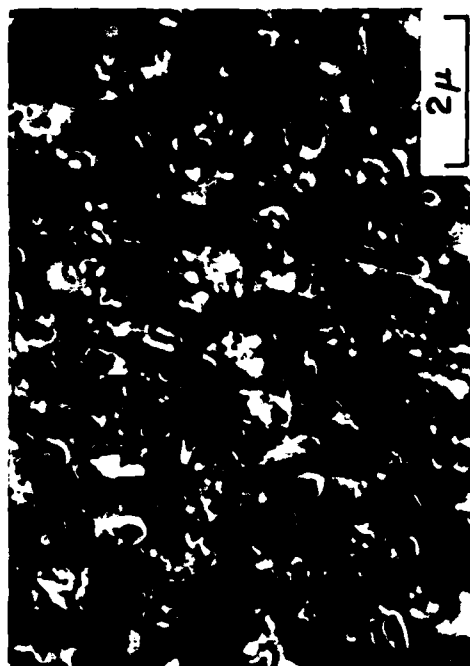


Fig. 8: SEM of columnar zone of ternary alloy annealed at 1000°F-2 hr. Particles aligned in direction of heat flow.



Fig. 9: SEM of longitudinal section of as-cast quaternary alloy. Shows oxide, equiaxed, columnar, and chill zones (top to bottom).



Fig. 11: SEM of equiaxed zone in as-cast quaternary alloy showing cruciform-shaped particles.

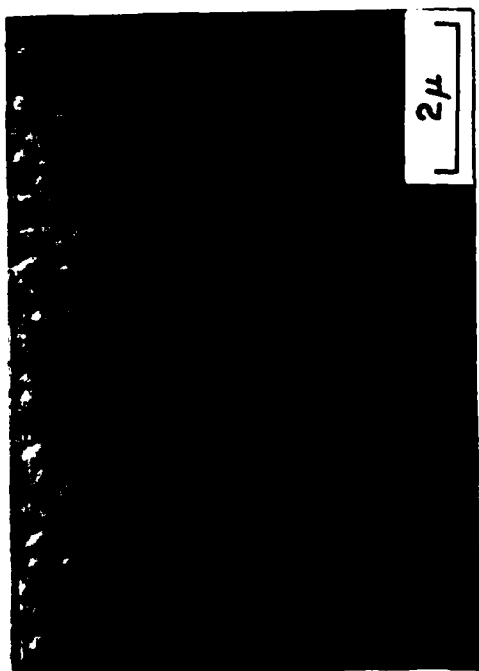


Fig. 10: SEM of chill zone of as-cast quaternary alloy with dispersion of particles.



Fig. 12: SEM of cruciform-shaped particle showing symmetry. Adjacent to field shown in Fig. 11.

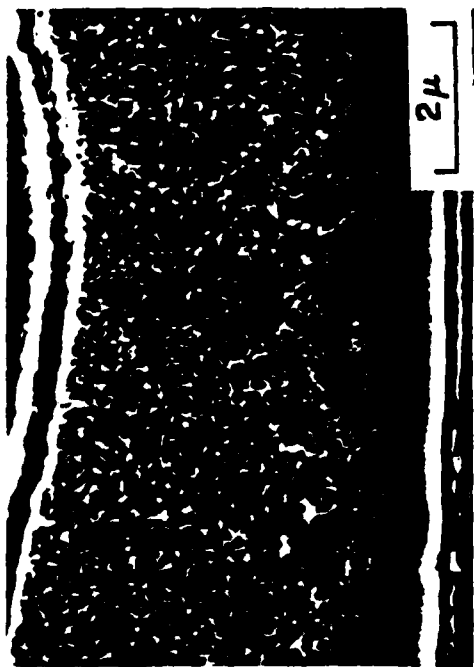


Fig. 13: SEM of quaternary alloy after annealing at 400°F-2 hr. Shows substantial coarsening in equiaxed and columnar zones.

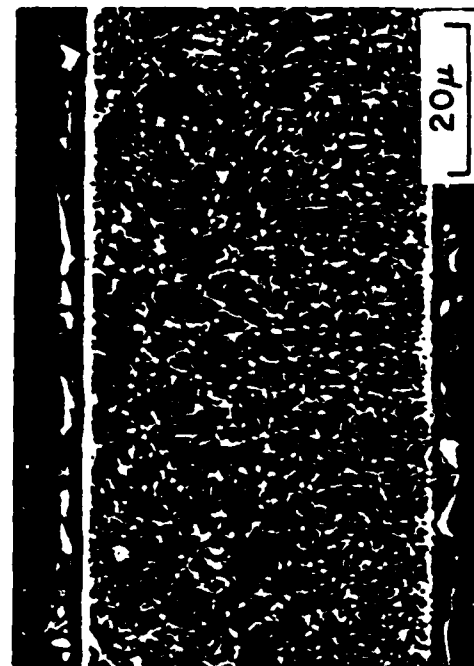


Fig. 15: SEM of longitudinal section of quaternary alloy after annealing at 1000°F-2 hr. Shows similar structure in all regions.



Fig. 14: SEM of equiaxed region of quaternary alloy after annealing at 400°F-2 hr.



Fig. 16: SEM of chill zone of quaternary alloy annealed at 1000°F-2 hr. Shows acicular as well as equiaxed particles.

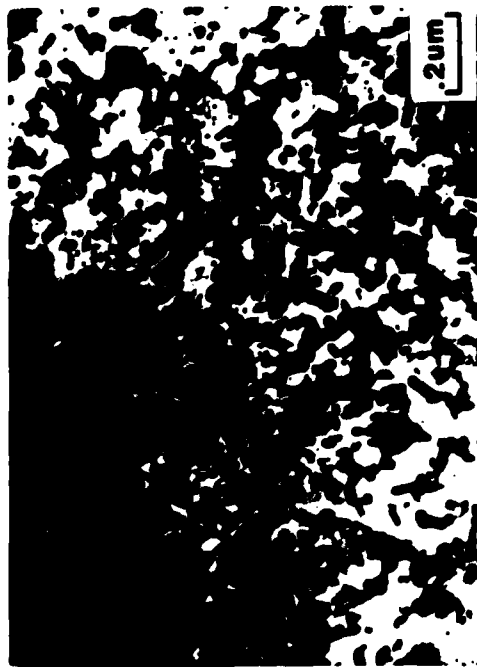


Fig. 17: TEM of as-cast ternary alloy. Shows particles in chill zone.



Fig. 18: TEM of as-cast ternary alloy, showing acicular particles.

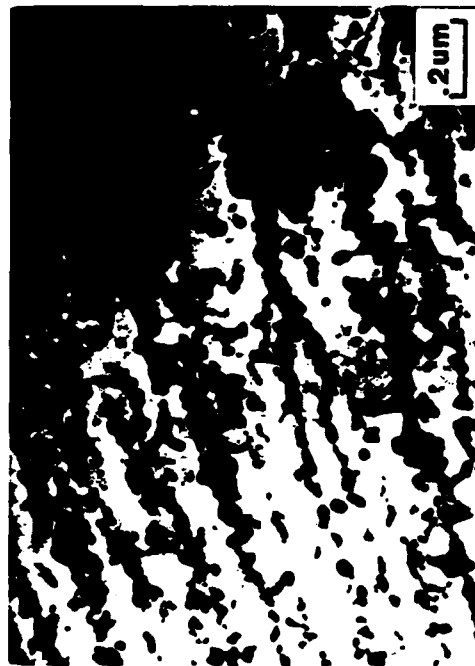


Fig. 19: TEM of chill-columnar transition region in ternary alloy after annealing at 800°F-2 hr.

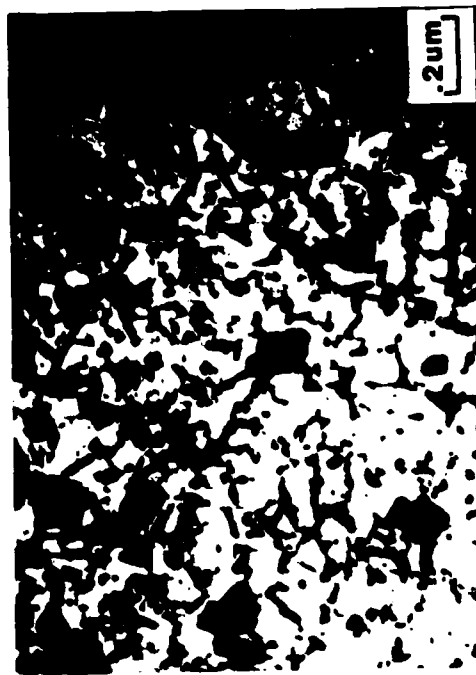


Fig. 20: TEM of ternary alloy after annealing at 800°F-2 hr. Shows larger (0.2 μ m) equiaxed particles.



Fig. 21: TEM of as-cast quaternary alloy with high density of fine particles.



Fig. 22: TEM of as-cast quaternary alloy with large (0.2 μm) equiaxed and smaller elongated particles.



Fig. 23: TEM of quaternary alloy after annealing at 800°F-2 hr., showing acicular particles.

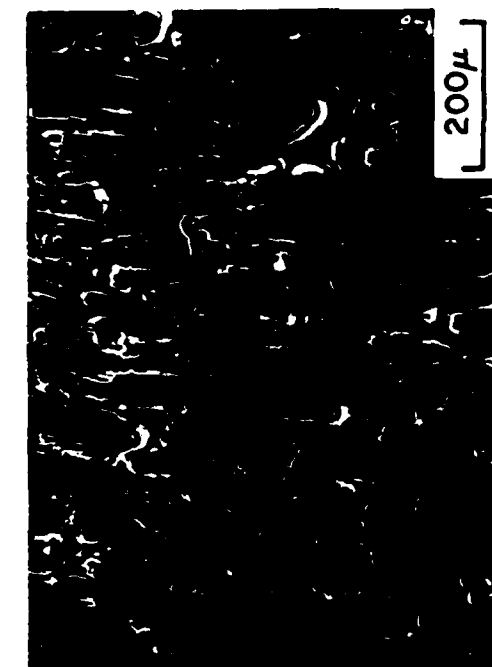


Fig. 24: SEM of wheel side of as-cast ternary ribbon.

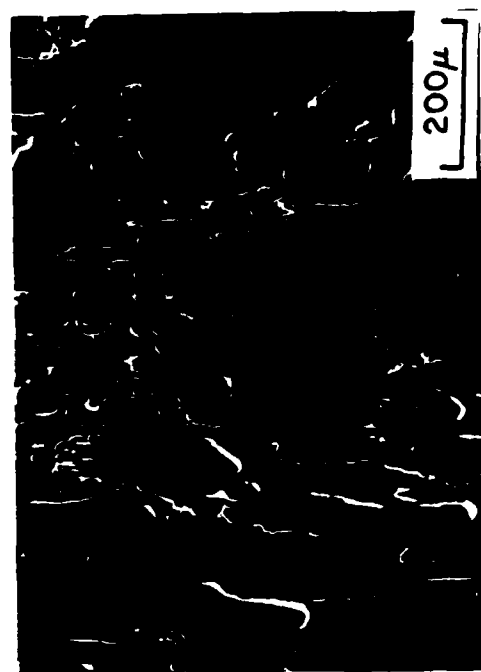


Fig. 25: SEM of wheel side of as-cast quaternary ribbon.

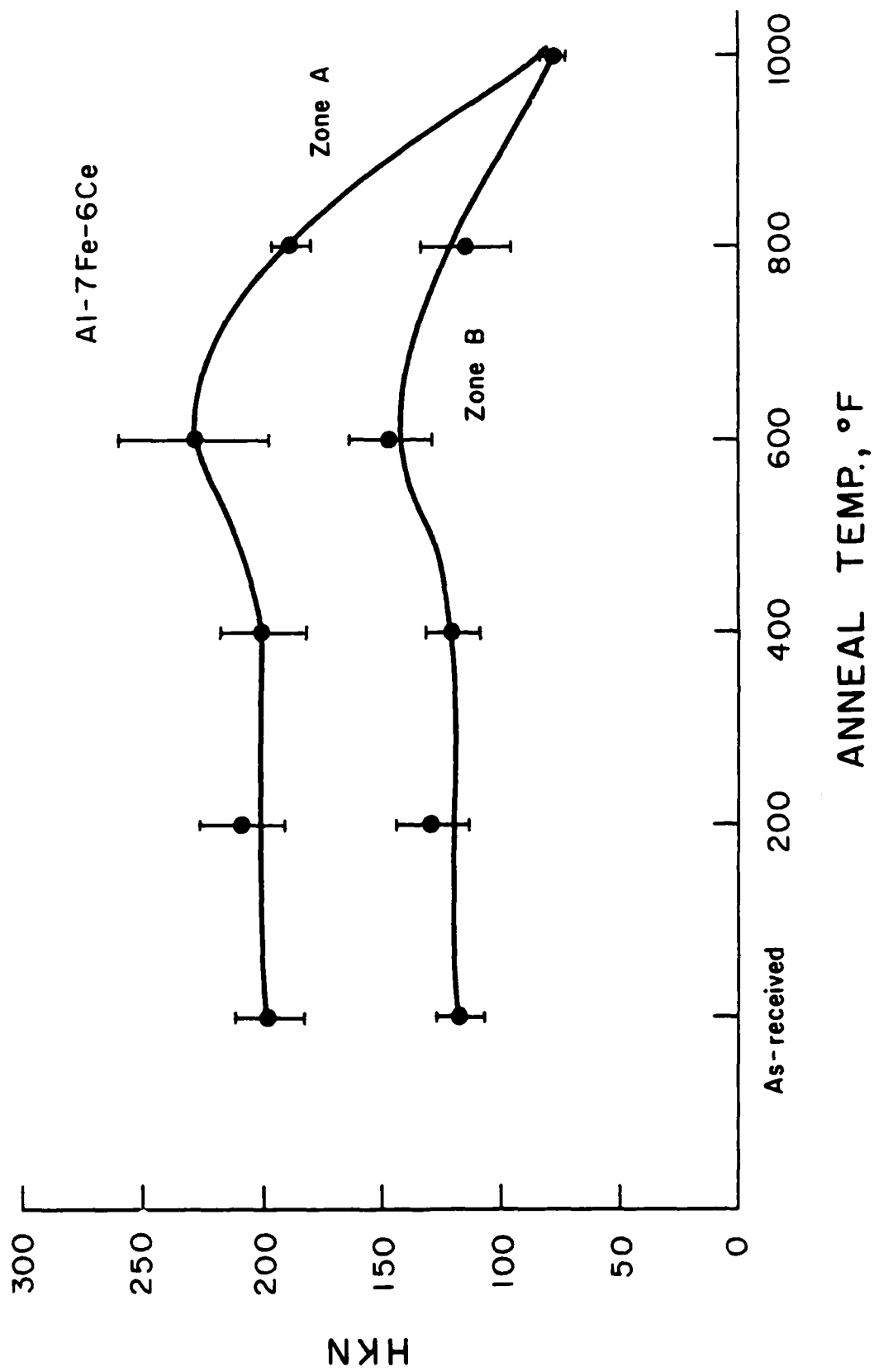


Figure 26: Microhardness curves for ternary alloy

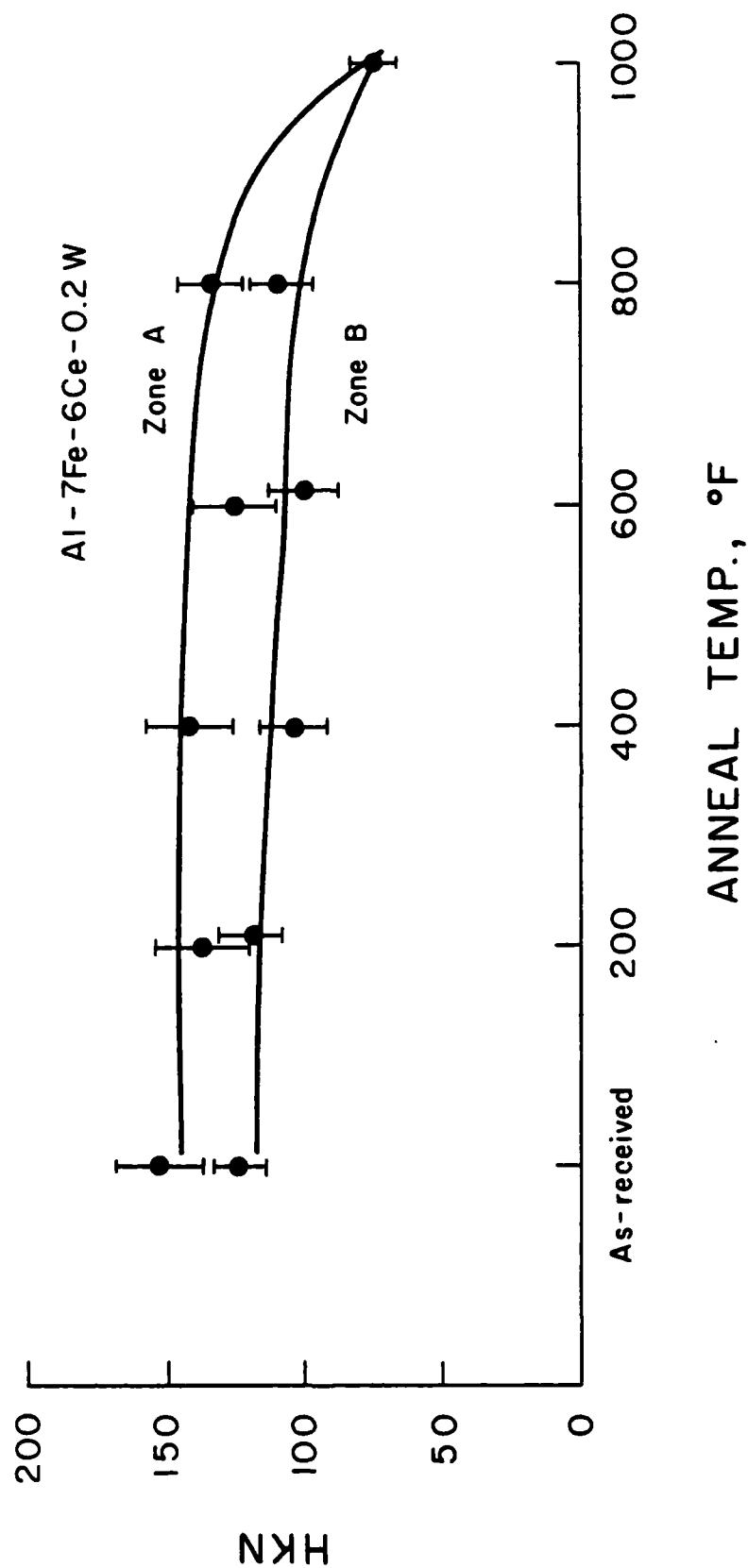


Figure 27: Microhardness curves for quaternary alloy.

1985 USAF-UES SUMMER FACULTY RESEARCH PROGRAM/
GRADUATE STUDENT SUMMER SUPPORT PROGRAM

Sponsored by the
AIR FORCE OFFICE OF SCIENTIFIC RESEARCH

Conducted by the
UNIVERSAL ENERGY SYSTEMS, INC.

FINAL REPORT

The F-15 SPO Support Equipment "Tiger Team"

Prepared by:	Patrick J. Sweeney, Ph.D. & R. Simon Insley, B.A.
Academic Rank:	Professor/Graduate Student
Department and	Engineering Management & Systems
University:	University of Dayton
Research Location:	Air Force Business Research Management Center
USAF Research:	Lt. Col. Robert Skipp
Date:	25 July 1985
Contract No:	F49620-85-C-0013

The F-15 SPO Support Equipment "Tiger Team"

by

Patrick J. Sweeney, Ph.D.
R. Simon Insley, B.A.

ABSTRACT

As a result of the news media's recent exposure of a number of "overpriced" items purchased by the government and the subsequent pressure to avoid such news stories, the F-15 System Program Office (SPO) formed a "Tiger Team" to explore alternative methods of procuring support equipment (SE). The objectives of the team were to reduce costs on support equipment, eliminate overpricing, and serve as a test for developing a methodology for determining fair prices for SE.

Using component breakout procedures and criteria of criticality, complexity, drawing availability, and prime contractor termination cost reasonability, the team selected for consideration 118 of the over 3300 F-15 SE items. These 118 were identified to be procured from other than the prime contractor. It was not possible to compute the offsetting government costs as a result of these procurements from a small disadvantaged 8(a) firm, however, the gross savings were 78 percent.

The F-15 SPO is developing a checklist that should assist in future determinations of fair SE prices.

ACKNOWLEDGEMENT

The authors wish to thank Lt. Col. Robert Skipp and Mrs. Linda McLaughlin of the Air Force Business Research Management Center at Wright-Patterson AFB, Ohio for their personal involvement and support in this effort. The cooperation of the F-15 SPO personnel from Mr. Harry Shulte, Deputy Director, to Lt. Col. Dennis Coggburn, Mrs. Pat Deschaine, and Lt. Brenda Haven was absolutely essential and graciously granted. Mrs. Peggy Conners also of the F-15 office provided most of the data and many of the leads required of this study. The assistance of these professionals is greatly appreciated.

The excellent support that the "Tiger Team" received from McDonnell-Douglas also aided the authors in this study.

We offer special thanks to Mr. Rod Darrah and his competent staff at UES who provided us what we needed when we needed it.

I. INTRODUCTION

Although overpricing by contractors of government support equipment (SE) may have existed since before Hannibal's crossing of the Alps, the fall of Troy, or Caesar's excursions into Gaul, this introduction begins with a letter from U.S. Senator William V. Roth to Deputy Defense Secretary Paul Thayer dated October 6, 1983. "...I have great difficulty in justifying proposed prices of \$9,600 for a 12 cent Allen wrench, \$900 for a \$7 cutting tool, \$1,100 for a \$5 spotface cutter pilot and \$9,800 for a \$1 spacer, even if these prices include engineering and data costs."

As reported in the Dayton (Ohio) Daily News Col. Michael Butchko, Director of the F-15 System Program Office (SPO), was faced with the problem of purchasing 350 support items from McDonnell-Douglas (McAair) at a cost of \$30 million. He formed a "Tiger Team" of six experts which identified 118 items that could be purchased quicker, cheaper, and at equal quality from an 8(a) small disadvantaged businesses instead of from McAair. As of the date of this report the F-15 Office had 35 of these items on contract and another 12 identified for one 8(a) contractor, and 15 items identified for a second 8(a) contractor.

II. OBJECTIVE

The objective of this study was to examine the F-15 SPO support equipment "Tiger Team" activity and to report on its successes, shortcomings, and lessons learned.

III. RESEARCH METHODOLOGY

The researchers accomplished a literature search and

review that was highlighted by the recent government studies, internal correspondence, news releases, and GAO reports. Next the researchers interviewed members of the F-15 SPO familiar with the "Tiger Team" activities. These people provided not only their personal perceptions but also non-classified files and data concerning the team actions.

All of the above data were studied, appropriate costs and quantities were tabulated, and the researchers developed their conclusions and recommendations.

IV. RESEARCH FINDINGS

The continuous news stories of the overpricing on government contracts sparked several congressional inquiries concerning these "horror stories". See Figure 1.

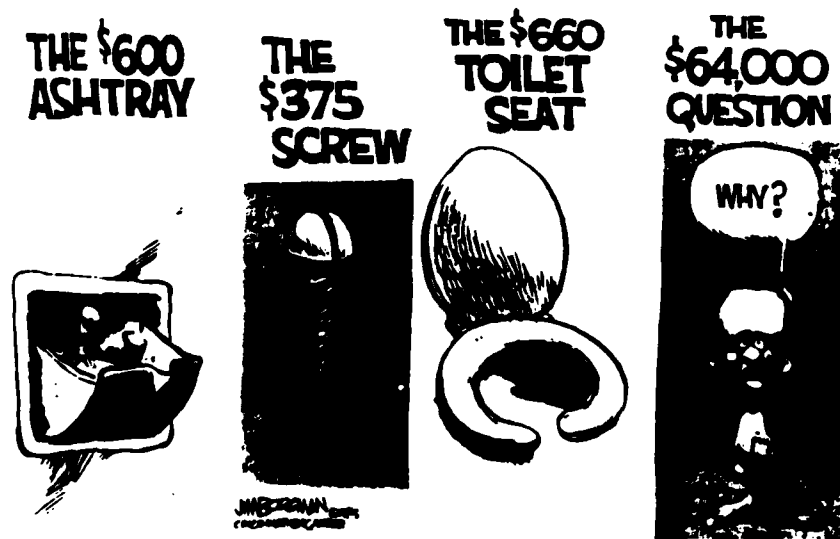


Figure 1. A cartoonist's view of government procurement.

Note: This appeared in The Dayton Daily News in June of 1985. Reprinted with special permission of King Feature Syndicate, Inc.

Embarrassing news stories are published when the

government purchases items familiar to readers at significantly higher prices than the readers might pay or think is a fair price. Taxpayers have recently read of \$7600 coffee-pots, \$660 toilet seat covers, \$435 claw hammers, and \$748 pliers. These prices are "terribly demoralizing to the American public," according to Rep. Bill Nichols (D-AL). Meg Greenfield, an editorialist wrote, "But the scandals and actual corruption that were revealed in a seemingly unending flow this year finally registered with the public and reinforced the growing displeasure being expressed by one-time Pentagon helpers on the Hill." (1) She inferred that the public has lost faith in the government defense procurement. This is unfortunate, since as stated by Asst. Defense Secretary Mary Ann Gilleece in June 1985, less than 1 percent of all DOD procurements could be categorized as overpriced. (3) However, even this small percentage when widely publicized is enough to cause the public to lose confidence in the government procurement system.

Secretary of the Navy, John Lehman, has been quite vocal about these "horror stories". To the press and in letters to company officials, Sec. Lehman has criticized the ethics of contractors. "...What we find is a pervasive corporate attitude that we find inappropriate to the public trust...Caveat emptor (buyer beware) is not a high enough standard for a defense contractor." (2) In a letter, 21 May 85, to General Dynamics Sec. Lehman ordered that a condition for future contracts would be the "establishment and enforcement of a rigorous code of ethics for all General Dynamics officers and employees with mandatory sanctions for violations." (2)

Earlier, General Marsh, AFSC Commander, in a letter dated 30 Oct 83 instructed that Air Force efforts paralleling the spare parts acquisition pricing control be taken on SE acquisition pricing. SPOs were to "Breakout for direct procurement from the manufacturer those non-complex, non-critical items where the prime contractor provides no value added."

In direct response to the General's instructions the F-15 SPO with the gracious assistance of MCAir set about acquiring non-complex SE from direct sources. In order to do this the SPO created a "Tiger Team" with the objectives of identifying and procuring non-complex SE from non-Prime contractors and to experiment in determining more accurate prices for these items. The first objective would reduce costs for the overhead from a small company would probably be less than that of a prime contractor. This objective would also reduce the probability that a F-15 "horror story" would occur. The second objective would serve as a test for future cost estimating and contracting procedures and, if successful, would also reduce the probability of future "horror stories".

The team of initially five personnel originally chartered for 90 days but eventually extended to about 180 days was not positioned to analyze the cost of the more than 3300 F-15 support equipment items. From these 3300 SE items the team selected the 350 items on current procurement lists. Then following the General's instructions selected 135 items. Evaluating these items against the criteria of drawing availability and termination costs reduced the total

number to 118. These SE items could be procured less expensively using component breakout type procedures. The final list of items to be procured by the "Tiger Team" consisted of non-complex items that could be manufactured in a typical machine shop from drawings owned by the Air Force without incurring a prime contractor termination costs exceeding 25 percent of the current item price from the prime contractor.

Probably more than 500 American companies are capable of producing these items so to get them on contract using DAR and FAR Supplement procedures for competition would have cost the SPO far more time and effort than a direct purchase from McAir. A gross savings may have resulted from this effort, however, lost opportunity costs would have been significant (More on lost opportunity costs later). An alternative which reduced the time and other costs associated with competition was to use a Small Business Administration (SBA) section 8(a) firm. Using this alternative the "Tiger Team" reduced the time commitment associated with competitive contracting and better controlled which company was awarded a contract.

The SBA identified six 8(a) firms to the "Tiger Team" and two were selected. Ver-Val Enterprises, Inc., Fort Walton Beach, Florida, the only company on contract at the outset of this effort, received an indefinite delivery-indefinite quantity contract. Wage and overhead rates were predetermined and the prices of items were to be negotiated as needed by the SPO. The contract ranges from a minimum

level of effort of \$.5 million to a maximum of \$6.5 million and extends from mid 1985 through fiscal year 1987.

The normal contracting procedures with a prime contractor and sub-contractors are shown in Figure 2. This figure shows that if the sub charges the prime \$400 (hypothetical) for an item the prime adds a pass through cost (similar to a handling charge) of \$200 (hypothetical) and bills the government \$600. This is a simple but potentially costly procedure, for there is no competition and in many cases the prime does not add value to the item only additional cost.

AIR FORCE/CONTRACTOR RELATIONSHIPS

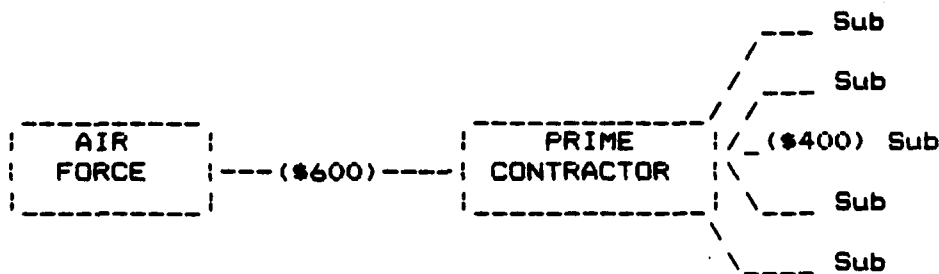


Figure 2. Typical Air Force/Prime Contractor Relationship

Figure 3 shows a similar hypothetical cost model when an 8(a) firm is introduced into the procurement process. The cost of the item is still \$400 from the subcontractor plus \$100 from the 8(a) firm for a total cost to the Air Force of \$500 for the item. It is possible that because of the 8(a) firm's typically small order quantity, the price from the sub may be higher to the 8(a) than a large prime

contractor. Figure 3 shows a savings when compared to Figure 2, however, the cost of coordination between the 8(a) and the prime is unknown. It is well known that the prime will not be assisting with this coordination without charging the Air Force for its efforts. This fee may exceed the \$100 savings in our hypothetical case. Regardless, this coordination fee will never be associated with the cost of the 8(a) procured items. This may tend to eliminate some items from the "horror story" list. However, it is more like reducing the price of a \$600 item to \$500, when in reality a fair price would have been \$300.

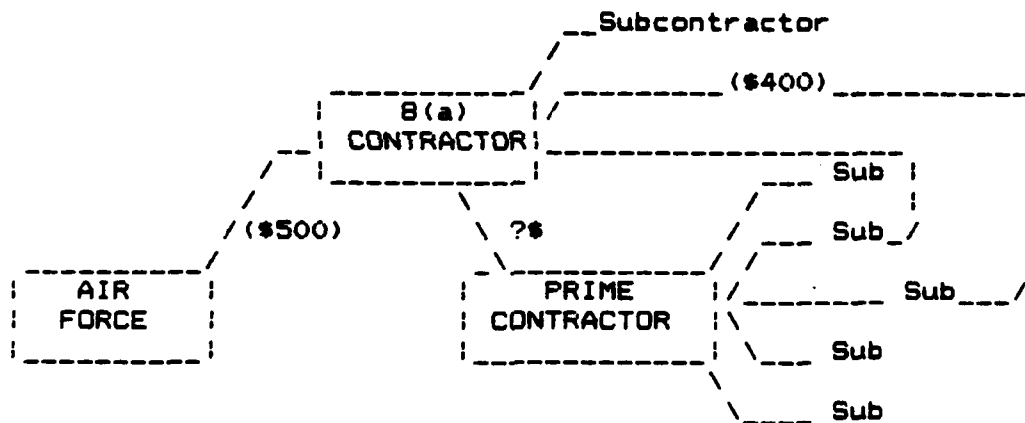


Figure 3. Typical Air Force/B(a) & Prime Contractor Relationship

At the time these data were gathered Ver-Val was on contract for delivery of 35 items. Comparing the most recent unit purchase prices paid by the Aeronautics System Division (ASD) and the negotiated price per unit from Ver-Val, the 35 items were analyzed for cost savings. (See Table 1.)

Table 1. Air Force ASD/ 8(a) Parts Price Comparison

* Assumed to include all costs to the Air Force.

**** Does not include all costs to the Air Force.**

ORD	NO.	DIV	PRICE*	SBA/MRECUR	SBA/RECUR	HIST/ORDER	SBA/ORDER	TOT SBA**	SAVING	% SAVING
24	0007		3904.00	5156.00	5800.00	936336.00	139372.00	140340.00	791700.00	84.56242
15	00177		9190.00	2500.00	2111.00	137850.00	31645.00	34245.00	103605.00	75.15701
16	00262		21080.00	3012.00	2307.00	350200.00	36912.00	39724.00	310200.00	80.59992
11	00390		9107.00	1450.00	1076.00	101057.00	20636.00	22094.00	70963.00	70.13712
5	00399		7059.00	297.00	1456.00	35295.00	7200.00	7572.00	27723.00	70.54691
0	00804		11292.00	1771.00	1932.00	90336.00	15956.00	17227.00	73109.00	80.93012
0	11392		3510.00	623.00	1377.00	20000.00	11016.00	11639.00	16441.00	50.35062
12	2442		2522.00		1010.00	30264.00	21016.00	21016.00	0440.00	27.91444
22	2405		40271.00	3733.00	6694.00	805962.00	147060.00	151001.00	734961.00	82.95632
6	2406		2054.00	1329.00	476.00	17126.00	2056.00	4105.00	12939.00	75.56062
2	2722		2266.00	1503.00	2009.00	4532.00	4170.00	5601.00	-1149.00	-25.35302
3	2962		3724.00	671.00	627.00	11172.00	1001.00	2552.00	0620.00	77.15722
0	2989		1626.00	430.00	340.00	13000.00	2720.00	3154.00	9054.00	75.75342
6	3112		4766.00	1007.00	972.00	20596.00	5032.00	7639.00	20937.00	73.20632
27	3247		10294.00	8670.00	7499.00	493930.00	202073.00	211103.00	202795.00	57.25312
5	3546		1517.00	505.00	640.00	7505.00	3240.00	3005.00	3700.00	49.03522
2	3669		12743.00	2052.00	6972.00	25006.00	13944.00	15996.00	9490.00	37.23612
5	3715		737.00	029.00	751.00	3915.00	3755.00	4504.00	-645.00	-17.00012
3	3790		8058.00	039.00	5535.00	20574.00	16405.00	17464.00	3110.00	15.11622
16	00004		4534.00	500.00	3491.00	72544.00	55056.00	56416.00	16120.00	22.23202
16	0123		2904.00	500.00	3267.00	46464.00	52272.00	52032.00	-6340.00	-13.70522
16	0124		3006.00	500.00	3977.00	60096.00	63032.00	64192.00	-3290.00	-5.41252
25	2113		3041.00	1359.00	677.00	76025.00	16925.00	10264.00	57761.00	75.97632
16	0751		3150.00	500.00	2376.00	50400.00	30016.00	30576.00	11024.00	23.46032
16	0752		1616.00	500.00	1473.00	25056.00	23560.00	24120.00	1720.00	6.60322
16	0766		1996.00	500.00	1721.00	31936.00	27536.00	20096.00	3040.00	12.02402
16	0767		769.00	330.00	300.00	12304.00	6200.00	6530.00	5766.00	46.06202
16	0768		2250.00	500.00	2305.00	36000.00	30160.00	30720.00	-2720.00	-7.55562
16	0769		3649.00	559.00	3047.00	50300.00	40752.00	49311.00	9073.00	15.50022
13	2306		2306.00	599.00	1997.00	29970.00	23561.00	23910.00	6000.00	20.24152
4	0961		1030.00	416.00	952.00	4120.00	3000.00	4224.00	-104.00	-2.52452
37	0995		15100.00	4735.00	1257.00	560920.00	46509.00	51234.00	509600.00	90.06612
20	09506		90865.00	22455.00	5285.00	1097300.00	105700.00	120135.00	1769165.00	93.74652
7	0627		165.00	1777.00	2431.00	1155.00	17017.00	10794.00	-17639.00	>>&

This showed a 78% gross savings as the former ASD cost would have been \$6.3 million whereas the Ver-Val procurement amounted to only \$1.3 million. This is significant, however, the researchers were unable to find any data that indicated that the SPO had ever determined a fair price for these items by any government analysis. Items were submitted to Ver-Val for price quotes and if these prices were less than had been paid by ASD, the team accepted the Ver-Val quote.

The above very significant savings does not include the offsetting costs to the AF associated with this effort. The "Tiger Team" consisted of five people at least 1/2 time for 180 days. Many trips to potential 8(a) sites were required to evaluate and qualify the 8(a) firms. Other costs include the expenses of personnel from TAEE, TAFK, DCAS, DCSMAS in Alabama, SBA, the NAVPRO and McAir. No costs have even been estimated for managing the SE after delivery, a function previously accomplished by McAir.

An AFIT Masters Thesis by Johnson and Molina identified and prioritized by cost a listing of 14 offsetting cost categories, see Table 2.

A number of references indicate that an analysis of each cost should be accomplished in order to estimate the magnitude of these costs and their effect upon the actual savings. These references further state that methodologies and guidelines are not currently available for accomplishing

these estimates accurately. Thus computation of these offsetting costs for the 35 items under contract with Ver-Val was not possible.

SUMMARY OF EXPERT "IMPORTANCE" RANKINGS

Rank	Offsetting Costs
1	Manpower (for component breakout team)
2	Reprocurement Costs
3	Data
4	Equipment/Tooling
5	Technical Reviews
6	Out-of-Station Costs
7	Partial Termination of Prime Contractor
8	Air Force Overhead
9	Special Air Force Requirements
10	Air Force General & Administrative (G&A)
11	Contract Administration & Audit Personnel
12	Transportation/Distribution
13	Storage
14	Security

Table 2. Offsetting Costs in Priority.

To have the highest probability of saving the greatest amount for the government, cost cutters should concentrate on the big dollar items. The greatest dollar savings will likely occur where the most is spent. However, concentrating in the support equipment area in hopes of reducing costs is accomplished at the expense of working in the high dollar value areas like engine parts, avionics, etc. This choice is accomplished at an expense termed lost opportunity cost---what could possibly be saved if the amount of effort exerted in SE were devoted to the high dollar items. See Figure 4 for a typical comparison of the SE costs when compared to total weapon system costs.

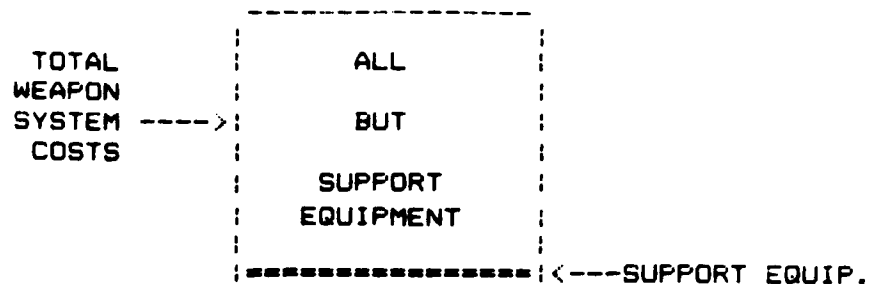


Figure 4. SE Costs and Total Weapon System Costs

A further division of these SE items typically indicates that the prime contractor is procuring about 88% of the total SE dollar amount. Of the remaining, approximately 10% is contracted to 8(a) firms and 2% is bought directly from the manufacturer, see Figure 5.

Based upon the pricing structure recommended in the 1983 AFMAG study on spare parts acquisition, the F-15 SPO is using a number of initiatives to attack overpricing problems in both the short and long term. A particularly interesting ASD initiative directs that total item cost be proportioned into recurring, non-recurring and pass through costs. Each cost is to appear as a separate contract line item number (CLIN). The recurring cost includes labor, materials, parts, and production costs. Non-recurring costs is traditionally tied to the cost of the first item and consists of the engineering design, data and initial test costs. Pass through cost is the cost added by a higher-tiered contractor to a purchased item without physically altering it material-

ly or functionally. This method is referred to as the 3 CLIN structure in a 9 January 85 ASD letter.

SUPPORT EQUIPMENT DISTRIBUTION

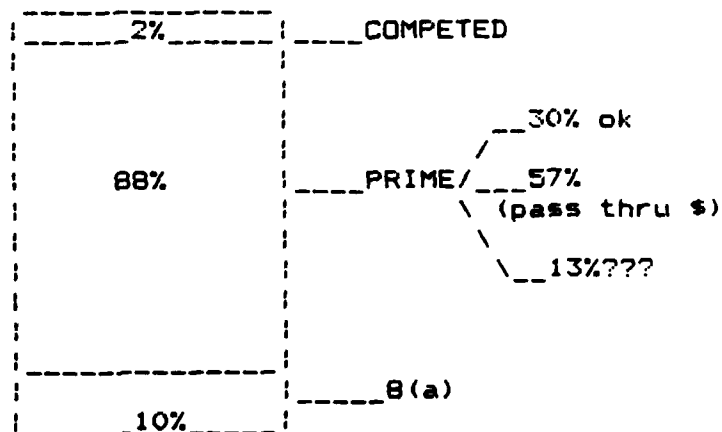


Figure 5. Typical Support Equipment Distribution.

Previous reports that evaluated several prime contractors' costs based upon this 3 CLIN structure revealed a general picture of SE pricing. Only 30% of the items evaluated had acceptable pricing. Another 57% were questionable in terms of pass through costs and would require more in-depth study to determine acceptability. The last 13% appeared to have inherent serious and unexplained pricing discrepancies, see Figure 5.

The Air Force is well aware of its duty to spend taxpayers' money wisely and many studies have proposed solutions to overpricing. Congress also has a responsibility in this area and has tried to help by legislating more and more constraints. Much of this legislation has succeeded in virtually slowing the procurement process to a snail's pace

within the SPO environment. The SPO cannot simultaneously implement all of the recommendations of the studies, the government regulations, and still procure SE for the weapon systems in an efficient manner---there are neither time nor personnel available to do this.

V. CONCLUSIONS AND RECOMMENDATIONS

a. Successes

This was a laudable experiment in cost savings as the gross savings amounted to 78% or nearly \$5 million from a potential \$6.2 million procurement.

The utilization of the SBA 8(a) firm serves a major goal of the U. S. government in supporting economically and socially disadvantaged businesses. However, the SPO utilized the 8(a) because of the ease of contracting when compared to all other available options not because of cost savings.

The 3 CLIN structure more truly reflects actual costs for support equipment items and should reduce the number of "horror stories" in the future, but it may not eliminate them.

b. Failures

The use of 8(a) firms did not increase competition, for only a single firm was ask to quote on each SE item. Apparently it is not possible to develop competition among 8(a) firms due to current procurement law.

The lost opportunity costs may have exceeded the savings reported in this study. If cost savings is the objective, it makes little sense trying to save dollars in the small dollar area of SE at the expense of ignoring the potential large savings associated with the much more costly items.

Although the prices by Ver-Val were considerably lower than from the prime contractor, there is no evidence that the SPO or anyone else for that matter ever computed a fair price for the items under contract with Ver-Val.

Since only 118 of the over 3300 support items were identified by the team for non-prime contractor procurement, nearly 3200 items have not been reviewed and are potentially new "horror stories."

c. Lessons Learned

The "Tiger Team" concept works very well when the mission is well defined, the team is well led, the priority for the work is high, and the task can be accomplished in a relatively short time.

The researchers were impressed with the knowledge, dedication, and professionalism of the Air Force personnel interviewed during this study. The procurement operation is in good hands if these ASD people are typical of all their contemporaries throughout the Air Force.

The Congress continues to legislate new procurement law and the quantity, unfortunately, seems to be a

function of the pressure applied by the press and subsequently the public. Recent legislation has slowed the procurement process at ASD to a crawl. More legislation is probably not the solution to fair prices for government procurements.

d. Recommendations

Transitioning (PMRT) support equipment to AFLC as early as possible in the weapon system development process will lead to lower prices as AFLC is better staffed and has more experience in this type of competition than ASD or AFSC. PMRT should be accomplished early in the weapon system development process. The F-15 SPO has altered a previous policy and is attempting to transition items at an increasing rate.

The use of the 8(a) firms would be greatly increased if there were a well staffed central SBA 8(a) office at ASD for SPO support. This office should have a significant list of 8(a) firms that are qualified, ready, and able to support the weapon system acquisition process when they are needed. The "Tiger Team" expended quite an effort in selecting the two 8(a) firms and negotiating rates.

The identification of the 4950th Test Wing as a source of procuring items highlights the fact that the government has a great number of manufacturing operations that in some cases may be less expensive than a prime contractor. These facilities should be used when economically

feasible.

The "horror stories" must be eliminated for they destroy the confidence of the public in government procurement and as noted recently, can significantly affect the Defense Department Budget in a negative manner. Rather than screening all non-complex items for cost abuses, it may be more prudent to review only those items familiar to the public who can identify and relate costs to their personal experience.

It was impossible to compute the offsetting costs due to the lack of guidelines, data, and time. However, the termination costs of the 35 contracted items exceeded \$300,000, thus it is highly likely that the offsetting costs are significant. Offsetting cost computing guidelines and methodologies should be developed.

Selected Bibliography

AeroSpace Daily. Jan 1985 to June 1985.

Air Force Management Analysis Group. "Spare Parts Acquisition," Defense Logistics Agency. 1983.

(3) Dayton Daily News. June 1985.

(2) Federal Contracts Report. Jan 1985 to June 1985.

General Accounting Office. "Air Force Breakout Efforts Are Ineffective." GOA/PLRD-83-82. B-208191. June 1983.

Johnson, Lieutenant Kathryn M. USAF and Captain Joseph R. Molina USAF. "Identification and Importance of Offsetting Costs in Component Breakout." Unpublished master's thesis. AFIT/GLM/LSM/85S-31. September 1984.

(1) Newsweek. May and June issues.

Support Equipment Acquisition Review Group, Final Report. Air Force Systems Command. July 1984.

Time. May and June issues.

Zamperelli, Captain Steven J. USAF. "Competition in the Acquisition of Replenishment of Spare Parts." Unpublished master's thesis. AFIT/LSSR 102-83. September 1983.

Personal Interviews

Lieutenant Colonel Dennis Cogburn, ASD/YZK

Mrs. Peggy Conners, Contract Negotiator, Tiger team member, TAFK

Mrs. Patricia Deschaine, Small Disadvantaged Business Office PMWA

Mr. Fred MacLeod, Program Manager Support Equipment, Tiger leader, TAFH

Mr. Harry Schulte, Deputy Director, F-15 SPO.

1985 USAF-UES SUMMER FACULTY RESEARCH PROGRAM/
GRADUATE STUDENT SUMMER SUPPORT PROGRAM

Sponsored by the
AIR FORCE OFFICE OF SCIENTIFIC RESEARCH
Conducted by the
UNIVERSAL ENERGY SYSTEMS, INC.

FINAL REPORT

STUDIES IN HOLOGRAPHIC PROCEDURES

Prepared by:	Charles E Taylor
Academic Rank:	Professor
Department and	Department of Engineering Sciences
University:	University of Florida
Research Location:	Air Force Armament Laboratory, DLM/DLMI
USAF Research:	Steven Butler
Date:	31 July 1985
Contract No:	F49620-85-C-0013

STUDIES IN HOLOGRAPHIC PROCEDURES

by

Charles E. Taylor

ABSTRACT

The use of dichromated gelatins has many advantages for recording holograms, especially when it is necessary to optimize the efficiency of the process. John Lushetsky, under my general supervision, conducted studies which are described in detail in his report.

James Sirkis conducted studies on the use of fiber optics as strain sensors. The feasibility had been established previously and the purpose of the continued work was to develop the necessary recording instrumentation. The latter will be included in his report.

In addition, I developed some display holograms to emphasize the potential of the method. Particular attention was given to recording multiple holograms on a single plate.

ACKNOWLEDGMENTS:

This work was conducted under the sponsorship of the Air Force Systems Command, Air Force Office of Scientific Research and the Air Force Armament Laboratory. The help and advice of Mr. Steven F. Butler is gratefully acknowledged.

I. INTRODUCTION: For the Advance Sensor group in the Armament Laboratory, it is of paramount importance to optimized the signal-to-noise ratio in the images which must be interpreted. For this purpose matched holographic filtering is used and it is highly desirable to used the full dynamic range of the recording media available. Extensive studies have indicated that dichromated gelatin have the best combination of properties for recording such holograms. The work conducted by John Lushetsky addressed that general problem.

Another area of interest, originally suggested to me by members of the Armament Laboratory, was the use of fiber optics as strain sensors. Since modern composite materials include elements very similar to the fibers used in fiber optics, it was thought that conceptually it may be possible to use part of the structure itself to monitor highly stresses areas or possibly damaged areas. Tests have confirmed that fiber optical elements can indeed be used to measure strain. However, it was necessary to develop associated instrumentation in order to make the method practical. James Sirkis spent some of his time during the summer to make a first step toward the development of the sensing, recording, and interpreting instruments. A brief description will be included in his report

Although I have used holography for several years as a means to study stresses in solids, my main effort has been to interpret the meaning of the fringes for various setups for holographic interferometry. Use of the linear region of commercially available films was never a serious limitation. Work with the

Advanced Sensor group was useful in broadening my background. My background in mechanics was of less direct use, because the local interest was in identifying whether a given object was a tank or a non-interesting target, and there was no interest in determining the strain in the tank. It is hoped that my general background in optical methods of stress analysis had some beneficial effects.

Some of my time was spent in making display holograms. One purpose was to explain the advantages of holography to a typical person not familiar with the methods. Several such holograms were made, and the procedures for recording more than one hologram on the same plate were investigated with some success.

II. OBJECTIVES OF THE RESEARCH EFFORT: The objectives in all cases was to learn what has been done by previous members of the Laboratory, conduct additional experiments, and to seek ways to improve the results.

III. RECOMMENDATIONS :

- A. Studies with dichromated gelatin involve the chemistry of the gells, temperatures and processing times. Specific recommendations are included in the report by John Lushetsky.
- B. The instrumentation for the fiber optic sensors is still being tested. James Sirkis will make recommendations after his tests are complete.
- C. Placing several holograms on a single plate is not a new idea. It was shown possible to provide additional effectiveness in emphasizing the power and versatility of holography.

1985 USAF-UES SUMMER FACULTY RESEARCH PROGRAM/
GRADUATE STUDENT SUMMER SUPPORT PROGRAM

Sponsored by the
AIR FORCE OFFICE OF SCIENTIFIC RESEARCH

Conducted by the
UNIVERSAL ENERGY SYSTEMS, INC.

FINAL REPORT

DYNAMIC STRESS ANALYSIS OF LAYERED STRUCTURES

Prepared by:	Joseph W. Tedesco
Academic Rank:	Assistant Professor
Department and University:	Department of Civil Engineering Auburn University
Research Location:	HQ AFESC/RDCS Tyndall AFB Panama City, Florida
USAF Research:	LDCR. Tom Hilferty Mr. Jack Hayes
Date:	September 1985
Contractor No.:	F49620-85-C-0013

DYNAMIC STRESS ANALYSIS OF LAYERED STRUCTURES

by

Joseph W. Tedesco

ABSTRACT

Protective military structures are typically constructed of massive, monolithic reinforced concrete slabs. This practice is considered necessary in order to protect personnel and/or vital equipment within the structure from the harmful effects of conventional weaponry. Recent studies have indicated, however, that "layered structures" may provide a viable alternative to conventionally hardened structures in certain environments.

This report presents the results of a finite element method (FEM) analysis of blast loading on layered structures. The results of this study indicate that layered structures are a viable alternative to conventional designs of hardened or semi-hardened facilities. However, due to the limited scope of this study, a follow-up, more comprehensive numerical analysis is recommended.

ACKNOWLEDGEMENTS

The author would like to express his appreciation to the Research Engineering Division, Research Directorate, U. S. Air Force Engineering and Services Center, Tyndall AFB, Florida for the hospitality during his stay as a summer fellow. Special thanks are due to LDCR. Tom Hilferty, Mr. Jack Hayes, and Dr. Paul Thompson for their assistances and fruitful discussions.

Appreciation is also extended to the Air Force System Command, Air Force Office of Scientific Research for sponsoring the program and providing such a unique opportunity.

SECTION I
INTRODUCTION

The author is an Assistant Professor of Civil Engineering at Auburn University. He received his B.S. degree in Civil Engineering from the University of Notre Dame; his M.S. degree in Structural Engineering from Tufts University; and his Ph.D. in Structural Engineering from Lehigh University. Prior to his M.S. study, the author worked as a design engineer at Souza and True, Inc., Consulting Engineers. After his M.S. study and prior to his Ph.D. study, the author worked as a senior engineer at United Engineers and Constructors Inc. His research interest has primarily been focused on the dynamic response of structures, with special emphasis on finite element analysis. The author has published articles in various topics such as marine pipeline stability, vibrational characteristics and seismic analysis of liquid storage tanks, and nonlinear dynamic analysis of concrete armor units. Currently the author serves on one technical committee, A.S.C.E. Technical Committee for Computing Practices, Software Verification Committee.

The author performed the attached study at the Air Base Survivability Branch, Research Engineering Division of U. S. Air Force Engineering and Services Center, Tyndall AFB. One of the Branch's objectives is to identify new and improved structural systems for protective shelters to withstand the destructive effects of non-nuclear weaponry. In order to achieve this end, an understanding of the dynamic response mechanisms of newly proposed structural systems is required.

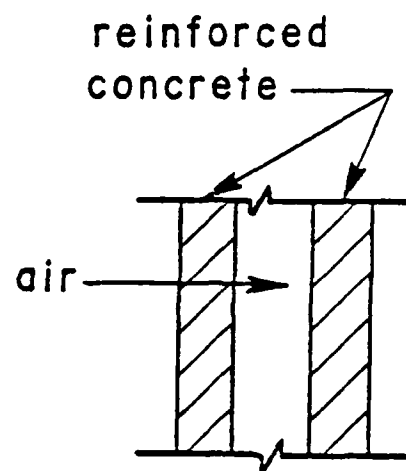
SECTION II

OBJECTIVES

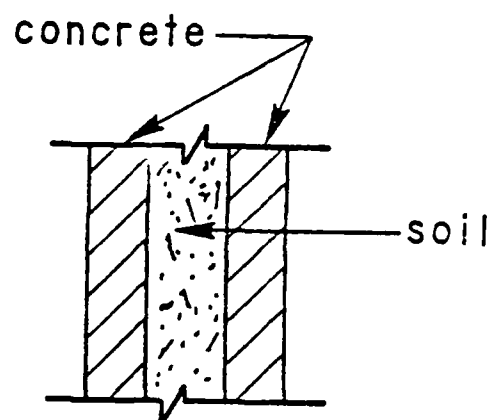
Protective military structures are designed to house vital functions and/or equipment of extreme value. Consequently, survivability takes precedence over appearance and the structures are usually massive, with soil and concrete the main building materials. Damage to protective shelters resulting from non-nuclear weapons occurs as a result of one or more of the following effects: penetration, fragmentation, ground shock, and blast (Ref. 6 and 8). In this study, only the effects of blast are considered.

Conventional protective structures are invariably constructed of massive, monolithic concrete slabs. This practice is considered necessary in order to protect the personnel and/or equipment within the structure from the harmful effects of overpressure and interior spalling of the concrete walls. Recent studies (Ref. 1, 7) however, have indicated that, in certain situations, "layered structures" may provide a viable alternative to conventionally hardened structures. (Typical details of several types of layered structures are illustrated in Fig. 1). The intent of the proposed study is to examine the effectiveness of various layered structures for protective shelters.

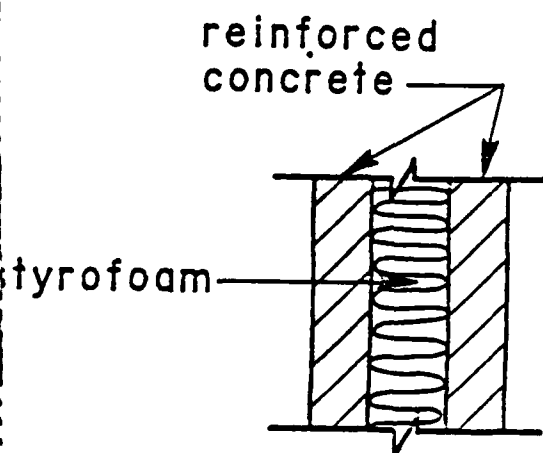
The use of layered structures in the building industry of the civilian sector is well established (Ref. 3, 9, 12, and 13). However, applications of layered structures for protective military shelters have received little attention. The primary objective of the proposed research is to evaluate the effectiveness of layered structures to resist blast from conventional weapons. Of primary concern in this study is the



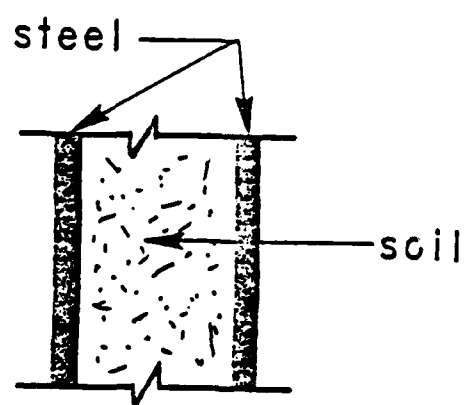
a) Type I



b) Type II



c) Type III



d) Type IV

Fig. 1. Details of layered structures

assessment of the capability of a layered structure to substantially reduce or eliminate the incidence of interior spalling of the concrete walls.

Current procedures to minimize spalling in protective shelters include (Ref. 4), (a) the construction of earth berms on the exterior face of the shelter walls, (b) the installation of steel spall plates on the interior face of the shelter walls, and (c) increase the total wall thickness. All three methods exhibited some degree of effectiveness in reducing or eliminating spalling of the interior wall, with earth berms being the most effective, and increasing the wall thickness being the least effective. The results of this study will show layered structures to be a viable alternative for reducing and/or eliminating spalling.

SECTION III

DESCRIPTION OF STUDY

As was previously stated in Section II of this report, the emphasis of this study is focused on reducing or eliminating spalling of the interior walls of protective shelters by implementing a layered structure concept. Spalling is defined (Ref. 14) as fracturing caused when a high intensity transient stress wave reflects from a free surface. In the specific case of a blast, the compressive longitudinal wave strikes the exterior surface of the wall and is transmitted through the wall until it reaches a free surface (the interior face of the wall). At this instant, continuity of stress and continuity of particle velocity will be preserved only if the wave is reflected as a tensile longitudinal wave of equal strength. It is this reflected tensile wave which causes the concrete to spall at the interior face.

When a plane elastic wave strikes a plane interface between two dissimilar materials, the interaction is regulated by the following boundary condition (Ref. 15):

$$(\sigma_I)_1 + (\sigma_R)_1 = (\sigma_T)_2 \quad (1)$$

where $(\sigma_I)_1$ and $(\sigma_R)_1$ are the instantaneous values of stress for the incident and reflected wave in medium one, respectively, and $(\sigma_T)_2$ is the instantaneous value of stress for the transmitted wave in medium two.

The fundamental equations governing the portioning of stress at an abrupt change in media are given by (Ref. 11):

$$(\sigma_T)_2 = [2\rho_2 c_2 / (\rho_2 c_2 + \rho_1 c_1)] (\sigma_I)_1 \quad (2)$$

and

$$(\sigma_R)_1 = [(\rho_2 c_2 - \rho_1 c_1) / (\rho_2 c_2 + \rho_1 c_1)] (\sigma_I)_1 \quad (3)$$

where ρ and c are the mass density of the material and velocity of propagation of the wave, respectively; the subscripts 1 and 2 denote the two different mediums. From Eqs. (2) and (3), the ratio of transmitted to reflected stress is given by:

$$(\sigma_T)_2 / (\sigma_R)_1 = 2\rho_2 c_2 / (\rho_2 c_2 - \rho_1 c_1) \quad (4)$$

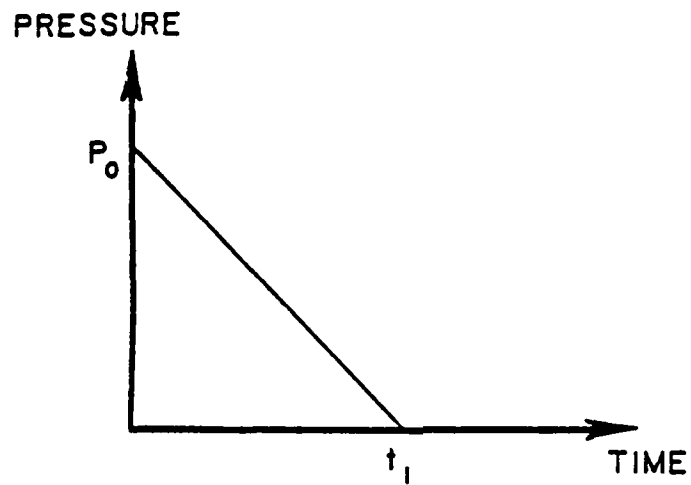
A number of important conclusions can be drawn from Eqs. (2), (3), and (4). When the two products $\rho_1 c_1$ and $\rho_2 c_2$ are equal, the ratio σ_R / σ_I is zero, and there is no reflected wave. The incident wave is transmitted at full intensity such as when the material is identical on both sides of the boundary. When $\rho_1 c_1 < \rho_2 c_2$ the ratio σ_R / σ_I is positive; implying that if σ_I is originally a compressive wave, the reflected wave will also be compressive. When $\rho_1 c_1 > \rho_2 c_2$ compressive waves will be reflected as tensions waves, and vice versa. When $\rho_2 c_2$ is zero, the condition for a free surface, $(\sigma_R)_1 = -(\sigma_I)_1$, a compressive wave is reflected at full stress level as a tension wave, and vice versa. The transmitted stress (Eq. 2) will always have the same sign as the incident stress, compression resulting in compression and tension in tension. For $\rho_1 c_1 < \rho_2 c_2$, σ_R is tension $\sigma_T < \sigma_I$; for $\rho_1 c_1 > \rho_2 c_2$, σ_R is compression and $\sigma_T > \sigma_I$.

In the present study, a finite element method (FEM) parametric study has been conducted to evaluate the effectiveness of a "layered structure" to reduce or minimize the reflected tensile wave at the interior surface of a shelter wall. The structure considered for this

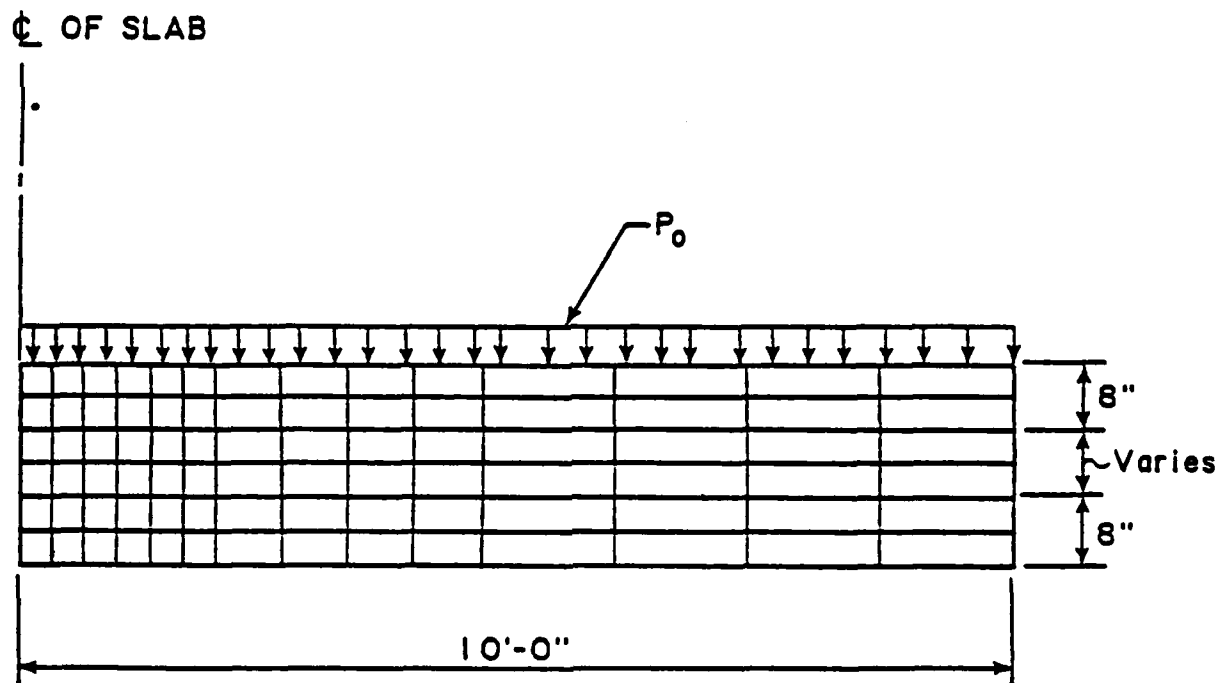
study is a twenty foot diameter circular wall of variable thickness subject to a uniform dynamic pressure (Fig. 2b). The load history for the dynamic pressure is given in Fig. 2a. The maximum value of the dynamic pressure, P_0 , is 2500 psi and the duration of the load, t_1 , is one millisecond (10^{-3} sec).

Four different FEM models were analyzed in this study (Fig. 3). Each model consisted of an outer layer (layer 3) and inner layer (layer 1) of concrete having a thickness of eight inches, modulus of elasticity of 3200.0 ksi, mass density of $0.000225 \text{ lb-sec}^2/\text{in}^4$; and Poisson's ratio of 0.18. The thickness of the inner layer (layer 2) varied for each model. The thickness of the inner layer was eight inches, sixteen inches, twenty-four inches, and thirty-two inches for Model 1, Model 2, Model 3, and Model 4, respectively. The material properties and mass densities of the intermediate layers were also varied. The thickness and material property parameters for the intermediate layer (layer 2) for each model are summarized in Table 1.

The FEM analyses were conducted through implementation of the ABAQUS computer programs. Each model was comprised of eighty-four CAX8 axis-symmetric elements. Since the analyses were dynamic in nature, the solutions of the governing differential equations were obtained by direct numerical integration. Dynamic integration operators are broadly classified as implicit or explicit. Explicit schemes obtain values for dynamic quantities at $t + \Delta t$, based entirely on available values at time t . This places an upper bound on the time step size in order to maintain numerical stability. Implicit schemes remove the upper bound on time step size by solving for dynamic quantities at time $t + \Delta t$ based not only at t , but also on these same quantities at $t + \Delta t$. For this study, the

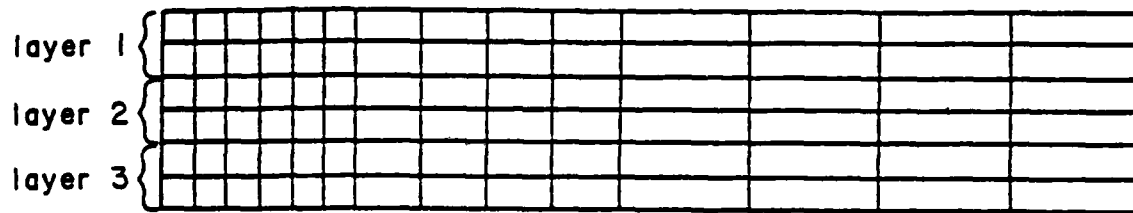


a) Load History

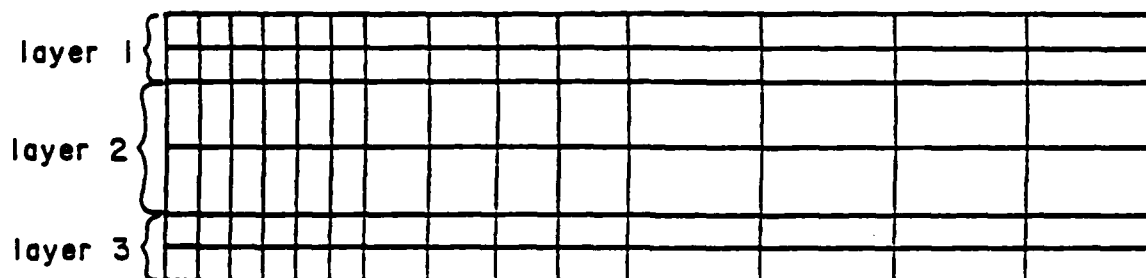


b) Loading Configuration

Fig. 2. Layered structure and load history

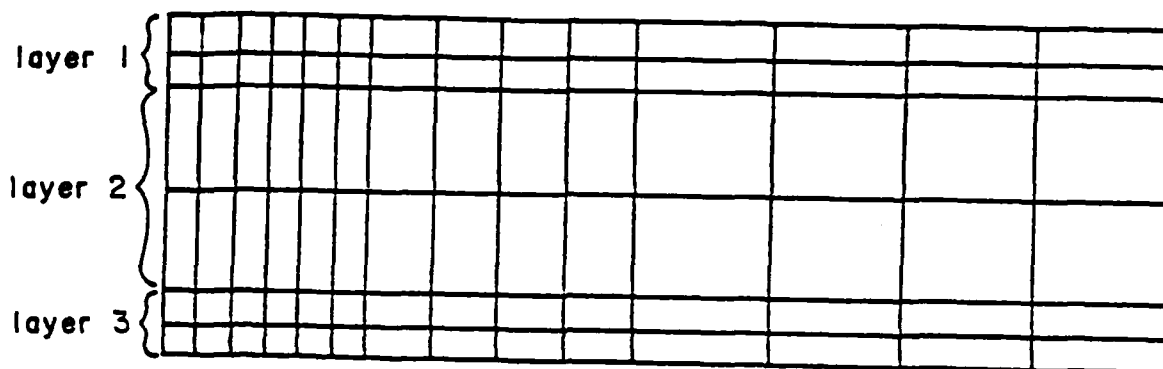


a) Model 1

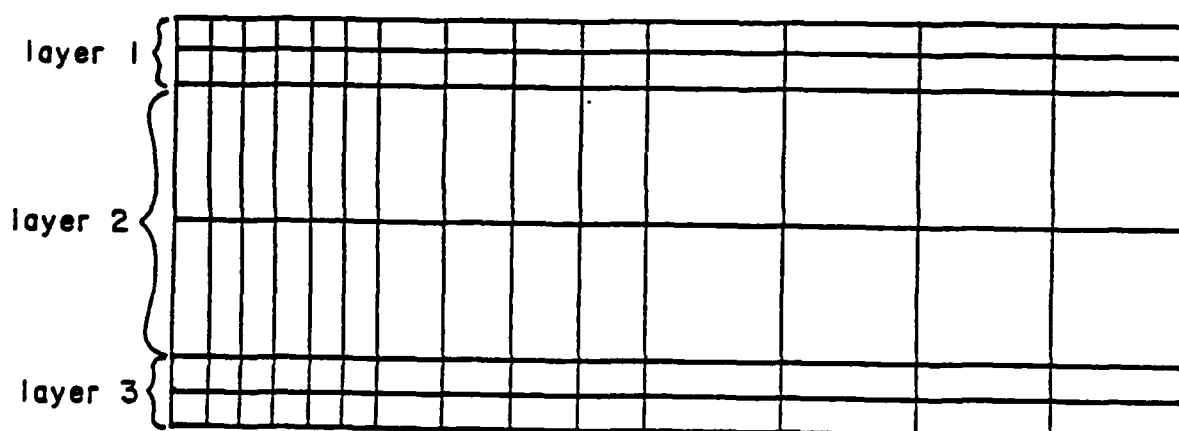


b) Model 2

Fig. 3. FEM Models



c) Model 3



d) Model 4

Fig. 3. (continued)

Model	Thickness (in) (layer 2)	Modulus of Elasticity, E (ksi)	Mass Density, ρ (lbs-sec ² /in ⁴)	Poisson's Ratio ν
1	8	3200.0*	.000225**	0.18*
	8	1600.0**	.000225**	0.18**
	8	800.0***	.0001175***	0.36***
2	16	1600.0	.000225	0.18
	16	800.0	.0001175	0.36
3	24	1600.0	.000225	0.18
	24	800.0	.0001175	0.36
4	32	1600.0	.000225	0.18
	32	800.0	.0001175	0.36

* material 1
 ** material 2
 *** material 3

Table 1. Dimensions and material properties for FEM models

Hilber-Hughes (Ref. 2, 10) implicit operator was used for time integration. The time step used in each analysis was 1×10^{-5} sec.

SECTION IV

RESULTS OF STUDY

The results of the analyses are summarized in Table 2. The stresses presented in Table 2 are the maximum values of the reflected tensile stresses at the inside surface (layer 3) of the wall. From these results it is apparent that increasing the wall thickness and changing the material characteristics of the middle layer (layer 2), significantly effect the maximum value of reflected tensile stress.

It is apparent that the reflected tensile stresses cannot be totally eliminated, however, they can be reduced to a level which is below the spall threshold level of concrete. In this manner, the incidence of spall can be reduced to an acceptable level or eliminated completely.

The results of this study indicate that layered structures are a viable alternative, at least in terms of reducing or eliminating interior concrete spalling, to conventional designs of hardened or semi-hardened facilities. However, due to the limited scope of this study, no general design recommendations for layered structures to resist blast effects from non-nuclear weaponry can be proposed.

Model	Material 1*	Material 2*	Material 3*
1	1250	1100	900
2	----	700	600
3	----	475	300
4	----	95	----

. All stresses in psi

* refer to Table 1 for material properties

Table 2. Summary of reflected tensile stresses
at inner surface of wall

SECTION V
RECOMMENDATIONS

Structural designs for protective military structures have essentially not changed over the past 40 years. The majority of protective shelters are constructed of massive, monolithic, cast-in-place concrete slabs. This type of construction may not always be the best alternative, either in terms of safety or economy, or both.

The concept of a layered structure was presented and analyzed in this report. The results of the analyses indicate that layered structures are potentially a viable alternative in the construction of hardened or semi-hardened facilities. Although encouraging, the results of the present study are by no means conclusive. Additional studies in this area are required.

It is recommended that a comprehensive analytical investigation be conducted on several types of layered structures (such as those illustrated in Fig. 1) in order to develop an understanding of the dynamic response mechanisms and investigate the effectiveness of layered structures to resist blast from conventional weapons. It is further recommended that a follow-up experimental study be conducted, either in a laboratory or in the field, to confirm the results of the proposed analytical investigation.

REFERENCES

1. Balags, P. and Vretblad, B., Model Tests on Composite Slabs of Light Gauge Metal and Concrete Subjected to Blast Loading, Proceedings of the Second Symposium on the Interaction of Nonnuclear Munitions with Structures, Panama City Beach, FL, April 15-18, 1985, pp. 143-148.
2. Belytschko, T., "A Survey of Numerical Methods and Computer Programs for Dynamic Structural Analysis", Nuclear Engineering and Design, Vol. 37, 1976, pp. 23-34.
3. Chong, K. P., Wang, K. A., and Griffith, G. R., "Analysis of Continuous Sandwich Panels in Building Systems", Building and Environment, Vol. 44, 1979, pp. 125-130.
4. Colthorp, D. R., Kiger, S. A., Vitayaudom, K. P., and Hilferty, T. J., "Blast Response Tests of Reinforced Concrete Box Structures", Proceedings of the Second Symposium on the Interaction of Non-Nuclear Munitions with Structures, Panama City Beach, Florida, April 15-18, 1985, pp. 95-100.
5. Colthorp, D. R., Vitayaudom, K. P., and Kiger, S. A. NATO Semihardened Facility Design Criteria Improvement, Final Report, Air Force Engineering and Services Center, Tyndall Air Force Base, Florida, June 1985.
6. Crawford, Robert E. et al, Protection From Nonnuclear Weapons, Technical Report No. AFWL-TR-70-127, Air Force Weapons Laboratory, Kirtland Air Force Base, New Mexico, February 1971.
7. Eytan, Reuben, Design of Layered Structures Against Conventional Weapons, Proceedings of the Second Symposium on the Interaction of Nonnuclear Munitions with Structures, Panama City Beach, FL, April 15-18, 1985, pp. 68-73.
8. Fundamentals of Protective Design for Conventional Weapons, Department of the Army, Waterways Experimentation Station, Corps of Engineers, Vicksburg, MS, July 1984.
9. Ha, K. H., Hussein, R., and Fazio, P., Analytic Solutions for Continuous Sandwich Plates, ASCE, Journal of the Engineering Mechanics Division, Vol. 108, No. EM2, April 1982, pp. 228-241.
10. Hiber, H. M., Hughes, T. J. R., and Taylor, R. L., "Collocation, Dissipation and Overshoot for Time Integration Schemes in Structural Dynamics", Earthquake Engineering and Structural Dynamics, Vol. 6, 1978, pp. 99-117.

11. Kolsky, H., Stress Waves in Solids, New York, New York, 1963, Dover Publications, Inc.
12. Plantema, F. J., Sandwich Construction, John Wiley & Sons, Inc., New York, NY, 1966.
13. Rizzo, S. and Fazio, P., Sandwich-Panel Assemblies: Analytical Model, ASCE, Journal of the Structural Division, Vol. 109, No. 11, November 1983, pp. 2715-2732.
14. Rhinehart, J. S., Stress Transients in Solids, Santa Fe, New Mexico, Hyper Dynamics, 1975.
15. Wasley, R. J., Stress Wave Propagation in Solids, New York, New York, 1973, Marcel Dekker, Inc.

1985 USAF-UES Summer Faculty Research Program/
Graduate Student Summer Support Program

Sponsored by the
Air Force Office of Scientific Research

Conducted by the
Universal Energy Systems, Inc.

Final Report

An EPR Study of the Decomposition of Various
Dinitrotoluenes and the Synthesis of Azo Compounds

Prepared by: Walter E. Trafton, Jr.
Academic Rank: Associate Professor
Department and Department of Chemistry
University: Gallaudet College
Research Location: The Frank J. Seiler Research Laboratory,
NC, X, United States Air Force Academy
USAF Research: Captain Jon T. Swanson
Date: August 26, 1985
Contract No.: F49620-85-C-0013

An EPR Study of the Decomposition of Various
Dinitrotoluenes and the Synthesis of Azo Compounds

by

Walter E. Trafton, Jr.

ABSTRACT

The rates of decomposition of several dinitrotoluenes were studied and compared with the rate of decomposition of TNT. It was found that 2,4-dinitrotoluene behaved the most like TNT. Activation energies for all dinitrotoluenes were determined. Five different azo compounds were synthesized by reacting lithium aluminum hydride with aromatic nitro compounds. Work still remains to recrystallize and obtain the EPR spectra of these compounds. The intention here is to generate phenyl radicals when the azo compound is heated. Finally, a preliminary study of the reaction of t-butyl peroxide and TNT was performed. The reaction was found safe to run in the EPR cavity, although no signal was obtained when this was done. More work needs to be done in this area.

Acknowledgments

I would like to thank the Air Force Systems Command and the Air Force Office of Scientific Research for sponsorship of my research. In order to be meaningful, scientific research must be conducted in an intellectually stimulating environment. The Frank J. Seiler Research Laboratory provided this environment. I would like to thank several members of the Seiler staff, Lieutenant Colonel Chet Dymek, Captain Jon Swanson, and Captain Joe Zirrolli, for giving me the opportunity and the guidance necessary for my research.

Finally, I would like to thank my wife, Barbara, and my daughters, Becky and Jill, for their willingness to re-locate and for their support and encouragement throughout the summer.

I. Introduction

I received my Ph.D. from the University of Illinois studying the kinetics of the decomposition of nitrous oxide, carbonyl sulfide, and carbon disulfide. I later was a post-doctoral fellow at the University of Toronto. Here I studied the kinetics of the decomposition of cyanogen bromide and the kinetics of the isomerization of cyclopropane.

The research problem at the Frank J. Seiler Research Laboratory involved the kinetics of the decomposition of TNT. What is the mechanism of this decomposition? What intermediates are formed?

The problem under investigation at Seiler was, therefore, very similar to the problems I had studied at Illinois and Toronto. Because of this similarity I was assigned to work on the decomposition of TNT at Seiler Lab.

II. Objectives of the Research Effort

The overall objective of the Energetic Materials research project is the synthesis of a more energetic and yet more stable explosive. We feel this can be done if the decomposition mechanism of explosives like TNT is better understood.

My individual objectives were:

1. A study of the rates of decomposition of various dinitrotoluenes and comparison of these rates with the rate of decomposition of TNT.
2. Synthesis of various azo compounds which when heated in the EPR cavity will produce phenyl radicals. A comparison of the spectra of these compounds with the EPR spectrum of TNT will help us determine if TNT forms a phenyl radical during decomposition.

3. A preliminary study of t-butyl peroxide and TNT. This should produce a benzyl radical which may appear during TNT decomposition.

III. Dinitrotoluenes

In order to compare structure with reactivity, I studied several dinitrotoluenes at different temperatures in the EPR. The specific dinitrotoluenes studied are 2,4-dinitrotoluene, 2,6-dinitrotoluene, 3,4-dinitrotoluene, and 2,3-dinitrotoluene.

First, all four dinitrotoluenes were studied at 240°C. The 2,4 isomer shows fine structure at early times (the first hour) and then slowly changes into a singlet. This is very similar to TNT. The singlet corresponds to the final polymeric product.

The other three isomers show very little signal early in the decomposition, although they all develop a singlet after 2 to 3 hours. It appears that both an *ortho* and a *para* nitro group are necessary for behavior like TNT.

I then ran all four dinitrotoluenes in the EPR at temperatures above 240°C. The 3,4 isomer was studied at 250°, 260°, and 270°C. The other three isomers, because they have lower activation energies, were studied at 255°, 270°, and 285°C.

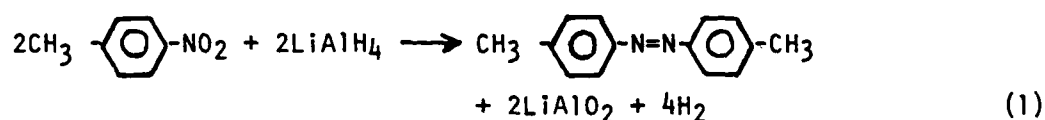
Each EPR experiment is done at a constant temperature. A spectrum is recorded at given time intervals (usually 4 to 8 minutes). The computer calculates the height of the largest peak. We then graph \ln of this peak height vs. time. The slope of this graph gives us the rate constant. After measuring rate constants at several temperatures, we can graph $\ln k$ vs. $1/T$. The activation energy is obtained from the slope of this graph.

Here is a table of activation energies for the dinitrotoluenes. The activation energy for the post-induction period of TNT is included for comparison.

<u>Compound</u>	<u>Ea (kcal/mole)</u>
TNT	30.2
2,4-DNT	32.2
2,6-DNT	36.5
3,4-DNT	37.5
2,3-DNT	18.5

IV. Azo Compounds

Azo compounds are synthesized by reacting aromatic nitro compounds with lithium aluminum hydride. The equation for the reaction of p-nitrotoluene with LiAlH_4 is:



I made azo compounds out of p-nitrotoluene, o-nitrotoluene, 2,6-dinitrotoluene, 2,4-dinitrotoluene, and TNT. The last three tend to form polymers so the yield is fairly small.

The procedure for the synthesis of an azo compound is as follows. One half gram of LAH is dissolved in 60 ml of ether and placed in a 3 neck round bottom flask fitted with condenser and dropping funnel. The mixture is kept under argon and cooled to -78°C with a dry ice isopropyl alcohol bath.

Approximately one tenth of a mole of aromatic nitro compound is dissolved in 40 ml of ether (more ether is required for TNT) and placed in the dropping funnel. This mixture is added to the LAH over a period of thirty minutes. Then we allowed the mixture to warm to room temperature.

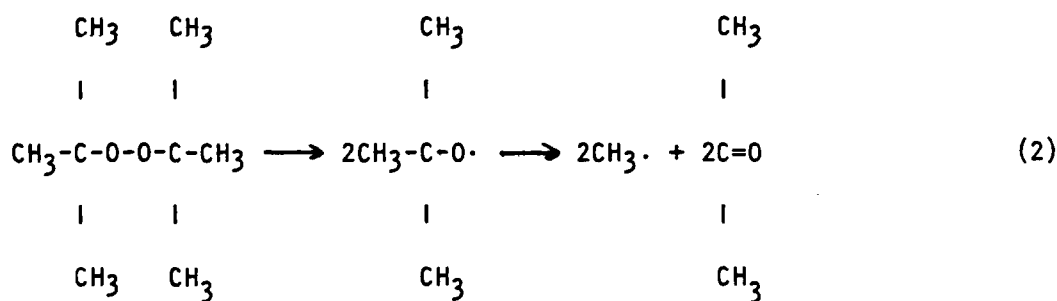
First, 40 ml of water and then 25 ml of 10% H₂SO₄ are added slowly to the reaction mixture. We put the mixture in a separatory funnel and removed the ether layer. We extracted the aqueous layer twice more with 50 ml of ether each time. All ether layers were combined and the ether evaporated. The product in some cases is a solid and in other cases is a tar.

The azo compound made from p-nitrotoluene was recrystallized from 40 ml of absolute ethanol. This was run in the EPR, but the spectrum proved difficult to interpret.

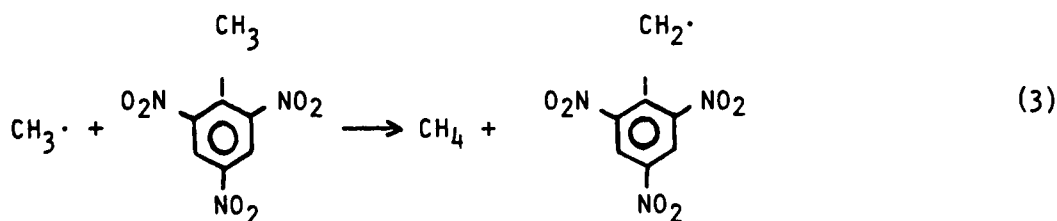
The other azo compounds need to be recrystallized and purified. All experiments stopped because of loss of hood space.

IV. T-Butyl Peroxide

T-butyl peroxide decomposes into acetone and a methyl radical.



The methyl radical will react with TNT to produce a benzyl radical. This is more stable than a phenyl radical.



I mixed 25 mg of TNT and 10 μ l of t-butyl peroxide in one ml of benzene. The mixture was placed in a glass tube and heated to 60°C in a fluidized sand bath for one hour. The mixture did not explode. Therefore we concluded that it was safe to do this experiment in the EPR.

I mixed 25 mg of TNT, 10 μ l of t-butyl peroxide, and 0.3 ml of benzene in an EPR tube. The tube was heated to 50°C in the EPR cavity. The experiment ran for two and one half hours, and no signal was observed at any time during this period. This line of experimentation could not be continued because of lack of time.

VI. Recommendations

1. The experiments with the dinitrotoluenes are almost finished. With the 2,3-dinitrotoluene a second experiment should be done at each temperature. Average rate constants at each temperature can be used to calculate an improved activation energy.

Also with 2,4-dinitrotoluene the zero order rate constant needs to be determined. This can be done simply by looking back at the spectra already obtained. The decrease in height with respect to time of one of the peaks on the wings of the spectrum will give this rate constant.

2. Much work remains to be done with the azo compounds. The azo compounds made from o-nitrotoluene, 2,4-dinitrotoluene, 2,6-dinitrotoluene, and TNT need to be purified. Appropriate solvents need to be found for recrystallization.

Many of these azo compounds are light sensitive. Indeed the azo compound made from 2,6-dinitrotoluene may already have decomposed photolytically. This compound may have to be re-synthesized.

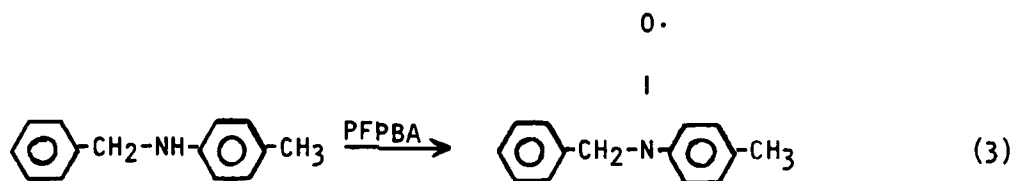
Once purified all the azo compounds need to be run on the EPR.

I suggest a concentration of 4 or 5 mg of azo compound dissolved in a ml of benzene.

3. The mixture of t-butyl peroxide and TNT produced no signal when run through the EPR. This may be because everything decomposed in the first four minutes (before a spectrum was taken). If this is true, running the experiment at a lower temperature, like perhaps 40°C, would give a satisfactory spectrum.

Another possibility is that the reaction is too slow at 50° and requires a higher temperature. A third possibility is that the concentrations of TNT and t-butyl peroxide need to be increased.

4. In addition to benzyl and phenyl radicals, a third type of free radical of interest is the nitroxyl radical. Researchers at the Seiler Laboratory strongly suspect that this type of radical is an intermediate in the decomposition of TNT. Nitroxyl radicals can be formed from secondary amines by reaction with parafluoroperbenzoic acid (PFPBA).



I strongly recommend that someone synthesize several different nitroxyl radicals, record the EPR spectrum, and compare with the spectrum of TNT. This would provide conclusive evidence as to whether nitroxyl radicals actually are part of the decomposition mechanism of TNT.

References

1. Guidry, R. M. and L. P. Davis, "Thermochemical Decomposition of Explosives. I. TNT Kinetic Parameters Determined from ESR Investigations," Thermochimica Acta, 32 (1979) 1-18.
2. Nystrom, R. F. and W. G. Brown, "Reduction of Organic Compounds by Lithium Aluminum Hydride. I. Aldehydes, Ketones, Esters, Acid Chlorides and Acid Anhydrides," Journal of the American Chemical Society, 69 (1947) 1197-1199
3. Nystrom, R. F. and W. G. Brown, "Reduction of Organic Compounds by Lithium Aluminum Hydride. III. Halides, Quinones, Miscellaneous Nitrogen Compounds," Journal of the American Chemical Society, 70 (1948) 3738-3740.
4. Ahlam, M.J.A. and Z.Y. Al-Saigh, "Photodecomposition of Azobenzenes," J. Chem. Tech. Biotechnol., 30 (1980) 440-446.
5. Horning, E. C. (Ed.), Organic Syntheses Collective Volume 3, New York, John Wiley and Sons, Inc., 1955.
6. Cuthbertson, M. J., E. Rizzardo, and D. H. Solomon, "The Reactions of t-Butoxyl with Unsaturated Hydrocarbons: Structure and Reactivity of Allylic Radicals," Aust. J. Chem., 36 (1983) 1957-73.

1985 USAF-UES SUMMER FACULTY RESEARCH PROGRAM/
GRADUATE STUDENT SUMMER SUPPORT PROGRAM

Sponsored by the
AIR FORCE OFFICE OF SCIENTIFIC RESEARCH

Conducted by the
UNIVERSAL ENERGY SYSTEMS, INC.

FINAL REPORT

A COMPARISON OF MEASURED AND CALCULATED ATTENUATION
OF 28 GHZ BEACON SIGNALS IN THREE CALIFORNIA STORMS

Prepared by:	LARRY VARDIMAN	and	MATTHEW PETERSON
Academic Rank:	Associate Professor		Graduate Research Assistant
Department and	Dept of Physical Science		Geophysics Department
University:	Christian Heritage College El Cajon, CA 92021		Institute for Creation Research El Cajon, CA 92021
Research Locations:	Air Force Geophysics Laboratory Atmospheric Sciences Division Cloud Physics Branch		
USAF Research	Dr. Arnold A. Barnes, Jr.		
Date:	19 August 1985		
Contract No:	F49620-85-C-0013		

A COMPARISON OF MEASURED AND CALCULATED
ATTENUATION OF 28 GHZ BEACON SIGNALS
IN THREE CALIFORNIA STORMS

by

Larry Vardiman
and
Matthew Peterson

ABSTRACT

Three case studies of attenuation through stratiform and convective Sierra Nevada storms from the winter of 1979-1980 were studied. A 28 GHz (1.05cm) dual channel radiometer was positioned on the Sacramento Valley floor just upwind of the central Sierra. It measured the signal strength from the COMSTAR satellite and brightness temperature from the cloud along the same path. Microphysics data from a cloud physics aircraft were used to calculate attenuation and brightness temperature from the same cloud volume.

Measured and calculated values of attenuation for weak precipitation agree, however large differences for heavier precipitation do not permit a conclusion regarding the importance of snow above the melting layer on attenuation. Flight patterns used to acquire the hydrometeor data may have contributed to the differences.

I. INTRODUCTION:

The United States Air Force (USAF) is concerned about the effect of storms on the transmission of millimeter wave-length signals from satellite to-ground and ground-to-ground systems. In the frequency band from 20 to 100 GHz the effect of rain and snow can be important. In this frequency band the wave length of the signal is on the same order as the size of the precipitation particles. A combination of Mie and Raleigh scattering theory applies and consideration of both ice and water phases must be made. Descriptions of the effects of hydrometeors on millimeter wave communication in the atmosphere have been reported by Hogg (1968), Hogg and Chu (1975), Tiffany (1983), and Ebersole et. al. (1985).

Although the theory of attenuation of radio waves through a scattering medium has been fairly well developed, the simultaneous measurement of attenuation and in-situ particle distributions over long path lengths in precipitating events is relatively scarce.

In discussing possible research topics for a summer appointment at the Air Force Geophysics Laboratory (AFGL), I recalled that such measurements had been made as part of the Sierra Cooperative Pilot Project (SCPP) during the winter of 1979-80 in northern California. The purpose of the original measurements was to develop a remote sensing technique for identifying super-cooled liquid water in support of cloud-seeding experiments in the Sierra Nevada. Cloud liquid measurement by microwave sensors is described by Snider, Burdick, and Hogg (1980), Snider, Guiraud, and Hogg (1980), and Hogg et. al. (1983). The description of the deployment and analysis of the radiometer system in the SCPP is given in Snider and Hogg (1981) and the SCPP Data Inventory (1979-80). In summary, the system was a dual channel radiometer which measured

the signal strength of the 28.56 GHz beacon on the COMSTAR Satellite (see Cox, 1978) while simultaneously measuring the brightness temperature of the cloud and precipitation particles along the same path at the same frequency.

A full compliment of meteorological and cloud physics measurements were made in association with the radiometer data (see the SCPP data inventory 1979-80). The most important measurements for the purposes of this study were the microphysics measurements made with the University of Wyoming cloud physics aircraft. Discussions of the instrumentation flown on this aircraft are given in Cooper (1978) and Gordon and Marwitz (1984). Analysis and interpretation of data in support of the SCPP are reported in Stewart and Marwitz (1980), Pace (1980), Parish et. al. (1981), Stewart and Marwitz (1982), Bradford (1982), Stewart, Marwitz and Pace (1984), and Gordon and Marwitz (1985).

It was decided that these data sources should provide a unique opportunity to compare the direct measurement of signal attenuation through precipitating storms with the attenuation calculated from the particle distributions measured in-situ.

My selection for this research was based on the background in cloud physics developed over five years with the USAF Air Weather Service working on fog dispersal applications, five years of graduate research at Colorado State University in orographic cloud seeding, and eight years with the US Bureau of Reclamation working on cloud physics research in the Sierra Nevada.

II. OBJECTIVES OF THE RESEARCH EFFORT:

The goal of this research was to compare measured and calculated attenuation in California storms using data from the SCPP. This was to

AD-A166 178

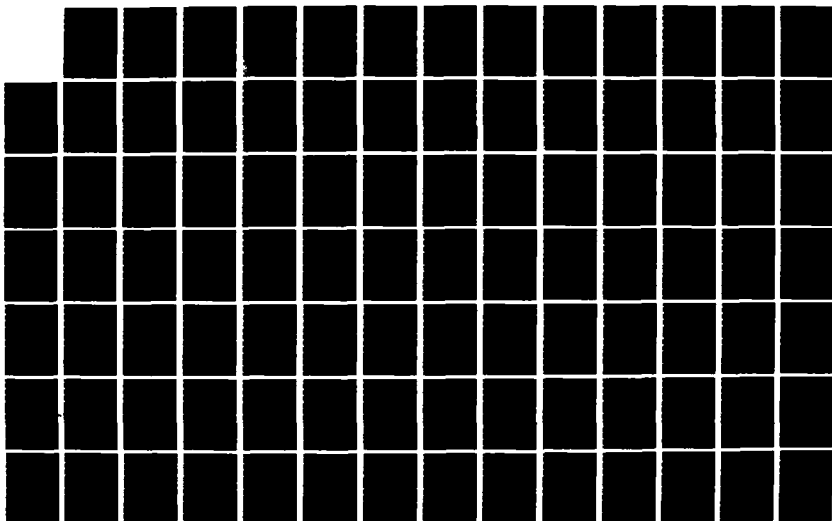
UNITED STATES AIR FORCE SUMMER FACULTY RESEARCH PROGRAM
1985 TECHNICAL RE (U) UNIVERSAL ENERGY SYSTEMS INC
DAYTON OH R C DARRAH ET AL DEC 85 AFOSR-TR-86-0141
F49620-85-C-0013

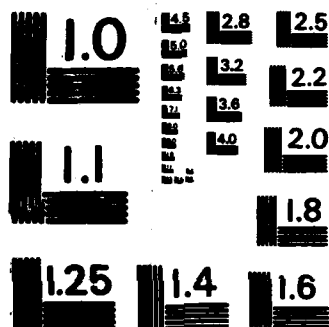
9/ //

UNCLASSIFIED

F/G 5/9

NL





MICROCOPY RESOLUTION TEST CHART
NATIONAL BUREAU OF STANDARDS-1963-A

be accomplished for at least two cases at the frequency of the COMSTAR beacon (28.56 GHz/1.05cm).

The objectives under this goal were to:

- a. Identify at least one stratiform and one convective case with adequate data to justify a full analysis.
- b. Reduce aircraft data and calculate vertical distributions of cloud and hydrometeor water contents.
- c. Develop a simple computer model to compute attenuation and brightness temperature expected along the signal path from the satellite beacon to the radiometer.
- d. Compute the attenuation and brightness temperature for the same conditions using a standard model developed at AFGL called RADTRAN.
- e. Compare the computed values with the measured values.
- f. Develop recommendations for future field research on attenuation.

III. Analysis:

a. Identification of Case Studies

An initial selection of case studies was made using the Project SKYWATER Data Inventory (1980), the radiometer logs in Snider and Hogg (1981), and the meteorological descriptions found in Rhea et. al. (1980). The initial criteria used to select cases were that the radiometer and microphysics aircraft operated simultaneously in a precipitation event and the aircraft was flown approximately along the beam from the COMSTAR satellite to the radiometer. Upon more careful analysis of the data after arriving at AFGL, it was discovered that all of the cases initially selected were flown in light precipitation. Since the attenuation of millimeter signals is only a problem in moderate to

heavy precipitation, it was decided that a new search for heavier precipitation cases would be initiated. This time the requirement that the aircraft flight be along the beam was relaxed so that soundings by the aircraft through cloud in the vicinity of the radiometer would be satisfactory. Two cases were identified which met these criteria -- 9 January 1980 and 14 January 1980. One light precipitation case from the earlier search -16 February 1980 -- was retained for comparative purposes. The 9 January and 16 February cases were both stratiform and the 14 January case was convective. The attenuation and brightness temperature measured by the radiometer and the precipitation rate at the radiometer site are shown in Figure 1 for the three cases.

b. Reduction of Aircraft Data

The processing of aircraft microphysics data was a sizable task. Over 200 variables were available for each second of flight during the 20 hours of archived aircraft data received. This massive amount of data was reduced to selected variables and flight times of interest by several programs written on the CYBER computer at AFGL. Averages of many of the variables were made over time intervals determined by the aircraft flight patterns and sample volumes of the hydrometeor probes. The selection of appropriate averaging times was an integral part of the analysis. If the time interval was too short, an insufficient number of particles would be sampled in the large size bins of the hydrometeor probes, causing a significant error. If the time interval was too long, the vertical resolution in computed variables would be too great. This problem will be addressed in the recommendations section regarding flight patterns for data collection. The final averaging interval of 30 seconds was selected for the 9 January

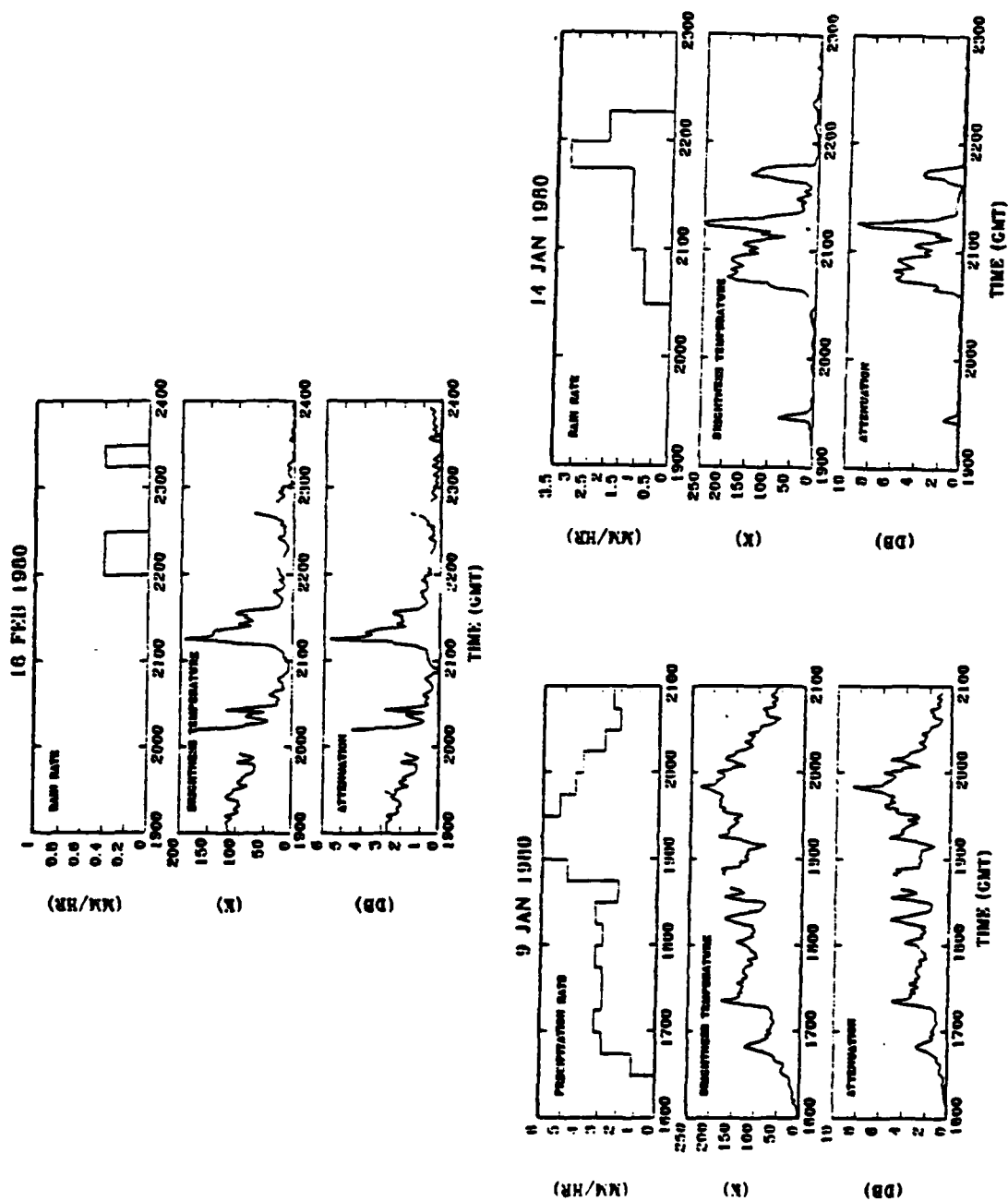


Figure 1. Attenuation, brightness temperature, and precipitation versus time near Sheridan, California.

and 16 February cases. In both of these cases the aircraft had been flown in an ascending pattern at a rate of about 1000-1500 ft/min. For the 14 January case the aircraft was flown at seven levels through a banded feature. The variables were averaged over 4 minutes centered on the band. This provided excellent microphysics data but poor vertical resolution.

The end product desired from the aircraft microphysics data was a vertical distribution of cloud and hydrometeor equivalent water contents for the three cases. It was initially assumed that the variables calculated by the University of Wyoming would be adequate for this study, but after some effort to use their values it was realized that we would have to use the particle spectra from the hydrometeor probes and calculate our own. The first effort at calculating hydrometeor contents used only the 2DC PMS probe. This was an improvement, but the sample volume for the large bins was inadequate. Therefore, PMS-2DP size spectra were then included. With this inclusion of the 2DP probe, however, hydrometeor contents were only stable if bins which contained less than 10 particles in a sample were excluded. One other adjustment was made near the end of the analysis. The University of Wyoming provides two types of size spectra for each hydrometeor probe. The first rejects artifact images caused by water "streaking" off the edges of the probes. The second rejects images, in addition to the "streakers", which do not have a certain degree of circularity. For a full discussion of the criteria for rejection of artifacts, see Cooper (1978). Since in this analysis we wanted to include all real particles, including angular ice crystals, we chose the first type of spectra for our calculations. However, we found that one of the passes just below the melting level on the 14 January case gave extremely high values of

hydrometeor water content unless we used the second type of spectra. In looking at the particle images, we discovered that some of them were gigantic (up to 8 cm) and appeared to be either large, wet snowflakes or artifacts. By using the second type of spectra these peculiar particles were rejected, thus not affecting the calculation of water contents. Such particles, if they are real however, could have an important effect on attenuation because of their large size. The greatest degree of uncertainty in making these calculations occurs in the melting layer because of the difficulty in identifying particle type, shape, and size.

The calculation of liquid water content below the melting layer is quite straightforward since the particles are mostly spherical. In the melting layer and above, however, the particle shape and density are highly speculative causing a great degree of uncertainty in calculating equivalent water content. After, several unsuccessful attempts to calculate water contents using the size to mass conversion equations of Nakaya (1954), we elected to use the conversion equations developed by Berthel (1981), at AFGL. We used his needle equation fitted to a gamma distribution for the 14 January and 16 February cases and the plate family equation for the 9 January case. It is obvious when looking at the particle images that a mixture of particle types is present and no single equation will properly apply to any given case. The 16 February case contained mostly needles and probably fits the equation better than the others.

The assumption was made in these calculations that all particles above the 0°C level were ice crystals and all particles below were water drops. In Sierra Nevada storms relatively few water drops occur above the 0°C because of the abundance of ice crystals, which will quickly

nucleate any supercooled drops. The assumption above the 0°C level is probably quite good. Below the 0° level, however, melting snow can take several hundreds of meters to completely melt, forming liquid drops. The assumption that all particles below the 0°C level are liquid probably overestimates the liquid water content. However, the attenuation based on this inflated hydrometeor liquid water content may not be far from reality because an electromagnetic wave "sees" a water-coated ice particle, almost as if it were a spherical water drop of the same size. Therefore, this assumption should be appropriate for use in calculating attenuation even though the actual hydrometeor liquid water content would probably be less.

Cloud liquid water content was measured by the PMS Forward Scattering Spectrometer Probe (FSSP) and is assumed to be liquid throughout the entire depth of the cloud. Because the cloud liquid water contents in Sierra Nevada storms are seldom greater than .1 gm/m³, the integration of the FSSP spectra is considered to be more accurate than the Johnson-Williams liquid water content measurements.

c. Development of a Simple Attenuation Model

The attenuation of an electromagnetic signal in cloud and precipitation as a function of temperature and wavelength has been reported by Gunn and East (1954). Snider, Burdick and Hogg (1980) fit a quadratic equation to this data to develop the attenuation coefficient for cloud water at 28.56GHz as a function of temperature.

$$\alpha_w(T) = (43.164 - .287T + .000482T^2)LWC \quad (1)$$

where α_w = db/km

LWC = gm/m³

By fitting the data from Gunn and East (1954) or the data from Tiffany

(1983) to a log-log plot the attenuation coefficient for rain at 28.56 GHz can be found.

$$\alpha_R = .21 R_r^{.9666} \quad (2)$$

where $\alpha_R = \text{dB/km}$

$R_r = \text{mm/hr}$

Although most investigators have discounted the contribution of snow on attenuation because of its low index of refraction, a recent analysis of data from the SNOW experiments by Ebersole et. al. (1985) has indicated that "attenuation due to falling snow will be significant at some frequencies if the path length is several kilometers." Fitting a straight line through the center of Ebersole's data gives the following equation for the attenuation coefficient of snow at 35GHz.

$$\alpha_s = .6 \text{ IWC}^{.9445} \quad (3)$$

where $\alpha_s = \text{dB/km}$

$\text{IWC} = \text{gm/m}^3$

Note, that Ebersole's attenuation coefficient for snow is in terms of a mass density rather than a precipitation rate. This formulation would seem to be more appropriate for rain as well, since the estimate of precipitation rates from aircraft or radar data introduce additional error due to uncertainties in fall velocity.

If we can now assume that we have accurate attenuation coefficients, we need only multiply the appropriate value of attenuation coefficient for cloud, rain, and snow by the thickness of each layer in the storm. The total vertical attenuation is then the sum of all layers. Since the radiometer was "looking" through the storm at an angle of 32.6° from the horizontal, the actual attenuation along the

beam is the vertical attenuation divided by the sine of 32.6°. This model does not take into account the attenuation due to water vapor.

If γ is the attenuation in each layer due to the cloud water, rain, and snow; then the contribution of each layer to the brightness temperature seen by the radiometer is:

$$T_B = (1 - \exp(\gamma/4.343)) T_m \quad (4)$$

where $T_B = ^\circ K$
 $\gamma = \text{dB}$
 $T_m = ^\circ K$

T_m is the mass weighted temperature of each layer in the storm. The total brightness temperature seen by the radiometer is then the sum of the contributions from each layer.

A computerized model based upon the preceeding discussion was formulated to calculate the attenuation and brightness temperature in each layer and find the totals "seen" by the radiometer.

d. Computation of Attenuation on RADTRAN

The same vertical distribution of cloud and hydrometeor water contents used in the simple model was also input to a standard attenuation model developed by Falcone et. al. (1982) called RADTRAN. RADTRAN is a fast computer code designed to model atmospheric microwave transmission and emission. The model considers attenuation by atmospheric gases including water vapor, which was not handled by the simple model above. Attenuation for rain is determined by table interpolation and for cloud water by multiplication of a factor times the liquid water content. The model does not calculate attenuation for snow or ice.

IV. RESULTS:

Tables 1 and 2 show the calculated and measured values of attenua-

tion and brightness temperature for the three cases studies. Note that the simple model did not compute attenuation due to water vapor and RADTRAN did not compute attenuation due to snow. The radiometer values are averages of observed attenuation and brightness temperature during the period of aircraft sampling for the 16 February and 9 January cases. For the 14 January case the radiometer values are averages during the 40 minute period from 2040 to 2120 GMT when the precipitation band was estimated to have been in the radiometer beam.

The calculated values of the attenuation for cloud and rain agree quite well between the two models, although the simple model is consistently higher. Uncorrected values from RADTRAN are consistently less than observed by the radiometer. Uncorrected values from the simple model are also less than observed by the radiometer except for the 14 January case. Rain is the primary contributor to attenuation for the two heavy precipitation cases. Water vapor and possibly snow are the main contributors to attenuation for the 16 February light precipitation case.

A best estimate of attenuation for each case was made by combining results from the two models and correcting for a wet antenna. The attenuation for water vapor from RADTRAN was added to the total attenuation calculated by the simple model. In addition, .3dB was added to correct for a wet antenna for the 9 January and 14 January cases, as suggested by Snider and Hogg (1981). With these adjustments, best estimates of attenuation are still low for the two stratiform cases on 16 February and 9 January, but quite high for the 14 January convective case compared to the measured attenuation. The relative error is small for the weakest case on 16 February but much larger for the heavier

precipitation cases.

No effort was made to evaluate the relative values of brightness temperature because of the divergent values of attenuation.

		16 FEB	9 JAN	14 JAN
S I M P L E	CLOUD	.109	.183	.254
	RAIN	.003	.739	3.753
	SNOW	.183	.341	1.166
	TOTAL	.295	1.263	5.173
R A D T R A N	CLOUD	.099	.178	.226
	RAIN	.000	.597	3.327
	WATER VAPOR	.292	.386	.413
	TOTAL	.391	1.151	3.966
RADIOMETER		.62	2.68	4.17
BEST ESTIMATE		.6	2.0	5.9
REL. ERROR		-5%	-25%	+41%

Table 1 Measured and Calculated Attenuation in dB

	16 FEB	9 JAN	14 JAN
SIMPLE MODEL	17.8	74.8	236.9
RADTRAN	27.1	69.6	160.4
RADIOMETER	22.9	114.7	153.9
REL. ERROR	-22%	-35%	+54%

Table 2. Measured and Calculated Brightness Temperature in °K.

V. CONCLUSIONS:

Based on the values in Table 1, it is concluded that measured and

calculated values of attenuation for weak precipitation agree quite well. However, for heavier precipitation cases, which are the more important, agreement is not as good. Because the relative errors for the two heavier precipitating cases are large and of opposite sign, it is not possible to conclude whether snow is a factor which should be considered in attenuation calculations or not. Since rain is the primary contributor to attenuation when it occurs, any error in its calculation will sway the results markedly. Unfortunately, the aircraft data taken below the melting level were relatively poor. The flight patterns used for the 9 January and 14 January cases were not intended for this study. One reason the 16 February case agrees as well as it does may be because it was specifically designed for this purpose. The 14 January case only had passes at two levels from which hydrometeor water contents and precipitation rates were estimated over a vertical distance of approximately 2 kilometers. In addition, it would appear that from an overlay of the aircraft flight track on the radar PPI, the aircraft was directed through heavier precipitation at and below the melting layer. The radiometer likely observed weaker precipitation than the aircraft, on the average. For the 9 January case the precipitation rate below the melting level appears to have been seriously underestimated from the aircraft data because the aircraft sounding was made in such a way that the low end of the track was in a weaker region of precipitation. The aircraft ascended from southwest to northeast in an orographic cloud where the precipitation rate increased markedly in the same direction.

Considering the problems with the data cited above, it is remarkable that the results are as close as they appear. However, the reader

is cautioned to remember that the relative errors are calculated on attenuation in decibels. Averages and relative differences of logarithmic variables always appear better than they really are.

Assuming the data acquisition problems can be resolved, the next major source of error is probably the calculation of hydrometeor water content from the PMS probes. Rain water content below the melting layer is probably not too bad because the particles are spherical. However, in the melting layer and above, the conversion from particle size spectra to water content is a major problem. The use of a single crystal-type equation for each case seemed to give reasonable results, but the water contents and precipitation rates could easily be wrong by a factor of two or more. One possible calibration of these quantities would be the detailed investigation of the radar reflectivity in the vicinity of the aircraft. Both the SKYWATER radar and the NCAR CP-2 doppler radar were operating during this season. Unfortunately, neither of these comparisons would provide an absolute calibration, since the crystal type and conversion equations must again be considered in these data. A better calibration would probably be the comparison of calculated precipitation rates from the PMS probes with measured precipitation rates in gauges located in the Sierra Nevada in and above the melting layer. Some 75 gauges were operated in the SCPP downwind of the Sheridan radar during 1979-80 with .25mm and 15 minute resolution.

VI. RECOMMENDATIONS:

The results and conclusions of this study have led to several recommendations for further research. These recommendations can be divided into two main categories.

a. Future Data Acquisition Procedures

Since rain is the primary contributor to attenuation, measurement of its spatial and temporal characteristics are crucial to estimates of its effect on attenuation. Flight patterns should be designed which allow sampling all the way to ground level in the vicinity of project radiometers. Missed approaches to nearby airports or launch and recovery from fields near the radiometers are possibilities. Precipitation gauges in the same location with as fine a time and precipitation resolution as possible are necessary to calibrate calculations with the PMS probes. Flights should be made in as uniform conditions as possible with the long dimension of any flight patterns in the direction of greatest uniformity. Vertical ascents or descents should be made slowly (no more than 300 ft/min, if continuous) or in shallow increments (in 1000 ft levels, if discontinuous). If flights are made in vertical increments, sampling should be done for 2-4 minutes at each level, depending on the particle concentration. Sufficient sampling at the large bin sizes will take times of this order. Flights should be made entirely through the top of a storm, if possible. Such a flight will take an hour or more, so meteorological features measured should be on the scale of 25 km or more in horizontal size. Race track or corkscrew flight patterns are recommended.

b. Further Data Analysis Approaches

It would seem beneficial to analyze two or three additional cases from the SCPP similar to those contained in this report. However, several additional guidelines should be added to the search for cases. First, the aircraft ascents or descents should be parallel to the barrier. Second, the ascents or descents should be as slow as possible.

Third, they should extend from above cloud top to ground level.

Calibration of calculated precipitation rates should be made using the precipitation gauges in and above the melting level in the Sierra. Adjustments could be made in the calculated precipitation rates by selecting equations more closely matching crystal types observed and adjusting fall velocities to take into account average orographic ascent.

ACKNOWLEDGMENTS

This research was accomplished under the sponsorship of the Air Force Systems Command, Air Force Office of Scientific Research, while the authors were on summer faculty appointments to the Air Force Geophysics Laboratory at Hanscom AFB, MA. Appreciation is expressed to Dr. Arnold A. Barnes, Jr. for his encouragement and discussions during the effort. Several individuals and organizations provided data and advice for this study. John Marwitz of the University of Wyoming, provided microphysics data and guidance for its use. Jack Snider from the Wave Propagation Laboratory of the National Oceanic and Atmospheric Administration provided the radiometer data. The Office of Atmospheric Resources Research of the Bureau of Reclamation provided archived radar and aircraft data. Owen Rhea of Electronic Techniques, Inc. gave permission to use the meteorological descriptions for the case studies. Vincent Falcone of AFGL/LYS made his program RADTRAN available for calculating attenuation and brightness temperature. Morton Glass, Vernon Plank, and Robert Berthel of AFGL/LYC helped the effort with their discussions on crystal mass calculations and size spectra manipulations. Finally, the staff of the Ophir Corporation is appreciated for their help on the AFGL computers and Carolyn Fadden for typing this report.

REFERENCES

- Berthel, R.O. "The Conversion of Aircraft Ice Crystal Measurements into Terms of Liquid Water Using Simulated Data", AFGL Environmental Research Paper No. 745, AFGL-TR-81-0173, 1981.
- Bradford, M.L. "Hydrometeor Characteristics of Orographic Clouds and Rainbands in California", M.S. Thesis, Dept. of Atmospheric Science, University of Wyoming, 145 pp, 1982.
- Cooper, W.A., "Cloud Physics Investigations by the University of Wyoming in HIPLEX 1977", Annual Report to Water and Power Resources Service (formerly Bureau of Reclamation), Contract No. 7-07-93-V0001, Dept. of Atmospheric Science, Univ. of Wyoming, 320pp, 1978.
- Cooper, W.A. and C.P.R. Saunders, "Winter Storms over the San Juan Mountains, Part II: Microphysical Processes", J. Appl. Meteor., 19(8) 927-941pp, 1980.
- Cox, D.C., "An Overview of the Bell Laboratories 19- and 28- GHz COMSTAR Beacon Propagation Experiments", The Bell System Technical Journal, Vol 57, No. 5, 1231-1255pp, 1978.
- Ebersole, J.F., W.K. Cheng, J. Hallett, and R.G. Hohlfeld, "Effects of Hydrometeors on Electromagnetic Wave Propagation", Final Report, AFGL-TR-84-0318, 74pp, 1985.
- Falcone, V.J., L.W. Abreu, E.P. Shettle, "Atmospheric Attenuation in the 30 to 300 GHz region using RADTRAN and MWTRAN," Proceedings of SPIE, Vol. 337, 62-66pp, 1982.
- Gordon, G.L. and J.D. Marwitz, "An Airborne Comparison of Three PMS Probes", J. of Atmos. and Ocean. Technol., 1, 22-27pp, 1984.
- Gordon, G.L. and J.D. Marwitz, "Hydrometeor Evolution in Rainbands Over the California Valley", Manuscript submitted to J. Atm. Sci., 1985.
- Gunn, K.L.S., and T.W.R. East, "The Microwave Properties of Precipitation Particles", Quart. J. Roy. Meteor. Soc., Vol 80, 522-545pp, 1954.
- Henderson, T.J. et. al., "SCPP Data Collection and Analysis for the period July 1, 1979 through June 30, 1980", Interim Progress Report, Atmospheric, Inc., Fresno, California, 1980.
- Hogg, D.C., "Millimeter-Wave Communication through the Atmosphere", Science, Vol. 159, No. 3810, 39-46pp, 1968.
- Hogg, D.C. and T. Chu, "The Role of Rain in Satellite Communications", Proceedings of the IEEE, Vol 63, No. 9, 1308-1331pp, 1975.

Hogg, D.C., F.O. Guiraud, J.B. Snider, M.T. Decker and E.R. Westwater, "A Steerable Dual-Channel Microwave Radiometer for Measurement of Water Vapor and Liquid in the Troposphere", J. of Climate and Appl. Meteor., Vol 22, 789-806pp, 1983.

Nakaya, Ukichiro, Snow Crystals, Cambridge, Harvard University Press, 1954.

Pace, John C., "Microphysical and Thermodynamic Characteristics through the Melting Layer", Report No. AS126 to the Water and Power Resources Service (formerly Bureau of Reclamation), Dept. of Atmospheric Science, Univ. of Wyoming, Contract No. 7-07-83-V0001, 204pp, 1980.

Parish, T.R., J.D. Marwitz, R.L. Lee, G.L. Gordon and A.R. Rodi, "Cloud Physics Studies in SSCP During 1980-81", Report No. AS132 to the Bureau of Reclamation, Dept. of Atmospheric Science, Univ. of Wyoming, Contract No. 7-07-83-V0001, 149pp, 1981.

Rhea, O.J., et.al., "Interim Progress Report, SSCP Forecasting Support for the period July 1, 1979-June 30, 1980", Electronic Techniques, Inc. Fort Collins, Colorado. 1980.

Sierra Cooperative Pilot Project Data Inventory for 1979-80, Office of Atmospheric Resources Research, Water and Power Resources, U.S. Dept. of the Interior, Denver, CO, 1980.

Sierra Cooperative Pilot Project, "Operations Plan, 1979-80", Office of Atmospheric Resources Management, Bureau of Reclamation, U.S. Dept. of Interior, Denver, Colorado, 1979.

Snider, J.B., F.O. Guiraud, and D.C. Hogg, "Comparison of Cloud Liquid Content Measured by Two Independent Ground-based Systems", J. Appl. Meteor., Vol 19, 577-579pp, 1980.

Snider, J.B., H.M. Burdick, and D.C. Hogg, "Cloud Liquid Measurement with a Ground-based Microwave Instrument", Radio Science, Vol. 15, No. 3, 683-693pp, 1980.

Snider, J.B. and D.C. Hogg, "Ground-based Radiometric Observations of Cloud Liquid in the Sierra Nevada", NOAA Technical Memorandum ERL/WPL72, Boulder, Colorado, 46pp, 1981.

Stewart, R.E. and J.D. Marwitz, "Cloud Physics Studies in SSCP During 1979-80", Report No. AS125 to the Water and Power Resources Service (formerly Bureau of Reclamation), Dept. of Atmospheric Science, Univ. of Wyoming, Contract No. 7-07-83-V0001, 96pp, 1980.

Stewart, R.E. and J.D. Marwitz, "Microphysical Effects of Seeding Winter-time Stratiform Cloud Near the Sierra Nevada Mountains", J. of Appl. Meteor., Vol 21, 874-880pp, 1982.

Stewart, R.E., J.D. Marwitz, and J.C. Pace, "Characteristics through the Melting Layer of Stratiform Clouds", J. of Atmospheric Science, Vol 41, No. 22, 3227-3237pp, 1984.

Tiffany, G.B., "Most Reliable Messenger: MM-Waves Get Through", Micro-waves and R.F., 64pp, 1983.

1985 USAF-UES SUMMER FACULTY RESEARCH PROGRAM/
GRADUATE STUDENT SUMMER SUPPORT PROGRAM

Sponsored by the
AIR FORCE OFFICE OF SCIENTIFIC RESEARCH

Conducted by the
UNIVERSAL ENERGY SYSTEMS, INC.

FINAL REPORT

ALLOCATION AND ASSESSMENT OF LOGISTICS RESOURCES

Prepared by:	Dr. Daniel T. Voss
Academic Rank:	Assistant Professor
Department and	Department of Mathematics and
University:	Statistics, Wright State University
Research Location:	Hq Air Force Logistics Command, DCS/Plans and Programs, Directorate of Management Sciences, Consultant Services Division (XRSM), Wright Patterson Air Force Base
USAF Research:	John Madden
Date:	23 August 1985
Contract No:	F49620-85-C-0013

ALLOCATION AND ASSESSMENT OF LOGISTICS RESOURCES

by

Dr. Daniel T. Voss

ABSTRACT

The Air Force Logistics Command uses analytic simulation models and marginal analysis techniques for balanced acquisition of reparable aircraft parts and assessment of resource levels. In this paper, inclusion of acquisition of such support resources as repair, transportation and administration is considered. Conditions are explored under which marginal analysis is optimal for acquisition of such resources, in light of a nonseparable objective function. Two marginal analysis based algorithms are recommended. Different methods are suggested for estimating demand rates and variance-to-mean ratios for reparable parts.

ACKNOWLEDGMENTS

I would like to express my thanks to the Air Force Systems Command, the Air Force Office of Scientific Research and the Directorate of Management Sciences of the Air Force Logistics Command for the opportunity to conduct research in the Logistics Command. Special thanks are due to Victor Presutti, John Madden, Major Ron Stokes and all the personnel of XRS for their warm welcome and tremendous level of cooperation.

I. INTRODUCTION:

This author received a B.S. in Mathematics from The University of Dayton in April of 1979, an M.S. in Statistics from The Ohio State University in December of 1981 and a Ph.D. in Statistics from The Ohio State University in March of 1984. The Ph.D. dissertation, "Confounding in Single Replicate Factorial Designs," was completed under the guidance of Dr. Angela Dean. Continued research activities have extended results obtained in the dissertation, with emphasis on both a comparison of classes of single replicate factorial designs in blocks as generated by various methods in the literature and development of new techniques of design construction.

According to the AFOSR brochure, the Logistics Command at Wright Patterson Air Force Base . . . "Uses mathematical models, Monte Carlo Simulation and other scientific techniques to analyze the traditional functional areas of supply, maintenance, transportation, material management, and logistics operations with the objective of relating logistics resource decisions to operational effectiveness." The brochure also advertised a desire for expertise in various fields, including mathematics and statistics.

Having degrees in mathematics and statistics, including

coursework in Monte Carlo Simulation and the theory of linear models, my abilities and interests are closely related to the activities and interests of the Logistics Command.

II. OBJECTIVES OF THE RESEARCH EFFORT:

The primary objectives during the summer program have been: (1) To develop familiarity with the projects of interest to and the techniques used by the Logistics Command; and (2) To focus on the INTEGRATE project so as to add structure and direction in its early stages.

The activities of the AFLC/XRS include making capability assessments for given resource mixes and determining balanced resource allocations, the objective being to maximize aircraft availability. An aircraft is modeled as consisting of reparable parts, with failure of parts treated as being stochastically independent events. For both assessment and allocation, a scenario is specified which includes flying program, parts failure rates, and time distributions for repair, transportation and administration. Aircraft availability, being the product of the probabilities of availability of the component parts, can be expressed as a separable function of individual parts availability rates. The Aircraft Availability Procurement Model (AAPM), a marginal analysis based computer model, is currently used for allocation of funds for reparable parts, and

Dyna-METRIC, an analytic simulation model, is currently used for assessment of aircraft availability for specified stock levels of reparable parts.

The objectives of the INTEGRATE project are to expand the capabilities of the AFLC/XRS for both allocation of funds and assessment of expenditures to include such support resources as repair, transportation and administration. The problems of the INTEGRATE project are primarily twofold: (1) The objective function, aircraft availability, can not be expressed as a separable function of reparable parts, repair, transportation and administration; and (2) Little information is available on the consequences of expenditures in the 'support resource' areas of repair, transportation or administration.

Two new goals were established during the summer directly concerning the INTEGRATE project. The first goal was to explore conditions under which marginal analysis techniques would be optimal, given a nonseparable objective function. The second goal was to formulate algorithmic approaches to marginal analysis in the setting of INTEGRATE.

The last goal established is to research improved techniques for the estimation of demand rates and variance-to-mean ratios. In currently utilized AFLC models as well as the INTEGRATE project, it is necessary to estimate the rate at which aircraft parts fail, called the 'demand rate,'

and the corresponding variance-to-mean ratio. Models currently utilize a moving average estimator of the demand rate and a power function relationship between demand rate and variance-to-mean ratio to estimate the variance-to-mean ratio, based on a 1973 study by Stevens and Hill. In a 1984 study, Sherbrooke recommended using single exponential smoothing to estimate demand rate and a similar power function relationship to estimate the variance-to-mean ratio. The recommendations of Sherbrooke warrant further consideration. The final goal is to evaluate several smoothed estimators of demand rate, establish a corresponding power function relationship between demand rate and variance-to-mean ratio, then develop a variance-to-mean ratio or variance estimator based on individual part data to be shrunk toward the power function estimate to improve accuracy while maintaining reasonable stability.

III. MARGINAL ANALYSIS WITH A NONSEPARABLE OBJECTIVE FUNCTION:

As indicated in Section II, Aircraft availability is not a separable function of the logistics resources of interest, namely reparable parts, repair, transportation and administration. Hence, marginal analysis techniques are not necessarily theoretically optimal. The purpose of this section is to explore alternate conditions under which marginal analysis will yield optimal results.

For simplicity, consider one aircraft type, with aircraft availability depending only on one line reparable unit (LRU). Allocation of resources will include acquisition of stock supply of LRU's versus expenditures on repair resources. Thus aircraft availability depends on the stock level, x , and the level of repair, y .

If each expenditure is one LRU's worth, whether on stock or repair, then the possible combinations of expenditures on stock and repair can be represented by the set of points $\{(x,y) : x,y \text{ are nonnegative integers}\}$. Let $a(x,y)$ denote aircraft availability achievable by acquisition of x LRU's and an expenditure of y LRU's worths on repair. Then the objective is, for each positive integer k , to determine the point (x,y) which maximizes $a(x,y)$ subject to the constraint $x+y=k$.

Let $h(x,y)=a(x+1,y)-a(x,y)$ and $v(x,y)=a(x,y+1)-a(x,y)$ denote the increments in aircraft availability obtainable by acquiring one LRU's worth of stock and one of repair, respectively, given x LRU's and y LRU's worth of repair before acquisition. Thus, $h(x,y)$ and $v(x,y)$ denote the change in aircraft availability for a movement one unit from the point (x,y) in the horizontal and vertical directions, respectively.

In this setting, marginal analysis consists of starting at the point $(0,0)$ and at each stage moving one step either

horizontally or vertically on the grid. From a point (x,y) , a vertical step is taken if $v(x,y) > h(x,y)$ and a horizontal step is taken otherwise. Hence, the problem can be re-phrased as follows: Under what conditions on the functions $h(x,y)$ and $v(x,y)$ does marginal analysis determine an optimal path through the (x,y) grid?

One set of sufficient conditions follows:

- (C1) For fixed y , $h(x,y)$ is a decreasing function in x ;
- (C2) For fixed x , $v(x,y)$ is a decreasing function in y ;
- (C3*) For fixed x , $h(x,y)$ is an increasing function in y ;
- (C4*) For fixed y , $v(x,y)$ is an increasing function in x .

(C1) and (C2) are conditions of diminishing returns. Thus, for a fixed number of LRU's worths of repair, each additional LRU acquired yields a smaller increase in aircraft availability; Similarity, for a fixed number of LRU's, each additional LRU's worth of repair yields a smaller increase in aircraft availability. For sufficiently large values of x and y to overcome any flushout effect, (C1) and (C2) are probably reasonable conditions.

(C3*) and (C4*) are conditions of combined benefits. Thus, an expense on one resource causes an increase in the marginal benefit of an expenditure on the other resource. Just the opposite conditions are probably appropriate, that is, an expenditure on repair would probably decrease the need for LRU's in stock, and increased stock levels would probably decrease the need for efficient repair.

A preferable set of conditions would be as follows:

- (C1) For fixed y , $h(x,y)$ is a decreasing function in x ;
- (C2) For fixed x , $v(x,y)$ is a decreasing function in y ;
- (C3) For fixed x , $h(x,y)$ is a decreasing function in y ;
- (C4) For fixed y , $v(x,y)$ is a decreasing function in x .

(C1) and (C2) are the conditions of diminishing returns given previously. (C3) and (C4) are the conditions of combined diminishing returns. Thus, an expense on one resource causes a decrease in the marginal benefit of an expenditure on the other resource.

While conditions (C1-C4) seem realistic, they are not sufficient conditions for marginal analysis to be optimal.

Another condition which is by itself sufficient to insure optimality of marginal analysis is the following:

- (C5) For any point (x,y) , any relation θ in the set $\{<,=,>\}$, and any positive integer k , $v(x,y)\theta h(x,y)$ implies $(v(x,y)+\dots+v(x,y+k))\theta(h(x,y)+\dots+h(x,y+k))$.

Condition (C5) is a condition of multiplicity. Thus, if it is better at some stage to acquire one LRU than one LRU's worth of repair, it is also preferable to acquire k LRUs than k LRUs' worths of repair, and vice versa. Unfortunately, (C5) does not in general seem realistic.

The effect of (C5) during marginal analysis is, at each stage of movement in either a horizontal or vertical direction in the grid, to eliminate from future consider-

ation either a column or a row of points on the grid. There is an analogue to (C5) for $r > 2$ resources which is also a sufficient condition for marginal analysis to be optimal, in which case an $r-1$ dimensional subspace is eliminated from future consideration at each step.

IV. TWO ALGORITHMS FOR THE ALLOCATION OF RESOURCES:

An essential preliminary task to either assessment or allocation of resources is to determine the effects of possible expenditures on each of repair, transportation and administration. For example, if a fixed number of dollars is to be spent on repair, how should the money optimally be spent and what is the consequence for repair capabilities with respect to such items as 'percentage of items repaired at base level' and 'repair times.'

Having accomplished the above, the task of making capability assessments for given resource mixes could conceivably be achieved with the Dyna-METRIC model. For given expenditures on such resources as repair and transportation, one could determine the appropriate repair and transportation parameter values. Stock levels would also be determined based on corresponding expenditures in the obvious manner. This information could then be input to Dyna-METRIC for evaluation.

Hence, assuming the effects of possible expenditures on repair and transportation can be modeled, the principle task

facing the INTEGRATE project is that of determining balanced resource allocations. Concerning said task, let me suggest two possible procedures which might be implemented separately or in tandem, with the reservation that each would likely be computationally inefficient.

The first suggested procedure for allocation of resources is to apply marginal analysis in the usual way, that is, sequentially acquire resources, at each stage acquiring that resource which provides the maximum marginal increase in aircraft availability per cost.

The second suggested procedure for allocation of resources is to develop an algorithm which, when given an initial configuration of resource allocation, a corresponding cost and a target level of expenditure, iteratively uses marginal analysis to move toward the target level of expenditure. Thus, if the cost of the current allocation is below the target level of expenditure, marginal analysis is used to 'acquire' additional resources, and if the cost of the current allocation is above the target level of expenditure, marginal analysis is used to remove 'previously acquired' resources from the current allocation. Such an algorithm would oscillate about the target level of expenditure while moving towards a more balanced allocation of resources, similar to the procedure considered by Van Slyke (1982).

Several comments are now in order. Firstly, even considering only one aircraft type, aircraft availability is not a separable function of the resources under consideration. Thus, use of marginal analysis does not guarantee either procedure to reach an optimal solution. For the same reason, program implementation of either procedure will be less efficient than current procedures for parts allocation. In particular, while the usual sort values could be used to decide which aircraft part is marginally best to acquire at any stage, the marginal benefit of acquiring that part versus expenditures on repair, transportation or administration must be based on marginal change in aircraft availability per cost for each possible expenditure, and any expenditure on repair, transportation or administration would cause a need for recalculation of all sort values. The algorithm efficiency could be improved somewhat by recomputing sort values less often, probably with little or no loss of quality of the results.

Secondly, the two procedures each have inherent advantages and disadvantages. The principle advantage of the first procedure is that it conveniently yields allocations for the complete spectrum of expenditure levels, while the second procedure must be run separately for each expenditure level of interest. The principle advantages of the second procedure are accuracy and 'local' efficiency. The use of marginal analysis in both forward and backward

directions would presumably yield greater accuracy than using only forward marginal analysis, if the first procedure does not yield optimal solutions. Also, for a given level of expenditure, the second procedure could be more efficient if the initial configuration of resource allocation is good.

Finally, while the first procedure seems more attractive pragmatically, the second procedure could be implemented in tandem with the first for various levels of expenditure as verification of the results. Thus, forward marginal analysis could be used to construct a 'shopping list' for a broad spectrum of levels of expenditure, than the results for each level of expenditure of interest could be used as the initial configuration of resource allocation in the second procedure to try to improve the balance of resource allocation.

V. ESTIMATION OF DEMAND RATES AND VARIANCE-TO-MEAN RATIOS:

Implicit in the allocation and assessment of resources, whether just stock levels or also such resources as repair, transportation and administration, is the need to estimate the demand rate of each part and the corresponding variance-to-mean ratio (V/M). The currently implemented methods are based on the report of Stevens and Hill (1973). A moving average is used to estimate demand rate. Due to a typically limited history of data, the usual variance estimator was

considered to be too unstable. Hence, variance was assumed to be a function of the demand rate, then parts of comparable demand rate were pooled to obtain a more stable variance estimator, resulting in a power function relationship between demand rate and V/M . Sherbrooke (1984) suggested that, since demand rate may change with respect to time, it should be estimated using single exponential smoothing with a constant of 0.4, then V/M should be estimated by a power function of demand rate similar to that used by Stevens and Hill (1973). In each case, a 'proportion' method was used to help take into account the changing mean demand rates in the estimation of V/M .

Historical data suggests that mean demand rates do change with respect to time. As supporting evidence, R.G. Brown (1963) states that a smoothing constant larger than 0.3 for single exponential smoothing indicates a trend in the data, while Sherbrooke (1984) suggests using 0.4. As such, it would seem preferable to estimate the demand rate, M , using some smoothing technique that accounts for trends, such as double exponential smoothing. Various estimators of V/M should be evaluated using artificial data, perhaps including each of the following trend types for M : (i) constant, (ii) linear, (iii) quasi-exponential, (iv) sinusoidal, and (v) constant except for stepwise jumps. For each, various levels of variability could be investigated, including variances consistent with the currently implemented rela-

tionship between M and V/M . Some judgment will be required as to how conservative the estimator of M should be with respect to response to trends, preferably based on investigation of prevalence of various trend types in real data.

Having determined an estimator of the mean demand rate, the individual part demand rate should be used more directly to estimate the variance-to-mean ratio. It seems realistic to believe that any power function relationship used to estimate V/M from M would only provide approximate models to reality, leaving the accuracy of the models open to question. It would seem preferable to use the individual data for each reparable part to estimate the corresponding V/M . Stevens and Hill (1973) argue against such an approach on the grounds that the small amount of available data would yield an unstable, unreliable estimate. My suggestion is to use the data, but in the following conservative manner.

Having determined an estimator, $m(s)$, of the mean demand rate $M(s)$ at time s for each s less than some time t , one could use the squared differences between each $m(s)$ and the corresponding observed demand rate at time s , combined by some smoothing technique, as an estimator of variance at time t . Note that the variance estimate may change with time, as seems desirable, but would also be rather unstable. To stabilize the variance estimator, it could than be 'shrunk' towards the estimate of variance obtainable

from the power function estimate of V/M ('shrinking' is a Bayesian technique for taking a weighted average of an estimate based on collected data and one based on prior beliefs). Comparisons should be made between the relative magnitudes of the two variance estimators using real data in order to: (1) Identify any magnitude bias in the power function estimator; (2) Evaluate the stability of the 'real-data' estimator of variance; and (3) Determine the type and degree of shrinkage appropriate.

VI. MISCELLANEOUS TOPICS:

This section consists of brief comments on a variety of topics and problems encountered during the summer research period. These tend to be the less tractable of problems encountered.

A problem of potentially great interest is how to allocate or assess allocation of stock levels to multiple aircraft types simultaneously. While aircraft availability is a separable function of stock levels for one aircraft type, choice of the appropriate objective function for multiple aircraft types is less clear, and various somewhat reasonable objective functions are not separable. For example, rather than considering the probability, P_i , that the i th aircraft type is available, if there are N_i aircraft of the i th type, one could equivalently consider the expected number of aircraft, $N_i P_i$, of the i th type as the

objective function to be maximized. A reasonable but nonseparable extension to k aircraft types would be the objective function $w_1 N_1 P_1 + \dots + w_k N_k P_k$, where w_i is some weighting constant for $i=1, \dots, k$. Perhaps a more tractable approach would be, if the i th aircraft type requires q_i parts to be operational, to take the q_i th root of each sort value for that aircraft type. Then the order of sort values within an aircraft type would be unchanged, but parts for more sophisticated aircraft types would receive higher priority, perhaps with optimal allocation of resources for equal availability rates of those aircraft involved. A similar well planned modification of sort values could perhaps give a desired mix of unequal availability rates.

An interesting modification to the algorithms for allocation of funds for purchase of reparable units would be to include as an option the purchase of whole aircraft. Currently, some number of aircraft are acquired, then some level of availability is strived for by expenditures on reparable parts and other resources. One could conceivably have the same number of available aircraft at lower cost by achieving a better balance of number of aircraft versus support resources. Since the support cost involves more than just reparable parts, one must either include other resources such as EOQ items and manpower in the model, or the proportion of support cost attributable to reparable

parts must be estimated.

Assumptions such as infinite repair capacity in both allocation and assessment algorithms must be questioned. Some adjustment is made by increasing the mean repair time to include time waiting for availability of repair resources. However, if items are actually queued for repair, the Poisson distribution assumptions for pipeline segment contents may be less valid, as well as any assumptions concerning stochastic independence of contents of different pipeline segments.

How to prorate shared parts is a difficult problem. The current method is to decrease the cost of a shared part based on the percentage of use of that part by the aircraft type under consideration, causing more to be 'needed' by each applicable aircraft type. Then the maximum amount 'needed' by any aircraft type is acquired. Perhaps a more intuitively appealing approach would be to increase the cost of a shared part based on the percentage of use of that part by the aircraft type under consideration, causing less to be 'needed' by each aircraft type. Then one would acquire the sum amount dictated by all aircraft types. The latter approach seems more consistent with the benefits of commonality of parts and would require no adjustment of levels of expenditures for those aircraft types not driving the purchase level. As yet, I can not give theoretical justification for either approach.

A final problem worthy of mention is the 'flushout effect,' the effect that the marginal benefit of acquiring a specific reparable part does not necessarily decrease as the number in stock increases. For large acquisitions, the convexification of sort values currently employed in AAPM forces the marginal analysis approach to be optimal. However, concern should be expressed for models in which limited reparable parts are acquired, for example the WARS model.

VII. RECOMMENDATIONS:

These final recommendations concern both the INTEGRATE project and the estimation of demand rates and variance-to-mean ratios.

Concerning the INTEGRATE project, emphasis should be placed more heavily on the support resources such as repair, transportation and administration. The reasons are twofold. Firstly and of great importance, the structure required to integrate the various computer models for resources will depend on the type of information available concerning these resources. Comments herein have assumed that expenditure on repair can for example be done in some optimal way to reduce repair time or the proportion of parts not reparable at base level. However, optimal expenditure on repair may depend on other resources. Secondly, expenditure on support resources

may change with availability of new support resources, for example, the availability of new equipment such as new testing devices. Keeping an inventory of current resources and a list of new available resources will probably be both an important and difficult task. Let it be emphasized that the problems associated with the support resources are not yet even well identified.

Concerning the estimation of demand rates and variance-to-mean ratios, the power function used to estimate V/M from the demand rate was obtained in a rather ingenious way by Stevens and Hill (1973). However, it is based on the assumption that such a relationship holds for all parts, an assumption which is difficult to justify. It could be preferable to combine a real-data estimator for each individual part with the power-function estimator using a weighted average. The real-data component would allow for variation from the power function estimate, while the power-function component would force some stability, otherwise lacking in a purely real-data estimator based on a small sample. Ten years of A-7 data is being assembled and would serve as a useful data base. More accurate estimation of demand rate and variance-to-mean ratio would lead to better allocation and assessment of logistics resources, and hence is worthy of further study.

REFERENCES

1. Brown, R.G., Smoothing, Forecasting and Prediction of Discrete Time Series, Englewood Cliffs, New Jersey, Prentice-Hall, Inc., 1963.
2. O'Malley, T.J., "The Aircraft Availability Model: Conceptual Framework and Mathematics," Logistics Management Institute, Washington, D.C., 1983.
3. Pyles, Raymond, "The Dyna-METRIC Readiness Assessment Model," The Rand Corporation, Santa Monica, California, July 1984.
4. Sherbrooke, C.C., "Estimation of the Variance-to-mean Ratio for AFLC Recoverable Items," Final Report, AFLC/MMMA, January 1984.
5. Stevens, R.J., and J.M. Hill, "Estimating the Variance-to-mean Ratio for Recoverable Items in the ALS Marginal Analysis Algorithms," Working Paper Number 49, Systems Studies Branch, Office of DCS/Comptroller, AFLC, WPAFB, March 1973.
6. Van Slyke, R.M., "Calculating Change Vectors for the Exchange Method," Information Systems Consultant, Brooklyn, New York, November 1982.

1985 USAF-UES SUMMER FACULTY RESEARCH PROGRAM/

GRADUATE STUDENT SUMMER SUPPORT PROGRAM

Sponsored by the

AIR FORCE OFFICE OF SCIENTIFIC RESEARCH

Conducted by the

UNIVERSAL ENERGY SYSTEMS, INC.

FINAL REPORT

NATURAL LANGUAGE UNDERSTANDING USING RESIDENTIAL GRAMMAR AND
ITS USE IN AUTOMATIC PROGRAMMING

Prepared by: Dr. Christian C. Wagner
Academic Rank: Assistant Professor
Department and School of Engineering and Computer Science
University: Oakland University, Rochester, MI 48063

Prepared by: Dr. Peter J. Binkert
Academic Rank: Associate Professor
Department and Department of Linguistics
University: Oakland University, Rochester, MI 48063

Prepared by: Ms. Kathleen A. Malin
Academic Rank: MS Candidate in Linguistics
Department and Department of Linguistics
University: Oakland University, Rochester, MI 48063

Prepared by: Ms. Frances M. Vallyly
Academic Rank: MS Candidate in Computer Science
Department and School of Engineering and Computer Science
University: Oakland University, Rochester, MI 48063

Prepared by: Mr. Thomas L. Schnesk
Academic Rank: MS Candidate in Computer Science
Department and School of Engineering and Computer Science
University: Oakland University, Rochester, MI 48063

Research Location: Air Force Human Resources Laboratory
Training Systems Division
Lowry Air Force Base, CO 80230-5000

USAF Research: Hugh L. Burns, Major, USAF

Date: August 28, 1985

Contract No: F49620-85-C-0013

ABSTRACT

NATURAL LANGUAGE UNDERSTANDING USING RESIDENTIAL GRAMMAR AND
ITS USE IN AUTOMATIC PROGRAMMING

by

Dr. Peter J. Binkert
Dr. Christian C. Wagner

Mr. Thomas L. Schnesk
Ms. Frances M. Vallely
Ms. Kathleen A. Malin

The research outlined here focuses on the development of a methodology for the creation of a natural language interface. It includes a set of software tools and procedures based on a non-transformational theory of language called Residential Grammar (RG; Binkert, 1983, 1984, 1985). The development of the natural language tools began with two parallel efforts. The computer science team worked on the implementation of the LISP version of the RG syntactic parser of English, while the linguistic team concentrated on the development of a first set of semantic features out of which the case relations of language could be defined. Once completed, the natural language understanding tool could be integrated into a computer's operating system to act as an interface between a computer system and a computer user. This would reduce the confusion caused by the various command languages on different computer systems.

ACKNOWLEDGEMENTS

The entire research team would like to thank the Air Force Systems Command, Air Force Office of Scientific Research and the Human Resources Laboratory, Training Systems Division for a most exciting summer of research away from the ordinary cares of academic life. Major Hugh Burns and Colonel Crow should be especially commended for providing us with an environment of people, computers, and resources well-suited to our needs and they did so with a concern and courtesy that we all appreciated.

Although it may seem like a long list, we felt so welcomed by the people at the Air Force Human Resources Laboratory that we wish to thank a number of other people for the help they have given us:

Captain Massey, Captain Griffith, Master Sergeant Cruz

Dr. Martha Polson

Ms. Betty Slye

Mr. Rodney Darrah, Ms. Sue Espy

Dr. Roger Pennell, Dr. Joe Yasutake, Mr. Joe Gordon,
Mr. Alan Marshall

I. INTRODUCTION

In the summer of 1985, the Air Force Human Resources Laboratory (AFHRL), Training Systems Division, served as the host for a research project funded by the Air Force Office of Scientific Research through the Summer Faculty Research Program / Graduate Student Summer Support Program. The research was conducted by two faculty members and three graduate students from Oakland University, Rochester, MI. The central problem addressed by this research team was the understanding of natural language by computer. The goal of the research was to begin the development of a set of software tools for natural language understanding that could be applied to arbitrary software settings, thus, eliminating much of the redundant research now being carried on in natural language processing.

To the degree that natural language understanding tools could be built, a wide variety of Air Force and Human Resources Laboratory goals could be advanced. For example, a natural language understanding tool could be integrated into a computer's operating system to act as an interface between a computer system and a computer user. This could greatly reduce the confusion caused by the widely differing command languages on different computer systems like the VAX, the IBM and the Cyber systems available at AFHRL. Another place

in which a natural language tool could be of great service is in the many training activities of the Air Force. At the AFHRL, the tools would allow a more human-like communication between student and automated tutor as in the Rule-Kit expert system developed for them by General Dynamics. A natural language interface would allow responses to a wider range of arbitrary requests from the user of the expert system. As these few examples illustrate, once the natural language tools are developed, projects within the AFHRL need no longer create their own natural language systems but, instead, need only use the expanding set of tools.

The research team from Oakland was an interdisciplinary group consisting of three members from the field of computer science and two from linguistics. Dr. Christian Wagner, an assistant professor of engineering and computer science at Oakland University, has been an active researcher in artificial intelligence for twelve years and worked on externally funded research in applying AI to medical diagnosis and treatment as well as decision making in education. With colleagues at Oakland University he has co-chaired major artificial intelligence conferences, developed graduate and undergraduate courses in AI, and run professional development seminars on robotics and advanced automation. Recent research interests have included the

problems of automatic programming and the control of computer and robotic systems through natural language systems with hardware based semantics. Working with Dr. Wagner were two masters degree candidates in computer science, Frances Vallyely and Thomas Schnesk. Ms. Vallyely has extensive experience in LISP and training in artificial intelligence with an MS in mathematics. She is a university faculty member in computer science and mathematics at Lawrence Institute of Technology and The University of Michigan - Dearborn. With a BS in computer science, Mr. Schnesk has worked as a systems analyst for General Motors. During the last year he has served as a graduate teaching assistant at Oakland University, and faculty member in computer science at The University of Michigan - Flint campus.

Dr. Peter Binkert is an associate professor in linguistics at Oakland University. His theory of Residential Grammar, RG, (Binkert, 1983, 1984, 1985) is the basis for the syntactic parsing tool; the feature-based style of analysis begun in RG is also the basis for the first part of the semantic feature system, those defining cases. His vast knowledge of syntactic theory and extensive research experience were an absolute necessity for the project's progress. Kathleen Malin, a graduate student with an MS in linguistics, has been working with the theory of Residential

Grammar for the past year. Together with Dr. Binkert, she has been involved in the creation of a semantic feature system as well as in the perfection of a case feature system.

II. OBJECTIVES

The stated objectives for the summer research at Lowry Air Force Base were as follows:

1) Case Feature System - A major effort in the linguistic side of the research was the elaboration and clarification of a set of linguistic features out of which the case relations across human languages can be constructed. The use of features for the definition of case relations was to parallel the syntactic feature matrix of Residential Grammar.

2) Semantic Feature System - A central idea behind the planned research in machine understanding of language was that the semantic features for an artificially intelligent system must be grounded in reality. Two different methods for such grounding were attempted: grounding in the universals across human languages and grounding in the physical capabilities of a computer system. This effort

involved expertise in both linguistics and computer science as well as extensive exploration of semantic relationships.

3) LISP Implementation of RG Parser - Because LISP is (a) the language of choice for artificial intelligence in the United States, (b) is definable in the DOD language Ada (Reeker, 1985), and (c) is an easy language in which to implement feature-based systems, a major effort of the research was to translate an existing RG parser written in the language PL-1 into the language LISP.

4) LISP Implementation and Testing of Semantic Feature System - As the semantic feature system for defining cases was completed, it was to be implemented in LISP and integrated with the LISP version of the RG parser.

5) Design and Implementation of Natural Language Front End to an Automatic Programming Systems - The ultimate goal of this phase of the research was to connect the natural language understanding tool (including the syntactic and semantic components) to an automatic programming system.

As the research progressed, modification of the original objectives was required due to resource and time constraints. First, it was discovered that the current LISP capabilities at the Human Resources Laboratory were not

adequate, specifically, no supported and viable version of a LISP processor was available on their VAX computer system. The power of a VAX is generally required for natural language processing because of the large size of dictionary and encyclopedic entries for the words and concepts of the language. Contact was made with DECUS (the DEC users group) to see if a free version of LISP were available for VMS4.0 on the VAX. Unfortunately, it was not. The development of the computer systems, therefore, had to remain bound on the IBM-PC microcomputers for the duration of the project at Lowry.

As translation of the parser from PL-1 into LISP progressed, an unanticipated new objective arose, namely, the redesign of parts of the parser. As the graduate students worked to translate the parser, it became evident that changes had to be made to the parser to more clearly reflect the framework of the syntactic theory. For example, the format of the dictionary entries was modified to allow for the link between semantically related nouns, noun forms, verbs, verb forms, etc. Where words such as "think," "thinker" and "thought" were originally treated as three separate lexical entries, the revised dictionary now lists them all under "think," as subforms of one entry. In addition, the syntactic categories were slightly revised to not only

account for the change in the dictionary entries, but also to more accurately represent links between similar grammatical forms. For example, words indicating temporal and positional location such as "here," "there," "now" and "then" were previously classified only as nouns with the added feature of either +LOCATIVE OF TIME or +LOCATIVE OF PLACE. It became apparent that parsing could be facilitated if new quantifier categories were added to account for these concepts.

III. APPROACHES AND RESULTS

The development of the natural language tools began with two parallel efforts: one by the computer science team to work on the implementation of the LISP version of the syntactic parser of English, the second by the linguistic team to work on the definition of a first set of semantic features out of which the case relations of language could be defined. The results of these efforts are summarized below, by objective.

1) Case Feature System - The approach taken in the definition of a case feature system parallels the successful approach taken in the development of the feature system for the RG syntactic model: a search was made for a set of

semantic features out of which case relations could be defined. As the search proceeded, the two criteria constantly applied to the possible feature systems were the ability to explain case differences across natural languages and the expressibility of the features in terms of the hardware capabilities of computer and robotic systems.

Although not considered by the research team to be in its final form, a set of very promising semantic features has been specified out of which the case relations across natural languages can be defined. Even more, the proposed feature system seems to capture the generalizations of Fillmore's (1966, 1967, 1977) and Gruber's (1965, 1976) case theories and Schank's (1975, 1977) conceptual dependency theory without containing some of the inherent redundancy.

The current feature system provides a complete specification of the case or thematic relation played by every argument (noun phrase) in association with every predicate in the sentence. It provides a means for associating the syntactic components of the sentence such as "subject" and "object" with thematic roles such as "agent" and "patient." The system utilizes twelve binary features which are highly transportable across natural languages and across other conceptual models (e.g., case grammar and conceptual

dependency theory). The theory states that each case relation is an abbreviation for a group of semantic features, just as each syntactic category is represented by an abbreviation of syntactic features. For each semantic entry, all features are specified with one of three possible values: "+", "-", or "+/-". At the current time the twelve semantic features are divided into six primary features and six secondary features. Brief and informal definitions of the features, based on precise and technical specifications, are provided below:

PRIMARY SEMANTIC FEATURES:

POSITIONAL: + having a primary focus on location, orientation, or movement in space or time
- not having a primary focus on location, orientation, or movement in space or time

DISJUNCTIVE: + emphasizing separation
- separation not emphasized

CONJUNCTIVE: + emphasizing union or association
- union or association not emphasized

EXTENSIONAL: + emphasizing the extent of space
- extent of space not emphasized

PROXIMAL: + involving contact
- non involving contact

FIRST ORDER: + involving relationships relative to a point, line or surface
- involving relationships relative to area or volume

SECONDARY SEMANTIC FEATURES:

TEMPORAL: + focusing on time
 - focusing on place

Relating to the x, y, z axes:

VERTICAL: + a positive value on the z axis
 - a negative value on the z axis

HORIZONTAL: + a positive value on the x axis
 - a negative value on the x axis

FRONTAL: + a positive value on the y axis
 - a negative value on the y axis

INTERVAL: + involving a medial position
 - not involving a medial position

INTENSIVE: + involving a range from average to
 maximal
 - involving a range from minimal to
 average

Given the existing case feature system, a classification scheme for verbs and prepositions is being created for the efficient storage of large numbers of syntactic and semantic features through simple inheritance networks.

The case feature system proposes that case relations like GOAL, EXPERIENCER, SOURCE, AGENT, et cetera, are actually labels for constellations of semantic features. The commonality in GOAL and EXPERIENCER is the feature [+CONJUNCTIVE] which denotes association or union; the

commonality in SOURCE and AGENT is [+DISJUNCTIVE], which denotes dissociation or separation. Therefore, the fact that the same thematic marker (preposition, postposition, grammatical case, etc.) is used for a variety of thematic relations can be attributed to the presence in those relations of the same feature. The loss of descriptive adequacy in theories of case grammar is shared by other related theories and semantic systems; the common features associated with thematic relations are not expressible, and it becomes a complete accident that the same marker is used across relations.

In addition to the loss of descriptive adequacy, there is a loss of explanatory adequacy in other theoretical frameworks. Thematic relations like SOURCE and GOAL cannot be related in any direct way to the concepts which form semantic networks or to the concepts which underlie other semantic constructs, e.g., the primitives in conceptual dependency theory (Schank 1975, 1977). In short, there is little transportability between the systems, so that the valuable insights of each cannot be gathered into one framework.

For example, it is clear that thematic relations like SOURCE and GOAL from case theory are associated with primitives like EXPEL and INGEST from conceptual dependency theory. But

the two theories are constructed in such a way that this association cannot be specified. Yet, the grammatical facts of natural language, in particular, the distribution of thematic markers, clearly indicate that there must be a connection between thematic relations and semantic fields in general. The same feature which shows up in relations like SOURCE and AGENT ([+DISJUNCTIVE], e.g., "from") should form part of the definition of words like "aversion," "deprive," "need," and so on; and, that feature should also show up in the definition of a primitive like EXPEL if a theory contains such a primitive. Similarly, the same feature that shows up in relations like GOAL and EXPERIENCER ([+CONJUNCTIVE], e.g., "to") should form part of the definition of words like "inclination," "supply," "abundance," and the like and show up in a proposed primitive like INGEST. This feature-based approach to thematic relations provides an explanation for why the same groupings of markers occur repeatedly in natural languages.

The feature system has been challenged through native speaker intuition and comparison to other languages, specifically Japanese. It appears, at this time, that the case feature system proposed here has an advantage over other case grammars. Since the system asserts that the [-POSITIONAL] relations are based on the [+POSITIONAL] ones,

at least the framework for [-POSITIONAL] is given by the existing one for [+POSITIONAL]. As a result, any number of nonpositional thematic relations can and have been posited. The case feature system can explain why the same grammatical case, preposition or postposition ("from" in examples a-g below) embraces both positional and nonpositional relations in examples such as the following:

- a. He ran from his office.
- b. He is back from Europe.
- c. Keep this away from the children.
- d. She can't tell red from orange.
- e. He can't find any relief from pain.
- f. They will be here an hour from now.
- g. We got a note from the dean.

It explains why a class like "separative notions" should remain intact diachronically and dialectally.

In addition to the above linguistic support for the case feature system, given a perceptual apparatus (human or machine), the feature definitions can be made very precise. The feature [+/-POSITIONAL] (an intentional renaming of +/-

CONCRETE to emphasize the hardware grounding of the feature) divides semantic concepts into two sets: those that are abstract ([-POSITIONAL]) and those that are concrete ([+POSITIONAL]). This opposition can be precisely defined in terms of the physical capacities of real computing systems. At Oakland University, our Automatrix Vision system can compute the area of any object in its visual field with a call to the system function TOTAL_AREA. If, in the computer's memory, a concept has been associated with a non-zero area, it must be concrete ([+POSITIONAL]), i.e., the computer has seen one or been informed that it is possible to see one. If no such association exists, the concept must be abstract ([-POSITIONAL]). By relating as many of the features as possible to the physical capacities of the system in this way, we can begin to attribute real understanding to the computer system, in particular, understanding that makes possible independent verification of natural language statements it receives. Though the entire system has yet to be completed, the case features will be applied to all syntactic categories in hopes of producing a comprehensive semantic description of any given language. The case feature system must be integrated into the larger semantic model and semantic net.

2) Semantic Feature System - Outside of the semantic features defining case relations, little explicit or

extended work was possible on semantic features. We discovered, however, the existing semantic features do, in fact, provide an explanation for the multiple senses and wide range of associations typically given to verbal expressions. It provides a means for specifying higher cognitive concepts such as comparison and quantification. For example, given the verb pair "enter/exit," an adequate semantic mapping of the pair would include the following information:

- a. They are motion verbs.
- b. 1. "enter" indicates motion forward;
2. "exit" indicates motion away.
- c. They indicate contact with the location.
- d. They require three dimensions.
- e. The dimension of the location varies.
- f. They are related to the prepositions "into/out of" respectively.
- g. They mean "go into/go out of."

The RG case feature system represents these relations as follows:

- a. [xDISJUNCTIVE, -xCONJUNCTIVE] (Where -x implies the opposite value of x and x may be +/-)
- b. 1. "enter" is [-DISJUNCTIVE, +CONJUNCTIVE]
2. "exit" is [+DISJUNCTIVE, -CONJUNCTIVE]
- c. [+PROXIMAL]
- d. [-FIRST ORDER]
- e. [-EXTENSIONAL]

- f. "into/out of" have the same features
- g. go is [xDISJUNCTIVE, -xCONJUNCTIVE]

In order for a semantic parser to be utilized in a natural language processor, there must be a theory of semantics as its underlying base. The notion of semantic nets became the model for the base.

A semantic net is a graphical method used for the representation of knowledge. A net consists of nodes representing objects, concepts, or events, and links between the nodes, representing their interrelations. One key feature of the semantic net representation is that important associations can be made explicitly and succinctly: relevant facts about an object or concept can be inferred from the nodes to which they are directly linked, without a search through a large database.

The theoretical aspects of the semantic theory for parsing natural language are in the final stages of formalization. Unfortunately, due to time restrictions, we were unable to complete the implementation of a semantic feature system that would adequately represent the scope of human perceptions within the framework of semantic nets.

3) LISP Implementation of RG Parser - One of the primary objectives of the research to be carried out at Lowry AFB was to translate the existing RG syntactic parser into LISP. Initially the RG parser was implemented using PL/I on the MULTICS system at Oakland University.

The motivation for selecting LISP, as the language of choice over the PL/I version was several fold. LISP is generally acknowledged as the standard U.S. language for work done in the realm of artificial intelligence. A LISP representation facilitates the introduction of semantic features. Also, variations on LISP written in ADA are currently under consideration.

Initially the focus of the work on the parser was viewed as a straight forward task of translation from PL/I into LISP. As the translation process proceeded, however, several problems arose. It became clear that the implementation of the original parser was not conducive to a simple translation into a transportable LISP system. The PL/I parser used character strings and non-portable system calls to the MULTICS mainframe system extensively. Indexing, rather than recursion, was used throughout for the purpose of searching forward and backward over a given sentence. The PL/I routines were excessively large and used deeply nested if-then constructions. Finally, the theoretical basis for

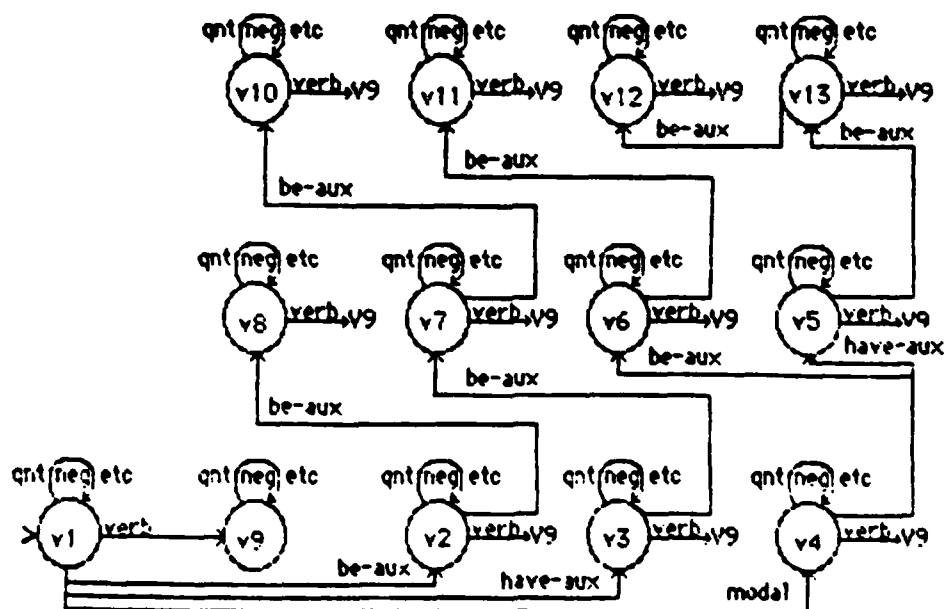
the parser, the RG model, had taken on several important improvements and modifications since the original parser was written. Because of these and other design considerations, an alternate format and some extensive redesign of the system became necessary to take full advantage of LISP as well as the theory of Residential Grammar.

The first step in the design of the LISP system was an investigation into an appropriate global data structure for the representation of the required graphemic, syntactic and semantic knowledge required. As with most LISP systems, the choice of data structures was essentially a semantic network. The net centered on five major node types: word nodes, concept nodes, syntactic nodes, semantic nodes, and functional nodes. Word nodes represented the graphemic input that the system could receive. Each word node was hooked to one or more concept nodes that contained all information relative to the word. The concept node pointed to the various syntactic types of the concept which, in turn, were connected to the various semantic meanings for the given syntactic type. Finally, the semantic meaning was hooked to a functional node which specified the precise function call and argument list required to perform any action.

This data structure required the creation and implementation of numerous constructor and selector functions. Once these

were complete, a dictionary of several hundred concepts was prepared. These concepts contained virtually all of the functions words of the language and enough of the content words to provide an adequate test of the system software.

As the LISP parser evolved, the use and control of these data structures was managed in a way different than the original PL/I parser, specifically, an augmented transition network (ATN) system was created and various, separate ATNs were created to handle the problems of word disambiguation and functional analysis. The following is a graphical representation of an existing ATN designed for the purpose of disambiguating verbs:



The many, small ATNs that were created each performed specific tiny tasks. The decisions made by the ATNs were only those decisions that were certain so that no backup and no unnecessary searching was performed. The ATN formalism provided a means for specifying the logic of parsing in a manner that more closely reflected the role of the syntactic categories of RG theory. The modularity of the independent ATNs also helped to clarify the grammatical disambiguation process and enhance the possibilities for alteration or expansion of the disambiguation process at a later time if it becomes necessary. Although extensive testing has not been completed, we feel that the benefits of the change from the PL/I design to the ATN design in LISP will be quite notable. This change in objective has required substantially more time than anticipated since the control flow of the PL/I program was no longer very useful in the translation process.

The balance of the effort involving the LISP parser was centered on the implementation of routines to handle the functional analysis process.

4) LISP Implementation and Testing of Case and Semantic Feature System - This is the one objective that could not be realized during the summer research. The primary reason for this was the greater than expected time commitment required

for the translation of the PL/I parser into LISP. Although the objective was not met, a great deal was learned about the problem that will make the eventual solution more correct and rapid. First, the ATN system for manipulating the syntactic parsing provides a straightforward formalism for the statement of the case relationship and semantic processing we will require. Second, the delay will provide us with greater time to study the proposed semantic feature system before attempting to implement them. There is a degree of uncertainty, at this time, as to the correctness of the specific features chosen for case analysis since there is no underlying model yet developed that will predict what these features should be (as there was a specific tree model that predicted the twelve syntactic features of the original parsing system).

5) Design and Implementation of Natural Language Front End to an Automatic Programming Systems - Research efforts for the design and implementation of a natural language front end to an automatic programming system had to begin, obviously, with the development of an automatic programming system itself. The design chosen centered on the concept that a computer's understanding must be grounded in the primitive processes that it can perform.

The design and implementation of the automatic programming system (AUTOP) is still in its formative stages; however, many of its characteristics have been defined. The overall model of the system design process will be based on the PSL/PSA system developed by Teichroew (1978). This system has been widely used in industry and government and seems to have the expressive power to describe an information processing environment. The focus of AUTOP will be to develop a running computer system in a top down fashion that eventually connects to primitive functions of which the underlying computer system is capable. This development will be based on an interactive dialog between the user and the program environment concerning, initially, the five major aspects of a computing system: input, storage, processing, output, and control.

During this short summer session, only a few of the AUTOP components were designed and tested. This allowed a small automatic programming system to be written and tested in a short amount of time. More interestingly, however, the components developed during the ten weeks now act as new primitives available to the AUTOP user in the creation of other new system. For example, in the creation of the program AUTOP, a set of menu driving functions were created (i.e., functions for the construction of data structures required by a menu and routines for the use of these

structures to display a menu, get a selection, and take the designated action). These menu routines are used by AUTOP to perform its functions. In addition, however, these menu routines are now available for AUTOP to use, itself, as it helps another user create a new system. Indeed, in typical computer science style, it might be possible to specify the AUTOP program itself using the AUTOP system. As the AUTOP system expands, the set of "basic primitives" that become the foundation for other systems expands in size and complexity.

At the current time, the basic primitives are divided into two classes: selector and constructor functions. As their names imply, constructor functions enable the user to define and build the basic data structures required and the selector functions query the data structures. The overall goal of an automatic programming system is to define these two basic primitive classes for the user's data and connect them together into a comprehensive working system whereby the user can interactively interface with a computer and design a functional problem solving tool.

The implemented parts of the main system provide control over initial start up (access) of the system and, then, allow eight possible activities. These activities center on the definition of the computing task required by the

user. They are as follows:

1. Create a new system
2. Work on an existing system
3. List existing systems
4. Save a system to a disk
5. Load a system from a disk
6. Run an existing system
7. List data in an existing system
8. Terminate the programming session

These eight options are developed and accessed by the constructor and selector functions that are recursively linked.

Since the main system is divided into separate activities that, in turn, will need to be subdivided, it was only logical that one of the first constructor functions required was that of a menu builder. Menu listing and selecting functions logically followed. These functions can, then, be accessed by the user to develop and build menus as necessary for his individual programming needs while accessing the system, thus utilizing the recursive features of the system. To date in the project, development includes the ability to control and limit access to the system, create a subsystem and establish security for that subsystem, list all

subsystems and save subsystems to a disk for later access.

Work is continuing in the area of describing and building the actual data structures required for the subsystems. The development of data structures is heading in the form of menu and form type input. Eventually, it is the goal of the team to incorporate the natural language tools described earlier into the automatic programming system.

IV. RECOMMENDATIONS AND FUTURE RESEARCH

Our comments on the summer research center on two different areas: the success and future directions of the research performed over the summer and an evaluation of the summer faculty research program and the graduate summer program as well.

Overall, the research effort over the summer was quite successful. Major sections of the RG parser have been implemented in LISP using the ATN formalisms, a tentative set of semantic features for defining case relations is complete, the ATN formalism is ready for the implementation of the case relation data, and the automatic programming system which can eventually be connected to the natural language understanding system has been started.

The current research will continue on several fronts. The natural language understanding tools being developed will be extended to: (1)implement the semantic feature system and extend the semantic framework beyond features associated primarily with verbs to features of other categories; (2)construct semantic nets from the new features; and (3)connect the features and nets to the hardware and software capabilities of existing computer systems. The parsing system will also be examined from another angle, to see if it would be possible for the syntactic parsing program to build the actual RG tree structures as an outcome of parsing the sentences. This would guarantee the correctness of the parser, demonstrate the strengths of the RG theory, and provide a visual demonstration of the same theory. Finally, the automatic programming system will be refined and expanded, possibly as part of a doctoral dissertation, to allow for the creation of simple computer systems under computer control.

The extension to the semantic features for our system will begin with the primitive perceptual, motor, and reasoning capabilities of a network of hardware and software available at Oakland University. This network will serve as a useful target at which our initial investigations of higher level semantic concepts will be aimed, but should in no way be viewed as a limiting or final choice. On this network, we

have an AUTOVISION II system from Automatix, Inc., a PUMA robotic manipulator from Unimation, and a MACLISP programming environment from Honeywell. These hardware and software resources provide us with approximately 45 visual parameters for sensing visual data about an object in a computer's field of view, ten manipulator parameters for sensing position of the arm and controlling its operation, and hundreds of MACLISP functions for sensory, reasoning and control functions.

The reexamination of the parsing method has been suggested by the staff because of the non-obvious way in which the RG model is currently implemented. As a series of separate ATNs, the present LISP parser more clearly isolates the syntactic features of RG. However, a much more concise description of RG is possible now that the ATN formalism has been implemented. Once the co-occurrence restrictions of the various parts of speech are specified, the tree structure defining the functional structure of a sentence can be specified. Therefore, if possible, we hope to examine a method of parsing by the merging of RG trees.

The automatic programming system will continue to expand in the five areas described earlier: input, storage, process, output, and control. Essentially, the varieties of inputs

are relatively limited, i.e., a menu input, a form input, a prompt-response input, an analog input, and maybe a few others. The storage types are similarly limited to a small set of primitive types and then a construction mechanism for building arrays and structures from them. As all of the five areas are examined, it becomes clear that recursive nets of inputs within inputs, outputs within outputs, etc. combined with the constraints of the type from PSL/PSA can adequately describe a system. The key is that the bottom of these hierarchies must be in the physical capacities of the software/hardware system on which the program is being developed.

In essence, the purpose of our future research is to develop a system whose understanding is built upon a particular set of hardware capabilities so that it can comprehend not only concrete relationships but also abstract ones. There is a continuous thread from the RG syntactic features that specify grammatical relations to the semantic features that specify case relations to the semantic relations that specify higher cognitive concepts. This entire progression is grounded in the sensory, motor and reasoning capacities of a hardware system.

As for the USAF program and the UES contractors, we have only praise. The members of the Air Force at Lowry were

exceptionally open and helpful in getting us set up and giving us a place to work, supplies, and people to work with. From Colonel Crow and Major Burns to the enlisted personnel, from other university faculty at the HRL to civilian employees, the courtesy and concern for our work was refreshing and appreciated. The contractors from UES were flexible, friendly and demonstrated an efficiency that we at a university greatly envied. The possibilities for integrating our research into the programs of the USAF are much greater as we have made many contacts with members of the military and artificial intelligence researchers here in the University of Colorado. We all feel that the program offered by the Air Force for summer faculty and graduate student research is outstanding and are very glad that we were given the opportunity to participate.

REFERENCES

- Binkert, P.J. (1983). Syntactic features in nontransformational grammar. In A. Chukerman, M. Marks & J. Richardson (Eds.), CLS 19, Papers from the nineteenth regional meeting, Ann Arbor, MI: Edwards Brothers.
- Binkert, P.J. (1984). Generative grammar without transformations, New York: Mouton Publishers.
- Binkert, P.J. (1985). Categorical versus feature-based parsing. To appear in Proceedings of the third annual conference on intelligence systems and machines, Oakland University, Rochester, MI.
- Fillmore, C. (1966). Toward a modern theory of case. In D. Reibel and S. Schane (Eds.), Modern studies in English. Englewood Cliffs, NJ: Prentice-Hall.
- Fillmore, C. (1967). The case for case. In E. Bach and R. Harms (Eds.), Universals in Linguistic Theory. New York: Holt, Rinehart and Winston.
- Fillmore, C. (1977). The case for case reopened. In P. Cole and J. Sadock (Eds.), Syntax and semantics, vol. 8. New York: Academic Press.
- Gruber, J. (1965). Studies in lexical relations. Doctoral dissertation, MIT. Bloomington: Indiana University Linguistics Club.
- Gruber, J. (1976). Lexical structures in syntax and semantics. New York: North-Holland.
- Schank, R.C. (1975). Conceptual information processing. New York: American Elsevier.
- Schank, R.C. & Abelson, R.P. (1977). Scripts, plans, goals, and understanding. Hillsdale, N.J.: Lawrence Erlbaum.
- Teichroew, E. (1978). PSL/PSA. ISDOS Project, Department of Industrial and Operations Engineering, The University of Michigan, Ann Arbor, MI.

1985 USAF-UES SUMMER FACULTY RESEARCH PROGRAM/
GRADUATE STUDENT SUMMER SUPPORT PROGRAM

Sponsored by the
AIR FORCE OFFICE OF SCIENTIFIC RESEARCH

Conducted by the
UNIVERSAL ENERGY SYSTEMS, INC.

FINAL REPORT

STABILITY AND CONTROL COMPUTER PROGRAM FOR
CONCEPTUAL AIRCRAFT DESIGN

Prepared by:	Dr. Richard C. Walker
Academic Rank:	Associate Professor
Department and University:	Department of Aeronautics Miami University, Oxford, Ohio
Research Location:	Flight Dynamics Laboratory, Office of Technology Assessment, Design Branch, Wright-Patterson AFB
USAF Research:	Mr. Terry Smith
Date:	15 September 1985
Contract No:	F49620-85-C-0013

STABILITY AND CONTROL PROGRAM FOR
CONCEPTUAL AIRCRAFT DESIGN

By

Dr. Richard C. Walker

ABSTRACT

The report is concerned with the method and code verification phase in the development of a computer program-SACP-which computes aerodynamic parameters and stability and control derivatives, for aircraft at the conceptual design level. A comparison of stability parameters obtained using SACP and the well established Digital Datcom is presented for a wing-body-tail configuration, as well as a comparison of SACP results with F-15 data. The generally good agreement of the comparisons indicates that SACP can be used with a good degree of confidence at the conceptual design level for the class of configuration investigated.

ACKNOWLEDGMENTS

The author thanks the Air Force System Command, the Air Force Office of Scientific Research, the Air Force Flight Dynamics Laboratory, The Office of Technology Assessment and the Design Branch for the opportunity to spend a very interesting summer with people interested in aircraft design at Wright-Patterson AFB, Ohio.

Many thanks are extended to Mr. James Parker, chief of the Design Branch, for his part in arranging the fellowship and his support during the research activity. Special thanks are also due to Mr. Terry Smith, principal developer of SACP, for his input and assistance.

I. INTRODUCTION

As part of a continuing program to improve its in-house aircraft design methodologies, the Design Branch of the Air Force Flight Dynamics Laboratory is developing a stability and control analysis computer program-SACP⁽¹⁾-appropriate to the conceptual and early phases of preliminary aircraft design.

In general, a detailed stability and control analysis of an aircraft configuration is necessary to ensure it meets all handling qualities and airworthiness requirements. In the conceptual design phase however, a rapid-less detailed analysis is performed to:

- 1). size and locate the vertical and horizontal surfaces
- 2). size control surfaces
- 3). determine if artificial stability and control augmentation devices will be required.

Roskam⁽²⁾ lists three methods (in order of increasing complexity) to ensure that stabilizing and control surfaces are adequate:

- 1). Volume coefficient method - developed on the premise that similar class aircraft will have a similar value of tail volume coefficient.
- 2). Static stability and control power criteria method - requires data and analysis to determine:
 - a). minimum static margin
 - b). adequate rotation at take-off
 - c). engine-out flight
 - d). cross-wind landing capability
 - e). trim drag

3). Dynamic stability criteria methods - require data and analysis to determine:

- a). short period motion
- b). phugoid motion
- c). roll, spiral and dutch roll stability

The stability and control program being developed by the Design Branch is at the method 2 and 3 analysis level with major emphasis on method 2. My involvement in the project came about because of my interest and background in aerodynamics, aircraft design and computers. The point at which I joined the effort was at the verification and validation of methodology and program code.

II. OBJECTIVES OF THE RESEARCH EFFORT:

The overall objective of my summer research effort was to continue development of a stability and control computer program to aid in aircraft design at the conceptual design level. Although the stability and control program-SACP-which runs on a PRIME 750 mini-computer has been under development for some time, it had not yet been developed to the point to make it useful in the design process. My specific objective was to verify and validate SACP for a wing-body-horizontal-tail-aircraft configuration.

III. APPROACH

The approach taken to validate the methods and code of SACP was to:

a) review and update, where necessary, methods of computing the aerodynamic parameters and stability derivatives and, b) run and compare test cases ranging from a simple configuration in Digital Datcom⁽³⁾ to a more complex F-15 configuration. Intermediate and final values of parameters calculated by SACP were compared with independently determined values. Any errors in coding or methodology were corrected as they were encountered.

A summary of the main computation sources incorporated in SACP is presented next, and then a comparison of results of the test cases.

IV. AERODYNAMIC AND STABILITY DERIVATIVE METHODS

The construction of SACP is modular so that when a more attractive method of computing a parameter becomes available, it can easily replace the existing method. Current methods incorporated in SACP to compute aerodynamic parameters and stability derivatives come from three main sources^(4,5,6).

Methods of Reference 4 are empirically based and are used in SACP to compute zero angle of attack aerodynamic coefficients: drag, C_{D_0} ; lift, C_{L_0} ; and moment, C_{M_0} .

Reference 5 methods are semi-empirical and were developed to estimate aerodynamics forces in all speed regimes, including transonic, and at high angles of attack. These methods are incorporated in SACP to compute the lift coefficient, C_L , and the change in lift coefficient with angle of attack, C_{L_α} , for each aircraft surface. Methods from this reference are also used to compute the induced drag coefficient, C_{D_i} , and the downwash at the horizontal tail.

V. RESULTS

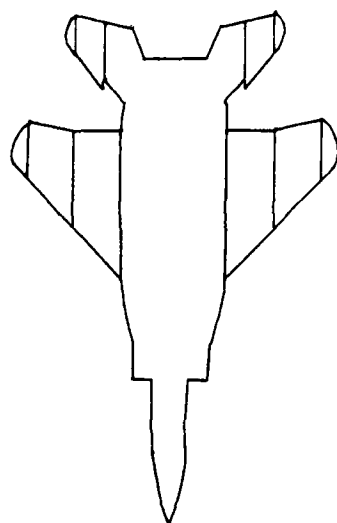
Table I contains a comparison of stability derivatives computed by SACP and Digital Datcom⁽³⁾ for the wing-body-horizontal-tail-vertical-tail configuration used as one of the test cases in this study. The data is presented for a flight Mach number of .6 and an angle-of-attack of 2 degrees, with similar Reynolds number for both computations. Aerodynamic and stability derivatives carry a conventional sign notation such as those used in Digital Datcom. Except for C_{L_α} , the difference in the values of the stability derivatives calculated by the two computer programs, as shown in Table 1, are well within the prediction accuracy Roskam⁽⁷⁾ believes attainable using theoretical methods. The difference in the C_{L_α} values indicated in Table 1 does not appear to have a large effect in the difference in the C_L vs α curves computed by SACP and Digital Datcom as shown in Figure 1. Good agreement between the two methods is indicated up to 20° angle-of-attack.

Figure 2 indicates excellent agreement in C_L data between that calculated by SACP and that reported in Reference 8 for the F-15 at $M = 1.6$.

Tables 2 and 3 contain a comparison of aerodynamic center data for the two test cases. The close agreement in the F-15 test case at $Mach = .9$ is probably fortunate, considering the uncertainties in in transonic aerodynamic force prediction methods.

Table I Comparison of stability derivative Digital Datcom example problem 3,
Flight Mach = 6, Angle of Attack = 2°

Derivative	DATCOM ⁽³⁾ (per degree)	SACP (per degree)	Difference (%)	Predicted Accuracy ⁽⁷⁾ (%)
Lift coefficient w.r.t. angle of attack, C_{L_α}	6.59×10^{-2}	7.42×10^{-2}	13	±5
Pitching moment coefficient w.r.t. angle of attack, C_{M_α}	-1.35×10^{-2}	-1.32×10^{-2}	2	±10
Yawing moment coefficient w.r.t. side slip angle, C_{N_β}	3.82×10^{-3}	4.31×10^{-3}	13	±15
Rolling moment coefficient w.r.t. side slip angle, C_{l_β}	-2.08×10^{-3}	-2.16×10^{-3}	4	±20
Pitching moment coefficient w.r.t. pitch rate, C_{M_q}	-1.38×10^{-1}	-1.37×10^{-1}	.7	±20
Pitching moment coefficient w.r.t. angle of attack rate, $C_{M_{\dot{\alpha}}}$	-6.46×10^{-2}	-7.03×10^{-2}	9	±40
Rolling moment coefficient w.r.t. roll rate, C_{l_p}	-8.38×10^{-3}	-7.47×10^{-3}	13	±15
Yawing moment coefficient w.r.t. Yaw rate, C_{N_r}	$-.4.55 \times 10^{-3}$	-5.19×10^{-3}	14	±25



MACH NO
□ — 1.6

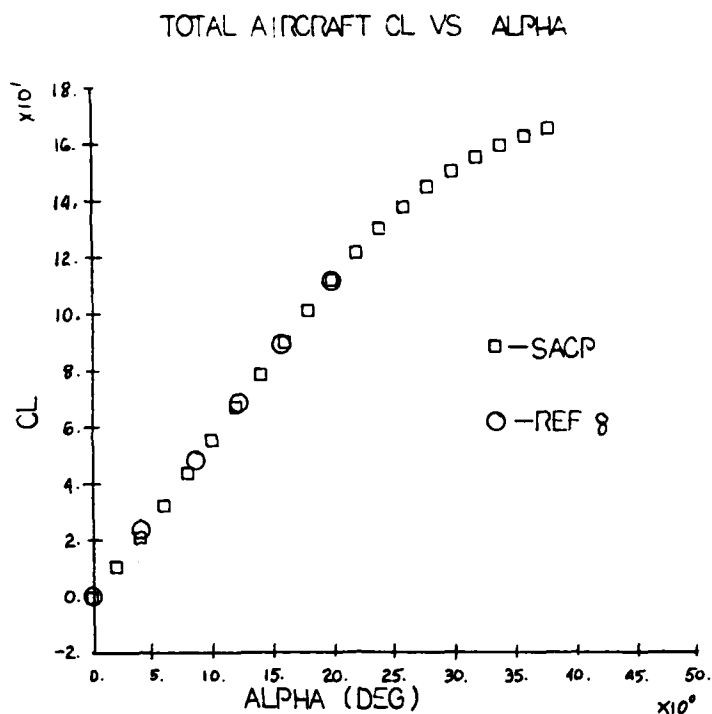
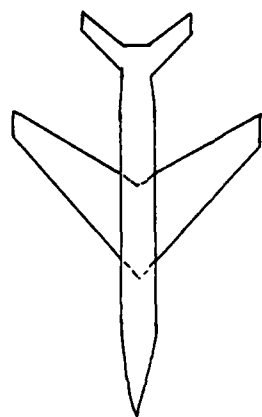


Figure 2. Digital Datcom configuration test case



MACH NO
□ — .6

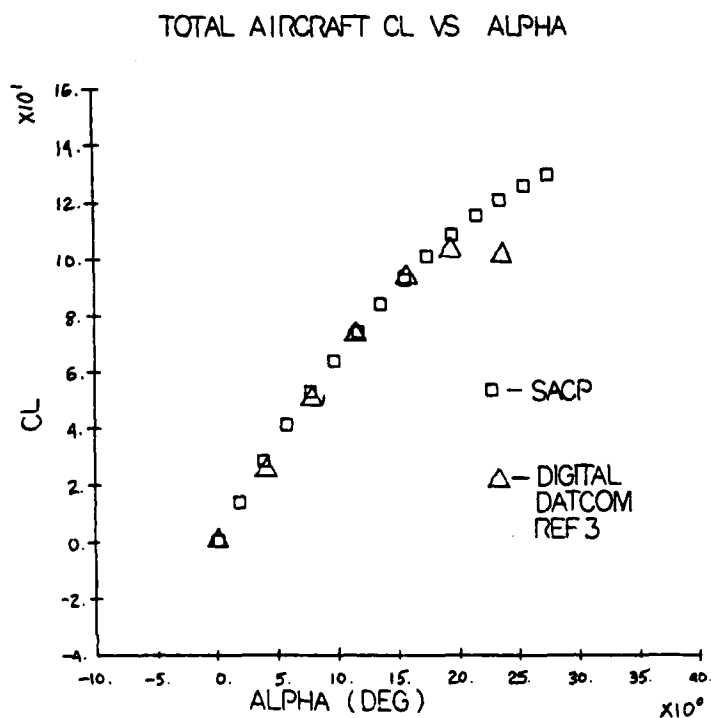


Figure 1. F-15 test case

Table 2 F-15 Test Case - Aerodynamic center comparison

FLIGHT MACH	SACP	REFERENCE 8
	% mean aerodynamic chord	% mean aerodynamic chord
.227	.334	.328
.9	.352	.325
1.6	.542	.568

Table 3 Digital Datcom configuration test case - Aerodynamic comparison

FLIGHT MACH	SACP	Digital Datcom ⁽³⁾
	% mean aerodynamic chord	% mean aerodynamic chord
.6	.422	.423

VI. RECOMMENDATIONS

Based on the data presented in this report and experience gained with the stability and control program (SACP) during my summer research activity, the following recommendations are made:

- 1). Use SACP in conceptual aircraft design studies to calculate stability parameters for wing-body-horizontal tail-vertical tail configurations.
- 2). Continue the development of SACP with the verification of methods and code for wing-body-canard and wing-body-canard-horizontal tail configurations.
- 3). Verify code and methods for computing control derivatives, and add spoilers and differential horizontal tail methods for roll control.

- 4). Check analysis methods which determine: rotation at take-off engine-out flight, cross-wind landing capability, trim drag and rolling capability.

The list for further development of SACP could of course be added to, like adding: multiple element high lift devices, ground effect, propulsive trimming, interface with a computer aided design geometry package and criteria for augmented stability vehicles. Completion of recommendations 2 through 4, however, would result in a very useful computer program for the stability and control analysis of general classes of configurations.

REFERENCES

1. Smith, Terry S., "Stability and Control Methodology for Conceptual Design," AFWAL-TR-(in progress).
2. Roskam, J., "Stability and Control", Classnotes-Aircraft Design Short Course, Bergamo Conference Center, Dayton, Ohio, July 1982.
3. William, John E. and Steven K. Vukelicha, "USAF Stability and Control Digital Datcom", Vol.II. AFFDL-TR-79-3032, April 1979.
4. Schemensky, R.T., "Development of An Empirical Based Computer Program to Predict the Aerodynamic Characteristics of Aircraft" Vol. I., AFFDL-TR-73-144, November 1973.
5. Axelson, John A., "AEROX-Computer Program for Transonic Aircraft Aerodynamics to High Angles Of Attack", Vol.I. NASA TM X-73,208, February 1977.
6. Hoak, D.E., "USAF Stability and Control DATCOM", October 1960, revised 1975.
7. Roskam, J.; Airplane Flight Dynamics and Automatic Flight Control Systems; Parts I and II, 1979; Roskam Aviation and Engineering Corporation, Route 4, Ottawa, Kansas 66067.
8. Thomas, R.W., "Analysis of Aircraft Stability and Control Design Methods", Vol.II, AFWAL-TR-84-338, May 1984.

1985 USAF-UES SUMMER FACULTY RESEARCH PROGRAM

Sponsored by the
AIR FORCE OFFICE OF SCIENTIFIC RESEARCH

Conducted by the
UNIVERSAL ENERGY SYSTEMS, INC.

FINAL REPORT

Compilation of Select Aspects of the Air Force
Weapons Laboratory's 1984 History

Prepared by:	Doris J. Walker-Dalhouse
Academic Rank:	Associate Professor
Department and University:	Early Childhood, Elementary Education and Reading
Research Location:	Air Force Weapons Laboratory History Office Kirtland AFB, NM 87117-6008
USAF Research:	Dr. Robert W. Duffner
Date:	2 August 1985
Contract No.:	F49620-85-C-0013

Abstract

Compilation of Select Aspects of the 1984
Air Force Weapons Laboratory History

by

Doris J. Walker-Dalhouse

The overall goal of the research appointment was to provide technical assistance in the collection of historical information pertinent to the mission of the Air Force Weapons Laboratory (AFWL) and in the writing of historical narratives on select AFWL programs assigned by the AFWL historian. To accomplish the designated task, interviews were conducted with specified Air Force personnel associated with the following administrative and technological units: AFWL Safety Office, AFWL Finances, the Rio Grande Research Corridor, and the Hard Mobile Launch Program. Subsequent historical narratives were written for inclusion in the 1984 AFWL History.

Acknowledgements

The writer wishes to thank the Air Force Systems Command, the Air Force Office of Scientific Research, Universal Energy Systems, and the Office of the Chief Scientist, Kirtland AFB, NM, for the opportunity to assist in the compilation of historical data at the Air Force Weapons Laboratory (AFWL), Kirtland Air Force Base, New Mexico. Special thanks are accorded to Dr. Robert W. Duffner, AFWL Chief Historian, for the cooperative rapport established in the delegation and review of assignments completed during the period of appointment. Accolades are also extended to Mrs. Ida Houseknecht for the quality supportive assistance which she provided in the typing of various historical narratives, in addition, to the final report.

I. INTRODUCTION

AFWL's mission entails planning and implementing the Air Force's exploratory, advanced, engineering development programs in nuclear and laser weapons, and advanced weapons concepts. The historian is responsible for developing, formulating, and monitoring the AFWL historical program to include researching and writing annual histories and monographs, as well as collecting and preserving those documents of historical significance. Due to the magnitude of the specified task, assistance in related disciplines was used in the preparation of the current historical volume and in the search for designated topic areas fundamental to the development of prospective historical narratives and monographs.

The author's academic training in Reading Education proved to be of immeasurable assistance in the application of comprehension and notetaking skills (summarization of main ideas, identification of supporting details, and the critical analysis of information) to the recording and understanding of information from both primary and secondary sources pertaining to the administrative operation of AFWL, its relationship to the technical community, and nuclear weapon effects studies.

Having taught communication skills (reading, writing, and speaking) courses in higher education, the author was

cognizant of the need to insure that historical narratives established clear lines of communication between the writer and prospective readers. Consideration of the need to provide sufficient background information and to use a clear writing style to promote an understanding of AFWL programs was foremost in the author's mind during the phases of writing (prewriting, writing, and rewriting) select aspects of the 1984 AFWL History.

II. OBJECTIVES

Specific objectives to be achieved during the period were to complete the following tasks:

1. Establish a historical data base by conducting research in open literature (secondary sources, Air Force documents, New York Times, Aviation Week & Space Technology, Air University Review, etc.) in order to collect key information on research and development activities (lasers, particle beams, nuclear weapons effects, advanced weapons, etc.) relating to the AFWL mission. Later, this objective was modified to focus specifically on nuclear weapons effects.
2. Use historical data collected and interviews with key AFWL program managers to write historical narrative covering select topics (administrative and technology activities) on select topics assigned by the AFWL chief historian.

The primary goal was to provide technical assistance in the ongoing preparation of the 1984 Air Force Weapons Laboratory History, a document containing historical information relative to AFWL's mission.

III. METHODOLOGY

After review of the research objectives with Dr. Robert W. Duffner, AFWL Chief Historian, the author began a search of unclassified literature pertaining to nuclear weapon effects, with specific emphasis focused on the MX and Hard Mobile Launcher. Main ideas and supporting details were extracted and summarized before cataloguing for future use.

Work relative to the fulfillment of the second objective involved conducting interviews with AFWL program managers regarding progress made by their offices during Fiscal Year 1984, 1 October 1983 to 30 September 1984. Topic areas covered included the AFWL Safety Office, Rio Grande Research Corridor, AFWL Finances, Nuclear Criteria Group Secretariat, and the Hard Mobile Launcher Program.

Interview tapes were transcribed and later utilized along with additional information ascertained from unclassified documents to draft historical narratives of each area. Drafts were placed on the word processor and later reviewed with respective project managers and the AFWL historian. Suggested changes were incorporated in the original draft and stored along with other completed segments of the history.

Said research should have direct implications at the university level for the educational training of Air Force civilian and military personnel, as well as in the subsequent tailoring of secondary and postsecondary educational programs.

IV. RECOMMENDATIONS

In reflecting upon potential obstacles encountered in the completion of responsibilities relative to the drafting of historical narratives relative to AFWL's achievements and in the survey of related literature, the author believes that the following recommendations should be considered for future Summer Faculty Research Program (SFRP) appointments:

1. Provide prior background reading from unclassified materials relative to topics to be investigated during the specified period.
2. Study ways to acquire temporary security clearances prior to, or in the early stages of, the research appointment in order to provide future research associates with access to classified documents essential for the preparation of historical narratives.

Ultimately, other individuals trained in education-related fields, such as reading, an applied discipline which derives its content from other subject fields, should be selected to participate in the SFRP to utilize their knowledge about factors (concept load, writing patterns, and vocabulary) which affect readability and subsequent comprehension in the development and/or evaluation of Air Force documents and histories. The interdisciplinary nature of these appointments could lead to the promotion of additional research on the reading skills of military personnel as it relates to the ever expanding reading demands associated with the technical nature of military documents.

1985 USAF-UES SUMMER FACULTY RESEARCH PROGRAM

Sponsored by the
AIR FORCE OFFICE OF SCIENTIFIC RESEARCH

Conducted by the
UNIVERSAL ENERGY SYSTEMS, INC.

FINAL REPORT

THE PLANNING OF A R & D OFFICE INFORMATION SYSTEM

Prepared by:	Yin-min Wei
Academic Rank:	Professor
Department and University:	Department of Computer Science Ohio University
Research Location:	Armstrong Aerospace Medical Research Laboratory, Technical Integration Division, Technical Integration Director's Office
USAF Research:	Mr. Robert F. Bachert
Date:	August, 1985
Contract No:	F49620-85-C-0013

THE PLANNING OF A R & D OFFICE INFORMATION SYSTEM

BY

Yin-min Wei

ABSTRACT

This study examined the needs of researchers and managers in a research organization for information and for information management support, and proposed a plan to provide those needs.

The principal components in the plan are: management information system with an hierarchical structure, direct online literature searches for the researchers, and establishing technical information analysis centers to provide local information needs as well as to serve other researchers in the country. In addition, if calendars of events of work-units and individuals are available in the computer network (even if partially) would improve communication within the organization and thus to quicken the flow of information. After all, the primary responsibility of a research organization is to search for new information.

Since computerized information storage and retrieval systems are used to complement the information in human brains. Thus information systems need the capabilities of human intelligence, and artificial intelligence is an important research area for information systems builders.

ACKNOWLEDGEMENT

The author would like to thank the Air Force Systems Command, the Air Force Office of Scientific Research and Universal Energy Systems, Inc. for providing him the opportunity to spend a very stimulating and fruitful summer at the Armstrong Aerospace Medical Research Laboratory. He would like to express his appreciation to the laboratory, in particular to the Technical Integration Directors' Office for its hospitality.

Further, he would like to thank Mr. Robert Bachert for encouraging this area of research and for his support and guidance. His appreciation goes to Dr. Billy Crawford, Mr. Dave Brungart and Mr. Richard Bennett for many of the helpful discussions; and, in particular, to Dr. George Mohr, Commander of the laboratory, for his discussion of his expectations of the laboratory information system.

His appreciation also goes to Col. Mary Sanders, Mr. Thoele and Sgt. Jones, and Mrs. Sears, Mrs. Trnka, Mrs. Cross and Mrs. Bohannon. They together have made his summer assignment a pleasant memory in the future.

The last, but not the least, he likes to thank Dr. Van Pattan, Dr. Warren, Dr. Boff, Mr. Monk, Mr. Sharp, Mr. Linhart, Dr. McDaniel, Dr. Moore, Dr. Nixon, Dr. Mattie, Mrs. Pinkerton, and Mrs. George for opportunity in discussing their information needs, and their ideas, plans and current practice for information acquisition and management.

I. INTRODUCTION

Every organization, whether it is in research, manufacturing, or service, can benefit from a good computerized information system network for information storage and retrieval, as well as for communication between all the offices and workers. As a university faculty member, teaching information systems, my long range goal is to design better information systems.

We have heard people saying in recent years that if all the public information are readily available for access, most of us can be twice as productive in contributing to the well-being of the mankind. However, we need enough convincing examples to illustrate this. One of the best examples perhaps is the importance of information system to the research workers. Without knowing exactly what have been accomplished and what are being done by others, the researchers often wasted most of their effort in duplicating the work of others.

Last summer, at the invitation of Mr. Robert Bachert, I participated in planning a computer network for the Armstrong Aerospace Medical Research Laboratory (AAMRL). That planning experience provided me a clearer view of the managers' needs of information of any organization similiar to AAMRL. As an extension of the last summer's effort, we are examining the information needs of the researchers and managers as a whole this time.

II. OBJECTIVES OF EFFORT

This effort examines the needs for computerized information system support of the researchers and the managers at AAMRL as a whole, and proposes a preliminary plan to provide that support.

This proposed support is supposed to make researcher's and manager's work more pleasant, and as a result multiply the amount of their accomplishments.

III. AN OVERVIEW OF OFFICE INFORMATION SYSTEMS

The office information system for an organization supports the information needs of all its workers. The Management Information System (MIS) which provides the information needs of the managers is the most important component of the Office Information System (OIS). In our mind, the major components of OIS for AAMRL would include :

- a) The Management Information System (MIS)
- b) The technical literature access for the researchers
- c) The research publications file
- d) The communication files, such as letters, memoranda, requests on special forms
- e) The calendar of events for the laboratory, the divisions, the branches and the individuals.

The above topics are to be discussed in the following.

IV. MANAGEMENT INFORMATION SYSTEM (MIS)

The computerized management information system for AAMRL would have the proposed hardware configuration (Figure 1). The configuration patterns after the organizational structure of the laboratory to provide direct communication channels for the most frequent communications. The communication between divisions are routed through the laboratory Commander's computer. Similarly, communication between branches are routed through their divisions' computer.

Notice that this computer configuration has been proposed only for the managers of the laboratory. Hardwares can be added to provide additional services. For example, a microcomputer can be provided for each individual who can justify his/her need. [Note: For convenience, from now on, HIS will be used in place of HIS/HER, HE in place of HE/SHE, and HIM in place of HIM/HER.]

AD-A166 178

UNITED STATES AIR FORCE SUMMER FACULTY RESEARCH PROGRAM

10/1

1985 TECHNICAL RE. (U) UNIVERSAL ENERGY SYSTEMS INC

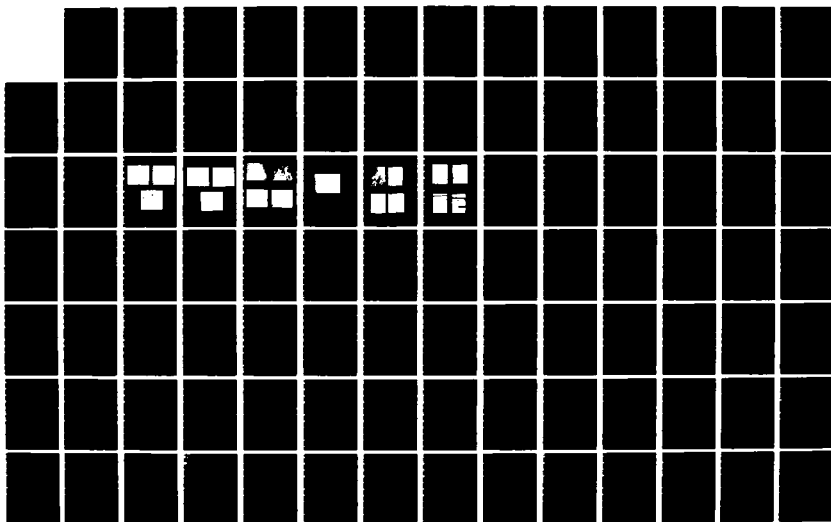
DAYTON OH R C DARRAH ET AL DEC 85 AFOSR-TR-86-0141

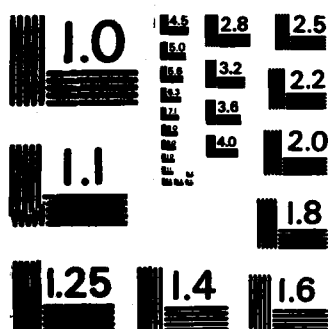
UNCLASSIFIED

F49620-85-C-0013

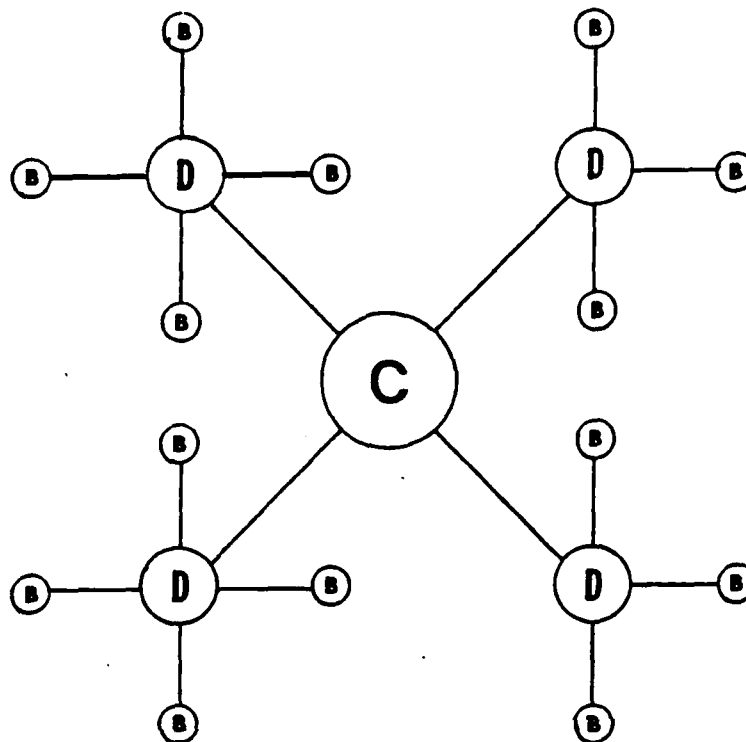
F/G 5/9

NL





MICROCOPY RESOLUTION TEST CHART
NATIONAL BUREAU OF STANDARDS-1963-A



WHERE C=Computer for the Commander
 D=Computer for each Division
 B=Computer for each Branch

FIGURE 1: HARDWARE CONFIGURATION FOR THE AMRL COMPUTERIZED MIS

Each individual's micro-computer is to be linked to the computer of the work-unit (which may be a branch, a division or the laboratory) to which the individual belongs.

V. TECHNICAL LITERATURE ACCESS FOR RESEARCHERS

Easy and quick access to the most up-to-date literature is of high-order importance to the researchers. Thus, each research project can begin at a higher ground and will be easier to reach a higher goal. However, access to technical literature had and still has problems. The problems are of three kinds:

a) No Direct Access. The researchers don't have direct access to the online databases (most of these are journal-paper titles with abstracts). They must wait in line for a time-slot of a professional online searcher. This waiting means time-delay for research progress and often is the cause for anxiety.

b) Inaccurate Indexing. The indexing of journal papers listed in online databases were mostly accomplished by professionals being non-experts in the subject area of the collection. As a result, a list of journal papers retrieved from online search are mostly irrelevant to the needs of the researcher. Therefore, he has the need to do more searches; and often is discouraged and frustrated.

The situation would improve if each researcher has direct access to the online databases himself. Of course, there is always budget problems for the online searches. This problem is similar to the budgeting for using computer resources.

However, (Pope, 1985) [1] reported the results of his study, at IBM research laboratories, of a group of managers and researchers during their interactive sessions on computer terminals. According to him, during those interactive computing sessions, the total cost of the human users' times comes to be about 7 times of the total cost of the computer resources they have consumed.

The search of online databases located across the country would consume computer as well as communication resources. However, according to the experience of a professional online searcher, during searches, the communication cost usually only amounts to about $1/3$ to $1/2$ of the computing cost. Thus, we can conclude with confidence that the online search cost would not exceed a researcher's time cost for online literature searches most of the time.

In summary, it would be a good practice to allow researchers to do literature searches from their own micro-computer based terminals (i.e. work-stations). Of course, the cost for searches needs to be budgeted and controlled as other costs. Those researchers who are used to delegate literature searches to others would be free to continue their present practice.

c) Indexing Vocabulary. The researchers are experts in their own subject areas. But they may not have time to memorize the special set of terms selected by others for indexing the published literature in their own subject areas. They know even less about the indexing of literature in other areas, from which they may need information at times to support their research.

To search for information into an unfamiliar area of knowledge, each person may try to do search with any term that happens to come into his mind and that appears to be related to the desired information. More often than not, this term does not belong to the selected vocabulary being used by the indexers and the librarians.

This road block to searches was recognized by (Doyle,1961) [2]. She proposed to provide a semantic road-map to guide the literature searchers, but did not include a method for implementation. In 1974, Wei [3,4] conceived (and lectured in his class) the idea of creating concept-atoms and letting computer to automatically assembly them into a semantic road map to assist literature searches.

At the beginning of a semantic road map creation, it might be composed of a number of isolated semantic patches, much like the isolated continents on the surface of earth. As an illustration, Figure 2 contains one concept-atom. It has "computer" as its nucleus, and "computer programming", "brain", and "office automation" are its satellites. Figure 3 contains another concept-atom which has "brain" as its nucleus, and "computer", "psychology", and "intelligence" are its satellites.

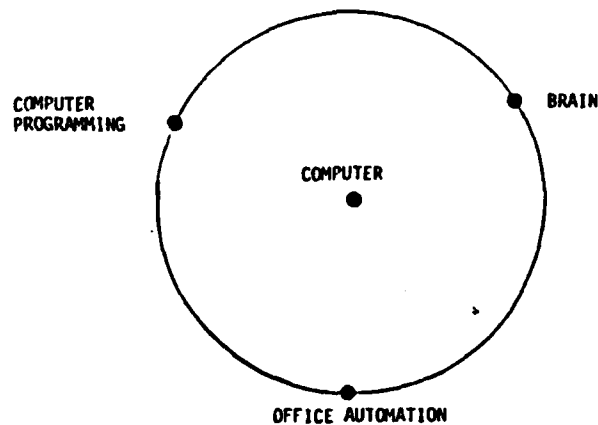


FIGURE 2: A Concept-atom

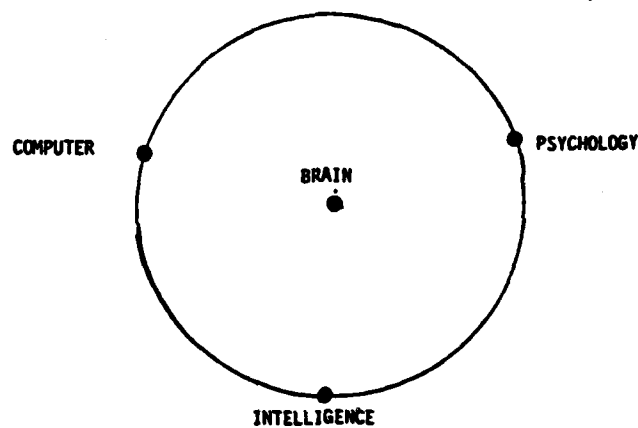


FIGURE 3: Another Concept-atom

Those two concept-atoms are automatically linked together by computer to form up the semantic patch (Figure 4). Beginning at the term, "office automation", one can be led through "computer" and "brain" to reach either "intelligence" or "psychology". One or more terms in the semantic patch might describe more accurately a researcher's search interest. Alternately, the literature of interest to the researcher might be indexed under one or another term in the patch.

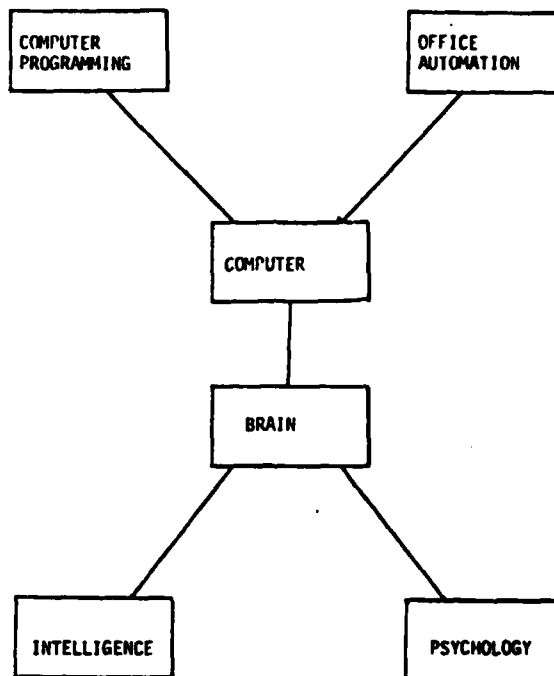


FIGURE 4: A Semantic Patch Automatically Composed from the Two Concept-atoms in Figures 2 and 3.

A large collection of concept-atoms would automatically form up a large semantic road map to guide literature searchers. Like a road map, it must be accurate and detailed enough to serve the purpose.

Road and street maps have been made by many people over many years. Semantic road maps can require investments over years too. Concept-atoms are only building blocks for the semantic road maps. We need to develop methods and skills to speed up the semantic map making process, as well as to ease the tasks for making changes. May be we should learn from the map makers too?

At the proposal of Dr. Ken Boff, the laboratory director Dr. Mohr of AAMRL plan [5] to establish a Crew Systems Ergonomics Information Analysis Center for engineers who occasionally need special knowledge in the area of human factors. Because they are alien to the human factors literature, they are even not familiar with the technical terms being used in that area.

Consequently, they have more difficulty in finding the information needed. As a remedy to this situation, a semantic road map for the human factors literature can be used to guide the engineers for their literature searches. From this point of view, the semantic map complements the semantic script structure in the human brains (Schank, 1982) [6]. As you can expect, the man made semantic road map can never be perfected. But, it can be continually improved by collecting information on user's search failures online, and using that information to improve the semantic map built into the systems for online literature searches.

VI. RESEARCH PUBLICATION COLLECTIONS

Keeping track of research publications by a researcher has been a problem as reported by Malone [7]. In a 1985 paper, "Emerging Office Automation Systems," [9], Helander stated that "the cost of providing each knowledge worker with a 32-bit microcomputer will be from 5% to 10% of annual salary". In view of his statement, we can anticipate each researcher to have a microcomputer in his office in the near future. Then it will be easy for each one of them to have computerized indexing file for his own research literature collection.

Through its connection to the laboratory MIS network, each microcomputer can communicate with other microcomputers in the laboratory. Thus, by entering into agreement with one another, the researchers can share one another's research literature collection. The sharing arrangement would not only save time for each participating individual, but will enhance his research progress. "Sharing" as emphasized by the authors of the book, IN SEARCH OF EXCELLENCE [8], is

central to the success of any organization . It has been placed in the center of a 7-S diagram (see Figure 5) which contains the seven most important ingredients: shared values, structure, strategy, skills, staff, style, and systems (all beginning with S) for any organization to be successful.

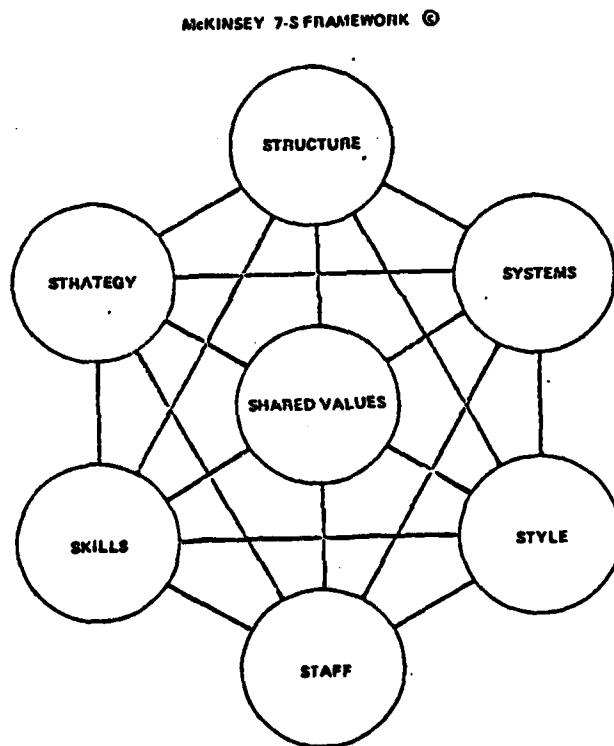


Figure 5: 7 - S Diagram

VII. THE OFFICE COMMUNICATION FILES

Each one of us receives/sends letters, memoranda and requests on special forms. These items usually make up the piles on our desks and on top of our file cabinets. Searching through these files were often chores that caused frustrations and disappointment because the items being searched for did not turn up.

In a 1983 paper, "How do People Organize Their Desks ?" [7], Malone reported that purchasing agents handled requests on special forms easily and efficiently, because these forms can be easily sorted for processing in order of their arrival. Thus, we need not to worry about processing of requests on forms. According to him, the researchers have messy desks, because their document collections are difficult to be categorized and stored. This kind of researcher's dilemma, we have already discussed under the title, "Research Publication Collections" in section VI.

The letters and memoranda can be very diversified in their subject content. The fact, their subject can often be classified into more than one category, makes their subject indexing a difficult task. Further, because most of them have only temporary value, they are not worth any great amount of indexing effort. Nevertheless, as pointed by Malone [7], they can be easily categorized by author, title, date of origination, and date of receiving. The fact that people often try to recall events by the time-frame of their occurrence, helps the effectiveness of indexing by time-frames. A personal microcomputer can be used to handle these indexing beautifully. As is often done in the past, the letters and memoranda can be numbered in sequence as L1, L2,..., and M1, M2,... respectively.

As the performance of voice recognition devices are being improved, their availability will ease individual's effort in indexing their own documents.

VIII. THE CALENDAR OF EVENTS FOR THE LABORATORY, THE DIVISIONS,
AND THE BRANCHES

To promote and ease the communications among individuals in the laboratory, calendar of events, similiar to the reservation system of the airlines, can be stored in the computer system for ready access by others.

It is proposed that each work-unit (laboratory, division, or branch) will have its calendar of events stored in its own central computer. Each individual has the option to send his own calendar showing the times and days , he will not be available (such as appointment in or out of office).

Information in general, can be classified into public or private. There are times, however, certain category of information may belong to the twilight zone (i.e. neither public or private). Individuals can have different judgement as to the nature of a certain kind of information. Therefore, it might be a good idea to encourage, but not require, individual calendars be made public.

IX. PROCEDURE FOR OFFICE INFORMATION SYSTEM IMPLEMENTATION

The office information system for AAMRL would have two distinct components. One component is to keep records on personnel, tasks, budgets, and inventories; and to manage internal communication and communication with other organizations. The other component is to provide quickly for the researchers with the most up-to-date information related to their research (which means search for new information).

a) Implementation of the Management Component of Office Information System

The basic strategy for implementing the management component (i.e. the first component) is to grow the computerized system slowly in parallel with the existing manual system, and to phase out the manual

system gradually at the same time. This approach seems to have best chance to succeed, because it takes time for people to break away from their cultural traditions. The validity of this approach has been supported by statements of Sprague and Carlson, in their book, Building Effective Decision Support System [10].

In fact, the implementation of this management component has already begun at AAMRL. However, to use the system beyond simple data retrieval, but to provide also decision support will require further research studies. Mr. Brungart who manages the MIS, has envisioned an expert system structure for the future management information system at AAMRL. That means the rules for selecting data-items for retrieval, and the retrieval programs are stored separately. So that the rules can be modified quickly and easily.

b) Implementation of the Research Component of Office Information System

The information needs of researchers is by nature very diversified. This kind of needs can never be completely satisfied. However, improvements and progresses in providing the needs are possible.

A number of researchers at AAMRL are anxious to do online literature search themselves. So that search time-delays can be eliminated, and the quality of search results improved. The quality improvement would be the direct result of the fact that researchers knowing more about the subject area of their interest than the online search intermediaries.

Of course, there is price for the quality improvement in search results. The researchers need to learn "how to interact with the online systems." Fortunately, help to this kind of learning process has begun appearing on the horizon. Charles Meadow described: the design and evaluation of an experimental online search assistance system, in a two-part article, "A Computer Intermediary for Interactive Database Searching," [11].

As mentioned earlier, Dr. Boff of AAMRL has been addressing the difficult problem of literature search into an unfamiliar subject area by researchers. In this case, a semantic road map containing various common and specialized terms could be used to guide the literature searchers. However, "how to construct good semantic road map" is still a research

problem, even though progress in the construction process is being made [4]. The semantic road map is to complement the semantic script in human memory.

Dr. Boff's proposal for an Information Analysis Center is to help engineers finding information in the area of human factors. Since methodologies and tools needed by Dr. Boff for his project can be applied equally well to research literatures in other areas, Information Analysis Centers could be established at AAMRL for other literature areas such as, biodynamics and toxic hazards. These centers would enhance local research as well as providing assistance to others in the country.

X. RECOMMENDATIONS FOR FUTURE RESEARCH

Our research goal is to extend our abilities for building better and better information systems. Naturally, the question, "what is a good information system," would arise. Since information systems are used to complement the information storage and processing capabilities of human brains, a good information system should possess all the capabilities of a human being if possible.

That means information systems should be made intelligent by some artificial means. Thus, the study of all aspects of artificial intelligence (AI) are within the domain of information system research.

Sowa states in his book [12] that, "artificial intelligence is the study of knowledge representation and their use in language, reasoning, learning, and problem solving." Thus there are five broad areas for our future research. Among those five, knowledge representation is the most fundamental element of them all. Since 1974, this writer has begun research on semantic network which is a sub-area of knowledge representation. He plans to continue that research, because semantic network is not only an entity that aids information search, it also is the foundation for user language to system language translation. Further it can be a good tool for documenting the structure of evolutionary information systems[13]. On the other hand, this writer is interested in the use of expert system (another AI application area) methodologies in MIS to enhance the system capabilities and its flexibility for modifications.

REFERENCES

1. Pope, Bucky, A Study of Where Users Spend Their Time Using VM/CMS, IBM Research Report 10953, Jan. 29, 1985.
2. Doyle, L.B., "Semantic Road Maps for Literature Searches," Journal of ACM , Vol.8, No.4, 1961; pp.553-576.
3. Wei, Y., "Concept Atom -- A Component in Information Organization and Retrieval," Computer Science Department, Ohio University (unpublished); 1975.
4. Wei, Y. etc. "An Experimental Interactive Information Retrieval System Utilizing Concept-atoms," Policy and Information, Vol.7, No.1, 1983; pp.17-24.
5. Mohr, George C., Information Analysis Centers, a memo. for a survey of the opinion of human-factors professionals, April 9, 1985.
6. Schank, Roger C., Dynamic Memory, Cambridge University Press, New York, 1982.
7. Malone, Thomas, W., "How do People Organize Their Desks ? Implications for the Design of Office Information System." ACM Transactions on Office Information Systems, Vol. 1, No. 1, Jan. 1983; pp. 99-112.
8. Peters, T. J. and R. H. Waterman, In search of Excellence, Warner Books, New York, 1982.
9. Helander, M. G. , "Emerging Office Automation System," Human Factors, Vol.27, No.1, 1985; pp. 3-20.
10. Sprague, R. H. and E. D. Carlson, Building Effective Decision Support System, Prentice-Hall, 1982; p.4 and pp. 155-7.

11. Meadow, C. T. etc. "A Computer Intermediary for Interactive Searching, Part I -- Design, Part II -- Evaluation." Jour. of the American Society for Information Science, Vol.33, No.5, pp.325-332, and No.6, pp. 357-364; 1982.
12. Sowa, J. F., Conceptual Structures -- Information Processing in Mind and Machine, Addison-Wesley, 1984; p.22.
13. Mettermair, R. T., "Semantic Nets for Modeling the Requirements of Evolvable Systems -- An Example," in Evolutionary Information Systems edited by J. Hawgood, North-Holland, 1982; pp. 193-216.

1985 USAF - UES SUMMER FACULTY RESEARCH PROGRAM

Sponsored by the

AIR FORCE OFFICE OF SCIENTIFIC RESEARCH

Conducted by the

UNIVERSAL ENERGY SYSTEMS, INC.

FINAL REPORT

DEVELOPMENT OF HIGH STRENGTH TITANIUM ALLOYS
VIA RAPID SOLIDIFICATION PROCESSING

Prepared by: I. Weiss
Academic Rank: Associate Professor
Department and Materials Science and Engineering
University: Wright State University
Research Location: AFWAL/ML Metals and Ceramic Division
Structural Metals Branch.
USAF Reasearch: Dr. F.H. Froes *Handwritten signature*
Date: September 20, 1985 *30 Sept '85*
Contract No: F49620-85-C-0013

DEVELOPMENT OF HIGH STRENGTH BETA TITANIUM ALLOYS VIA RAPID
SOLIDIFICATION PROCESSING

BY

I. Weiss

ABSTRACT

The development of high strength beta titanium alloys using rapid solidification (RS) approach is being addressed. Additions of boron, carbon, cerium and erbium have been made to Ti-6Al-4V, Ti-10V-2Fe-3Al, Ti-15V-3Cr-3Sn-3Al and Ti-20Mo in an attempt to dispersion or precipitation strengthen these alloys.

The primary concern in alloy preparation is uniformity of composition. The problem of segregation has been evaluated for the different alloys. Large scale macro segregation is found in Carbon and Boron containing alloys. Metastable supersaturation has been obtained by RS conversion utilizing the pendent drop melt extraction (PDME) process. The production of homogeneous RS material and the difficulties encountered are presented. The effect of various quench wheel materials on the cooling rate is examined. Thermal conductivity and thermal expansion are important parameters to consider in selecting quench wheel material. The finest RS microstructure with columnar grains 7 μ m thick is obtained utilizing mild steel quench wheel.

I. INTRODUCTION

It has long been recognized that the high strength to density ratio of titanium alloys makes these alloys an excellent material for aerospace application.

Further improvement of properties requires either a reduction in density or an increase in strength. The present work attempts to increase the room temperature strength of beta titanium alloys (Ti-6-4, Ti-10-2-3, Ti-15-3-3-3, and Ti-20) using a rapid solidification (RS) approach.

Dispersion strengthening of titanium alloys has received little attention because of the experimental difficulties in producing the desired size and distribution of dispersoids by conventional techniques. Production of dispersoids by solid state precipitation [1], precipitation from the liquid [2,3] and internal oxidation [4] has generally resulted in unstable and coarse particles. Such precipitation also exhibits low nucleation rate, heterogeneous nucleation and insufficient supersaturation in the as quenched condition. Rapid solidification processing provides a mean to overcome the above limitations. By increasing the solidification rate, meta stable supersaturation of dispersoid-forming elements such as; Ce, Er, Be, Fe, Nd, Th, Y, C, B can be achieved in addition to fine grain size microstructure. Upon subsequent annealing, the supersaturated solid solution decomposes to form large volume fraction of fine uniform dispersoids which in turn will strengthen the alloy by an orowan by passing mechanisms .

II. OBJECTIVES OF THE RESEARCH EFFORT

Primary goals of Phase I;

1. Production of homogeneous titanium base alloys with addition of boron, carbon or erbium for RS conversion by the PDME process.
2. RS conversion of four titanium alloys (Ti-6-4, Ti-10-2-3, Ti-15-3-3-3 and Ti-20) each containing addition of 0.5, 1.5 and 3 %/o erbium, boron or carbon.

III. EXPERIMENTAL APPROACH

Base alloys (Ti-6Al-4V, Ti-10V-2Fe-3Al, Ti-15V-3Cr-3Sn-3Al, Ti-20Mo) were used as starting materials. Elemental boron or erbium was added to each base alloy. The charges were arc melted with a non-consumable tungsten electrode. Melting was done in a vacuum chamber over a water-cooled copper hearth. The chamber had been backfilled with argon in order to maintain a stable arc during melting. The alloys were melted in a circular mold, solidified, and flipped before remelting. Subsequent passes were made utilizing an elliptical mold and finally a cigar shaped mold was used in order to produce an ingot which is appropriate for swaging. (See Table 1 for the number of passes per mold geometry). Typical melting currents were

550-700 amps DCSP and the duration of each pass was about 5 min. The resulting product was a cigar-melt roughly 5" long and 3/4" in diameter. Following melting, the cigars were homogenized at 1875°F for 24 hrs. in vacuum. The homogenized cigars were canned in commercially pure titanium tubing in preparation for hot swaging. The canned cigars were annealed for 30 min. at the swaging temperature (Table 2) and subsequently swaged for 10 to 20 % reduction followed by annealing at the same temperature for 15 min. This sequence was continued until a bar 3/8" in diameter was obtained. The CP titanium was then removed by machining. A second homogenization was carried out at 1875°F for 24 hrs. Throughout alloy preparation, chemistry and segregation were checked. A piece was sectioned from each end of the cigar-melt for wet chemical analysis. An additional piece was sectioned from one of the ends for optical and SEM microscopy.

RS conversion was carried out utilizing the PDME process. The PDME unit converts rod material into ribbons. The rod was melted at its tip by an electron beam. The approximately 0.5 cm³ molten pool was carried away by a rotating wheel. The rod was mechanically lowered at a rate which was expected to best yield continuous production of ribbon. The chemistry of the ribbons was found to be a direct result of the chemistry of the rod.

IV. RESULTS AND DISCUSSION:

Erbium Containing Alloys

The effect of Er levels for a given base alloy on dispersoid size and distribution will be examined. Microstructural analysis of the cigar-melts have shown an increase in the number of coarse dispersoids ($> 1\mu$ m. diameter) with increasing of amounts of Er (Figure 1). It was assumed that the dispersoids are Er_2O_3 due to the scavenging of interstitial oxygen by Er. The larger dispersoids resulted from the low solubility of Er in Ti and the coarsening of Er_2O_3 during slow cooling of the melt. It was also observed that an increase in Er levels resulted in segregation of Er_2O_3 at the grain boundaries (Figure 2). Figures 2b, 3a, and 3b show Er_2O_3 dispersions in two of the four base alloy systems with additions of 1.5 w/o Er. The nature of the dispersion appears independent of the base composition for a given Er level. After a full processing cycle (heat treatment, swaging, heat treatment), the dispersoids were of consistent size and were uniformly distributed. (Figure 3c and 3d). This has been observed in all four base alloy systems. This processing cycle eliminated grain boundary segregation and fully spherodized the Er_2O_3 particles. Chemical analysis (Table 3) of the cigar melt showed satisfactory results and was assumed to represent the final rod.

are also important. In order to optimize the cooling rate while all other controllable parameters are constant, the following quench wheel materials were chosen : copper, brass, aluminum, titanium, nickel coated copper, and mild steel. All wheels had a 600 grit surface finish. As anticipated, various ribbon thicknesses (Ti-6Al-4V alloy) were produced in each run. To ensure that legitimate comparison would be made from wheel to wheel, ribbons of similar thicknesses range (76-89 μm) were selected from each run except that with a titanium quench wheel. (Ribbon produced using a titanium quench wheel was consistently thicker than ribbon produced using the other five wheels).

Optical microscopy was performed on longitudinal cross section of Ti-6-4 ribbons produced using each wheel material. The microstructures observed were martensitic with prior β grain boundaries outlined with α phase. Morphology of prior β grains (Figures 5 and 6) ranged from columnar to equiaxed, a direct result of different cooling rates. A line intercept method was used to measure prior grain size. The ribbons' thicknesses imposed a limit on the columnar grain size in the direction perpendicular to the wheel. Thus, only the width of the columnar grains is meaningful. A minimum of fifty measurements was taken for each wheel material. Ribbon thickness and width variations per wheel were also measured (Table 4). Use of a copper quench wheel for rapid solidification conversion has been predominate in the past based on its high thermal conductivity relative to other materials (Table 5).

Boron Containing Alloys

Microstructural analysis of the cigar-melts containing boron revealed large scale segregation at all levels of boron. Figure 4 shows macrosegregation in Ti-6Al-4V with a small addition of B(0.05%). It is apparent that the standard melting procedure was inadequate for the incorporation of boron. Solution to the problem involved a proper selection of melting mold. During melting in the cigar shaped mold, only a portion of the material was molted at any given time. The liquid portion of the material was circular and was moved along the length of the cigar with the arc. Because of the radial nature of the heat flow, the melt pool will always be approximately round. The largest portion of material will be liquid in the round-shaped mold. Therefore it is suggested that the round mold will allow for the best mixing while remelting in the cigar mold results in redistribution of boron to the ends of the melt.

Specification of Adjustable Parameters of PDME Unit

High solidification rates yield fine microstructure, i.e. grains, precipitate, and dispersoid sizes. Changes in microstructure during solid state cooling are particularly important when cooling is slow such as radiative cooling in a vacuum.. The PDME unit has four controllable variables: heating rate (accelerating voltage), wheel speed, descending rate of the stock material, and cooling rate. In addition, parameters such as melt drop size and melt superheating,

However, in this study the finest microstructure was obtained using a mild steel quench wheel. Therefore, wheel thermal conductivities cannot be the sole criteria for quench wheel material selection. The residence time of the ribbon on the wheel is an important factor when considering the heat transferred. During the quench process the ribbon is effectively brazed to the wheel. Ribbon residence time is a function of the ribbon wheel bond strength. This bond is broken by forces developed by simultaneous expansion of the heating wheel and contraction of the cooling ribbon. This expansion and contraction depends on thermal expansion coefficients (Table 2). The titanium-titanium and titanium-nickel bond strengths were great enough that the ribbon stuck to the wheel to such a degree that production of ribbon was difficult. Cooling while the ribbon is on the wheel depends not only on the thermal conductivity of the wheel, but also on the ribbon-wheel contact area per volume of ribbon (i.e. wettability). The ribbon contact sides were examined by SEM techniques. Comparison of the contact sides of ribbons quenched on the brass and mild steel wheels shows differences in ribbon-wheel contact areas (Figure 7). The ribbon quenched on the brass wheel shows that less of its surface was in contact with the wheel than the surface of the ribbon quenched on mild steel. The microstructures observed, large equiaxed grains in ribbon quenched on the mild steel wheel, correlate with the relative contact areas (Figure 5).

V. RECOMMENDATION

1. Base alloys with erbium additions show uniform chemical composition and microstructure (Ti-20Mo-1.5Er is excluded here due to anomaly in chemical analysis). Processing of these alloys should be continued as planned.

2. A new cigar-melt is needed for the nominal composition of Ti-20Mo-1.5Er because of undesirable erbium levels in previous melt.

3. Because of segregation and poor chemical analysis results, the cigar-melts containing boron are not satisfactory for further processing. It is recommended that lower levels of boron be added (0.2, 0.8 and 1.5 w/o) as a partial solution to the segregation problem.

4. Macrosegregation may be reduced in cigar-melts by melting 4 to 5 times in the round mold, once in the elliptical mold and once in the cigar mold. This could limit the high concentration of additions in the end of the cigar-melt.

5. Factors which determine the ribbon-wheel bond strength should be identified and studied.

6. Based on the fine microstructure obtained using a mild steel quench wheel, Steel plated copper wheel can yeild a very fine microstructure. This is the result of the combination of large residence time due to the steel and high thermal conductivity of copper.

Table 1:
NUMBER OF PASSES PER MOLD GEOMETRY
550-700 amps DCSP, 5 min. per pass

<u>Melt No.</u>	<u>Nominal Composition (w/o)</u>	<u>Number of Passes per Mold Geometry</u>			<u>Total No. of Passes</u>
		<u>Circular</u>	<u>Ellipitcal</u>	<u>Cigar</u>	
2116	Ti-6Al-4V-0.5Er	1	1	1	3
2117	Ti-6Al-4V-1.5Er	1	1	1	3
2118	Ti-6Al-4V-3.0Er	1	1	1	3
2119	Ti-6Al-4V-0.5B	1	1	1	3
2120	Ti-6Al-4V-1.5B	1	1	1	3
2121	Ti-6Al-4V-3.0B	1	1	1	3
2128	Ti-10V-2Fe-3Al-0.5Er*	2	1	2	5
2122	Ti-10V-2Fe-3Al-1.5Er*	1	1	1	3
2159	Ti-10V-2Fe-3Al-1.5Er *	2	1	2	5
2129	Ti-10V-2Fe-3Al-3.0Er *	2	1	2	5
2123	Ti-10V-2Fe-3Al-1.5B*	2	1	2	5
2130	Ti-15V-3Cr-3Sn-3Al-0.5Er *	2	1	2	5
2126	Ti-15V-3Cr-3Sn-3Al-1.5Er*	2	1	2	5
2131	Ti-15V-3Cr-3Sn-3Al-3.0Er*	2	1	2	5
2146	Ti-15V-3Cr-3Sn-3Al-0.5B	2	1	5	8
2125	Ti-15V-3Cr-3Sn-3Al-1.5B *	2	1	2	5
2144	Ti-20Mo-0.5Er	2	1	4	7
2124	Ti-20Mo-1.5Er	2	1	2	5
2145	Ti-20Mo-3.0Er	2	1	5	8
2127	Ti-20Mo-1.5B	2	1	2	5

*Indicates those where holes were drilled in the base material to accommodate the additions.

Table 2:
SWAGING TEMPERATURES

<u>Melt No.</u>	<u>Nominal Composition (w/o)</u>	<u>Transus Temperature*</u>	<u>Swaging Temperature</u>
2116	Ti-6Al-4V-0.5Er	1830° F	1750° F
2117	Ti-6Al-4V-1.5Er	1830° F	1750° F
2118	Ti-6Al-4V-3.0Er	1830° F	1750° F
2128	Ti-10V-2Fe-3Al-0.5Er	1480° F	1425° F
2159	Ti-10V-2Fe-3Al-1.5Er	1480° F	1425° F
2130	Ti-15V-3Cr-3Sn-3Al-0.5Er	1400° F	1350° F
2126	Ti-15V-3Cr-3Sn-3Al-1.5Er	1400° F	1350° F
2144	Ti-20Mo-0.5Er	**	1350° F
2124	Ti-20Mo-1.5Er	**	

* transus temperatures will vary with O₂ content.

** In phase field at room temperature.

Table 3:
CHEMICAL ANALYSIS RESULTS FOR CIGAR MELTS

Composition w/o

<u>Melt No.</u>	<u>Nominal</u>	<u>Chemical Analysis</u>
2116	Ti-6Al-4V-0.5Er	Ti-5.9Al-4.0V-.57Er
2117	Ti-6Al-4V-1.5Er	Ti-6.1Al-3.9V-1.6Er
2118	Ti-6Al-4V-3.0Er	Ti-6.3Al-3.8V-2.7Er
2119	Ti-6Al-4V-0.5B	Ti- Al- V-2.4B**
2120	Ti-6Al-4V-1.5B	Ti- Al- V-3.6B**
2121	Ti-6Al-4V-3.0B	Ti- Al- V-4.4B**
2128	Ti-10V-2Fe-3Al-0.5Er*	Ti-10.0V-2.0Fe-3.3Al-.63Er
2122	Ti-10V-2Fe-3Al-1.5Er*	Ti-9.9V-2.2Fe-3.5Al-1.5Er
2159	Ti-10V-2Fe-3Al-1.5Er	Ti-9.9V-2.0Fe-3.4Al-1.6Er
2129	Ti-10V-2Fe-3Al-3.0Er*	Ti-10.2V-2.2Fe-3.5Al-2.8Er
2123	Ti-10V-2Fe-3Al-1.5B*	Ti- V- Fe- Al-2.9B**
2130	Ti-15V-3Cr-3Sn-3Al-0.5Er*	Ti-14.2V-2.8Cr-2.9Sn-3.6Al-.56Er
2126	Ti-15V-3Cr-3Sn-3Al-1.5Er*	Ti-14.6V-2.8Cr-2.8Sn-3.6Al-1.4Er
2131	Ti-15V-3Cr-3Sn-3Al-3.0Er*	Ti-14.4V-2.8Cr-2.7Sn-3.5Al-3.0Er
2146	Ti-15V-3Cr-3Sn-3Al-0.5B	Ti-15.3V-3.0Cr-2.9Sn-3.2Al-.43B
2125	Ti-15V-3Cr-3Sn-3Al-1.5B*	Ti-14.5V-2.9Cr-2.8Sn-3.3Al-2.6B
2144	Ti-20Mo-0.5Er	Ti-21.3Mo-.47Er
2124	Ti-20Mo-1.5Er	Ti-21.6Mo-.77Er
2145	Ti-20Mo-3.0Er	Ti-21.0Mo-2.8Er
2127	Ti-20Mo-1.5B	Ti-20.0Mo-2.5B

* Indicates those melts where holes were drilled in the base material to accomodate the additions.

** Complete chemical analysis not available.

Table 4:

PHYSICAL DIMENSIONS OF RIBBONS

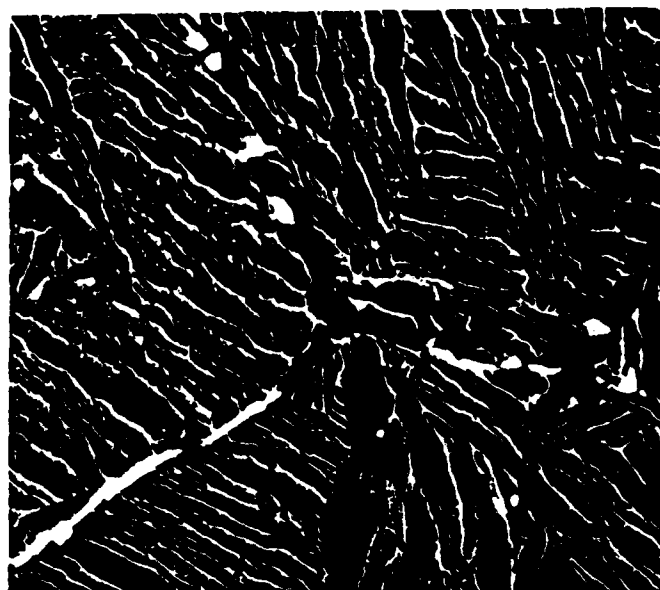
Wheel Material	Average Grain Width μm	<u>Ribbon Thickness</u>		<u>Ribbon Width</u>	
		Mean μm	Standard Deviation μm	Mean μm	Standard Deviation μm
Mild Steel	6.90	69	20	953	345
Aluminum (6061)	8.28	66	47	969	318
Titanium	8.47	178	108	1069	526
Copper	8.82	78	20	1060	354
Nickel Coated Copper	8.84	84	25	1110	469
Brass	29.95	89	27	1020	364

Table 5:
PHYSICAL CONSTANTS²

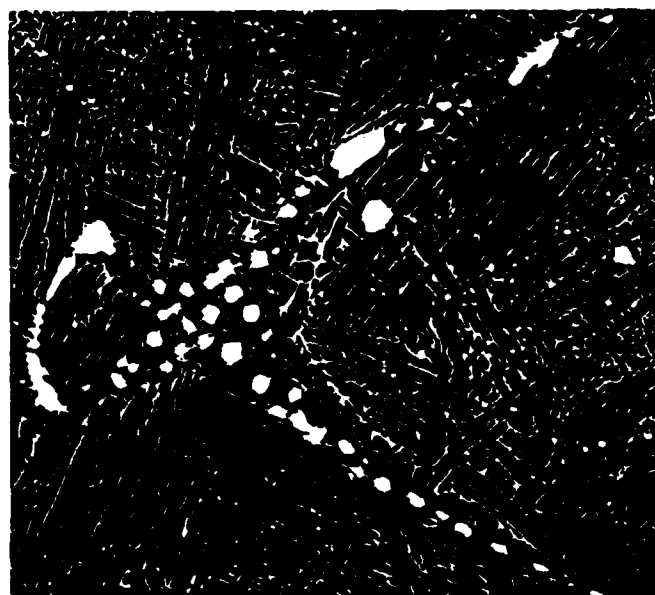
Material (Wheel)	Thermal Conductivity	Thermal Expansion Coefficient
	Btu in/hr ft ² °F	(in/in/°F) × 10 ⁻⁶
Aluminum	840	13.0
Mild Steel	460	6.7
Titanium	112	4.7
Nickel	520	5.8
Brass	830	11.2
Copper	2680	9.8



a



b

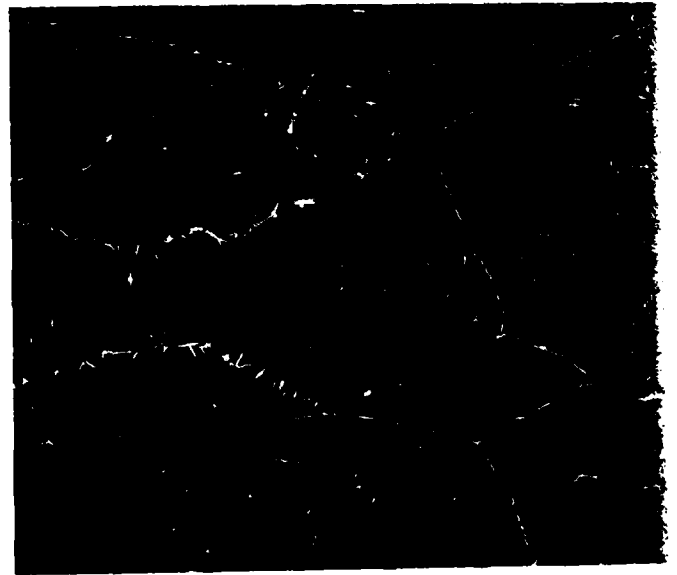


c

Fig. 1. SEM micrographs of Ti-6Al-4V cigar-melts with additions of (a) 0.5 wt% Er (2000x), (b) 1.5 wt.% Er (2000x) and (c) 3.0 wt.% Er (1500x).



a

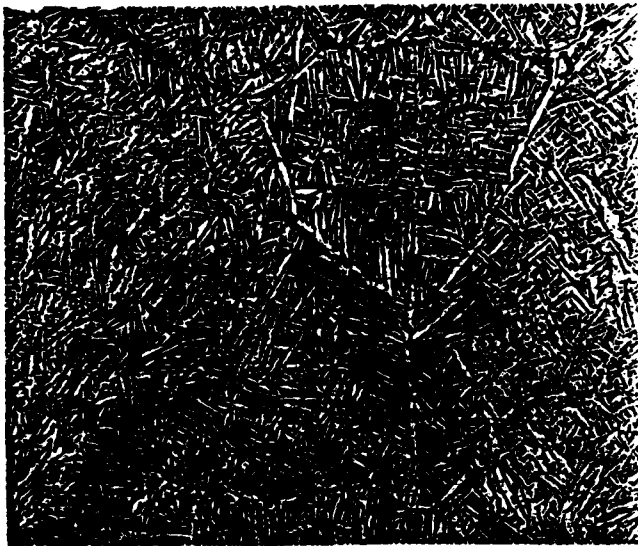


b



c

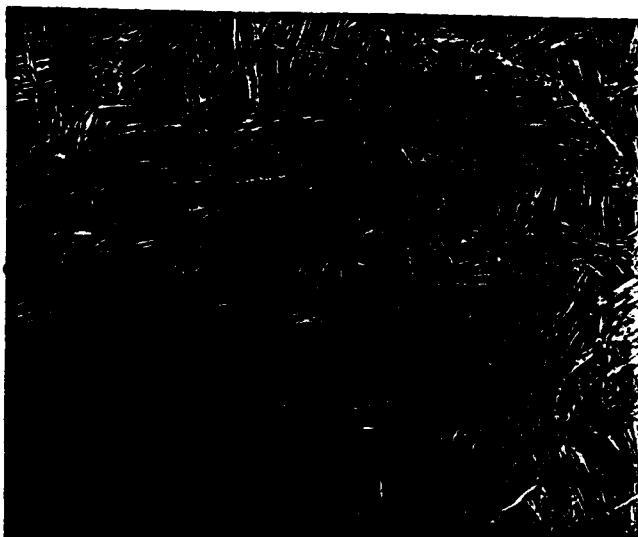
Fig. 2. SEM micrographs (200x) of Ti-6Al-4V cigar-melts with additions of (a) 0.5 wt.% Er, (b) 1.5 wt.% Er and (c) 3.0 wt.% Er.



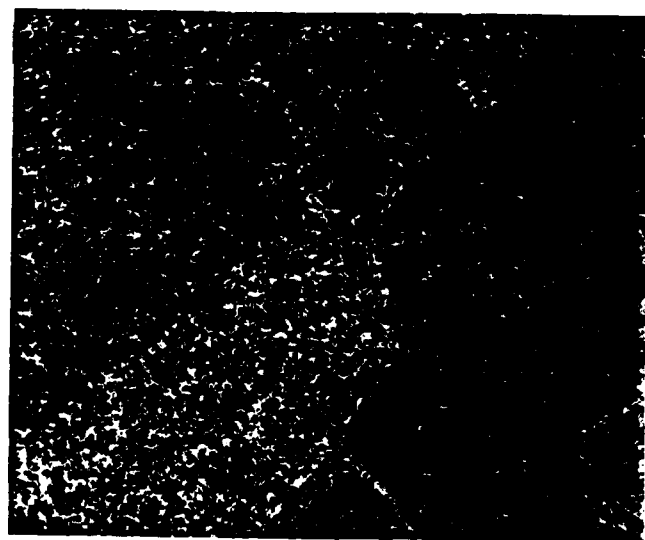
a



b



c



d

Fig. 3. Light micrographs of (a) Ti-6Al-4V-1.5Er cigar-melt (400x), (b) Ti-10V-2Fe-3Al-1.5Er cigar-melt (400x), (c) fully homogenized Ti-6Al-4V-1.5Er (200x) and (d) fully homogenized Ti-10V-2Fe-3Al-1.5Er (200x).

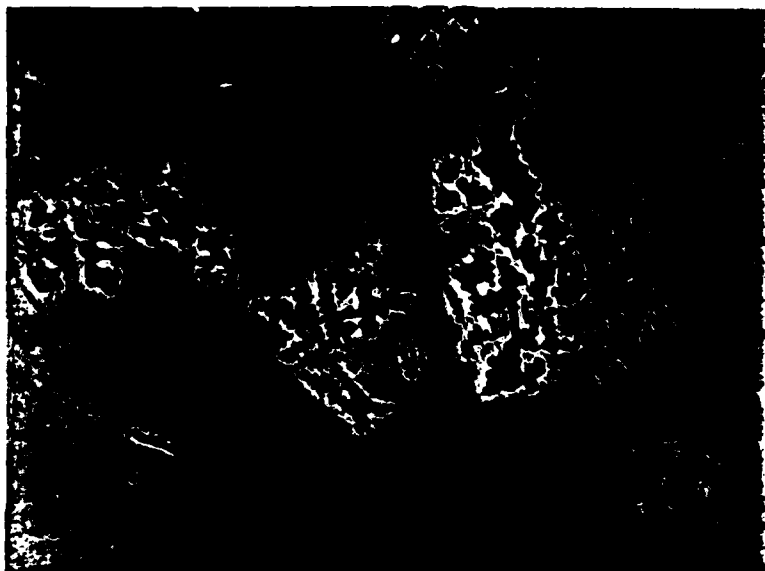


Fig. 4 Light micrograph (50x) of Ti-6Al-4V-0.5B cigar-melt.

FIGURE 5

Typical Microstructures



a) Ti-6Al-4V ribbon quenched
on mild steel (800x).



b) Ti-6Al-4V ribbon quenched
on aluminum (800x).



c) Ti-6Al-4V ribbon quenched
on copper (800x).



d) Ti-6Al-4V ribbon quenched
on brass (400x).

FIGURE 6

Typical Microstructures



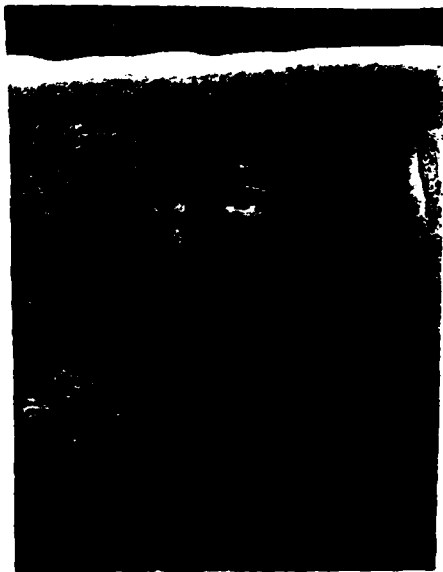
a) Ti-6Al-4V ribbon quenched
on titanium (400x).



b) Ti-6Al-4V ribbon quenched
on nickel coated copper (800x).

FIGURE 7

SEM of Ribbon Contact Side



a) Ti-6Al-4V ribbon quenched
on mild steel (70x).



b) Ti-6Al-4V ribbon quenched
on brass (70x).

1985 USAF-UES SUMMER FACULTY RESEARCH PROGRAM

Sponsored by the
AIR FORCE OFFICE OF SCIENTIFIC RESEARCH

Conducted by the
UNIVERSAL ENERGY SYSTEMS, INC.

FINAL REPORT

"POPCORN" AS A TOOL FOR FUTURE COGNITIVE WORKLOAD ASSESSMENT:

A CONCEPTUAL ANALYSIS

Prepared by:	Shih-sung Wen
Academic Rank:	Professor of Psychology
Department and University:	Department of Psychology Jackson State University
Research Location:	School of Aerospace Medicine/NGN Brooks AFB, San Antonio, TX
USAF Research:	John C. Patterson
Date:	August 7, 1985
Contract No:	F49620-85-C-0013

"POPCORN" AS A TOOL FOR FUTURE COGNITIVE WORKLOAD ASSESSMENT:

A CONCEPTUAL ANALYSIS

by

SHIH-SUNG WEN

ABSTRACT

The present study was aimed at conceptually analyzing the degree to which the POPCORN, a supervisory control simulation system developed by NASA Ames Research Center, measures the cognitive processes of piloting. In light of the weakness of current measurement approaches and the characteristic cognitive demands of future aircraft and combat tactics, the result of analysis suggests that the POPCORN is capable of assessing both low and high cognitive processes and is a man-machine interactive measurement tool for the future. It was considered especially suitable for monitoring metacognitive ability of the pilot. The author strongly recommended that the POPCORN be validated through empirical data analysis. It was further suggested that a short-term study be conducted to investigate conditions under which metacognition is being monitored by the POPCORN.

ACKNOWLEDGEMENTS

This research was supported by the Air Force Systems Command, Air Force Office of Scientific Research, through Summer Faculty Research Program which was conducted by Univesal Energy System under Contract F49620-85-C-0013.

Thanks are due to Dr. Bryce Hartman for his support and encouragement, to Dr. John C. Patterson for introducing the POPCORN simulation program and for his generous support, comments and valuable suggestions throughout the research, and to Mrs. Rosie M. Anguiano for typing the report. The research experience at the School of Aerospace Medicine/NGN, Brooks AFB, San Antonio has been a very meaningful and productive one.

I. INTRODUCTION

A. Importance of Cognitive Workload Assessment

Workload assessment is of great interest to cognitive psychologists. Although "workload" has not been clearly defined, it consists of a set of task demands, operator efforts, and task performance (Gartner & Murphy, 1979). Cognitive psychologists try to understand how the intended task demands are perceived, processed, and performed by an aircraft operator.

Recent advancement in avionic technology has altered a great deal of the traditional man-machine relationship in cockpit. The computer hardwares and softwares in the aircraft can assume control and monitoring of a routine flight, handle repetitive tasks, and automatically diagnose, adjust, and correct mechanical errors. This achievement in automation has drastically reduced a large number of psychomotor or physical task demands (Hart & Sheridan, 1984). Cognitive demands, on the other hand, have greatly increased and become a major concern for the pilot.

Today, computer-automation and its display systems constitute the key element of cockpit environment. The automated, yet sophisticated, highspeed man-made "brain" could constantly interact with the pilot and be ready to receive commands under critical flight conditions. For this, piloting is no longer a one-way communication from the pilot to the instrument. In most cases, it is neither a direct nor an analog control of the aircraft. The versatility of the artificial brain provides the pilot with instant messages for actions or reactions. It also lists

various options for pilots to judge, choose, or reject in decision-making. This constant feedforward and feedback between the human brain and the artificial brain inevitably means that cognitive processes, such as attention, perception, comprehension, reasoning, judgment, memory, learning, decision-making, and problem-solving, are dominant features in piloting.

Psychologists are increasingly aware of the types of task demands imposed on pilots. Questions they are trying to answer are: what cognitive processes are being involved and how much cognitive resources are available for a mission flight? The former is concerned with simulation of cognitive demands and the latter resources identification and utilization. Understanding the underlying cognitive processes of complex flight tasks would benefit pilot training by identifying and structuring priorities of tasks and specifying conditions under which optimal cognitive functions and outcomes could be achieved. Similarly, knowledge of a pilot's resources available for a mission flight could assist aviation engineers in designing a friendly cockpit environment with a feasible flight model which would best utilize human resources without causing overload (performance deterioration) or underload (boredom). Hence, the importance of cognitive workload assessment could never be understated.

B. Current Approaches to Workload Assessment

According to Wierwille, et al (1979), workload assessment techniques could be evaluated by a matrix of two dimensions: workload methodology and operator behavior. Methods of workload assessment include subjective opinion (rating scale, interview, or questionnaire), spare mental capacity (task analytic, secondary-task, occlusion), primary task measures (single

or multiple measure, mathematical modeling), and physiological measures (single or combined measure). Berliner, et al (1964) categorized operator behavior into perceptual (searching for and receiving information, identifying objects, actions, events), mediational (information processing, problem-solving and decision-making), communication, and motor (simple/discrete, complex/continuous).

C. Critical Problems Associated with Current Assessment Approaches

Most workload measures, in terms of measuring perceptual, cognitive, and communication workload, are having limited success (Casali & Wierwille, 1984; Hart & Sheridan, 1984; Hartman & McKenzie, 1979; McKenzie & Hartman, 1979; Rahimi & Wierwille, 1982; Wierwille, Williges, & Schiflett, 1979). The underlying causes of failure to validly assess or predict a pilot's task performance in reality can be attributed to: (a) the lacking of a consensus on the definition of workload and its performance standards (McKenzie & Hartman, 1979), (b) no theoretical foundation for the test development (Hart & Sheridan, 1984), (c) issues with sensitivity and intrusion in simulation procedures (Casali & Wierwille, 1984; Heffley, Clement, & Jewell, 1982), (d) inadequate attention to interactions between task loading and operator factors (O'Donnell, 1982), (e) irrelevance or meaningless in task assignment (Rabbitt, 1984; Witlin, 1984), and (f) a general dissociation between objective and subjective measures (Gopher & Braune, 1984; Vidulich & Wickins, 1983).

A review, by this author, of task descriptions of some latest assessment batteries, such as Criterion Task Sets (CTS), Unified Tri-Service Cognitive Performance Assessment Battery (TS-CPAB), Basic Attributes Tests (BAT-Version 4), and other similar instruments has revealed a number of

psychometric flaws for their intended applications. First, most subscales or subcategory tasks were put together in a piecemeal fashion without clear rationale behind the arrangement. While each test has an empirical literature, the "battery" suffers from lack of validity studies. This was especially critical in dual-task or secondary-task assignments. Lack of Gestalt in task arrangement is distractive and could negatively affect the subject's willingness to actively participate in assessment and hence reduce the face validity of the instrument. Second, tasks were essentially measures of basic perceptual skills leaving many high-level cognitive processes untouched. Although cockpit facilities have been greatly reduced by introducing multifunctions display systems (Statler, 1984), many test developers remained committed to developing tasks of monitoring constancy or detecting changes on traditional panel displays. Thus, many high-level cognitive tasks, which the automation is unable to do (Hart & Sheridan, 1984), have been seriously ignored. Finally, the pilot's knowledge base which affects an individual's perception and performance of task demands (Hart & Sheridan, 1984; Santilli, 1985) was omitted from current measures. Lack of, or inadequate knowledge of specific task demands or unexpected task conditions could cause errors which might either lead to irreversible accidents or become an extraneous source of mental workload (Hart & Bortolucci, 1984).

D. Principles of an Effective Cognitive Workload Assessment

Flight is a purposive behavior. To validly measure cognitive workload in flight, the principles listed below should be followed.

1. A comprehensive flight model should be established to guide the development of assessment tasks. A comprehensive flight model should clearly define workload, specify hierarchical structures of man-machine

relationship, describe conditions under which optimal results can be reached, and identify criteria against which behavior outcomes can be evaluated.

2. Lower-level cognitive processes, such as perceptual skills and attentional distributions, should be measured within a contextual framework of higher-level cognitive processes, such as metacognition, decision-making, or problem-solving. This will insure that all aspects of assessment are meaningful and relevant to the goal of flight and hence the result can be interpreted in a significant manner.

3. Task performance should reflect a human-environment dynamic system of interactions. Since cognitive processes in flight are constantly modified by results of interactions between the pilot and his environment, simulation tasks should allow the subject to see results of his actions and show records of his inputs.

4. Measurement instrument should be periodically revised in light of both technological advancement and strategic innovation. Recent development in workload assessment did reflect some degrees of concerns for technological advancement. However, the strategic innovation which is closely associated with the technological upgrade was very much unattended. What does automation mean to the pilot? How does the pilot perceive enemy threats when the integrated fire/flight (IFF) system is on hand? Issues related to new aircombat strategies should be addressed in the development of assessment instruments.

E. POPCORN as an Assessment Tool for Future

Recently, a Supervisory Control Simulation program (POPCORN) was developed by NASA Ames Research Center (Hart, 1984). It was designed to

simulate the cockpit environment of the future. The program, according to its developer, will measure such cognitive processes as attention, monitoring, memory, rule learning and application, predicting, decision-making, problem-solving, and automated system management.

II. OBJECTIVE OF THE RESEARCH EFFORT

The objective of the present research was to conceptually analyze the POPCORN as a cognitive workload assessment instrument by mapping its task performance into cognitive processes of piloting. This was an initial step toward validation of the instrument.

III. METHOD

A. An Examination of Cognitive Demands in Future Cockpit Environment

An Aerospace Medical Panel Symposium was recently held to address "Human Factors Considerations in High Performance Aircraft" (Hennessy, 1984). The symposium generally agreed that the future aircraft design and aircombat tactics would impose many more cognitive demands than did traditional ones. The cognitive demands that were specifically mentioned for future flight are: selectivity of perception (attention), interpretation (comprehension), monitoring (supervisory control), anticipation, prediction, recognition and diagnosis of unexpected situations, learning and memory, inductive reasoning, judgment, rule application, risk, decision making, problem solving, and self-regulation.

B. Task Analysis of the POPCORN

1. Basic features

The POPCORN consists of computer-generated performance tasks to simulate cognitive processes of future cockpit environment. According to its 1984 experimental version, the POPCORN includes five tasks and fif-

teen functions for each task. The five tasks are displayed horizontally at the bottom of the cathode-ray tube (CRT), and the fifteen functions are displayed vertically in top-down sequence on the right edge of the CRT. Each task is represented by a box which contains up to 20 events ("kernels"). When a task (e.g. Box *) and a function (e.g. "Open" a lid) are sequentially activated by a magnetic pen on a pad (with similar displays on the CRT), kernels will start "popping" out of the box and can be "consumed" (scored) by touching the PERFORM key at the bottom-right corner, otherwise they will "die" (scored as error). The kernels in the activated box will begin to mill around with increasing speed the longer they remain in the box unperformed. Boxes can be simultaneously activated (linked) and can be stopped or delayed or changed. The experimenter can, by modifying task instructions or computer softwares, change the nature, speed, meanings, and values of tasks and functions to increase the flexibility, complexity, and demands of task performance.

2. Independent variables

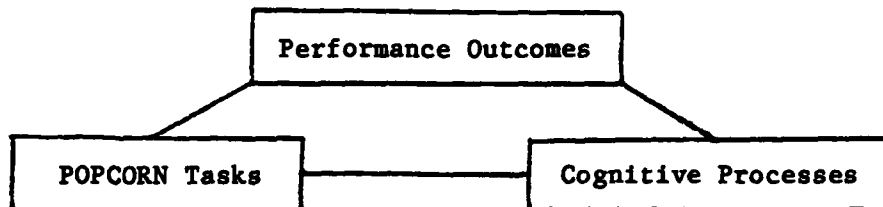
- a. Number of tasks in action
- b. Number of functions used: OPEN (box), CLOSE (box), STUFF (elements), REMOVE (barriers from elements), STOP, CHANGE (colors), ADD (elements), SHED (elements), LINK (tasks), UNLINK (tasks), BACKUP (for diagnosis), CYCLE (door), MANUAL (for problem-solving).
- c. Number of touching PERFORMANCE key
- d. Task difficulty (Number of tasks X Number of functions)
- e. Strategies (combinations of tasks and functions in various orders at different time)

3. Dependent variables

- a. Score or penalty point (objective measure)
- b. Satisfaction (subjective measure)
- c. Stress (subjective measure)
- d. Fatigue (subjective measure)

C. Mapping POPCORN Tasks into Cognitive Processes

Since the POPCORN is a set of dynamic simulation tasks, it can only be evaluated through an analysis of interactions among tasks, cognitive (mediational) processes, and task performance outcomes. The following diagram was used to depict the dynamic relationship among variables of interest.



To proceed with the mapping, each task performance was conceptually simulated and sequentially checked with cognitive processes to find out the most appropriate matches in light of possible outcomes.

IV. RESULT

A. Cognitive Processes Measured by the POPCORN

- 1. Selective Attention: Attending to tasks selected, procedures to be followed, and outcomes to be expected.
- 2. Divided Attention: Attending to two or more tasks simultaneously activated.
- 3. Basic perceptual skills: Recognizing tasks to be completed, functions available for uses, and warnings of penalty; estimating speeds

of popping kernels and possible scores can be earned; classifying tasks into various classes (completed vs. incomplete, active vs. inactive or delayed, regular vs. added, linked vs. unlinked); monitoring progress of each task; and predicting success against failure.

4. Judgment and decision making: Judging the quality and quantity of strategies used; determining underload, overload, or just-right workload; and deciding which options to choose to facilitate scoring or avoid penalty.

5. Cognitive strategies: Formulating or modifying task strategies to achieve maximum scores with high satisfaction but low stress and fatigue.

6. Learning: Acquiring and applying tasks-related rules; and modifying behavior through feedbacks.

7. Memory: Sensory store for each popping kernel; short-term memory for each action taken or score earned; and long-term memory of strategies used, rules followed, problems solved, mistakes made, and total scores accumulated.

8. Problem solving: Solving the built-in problems in tasks by following predetermined procedures.

9. Metacognition: Knowing what one wants to do, what one has done, how tasks are to be done, and how much mental resources are still available; and knowing what one knows and what one does not know in dealing with tasks.

In summary, as the result of this conceptual analysis, the POPCORN appears to be able to meet the need of assessing major cognitive demands of future cockpit environment, although some are more adequately measured

than others.

B. Unique Characteristics of the POPCORN

The impressive capacity of the POPCORN to measure a broad range of cognitive processes could be attributed to, among other things, its three unique features.

1. Man-machine interaction: From the beginning to the end the whole simulation program is a process of action-and-interaction between the operator and the task. Perceptions, efforts, and outcomes are changing as time and tasks progress. It considers the operator as an active, purposive, and adaptive information processing system as did Newell and Simon (1972). As the result, all efforts, decision-making, strategies and other cognitive processes are "naturally" imbedded in the seemingly non-intrusive, game-like task performance. Consequently, human interest can be maintained; the process of task attainments can be analyzed; and the outcome can be meaningfully interpreted.

2. Metacognition assessment: One advantage of having a complete, meaningful, and interactive simulation system is that it can be used to measure the pilot's metacognition. Metacognition is a superordinate executive system which overview and guide on-going cognitive activities (Meichenbaum, 1977). For a pilot, knowing what he knows, what he is doing, and how things can be done is essential in determining courses of action. Perhaps, it can decide how much a pilot will benefit from his own experience.

3. Future assessment tool: The POPCORN was designed with considerations of high degree of automation and high demands of cognitive processes in future aircraft. In cockpit, automation lets the pilot "fall behind,"

he has to manage to "stay ahead" (Richter, 1984). This is also true in the case of workload assessment. The POPCORN is the one that stays ahead.

V. SUMMARY, CONCLUSION, AND RECOMMENDATION

A. Summary and Conclusion

Although many current workload assessment instruments are having some degree of success, they are characterized by a number of problems: a consensus on the definition of workload is still lacking; a comprehensive theoretical foundation for simulation is not available; intrusion effects on measurement sensitivity are unsolved; man-machine interactions are ignored; task assignments are mostly irrelevant or meaningless; discrete molecular tasks are put together in a piecemeal manner to simulate the continuous and complex molar task of flying; few high-level cognitive skills are being measured; and the knowledge base of piloting is not properly included.

An analysis of the cognitive demands of future aircrafts and combat strategies indicates that a new workload measurement instrument is needed to adequately assess high-level cognitive processes of piloting. Further analysis of a recently developed workload assessment tool, POPCORN, shows that it can monitor selective and divided attention, basic perceptual skills, judging and decision-making, cognitive strategies, learning, memory, problem solving and metacognition. The study concluded that the POPCORN is an interactive simulation system, capable of measuring meta-cognition, and that it is an assessment tool of the future.

B. Recommendation

Validity is the major quality with which a measurement can be properly evaluated. Low validity and poor generalizability of current workload

assessment instruments have prompted two possible options: continuously modifying current instruments or constructing a new-generation assessment tool. The Basic Attributes Tests (BAT) and Unified Tri-Service Cognitive Performance Assessment Battery (CPAB) and other similar instruments are the result of the former attempt and the POPCORN the latter. On the ground specified in the present analysis, this writer favors the POPCORN as a cognitive workload assessment tool of the future.

The result of this study has suggested that the POPCORN is capable of measuring a large number of important cognitive processes of piloting. Since this study was only a first step toward validation of the instrument, a long-term empirical validity study should follow. To achieve this goal, however, a short-term empirical study is recommended to systematically investigate how a selected cognitive process is being simulated by POPCORN tasks.

REFERENCES

- Berliner, C., Angell, D., & Shearer, D.J. (1964). Behaviors, measures, and instruments for performance evaluation in simulated environment. Paper presented at the Symposium and Workshop on the Quantification of Human Performance, Albuquerque, New Mexico, August, 1964.
- Casali, J.G., & Wierwille, W. W. (1984). On the measurement of pilot perceptual workload: A comparison of assessment technique addressing sensitivity and intrusion issues. Ergonomics, 27, 1033-1050.
- Gartner, W.B., & Murphy, M.R. (1979). Contents of workload. In B.O. Hartman & R.E. McKenzie (Eds), Survey of methods to assess workload, AGARD-AG-246.
- Gopher, D., & Braune, R. (1984). On the psychophysics of workload: Why bother with subjective measures? Human Factors, 26, 519-532
- Hart, S.G. (1984). POPCORN: Subtask definition for a supervisory control simulation. NASA Ames Research Center, Moffett Field, CA.
- Hart, S.G., & Bortolussi, M.R. (1984). Pilot errors are a source of workload. Human Factors, 26, 545-556.
- Hart, S.G., & Sheridan, T.B. (1984). Pilot workload, performance, and aircraft control automation. In R. T. Hennessy (ED), Human factors considerations in high performance aircraft, AGARD-CP-371.
- Hartman, B.O., & McKenzie, R.E. (1979). Survey of methods to assess workload. AGARD-AG-246.
- Heffley, R.K., Clement, W. F. & Jewell, W.F. (1982). Overview of work in progress on non-intrusive assessment of pilot workload and pilot dynamics. Proceedings of the workshop on flight testing to identify pilot workload and pilot dynamics. AD-129-333.

- Hennessey, R. T. (1984). Human factor considerations in high performance aircraft. AGARD-CP-371.
- McKenzie, R.E., & Hartman, B.O. (1979). Some insights relative to the man-machine system: An overview of ten years of research. In B.O. Hartman & .E. McKenzie (Eds), Survey of methods to assess workload. AGARD-AG-246.
- Meichenbaum, D. (1977). Cognitive-behavior modification: An integrative approach. New York: Plenum Press.
- Newell, A., & Simon, H.A. (1972). Human problem solving. Englewood Cliffs, N.J.: Prentice-Hall.
- O'Donnell, R.D. (1982). Historical foundations of the AFAMRL workload program. Proceedings of the workshop on flight testing to identify pilot workload and pilot dynamics, 53-67.
- Rabbitt, P. (1984). The control of attention in visual search. In R. Parasuraman & D.R. Davies (Eds), Varieties of attention, New York: Academic Press.
- Rahini, M., & Wierwille, W.W. (1982). Evaluation of the sensitivity and intrusion of workload estimation techniques in piloting tasks emphasizing mediational activity. Proceeding of the 1982 international conference on cybernetics and society, 593-597.
- Richter, K. (1984). Impact of future aircraft characteristics on pilot performance and cockpit design. In R.T. Hennessey (ED), Human factors considerations in high performance aircraft. AGARD-CP-371.
- Santilli, S.R. (1984). Information processing and you. Tac Attack. June, 6-11.

- Statler, I.C. (1984). Military pilot ergonomics. In R.T. Hennessy (Ed),
Human factors considerations in high performance aircraft. AGARD-CP-371.
- Vidulich, M.D., & Wickens, C.D. (1983). Processing phenomena and the
dissociation between subjective and objective workload measures.
Engineering-Psychology Research Laboratory Technical Report, University
of Illinois at Urbana-Champaign.
- Wierwille, W.W., Williges, R.C., & Schiflett, S.G. (1979). yAircrew
workload assessment techniques. In B.O. Hartman and R. E. McKenzie
(Eds), Survey of methods to assess workload, AGARD-AG-246.
- Wittlin, A.S. (1984). Are the limits of the mind expandable?
Behavioral Science, 29, 51-60.

1985 USAF-UES FACULTY SUMMER SUPPORT PROGRAM

Sponsored by the

AIR FORCE OFFICE OF SCIENTIFIC RESEARCH

Conducted by

UNIVERSAL ENERGY SYSTEMS, INC.

FINAL REPORT

LABELING THE TOPOGRAPHIC FEATURES OF A GRAY-LEVEL IMAGE

Prepared by:	Dr. David C. Wilson
Academic rank:	Associate Professor
Department and	Department of Mathematics,
University:	University of Florida
Research Location:	Air Force Armament Laboratory, Eglin AFB
	Guided Weapons Division
	Electro-Optical Terminal Guidance Branch
USAF Research Contact:	Mr. Neal Urquhart
Date:	July 29, 1985
Contract No:	F49620-85-C-0013

LABELING THE TOPOGRAPHIC FEATURES OF

A GRAY-LEVEL IMAGE

by

David C. Wilson

ABSTRACT

The purpose of this paper is to describe a method for labeling the topographic features of a gray-level image. The topographic features considered include peaks, ridges, cliffs, prairies, valleys, canyons, ravines, and sinks. This approach to Image Processing grew out of the Eglin Armament Laboratory's interest in identifying such high-value targets as buildings, bridges, petroleum tanks, and runways. In an infrared image buildings and petroleum tanks tend to appear as peaks and small ridges topographically, while bridges and runways tend to appear as large ridges. Since these peaks and ridges represent pixels higher than the average, the algorithm presented here is designed to focus on the connected components of those pixels at least one standard deviation above the mean. (The algorithm also considers components one standard deviation below the mean.) These connected components are then labeled according to the local topographic content of their pixels. For example, if a component has a significant percentage of peak pixels or ridge pixels, then it will be labeled a peak or ridge, respectively. The algorithm was successful in accurately labeling most components.

Acknowledgements

The author would like to express his appreciation and gratitude to the Air Force Systems Command and the Air Force Office of Scientific Research for providing the opportunity to spend a very interesting and valuable summer at the Air Force Armament Laboratory, Eglin AFB, Florida. In particular, he would like to acknowledge Mr. Neal Urquhart who conceived, encouraged, and pushed the project to its successful conclusion. The author would also like to thank Professor Gerhard Ritter for his many helpful comments and suggestions and Mr. Dennis Garbo who provided solutions to the endless computer problems encountered. Finally, the author would like to acknowledge the assistance of Mrs. Mildred Campbell in the preparation of this manuscript.

I. INTRODUCTION

The primary goal of this research effort is to develop an algorithm which accurately labels the topographic features of a gray-level image. The topographic features of interest include peaks, ridges, cliffs, prairies (level regions), valleys, canyons, ravines, and sinks. The motivation behind this project grew out of the Air Force's desire to recognize high-value targets in an infrared image. This approach is natural in this type of target recognition because when infrared images of high-value targets are plotted on the DeAnza color graphics CRT, the buildings and petroleum tanks tend to appear as very high peaks and small ridges, while the runways and bridges tend to appear as large high ridges. In fact, when a gray-level image is plotted on a CRT, the resulting picture looks like a topographic map with not only peaks and ridges, but also cliffs, prairies, valleys, canyons, ravines, and sinks. In the case of infrared images of high-value targets the buildings, and petroleum tanks showed up as peaks and small ridges because they are very hot relative to the natural background and not very large. Since runways and bridges are usually long, narrow, and also hot relative to the natural background, they appear as large high ridges. When these infrared images are plotted, ravines, canyons, and valleys tend to occur in the regions between the buildings and runways. The natural background frequently occurs as one or more large prairies and sometimes sinks appear near petroleum tanks.

At this point several remarks seem to be in order. First, while

this topographic approach is motivated by target recognition, any gray-level image can be analyzed and labeled. Thus, the methods presented here are completely general and could possibly be utilized in other fields such as medicine. This comment leads to the second remark. While the topographic terminology is familiar and convenient to use, let us be clear that when we mention peaks, ridges, and cliffs in a gray-level image we do not mean that the image is a picture of a peak in Rocky Mountain National Park, a ridge on the Appalachian Trail, etc. The image could represent virtually anything.

As part of the research effort an extensive literature search was undertaken to locate articles which study gray-level images from a topographic point of view. While conducting this search, we found a variety of references to many of the standard methods of feature extraction. For example, Rosenfeld and Weszka give an overview of some of these methods in their articles "Picture Recognition," [1,2]. They discuss edge detection, template matching, region growing, connectedness tests, size tests, and statistical tests. Gonzalez and Tou [3] discuss decision functions. Serra [4] reviews the basic theory of the rolling ball algorithm, erosions, dilations, and the medial axis transform. In the topographic approach presented here we make little use of these well-known methods. In fact, from the above list only the most elementary connectedness and size tests are employed. However, we did locate a few papers with a topographic point of view. First, Serra [4] briefly mentions the work of Lantuejoul [5], who studies the notions of watershed, summits, sinks, divides, etc. Also, the paper by

Laffey, Haralick, and Watson [6] may be pertinent to our investigation. Since neither of these papers [5],[6] was published as a journal article, we were unable to obtain copies. Consequently, there is no way to compare their methods with ours. We did find a brief paper by Johnston and Rosenfeld [7], which takes a topographic approach. They define peaks, ridges, ravines, and pits. However, even though they use terminology similar to ours, they left out many other terms such as mesas, canyons, valleys, and prairies that we made use of. However, the main difference between the two papers is that they did not make use of the "elevation information" that we did.

As part of our approach to the labeling of a gray-level image by its topographic features, we felt that our terminology should be consistent with that used in Physical Geography. Thus, we contacted the Defense Mapping Agency in both Washington, D.C., and St. Louis, Missouri, to see if they had a glossary or dictionary of such terms. As far as we could determine, they did not have any such reference volume. In place of an official document we used the "Dictionary of Physical Geography" by W.G. Moore [8]. The terms we chose to use for our labeling scheme are defined at the end of Section III.

Dr. David C. Wilson received his Ph.D. in Mathematics from Rutgers in 1969. His area of specialization was Geometric Topology. Since that time, he has published over 15 papers in Topology and one paper in the area of Grid Generation (a subfield of Computational Fluid Dynamics). Teaching responsibilities during his 13 years as a member of the Mathematics Department at the University of Florida have

included courses ranging in difficulty from Freshman Calculus to Algebraic Topology. Applied mathematics courses taught include Differential Equations, Partial Differential Equations, Intermediate Differential Equations, Numerical Methods in Differential Equations, Vector Analysis, Computational Linear Algebra, and Complex Variables. During the last year at the University of Florida he attended weekly seminars on Image Processing, Partial Differential Equations, and Computer Science. He was assigned to the Image Processing Lab at Eglin AFB during the Summer of 1985. One concern of this Laboratory is to develop and apply Image Processing techniques to the problem of automatic recognition of high-value targets.

II. Objectives of the Research Effort

The primary objective of our research effort this summer was to investigate the feasibility of identifying and labeling the topographic content of a gray-level image. A necessary aspect of this investigation would be the implementation of an algorithm which would accurately label topographic features such as peaks, ridges, valleys, and cliffs.

A second objective was to conduct an extensive literature search for any articles, technical reports, or government documents related to our research effort.

A third objective was to locate an official dictionary of topographic terms to insure that our labeling scheme is consistent with the definitions and terminology presently used in the area of physical

geography. In particular, the Defense Mapping Agency was to be contacted for such information.

Objectives 2 and 3 are discussed in Section I, while the primary objective is discussed in Sections III and IV.

III. An Overview of the Labeling Algorithm

The discussion presented in this section will use the subroutine and array names exactly as they appear in the Fortran source code. The two main aspects of the algorithm are the level slicing and the probe.

First, the probe value at each pixel is determined in subroutines PROBE and TEST. The subroutine PROBE looks at each pixel in the filtered version of the input array, reaches out in 8 different directions, and then selects one neighbor from each direction. The subroutine PROBE can be thought of as an octopus sitting at the center pixel reaching out in 8 different directions with 8 different arms, grasping 8 unwilling neighbors, and drawing them into her lair. The subroutine TEST analyses these 8 neighbors and determines whether or not the center pixel is on a peak, on a ridge, at the top of a cliff, on a steep slope, on a gentle slope, on a flat area, at the bottom of a cliff, in a ravine, or in a sink. While the rules given in TEST are very specific, they can each be visualized in a natural way. In particular, a pixel will be declared a peak point if it is higher than all 8 of its neighbors. A pixel is on a ridge if it is in a region which is long, narrow, and fairly level with steep slopes on each side. A pixel is on a cliff if it is on a flat area with a sheer almost

vertical drop on one side. A pixel is on a steep slope if part of the terrain is above it, part on the same level, and part below. A pixel is on a gentle slope if it has some neighbors above (or below) but also some others at about the same level. A pixel is on a flat area if all its neighbors are at the same level. A pixel is in a ravine if it is in a region that is long, narrow, and level with steep upward slopes on each side. (A ravine is the opposite of a ridge.) A sink is the opposite of a peak. Thus, a pixel is in a sink if it is lower than each of its 8 neighbors.

Second, the subroutines SLICE and LABEL are combined to find the connected components of all pixels in the input array which are two standard deviations above the mean. Components with fewer than 30 pixels are discarded. Subroutine SCRIPT2 is now called. While the primary purpose of SCRIPT2 is to tabulate the data generated in LABEL, it also calls the subroutine VERYHIGH. This subroutine computes such quantities as the percentage of peak points in each component, the percentage of ridge points in each component, and the percentage of flat points in each component. If 10% of the pixels in the component are peak points, then it is declared a peak. If 20% of the pixels in the component are ridge points, then it is declared a very high ridge. If 40% of the pixels are flat points, then it is declared a very high mesa. The subroutine VERYHIGH also makes size estimates to determine if a component is small, medium, or large. If a component is left unlabeled then subroutine SHAPE is called to take a second look to check whether it should be labeled a peak or ridge. If the component

is "long" and "thin," it is labeled a ridge; if it is more rounded, it is labeled a peak. The subroutines SLICE and LABEL are combined 3 more times to investigate the connected components of the peaks one standard deviation above the mean, two standard deviations below the mean, and one standard deviation below the mean. As before the subroutine SCRIPT2 calls the subroutines HIGH, VERYLOW, and LOW at the appropriate moment to label these 3 new sets of components. The rules are very similar to those just described for VERYHIGH. The 5th and last time LABEL is called it is used to locate the components of the cliff points. The subroutine SCRIPT3 writes out the results to the output file.

The following are our definitions of the topographical terms we used in this report. We used the "A Dictionary of Geography" by W.G. Moore [8] as a guide.

canyon: a deep, narrow valley with precipitous sides or a ravine of considerable size bounded by steep slopes

cliff: a high and extremely steep face, approaching the vertical

crest: the highest line of a range of mountains, very high ridge

mesa: a flat, table-like mountain, which falls away steeply on all sides

peak: the top of a hill or mountain; a whole hill or mountain, especially when standing above the level of the surrounding country

prairie: an extensive tract of level or rolling land

ravine: a small, narrow, steep-sided valley that is larger than a

gully but smaller than a canyon

ridge: a long narrow, level, high region with steep slopes on each side

sink: a depression in the land surface bounded by steep slopes on all sides

valley: an elongate depression of the earth's surface commonly situated between ranges of hills or mountains

IV. Details of the Algorithm

This section of the report is devoted to a detailed discussion of the Fortran program that was used in the labeling algorithm. The name of the subroutines and arrays will be used here exactly as they appear in the source code.

Since the images we studied were taken from the IRHVTA library, the data was image-formatted. The subroutine NUMBERIMG reads this data and converts it into integer format. The resulting array is immediately converted to floating point and stored in the array AMATRIX. Next, the mean and standard deviation of the array AMATRIX are computed and stored in XMEAN and STDV, respectively. The values XMIN and XMAX are the minimum and maximum values in AMATRIX. Using a mean filter with a 3x3 window the array AMATRIX is smoothed and stored in the array BMATRIX. The subroutine SLICE is used to compute the height of each pixel relative to the mean and standard deviation. The output of SLICE is the array LEVEL which has values between 0 and 9. The entries in LEVEL are determined by the following rules. If

AMATRIX(I,J) is greater than or equal to $XMAX - STDV/2$, then $LEVEL(I,J) = 9$. If AMATRIX(I,J) is greater than or equal to $XMEAN + 3.0*stdv$, then $LEVEL(I,J) = 8$. If AMATRIX(I,J) is greater than or equal to $XMEAN + 2.0*STDV$, then $LEVEL(I,J) = 7$, etc.

The subroutines PROBE and TEST combine to approximate the local topographic content at the pixel $a(i,j)$ in BMATRIX. More specifically PROBE and TEST determine if the pixel $a(i,j)$ is a peak point a ridge point, a cliff point, etc. The parameter L is the "reach." It is used to locate the 8 immediate neighbors of $a(i,j)$. These neighbors are computed and stored in the array A according to the following rules: (The parameter L was usually chosen to equal 5.)

center pixel= $a(i,j)$
 $A(1) = a(i,j+L)$
 $A(2) = a(i-L,j+L)$
 $A(3) = a(i-L,j)$
 $A(4) = a(i-L,j-L)$
 $A(5) = a(i,j-L)$
 $A(6) = a(i+L,j-L)$
 $A(7) = a(i+L,j)$
 $A(8) = a(i+L,j+L)$

SCHEMATIC REPRESENTATION

$A(4)$	$A(3)$	$A(2)$
$A(5)$	$a(i,j)$	$A(1)$
$A(6)$	$A(7)$	$A(8)$

The next step is to construct the array IVECT. The entries in IVECT will be selected from among the integers -1, 0, and +1. If $IVECT(k)$ is less than or equal to $a(i,j) - ALPHA$, then $IVECT(k) = -1$. If $IVECT(k)$ is greater than or equal to $a(i,j) + ALPHA$, then $IVECT(k) = +1$. Otherwise, $IVECT(k) = 0$. In the data we tested we found that the variable ALPHA should be about twice the size of the parameter L. Thus, we set $ALPHA = 10.0$. Note that if B is the angle of inclination from the center pixel to a nearest neighbor, then $IVECT(k) = +1$ implies that $\tan(B)$ is greater than or equal to $ALPHA/L$. Hence, B is approximately equal to 64 degrees.

Six parameters computed in TEST are:

- 1) IPOS counts the total number of 1's in IVECT
- 2) INEG counts the total number of -1's in IVECT
- 3) IZERO counts the total number of 0's in IVECT
- 4) IDROP counts the total number of integers with the property that $IVECT(k)$ is less than or equal to $a(i,j) - 2.0*ALPHA$. Thus, IDROP counts the number of neighbors which are significantly below the center pixel.
- 5) IRISE counts the total number of integers with the property

that IVECT(k) is greater than or equal to $a(i,j) + 2.0*ALPHA$. Thus, IRISE counts the number of neighbors which are significantly above the center pixel.

6) ISIGN counts the total number of consecutive sign changes in the sequence IVECT(1), IVECT(2),..., IVECT(8), IVECT(1). Thus, for example, if IVECT(1), IVECT(2),..., IVECT(8), IVECT(1)= 1,1,1,0,-1,-1,-1,0,1, then ISIGN = 4, with sign changes occurring between IVECT(3) and IVECT(4), IVECT(4) and IVECT(5), IVECT(7) and IVECT(8), and IVECT(8) and IVECT(1).

Depending on the relations between these six parameters, the center pixel is labeled with an integer between 0 and 9. In the next paragraph, we give an indication of the rules used to assign the values in the array MATRIX. The correspondence between the topographic property and the value in the array MATRIX are listed in the following table:

<u>MATRIX(I,J)</u>	<u>TOPOGRAPHIC PROPERTY</u>
9	peak point
8	ridge point
7	top of cliff point
6	steep slope point
5	gentle slope point
4	relatively flat area
3	bottom of cliff point
2	ravine point
1	sink point
0	undefined

MATRIX(I,J) = 9: if INEG = 8, that is, if all values of IVECT(k), k from 1 to 8, are -1. Example:

-1	-1	-1
-1	X	-1
-1	-1	-1

MATRIX(I,J) = 1: if IPOS = 8, that is, if all values of IVECT(k) are 1. Example:

1	1	1
1	X	1
1	1	1

A '1' signifies the reverse topographic feature of the '9', since a 1 is a local minimum, and a 9 is a local maximum.

MATRIX(I,J) = 8: if IPOS = 0, and ISIGN = 4. Examples:

-1	-1	0		-1	-1	0
-1	X	-1	OR	0	X	0
0	-1	-1		-1	-1	-1

MATRIX(I,J) = 2: if INEG = 0 and ISIGN = 4. Examples:

0	1	1		1	1	1
0	X	1	OR	0	X	0
1	0	0		1	1	1

Note that a '2' signifies the reverse topographic feature of the '8'.

MATRIX(I,J) = 7: if IPOS = 0, ISIGN = 2, and IDROP is at least = 2.

Examples:

-1	-1	<u>-1</u>		0	0	0
<u>-1</u>	X	<u>0</u>	OR	0	X	0
0	0	0		<u>-1</u>	<u>-1</u>	0

where an underlined number means that the corresponding gray-level value is less than or equal to $a(i,j) - 2.0 \cdot \text{ALPHA}$. Thus

IDROP is greater than or equal to 2 in the above example.

MATRIX(I,J) = 6: There are 2 sets of conditions that if satisfied will label a pixel a six:

1) IPOS = at least 1, and INEG = at least 1, and IZERO = at least 1, and ISIGN = 4. Examples:

1	1	1		-1	0	0
0	X	0	OR	-1	X	1
-1	-1	-1		0	0	0

2) if IPOS + INEG = at least 2, which is equivalent to IZERO is less than or equal to 6; and ISIGN = 3. Examples:

-1	-1	1		1	0	-1
0	X	1	OR	1	X	-1
0	0	0		-1	-1	-1

MATRIX(I,J) = 5: There are two sets of conditions that if satisfied will label a pixel a five:

1) if INEG = 0, and ISIGN = 2, and IRISE is less than 2.

Example:

1	1	1
0	X	1
0	0	0

2) if IPOS = 0, and ISIGN = 2, and IDROP is less than 2.

Example:

0	0	0
0	X	0
0	-1	<u>-1</u>

Note that IDROP = 1.

MATRIX(I,J) = 4: if IZERO = 8. Example:

0	0	0
0	X	0
0	0	0

The subroutine SCRIPT1 prints out the values of the array MATRIX.

Subroutine LABEL is probably the most important subroutine in the algorithm. This subroutine is called 5 times during the execution of the program to determine and label the (8 connected) components of certain subsets of pixels in the image. For example, the first time LABEL is called the parameters ILOW = 7 and IHIGH = 9. With this choice of parameters the components of all pixels in AMATRIX at least two standard deviations above the mean will be found. (Recall that if LEVEL(I,J) is 7,8, or 9, then AMATRIX(I,J) is greater than or equal to XMEAN + 2.0*STDV.) The subroutine SCRIPT2 together with subroutine VERYHIGH prints out the components with at least 30 pixels in the array LAB. The decision whether a component is a peak, ridge, crest, or mesa is made in VERYHIGH.

The following are the Fortran criterion used to determine the label of a component:

a high peak: a component whose pixel gray-level values are all greater than or equal to the mean plus one standard deviation of the image and where 10% of the component's pixels are peak points (9's)

a very high peak: a component whose pixel values are all greater than or equal to the mean plus two standard deviations and where 10% of the component's pixels are peak points; or, where 50% of pixels have values greater than or equal to either mean plus three standard deviations or

XMAX minus one-half standard deviation.

ridge: twenty percent of the component's pixels are ridge points (8's). Again, we have high ridges or very high ridges.

crest: the component is both a peak and a ridge

mesa: forty percent of the component's pixels are 4's. A very high mesa has all its pixel values greater than or equal to mean plus two standard deviations. A high mesa has all its pixel values greater than or equal to mean plus one standard deviation.

cliff: all the component's pixels are 7's in the array MATRIX

The subroutine VERYHIGH also makes certain size estimates. In particular, if the number of pixels in the component is less than 1.5% of TOTAL, then the component is considered small. The variable TOTAL is the number of pixels in the entire array. If the number of pixels in the component is less than 3.0% of TOTAL but greater than 1.5%, then it is considered medium sized. If the number of pixels in the component has more than 3.0% of TOTAL, then it is considered large. If the component is unlabeled and 70% of its pixels are either peak points, ridge points, cliff points or steep slopes, then subroutine SHAPE is called. In SHAPE two additional tests are applied to a component to check whether it should be classified as a ridge or peak. The second time LABEL is called ILOW = 6 and IHIGH = 9 so that only pixels at least one standard deviation above the mean are considered. The subroutine SCRIPT2 together with subroutine HIGH labels the components and prints out the results. The third time LABEL is called ILOW = 0 and IHIGH = 3 so that only pixels at least two standard

deviations below the mean are considered. SCRIPT2 together with subroutine VERYLOW labels the components as very low level regions, ravines and sinks. If 40% of the pixels in a component are either flat points or gentle slopes, then it is labeled a very low level region. If 20% of the pixels are ravines points, then it is labeled a ravine. If 10% are labeled sink points, then the component is labeled a sink. The fourth time LABEL is called only pixels at least one standard deviation below the mean are considered. SCRIPT2 together with subroutine LOW labels the components as sinks, ravines, canyons, valleys and prairies.

The following are the Fortran criterion used to determine the label of a component:

sink: ten percent of the pixels in a component are sink points

ravine: twenty percent of the pixels in the component are ravine points, and the sum of the ravine points, steep slope points and bottom of cliff points is at least 50%

prairie: fifty-five percent of the pixels are flat points

canyon: twenty-five percent of the pixels are flat points or gently sloping points, and the sum of the ravine points, bottom of cliff points, or steep slope points is at least 30%

valley: forty percent of the pixels are flat points or gently sloping points and 20% of the pixels are ravine points, bottom of cliff points, or steep slope points

The fifth and last time LABEL is called the components of the cliff points are identified. The subroutine SCRIPT3 prints out a size

estimate of each component.

V. Analysis of Data and Conclusions

The algorithm described in sections III and IV was applied to over a dozen different images in the IRHVTA library. Since each image is 120 x 360, the quantity of output is enormous. It will be months before it can be carefully analyzed. A preliminary look at the data, however, has convinced us of several points. First, the local labeling of the pixels by their topographic content seems to be quite accurate. If a pixel is on a peak, then it is designated a peak point. If a pixel is on a ridge, then it is labeled a ridge point, etc. Second, components of the pixels two standard deviations above the mean were accurately labeled most of the time. However, even with the inclusion of subroutine SHAPE, some components remained unlabeled. Also, some components were labeled ridges, which should have been labeled peaks. While we are disappointed that our results were not perfect, we are not surprised. After all, we have based most of our decision making on crude percentage estimates. We have not employed any test which utilizes the proximity or relationships of the various types of pixels. Clearly this type of analysis needs to be done to improve our success rate.

VI. Recommendations

We feel that the main objective of the project has been achieved. The topographic labeling of a gray-level image is feasible and potentially very useful. We recommend the following steps for future

research.

1. A careful analysis of the success rate of the labeling should be made. Unlabeled and mislabeled components should be studied carefully to search for relationships which were overlooked before.

2. Proximity relationships between components should be introduced. In the ten weeks at Eglin we have not had time to investigate such notions as Hausdorff distance. These distance relationships become important when one is interested in questions of the type: "Is there a building near a runway?", "Is there a cluster of three buildings near one another?" .

3. Remark 2 above leads to the motivation underlying the entire project. Namely, can these topographic features give us insight into target recognition. Can we find features which characterize bridges, buildings, petroleum tanks and runways? Our feeling is that significant progress to this last question can be made if a careful analysis is done on the topographic features of infrared high-value targets.

References

1. Rosenfeld, A. and J.S. Weszka, Picture Recognition, Digital Image Processing for Remote Sensing, ed. by Ralph Bernstein, IEEE Press, New York, 1978, pp. 306-337.
2. Rosenfeld, A. and J.S. Weszka, Picture Recognition, Digital Pattern Recognition, Second Corrected and Updated Edition, ed. by K.S. Fu, Springer-Verlag, New York, 1980, pp. 135-166.
3. Gonzalez, R.C. and J.T. Tou, Pattern Recognition Techniques, Addison-Wesley Publishing Company, Reading, Massachusetts, 1974.
4. Serra, J, Image Analysis and Mathematical Morphology, New York, New York, Academic Press Inc., 1982.
5. Lantuejoul, Ch, "Detection automatique de lignes de défauts dans les systemes eutectiques lamellaires," Rapport interne, Centre de Morphologie Mathematique Fontainebleau, France, 1978.
6. Laffey, T.J., R.M. Haralick, L.T. Watson, "Topographic classification of digital image intensity surfaces," presented at the IEEE workshop on Computer Vision, Representation and Control, Rindge, New Hampshire, Aug. 1982, pp. 171-177.
7. Johnston, E.G. and A. Rosenfeld, "Digital Detection of Pits, Peaks, Ridges, and Ravines," IEEE Transactions on Systems, Man, and Cybernetics, July, 1975, pp. 472-480.

8. Moore, W.G, A Dictionary of Geography,

Frederick A. Preager, Publishers, New York.

1985 USAF-UES SUMMER FACULTY RESEARCH PROGRAM/
GRADUATE STUDENT SUMMER SUPPORT PROGRAM

Sponsored by the
AIR FORCE OFFICE OF SCIENTIFIC RESEARCH

Conducted by the
UNIVERSAL ENERGY SYSTEMS, INC.

FINAL REPORT
THE WAREHOUSE LAYOUT PROGRAM

Prepared by:	Jesse Williams
Academic Rank:	Associate Professor
Department and University:	Mathematics/Computer Science Cheyney University
Research Location:	Air Force Logistics Management Center AFLMC/LGS Gunter AFS, AL 36114-6693
USAF Research:	Maj. Douglas J. Blazer
Date:	12 July 1985
Contract No:	F49620-85-C-0013

THE WAREHOUSE LAYOUT PROBLEM

by

Jesse Williams

ABSTRACT

This paper is concerned with developing a microcomputer model that will rearrange items within an Air Force warehouse from their initial locations to desired locations. Such a rearrangement is necessary since the present arrangement of items within these Air Force warehouses was not designed by scientific principles. An efficient design would minimize the total travel distance, which is the number of times an item is picked up times the distance from the warehouse storage location to the pick up and delivery. As demands for items change it is not efficient to have low demand items near pick up and delivery. A heuristic technique is developed for a microcomputer model which is to be used by base level personnel in the warehouse. The technique relocates items with higher demand closer to the pick up and delivery area.

ACKNOWLEDGEMENTS

This research effort was made possible through the sponsorship of the Air Force Systems Command, Air Force Office of Scientific Research, and the Air Force Logistics Management Center. In particular, the contributions of Maj. Douglas J. Blazer have played an important role in this research effort.

I. INTRODUCTION: The United States Air Force (USAF) has determined that the location of items within its warehouses should be done with the objective that the warehouse is efficient in the use of manpower. The Air Force Logistics Management Center (AFLMC) was given this task to develop efficient warehouse layouts. The first phase of this project is to develop a microcomputer model that can be used by base level warehouse personnel. To develop such a model requires a person with an operations research background and, also, literacy with computers. My experiences include educational preparation in and the teaching of courses in operations research and in computer science. Additionally, my past efforts have included professional experience as an operations research analyst. The AFLMC is involved with many projects that require the use of operations research techniques and the development of computer models. Thus, the AFLMC would be able to provide the necessary assistance to an individual involved in developing the type of model it desired.

II. OBJECTIVES OF THE RESEARCH EFFORT: At the present time the USAF does not utilize any scientific principles with respect to the location of items within the warehouse. When items are sent to the warehouse the personnel at the facility will locate an item in the first open bin available. There is no systematic technique utilized to determine the location

that would be most efficient for the item. Demand for an item and distance traveled to pick up that item are not utilized when determining where an item should be located.

The AFLMC was given the task of developing a microcomputer model which would assist the warehouse personnel at the base level with determining the most efficient location for an item. Here efficiency is measured as total travel distance which is the product of the demand for an item and the distance the item is located from the pick up and delivery area. Reducing the total travel distance of an item, consequently, increases the efficiency of the warehouse.

In consultation with my USAF Research Colleague it was determined that I should develop a user friendly microcomputer model which would be used by base level warehouse personnel and which would rearrange items in the warehouse. This rearrangement would reduce the total travel distance of the present (initial) layout. This model was to have the capability of rearranging consecutive rows or selective (non-consecutive) rows. The model should also be able to handle up to approximately 10,000 items. In addition to developing the microcomputer model a User's Guide was to be developed that would enable the user of the model to do so with ease. The model would be tested on actual Air Force data.

III. HEURISTIC TECHNIQUE: The problem of warehouse layout can be described as follows. The total travel distance of an item is defined to be the product of trips (demand) made to pick up the item and the distance traveled to pick up the item. The total travel distance of the warehouse is the sum of the travel distances of the individual items in the warehouse. Our objective is to reduce this total distance (C) as much as possible. Formally, the problem is to

$$\text{minimize } C = \sum_{i=1}^N \sum_{j=1}^N T_{ij} D_{ij}, \quad (1)$$

where T_{ij} = trips between location i and location j ,

D_{ij} = distance from location

and N = number of locations..

In the literature, e.g. [1], a solution technique to this problem starts with an arbitrary initial layout and then obtains a new layout by interchanging locations pairwise. Compare the travel distance of this new layout to the initial layout and continue developing new layouts until the total travel distance of a layout can no longer be reduced.

The problem solution technique considered in this paper attempts to obtain an optimal or near optimal solution layout on the first rearrangement. The Williams' heuristic technique claims that the first rearrangement it produces is

optimal or near optimal with respect to reducing the total travel distance of the layout. This technique uses a sorting technique to solve the problem. The set of number of trips to pick up an item is sorted into descending order. The set of distances between bin locations and pick up and delivery is sorted into ascending order. The items are then located in the bins such that the item with highest demand is placed in the bin with the lowest distance. Then the item with the next highest demand is placed in the bin with the next lowest distance. This process is repeated until all items have been placed in bins and a complete layout has been obtained. This layout is claimed to have the minimum or near minimum total travel distance of all possible layouts.

Mathematically we show this technique as follows. Suppose we have two sets of nonnegative numbers defined as

$$i, i+a, i+b \text{ and } j, j+c, j+d,$$

where $a < b$ and $c < d$. If we multiply the three numbers in each set pairwise and sum the products we have

$$[3ij + (c+d)i + (a+b)j] + [ac + bd].$$

This is one of $3! (=6)$ possible sums of products. Of all these possible sums which is the minimum? The above sum is the maximum. The minimum can be obtained if we change the ordering of one of the given sets such that the orderings are inverse with respect to each other. By this we mean that one

set is in ascending order and the other set is in descending order. E.g.,

$$i, i+a, i+b \text{ and } j+d, j+c, j$$

are now multiplied pairwise and summed. The result is

$$[3ij + (c+d)i + (a+b)j] + [ac].$$

All $3!$ of the summations will have the same set of variable terms and will differ only in the constant terms. If all summations have the same variable terms, then we are interested in the constant terms to determine the minimum summation. The constants for the $3!$ summations are

$$ac + bd, ad + bc, bd, ad, bc, \text{ and } ac.$$

It can be seen that ac is the minimum of this set. It was implied above that $ac + bd$ is the maximum of this set. This can be shown by demonstrating that $ad + bc < ac + bd$. This is shown through the following steps.

Given that $a < b$ and $c < d$.

$$a < b$$

$$0 < b - a$$

$$c < d$$

$$(b-a)c < (b-a)d$$

$$bc - ac < bd - ad$$

$$ad+bc < ac+bd$$

q.e.d.

or

$$a < b$$

$$(d-c)a < (d-c)b$$

$$ad-ac < bd-bc$$

$$ad+bc < ac+bd$$

q.e.d.

Therefore, the summation obtained from pairwise multiplication with both sets sorted in ascending order (or both sets sorted in descending order) gives a maximum result. A minimum result is obtained if the sets are sorted inversely before multiplying and summing.

IV. MICROCOMPUTER MODEL* The program was written in FORTRAN 77 to run on a Zenith-100 microcomputer with a 10.4 megabyte hard disk drive. The microcomputer model sorts the demands of the items into descending order and places these items into bins according to distances of bins from pickup and delivery area. The user of the model selects the rows and bins to be rearranged within a specified area in the warehouse. The program generates distances in a matrix with respect to rows and bins selected by the user. The user must input distance or closest bin selection to pickup and delivery area. The program generates distances in an ordinal manner for each row. The user inputs the number of levels

desired for each bin. Flexibility is offered to the user since the user does not have to utilize all of the levels available in the bin. Additional flexibility is offered to the user in that the rows selected do not have to be consecutive in sequence.

Output by the program includes a recommended layout and comparisons of the total travel distance of initial layout versus total travel distance of recommended layout.

Data provided for the program consists of approximately 10,000 items records. In order to manipulate this size of records the Shell-Metzner sort routine was utilized, which is very efficient for sorting large amounts of data.

Calculations are made for the total travel distance of the initial layout and the total travel distance of the recommended layout.

V. RECOMMENDATIONS:

a. Since the program is user friendly, utilization by base level personnel would increase efficiency within Air Force warehouses. An efficient warehouse means more effective warehouse operations during emergency periods such as wartime.

b. Follow-on research needs to consider the weight and volume of items and how best to store items in a multilevel bin. The present program does not consider weight and volume and assumes that all items are of the same size. The user selects the number of levels in a bin and the program will place the number of items in the bin, but does not specify the level within the bin. The level selection decision is left to the warehouse personnel. Research needs to be done to determine if a microcomputer program can be developed that will specify levels and depth for locations in a bin by utilizing weight and volume data. I intend to apply for a mini grant to do such follow-on research.

REFERENCES

1. Adam, Everett E., Jr. and Ronald J. Ebert, Production and Operations Management: Concepts, Models, and Behavior, 2nd Edition, Englewood Cliffs, NJ, Prentice-Hall, Inc., 1982.
2. Buffa, Elwood S., Operations Management: Problems and Models, 2nd Edition, New York, John Wiley & Sons, Inc., 1968.
3. Christofides, Nicos and I. Colloff, "The Rearrangement of Items In a Warehouse," Operations Research Journal, v. 21, No. 2, Mar.-Apr. 1973, pp. 577-589.
4. Foulds, L.R., "Techniques for Facilities Layout: Deciding Which Pairs of Activities Should Be Adjacent," Management Science, Vol. 29, No. 12, December 1983, pp. 1414-1426.
5. Gaston, Gerry K., "Facility Layout Optimizes Space, Minimizes Cost," Industrial Engineering, Vol. 16, No. 5, 1984, pp. 22-25.
6. Johnson, Richard A., William T. Newell, and Roger C. Vergin, Operations Management: A System Concept, New York, Houghton Mifflin Co., 1972.
7. Manivannan, S. and Dipak Chaudhuri, "Computer-Aided Facility Layout Algorithm Generates Alternatives To Increase Firm's Productivity," Industrial Engineering, Vol. 16, No. 5, 1984, pp. 81-84.
8. Schroeder, Roger G., Operations Management: Decision Making in the Operations Function, New York, McGraw-Hill Book Company, 1981.

1985 USAF-UES SUMMER FACULTY RESEARCH PROGRAM/

GRADUATE STUDENT SUMMER SUPPORT PROGRAM

Sponsored by the

AIR FORCE OFFICE OF SCIENTIFIC RESEARCH

Conducted by the

UNIVERSAL ENERGY SYSTEMS, INC.

FINAL REPORT

A SUMMER'S STUDY ON NUCLEAR DEBRIS CLOUD

RADIATION AND LASER TRANSMISSION IN THE ATMOSPHERE

Prepared by:	Dr. Arthur Woodrum
Academic Rank:	Professor and Head
Department and	Department of Physics
University	Georgia Southern College
Research Location	Division of Radiation Science School of Aerospace Medicine Brooks Air Force Base
USAF	Lt. Peter Vanden Bosch and Dr. Donald Farrer
Date:	August 7, 1985
Contract No:	F49620-85-C-0013

A SUMMER'S STUDY ON NUCLEAR DEBRIS CLOUD
RADIATION AND LASER TRANSMISSION IN THE ATMOSPHERE

by

Arthur Woodrum
Professor of Physics
Georgia Southern College

ABSTRACT

A simple mathematical model for calculating the estimated radiation dose of an aircrew in an aircraft flying through a debris cloud from a single nuclear detonation is developed. Suggested ways of creating a computer model for the growth of clouds from nuclear multibursts are made. A study shows that a measure of the "strength" of turbulence affecting the transmission of lasers through the atmosphere near ground level is given by the refractive-index structure coefficient which can be measured from a vertical temperature profile or from the resolution angle of two point light sources.

I. INTRODUCTION

My research background involves much work on the study of wave motions in the upper atmosphere. Experimental data on winds, pressure, density and temperature variations in the atmosphere around 100 kilometers were obtained from artificial clouds put into the atmosphere with rockets. These data were analyzed to discover the systematic wave motions in each of the variables.

The most recent research prior to the Summer 1985 involved creating a worldwide computer model of the atmosphere depicting representative values of winds, pressure, density, temperature, and their variations for any latitude, longitude, day of year, time of day and any height from surface up to about 200 kilometers. This work was done for NASA in connection with the Space Shuttle program. It resulted in a computer model named GRAMS which is still being used.

Even though this last research was done ten years ago, the background has served well in performing the work at Brooks AFB during the Summer 1985. The Air Force is interested in modeling the clouds of nuclear bursts in the atmosphere for the purpose of studying radiation doses of objects penetrating the clouds. Many of the techniques learned earlier are also applicable in this work.

II. OBJECTIVE OF THE RESEARCH EFFORT

There were three main objectives for my work during the Summer 1985. Two (A & B) were determined prior to the Summer and the other (C) was added during the Summer.

Objective A: Analyze the results of the CASSANDRA nuclear scenerio and organize it into a useable product for Air Force Planners.

Objective B: Investigate and recommend a research path for the development of the computer model of cloud growth from a multiburst of nuclear explosions.

Objective C: Determine some easily measured parameter that will indicate the "strength" of turbulence in the atmosphere near ground level that affects the transmission properties of lasers.

III. PROCEDURE

Objective A involved debugging a computer program developed by Taboada et al (1) to calculate radiation doses of aircraft flying through nuclear debris clouds and then analyzing the results. Work had already begun on this problem prior to this Summer by Lt. Peter Vanden Bosch. I assisted him in completing the debugging of the program and the analysis of the data.

Objectives B and C required literature searches of current work on the problem of concern. Then, theoretical analysis was done to adapt the current knowledge to the particular problem of interest to the Air Force.

IV. RESULTS

The work for all three objectives was completed during the Summer with very good results.

The work on objective A resulted in a document which is being presented for governmental publication as a technical report. The analysis of the computer model developed by Taboada et al (1) yielded a simple mathematical model to calculate radiation doses of aircrews in aircraft passing through debris clouds from single nuclear bursts. The great advantage of the mathematical model is two-fold. First, there is time and money savings. The calculation of an estimated radiation dose to aircrew from the computer model takes about 15 to 20 minutes of computer time with many input parameters; whereas, the same calculation with a minimum of input parameters can be done with a hand calculator in less than one minute using the mathematical model. Secondly, the simplification of the calculations using the mathematical model enables mission planners, and even aircrews, to analyze different scenarios within a short timespan. This may become important during a nuclear attack.

The major points of interest in this research are the following. The estimated radiation dose of an aircrew flying a KC-135 aircraft through a debris cloud from a single nuclear burst of yield W (megatons) with a speed of 311 knots is

$$\text{Dose} = 1.96 W^{0.45} t^{-1.53} \quad (1)$$

where t is the time in hours after detonation. The estimated dose that will be accrued during the remainder of the mission due to onboard dust particles is

$$D(t,) = 5R, (t_a^{-0.2} - t_i^{-0.2}) \quad (2)$$

where $D(t,)$ is the dose in rads for the mission at time t , hours after detonation that the aircraft exits the debris cloud. $R,$ is a dose rate constant given by the equation:

$$R, = 1.19 W^{0.54} t^{-0.33} \quad (3)$$

The total estimated dose of the aircrew for the entire mission is the sum of the doses from equations (1) and (2). The estimated doses can be adjusted to accomodate different aircraft and for flying different speeds.

A copy of the document submitted for governmental publication is enclosed.

The next research problem worked on during the Summer was objective C. An analysis of the current literature on the effects of turbulence on the transmission properties of lasers in the atmosphere near ground level revealed that the best parameter to indicate the "strength" of turbulence is a quantity called the refractive-index structure coefficient. This coefficient can be measured by either a knowledge of the vertical temperature profile along the propagation path of the laser or from the resolution angle of two point light sources in the area of the laser path. Once the coefficient has been determined, other properties of the laser beam that can be calculated from it include the resolution, modulation transfer function, and the mean squared angular deviation.

A report of this work was given to Major Dennis A. Maier in the form of a memo dated July 30, 1985. A copy of the memo is enclosed.

The last project of the Summer was objective B. A review of the literature reveals that little work has been done on modeling the growth of nuclear clouds from multibursts other than by approximating them by superposition of individuals bursts. My recommendation is that a simple case be examined first. Consider a multiburst of many simultaneous detonations in a symmetry such as a circle. Let the initial energy from the bursts be distributed uniformly over the area of the multiburst. Let the initial growth of the cloud be adiabatically. The subsequent growth can be approximated by adapting the single burst model DELFIC to the multiburst. This adaptation will not be easy and will involve severe changes in the model during early times.

Once an understanding of this simple model is accomplished, one can then consider adaptations of it to more realistic, but more complicated, configurations.

V. RECOMMENDATIONS

The results of the work on objective A are significant and need to be made available to the scientific community as quickly and widely as possible. Steps have already been taken to publish it as a governmental report. However, it also needs to be published in a journal. Presentations of the material should be given to other governmental agencies concerned with this type of work.

The work on objective B was only a beginning to the solution of a complicated problem. An approach has been determined. I will request funds from the Mini Grant Program to continue this work.

From a theoretical point of view, the work for objective C has been accomplished. However, the correlation of theory and actual experiment is not always complete. The experiments for which this theoretical work was done will be conducted during late 1985 and early 1986. Thus, the correlation can be checked at that time. A request for follow-on work in this area will be made directly to Brooks AFB.

AD-A166 178

UNITED STATES AIR FORCE SUMMER FACULTY RESEARCH PROGRAM 11/11

1985 TECHNICAL RE (U) UNIVERSAL ENERGY SYSTEMS INC

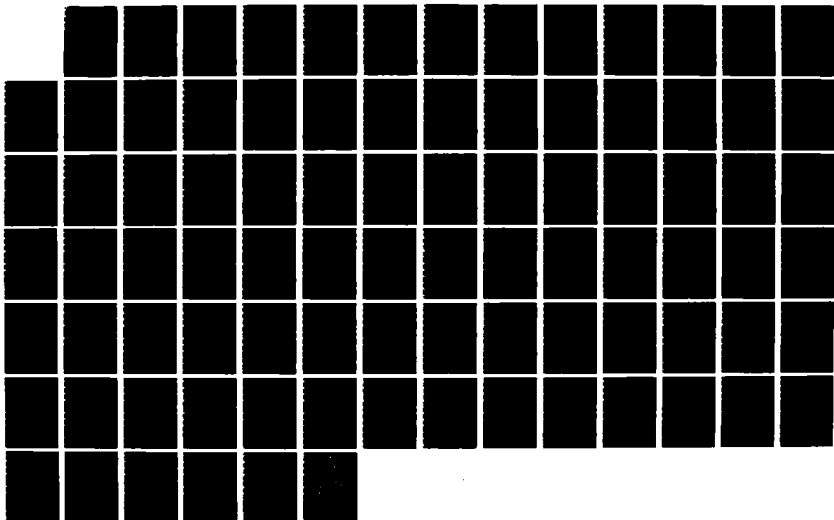
DAYTON OH R C DARRAH ET AL DEC 85 AFOSR-TR-86-0141

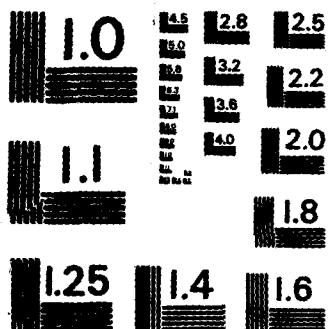
F49620-85-C-0013

F/G 5/9

NL

UNCLASSIFIED





MICROCOPY RESOLUTION TEST CHART
NATIONAL BUREAU OF STANDARDS - 1963-A

VI. ACKNOWLEDGEMENTS

I would like to extend a special thanks to Lt. Peter Vanden Bosch for his friendship and technical assistance during my summer visit. It has been an honor to work with him on the research and a pleasure to accompany him visiting many of the interesting sights around San Antonio.

Special thanks go also to Dr. Donald Farrer, Chief of the Vulnerability Assessment Branch. He was excellent as my Focal Effort Point and was always available for advice and help.

I would like to gratefully acknowledge the encouragements and technical assistance of Colonel (Ret.) J.E. Pickering, Chief of the Radiation Sciences Division of the School of Aerospace Medicine, Brooks Air Force Base. Even though I did not have the pleasure of meeting him until late in the Summer due to his sickness, his comments were most helpful. Appreciation and thanks are also given to Major Dennis A. Maier and Mr. Jack Labo for their technical advice.

Appreciation is extended to the personnel of the Radiation Science Laboratory for their courteous and helpful attitude. Special thanks goes to Sgt. Dlugokinski, my office mate. He was always willing to answer questions and do extra things to make my adjustment to the laboratory easier.

The Summer's activity was made possible by funds from the Air Force Systems Command, Air Force Office of Scientific Research under contract F 49620-85-C-0013. The management of the program was by Universal Energy System, Inc. under the leadership of Mr. Rodney Darrah and Ms. Sue Espey. Thanks go to them for a job well done. Thanks also go to Ms. Ann Mantia of UES for her concerned and courteous help to me by

telephone and to Mr. Harold B. Powell of San Antonio for his help.

VII. REFERENCE

1. Taboada, J., D. Hegedusich, and E. Bell, "Interactive scenario computer model for dose rates to aircrew in flight through nuclear debris cloud," Report USAFSAM-TR-85-49, School of Aerospace Medicine, Brooks AFB, Texas, 1985.

1985 USAF-UES SUMMER RESEARCH PROGRAM/
GRADUATE STUDENT SUMMER SUPPORT PROGRAM

Sponsored by the
AIR FORCE OFFICE OF SCIENTIFIC RESEARCH

Conducted by the
UNIVERSAL ENERGY SYSTEMS, INC.

FINAL REPORT

THE EFFECT OF WAVELENGTH ON LIGHT SCATTER IN THE HUMAN EYE

Prepared by:	B. R. Wooten
Academic Rank:	Associate Professor
Department and	Psychology
University:	Brown University
Research Location:	Human Resources Laboratory Williams Air Force Base
USAF Research:	Dr. George Geri
Date:	October 30, 1985
Contract No.	F49620-85-C-0013

The Effect of Wavelength on Light
Scatter in the Human Eye

by

B. R. Wooten

ABSTRACT

An optical system was constructed that allowed the psychophysical measurement of intra-ocular light scatter. Results showed that at the center of an annulus of 3 degrees inner and 8 degrees outer diameter light scatter was 1.3 percent and was independent of wavelength. These findings rule out Rayleigh scattering in the human eye.

The Effect of Wavelength on Light

Scatter in the Human Eye

This report constitutes a summary of research conducted in the summer of 1985 at the Human Resources Laboratory, Williams Air Force Base, Arizona. The author gratefully acknowledges support as a Summer Faculty Fellow sponsored by the U. S. Air Force Systems Command, Office of Scientific Research. Special thanks go to staff at HRL for making the visit pleasant and productive: Dr. George Geri, Dr. Tom Longridge, and Dr. Liz Martin. I am also grateful for the cooperation, mainly informal, of the Base Machine and Sheetmetal Shops.

Section II of the report describes some further validating and follow-up studies. It constitutes, in conjunction with Section I, a research proposal as part of the Mini-Grant Program.

Table of Contents

Section I	Preliminary Experiments	page
Section II	Proposed Experiments	page
Section III	References	page
Section IV	Figures	page
Section V	Proposed Budget	page

The Effect of Wavelength on Light

Scatter in the Human Eye

Section I: Preliminary Experiments

A. Introduction

Like any other image forming system, the human eye is imperfect. All of the ordinary optical imperfections, such as coma, spherical aberration, astigmatism, and chromatic aberration, are present. In addition, a significant amount of light is scattered outside the optic image to far retinal regions. The exact mechanism or mechanisms of optic scatter are not well understood, but most of the possibilities are clear. A small spread of the optic image is due to diffraction, but its extent is only several minutes of arc, at most (1). Genuine scatter refers to light distributed outside of an image predicted by the diffraction line-spread function. To distinguish this wide-spread scatter from the scatter near an edge, which would be added to the line spread function, I shall call it far scatter and define it as light outside the primary optic image by 0.2 degree of visual angle or more.

There are important reasons for being interested in the quality of the retinal image. The most basic one is simply that the retinal representation of the outside world is all that our visual sensory apparatus can respond to. That is, any information about the physical environment that is lost in the image-forming process of the eye is lost forever. In this sense, the retinal image is a kind of funnel between the real world and the perceived world. Any general theory or model of visual function must begin

with the information that is preserved in the optic image on the retina. In turn, this image can only be understood by direct observation or by measuring all of the factors that degrade it.

Scatter within the eye has been studied by several techniques (2). The most direct is to dissect a window in the rear pole of the eye and observe the image and scatter (3). It is also possible to dissect apart the various elements of the eye and examine their individual scattering properties (4). Both of these methods suffer from the problem that the structures begin to deteriorate at death. Several investigators have used modified ophthalmoscopes to measure the double-pass, reflected image (5). This method gives a good description of the image spread and near scatter, but is poor for the weaker far scatter because of a poor signal-to-noise level. A psychophysical technique, known as the glare method, obviates the difficulties of the direct and the reflection procedures (6). Basically, the glare method involves determining increment threshold in the area of interest at some distance from the image and then determining the level of a large homogeneous field that results in the same increment threshold. The ratio of the luminances of the homogeneous and the image fields determines the scatter estimate. (Details and assumptions of this procedure are given in the next section.)

The precise composition of the retinal image is of tremendous importance for both applied issues, e.g., visibility of displays, and for models of visual function. Thus, there have been many studies of the image spread function and of far scatter. The scatter data differ somewhat between authors, but Walraven has recently summarized the data for scatter

between 0.15 and 8.0 degrees of visual angle (7). These values are most relevant to the present work:

$$L = \frac{K \cdot E}{(a + .13)^{2.8}}$$

where E is the eye's illumination (lux), L is the luminance of the scattered light (cd/m^2), K is a constant with a value of 29, and a is the visual angle in degrees. Walraven's formula is useful and has been helpful in understanding certain visual phenomenon. Walraven, for example, has shown that for some conditions of simultaneous color contrast all of the effect can be attributed to the effects of stray light.

Vision in every day life generally involves a retinal image of scenes where not only luminance varies in a complex way, but also chromaticity. Since some mechanisms of scatter are wavelength dependent, it is critical to examine the eye for this possibility. If, for example, the optic media contains scattering particles smaller than the wavelength of light, Rayleigh scattering would occur. This mechanism, which is common in nature and accounts for the blue of the sky, predicts that scatter would be proportional to the inverse of the wavelength raised to the fourth power. Thus, if the eye exhibits Rayleigh scatter, violet light (420 nanometers) would scatter about 7.5 times more than red light (650 nm). Particles on the order of light's wavelength would exhibit slight wavelength dependency. Large particles would scatter all wavelengths equally. Good data on this issue do not exist. The only systematic examination of wavelength-dependent scattering is a study by Boettner (4) using excised human eyes. His results indeed indicate increased scatter at short wavelengths, but the validity of the study is questionable. Boettner's results show over 40%

scatter at 600 nm, a figure that is too high by at least a factor of ten. This impossibly high figure indicates that the eye, several hours dead, has probably suffered considerable degeneration and clouding. For the same reason, the wavelength dependency is also in question. Wyszecki and Stiles state, without a reference, that there is no evidence of wavelength dependent scattering in the human eye (1). After examination of the literature, I would summarize by saying that although most vision researchers (e.g., 7) are biased to expect increased scatter in the short-wave region (Rayleigh scatter), there is no reliable evidence for or against this expectation. The purpose of this study is to measure scatter as a function of wavelength.

B. Method

Procedure

To determine the dependency, if any, of intra-ocular light scatter upon wavelength we used a modification of the glare method. The configuration of the stimuli are shown in Fig. 1a. In Stage I, a steady, monochromatic annulus is presented with an outer diameter of 8 degrees and an inner diameter of 3 degrees. A fixation point is placed on the left margin of the annulus. A circular test flash of 20 minutes diameter is flashed for 0.5 sec every 1.5 sec. The test flash and the annulus are set at the same wavelength: 420, 430, 440, 450, 470, 490, 510, 530, 560, 590, 620, or 650 nanometers. For each wavelength the luminance of the annulus is set in steps of about 0.5 log unit. At each level, the subject sets the luminance of the flash at threshold using the method of adjustment. The basic idea is that the light scattered from the annulus to the immediate region of the test

determines the threshold of the test. The expected result is shown in Fig. 1b as the curve labelled "I": The threshold of the test rises as the luminance of the surround increases due to the corresponding increase of scattered light into the central zone.

In State II, a homogeneous field of the same wavelength and outer diameter is used. As in Stage I, the luminance of the large field is set in 0.5 log steps and the threshold of the test spot is set by the subject. The expected result is shown in Fig. 1b as the curve labelled "II": Its form is the same as for I except it is displaced to the left along the x-axis. The amount of the displacement is the estimate of the luminance of the scatter. For example, if the scatter luminance is 10 times less than the annular luminance, the displacement would be 1.0 log unit. By systematically varying wavelength, it is possible to determine the percent scatter versus wavelength function.

Apparatus

The apparatus was a 3 channel, maxwellian-view optical system that was constructed at the Human Resources Laboratory in the months of June and July. Fig. 2 is a schematic diagram of the system. The source (SI) was a 45-Watt, single-coil, tungsten-halogen lamp operated by a precision power supply at 6.5 Amps. The beam for the test flash was formed by a series of collimating and focussing lenses (L1 - L8) and was rendered monochromatic by a grating monochromator (MO1). Energy of the test was varied by a motor-driven, neutral-density, circular wedge (W1). An electro-mechanical shutter (SH), driven by appropriate timing circuits, formed the 0.5 sec flashes. The steady background field was provided by a series of collimating and focussing lenses (L9 - L13) and was rendered monochromatic by a grating monochromator (MO2). The small test flash was formed by a

metal aperture (A1) placed behind L8. The background field was formed by either an annular aperture or a circular aperture (A2) placed behind L13. The two beams were combined by a prism-type beam splitter (BS2). Energy of the background was controlled by a circular, neutral-density wedge (W2). A third channel (L14 - L20) could be combined with the test channel, but was not used in this study. All lenses were achromatic and all mirrors (M1 - M7) were front-surface type. A separate tungsten source (S2) was collimated (L21) and combined with the background channel by a thin microscope cover-slip (CS) to provide the dim fixation point. All channels were baffled and covered to minimize light scatter within the room. The subject's head was steadied by a bite-bar mounted on a three-dimensional movement, which provided movement for adjustment. All wedges and filters were calibrated at the test wavelengths. Light levels were determined by an electronic photometer. Stray light at the center of the annular image provided by the apparatus was determined to be less than one part in a thousand of the annular image itself. The exit pupil of the system was 1 mm wide and 2 mm high.

C. Results

Typical results are shown in Fig. 3a for 620 nm. Log threshold for the test flash (y-axis) is plotted against either log luminance of the annulus (open circles, curve I) or log luminance of the background (filled circles, curve II). The thresholds for both conditions rise in an orderly way with increasing luminance of the background or annulus. The same smooth curve

describes both sets of data well, implying that the same mechanism is mediating the responses. It also implies that a simple shift along the x-axis would result in superposition. This is shown in Fig. 3b in which the data points for the annulus (open circles) have been shifted to the left by 1.78 log unit, as indicated by the arrowhead in the lower right. Since the shift is to lower light levels, the value of 1.78 is negative. The anti-log of -1.78 is 0.017, which corresponds to a value of 1.7 percent. Thus, the estimate of the luminance of the scatter for these conditions, (i.e., 620 nm light at the center of a 3 degree-8 degree annulus) is 1.7 percent of the main image of the pattern.

Results for the other wavelengths are shown in Fig. 4 (420 - 490 nm) and Fig. 5 (510 - 650 nm). The data points for the annulus (open circles) have been shifted for maximum correspondence to the data points for the background (filled circles). The shift in log units and the corresponding scatter estimate in percent are indicated within parentheses below each wavelength designation. Each set of points for a given wavelength condition is shifted along the x- and y-axis for the sake of clarity. These figures are meant to show only the form and variability of the data. The estimates of per cent scatter range from 1.07 to 1.70 with a mean of 1.3.

D. Discussion

The glare method of measuring scattered light assumes that the threshold of the test beam is determined only by the light in the immediate region of the test beam. That is, it requires that the test spot be far enough from

the nearest edge, be it the inner edge of the annulus or the outer edge of the background, that its threshold is unaffected by the edge per se.

Based upon previous related experiments, it is a safe assumption for these experiments since the outer edge of our 20 min spot was 80 min from the inner edge of the annulus. This value is several times larger than the local interactions expected from results of the Westheimer paradigm.

Fig. 3 shows that for 650 nm the results for Stages I and II give the same shaped function. This is exactly what is expected given the assumption that the spot is well beyond the influence of the edges and that only the light in the immediate region determines the threshold. Figures 4 and 5 verify this conclusion for other wavelengths from 420 to 650 nm.

Figures 4 and 5 show that for each wavelength the threshold curve is the same shape for the annular and background conditions. It is also clear from the data that the shapes of the curves are not the same for all wavelengths. This result is neither unexpected nor troublesome. The test spot, being located 4 degrees on the nasal retina, will stimulate rods and cones. The degree to which rods versus cones are stimulated will clearly depend upon luminance level and wavelength. Due to the difference in photopic and scotopic spectral sensitivity, alone, different curve shapes would be expected. In addition, the curve relating threshold to luminance level is flat at low levels, slightly concave at intermediate levels, and linear at higher levels. Thus, if the whole curve is not sampled, different shapes would result. In our case, we needed to sample only a range that gave a reliable, non-zero slope so that the Stage I-II shift could be estimated. There was no attempt to manipulate luminance levels in order

to achieve similarity in shape across wavelength. The actual luminance values used were determined by two factors: The subject's criterion that the dimmest value be roughly comparable for the different wavelengths and the light available from the apparatus. The similarity of shape between the two conditions for each wavelength, despite differences across wavelengths, is impressive evidence that the fundamental assumption of the method is true (i.e., that thresholds are determined only by local light levels).

Although previous studies using comparable techniques have not examined wavelength dependency, several have estimated the overall amount of scatter. These values are remarkably close to our mean estimate of 1.3 percent. Walraven, for example, using a color contrast method estimated a value of 2 percent for a 3 degree annulus. Of particular interest is the study of Rushton and Gubish (8) since they verified the results of a glare procedure with reflection densitometry and their stimulus conditions were nearly identical to ours (i.e., a 3-8 degree annulus). Their estimate using both methods was 1.5 percent, which is practically identical to our value. Other less precise methods (2) are consistent with our result. Since our data agree with those of several other studies using diverse conditions and techniques, we feel confident that the method indeed is a valid measure of scattered light.

The most important and original result of our study pertains to the relation between scatter and wavelength. Although relevant data are scant, all vision researchers who I have polled predicted considerably more scattering for the short-wave spectral region. Indeed, it was my expectation

as well. There are several reasons for this. The human eye's performance is generally poorer in the violet and blue regions: Sensitivity is low, wavelength discrimination is poor, and chromatic aberration is severe. Thus, there is a bias to expect that scatter would be worse. Adding to this expectation is the well-known and wide-spread mechanism of Rayleigh scattering, which predicts that scatter is proportional to the inverse of the wavelength raised to the fourth power. This is why the sky is blue. Although there are no data showing that intra-ocular conditions are appropriate for extensive Rayleigh scattering, neither are there data to rule it out. This situation combined with a well-justified expectation of poor performance at short-waves has led most writers, e.g., Rodick (7), to assume more short-wave scattering. In addition, the study on excised eyes by Boettner (4) did in fact show increased scatter at short-waves, although less than predicted by the Rayleigh mechanism alone. As mentioned in the Introduction, however, this experiment is questionable due to the extremely large scatter found in all spectral regions, which suggests that the tissue was in poor condition.

The data presented in Figures 4 and 5 show that our estimates of scatter from 420 to 650 nm range only from 1.2 to 1.9 percent. These values are plotted (filled circles) as a function of wavelength in Fig. 6. As is clearly seen, there is no obvious trend in that a line of zero slope describes the data quite well. In the same figure, the scatter predicted by the Rayleigh mechanism assuming 1.3 percent at 650 nm is shown. This prediction is obviously a poor description of the data,

being too high at 420 nm by a factor of almost six. Our conclusion is quite clear: Since there is no measurable increase in scatter at short-waves, there is no appreciable Rayleigh scattering in the human eye. In turn, this conclusion necessarily implies that there are no scattering particles in the eye smaller than the wavelength of visible light. The wavelength-independent scatter that is found must be due to particles larger than the wavelength of light, inhomogeneities in the refractive index of the eye media, and reflection from the fundus. The relative contributions of these factors require further research.

In addition to their relevance to mechanisms of ocular scatter, these results are important for models of chromatic contrast. These theories attempt to understand how the color of a light is affected by the color of an adjacent stimulus. Most models propose lateral neural mechanisms at a receptor and at an opponent-process level. None incorporate the effects of scattered light even though the composition of the proximal stimulus is obviously critical. This study represents a beginning in that we have shown that the scattered light expression need not incorporate a wavelength term. This greatly simplifies the task ahead. Needless to say, however, these findings on a single subject must be verified on other observers.

Section II: Proposed Experiments

A. Introduction

The proposed experiments are primarily extensions of the work discussed in Section I. The experiments described in part A are needed to complete and validate the preliminary work. It had been hoped that these could have been completed in the summer of 1985 during my tenure as a Summer Faculty Fellow at the Human Resources Laboratory, Williams AFB. The apparatus needed for the study is, however, rather complex (Fig. 2) and required two months of hard work to design, build, calibrate, and test. It was only with the enthusiastic help of my colleague at HRL, Dr. George Geri, and the cooperation of several base machine shops that it was possible to complete the device during my visit. Following construction, we had only two weeks to do all of the work described in Section I. The results from that effort are certainly sound and, I think, important. They do, however, refer to just one subject. In addition, certain control experiments are virtually certain to validate the method, but must be done before the study can be regarded as complete. Once these experiments are completed, the study can be submitted for publication. The experiments described in part C are natural extensions of the basic study. They are not required as part of the first paper, but represent a distinct, second project.

Most of the proposed work would be done at the Walter S. Hunter Laboratory of Psychology, Brown University. Fortunately, an apparatus quite similar to that shown in Fig. 2 already exists in my laboratory.

Although some minor modifications and one major improvement (described in the Budget section) are needed, the proposed studies can be initiated quickly. Since vision research has been conducted at Brown for over 80 years, there is a large supply of lenses, filters, measuring devices, and calibration equipment. Machine and electrical shops are available.

The purpose of the Mini-Grant Program, as I understand it, is to serve as a follow-up to the Summer Program and as a transition for a possible larger future project to be submitted to the Air Force. The validating and extension studies proposed in this section are certainly follow-up experiments from the past summer. Furthermore, this whole examination of intra-ocular scattered light is really a part of a larger plan to explore the mechanisms of chromatic contrast, as discussed in Section I. In the Spring, I plan to submit a research proposal dealing with experiments and models on the spatial aspect of chromatic contrast to the USAF Office of Scientific Research. Last summer I discussed this plan with an official of that office and his initial response was highly favorable. Thus, the Mini-Grant would certainly serve its intended function.

B. Further Validating Experiments

1) For reasons discussed in the previous section, our preliminary work was done on only one subject. It is highly likely that such a basic aspect of the eye as scattering is similar in all normal, relatively young eyes. Nevertheless, before publication, it will be necessary to repeat the main experiment on at least three more subjects. Actually,

this work is now in progress on the apparatus at the HRL. Dr. Geri, with my collaboration, is conducting the experiments. The Mini-Grant would allow me to make the necessary visits to HRL for the completion of this phase of the research.

2) As discussed in Section I, the glare method of measuring scattered light requires that the test threshold be determined only by the light in the immediate region of the test field. That is, the test must be far enough from the inner edge of the annulus such that its threshold is not influenced by the edge itself. Based upon work in the literature dealing with edge effects, we feel that our distance of 80 min of visual angle is sufficient. Nevertheless, it would be prudent to verify this with our specific stimulus conditions. This could be done by determining test threshold on homogeneous backgrounds of varying size (i.e., the Westheimer paradigm). If our assumption is correct, the perturbation of the threshold by the edge of the background field would be complete well within 80 min. This study would be done at an eccentricity of 4 degrees, where the test was located in our study. In addition, it should be done with several widely spaced wavelengths (420, 520, and 650 nm) to verify that our assumption is valid across the visible spectrum. It would be adequate to do this on two subjects.

3) For each wavelength in the preliminary study, we sampled about a 2 log unit range of luminance of the annulus-background fields. The

similarity of the Stage I-Stage II data is strong evidence that the same mechanism is mediating the threshold in the annulus and background configurations (Figures 4 and 5). It would be worthwhile, however, to check this over a large range of luminance. This could best be done at about 510 nm where the largest luminance range is possible. In addition, at this wavelength one would expect a mixed response in that rods would mediate the response at low levels and cones would mediate the response at high levels. It would probably be possible to measure threshold over about 4 log units. If our assumption is correct, the resulting mixed curves for Stages I and II should have the same shape over the entire range. This experiment would be worth doing in two subjects.

4) The preliminary results show that intra-ocular scatter is independent of wavelength (Fig. 6). The main conclusion regarding mechanisms of scatter is that the Rayleigh process does not occur in the human eye. The preliminary data suggest and the validating study will almost certainly confirm that our method is solid. It would be comforting, however, to show directly that if Rayleigh scattering could be artificially created, our method could detect. This is possible by deliberately introducing Rayleigh scatter by simply placing a cell containing the appropriate solution in front of the eye. We are now researching what would be the best test scattering media for this purpose. One simple possibility is to use a milk solution, which is known to cause Rayleigh scattering. We would then

simply repeat the basic experiment and expect to detect the wavelength-dependent scattering shown in Fig. 6. This experiment should work and would be impressive validation of our procedure.

C. Extension Studies

1) The basic experiment outlined above will be done with normal, relatively young subjects. The results should be generally true for that class of observers. There is evidence in the literature, however, that older subjects show considerably more scatter than young subjects. Thus, there appears to be an age trend. This raises two possibilities that should be explored with our technique. The first is simply to carefully explore the age trend by studying a wide age range. This can easily be done. It would add generality to our study and may have important implications for the aging eye. The second study is to check for wavelength-dependent scattering in older eyes. Since older eyes exhibit increased scatter it is possible that whatever is causing this effect may show the Rayleigh effect. This can easily be done by simply repeating the basic experiment with older subjects. The task is easy and should be possible with elderly individuals.

2) Our basic study addressed primarily the issue of wavelength-dependent scattering. Thus, we did not examine the general issue of the exact spatial spread of intra-ocular scatter. We simply looked at scatter for one spatial condition (i.e., in the center of a 3-8 degree annulus). Other studies, e.g., Walraven (7), have explored the spatial

factor to some extent. Nevertheless, after a careful reading of the literature, I have not found a study that systematically measures the form and extent of far scatter over a large spatial range. I think that this is worth doing and our technique can easily be adapted to the task by simply varying the spatial dimensions of our annulus. This work would hopefully result in a single expression for far scatter from very small to large visual angles. It would also be worthwhile to check for wavelength dependency at a small and at two or three large visual angles. This would test the generality of our basic results.

Section III: References

- 1) Krauskopf, J. J. Opt. Soc. Am. 52, 1046, (1962)
- 2) Wyszecki, G. and Stiles, W. S. Color Science, John Wiley and Sons, New York, (1967).
- 3) De Mott, D. and Boynton, R. J. Opt. Soc. Am. 48, 13, (1958).
- 4) Boettner, E. University of Michigan, Contract AF41, USAF School of Aerospace Medicine, (1967).
- 5) Campbell, F. and Gubish, R. J. Physiol. 186, 558, (1966).
- 6) LeGrand, Y. Rev. d'Opt. 16, 201, (1937).
- 7) Walraven, J. Vis. Res. 13, 1739, (1973).
- 8) Rodieck, R. The Vertebrate Retina, W. H. Freeman, San Francisco, (1973).
- 9) Rushton, W. and Gubish, R. J. Opt. Soc. Am. 56, 104, (1965).

Section IV: Figures

Fig. 1. (a) Schematic of stimulus conditions for Stages I and II.
(b) Idealized results of log threshold versus log luminance for Stages I and II.

Fig. 2. Diagram of the apparatus: L - lenses, M - mirrors, MO - monochromators, W - wedges, A - apertures, SH - shutter, BS - beamsplitters, CS - converslip, S - sources.

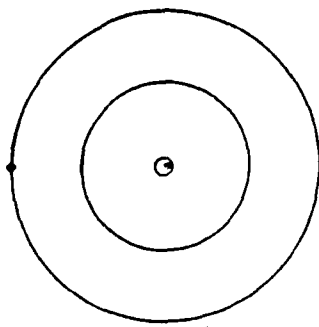
Fig. 3. (a) Results for Stages I and II at 650 nanometers
(b) Results with Stage I data shifted -1.78 log unit to show correspondence between Stages I and II.

Fig. 4. Results for wavelengths 420-490 nm. Stage I shown by open circles; Stage II shown by filled circles. Stage I data have been shifted by amount shown in parentheses for maximum correspondence with Stage II data. Both axes are in log relative units.

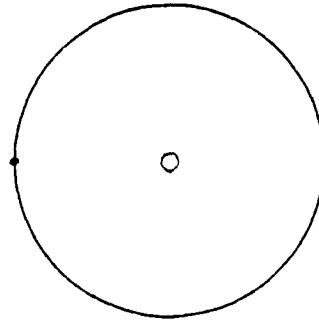
Fig. 5. Same as for Fig. 4 but for 510-650 nm.

Fig. 6. Filled circles show the measured percent scatter across the spectrum. X's indicate the percent scatter predicted by the Rayleigh mechanism.

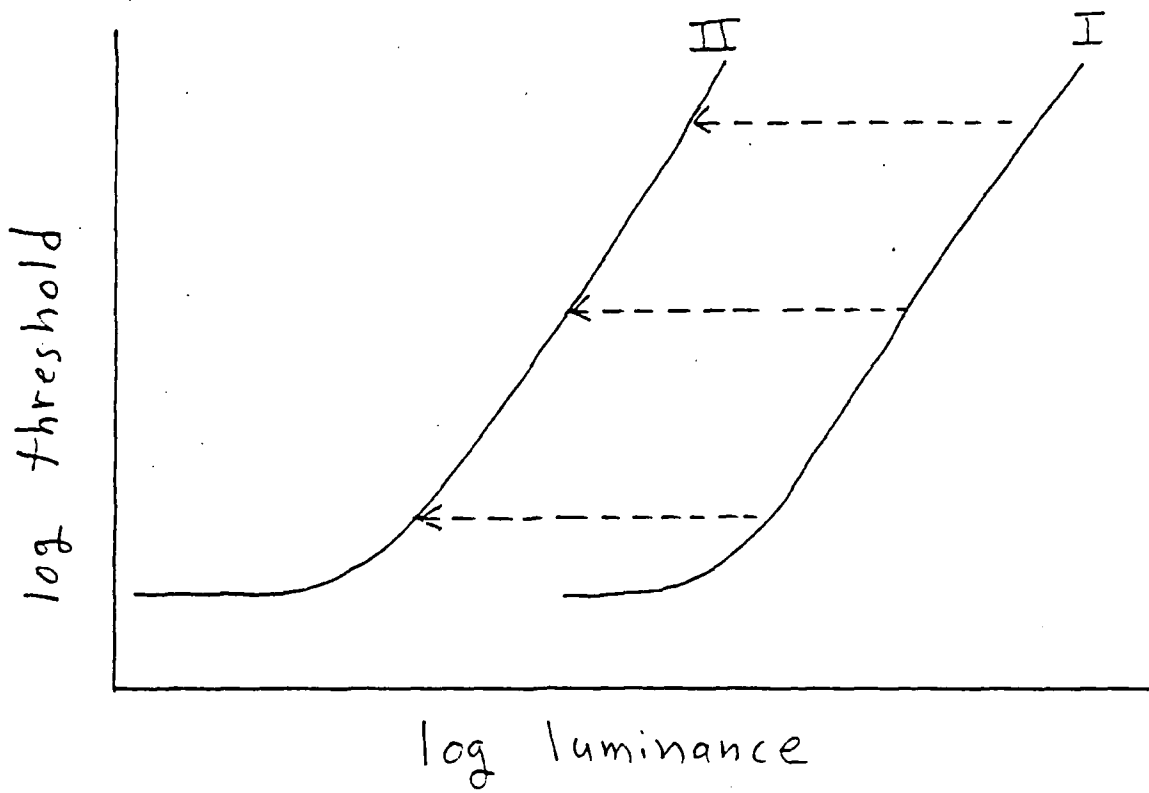
(a)



I



II



(b)

151-23

Fig 1

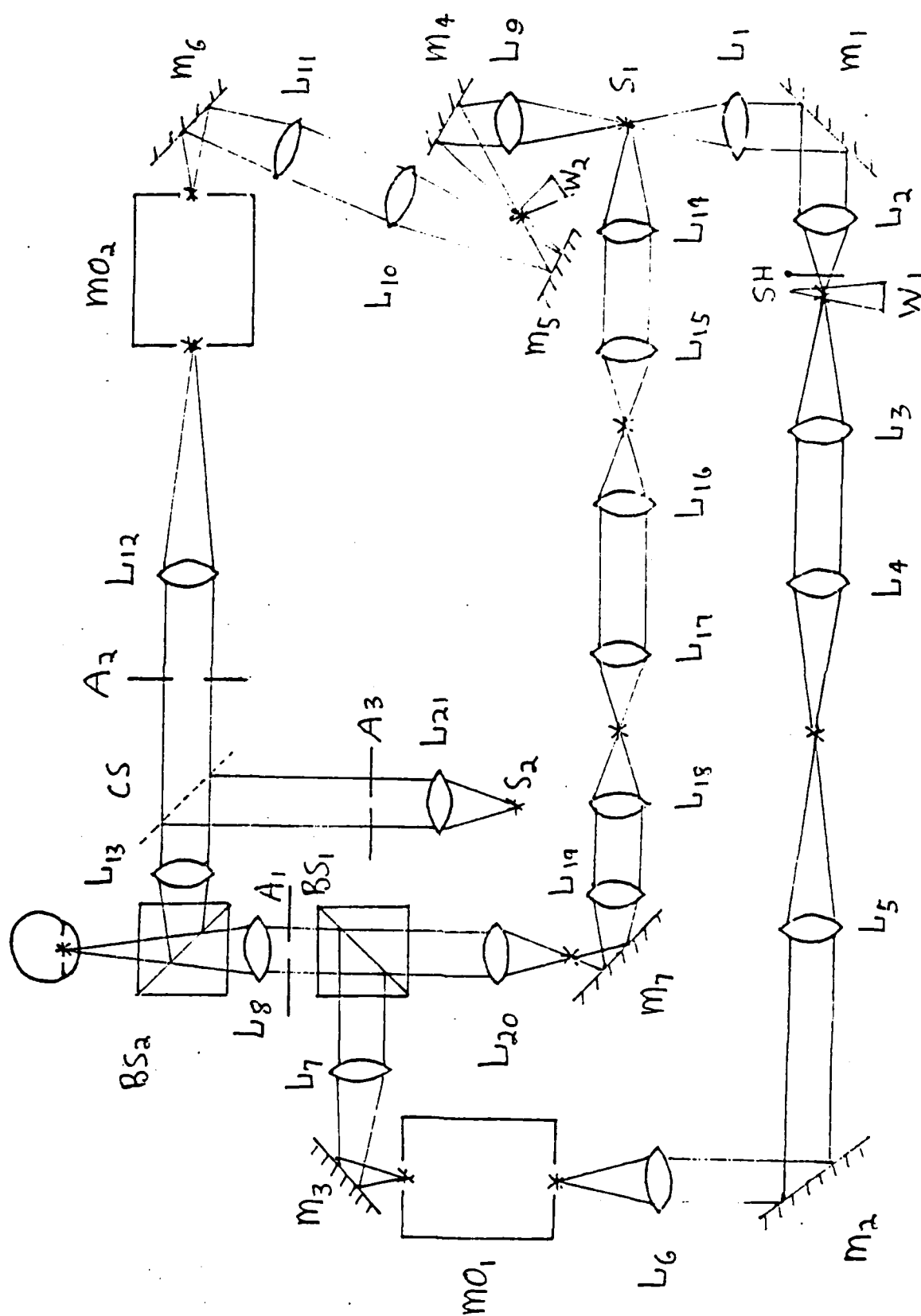


Fig 2

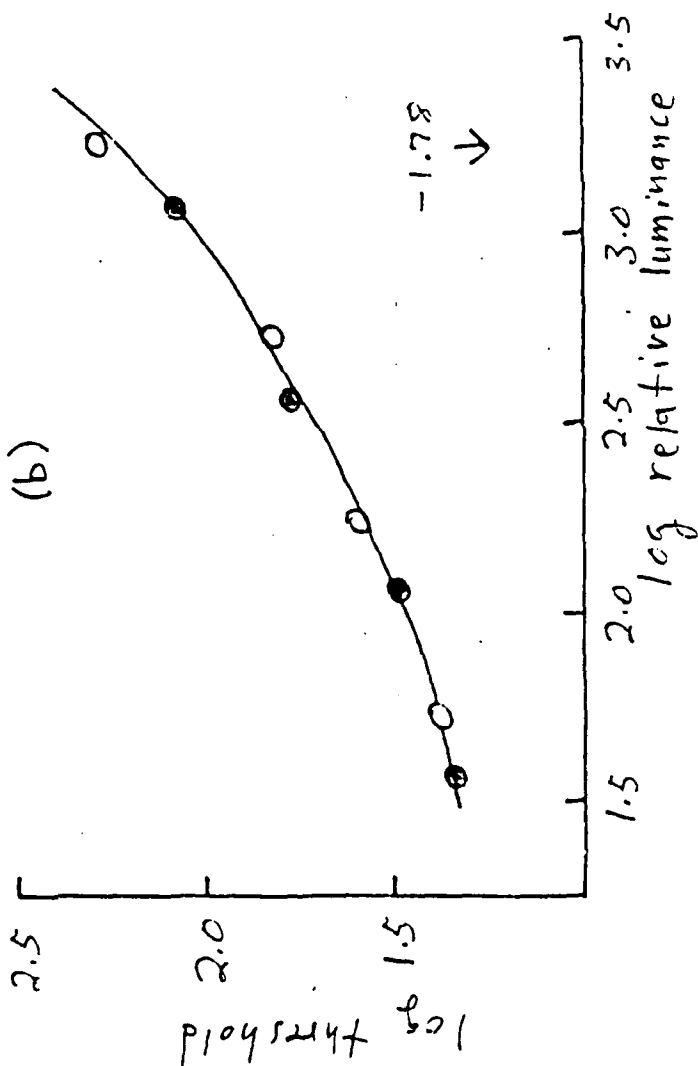
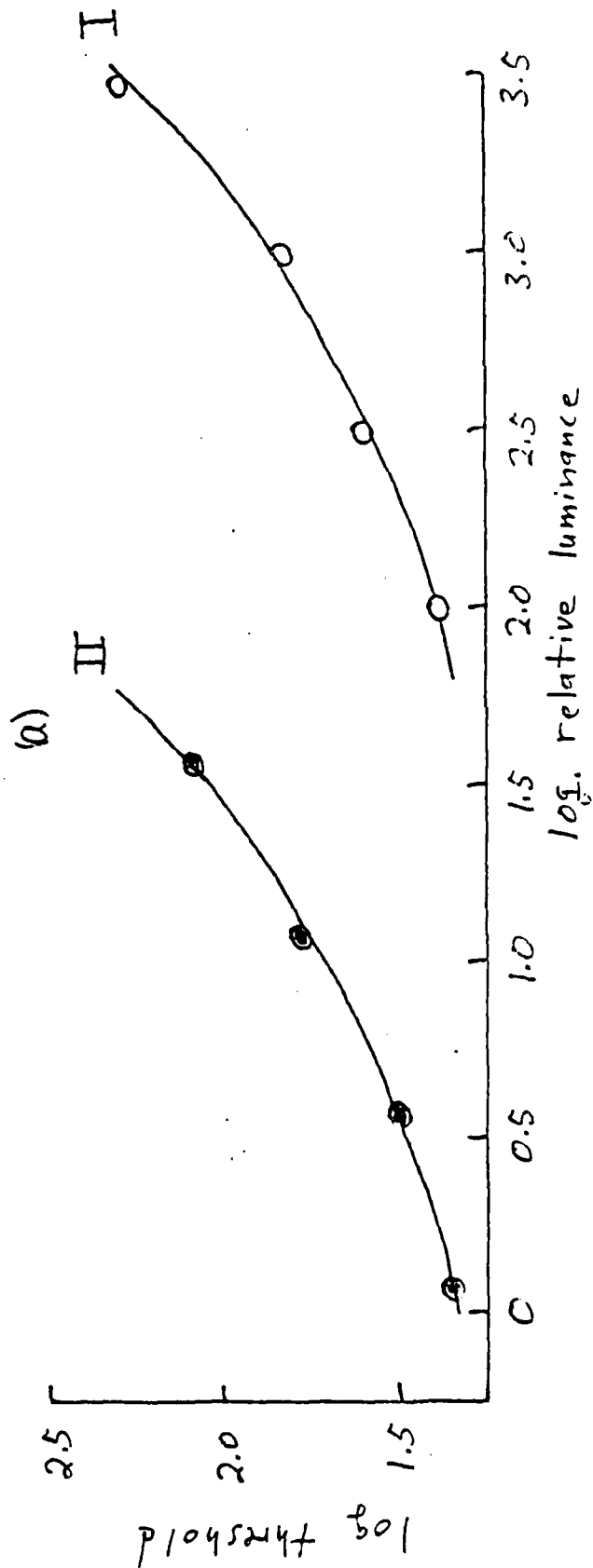


Fig 3

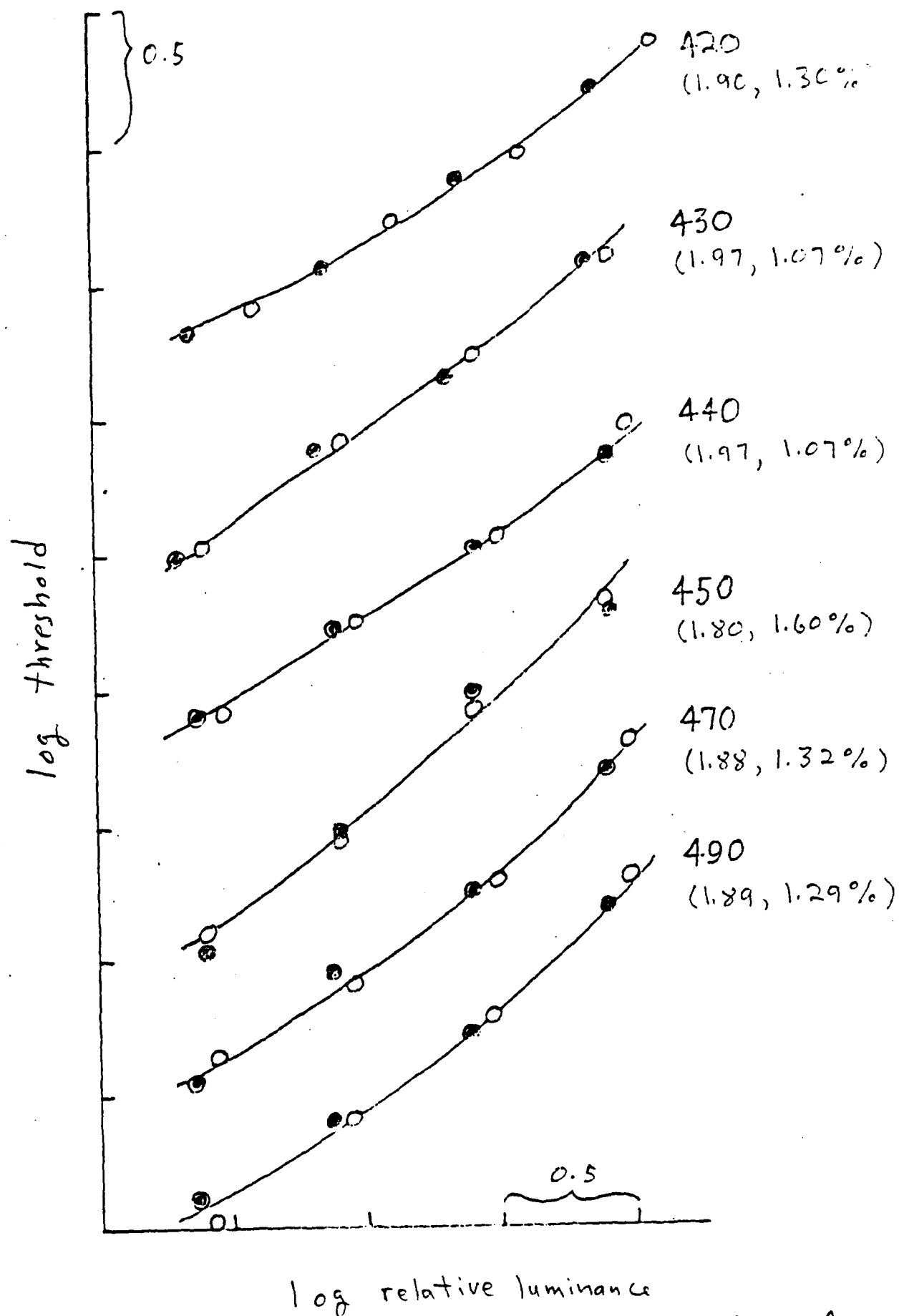


Fig 4

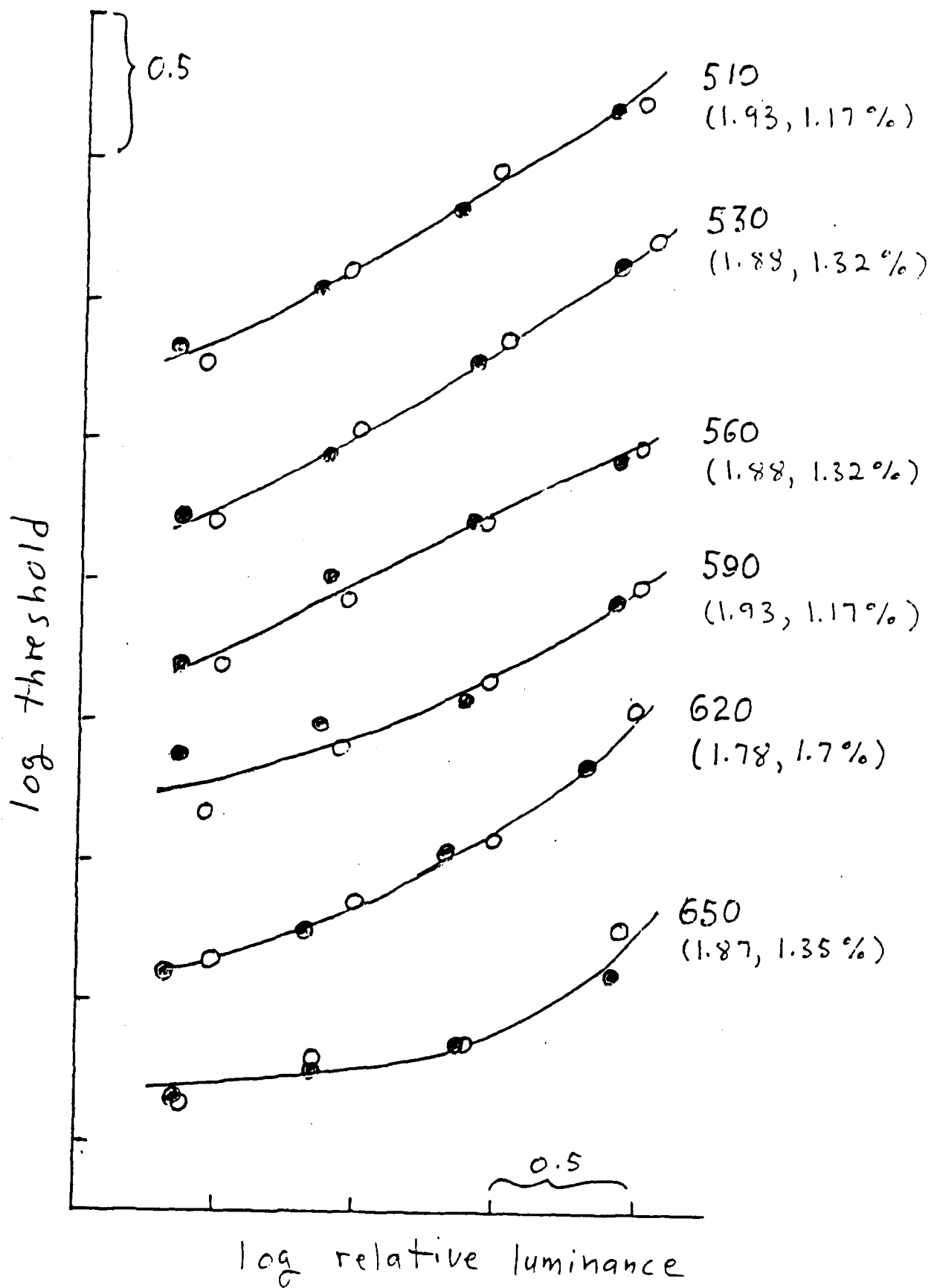


Fig 5

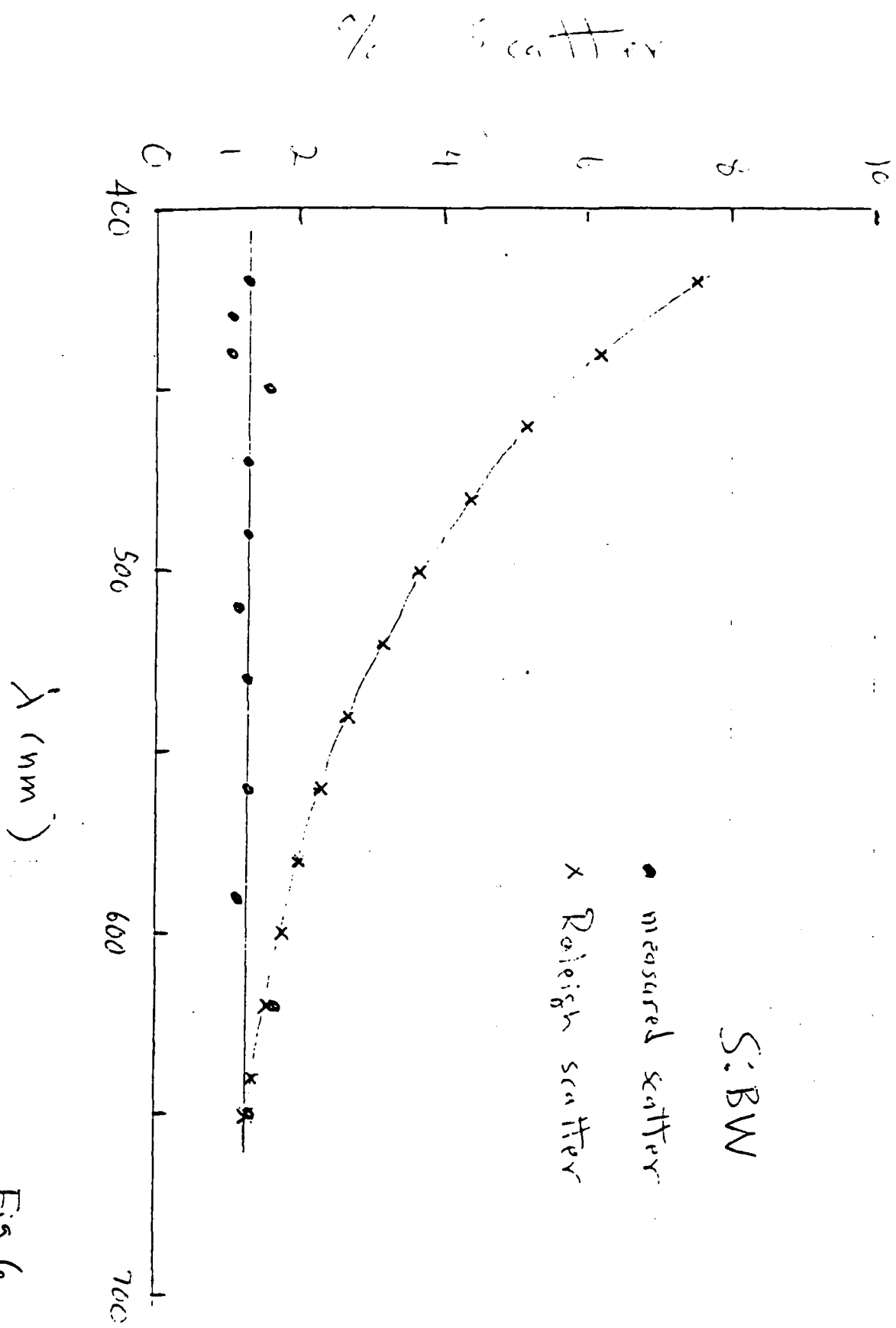


Fig 6

1985 USAF-UES SUMMER FACULTY RESEARCH PROGRAM/
GRADUATE STUDENT SUMMER SUPPORT PROGRAM

Sponsored by the
AIR FORCE OFFICE OF SCIENTIFIC RESEARCH

Conducted by the
UNIVERSAL ENERGY SYSTEMS, INC.

FINAL REPORT

MOLECULAR OPERATORS THAT MOVE NUCLEI
ALONG PATHS OF CONSTANT ORBITAL ENERGY

Prepared by:	Carl E. Wulfman
Academic Rank:	Professor
Department and	Department of Physics
University:	University of the Pacific
Research Location:	Frank J. Seiler Research Laboratory, United States Air Force Academy
USAF Research:	Dr. James Stewart, Dr. Almon Turner
Date:	July 30, 1985
Contract No:	F49620-85-C-0013

Molecular Operators That Move Nuclei
Along Paths of Constant Orbital Energy[#]

Carl E. Wulfman*

Frank J. Seiler Research Laboratory
United States Air Force Academy
Colorado Springs, Colo. 80940

ABSTRACT

Systematic methods have been developed for obtaining an increasingly accurate series of approximations to quantum mechanical operators with the following properties:

- i. Given an initial nuclear configuration, and corresponding electronic orbital, the operators move the nuclei of a molecule along paths of constant orbital energy.
- ii. The operators convert the initial orbital into eigenstates appropriate to each successive nuclear configuration.

Applying these methods to triatomics we have obtained a first approximation to such an operator. The accuracy of this and successive approximations is being assessed.

Acknowledgements

It is a pleasure to acknowledge the support of this research by the Air Force Systems Command. I would particularly like to thank Colonel Dymek, Dr. John Wilkes, and the staff of the F. J. Seiler Laboratory's Chemistry Section for their continual personal help. They, and the central administrative staff of the Laboratory have established a supportive atmosphere which makes it possible to concentrate every bit of one's attention on the scientific problems at hand. In addition, Dr. James Stewart and Dr. Almon Turner, NRC Fellows in the Chemistry Section, were ever ready to put their computer programming experience and extensive knowledge of quantum chemistry at the disposal of the author. Their support along with that provided by the Air Force personnel made it possible to do six months of work in ten weeks.

I. Introduction

In recent years it has become possible to use quantum mechanical methods to usefully approximate the properties of molecules of interest to a wide range of materials scientists. In fact it is now often quicker and less expensive to obtain knowledge of the properties of materials by these theoretical means than it is by experimental studies. The AFOSR clearly recognized this some time ago and has given strong support to the development of quantum mechanical methods and computer software designed to be of aid in the materials sciences. The Frank J. Seiler Laboratory at the U.S. Air Force Academy has been one of the beneficiaries of this support and is rapidly becoming known as a center of research in this area.

A key step in much quantum chemical work is the calculation of the dependence of the energy of a molecular system upon the relative positions of its nuclei - the calculation of molecular potential energy surfaces. Because most molecules of interest have many atomic nuclei these surfaces are multidimensional and it becomes difficult to locate those nuclear configurations that have interesting chemical or physical properties. In fact this is presently done by trial and error and only quite simple systems are manageable. This difficulty currently imposes a severe restriction on all available computer programs designed to search for chemically interesting regions of reaction surfaces. The difficulties are especially great when the systems of

interest are highly energetic or can for other reasons lead to the development of many reactants and transition states. Reactions in such systems develop such a variety of products as to suggest that the systems are effectively exploring a multidimensional potential energy surface. Dewar's investigation of the simple system C_4H_4 provides an example of this.⁽¹⁾

Because the methods currently used in quantum chemical calculations are completely numerical it is also very difficult for the theoretician to establish functional relations that will allow one to use knowledge about one potential surface to estimate properties of another related one, or to use knowledge of one region of a potential surface to obtain reliable knowledge of another region of the same surface. This is one of the great disappointments of modern quantum chemistry, because it is just such a transference of knowledge that has long been the natural habit of thought of the practicing chemist - the guidance to a large proportion of the discoveries made by chemists in the past two centuries.

This report describes the elements of one aspect of a new approach to molecular quantum mechanics which sets out from the beginning to determine functional relations - functional relations between the properties of one region of a potential energy surface and another region of the same surface, between one potential energy surface of a molecule and another between the properties of one molecule and those of another molecule.⁽²⁾

A key feature of the approach is its emphasis upon the determination of operators rather than wave functions. This is because wave functions fix the properties of unique quantum mechanical systems, in fact single states of such systems, while operators can be used to convert the wave function of one state into that of another and the wave functions of

one system to those of another. By seeking appropriate operators one can not only interconvert different quantum mechanical systems, one can also rather directly obtain functional relations between the properties of different systems.

The observations made in these paragraphs have guided the research program of the author and his students for more than a decade.⁽²⁾ Early on it became evident that until sophisticated symbol manipulating computer systems became available, it would not be practicable to obtain and use the operators envisaged; to obtain operators one must obtain functions (symbols) rather than numbers, and to use operators one must use functions rather than numbers. The development of symbol manipulating systems has progressed rapidly during this decade and there are now available very sophisticated artificial intelligence systems of this sort, such as MACSYMA and SMP which can be used on standard digital computers. All the algebra and differential and integral calculus described below was done with one of these expert systems (MACSYMA).

II. Objectives of this Research

This summer we set out to develop a systematic method for approximating operators that have the properties listed in the abstract and to test the validity of the approximations used in obtaining them. Additional desirable criteria set out were:

- i. It should be possible to determine the operators by both ab initio and semiempirical methods so that one can soundly assess their accuracy and yet also use them on systems of

practical interest that are too complicated for ab initio methods.

- ii. The operators should be directly applicable to MNDO and Gaussian type molecular orbitals obtainable by computer programs widely distributed in the quantum chemical community.

III. General Properties of the Operators

It is, of course, necessary to precisely define the properties of the operators U being sought before one can set about developing them. In reference (2) will be found most of the motivation that has led us to settle on the following requirements:

- i. U is of the form $\exp(iaQ)$, with Q a self-adjoint operator and a a real parameter.
- ii. U acts on both nuclear and electronic degrees of freedom.
- iii. The action of U on nuclear degrees of freedom depends only upon the position of the nuclei and upon constants of motion of the system.
- iv. Q satisfies

$$[H(p,r,R),Q]\psi(R,r) = 0 \quad (1.1a)$$

for every ψ_Y satisfying

$$H\psi_Y = E_Y(R)\psi_Y, \quad (1.1b)$$

where

$$H = \frac{p^2}{2} - \sum_j Z_j / |r - R_j|.$$

Here $R = (R_1, R_2, \dots)$ are nuclear coordinates, Z_j is the

charge of nucleus j , r is the electronic position operator and p is the electronic momentum operator.

We have obtained Q as a differential operator of the form

$$Q = \sum_j \xi_j(R, \gamma) \cdot \nabla_{R_j} + \eta(R, r, p) \quad (1.2)$$

Let us write

$$\exp(iaQ)R = \bar{R} = R'(a), \quad (1.3a)$$

$$\exp(iaQ)r = \bar{r} = r'(a), \quad \exp(iaQ)p = \bar{p} = p'(a)$$

Note that $a = 0$ yields the identity transformation, and that as a increases in magnitude the transformations of R , r , p become increasingly profound. The inverse of the transformation with parameter a is the transformation with parameter $-a$. In short the transformations are those of a Lie group.⁽³⁾

Arguments due to Lie establish that for analytic functions f

$$\exp(iaQ)f(r) = f(\bar{r}), \quad \exp(iaQ)f(R, r, p) = \bar{f}(\bar{R}, \bar{r}, \bar{p}). \quad (1.3b)$$

Note that in the first case the functional form of f is not altered, while in the second case it is. (It is necessary to use operators that may change the functional form of $\psi(R, r)$ as one changes nuclear positions because if one did not, it would, for example, be impossible for the wave function ψ to remain normalized.)

Now, by virtue of (1.1) one has:

$$H(\bar{R}, \bar{r}, \bar{p}) \bar{\psi}(\bar{R}, \bar{r}) = E(\bar{R}) \bar{\psi}(\bar{R}, \bar{r})$$

where

(1.4)

$$\bar{\psi}(\bar{R}, \bar{r}) = \exp(iaQ) \psi(R, r)$$

Thus as a varies U converts solutions of the Born-Oppenheimer Schroedinger equation for one nuclear configuration into solutions of the same energy at a succession of different nuclear configurations, and correspondingly moves the nuclei along paths of constant energy. By virtue of (1.1) U is universal in the sense that it will act in this way when applied to any eigenstate of H at any value of R.

Before turning to a specific example of such an operator, it is perhaps worthwhile pointing out how the operators Q may be used to determine contours of constant energy on a potential energy surface. If the equations $F(R_1, R_2, \dots) = C(E)$ describe a family of constant energy contours, then one can show that F satisfies the equation $QF = 0$ and the vector $\xi = (\xi_1, \xi_2, \dots)$ is tangent at R to the contour through R.⁽³⁾ The vector of steepest descent at R is orthogonal to ξ . Thus the coefficients ξ_j in the operator Q directly indicate the direction the nuclei should be moved if one wishes to keep the energy constant. The remaining term, η , in Q determines the changes in the electronic position and momenta and in the functional form of the wave function that are required as the nuclei are moved in the isoenergetic direction.

The reader may well wonder why we have not here chosen to study

operators that take into account nuclear repulsion effects as they move nuclei about. There are three reasons: 1. Orbital energy surfaces are much smoother and hence more easily approximated. 2. Lack of knowledge of the general properties of orbital energy surfaces in regions distant from energy minima is currently a major impediment in the search for chemically relevant portions of potential energy surfaces. 3. It is not difficult to take nuclear repulsions into account once one has learned how to handle the quantum mechanical problems associated with the determination of the Q.

One must, in general allow η in Q to be a differential operator of arbitrary order⁽⁴⁾. This has been the key impediment in applying Lie methods to molecular quantum mechanics. One of the major contributions of the work carried out during the summer at the F.J. Seiler Laboratory has been the discovery of a way to sidestep this difficulty. We have found that if one converts Schroedinger's equation into the corresponding dynamical equation in Fock's projective momentum space,⁽⁵⁾ then for the purposes at hand one may restrict Q to be a differential operator of at most first order.

A second major result of the summer has been the discovery of a method for partitioning a molecular Hamiltonian H into pieces H^0, H^1, H^2, \dots in such a way that one can conveniently determine operators Q^0, Q^1, Q^2, \dots that successively satisfy

$$\begin{aligned}
 [H^0, Q^0] &= 0, \quad [(H^0 + H^1), Q^1] = 0, \\
 [(H^0 + H^1 + H^2), Q^2] &= 0 \dots\dots
 \end{aligned}
 \tag{1.5}$$

to the same level of approximation that $H^0 + H^1$ approximates H . This makes it possible to systematically improve one's approximations by determining operators that are appropriate to increasingly sophisticated model Hamiltonians. It will throw much of the study of the accuracy of the approximations into a study of the accuracy of the model Hamiltonian itself. Furthermore, at any stage one can convert the analytically defined Hamiltonian into a semi-empirical one by a well defined process that will directly, without further calculation, convert the analytically determined generators Q into those belonging to the semiempirical Hamiltonian.

IV. A First-Order Approximate Operator U .

We have used the molecule H_3^{++} as a test case. Letting the positions of its nuclei be R_a, R_b, R_c we have obtained a Lie generator Q and group operator $U = \exp(a\tilde{Q})$ which acts on linear nuclear configurations to change bond lengths $R_{ab} = |R_a - R_b|, R_{bc} = |R_b - R_c|, R_{ca} = |R_c - R_a|$ while keeping the energy of the ground state molecular orbital approximately constant. The generator is $\tilde{Q} = iQ$ with

$$\tilde{Q} = \xi_{ab} \frac{\partial}{\partial s_{ab}} + \xi_{bc} \frac{\partial}{\partial s_{bc}} + \xi_{ca} \frac{\partial}{\partial s_{ca}} + \eta$$

where $s_{ij} = \alpha R_{ij}$ and

$$\begin{aligned}\xi_{ab} &= (s_{ab} - s_{bc}) \exp - (s_{ab} + 2s_{bc} + 2s_{ca}) \\ \xi_{bc} &= (s_{bc} - s_{ca}) \exp - (s_{bc} + 2s_{ca} + 2s_{ab}) \\ \xi_{ca} &= (s_{ca} - s_{ab}) \exp - (s_{ca} + 2s_{ab} + 2s_{bc})\end{aligned}$$

The reader may verify that $QF = 0$ for

$$F(s) = (1 + s_{ab})\exp(-s_{ab}) + (1 + s_{bc})\exp(-s_{bc}) + \\ (1 + s_{ca})\exp(-s_{ca}).$$

We have taken a semi-empirical approach which treats α as a parameter to be fixed so as to obtain the best approximate family of isoenergetic curves $F(s) = \text{const.}$ Figure 1 compares such a curve with the results of MNDO calculations for a region of the H_3^{++} potential energy surface where MNDO is expected to be most accurate. The parameter α was chosen to make the curve pass through the points $(R_{ab} = 2a_o, R_{bc} = 2a_o)$, and $(R_{ab} = 1.5a_o, R_{bc} = 2.95a_o)$ which have nearly identical MNDO orbital energies. MNDO energies at other points on the curve are seen to deviate from constancy by less than 1 kcal./mole! *

That such a simple approximate operator would so accurately determine an isoenergetic curve is quite astonishing. We expected much poorer results at this level of approximation, and we also expected that even for such a first-order approximate Q it would be necessary to determine the isoenergetic curves $F(s) = c$ by approximation methods.

Further comparisons are being made and a paper describing the work is being prepared for submission.

* The deviations are much greater than this along the level curves of $f(s)$ at smaller internuclear distances where the MNDO results are known to be inaccurate.

LEVEL CURVES OF $F(s)$ FOR THE GROUND STATE OF H_3^{++}

The numbers at points on the graph represent the difference between the MNDO orbital energy, in K.cal., at the point and the MNDO energy at the * point on the same level curve.

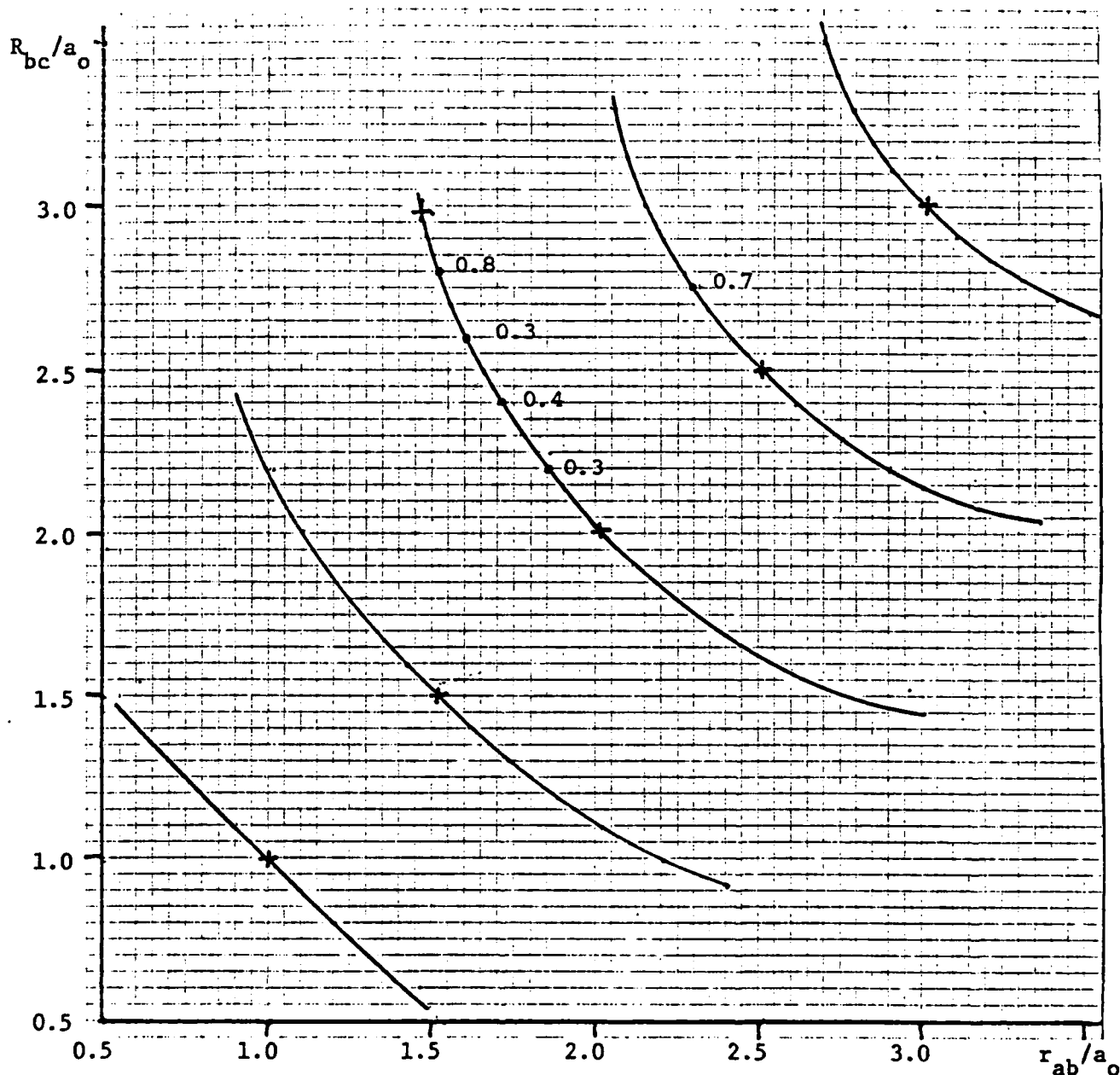


Figure 1

V. Recommendations

In order to more fully assess the utility of the approach presented here it is first of all necessary to more fully investigate the range of utility of the first approximation we have developed. Thereafter one should investigate more sophisticated approximate operators. From a practical standpoint one now needs answers to three questions:

1. What further chemical information can be obtained from the operators Q and U that it is difficult to obtain without them?
2. How expensive is it to obtain semiempirical and ab initio one-electron operators U that are able to produce orbital isoenergetic curves of chemical accuracy (E constant to a few kilocal./mole) in polyatomics?
3. Can less accurately determined operators be of use, e.g., for establishing chemical rules of thumb?

If the answers to these questions about one-electron operators indicate that the operator approach has general promise, then it is evident that one should begin the investigation of operators that move many-electron systems along isoenergetic paths in nuclear configuration space.

References:

1. M.J.S. Dewar, H. Kollmar, J.A.C.S. 97 2933 (1975).
2. C.E. Wulfman, "Dynamical Groups in Atomic and Molecular Physics", in "Recent Advances in Group Theory and Their Application to Spectroscopy", J.C. Donini, ed. Plenum, N.Y., 1979.
3. c.f., e.g., A. Cohen, "An Introduction to the Lie Theory of One-parameter Groups with Applications to the Solution of Differential Equations", Heath, Boston, 1911.
4. R.L. Anderson, S. Kumei, C.E. Wulfman, Phys. Rev. Lett. 28, 988 (1972).
5. T. Shibuya, C.E. Wulfman, Proc. Roy. Soc. A 286, 376 (1965).

1985 USAF-UES SUMMER FACULTY RESEARCH PROGRAM/
GRADUATE STUDENT SUMMER SUPPORT PROGRAM

Sponsored by the
AIR FORCE OFFICE OF SCIENTIFIC RESEARCH

Conducted by the
UNIVERSAL ENERGY SYSTEMS, INC.

FINAL REPORT

THE LQG/LTR DESIGN VIA H_2 -OPTIMIZATION

Prepared by: Hsi-Han Yeh
Academic Rank: Associate Professor
Department and Department of Electrical Engineering
University: University of Kentucky
Research Location: Control Analysis Group, Control Dynamics Branch
Flight Control Division, Flight Dynamics Lab
(AFWAL/FIGC)
USAF Research: Dr Siva S. Banda, Lt Tim McQuade USAF, and
Lt P.J. Lynch USAF
Date: August 16, 1985
Contract No. F49620-85-C-0013

THE LQG/LTR DESIGN VIA H_2 -OPTIMIZATION

by

HSI-HAN YEH

ABSTRACT

An H_2 -optimization technique is adapted to solve the LQG/LTR problem. Repetitive computations for the sequence of filter or controller gains as some parameter approaches zero or infinity are avoided. The limit values of the LQG/LTR compensator are obtained in one iteration without involving infinite filter or controller gains. The configurations of the H_2 -optimal compensator and the LQG/LTR compensator are compared.

I INTRODUCTION

The Linear-Quadratic-Gaussian synthesis with Loop Transfer Recovery (LQG/LTR) is an elegant method for achieving desired loop shapes and maximum robustness properties in the design of feedback control systems [1-2]. It involves essentially a two-step approach. First, a Kalman filter (or alternatively, a full-state linear quadratic (LQ) feedback regulator) with desired loop transfer properties is designed. Then a sequence of LQ feedback regulators (or alternatively, Kalman filters) approaching an ideal limit is designed and the combined Linear-Quadratic-Gaussian (LQG) compensator is selected with trade-offs.

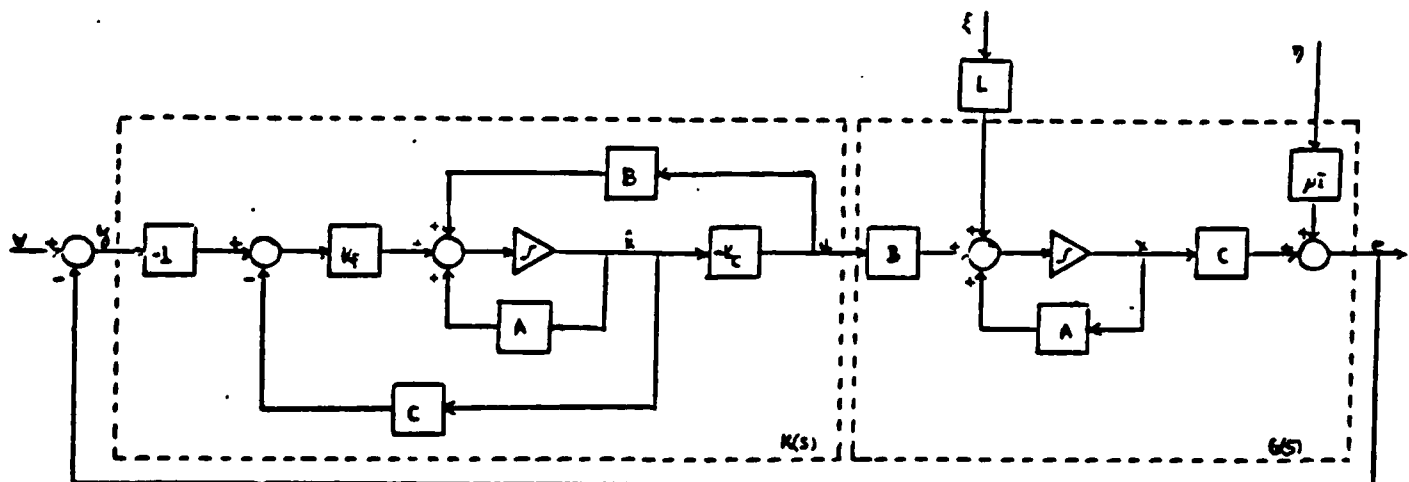
This design method is powerful in that for minimum phase systems, it offers essentially arbitrary freedom to shape the loop transfer characteristics in the high gain region, and it yields stability margins approaching those of the Kalman filter (or full state LQ regulator) in the limit. The compensator obtained from this design also has a one pole roll-off at high frequencies. This design method is easy to carry out because it primarily involves repeated solutions of algebraic Riccati equations. However, when computing the sequence of compensators as a certain parameter approaches zero or infinity in the limit, numerical difficulty may occur before the limit becomes apparent. In the numerical experiments conducted, it was observed that letting state weighting go to infinity more often resulted in computational difficulty than letting control weighting go to zero, when designing regulators to recover filter characteristics. The resultant sequence of compensators always involve some arbitrarily large values either in the regulator gain matrix or in the Kalman filter gain matrix.

In a recent paper [2], it is shown that the LQG integral performance index is equivalent to a 2-norm over the Hardy space of stable rational transfer functions (H_2 -space). Therefore, the LQG method (and in particular LQG/LTR procedures) may be regarded as one way of solving a particular H_2 -optimization problem.

The solutions of H_2 and H_∞ (Hardy space with infinity norm) optimization are treated extensively in a recent dissertation [3]. The techniques presented in [3] enables one to solve H_2 -optimization problems directly in H_2 -space without resorting to time domain optimization.

In this paper, the H_2 -optimization technique developed in [3] is adapted to solve the LQG/LTR problem. The objectives are twofold (1) to obtain the LQG/LTR compensator without involving infinite gains in the filter or controller, or the trade-offs thereof, and (2) to avoid repetitive computations for the sequence of filter or controller gains as some parameter approaches zero or infinity in the recovery procedure, and the numerical errors that may be associated with such a procedure.

II LQG/LTR Method vs H_2 -Optimization



153-4
Fig 1 Block Diagram of LQG System

In LQG Control (Fig 1), one selects the Kalman filter gain K_f and LQ controller gain K_c to minimize

$$J_{LQG} = E \left\{ \lim_{T \rightarrow \infty} \frac{1}{T} \int_0^T (x^T(t) H_o^T H_o x(t) + \rho^2 u^T(t) u(t) dt) \right\} \quad (1)$$

where superscript T denotes transpose, H_o is a constant column matrix, ρ a constant scalar, u and x are control and state vectors.

The optimal Kalman filter gain and LQ controller gain are given by

$$K_f = \Sigma C^T R_f^{-1} \quad (2)$$

$$A \Sigma + \Sigma A^T + Q_f - \Sigma C^T R_f^{-1} C \Sigma = 0 \quad (3)$$

$$K_c = \frac{1}{\rho^2} B^T P \quad (4)$$

$$A^T P + P A + H_o^T H_o - \frac{1}{\rho^2} P B B^T P = 0 \quad (5)$$

respectively, where

$$Q_f = L Q_o L^T \quad (6)$$

$$R_f = \mu^2 R_o \quad (7)$$

and $\xi(t)$ and $\eta(t)$ are Gaussian white noise vectors satisfying

$$E[\xi(t)\xi^T(\tau)] = Q_o \delta(t - \tau) \quad (8)$$

$$E[\eta(t)\eta^T(\tau)] = R_o \delta(t - \tau) \quad (9)$$

$$E[\eta(t)\xi^T(\tau)] = 0 \quad (10)$$

The frequency domain representation of J_{LQG} can be obtained through Parseval's Theorem as [2]

$$J_{LQG} = \frac{1}{\pi} \int_0^\infty \text{Tr}[M(j\omega)M^H(j\omega)]d\omega = \frac{1}{\pi} \int_0^\infty \text{Tr}[M^H(j\omega)M(j\omega)]d\omega = \|M(j\omega)\|_2^2 \quad (11)$$

where superscript H denotes Hermitian transpose, Tr denote the trace (sum of diagonal terms) of a matrix and

$$M(s) = \begin{bmatrix} m_{11}(s) & m_{12}(s) \\ m_{21}(s) & m_{22}(s) \end{bmatrix} \quad (12)$$

$$m_{11}(s) = H_o \Phi(s) L - H_o \Phi(s) B K(s) (I + G(s) K(s))^{-1} C \Phi(s) L \quad (13)$$

$$m_{12}(s) = -\mu H_o \Phi(s) B K(s) (I + G(s) K(s))^{-1} \quad (14)$$

$$m_{21}(s) = -\rho K(s) (I + G(s) K(s))^{-1} C \Phi(s) L \quad (15)$$

$$m_{22}(s) = -\mu \rho K(s) (I + G(s) K(s))^{-1} \quad (16)$$

$$\Phi = (sI - A)^{-1} \quad (17)$$

In LQG/LTR, (with the loop broken at the output) L and μ are chosen as

$$\frac{1}{\mu} C \Phi(s) L = W(s) \quad (18)$$

and H_o and ρ are chosen as

$$H_o = C \text{ and } \rho \rightarrow 0 \quad (19)$$

to make $G(s) K(s)$ recover the desired full-state loop transfer matrix. Here, $W(s)$ can be interpreted as a desired loop transfer matrix or a weighting transfer matrix.

Then $M(s)$ takes the form of $M_o(s)$

$$M_o(s) = \mu \begin{bmatrix} (I + G(s) K(s))^{-1} W(s) & -G(s) K(s) (I + G(s) K(s))^{-1} \\ 0 & 0 \end{bmatrix} \quad (20)$$

If the optimization is solved by computing K_f and K_C of (2) and (4), respectively subject to (18) and (19) (LQG/LTR procedure), then at least one component in K_C approaches infinity as ρ approaches zero in the limit.

In the output-breaking LOG/LTR problem, replacing (19) by

$$H_o = q C_o^T C, \quad \rho = 1, \quad q \rightarrow \infty \quad (21)$$

for any nonsingular C_o should yield the same result, theoretically.

However, experience shows that letting $q \rightarrow \infty$ tends to have numerical instability in the computational process.

It should also be noted that by duality, that LOG/LTR can also be formulated for the input-breaking problem. In this case, the desired full-state loop transfer matrix is 'recovered' by $K(s) G(s)$ through the proper choice of parameters. In both versions of the LQG/LTR procedure,

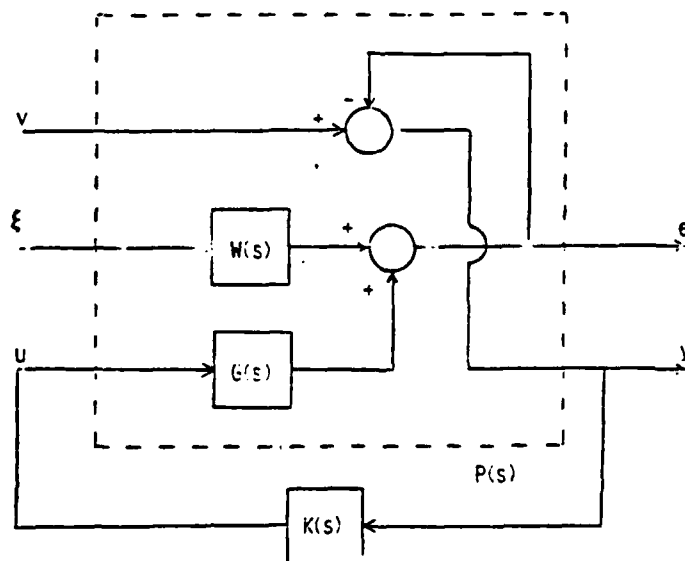
the singular values of the recovered loop transfer matrix approximate those of the weighting function $W(s)$ in the low frequency (high gain) region. Therefore, $W(s)$ is also regarded as the loop shape of the optimum system.

III FORMULATION OF H_2 -OPTIMIZATION PROBLEM THROUGH LINEAR FRACTIONAL TRANSFORMATION

The H_2 -optimization problem may be solved by either frequency domain projection method of Chang and Pearson [4], or the time-domain method of Doyle [3]. While Chang and Pearson's method applies to plants having equal number or more inputs than outputs, Doyle's method applies to plants having equal number or more outputs than inputs. In this paper, the application of Doyle's H_2 -optimization method to the LQG/LTR problem is explored.

The system of Fig 2 which is obtained from setting $\eta(t) = 0$, $C\Phi(s)L = W(s)$, and rearranging Fig 1, fits into the "linear fractional transformation" format. Let

$$\bar{v} = \begin{bmatrix} v \\ \xi \end{bmatrix} \quad (22)$$



153-7
Fig 2 Feedback System in Linear Fractional-Transformation Form

Then, in the frequency domain

$$\begin{bmatrix} c(s) \\ y(s) \end{bmatrix} = P(s) \begin{bmatrix} \tilde{v}(s) \\ u(s) \end{bmatrix} = \begin{bmatrix} p_{11}(s) & p_{12}(s) \\ p_{21}(s) & p_{22}(s) \end{bmatrix} \begin{bmatrix} \tilde{v}(s) \\ u(s) \end{bmatrix} \quad (23)$$

where

$$\begin{aligned} p_{11}(s) &= [0 \quad W(s)] & p_{12}(s) &= G(s) \\ p_{21}(s) &= [I \quad -W(s)] & p_{22}(s) &= -G(s) \end{aligned} \quad (24)$$

and

$$u(s) = K(s)y(s) \quad (25)$$

substituting (25) into (23) gives

$$c(s) = F_l(P(s), K(s)) \tilde{v} \quad (26)$$

$$\begin{aligned} F_l(P(s), K(s)) &= p_{11} + p_{12}K(I - p_{22}K)^{-1}p_{21} \\ &= [GK(I + GK)^{-1} \quad (I + GK)^{-1}W] \end{aligned} \quad (27)$$

In the right-hand side of (27), the Laplace transform variable has been suppressed for the sake of brevity. The same will be done in the subsequent development whenever no confusion may occur.

Comparison of (20) and (27) shows that

$$\mu \|F_l\|_2 = \|M_o\|_2 \quad (28)$$

Thus, the LOG/LTR design of Fig 1 may be achieved by H_2 -optimization of the system of Fig 2, when $\|F_l\|_2$ is chosen to be minimized.

It has been shown by Doyle [3] that every compensator $K(s)$ that yields an internally stable linear fractional transformation (Fig 2) can be represented by yet another linear fractional transformation shown in Fig 3, where J can be represented by parameters in the minimal realization (non-unique) of $P(s)$, viz,

$$P(s) = \begin{bmatrix} p_{11}(s) & p_{12}(s) \\ p_{21}(s) & p_{22}(s) \end{bmatrix} = \left[\begin{array}{c|cc} A_p & B_1 & B_2 \\ \hline C_1 & D_{11} & D_{12} \\ C_2 & D_{21} & D_{22} \end{array} \right] \quad (29)$$

$$J(s) = \begin{bmatrix} J_{11}(s) & J_{12}(s) \\ J_{21}(s) & J_{22}(s) \end{bmatrix} = \left[\begin{array}{c|cc} A_p + B_2 F + F C_2 + H D_{22} F & -H & B_2 + H D_{22} \\ \hline F & 0 & I \\ -(C_2 + D_{22} F) & I & -D_{22} \end{array} \right] \quad (30)$$

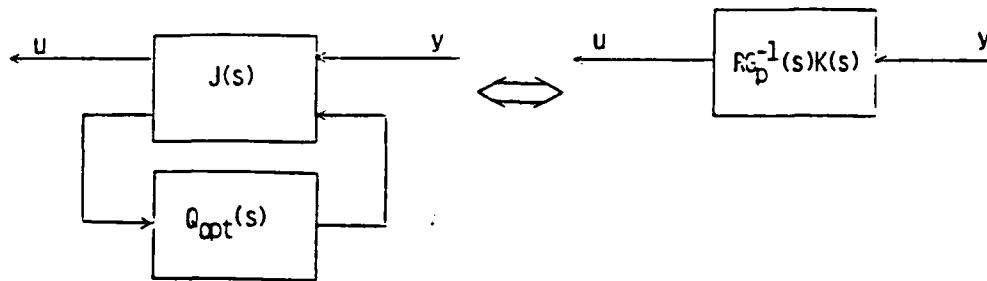


Fig 3 Compensator as a Linear Fractional Transformation

The right-hand sides of (29) and (30) are minimal realizations of $P(s)$ and $J(s)$, respectively. (A minimal realization has the minimal number of states.) F and H are any real matrices (of compatible sizes) that stabilize $A_p + B_2 F$ and $A_p + H C_2$, respectively. They may be obtained by solving a pair of matrix Riccati equations in which some coefficients are arbitrarily set [5].

The block $Q(s)$ in Fig 3 is any proper rational matrix of the same size as the transpose of $p_{22}(s)$, and is analytic and bounded in the right-half plan ($\text{Re } s > 0$) (asymptotically stable). The only other condition that $Q(s)$ must satisfy is that

$$\det[I + D_{22}Q(\infty)] \neq 0 \quad (31)$$

With J given in (30), the closed-loop transfer function F_L of Fig 2 is found [3] to be

$$F_L(s) = T_{11}(s) + T_{12}(s)Q(s)T_{21}(s) \quad (32)$$

where $T_1(s)$, $T_2(s)$ and $T_2(s)$ may be represented by the following realizations:

$$T_{11}(s) = \left[\begin{array}{c|c} A_p + B_2 F & -B_2 F \\ \hline 0 & A_p + H C_2 \end{array} \left| \begin{array}{c} B_1 \\ B_1 + H D_{21} \end{array} \right. \right] \quad (33)$$

$$T_{12}(s) = \left[\begin{array}{c|c} A_p + B_2 F & B_2 \\ \hline C_1 + D_{12} F & D_{12} \end{array} \right] \quad (34)$$

$$T_{21}(s) = \left[\begin{array}{c|c} A_p + H C_2 & B_1 + H D_{21} \\ \hline C_2 & D_{21} \end{array} \right] \quad (35)$$

IV THE H_2 -OPTIMAL CONTROLLER

It has been shown by Doyle [3] that if p_{12} and $p_{21}(s)$ have no transmission zeros on the $j\omega$ -axis (including infinity) and if

$$D_{12}^T D_{12} = I \quad (36)$$

$$D_{21} D_{21}^T = I \quad (37)$$

then the controller $Q(s)$ that minimizes $\|F_L\|_2$ of (32) is found to be

$$Q_{opt}(s) = -D_{12}^T D_{11} D_{21}^T \quad (38)$$

provided that F and H are selected as follows:

$$F = -(D_{12}^T C_1 + B_2^T X) \quad (39)$$

$$H = -(B_1 D_{21}^T + Y C_2^T) \quad (40)$$

where X and Y are the solutions of the following Riccati equations

$$(A_p - B_2 D_{12}^T C_1)^T X + X(A_p - B_2 D_{12}^T C_1) - X B_2 B_2^T X + C_1^T D_{\perp} D_{\perp}^T C_1 = 0 \quad (41)$$

$$(A_p - B_1 D_{21}^T C_2)^T Y + Y(A_p - B_1 D_{21}^T C_2) - Y C_2^T C_2 Y + B_1 \hat{D}_{\perp}^T \hat{D}_{\perp} B_1^T = 0 \quad (42)$$

where D_{\perp} is an orthogonal complement of D_{12} such that $(D_{\perp} = (D_{12})_{\perp})$,

$$[D_{12} \ D_{\perp}]^T [D_{12} \ D_{\perp}] = I \quad (43)$$

$$\begin{bmatrix} D_{21} \\ \hat{D}_{\perp} \end{bmatrix} \begin{bmatrix} D_{21} \\ \hat{D}_{\perp} \end{bmatrix}^T = I \quad (44)$$

A necessary condition for D_{12} to satisfy (36) is that D_{12} (and hence $p_{12}(s)$) must have at least as many rows as columns. Likewise (37) requires that D_{21} (and hence $p_{21}(s)$) must have at least as many columns as rows. Therefore, the plant $G(s)$ must have at least as many outputs as inputs (see Eq (24)).

It should be noted that for the case where $p_{12}(s)$ has more columns than rows and $p_{21}(s)$ has more rows than columns, B. C. Chang has shown [4] through the use of an example that a frequency domain inner-outer factorization and H_2 -projection method may be used to find the product $B_o(s) Q_{opt}(s) A_o(s)$, where $B_o(s)$ has a stable right inverse and $A_o(s)$ has a stable left inverse. In some special cases, $Q_{opt}(s)$ may be computed.

In this paper, $G(s)$ is assumed to have at least as many outputs as inputs so that Doyle's method is applicable. Since $p_{12}(s) = G(s)$, (36) and (37) cannot be satisfied for practical plants which are usually strictly proper. Therefore, the H_2 -optimization technique must be adapted to this case.

Manipulate Fig 2 into an equivalent form shown in Fig 4, where a constant matrix R and

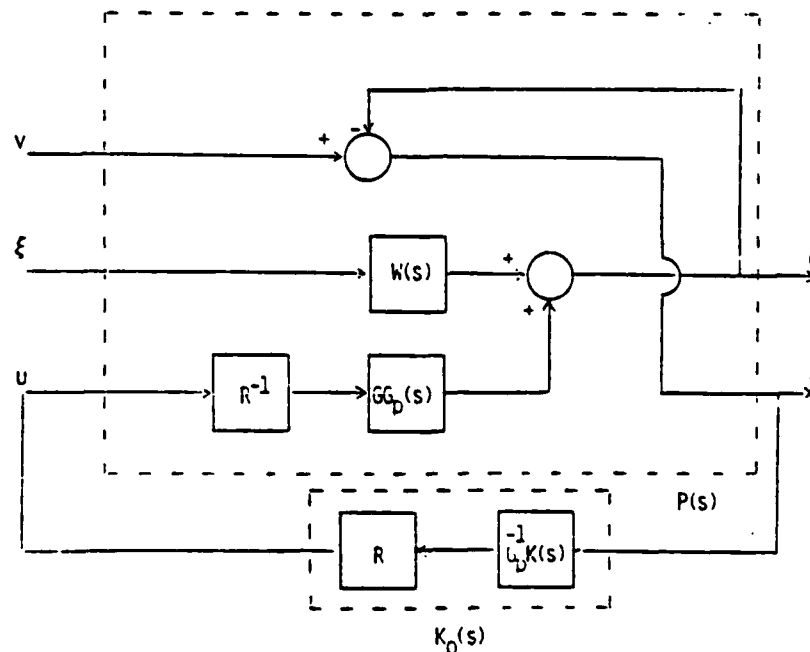


Fig 4 Treatment of a Strictly Proper Plant

a nonsingular diagonal polynomial matrix $G_p(s)$ is chosen to satisfy the following conditions:

$$G_p(s) = \text{diag}\{f_1(s) \ f_2(s) \ \dots \ f_n(s)\} \quad (45)$$

$$|G(j\omega)G_p(j\omega)|^* |G(j\omega)G_p(j\omega)| > 0 \quad (46)$$

$$f_i(s) \neq 0 \ ; \ \text{for } \text{Re } s > 0, \text{ all } i \quad (47)$$

$$D^o_{12} \equiv \lim_{s \rightarrow \infty} G(s)G_p(s) \neq 0 \quad (48)$$

$$\det[(D^o_{12})^T D^o_{12}] \neq 0 \quad (49)$$

$$R^T = R \quad (50)$$

$$RR = (D^o_{12})^T D^o_{12} \quad (51)$$

Condition (46) requires that $G(s)G_p(s)$ has no transmission zeros on the $j\omega$ -axis so that Eq (38) applies. Condition (47) requires that $G_p(s)$ does not introduce any right-half plane zeros to affect the projection results in the E_2 -space. Condition (48) is implied by (49). It is written there for notational convenience.

Now Define

$$D_{12} \equiv \lim_{s \rightarrow \infty} G(s)G_p(s)R^{-1} = D^o_{12}R^{-1} \quad (52)$$

Then

$$\begin{aligned} D_{12}^T D_{12} &= (D^o_{12}R^{-1})^T D^o_{12}R^{-1} \\ &= (R^{-1})^T (D^o_{12})^T D^o_{12}R^{-1} \\ &= R^{-1} (D^o_{12})^T D^o_{12} R^{-1} = I \end{aligned} \quad (53)$$

Moreover, since $W(s)$ is also the desired loop shape, it should always satisfy

$$W(\infty) = 0 \quad (54)$$

Therefore

$$D_{21}D_{21}^T = \begin{bmatrix} I & 0 \\ 0 & 0 \end{bmatrix} = I \quad (55)$$

Now, if the minimal realization of $P(s)$ is written for the system in Fig 4, then conditions (36) and (37) are met and $K(s)$ of Fig 4 becomes $R G_p(s) K(s)$, as represented in Fig 5, where $O_{opt}(s)$ is given by (38) and $J(s)$ is still represented by (30)

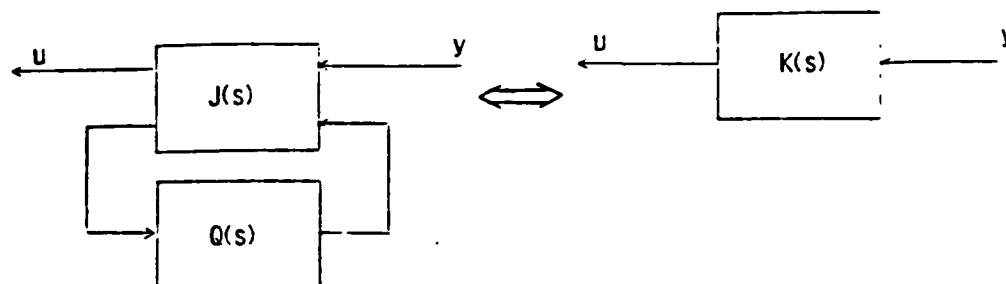


Fig 5 Optimal Compensator $K(s)$ of a Strictly Proper Plant

The linear fractional transformation of Fig 5 means

$$u(s) = K_o(s)y(s) \quad (56)$$

$$K_o(s) = J_{11}(s) + J_{12}(s)Q_{opt}(s)(I - J_{22}(s)Q_{opt}(s))^{-1}J_{21}(s) \quad (57)$$

Therefore, the controller of the strictly proper plant is given by

$$K(s) = G_p(s)R^{-1}K_o(s) \quad (58)$$

The configuration of the H_2 -optimal compensator can be obtained by combining Fig 4 and Fig 5 and using (30) as a realization of $J(s)$. The result is given in Fig 6. The similarity between Fig 6 and Fig 1 is obvious. However, for a strictly proper plant $G(s)$, the LQG compensator is always strictly proper, whereas the H_2 -optimal Compensator is proper if $D_{22} \neq 0$. As a result of the recovery procedure, LQG/LTR Compensators always result in some infinite gains in K_f or K_c , whereas the H_2 -optimal solution of the LQG/LTR problem still has all finite gains in the H and F matrices. This will be demonstrated in a numerical example after the H_2 -optimization procedure is summarized.

It is worth noting that the H_∞ -optimal compensator has the same configuration as in Fig 6. The difference between H_2 -Optimal compensator and H_∞ -optimal compensator is that they have different $Q_{opt}(s)$ block.

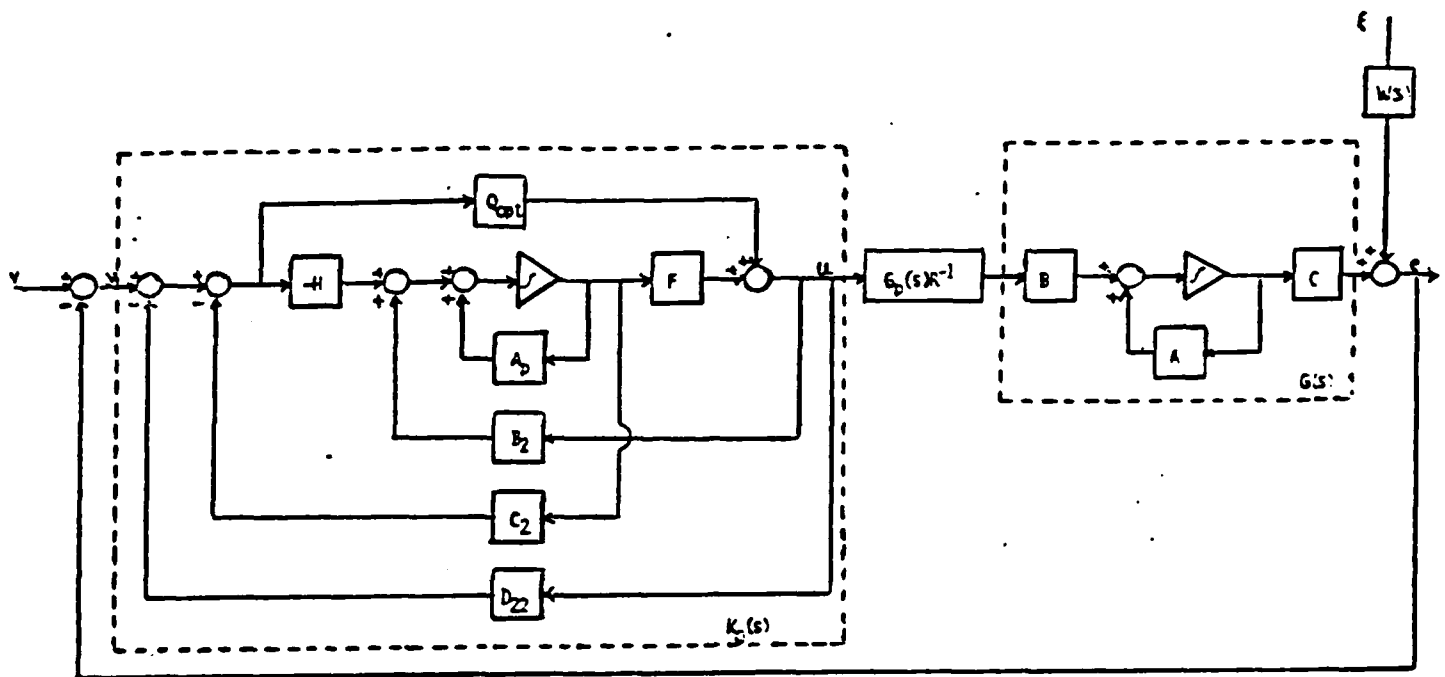


Fig 6 Configuration of an H_2 -Optimal Compensator

V H_2 -OPTIMIZATION PROCEDURE FOR THE LQG/LTR PROBLEM

The method developed in the above section (for plants having equal or more outputs than inputs) may be summarized into the following algorithm.

Step 1 Select a desired loop shape (or weighting function) matrix $W(s)$ for the system, with $W(\infty) = 0$. Some considerations for loop-shaping may be found in [1].

Step 2 If the plant $G(s)$ is strictly proper, skip this step and go to Step 3. Otherwise, compute a minimal realization of

$$P(s) = \begin{bmatrix} p_{11}(s) & p_{12}(s) \\ p_{21}(s) & p_{22}(s) \end{bmatrix} = \left[\begin{array}{c|cc} A_p & B_1 & B_2 \\ \hline C_1 & D_{11} & D_{12} \\ C_2 & D_{21} & D_{22} \end{array} \right] \quad (59)$$

where

$$p_{11}(s) = [0 \quad W(s)]; \quad p_{12}(s) = G(s) \quad (60)$$

$$p_{21}(s) = [I \quad -W(s)]; \quad p_{22}(s) = -G(s)$$

Step 3 If D_{12} has full rank, skip this step, re-name D_{12} as D_{12}^0 and go to Step 4. If $G(s)$ is strictly proper or D_{12} does not have full rank, select $G_p(s) = (s + a)I$ (for some $a > 0$) or $G_p(s) = \text{diag}[s + 1, s + 2, \dots]$, etc. until D_{12}^0 (see (48)) has full column rank.

Step 4 Compute

$$R = [(D_{12}^0)^T D_{12}^0]^{-1/2} \quad (61)$$

and substitute $G(s) G_p(s) R^{-1}$ for $G(s)$ in Step 2. Recompute the minimal realization of $P(s)$. The result should satisfy

$$D_{12}^T D_{12} = I \quad (62)$$

and

$$D_{21} D_{21}^T = I \quad (63)$$

Step 5 Compute D_{\perp} and \tilde{D}_{\perp} as

$$D_{\perp} = (D_{12})_{\perp} \quad (64)$$

$$\tilde{D}_{\perp} = (D_{21})_{\perp} \quad (65)$$

such that

$$[D_{12} \ D_{\perp}]^T [D_{12} \ D_{\perp}] = I \quad (66)$$

and

$$\begin{bmatrix} D_{21} \\ \tilde{D} \end{bmatrix} [L_{21}^T \ \tilde{D}_{\perp}^T] = I \quad (67)$$

Step 6 Solve the following Riccati equations

$$(A_p - B_2 D_{12}^T C_1)^T X + X(A_p - B_2 D_{12}^T C_1) - X B_2 B_2^T X + C_1^T D_{\perp} D_{\perp}^T C_1 = 0 \quad (68)$$

$$(A_p - B_1 D_{21}^T C_2) Y + Y(A_p - B_1 D_{21}^T C_2)^T - Y C_2^T C_2 Y + B_1 \tilde{D}_{\perp}^T \tilde{D}_{\perp} B_1^T = 0 \quad (69)$$

and compute

$$F = -(D_{12}^T C_1 + B_2^T X) \quad (70)$$

$$H = -(B_1 D_{21}^T + Y C_2^T) \quad (71)$$

$$\hat{A} = A_p + B_2 F + H C_2 + H D_{22} F \quad (72)$$

$$\hat{B} = B_2 + H D_{22} \quad (73)$$

$$\hat{C} = C_2 + D_{22} F \quad (74)$$

$$J(s) = \begin{bmatrix} J_{11}(s) & J_{12}(s) \\ J_{21}(s) & J_{22}(s) \end{bmatrix} \begin{bmatrix} \hat{A} & -H & \hat{B} \\ F & 0 & I \\ -\hat{C} & I & -D_{22} \end{bmatrix} \quad (75)$$

Step 7 Compute

$$Q_{opt}(s) = -D_{12}^T D_{11} D_{21}^T \quad (76)$$

$$K_o(s) = J_{11}(s) + J_{12}(s)Q_{opt}(s)(I - J_{22}(s)Q_{opt}(s))^{-1}J_{21}(s) \quad (77)$$

Finally, the optimal compensator is given by

$$K(s) = G_p(s)R^{-1}K_o(s) \quad (78)$$

Note that by virtue of (60), D_{11} is always zero since $W(\infty) = 0$.

Hence, Q_{opt} in the H_2 -optimization is always zero and

$$K_o(s) = J_{11}(s) \quad (79)$$

is always strictly proper.

VI EXAMPLE OF LOOP RECOVERY VIA H_2 -OPTIMIZATION

The mathematical development of the previous actions covers the general case of multiple-input multiple-output systems. A single-input single-output system will be used in the numerical example of this section for comparison of the recovery of the desired loop transfer function via H_2 -optimization versus the LQG/LTR procedure.

Let the plant be given by

$$\dot{x} = Ax + Bu + L\xi \quad (80)$$

$$y = Cz + \mu\eta \quad (81)$$

$$E[\xi(t)\xi^T(\tau)] = Q_o\delta(t - \tau) \quad (82)$$

$$E[\eta(t)\eta^T(\tau)] = R_o\delta(t - \tau) \quad (83)$$

$$E[\xi(t)\eta^T(\tau)] = 0 \quad (84)$$

where

$$A = \begin{bmatrix} 0 & 1 \\ -3 & -4 \end{bmatrix} \quad B = \begin{bmatrix} 0 \\ 1 \end{bmatrix} \quad \mu = 1 \quad (85)$$

$$C = [2 \ 1] \quad Q_o = 1 \quad R_o = 1 \quad (86)$$

$$G(s) = C(sI - A)^{-1}B = \frac{(s+2)}{(s+1)(s+3)} \quad (87)$$

The H_2 -optimization:

The H_2 -optimal compensator minimizing (11) with M given by M_0 of (20) is computed first:

Step 1 Choose

$$W(s) = \frac{10(s+5)}{(s+1)(s+2)} \quad (88)$$

by some loop shaping consideration which is not the concern of this paper.

Step 2 Since $G(s)$ is strictly proper, skip this step, and go to Step 3.

Step 3 Select

$$G_p(s) = (s+4)I \quad (89)$$

Then

$$G(s)G_p(s) = \frac{(s+2)(s+4)}{(s+1)(s+3)} \quad (90)$$

$$D^o_{12} = \lim_{s \rightarrow \infty} G(s)G_p(s) = 1 \quad (91)$$

Step 4

$$R = |(D^o_{12})^T D^o_{12}|^{\frac{1}{2}} = 1 \quad (92)$$

$$P(s) = \begin{bmatrix} 0 & \frac{10(s+5)}{(s-1)(s+3)} & \frac{(s+2)(s+4)}{(s-1)(s+3)} \\ 1 & \frac{-10(s-5)}{(s-1)(s+3)} & \frac{-(s+2)(s+4)}{(s-1)(s+3)} \end{bmatrix}$$

$$= \begin{bmatrix} -3.4538 & 3.5364 & 0 & .9578 & -.1182 \\ -.3149 & -.5462 & 0 & -.1950 & -.039 \\ 0 & -51.2738 & 0 & 0 & 1 \\ 0 & 51.2738 & 1 & 0 & -1 \end{bmatrix} \quad (93)$$

$$A_p = \begin{bmatrix} -3.4538 & 3.5364 \\ -.3149 & -.5462 \end{bmatrix}; \quad B_1 = \begin{bmatrix} 0 & .9578 \\ 0 & -.1950 \end{bmatrix}; \quad B_2 = \begin{bmatrix} -.1182 \\ -.0390 \end{bmatrix} \quad (94)$$

$$C_1 = [0 \quad -51.2738]; \quad D_{11} = [0 \quad 0]; \quad D_{12} = [1] \quad (95)$$

$$C_2 = [0 \quad 51.2738]; \quad D_{21} = [1 \quad 0]; \quad D_{22} = [-1] \quad (96)$$

Step 5 $D_{12} \in \mathbb{R}^{1 \times 1}$ implies that

$$D_{\perp} \equiv (D_{12})_{\perp} = 0 \quad (97)$$

By observation, we have

$$\hat{D}_{\perp} = (D_{21})_{\perp} = [0 \quad 1] \quad (98)$$

Step 6

$$X = \begin{bmatrix} 0 & 0 \\ 0 & 0 \end{bmatrix}; \quad Y = \begin{bmatrix} .0542 & -.0131 \\ -.0131 & .004 \end{bmatrix} \quad (99)$$

$$F = [0 \quad 51.2738] \quad (100)$$

$$H = \begin{bmatrix} .6717 \\ -.2047 \end{bmatrix} \quad (101)$$

$$\begin{aligned} J_{11}(s) &= \begin{bmatrix} -3.4538 & -2.5220 & -.6710 \\ -.3149 & -2.5462 & 2.2047 \\ 0 & 51.2738 & 0 \end{bmatrix} \\ &= \frac{10.4976(s + 4.4858)}{(s + 2)(s + 4)} \end{aligned} \quad (102)$$

Step 7

$$Q_{opt} = -D_{12}^T D_{11} D_{21}^T = 0 \quad (103)$$

$$K_o(s) = J_{11}(s) = \frac{10.4976(s + 4.4858)}{(s + 2)(s + 4)} \quad (104)$$

$$K(s) = (s + 4)K_o(s) = \frac{10.4976(s + 4.4858)}{(s + 2)} \quad (105)$$

The LOG/LTR Procedure:

To rework this problem via LQG/LTR procedure (minimizing (1) subject to the conditions of (18) and (19)), choose

$$L = \begin{bmatrix} 30 \\ -50 \end{bmatrix} \quad (106)$$

$$Q_f = LQ_c L^T = 100 \begin{bmatrix} 9 & -15 \\ -15 & 25 \end{bmatrix} \quad (107)$$

$$R_f = \mu^2 R_o = 1 \quad (108)$$

The LQ controller gain K_c is computed according to (2) and (3), and the filter gain K_f is computed according to (4) and (5), with $H_o = C$ and $\rho \rightarrow 0$. It is found that for $\rho^2 = 10^{-12}$

$$K_c = [2 \times 10^6 \quad 10^6] \quad (109)$$

$$K_f = \begin{bmatrix} 26.0948 \\ -41.6919 \end{bmatrix} \quad (110)$$

$$\begin{aligned} K(s) &= K_c (sI - A + BK_c + K_f C)^{-1} K_f \\ &= \frac{1.0498 \times 10^7 (s + 4.4853)}{(s + 10^6)(s + 2)} \end{aligned} \quad (111)$$

Thus, the LQG/LTR procedure and H_2 -optimization yield the same compensator at finite frequencies, but high gains are involved in the LQG/LTR compensators.

VII CONCLUSIONS

An H_2 -Optimization technique has been adapted to solve the LQG/LTR problem. This method gives the limit solution of the LQG/LTR problem in one iteration without requiring any parameters to approach zero or infinity in the limit. The H_2 -optimal compensator also does not involve any infinite gains as in the results of LQG/LTR procedure.

VIII RECOMMENDATIONS

The H_2 -optimization method presented in this paper may be used in conjunction with an LQG/LTR design to provide an additional point of reference to aid the designer in the choice of implementation.

Robust design for nonminimum phase system is a difficult problem because the impact of the right-half plane transmission zeros is not yet fully understood [2]. In the configuration of Fig 4, if $G_p(s)$ has no

transmission zero in the right-half plane, then the H_2 -optimal compensator $K_O(s)$ is independent of $G_p(s)$. However, if $G_p(s)$ has transmission zeros in the right-half plane, then due to the orthogonal projection made in the H_2 -space in the process of optimization, $K_O(s)$ is affected by the choice of $G_p(s)$. Therefore, the effect of a nonminimum phase $G_p(s)$ on the optimal compensator $K(s)$ may have a bearing on the design methodology of nonminimum phase system and should be studied, especially if the desired loop shape is chosen to be nonminimum phase.

ACKNOWLEDGEMENTS

This research was performed at the Flight Dynamics Laboratory, Wright-Patterson Air Force Base under the sponsorship of Air Force Office of Scientific Research, Air Force Systems Command. Inputs from Dr Siva S. Banda and Capt D. Brett Ridgely, USAF, and inputs and technical supports from Lt Tim McQuade, USAF, and Lt P. J. Lynch, USAF (all of Control Dynamics Branch, Flight Control Division) are acknowledged.

REFERENCES

- [1] Doyle J. C. and Stein G., "Multivariable Feedback Design Concepts for a Classical/Modern Synthesis", IEEE Trans. Auto. Contr., Feb 1981.
- [2] Stein G. and Athans M., "The LQG/LTR Procedure for Multivariable Feedback Control Design", Automatic Control Conference, May 1984, San Diego.
- [3] Doyle J. C., "Matrix Interpolation Theory and Optimal Control", Ph.D. Dissertation, University of California, Berkeley, Dec 1984.
- [4] Chang B. C. and Pearson J. B., "Optimal Disturbance Reduction in Linear Multivariable Systems", Conference on Decision and Control, Dec 1983.

[5] Nett C. N., Jacobson C.A. and Balas M. J., "A Connection Between State Space and Doubly Coprime Fractional Representations," IEEE Trans Auto Control, Vol AC-29, No 9, Sept 1984, pp 831-832.

1985 USAF-UES SUMMER FACULTY RESEARCH PROGRAM/
GRADUATE STUDENT SUMMER SUPPORT PROGRAM

Sponsored by the
AIR FORCE OFFICE OF SCIENTIFIC RESEARCH
Conducted by the
UNIVERSAL ENERGY SYSTEMS, INC.

FINAL REPORT

HEAT TRANSFER CORRELATION FOR NOSETIPS

WITH STAGNATION-POINT GAS INJECTION

Prepared by: Juin S. Yu

Academic Rank: Professor

Department and University: Mechanical Engineering
West Virginia Institute of Technology

Research Location: Arnold Engineering Development Center (AEDC)
Von Karman Facility (VKF)
Aerophysics Branch
Applied Computation Mechanics Group

USAF Research: Dr. Jim R. Maus, Jr.

Date: September 23, 1985

Contract No: F49620-85-C-0013

HEAT TRANSFER CORRELATION FOR NOSETIPS
WITH STAGNATION-POINT GAS INJECTION

by

Juin S. Yu

ABSTRACT

The test-inferred local heat transfer coefficient distributions over the surfaces of the BMO/Martin nosetip models at zero angle of attack have been correlated from the viewpoint of an attached stable turbulent boundary layer flow. Data included for correlation are obtained from the original data set after screening by using the tabulated heat transfer correlation coefficients. The correlation parameters are determined by applying the method of least squares. A total of twelve runs have been correlated covering injection rates corresponding to $p_c/p_{t2}=1, 1.5, 2, 3$. A reference flat plate boundary layer indicative of the local flow conditions is introduced and the boundary layer is projected to begin at a location on the surface having an axial distance x_o . Primary results show that $h/h_{fp} = \delta_{fp}/\delta \approx 1.3$ and that x_o increases slightly with increasing injection rates.

The method has so far proved to be reasonably effective. Implementation of the procedure to other test runs and follow-on work for better understanding the related processes are suggested.

ACKNOWLEDGEMENTS

This work was sponsored by the 1985 USAF-UES Summer Faculty Research Program under Contract F49620-85-C-0013. Part of the work was performed in conjunction with the Applied Computation Mechanics Group of the von Karman Facility at AEDC, with the last phase completed at West Virginia Institute of Technology. The author would like to take this opportunity to express his many thanks to Mr. M. K. Kingery, the AEDC Effort Focal Point, for giving him this assignment and all the sincere help whenever needed, and to Messrs. W. T. Strike and R. K. Matthews for briefing him with the major problems of immediate AEDC interest. He is deeply indebted to Dr. J. R. Maus, Jr., VKF/AP/VB5 Principal Engineer of Calspan, for everything he rendered (too many to mention here) during the course of this work. Finally, the author would like to thank all the summer colleagues at VKF, especially Mrs. F. A. Stewart and Dr. C. J. Fisher and his family, who did so much to comfort a person who was working away from home.

NOMENCLATURE

c_p	Constant pressure specific heat of air, Btu/lbm-°R
h	Local heat transfer coefficient, Btu/ft ² -sec-°R
h_{fp}	Reference flat-plate heat transfer coefficient, Btu/ft ² -sec-°R
N	Number of data points in correlation set
p_c	Absolute static pressure of jet gas supply chamber
Pr	Prandtl number
p_{t2}	Axial interface absolute pressure
p_w	Absolute wall pressure
r	Recovery factor
Re	Reynolds number
$R2$	Heat transfer correlation coefficient
T_1	Static temperature at outer edge of boundary layer, °R
T_{o1}	Stagnation temperature at outer edge of boundary layer, °R
T_r	Recovery temperature, °R
T^*	Boundary layer reference temperature, °R
x	Axial distance, in
x_o	Axial distance where boundary layer is projected to begin, in
s	Distance measured along surface of test model, in
s_o	Distance along surface where boundary layer is projected to begin, in
x_{min}	Minimum axial distance in data set used for correlation, in
u_1	Flow velocity at outer edge of boundary layer, ft/sec
δ	Boundary layer thickness
δ_{fp}	Reference flat-plate boundary layer thickness
μ	Dynamic viscosity, lbm/ft-sec
ρ	Density, lbm/ft ³

I. INTRODUCTION:

By going through formal graduate education programs, I have earned the basic knowledge necessary to work in the area of thermofluid engineering sciences, comprising fluid dynamics, heat transfer, thermodynamics, and transport properties. My master's thesis deals with the complete design of a small blowdown supersonic wind tunnel up to Mach 4 and my doctoral dissertation looks on the mass transport mechanisms of gases to and from a solid surface in a vacuum under cryogenic conditions. The latter work, performed at the Mechanical Engineering Department at the University of Illinois, was sponsored by the U.S. Air Force with equipment furnished by AEDC.

My particular interest is in the general area of transport processes, either at low speed characteristic of chemical processing or at high speed typified by vehicles traveling at hypersonic velocities. I have studied the Taylor dispersion problem, a mass transport process by simultaneous diffusion and convection within a transversely bounded region, for quite sometime. As a result, an exact solution has been formulated for the problem and the apparent gap between the previous small-time and large-time asymptotic solutions is closed on a fundamental basis. Part of this work was performed at the Mechanical Engineering Department of University of California at Berkley under a grant from the National Science Foundation. Some of the results have been published in the open literature. A general paper, including homogeneous and heterogeneous first order chemical reactions, is being prepared for immediate submission.

Mr. M. K. Kingery, the AEDC Effort Focal Point of the USAF-UES Summer Faculty Research Program, assigned me to work with the Aerophysics Branch of the von Karman Facility Division where major efforts have been devoted to investigating problems of transfer of mass, heat, and momentum in hypersonic flow fields. For a person with my background, I couldn't agree with Mr. Kingery any better on the assignment. There were many on-going projects with a wealth of data to be analyzed. The particular problem on which I turned out to spend the summer research period of ten weeks was to investigate the heat transfer over the surfaces of nosetips with gas injections counter-current to a

supersonic mainflow stream. The task belongs to the Applied Computation Mechanics Group of the Aerophysics Branch with Dr. J. R. Maus, Jr. as the principle engineer.

II. OBJECTIVES OF THE RESEARCH EFFORT:

The first phase of testing under wind tunnel conditions was completed in October 1984 by employing two different nosetip shapes attached to aft cones of identical configurations--the baseline model and the alternate model (Ref. 1). In these tests, air was used for both the main flow and the jet gas which was varied over a range of injection mass flow rates. The long-range goal of the project is, through analyzing the test data, to search for a method for predicting the heat transfer, and ultimately the wall temperatures in the course of time after the onset of the jet gas, over the surface of a full-size flight model under flight conditions, including the effects by using jet gases of different molecular weights. At present, however, major research activities have been aimed at an attempt to reproduce the AEDC test data by theoretically or empirically modeling the physical flow processes. Dr. Maus has been calculating the flow field from first principles by using computer codes modified to meet the conditions of the present problem. Very encouraging results have been obtained. A brief attempt with little success has been made to compare on a common basis the AEDC data with those inferred from the NASA Langley measurements (Ref. 2). After consultation with Dr. Maus, I concentrated my effort on physically modeling the boundary layer flow process by using the AEDC test data for the correlation of the experimentally inferred heat transfer coefficients. This report consists of the results for such correlations obtained over the portion of the model surface where a two-dimensional flow of the attached boundary-layer type is assumed to exist.

III. BOUNDARY-LAYER FLOW MODELING:

Figure 1 shows a sketch of the general flow pattern and for a configuration where a nosetip with a counter-flow sonic jet is placed in a supersonic airstream. The sonic jet expands into the region outside

the exit to a higher Mach number and experiences a normal shock at the axis. The bow shock, which is also normal at the axis, encountered by the airstream stands away at a distance upstream of the jet shock. The two streams decelerate toward each other and meet at the mutual stagnation point given by the intersection of the axis and the interface. The jet flow is deflected outward and rearward by the action of the main stream, and a separation region with flow recirculation is created around the jet emanating from the orifice and over a certain portion of the nosetip surface at the front. The flow near the downstream end of the separation region in the direction of the main flow reattaches to the wall, where the flow is supersonic, and a recompression shock occurs for flow readjustment. Beyond the point of reattachment, the flow over the surface is fully attached and a boundary layer is developed. However, the boundary layer may not be in stable equilibrium over some distance in the flow direction near the front because of possible shedding of streamwise vortices (Ref. 3). The contribution to heat transfer of these vortices has yet to be clarified. The flow velocity along the interface smooths out and increases steadily because normally the stagnation temperature, and therefore the flow velocity, of the jet gas is much lower than that of main airstream. Turbulent mixing thus takes place across the interface and the adiabatic wall temperature of the boundary layer over the surface increases steadily in the direction of the main flow.

The test data for the two models employed, the baseline and the alternate, are compiled in Ref. 4. In order to correlate the test-inferred heat transfer coefficients, it is necessary to devise a working scheme for determining the local properties characteristic of the outer edge of the boundary layer. It is proposed here that such local characteristic properties be fixed as follows:

- (1) the pressure variation across the boundary layer thickness is negligible,
- (2) the flow expands isentropically from the interface pressure at the mutual stagnation point to the locally measured wall pressure with a local stagnation temperature to be determined from the test-inferred recovery temperature,

the exit to a higher Mach number and experiences a normal shock at the axis. The bow shock, which is also normal at the axis, encountered by the airstream stands away at a distance upstream of the jet shock. The two streams decelerate toward each other and meet at the mutual stagnation point given by the intersection of the axis and the interface. The jet flow is deflected outward and rearward by the action of the main stream, and a separation region with flow recirculation is created around the jet emanating from the orifice and over a certain portion of the nosetip surface at the front. The flow near the downstream end of the separation region in the direction of the main flow reattaches to the wall, where the flow is supersonic, and a recompression shock occurs for flow readjustment. Beyond the point of reattachment, the flow over the surface is fully attached and a boundary layer is developed. However, the boundary layer may not be in stable equilibrium over some distance in the flow direction near the front because of possible shedding of streamwise vortices (Ref. 3). The contribution to heat transfer of these vortices has yet to be clarified. The flow velocity along the interface smooths out and increases steadily because normally the stagnation temperature, and therefore the flow velocity, of the jet gas is much lower than that of main airstream. Turbulent mixing thus takes place across the interface and the adiabatic wall temperature of the boundary layer over the surface increases steadily in the direction of the main flow.

The test data for the two models employed, the baseline and the alternate, are compiled in Ref. 4. In order to correlate the test-inferred heat transfer coefficients, it is necessary to devise a working scheme for determining the local properties characteristic of the outer edge of the boundary layer. It is proposed here that such local characteristic properties be fixed as follows:

- (1) the pressure variation across the boundary layer thickness is negligible,
- (2) the flow expands isentropically from the interface pressure at the mutual stagnation point to the locally measured wall pressure with a local stagnation temperature to be determined from the test-inferred recovery temperature,

- (3) the recovery factor is essentially constant which, for turbulent flow, ranges from 0.875 to 0.890 (Ref. 5), and
- (4) air may be treated as a perfect gas with constant specific heats.

Thus we can calculate

$$T_1/T_{01} = \left(\frac{P_w}{P_{t2}} \right)^{\frac{k-1}{k}} \quad (1)$$

which, with the input of the test-inferred recovery temperature, can be used to compute

$$T_1 = T_r / [1 + r(T_{01}/T_1 - 1)], \quad (2)$$

and then calculate

$$u_1 = 109.62 \sqrt{T_1 (T_{01}/T_1 - 1)}, \quad (3)$$

where $k = 1.4$ is the specific heat ratio of air and $r=0.875$ is arbitrarily selected (little changes occur as long as 0.875 r 0.890). By using the above procedure, a set of characteristic properties is thus completely defined for every local state at the outer edge of the boundary layer at every location along the surface of the test model where measurements are taken.

IV. HEAT TRANSFER CORRELATION:

The stable boundary layer is projected to have a starting point at a distance s_0 measured along the surface of the test model from the jet exit in the direction of the mainflow. For surface locations at $s > s_0$, a local flat-plate boundary layer thickness δ_{fp} is used to characterize the thickness of the actual boundary layer at the same location. The former is defined as the boundary layer thickness which would exist at the location s if a flow with a freestream velocity u_1 at a freestream condition (p_w, T_1) had taken place over a flat plate at zero incidence with a leading edge located at s_0 . In the above, p_w is the measured local wall pressure, and T_1 and u_1 are given by equations (2)

and (3), respectively. Following Eckert (Ref. 6), to effectively account for the influence of the temperature gradient on the boundary layer flow, the flow properties are evaluated at a reference temperature

$$T^* = T_1 + 0.5(T_w - T_1) + 0.22(T_r - T_1). \quad (4)$$

The boundary layer is assumed to be turbulent. Thus for the reference flat plate,

$$\delta_{fp} = 0.371(s - s_o) Re^{*-0.2}, \quad (5)$$

and

$$h_{fp} = 0.0288 \rho^* u_1 c_p Re^{*-0.2} Pr^{*-2/3}, \quad (6)$$

where

$$Re^* = \frac{\rho^* u_1 (s - s_o)}{\mu^*}, \quad (7)$$

and ρ^* , μ^* , and Pr^* are evaluated at the reference temperature T^* given by equation (4).

The boundary layer thickness δ_{fp} defined by the above flat-plate scheme has a one-to-one correspondence with that on the surface of the test model. As a first approximation, it is proposed to try out a linear relationship between these two quantities. Since the heat transfer coefficient is inversely proportional to the boundary thickness, the above approximation then leads to

$$h/h_{fp} = \delta_{fp}/\delta = F \quad (8)$$

where F is a constant. Use of equation (6) in equation (8) we can write

$$h = CH(s - s_o)^{-0.2}, \quad (9)$$

where

$$C = 0.0288 F c_p \quad , \quad (10)$$

and

$$H = (g^* u_1)^{0.8} \mu^*{}^{0.2} Pr^*{}^{-2/3} . \quad (11)$$

In order to make use of equation (9) for the correlation of the test-inferred heat transfer coefficients, it becomes necessary to determine the constant C, and therefore F, and the projected surface distance s_0 for the starting point of the stable boundary layer. The method of least squares is applied to achieve this purpose. The results are

$$C = \frac{\sum_{j=1}^N h_j H_j (s_j - s_0)^{-0.2}}{\sum_{j=1}^N H_j^2 (s_j - s_0)^{-0.4}} \quad , \quad (12)$$

$$\sum_{j=1}^N H_j (s_j - s_0)^{-1.2} [C H_j (s_j - s_0)^{-0.2} - h_j] = 0, \quad (13)$$

$$s_0 < \min_{1 \leq j \leq N} \{s_j\}, \quad (14)$$

where N is the total number of data points and s_j is the jth surface distance at the axial location x_j of the data set to be correlated, H_j is given by equation (11) evaluated at s_j , and equation (14) states the fact that s_0 must be smaller than the minimum in the set $\{s_j\}$ to be correlated.

A FORTRAN program has been written for calculating C according to equation (12) and solving for s_0 from equation (13). Incorporated in the program is an option for discriminating against those test-inferred heat transfer data which have low correlation coefficients (R^2 in Ref. 4). On output, all surface distances are converted to axial distances.

IV. RESULTS AND DISCUSSION:

The procedure described above has been applied to correlate the test-inferred heat transfer coefficient distributions over the surfaces of the nosetip models tested at nearly zero angle of attack. The constants x_o (axial distance) and F obtained by the least squares method together with the number of data points and the value of the heat transfer correlation coefficients used in the correlations are tabulated below.

Run	P_c/P_{t2}	x_o in	F	$R2$	N
Baseline Model, $M = 10.10$					
10	1.10	4.917	1.262	0.92	28
11	1.49	5.395	1.295	0.89	28
12	2.01	6.700	1.284	0.90	20
7	2.99	16.164	1.449	0.40	14
Baseline Model, $M = 5.98$					
52	1.08	4.664	1.304	0.85	29
53	1.53	6.700	1.359	0.31	19
54	1.99	6.700	1.302	0.34	18
58	2.98	17.918	0.807	0.40	7
Alternate Model, $M = 10.10$					
32	1.11	7.186	1.386	0.88	29
33	1.48	7.844	1.293	0.95	22
34	2.00	7.844	1.301	0.94	22
43	2.98	17.693	1.038	0.70	18

The number of data points used for correlation depends on the value of the correlation coefficient ($R2$ in above table) selected. The particular values listed are employed for the purpose of making the number of correlation data points as large as possible and, if it turns out to be the case, of excluding from the correlation set the test data in the immediate neighborhood of the fixed joint where the nosetip is linked to the aft cone. A value of $R2=0.95$ is recommended in Ref. 3 as the lower limit. Therefore, results obtained with an $R2$ value

substantially lower than 0.95 may be questionable. Ref. 7 may provide some clarifications to this problem.

The least-square parameters (x_o and F) are obtained by visual comparison between the distribution of the heat transfer coefficients obtained by correlation and that inferred from experiments (to be shown below). The test-inferred heat transfer data showed unexpected distortions upstream and downstream from the fixed joint between the nosetip and the aft cone, especially at high jet gas injection rates (high p_c/p_{t2} ratios). A possible reason for this occurrence has been conjectured (Ref. 8) but little proof can be ascertained without future tests.

Putting aside the results at the highest injection rate ($p_c/p_{t2} = 2$) and treating the rest of the results on an equal basis by disregarding the values of the correlation coefficients used, the present correlation shows that $F=h/h_{fp}$ falls in the range of 1.26 to 1.39 for both models tested and that x_o increases slightly with increasing injection rates. By excluding Run 53 because of its poor overall quality as indicated by the low correlation coefficient values (see Ref. 4), the tabulated results for the baseline model tend to indicate that effects on x_o and F due to Mach number are only slight.

Visual comparisons for the baseline model at Mach 10 between correlations and experiments are shown in Figures 2(a) to Figures 2(d). The other results are treated in similar fashion. Good agreement has been obtained at low injection rates, as shown in Figures 2(a) and 2(b), for all $x > x_o$ except at the locations $x=7.39$, 8.37 and 11.30 inches where the test data substantially fall below the general trend indicated by all the other data points. The same departures at these same locations also appeared in the Mach 6 runs with the same injection rates.

In Figure 2(c), where $p_c/p_{t2}=2.01$, there are plotted three sets of correlation results. A value of $R^2=0.90$ is used for all three cases but the test data used for correlation in each case include only those having axial distances equal to or greater than a specified value x_{min} . It can be observed that the comparisons are (1) $x_{min}=4.95$ " : partially favorable over the nosetip but not over the aft cone, (2) $x_{min}=9.35$ " : partially favorable over the nosetip and realistically reasonable over the aft cone, and (3) $x_{min}=13.27$ " : favorable over the aft cone only. If

the stable boundary layer starts on the nosetip, then Case (2) is the logical choice; otherwise, the choice must be narrowed down to Case (3). Case (2) is selected to represent the real picture by assuming that the fixed joint between the nosetip and the aft cone did not seriously disturb the boundary layer.

Figure 2(d) is the result obtained at the highest injection rate corresponding to $p_c/p_{t2}=2.99$. Correlation is possible only over the surface of the aft cone. This seems to imply that the boundary layer flow is highly disturbed by the fixed joint between the nosetip and the aft cone.

In Figure 2(a) and 2(b) where low injection rates are used, it appears that the projected starting point of the stable boundary layer x_0 can be identified approximately to fall in the region over the surface where the test-inferred heat transfer coefficient undergoes a sudden sharp rise. This feature of comparison, however, is somewhat lost at higher injection rates, as shown in Figure 2(c), and completely disappeared, illustrated in Figure 2(d), as the injection rate is raised further. The flow is expected to follow some regular pattern of change. The difference in the distributions of the test data obtained at low and high injection rates, whether it be due to the interference of the joint between the nosetip and the aft cone or be of a fundamental nature characteristic of an unstable boundary layer complicated with the existence of 3-dimensional effects, can not be pinpointed at present. It is hoped that this can be clarified by future tests.

VI. RECOMMENDATIONS:

The method can be immediately implemented to correlate all the AEDC runs if retrieval of test data from the computer datafile is permitted. This is considered to be worthwhile because it will help establish the range of the parameter $F=h/h_{fp}$ on a much broader basis than what has been reported here. The present computer program can be modified to search for the least-squares parameters in a systematic manner if a workable criterion of termination, such as the minimum of the average rms deviations, is used.

The present results indicate that the heat transfer data correlated do conform to the distributions characteristic of an attached stable turbulent boundary layer. The outcome of the 12 runs correlated, revealing $h/h_{fp} = \delta_{fp}/\delta \approx 1.3$, at present shows that the reference flow with zero pressure gradient connotive of the actual boundary layer is a rather effective measure for the purpose of correlation. To help understand its significance, it is necessary to investigate the actual boundary layer growth over the wall surface along which a rather substantial streamwise pressure drop exists. It will be proposed that such an investigation be considered as an item of work to follow on. The contention is that, by estimating the thickness of the actual boundary layer, the present method of correlation can be substantiated in essential details.

The axial location x_0 where the boundary layer is projected to start is a critical quantity for correlating the heat transfer downstream. The present results indicate that x_0 to a large extent depends on the geometry of the nosetip model with a slight increase as the injection rate of the jet gas increases, while its dependence on Mach number seems to be rather weak. The ratio of the jet exit diameter to the overall length of the two nose assemblies tested at AEDC is roughly ten times that of the flight-scale model tested at NASA Langley (Ref. 1 and 2). It is desirable to know how the heat transfer key parameters of these different geometries are related. However, if data of acceptable quality for the flight-scale model are available, then the results obtained by correlation can readily be used to predict, subject to the requirements of similarity, the possible outcome for a full size nose assembly at flight conditions. The heat transfer coefficient distributions obtained from the NASA Langley data for the flight-scale nose assembly (Ref. 2) showed little resemblance to what is expected of an attached boundary layer. It is not likely that this was caused by boundary layer instabilities. In any case, perhaps the NASA Langley data should be studied over in order to find a possible explanation for the unusual results in heat transfer.

Future tests have been planned at AEDC to use jet gases different from air. A problem to be looked into is then the dispersion of the jet gas in the flow stream. The diffusion-convection equations governing

the dispersion of the gaseous constituents must then be coupled with the equations of motion and energy conservation for the ultimate solution of the flow field. The present author would like to contribute, in whatever capacity necessary, his effort toward a solution to this problem.

REFERENCES

1. Hartman, A.S., "Heat-Transfer, Recovery Temperature, and Surface Pressure Measurements Obtained in Tunnels E & C on Nosetips with Stagnation Point Gas Injection Coding," AEDC-TSR-85-V3, December 1984.
2. Dunn, S., and Dunn, J., "Heat Transfer Test Results for a Flight-Scale GJNT with Mass Injection from HTST," PDA TR-1537-17-05, May 6, 1983.
3. Simpers, G., Vas, I., and Bogdonoff, S.M., "Turbulent Shear Layer Reattachment at M 3," AIAA Paper 77-43, 1977.
4. Hartman, A.S., "BMO/Martin Gasjet Nosetip Test," Vols. 1 and 2, ADEC Project No. CB35VC, Calspan Project No. V-3-3L, October 1984.
5. Schlichting, H., Boundary Layer Theory, Transl. J. Kestin, McGraw-Hill, 1968, p. 668.
6. Eckert, E.R.G., and Drake, R.M., Analysis of Heat and Mass Transfer, McGraw-Hill, 1972, p. 432.
7. Young, H.D., Statistical Treatment of Experimental Data, McGraw-Hill, 1962, pp. 126-131.
8. Memo to Dr. J.R. Maus from J.S. Yu, Aug. 21, 1985.

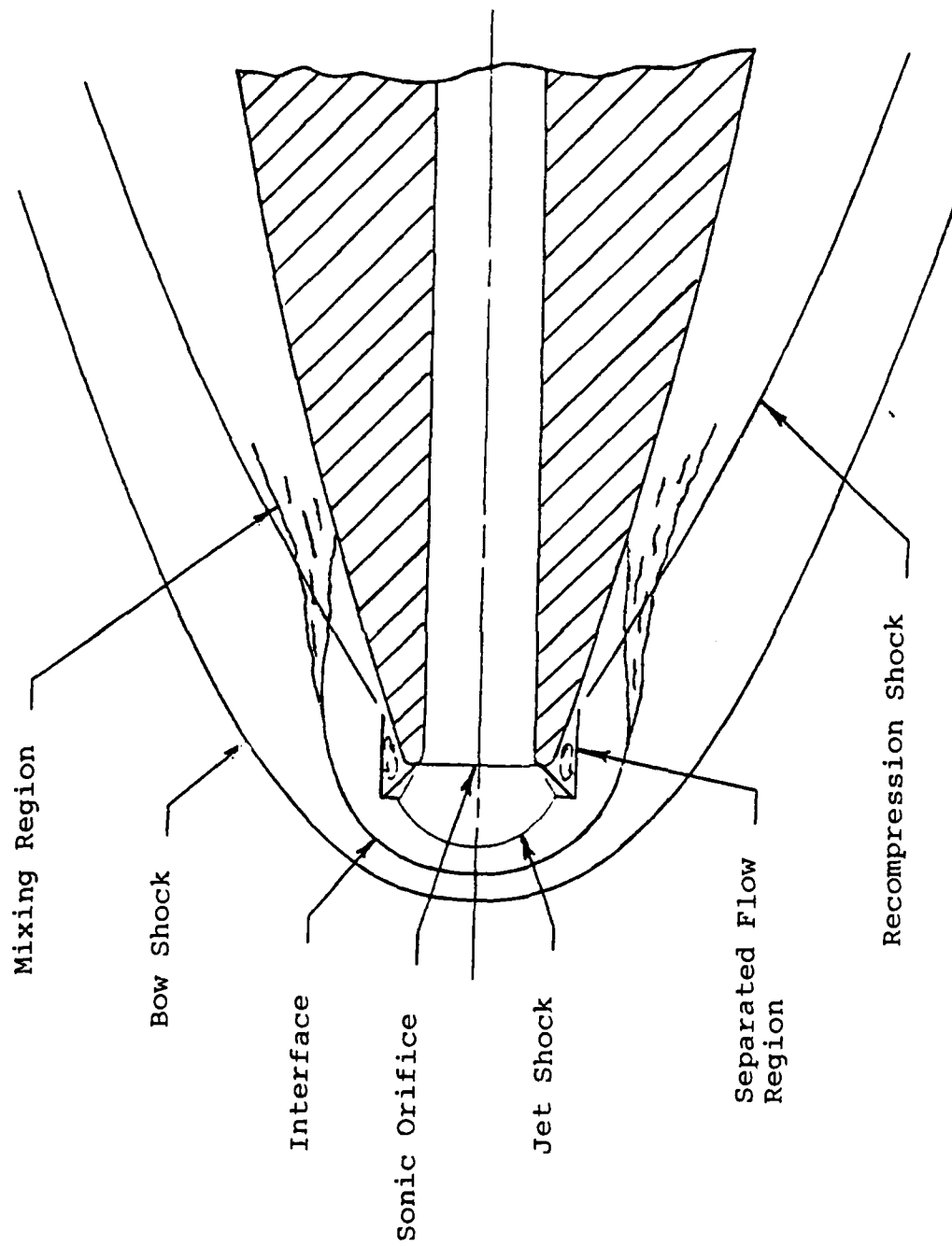


Figure 1. Principal flow features around nosetip with stagnation-point gas injection

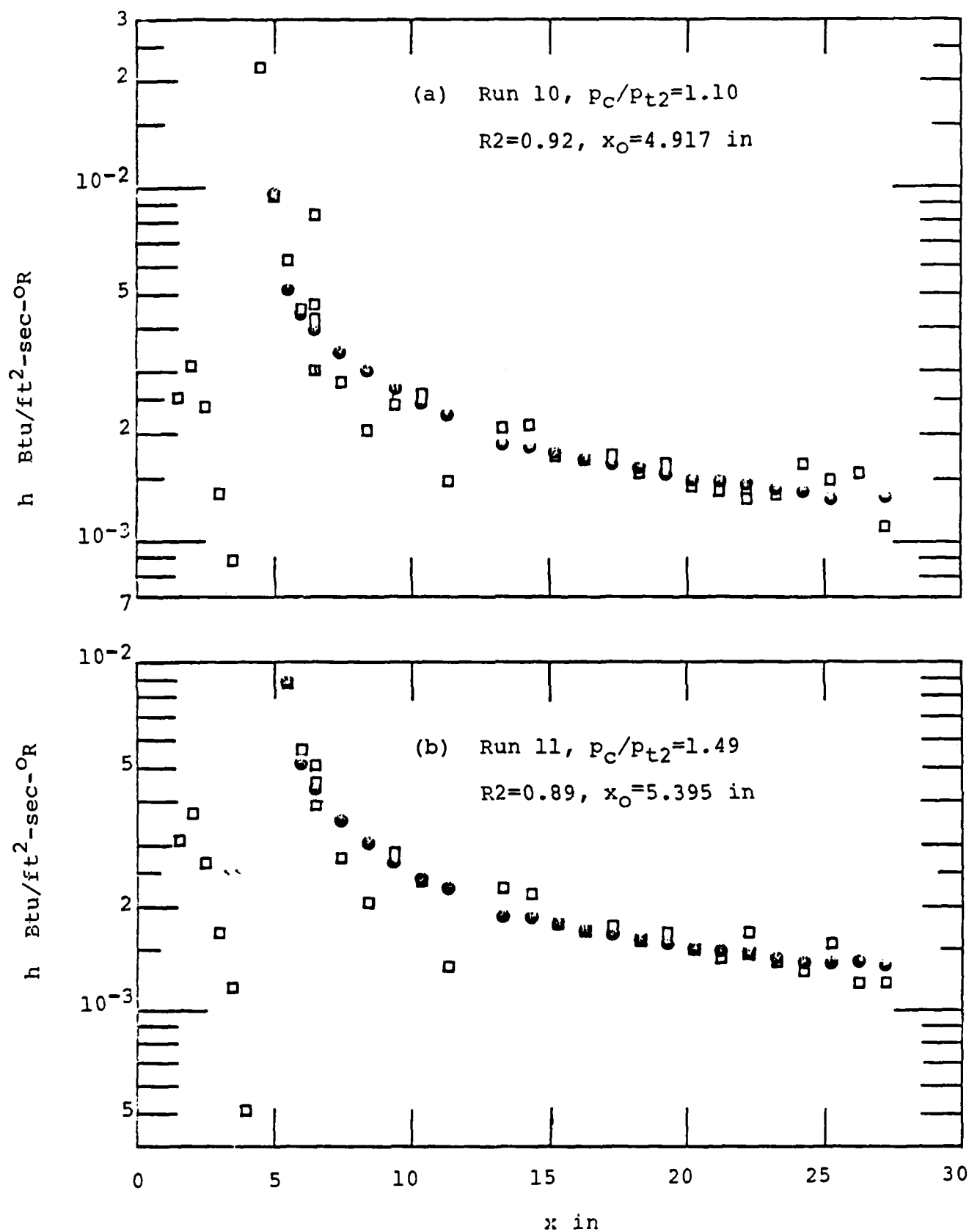


Figure 2. Comparison of heat transfer coefficient distributions, BMO/Martin Baseline model, $M = 10.10$, \square : test-inferred, \bullet : correlated.

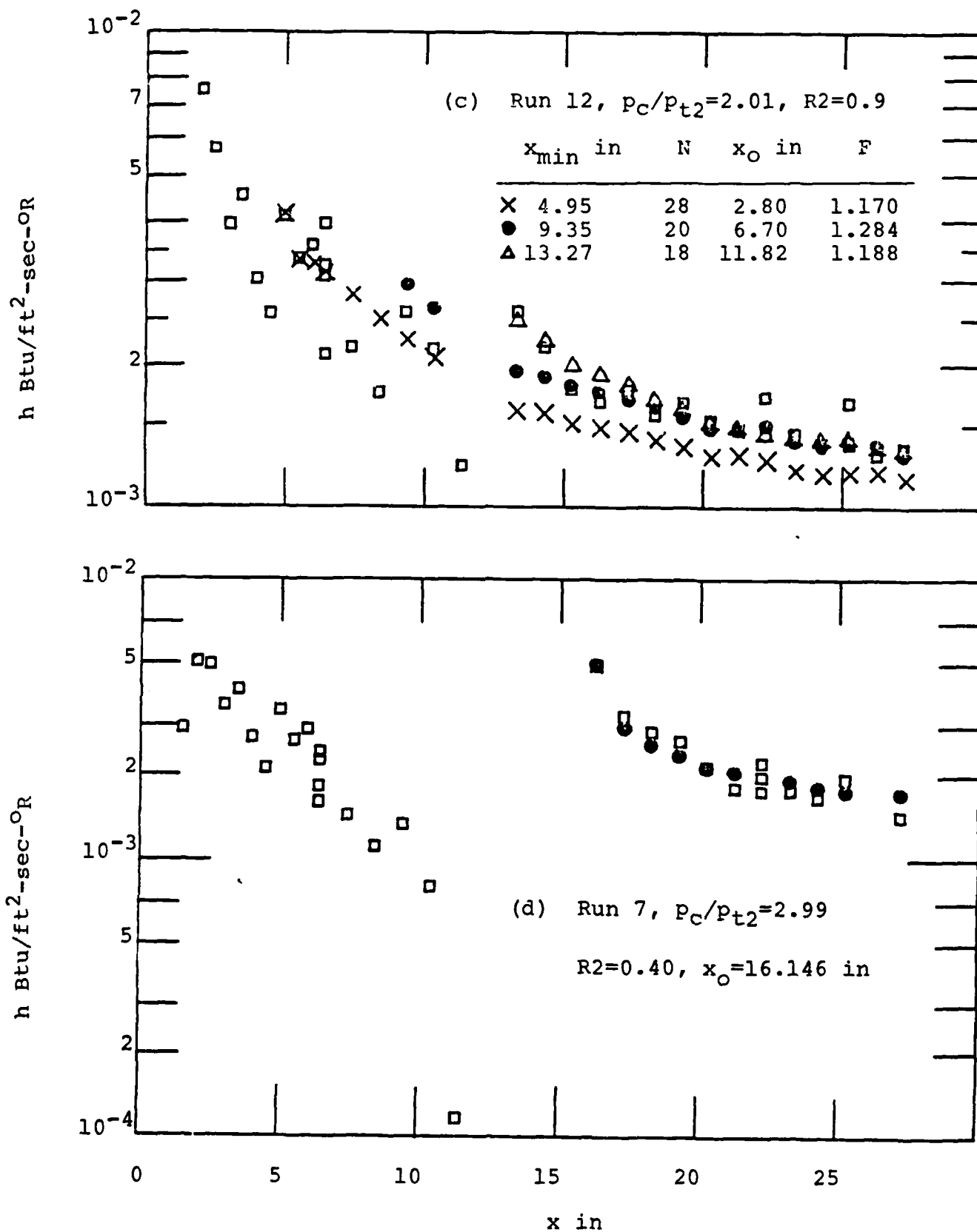


Figure 2. Concluded

END

DTic

5-86